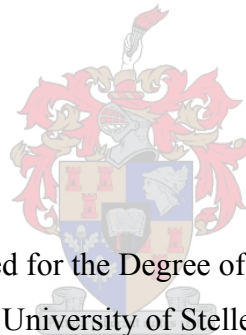


# **An Investigation of Myosin Binding Protein C Mutations in South Africa and a Search for Ligands Binding to Myosin Binding Protein C**

**W.J. de Lange**



Dissertation presented for the Degree of Doctor in Philosophy  
at the University of Stellenbosch

Promoter: Prof Valerie A. Corfield  
Co-promoter: Dr Johanna C. Moolman-Smook

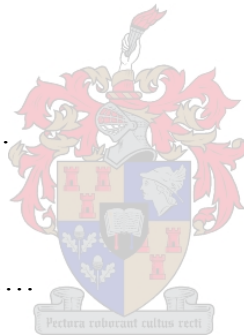
December 2004

# DECLARATION

I, the undersigned, hereby declare that the work contained in this dissertation is my own original work and that I have not previously in its entirety or in part submitted it at any university for a degree.

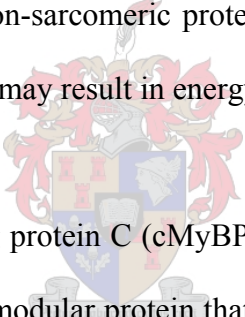
Signature: .....

Date: .....



## ABSTRACT

Hypertrophic cardiomyopathy (HCM) is an autosomal dominantly inherited primary cardiac disease. The primary features of HCM are left ventricular hypertrophy, myocardial disarray, fibrosis and an increased risk of sudden cardiac death. To date, more than 264 HCM-causing mutations, occurring in thirteen genes, have been identified. As the vast majority of HCM-causing mutations occur in components of the cardiac sarcomere, HCM has been considered a disease of the cardiac sarcomere. Functional analyses of HCM-causing mutations in sarcomeric protein-encoding genes revealed that HCM-causing mutations have a vast array of effects on contractile function. The discovery of HCM-causing mutations in the gamma two subunit of adenosine monophosphate activated protein kinase highlighted the fact that mutations in non-sarcomeric proteins can also cause HCM and supports a hypothesis that HCM-causing mutations may result in energy wastage leading to energy depletion.

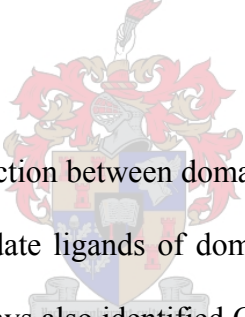


Mutations in the cardiac myosin binding protein C (cMyBPC) gene (*MYBPC3*) are the second most prevalent cause of HCM. cMyBPC is a modular protein that forms an integral part of the sarcomeric thick filament, where it acts as a regulator of thick filament structure and cardiac contractility. Although cMyBPC has been studied extensively, the mechanisms through which it fulfill these functions have remained elusive, largely due to a lack of a comprehensive understanding of its interactions with other sarcomeric components and its quaternary structure.

The aims of the present study were, firstly, to screen *MYBPC3* for HCM-causing mutations in a panel of HCM-affected individuals and, secondly, to identify the ligands of domains of cMyBPC in which HCM-causing mutations were found.

A panel of deoxyribonucleic acid (DNA) samples obtained from unrelated HCM-affected individuals was screened for HCM-causing mutations in *MYBPC3*, using polymerase chain reaction (PCR)-based single-strand conformation polymorphism method, as well as restriction enzyme digestion, DNA sequencing and reverse transcription PCR techniques. In order to identify the ligands of domains in which HCM-causing mutations were found, yeast two-hybrid (Y2H) candidate-ligand-and library-assays were performed.

Three novel and two previously described putative HCM-causing mutations were identified in *MYBPC3*. Data generated in this and other studies, however, suggest that two of these “mutations” are likely to be either polymorphisms, or disease-modifying factors, rather than main-locus HCM-causing mutations.



Recent findings showed a specific interaction between domains C5 and C8 of cMyBPC. This finding identified domains C6 or C10 as candidate ligands of domain C7. Y2H-assays revealed a specific C7:C10 interaction. Additional Y2H assays also identified C-zone titin as a ligand of domain C7 and domain C10 as a ligand of domain C3. Several other Y2H assays, however, yielded no known sarcomeric ligands of the N-terminal region of cMyBPC.

Identification of the ligands of specific domains of cMyBPC led to the development of detailed models of cMyBPC quaternary structure when cMyBPC is both unphosphorylated and fully phosphorylated. The integration of these models into an existing model of thick filament quaternary structure allows new insights into the functioning of cMyBPC as a regulator of both thick filament structure and cardiac contractility, as well as the pathophysiology of cMyBPC-associated HCM.

## OPSOMMING

Hipertrofiese kardiomiopatie (HKM) is 'n outosomaal dominante primêre hartsiekte. Die primêre kenmerke van HKM is linker ventrikulêre hipertrofie, miokardiale wanorde, fibrose en 'n verhoogde risiko van skielike dood. Tot dusver is 260 HKM-veroorsakende mutasies in 13 gene geïdentifiseer. Aangesien die oorgrote meerderheid van HKM-veroorsakende mutasies in komponente van die kardiaale sarkomeer voorkom, is HKM as 'n siekte van die kardiaale sarkomeer beskryf. Funksionele analise van HKM-veroorsakende mutasies in sarkomeriese proteïen-koderende gene het aan die lig gebring dat hierdie mutasies 'n wye spektrum van gevolge op kontraktiele funksie het. Die ontdekking van HKM-veroorsakende mutasies in die gamma-twee subeenheid van adenosien monofosfaat-geaktiveerde proteïen kinase het die feit dat mutasies nie-sarkomeriese proteïene ook HKM kan veroorsaak onderstreep en ondersteun 'n hipotese dat HKM-veroorsakende mutasies energievermorsing en energie uitputting tot gevolg het.

Mutasies in die kardiaale miosien-bindingsproteïen C (kMiBPC) geen (*MYBPC3*) is die tweede mees algemene oorsaak van HKM. kMiBPC is 'n modulêre proteïen wat 'n integrale deel van die sarkomeriese dik filament vorm, waar dit die struktuur van die dik filament en kardiaale kontraktiliteit reguleer. Nieteenstaande die feit dat kMiBPC intensief bestudeer is, word die meganismes hoe hierdie funksies vervul word swak verstaan, grotendeels weens die afwesigheid van 'n in diepte begrip van sy interaksies met ander komponente van die sarkomeer asook sy kwaternêre struktuur.

Die doelstellings van hierdie studie was, eerstens, om *MYBPC3* vir HKM-veroorsakende mutasies in 'n paneel van HKM-geaffekteerde individue te deursoek en tweedens, om die ligande van domeine van kMiBPC waarin HKM-veroorsakende mutasies gevind is te identifiseer.

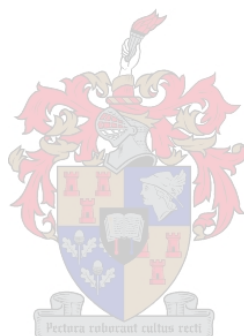
‘n Paneel van deoksiribonukleïensuur (DNS) monsters verkry van onverwante HKM-geaffekteerde individue is deursoek vir HKM-veroorsakende mutasies in *MYBPC3*, deur middel van die polimerase ketting-reaksie (PKR)-gebaseerde enkelstrand konformasie polimorfisme metode, sowel as restriksie ensiem vertering, DNS volgordebepaling en terugtranskripsie PKR tegnieke. Die ligande van domeine van kMiBPC waarin HKM-veroorsakende mutasies gevind is, is geïdentifiseer deur middel van gis twee-hibried (G2H) kandidaat-ligand en biblioteek-siftings eksperimente.

Drie onbeskryfde en twee voorheen beskryfde vermeende HKM-veroorsakende mutasies in *MYPBC3* is geïdentifiseer. Data gegenereer in hierdie en ander studies dui daarop dat twee van hierdie “mutasies” eerder polimorfismes, of siekte-modifiserende faktore, as hoof-lokus HKM-veroorsakende mutasies is.

Onlangse bevindings het ‘n spesifieke interaksie tussend die C5 en C8 domeine van kMiBPC getoon. Hierdie bevindings het óf domein C6, óf C10, as kandidaat-ligande van domein C7 geïdentifiseer. G2H eksperimente het ‘n spesifieke interaksie tussen domains C7 en C10 getoon. Addisionele G2H eksperimente het ook C-zone titin as ‘n ligand van domein C7 sowel as domein C10 as ‘n ligand van domein C3 geïdentifiseer. Verdere G2H eksperimente het egter geen sarkomeriese ligande van die N-terminale gedeelte van kMiBPC geïdentifiseer nie.

Die identifikasie van ligande van spesifieke domeins van kMiBPC het gelei tot die ontwikkeling van ‘n gedetailleerde model van kMiBPC kwaternêre struktuur wanneer kMiBPC beide ongefosforileerd en ten volle gefosforileerd is. Die intergrasie van hierdie modelle in bestaande modelle van dik filament kwaternêre struktuur werp nuwe lig op die funksionering van kMiBPC as ‘n reguleerder van beide dik filament struktuur en kardiaale kontraktiliteit, sowel as die patofisiologie van kMiBPC-geassosieerde HKM.

<b>INDEX</b>	<b>Page</b>
<b>ACKNOWLEDGEMENTS</b>	<b>viii</b>
<b>LIST OF ABBREVIATIONS</b>	<b>ix</b>
<b>LIST OF FIGURES</b>	<b>xvii</b>
<b>LIST OF TABLES</b>	<b>xxv</b>
<b>I. INTRODUCTION</b>	<b>4</b>
<b>II. METHODS AND MATERIALS</b>	<b>93</b>
<b>III. RESULTS</b>	<b>165</b>
<b>IV. DISCUSSION</b>	<b>262</b>
<b>APPENDIX A</b>	<b>345</b>
<b>APPENDIX B</b>	<b>360</b>
<b>APPENDIX C</b>	<b>361</b>
<b>REFERENCES</b>	<b>362</b>



## ACKNOWLEDGEMENTS

Firstly, I would like to thank my promoter, Prof Valerie Corfield, and co-promoter, Dr Hanlie Moolman-Smook, for all your support and advice throughout the course of the project, as well as in the preparation of this dissertation. Without your technical support, advice, guidance and linguistic skills, neither this study, nor this dissertation would have been possible.

Secondly, I want to thank everyone in the Department of Medical Biochemistry, and especially the members of Laboratory F445, both past and present, for all the technical support and intellectual discussions, all of which have contributed to this study and my scientific development. Specifically, I would like to thank Mrs Ina le Roux who performed DNA extractions and EBV transformations. Sr Althea Goosen who collected blood samples, did the tracing of family members of mutation carriers and constructed family trees, from time to time you did the seemingly impossible to make this study possible. Mrs Lundi Korki for all her help and technical assistance. Also Prof Paul Brink for his clinical insights, as well as stimulating numerous scientific discussions.

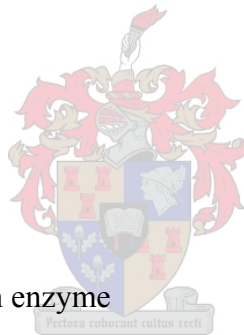
I would also like to thank Prof Hugh Watkins and his group at the Department of Cardiovascular Medicine, University of Oxford, where I performed most of the RNA and RT-PCR work in this study. Your technical expertise in this regard was invaluable and your hospitality impeccable. Also the advice and guidance received from Prof Watkins throughout the course of this study was invaluable.

I would also want to acknowledge Dr Peter Rogan, from the University of Missouri-Kansas City School of Medicine, who performed computational analysis of nucleotide sequence variants identified in *MYBPC3*, to establish whether these variants are likely to alter the splicing of the *MYBPC3* transcript.

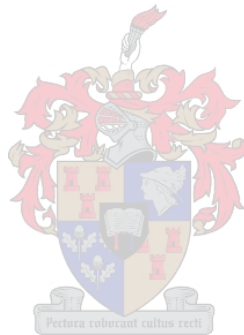
Finally, I would like to thank my family and close friends, especially Claris my mother, Marelette, Adam, Sara, Jean, Hendri and Inge. Without your support, this study would not have been possible.

## LIST OF ABBREVIATIONS

5' AMP-activated protein kinase	AMPK
5' AMP-activated protein kinase ( $\gamma_2$ subunit) gene	<i>PRKAG2</i>
5' AMP-activated protein kinase kinase	AMPKK
$\alpha$ -Cardiac actin gene	<i>ACTC</i>
$\alpha$ -Myosin heavy chain	$\alpha$ MHC
$\alpha$ -Myosin heavy chain gene	<i>MYH6</i>
$\alpha$ -Tropomyosin	$\alpha$ TM
$\alpha$ -Tropomyosin gene	<i>TPM1</i>
$\beta$ -Galactosidase	$\beta$ -Gal
$\beta$ -Myosin heavy chain	$\beta$ MHC
$\beta$ -Myosin heavy chain gene	<i>MYH7</i>
$\lambda$ DNA, digested with the <i>Pst</i> I restriction enzyme	$\lambda$ Pst
A-kinase anchoring proteins	AKAPS
Adenine hemisulphate	Ade
Adenosine	a
Adenosine monophosphate	AMP
Adenosine triphosphate	ATP
Adenosine triphosphatase	ATPase
Alanine	A
Allele-specific restriction enzyme analysis	ASREA
Ampicillin	Amp



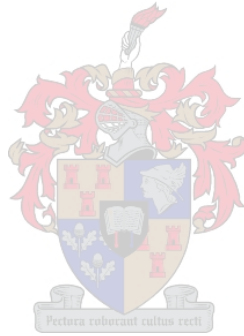
Annealing temperature	Ta
Asparagine	N
Aspartic acid	D
Arginine	R
Ca <sup>2+</sup> -activated phospholipid-dependent protein kinase	PKC
Ca <sup>2+</sup> /calmodulin-dependent protein kinase II	CaMK II
Calf intestinal alkaline phosphatase	CIP
Cardiac myosin binding protein C	cMyBPC
Cardiac myosin binding protein C gene	<i>MYBPC3</i>
Cardiac troponin C	cTNC
Cardiac troponin C gene	<i>TNNC1</i>
Cardiac troponin I	cTNI
Cardiac troponin I gene	<i>TNNI3</i>
Cardiac troponin T	cTNT
Cardiac troponin T gene	<i>TNNT2</i>
cAMP-dependent protein kinase	PKA
Centimetre	cm
Co-immunoprecipitation	CoIP
Colony forming units	cfu
Copy DNA	cDNA
Cyclic AMP	cAMP
Cyclic guanosine monophosphate	cGMP
Cysteine	C



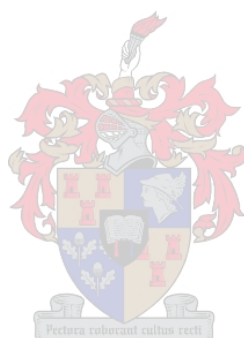
Cytosine	c
Deletion	Δ
Degrees Celsius	°C
Deoxyadenosine triphosphate	dATP
Deoxycytidine triphosphate	dCTP
Deoxyguanosine triphosphate	dGTP
Deoxythymidine triphosphate	dTTP
Deoxyribonucleic acid	DNA
Diethylpyrocarbonate	DEPC
Dilated cardiomyopathy	DCM
Dimethylsulphoxide	DMSO
Distilled deionised H <sub>2</sub> O	ddH <sub>2</sub> O
Electrocardiogram	ECG
Enzyme unit	U
Epstein-Barr virus	EBV
<i>Escherichia coli</i>	<i>E.coli</i>
Ethylene-diamine-tetra-acetic acid	EDTA
Fast skeletal MyBPC	fsMyBPC
Fast skeletal troponin I	fsTNI
Fibronectin type 3 domain	Fn3
Filamentous actin	F-actin
Glutamic acid	E
Glutamine	Q



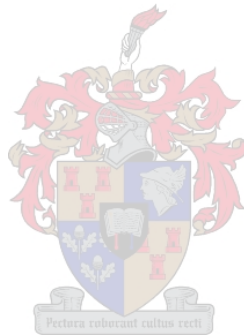
Gram(s)	g
Glycine	G
Guanosine	g
Heavy meromyosin	HMM
Histidine	H (His)
Hour(s)	h
Hypertrophic cardiomyopathy	HCM
Immunoglobulin type C2 domain	IgC2
Insertion	Ins
Interventricular septum	IVS
Isoleucine	I
Kanamycin	Kan
Kilo Dalton	kDa
Kilobase	kb
Left ventricular hypertrophy	LVH
Leucine	L (Leu)
Lithium acetate	LiAc
Litre	l
Light meromyosin	LMM
Luria-Bertani	LB
Lysine	K
Melting temperature	T <sub>m</sub>
Mega Dalton	MDa



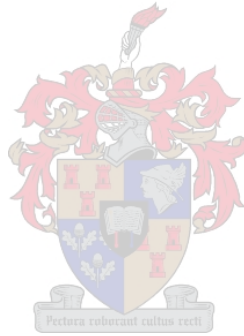
Megahertz	Mhz
Messenger RNA	mRNA
Methionine	M
Microgram	μg
Microlitre	μl
Micrometre	μm
Millilitre	ml
Millimetre	mm
Millimolar	mM
Minute(s)	min
Molar	M
Multiple cloning sites	MCS
Muscle LIM protein	MLP
Muscle LIM protein gene	<i>CSRP3</i>
Myosin binding protein	MyBP
Myosin binding protein C	MyBPC
Myosin binding protein H	MyBPH
Myosin essential light chain	MELC
Myosin heavy chain	MHC
Myosin regulatory light chain	MRLC
Myosin subfragment 1	S1
Myosin subfragment 2	S2
Myosin ventricular essential light chain 1 gene	<i>MYL3</i>



Myosin ventricular regulatory light chain 2 gene	<i>MYL2</i>
Nanogram	ng
Nanometre	nm
Non-insulin dependent diabetes mellitus	NIDDM
Nucleotide base pair	bp
O-nitrophenyl $\beta$ -D-galactopyranoside	ONPG
Open reading frame	ORF
Optical density	OD
Phenol:chloroform:isoamyl alcohol	PCI
Phosphocreatine	PCr
Phospholamban	PLB
Polyethylene glycol	PEG
Polymerase chain reaction	PCR
Posterior wall	PW
Professor	Prof
Proline	P
Quadruple dropout	QDO
Republic of South Africa	RSA
Reverse transcription PCR	RT-PCR
Revolutions per minute	rpm
Ribonuclease	RNase
Ribonucleic acid	RNA
Ryanodine receptor	RyR



Sarcoplasmic reticulum	SR
Second(s)	s
Selective dropout	SD
Serine	S
Single nucleotide substitution	SNS
Single strand conformation polymorphism	SSCP
Silent site sequence variations	ssSVs
Slow skeletal MyBPC	ssMyBPC
Slow skeletal troponin I	ssTNI
Sodium acetate	NaAc
Sodium dodecyl sulphate	SDS
Splice acceptor site	SaS
Splice branch point	SbP
Splice donor site	SdS
SR Ca <sup>2+</sup> -ATPase	SERCA2a
Sudden cardiac death	SCD
Termination codon	X
Threonine	T
Thymidine	t
Times	x
Titin gene	<i>TTN</i>
Triple dropout	TDO
Troponin C	TNC



Troponin I	TNI
Troponin T	TNT
Tryptophan	W (Trp)
Tyrosine	Y
United Kingdom	UK
United States of America	USA
Valine	V
Volt	V
Volume per volume	v/v
Watt	W
Weight per volume	w/v
Wolff-Parkinson-White syndrome	WPW
Wormlike chain	WLC
Yeast two-hybrid	Y2H



## LIST OF FIGURES

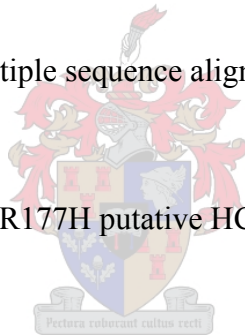
<b>Figure</b>	<b>Page</b>
Figure I.1. Regulation and function of 5' AMP-activated protein kinase	15
Figure I.2. Ca <sup>2+</sup> -regulation of cardiac contraction	19
Figure I.3. Structure of troponin complex and $\alpha$ -tropomyosin during diastole and systole	24
Figure I.4. Schematic representation of cardiac troponin I	25
Figure I.5. Proposed mechanisms involved in the cAMP-dependent phosphorylation and cGMP-dependent dephosphorylation of cTNI, as well as the effect thereof on Ca <sup>2+</sup> sensitivity	26
Figure I.6. Arrangement of titin in the sarcomere	28
Figure I.7. Domain organisation of C-terminal titin	29
Figure I.8. Organisation of D-zone titin	31
Figure I.9. Organisation of C-zone titin	32
Figure I.10. Organisation of P-zone titin	33
Figure I.11. Splice isoform diversity of the I-band regions of titin	37
Figure I.12. Model for passive tension development by N2B titin	41
Figure I.13. Proposed mechanism for the generation of restoring force facilitated by an interaction between the PVEK segment of N2B titin and F-actin.	43
Figure I.14. Domain organisation of Z-disk titin	44
Figure I.15. Proposed position of titin in the Z-disk	45



<b>Figure</b>	<b>Page</b>
Figure I.16. Structure of the MyBPC and MyBPH	48
Figure I.17. Distribution of MyBPs within the sarcomere	49
Figure I.18. Interaction-surface model between MyBPC domain C10 and LMM	51
Figure I.19. Structure of myosin II protein	54
Figure I.20. Location of phosphorylation sites in cMyBPC	57
Figure I.21. Effect of cMyBPC phosphorylation on thick filament structure	61
Figure I.22. Transition of myosin S2 from a coiled-coil conformation to a random coil conformation associated with the binding of an antibody to S2	63
Figure I.23. HCM-causing mutations in cMyBPC	75
Figure II.1. Flow-diagram depicting the mutation screening protocol followed	94
Figure II.2. Flow-diagram depicting the procedures followed for the generation of Y2H constructs	95
Figure II.3. Flow-diagram depicting the procedures followed for the Y2H screening of cDNA libraries	96
Figure II.4. Site-directed mutagenesis PCR	124
Figure II.5. Restriction map and multiple cloning site of pAS2.1	139
Figure II.6. Restriction map and multiple cloning site of pGBKT7	140
Figure II.7. Restriction map and multiple cloning site of pACT2	141
Figure II.8. Restriction map and multiple cloning site of pGADT7	142
Figure III.1. Identification of the novel t2510c polymorphism in intron 4 of <i>MYBPC3</i>	168

<b>Figure</b>	<b>Page</b>
Figure III.2. Identification of the novel ins/del c2735 polymorphism in intron 5 of <i>MYBPC3</i>	169
Figure III.3. Identification of the novel a4962g ssSV in intron 8 of <i>MYBPC3</i>	170
Figure III.4. Identification of the novel c6114a polymorphism in intron 11 of <i>MYBPC3</i>	171
Figure III.5. Identification of the novel g8168a polymorphism in intron13 of <i>MYBPC3</i>	172
Figure III.6. Identification of the novel c8612t polymorphism in intron 15 of <i>MYBPC3</i>	173
Figure III.7. Identification of the novel c13314g polymorphism in intron 24 of <i>MYBPC3</i>	174
Figure III.8. Identification of the novel g19143a polymorphism in intron 33 of <i>MYBPC3</i>	175
Figure III.9. Identification of the novel c19731t polymorphism in intron 34 of <i>MYBPC3</i>	176
Figure III.10. Identification of the novel g19706a ssSV in intron 34 of <i>MYBPC3</i>	177
Figure III.11. Identification of the novel T262T polymorphism in exon 8 of <i>MYBPC3</i>	178
Figure III.12. Identification of the novel A522A ssSV in <i>MYBPC3</i> exon 18	179
Figure III.13. Identification of the novel S708S polymorphism in <i>MYBPC3</i> exon 23	180

<b>Figure</b>	<b>Page</b>
Figure III.14. Identification of the novel T737T ssSV in exon 24 of <i>MYBPC3</i>	181
Figure III.15. Identification of the novel E1096E polymorphism in exon 31 of <i>MYBPC3</i>	182
Figure III.16. Identification of the novel V158M putative HCM-causing missense mutation in exon 5 of <i>MYBPC3</i>	184
Figure III.17. Cross-species/isoform multiple sequence alignment of a portion of the C1 domain of MyBPC	185
Figure III.18. Identification of the novel A181T putative HCM-causing mutation in exon 6 of <i>MYBPC3</i>	186
Figure III.19. Cross-species/isoform multiple sequence alignment of a portion of the C1 domain of MyBPC	187
Figure III.20. Identification of the novel R177H putative HCM-causing mutation in exon 6 of <i>MYBPC3</i>	188
Figure III.21. Cross-species/isoform multiple sequence alignment of a portion of the C1 domain of MyBPC	189
Figure III.22. Identification of the G278E polymorphism in exon 9 of <i>MYBPC3</i>	190
Figure III.23. Cross-species/isoform multiple sequence alignment of a portion of the MyBPC-motif of MyBPC	191
Figure III.24. Identification of the G507R putative HCM-causing mutation in exon 18 of <i>MYBPC3</i>	192



<b>Figure</b>	<b>Page</b>
Figure III.25. Cross-species/isoform multiple sequence alignment of a portion of the C3 domain of MyBPC	193
Figure III.26. Identification of the novel V896M putative HCM-causing mutation in exon 27 of <i>MYBPC3</i>	194
Figure III.27. Cross-species/isoform multiple sequence alignment of a portion of the C7 domain of MyBPC	195
Figure III.28. Identification of the exon 5 SdS -13 c>t putative HCM-causing splicing mutation	197
Figure III.29. RT-PCR analysis of the exon 5 SdS -13 c>t putative HCM-causing splicing mutation	198
Figure III.30. Identification of the exon 7 SaS +1 g>a putative HCM-causing splicing mutation in the <i>MYBPC3</i> exon 7 splice acceptor site	200
Figure III.31. RT-PCR analysis of the exon 7 SaS +1 g>a putative HCM-causing splicing mutation	201
Figure III.32. Identification of the novel intron 6 SbP +1 c>t putative HCM-causing mutation in intron 6 of <i>MYBPC3</i>	203
Figure III.33. RT-PCR analysis of the intron 6 SbP +1 c>t putative HCM-causing splicing mutation	204
Figure III.34. Identification of the novel $\Delta$ c 13255 HCM-causing mutation in exon 24 of <i>MYBPC3</i>	206

<b>Figure</b>	<b>Page</b>
Figure III.35. Pedigree 120 in which the <i>MYBPC3</i> V896M putative HCM-causing mutation segregates	208
Figure III.36. Pedigree 137 in which both the <i>TNNT2</i> R92W HCM-causing mutation and <i>MYBPC3</i> exon 7 SaS +1g>a putative HCM-causing splicing mutation were identified	211
Figure III.37. Linearised growth-curve of yeast strain PJ69-2A transformed with pAS2.1-based Y2H bait-vectors	215
Figure III.38. Linearised growth-curves of yeast strain AH109 transformed with pGBKT7-based Y2H bait-vectors	215
Figure III.39. Organisation of C-zone titin	243
Figure III.40. Multiple sequence alignment of cMyBPC domain C7 ligand 24 and C-zone domains of titin	245
Figure III.41. Identification of cMyBPC domain C10 as the ligand of the cMyBPC domain C7	247
Figure III.42. Detection of an interaction between domain C7 of cMyBPC and C-zone titin	249
Figure III.43. Quantitative ONPG $\beta$ -galactosidase assays performed to establish the effect of the V896M mutation in domain C7 of cMyBPC	252
Figure III.44. Detection of an interaction between domains C3 and C10 of cMyBPC	255

<b>Figure</b>	<b>Page</b>
Figure IV.1. Structure of the truncated cMyBPC protein predicted to be created by the exon 7 SaS+1 g>a putative HCM-causing splicing mutation	271
Figure IV.2. Structure of the truncated cMyBPC protein predicted to be created by the $\Delta$ c13255 frame-shift putative HCM-causing mutation	274
Figure IV.3. C5:C8 mediated dimerisation of cMyBPC molecules in an antiparallel and parallel fashion	276
Figure IV.4 Proposed model of cMyBPC quaternary structure	277
Figure I.5. Colour representation of a 42.9nm segment of the curved crystalline layer model of a vertebrate striated myosin muscle filament	287
Figure IV.6. Incorporation of A-band titin into the thick filament backbone	290
Figure IV.7 Incorporation of cMyBPC into the thick filament backbone	296
Figure IV.8. Dimensions of $\alpha$ -myosin “tight” and “loose” heavy chain containing cardiac thick filaments	298
Figure IV.9. Proposed mechanism of LMM thick filament expansion	301
Figure IV.10. Proposed positions of titin dimers on the “expanded” LMM thick filament backbone	303
Figure IV.11. Proposed arrangement of cMyBPC “loose collar” around the “expanded” thick filament backbone	306
Figure IV.12. Proposed orientation of the N-terminal portion of cMyBPC	315
Figure IV.13. Relative positions of HCM-causing missense mutations in the C3 IgC2 domain of cMyBPC	329

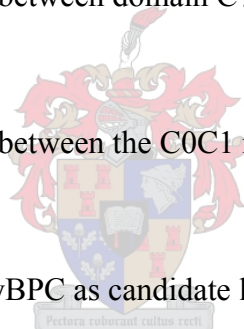
<b>Figure</b>	<b>Page</b>
Figure IV.14. Relative positions of HCM-causing missense mutations in the C5 IgC2 domain of cMyBPC	331
Figure IV.15. Proposed three-dimensional structures of domain C5 of cMyBPC	332
Figure IV.16. Relative positions of HCM-causing missense mutations in the C6 Fn3 domain of cMyBPC	334
Figure IV.17. Relative positions of the V897M putative disease-modifying factor in the C7 Fn3 domain of cMyBPC	335
Figure IV.18. Relative positions of HCM-causing missense mutations in the C8 IgC2 domain of cMyBPC	337
Figure IV.19. Relative position of the V1115I HCM-causing missense mutations in the C9 Fn3 domain of cMyBPC	338
Figure IV.20. Relative positions of HCM-causing missense mutations in the C10 IgC2 domain of cMyBPC	340
Figure IV.21. Proposed structure of the partial C10 domain identified as the ligand of the C7 domain	341

## LIST OF TABLES

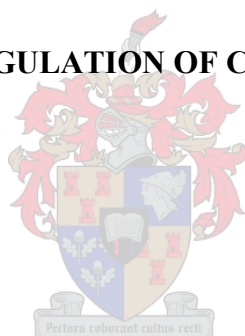
Table	Page
Table I.1. Genes and mutations responsible for causing HCM, their loci and estimated frequency	6
Table I.2. Functional analyses of HCM-causing mutations	11
Table I.3. Distribution of MyBP isoforms in various skeletal muscle types	50
Table I.4. Effect of cMyBPC phosphorylation on thick filament structure	65
Table I.5. Frequency of interactions between thick and thin filaments	70
Table I.6. HCM-causing mutations in <i>MYBPC3</i>	77
Table II.1. Primer sequences used in PCR amplification of protein-encoding exons of <i>MYBPC3</i>	110
Table II.2. <i>MYBPC3</i> RT-PCR primer sequences	112
Table II.3. Primer sequences used in PCR amplification of target sequences encoding proteins/protein domains used in Y2H-assays	113
Table II.4. Primer sequences used in the amplification of inserts present in Y2H cloning vectors	114
Table II.5. Primer sequences of site-directed mutagenesis primers	115
Table II.6. Primer-pairs used for the amplification of bait and prey constructs used in Y2H assays	118
Table II.7. RT-PCR primer pairs used	120
Table II.8. Restriction enzymes used	136
Table II.9. Characteristics of Y2H cloning plasmids	138

<b>Table</b>	<b>Page</b>
Table II.10. Generation of Y2H-constructs	144
Table III.1. Sequence variations identified in <i>MYBPC3</i>	166
Table III.2. Symptoms present in individuals carrying the V896M putative HCM-causing mutation	209
Table III.3. Echocardiographic and electrocardiographic features present in individuals with the V896M putative HCM-causing mutation	209
Table III.4. Symptoms present in individuals from pedigree 137 carrying the <i>TNNT2</i> R92W HCM-causing mutation	212
Table III.5. Echocardiographic and electrocardiographic features present in individuals from pedigree 137 with the <i>TNNT2</i> R92W HCM-causing mutation	212
Table III.6. Reporter gene self-activation tests of Y2H constructs	216
Table III.7. Effect of bait-peptides on yeast mating efficiency	217
Table III.8 cMyBPC C0C1 (1) putative interactor clones	219
Table III.9. Identification of cMyBPC C0C1 (1) primary putative interactor clones	220
Table III.10. Putative interactor clones from the Y2H library screen with the C0C1 (2) region of cMyBPC	223
Table III.11. Identification of primary putative interactor clones from the Y2H library screen (2) with the C0C1 region of cMyBPC	227
Table III.12. Putative interactor clones from the Y2H library screen with the C0 domain of cMyBPC	230

<b>Table</b>	<b>Page</b>
Table III.13. Identification of primary putative interactor clones from the Y2H library screen with the C0 domain of cMyBPC	231
Table III.14. Putative interactor clones identified in the cMyBPC domain C7 Y2H library-assay	236
Table III.15. Identification of primary interactor clones selected in the cMyBPC domain C7 Y2H library-assay	237
Table III.16. Amino acid homology shared between the 35 amino acid M-line titin peptide and specific C-zone titin domains	244
Table III.17. Assessment of interactions between domain C7 of cMyBPC and C-zone titin	250
Table III.18. Assessment of interactions between the C0C1 region of cMyBPC and C-zone titin	253
Table III.19. N-terminal domains of cMyBPC as candidate ligands of the C0C1 region of cMyBPC	256
Table III.20. Cardiac actin as a candidate ligand of the C0C1 region of cMyBPC	258
Table IV.1. Functions assigned to specific domains/regions of cMyBPC	322



<b>CHAPTER I: INTRODUCTION</b>	<b>Page</b>
<b>I.1. HYPERTROPHIC CARDIOMYOPATHY</b>	<b>4</b>
<b>I.1.1. MOLECULAR GENETICS OF HCM</b>	<b>5</b>
<b>I.1.1.1. Pathophysiology of HCM-causing mutations in sarcomeric protein-encoding genes</b>	<b>7</b>
<b>I.1.1.2. Pathophysiology of HCM-causing mutations in non-sarcomeric protein-encoding genes</b>	<b>10</b>
<b>I.2. EFFECT OF <math>\beta</math>-ADRENERGIC STIMULATION ON CARDIAC CONTRACTILITY</b>	<b>17</b>
<b>I.3. CALCIUM-DEPENDENT REGULATION OF CARDIAC CONTRACTION</b>	<b>18</b>
<b>I.4. PHOSPHOLAMBAN</b>	<b>19</b>
<b>I.5. CARDIAC TROPONIN I</b>	<b>21</b>
<b>I.5.1. STRUCTURE AND FUNCTION OF THE TROPONIN-TROPOMYOSIN COMPLEX</b>	<b>21</b>
<b>I.5.2. cTNI AS SUBSTRATE FOR PKA</b>	<b>22</b>
<b>I.6. TITIN</b>	<b>27</b>
<b>I.6.1. TITIN STRUCTURE</b>	<b>27</b>
<b>I.6.2. M-LINE TITIN</b>	<b>29</b>
<b>I.6.3. A-BAND TITIN</b>	<b>30</b>
<b>I.6.3.1. D-zone titin</b>	<b>31</b>
<b>I.6.3.2. C-zone titin</b>	<b>31</b>
<b>I.6.3.3. P-zone titin</b>	<b>32</b>
<b>I.6.4. I-BAND TITIN</b>	<b>34</b>



	<b>Page</b>
<b>I.6.4.1. I-band titin isoform diversity</b>	<b>34</b>
<b>I.6.4.2. I-Band titin as generator of passive tension</b>	<b>36</b>
I.6.4.2.i. <u>Tandem Ig domains acting as a rigid WLC</u>	<b>38</b>
I.6.4.2.ii. <u>PVEK as a WLC</u>	<b>38</b>
I.6.4.2.iii. <u>N2B element as an adjustable generator of passive tension</u>	<b>39</b>
I.6.4.2.iv. <u>Domain denaturation as a mechanism for generating passive tension</u>	<b>39</b>
<b>I.6.4.3. I-band titin as a generator of restoring force</b>	<b>40</b>
<b>I.6.5. Z-DISK TITIN</b>	<b>43</b>
<b>I.6.6. PKA-MEDIATED PHOSPHORYLATION OF TITIN</b>	<b>44</b>
<b>I.7. MYOSIN BINDING PROTEIN C</b>	<b>46</b>
<b>I.7.1. STRUCTURE OF THE MyBP FAMILY</b>	<b>46</b>
<b>I.7.2. C-ZONE LOCALISATION OF MyBPC</b>	<b>48</b>
<b>I.7.3. INTERACTIONS OF MyBPC WITH OTHER SARCOMERIC COMPONENTS</b>	<b>49</b>
<b>I.7.3.1. Interactions between MyBPC and LMM</b>	<b>49</b>
<b>I.7.3.2. Interaction between MyBPC and C-zone titin</b>	<b>52</b>
<b>I.7.3.3. Domain C7 of MyBPC essential for correct A-band incorporation</b>	<b>53</b>
<b>I.7.3.4. Interaction between the MyBPC-motif and the S2 region of myosin</b>	<b>53</b>
<b>I.7.3.5. Interaction between MyBPC and F-actin</b>	<b>54</b>
<b>I.7.4. PHOSPHORYLATION OF cMyBPC</b>	<b>55</b>
<b>I.7.5. DEPHOSPHORYLATION OF cMyBPC</b>	<b>58</b>
<b>I.7.6. FUNCTIONS OF cMyBPC</b>	<b>59</b>



<b>I.7.6.1. Effect of cMyBPC phosphorylation on thick filament structure</b>	<b>60</b>
I.7.6.1.i. <u>“Disordered” thick filament structure</u>	60
I.7.6.1.ii. <u>“Tight” thick filament structure</u>	62
I.7.6.1.iii. <u>“Loose” thick filament structure</u>	64
<b>I.7.7.    EFFECT OF cMyBPC PHOSPHORYLATION ON CARDIAC           CONTRACTILITY</b>	<b>66</b>
<b>I.7.7.1. Transition of thick filaments from a “disordered” to a “tight” structure</b>	<b>67</b>
<b>I.7.7.2. Transition of thick filaments from a “tight” to a “loose” structure</b>	<b>69</b>
<b>I.7.7.3. Interaction between cMyBPC domain C0 and actin as a regulator of cardiac           contractility</b>	<b>71</b>
<b>I.7.8.    HCM-CAUSING MUTATIONS IN cMyBPC</b>	<b>72</b>
<b>I.7.8.1. Phenotypic expression of cMyBPC-associated HCM</b>	<b>73</b>
<b>I.7.8.2. Pathogenesis of HCM-causing mutations resulting in the truncation of           cMyBPC</b>	<b>83</b>
<b>I.7.8.3. Pathogenesis of HCM-causing missense mutations in cMyBPC</b>	<b>85</b>
<b>I.8.      PRESENT STUDY</b>	<b>86</b>



# CHAPTER I: INTRODUCTION

## I.1. HYPERTROPHIC CARDIOMYOPATHY

Hypertrophic cardiomyopathy (HCM) is a primary cardiac disease, which is inherited in an autosomal dominant fashion (Spirito et al., 1997). It has been estimated that this disease, which is the most prevalent cause of sudden death in apparently healthy young individuals (Fananapazir and Epstein, 1991), affects about one in five hundred people in the general population (Maron et al., 1995; Seidman and Seidman, 2001). The primary features of HCM are left ventricular hypertrophy (LVH) in the absence of other aetiologies, myocardial disarray, fibrosis, diastolic dysfunction and an increased risk of both sudden cardiac death (SCD) and congestive heart failure (Fananapazir and Epstein, 1994; Davies and McKenna, 1995).

As the symptoms with which patients suffering from HCM present, such as angina, dyspnoea, palpitations, presyncope and syncope, are characteristic of several diseases, a positive diagnosis of HCM can only be made following electrocardiographic (ECG) and echocardiographic evaluation, if LVH, in the absence of other aetiologies, is present (Fananapazir and Epstein, 1989; Fananapazir et al., 1989; Fananapazir and Epstein, 1991; Fananapazir et al., 1992; Maron and Fananapazir, 1992). Diagnosis of HCM is further confounded by the fact that HCM shows reduced penetrance, rendering asymptomatic mutation carriers clinically undiagnosable (Maron et al., 1984; Davies and McKenna, 1995). Due to these difficulties in the clinical diagnosis of HCM, combined with the fact that clinically unaffected mutation carriers remain at risk of SCD (Watkins et al., 1995b; Moolman et al.,

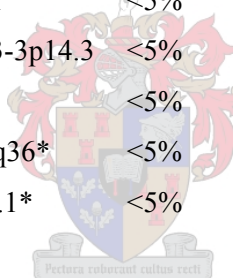
1997; Moolman-Smook et al., 2000), molecular diagnosis of HCM may be advantageous, as it facilitates counselling and patient management.

### I.1.1. MOLECULAR GENETICS OF HCM

To date, more than 264 different HCM-causing mutations, occurring in eleven different genes, have been identified (FHC Mutation Database, available at: <http://morgan.angis.su.oz.au/Databases/Heart/heartbreak.html>). The vast majority of these mutations occur in genes encoding components of the cardiac sarcomere, namely, the  $\beta$ -myosin heavy chain gene (*MYH7*) (Geisterfer-Lowrance et al., 1990), the cardiac troponin T gene (*TNNT2*) (Thierfelder et al., 1994), the  $\alpha$ -tropomyosin gene (*TPMI*) (Thierfelder et al., 1994), the cardiac myosin binding protein C gene (*MYBPC3*) (Bonne et al., 1995; Watkins et al., 1995a), the myosin ventricular essential light chain 1 gene (*MYL3*) (Poetter et al., 1996), the myosin ventricular regulatory light chain 2 gene (*MYL2*) (Poetter et al., 1996), the cardiac troponin I gene (*TNNI3*) (Kimura et al., 1997), the cardiac splicing isoform of the titin gene (*TTN*) (Satoh et al., 1999), the  $\alpha$ -cardiac actin gene (*ACTC*) (Mogensen et al., 1999) the cardiac troponin C gene (*TNNC1*) (Hoffmann et al., 2001) and the  $\alpha$ -myosin heavy chain gene (*MYH6*) (Niimura et al., 2002). The number and type of mutations, thus far identified in each of these genes, are summarised in table I.1. The identification of HCM-causing mutations in sarcomeric protein-encoding genes led to the formation of a hypothesis that HCM is a disease of the cardiac sarcomere (Thierfelder et al., 1994; Watkins et al., 1995c). Subsequently, however, HCM-causing mutations were also found in *CSRP3*, encoding muscle LIM protein (MLP) (Geier et al., 2003), and *PRKAG2*, encoding the  $\gamma_2$  subunit of 5' adenosine monophosphate (AMP)-activated protein kinase (AMPK) (Blair et al., 2001; Gollob et al., 2001; Arad et al., 2002).

**TABLE I.1. Genes and mutations responsible for causing HCM, their loci and estimated frequency (adapted from Marian and Roberts, 2001)**

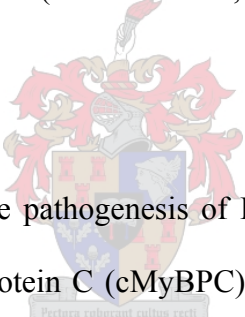
<b>Protein</b>	<b>Gene</b>	<b>Locus</b>	<b>Frequency</b>	<b># Mutations</b>	<b>Mutation Type</b>
$\beta$ -Myosin heavy chain	<i>MYH7</i>	14q12	~30% - ~40%	102	Mostly missense
Cardiac myosin binding protein C	<i>MYBPC3</i>	11p11.2	~20% - ~42%	93	Mostly truncation, some missense
Cardiac troponin T	<i>TNNT2</i>	1q32	~6% - ~20%	20	Mostly missense, some truncation
$\alpha$ -Tropomyosin	<i>TPMI</i>	15q22.1	~5%	7	Missense mutations
Cardiac troponin I	<i>TNNI3</i>	19q13.2	~5% - ~7%	14	Mostly missense
Myosin ventricular essential light chain 1	<i>MYL3</i>	3p21.3-p21.2	<5% - ~7%	3	Missense mutations
Myosin ventricular regulatory light chain 2	<i>MYL2</i>	12q23-q24.3	<5%	11	Mostly missense mutations
Cardiac $\alpha$ -actin	<i>ACTC</i>	11q	<5%	4	Missense mutation
Titin	<i>TTN</i>	2q24.1	<5%	1	Missense mutation
Cardiac troponin C	<i>TNNC1</i>	3p21.3-3p14.3	<5%	1	Missense mutation
$\alpha$ -Myosin heavy chain	<i>MYH6</i>	14q12	<5%	1	Missense mutation
5' AMP-activated protein kinase	<i>PRKAG2</i>	7q35-q36*	<5%	4	Missense mutations
Muscle LIM protein	<i>CSRP3</i>	11p15.1*	<5%	3	Missense mutations



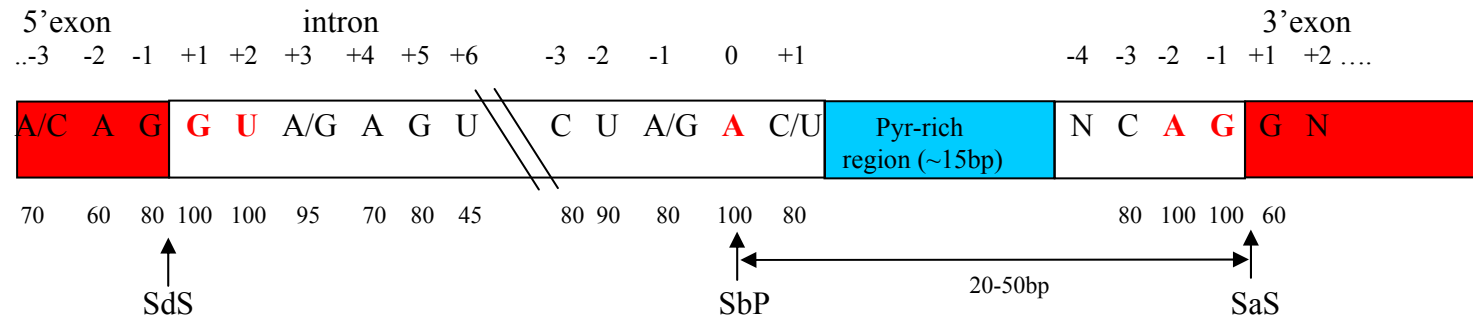
*Frequency = percentage of cases of HCM caused by mutations in a particular gene (from Marian and Roberts, 2001 and Richard et al., 2003); \* = human chromosomal location obtained from LocusLink available at: <http://www.ncbi.nih.gov/LocusLink/list.cgi>; # mutations = number of HCM-causing mutations thus far identified.*

### I.1.1.1. Pathophysiology of HCM-causing mutations in sarcomeric protein-encoding genes

With the exception of mutations in *MYBPC3*, the majority of HCM-causing mutations identified thus far are missense mutations or short in-frame deletions, resulting in the generation of mutant proteins that differ from the wild type protein by only one or a few amino acids (table I.1). Several studies have clearly shown that mutant proteins, generated by these mutations, are stably incorporated into the sarcomere, where they act as “poison peptides” resulting in a gain or loss of protein function (Seidman and Seidman, 2002) (table I.2 and references therein). Additionally, it was shown that truncated cardiac troponin T protein (cTNT), resulting from the *TNNT2* splice donor site (SdS)+1 g>a mutation (box 1) (Watkins et al., 1996), is also stably incorporated into the sarcomere and is, therefore, likely to act in a similar fashion (Watkins et al., 1996; Frey et al., 2000; Montgomery et al., 2001).

The image shows a faint watermark of a university crest in the center of the page. The crest features a shield with various symbols, topped with a crown and flanked by two figures. Below the shield is a motto scroll with the Latin text "Pectora cubant cibus recti".

The mechanisms involved in the disease pathogenesis of HCM-causing mutations resulting in the truncation of cardiac myosin binding protein C (cMyBPC), as a result of splice site, nonsense and frame-shift mutations in *MYBPC3*, is, however, controversial. As the majority of these cMyBPC truncation mutations result in the loss of the C-terminal region of the protein, essential for correct A-band incorporation of cMyBPC into the sarcomere (sections I.7.3.1, I.7.3.2 and I.7.3.3), it was proposed that these mutations may result in haploinsufficiency, rather than act as “poison peptides” (Carrier et al., 1997; Rottbauer et al., 1997). This hypothesis is supported by findings that truncated cMyBPC was not detected by Western analyses in myocardial biopsies from HCM-affected individuals, carrying HCM-causing truncation mutations in *MYBPC3* (Rottbauer et al., 1997; Moolman et al., 2000). Several studies have, however, shown that even though truncated cMyBPC is distributed more diffusely throughout the cardiomyocyte, truncated cMyBPC is incorporated into cardiac sarcomeres (Yang et al., 1998; Flavigny et al., 1999; Yang et al., 1999). Additionally, Harris

**BOX 1**

*Consensus sequences around splice donor sites (SdS), splice acceptor sites (SaS) and splice branch points (SbP). Nonvariant nucleotide sequences are indicated in bold red lettering. ■ = exons; ■ = pyrimidine-rich (Pyr-rich) region. The positions of nucleotide residues relative to SaS, SdS and SbPs are shown above the figure, while the percentage conservation of these residues are shown below the figure (from Lodish et al., 1995).*



et al., (2002) have shown that heterozygous *MYBPC3* knockout mice do not display LVH, disarray, fibrosis or contractile dysfunction, while these features were all present in homozygous *MYBPC3* knockout mice. This finding suggests that the loss of a single *MYBPC3* allele does not have any pathogenic effect and that other mechanisms may compensate for haploinsufficiency. In the light of these findings, it seems likely that mutations resulting in the truncation of cMyBPC also act as “poison peptides”, rather than acting through a mechanism of haploinsufficiency.

In order to establish the pathological effect of “poison peptides”, resulting from HCM-causing mutations in sarcomeric protein-encoding genes, several *in vitro*, *in situ* and *in vivo* functional studies have been conducted. Phenotypically the expression of these “poison peptides” in animal models generally caused disarray (at the sarcomeric, myocytic or myofibrillar levels), and fibrosis. However, LVH, arrhythmias and increased mortality were rare and often only induced following exercise (table I.2 and references therein). These findings indicate that disarray and fibrosis are in all likelihood the primary characteristics of HCM in humans, while LVH, the criterion that is generally used for clinical diagnosis, may be a secondary feature, caused by other cellular and physiological defects.

Furthermore, these studies investigated the effect of mutant peptides on a wide array of physiological and contractile parameters, including intrinsic myosin adenosine triphosphatase (ATPase) activity,  $\text{Ca}^{2+}$ -activated actomyosin ATPase activity, systolic function/contractility, diastolic function/relaxation, maximal  $\text{Ca}^{2+}$ -activated force, sliding velocity and  $\text{Ca}^{2+}$ -sensitivity of contraction. Surprisingly, it was shown that HCM-causing mutations, investigated in these studies, have a wide array of effects on the majority of these parameters, resulting in either hypo- or hypercontractility (table I.2 and references therein). The majority of these studies, however, found

that diastolic function was generally impaired, while  $\text{Ca}^{2+}$ -sensitivity of contraction was enhanced (table I.2 and references therein). It can, therefore, be concluded that HCM-causing mutations in sarcomeric protein-encoding genes result in contraction at lower intracellular  $\text{Ca}^{2+}$  concentrations, which may in turn result in impaired relaxation and diastolic function.

The mechanisms involved in this enhanced  $\text{Ca}^{2+}$ -sensitivity of the contractile apparatus, resulting from the presence of HCM-causing mutations in nine different sarcomeric protein-encoding genes, remain elusive.

#### **I.1.1.2. Pathophysiology of HCM-causing mutations in non-sarcomeric protein encoding genes**

The discovery of HCM-causing mutations in *CSRP3*, encoding muscle LIM protein (MLP) (Geier et al., 2003), and *PRKAG2*, encoding the  $\gamma_2$  subunit of 5' AMP-activated protein kinase (AMPK), (Blair et al., 2001; Gollob et al., 2001; Arad et al., 2002) has highlighted the fact that mutations in non-sarcomeric protein-encoding genes also cause HCM. Even though MLP is not classically regarded as a sarcomeric component, this protein plays an essential role in stabilising the interaction between the sarcomere and the cytoskeleton by binding to both  $\alpha$ -actinin (sarcomeric), telethonin (sarcomeric) and  $\beta$ I-spectrin (cytoskeletal) (Arber et al., 1994; Arber et al., 1997; Flick and Konieczny, 2000; Knoll et al., 2002; Geier et al., 2003). It is, therefore, possible that mutations in this protein cause HCM by disrupting sarcomeric assembly and integrity, a mechanism proposed for the disease pathogenesis of HCM-causing mutations in titin and the light meromyosin (LMM) subfragment of myosin (Blair et al., 2002; Watkins, 2003). This view is supported by the finding that myofibrillar disarray and fibrosis, considered characteristic features of HCM-caused by sarcomeric

**TABLE I.2. Functional analyses of HCM-causing mutations**

<b>Mutation</b>	<b>Type of study</b>	<b>M ATPase</b>	<b>AM ATPase</b>	<b>Sys/C</b>	<b>Dia/R</b>	<b>Ca<sup>2+</sup>-sens</b>	<b>F<sub>avg</sub></b>	<b>V<sub>max</sub></b>	<b>Phenotype</b>	<b>Ref</b>
MHC <sup>R403Q</sup>	<i>In vivo</i>	—	—	↓	↓	↑	—	↓	LVH, MH, ↑M, D, F, ECG, Arr	1-6
MHC <sup>R403Q</sup>	<i>In situ</i>	—	↓	↓	↓	↑	↓	—	D, F	7-9
MHC <sup>R403Q</sup>	<i>In vitro</i>	=	↑ <sup>8,12</sup> /↓	↓	↓	↑	↓ <sup>12</sup> /↓	↑ <sup>8</sup> /↓	—	10-14
MHC <sup>V606M</sup>	<i>In vitro</i>	=	=	—	—	—	—	↓	—	13
MHC <sup>R249Q</sup>	<i>In vitro</i>	↓	↓	—	—	—	—	↓	—	13
MHC <sup>R453C</sup>	<i>In vitro</i>	↓	↓	—	—	—	—	↓	—	13
MHC <sup>G716R</sup>	<i>In vitro</i>	—	↑	—	—	—	—	↓	—	14
MHC <sup>R719Q</sup>	<i>In vitro</i>	—	↑	—	—	—	—	↓	—	14
MHC <sup>R719W</sup>	<i>In vitro</i>	—	↑	—	—	—	—	↓	—	14
MHC <sup>F513C</sup>	<i>In vitro</i>	—	↓	—	—	—	—	↓	—	14
MHC <sup>G584R</sup>	<i>In vitro</i>	—	↑	—	—	—	—	↓	—	14
cTNT <sup>R92Q</sup>	<i>In vivo</i>	—	=	↑/↓ <sup>17</sup>	↓	↑	—	↓	F, D, ↓HW	15-17
cTNT <sup>R92Q</sup>	<i>In situ</i>	—	—	—	—	—	—	↓	—	18
cTNT <sup>R92Q</sup>	<i>In vitro</i>	—	=	—	—	↑	—	—	—	19-20
cTNT <sup>I79N</sup>	<i>In vitro</i>	—	=	—	—	↑/= <sup>18</sup>	—	↑	—	19-21
cTNT <sup>F110I</sup>	<i>In vitro</i>	—	↑	—	—	=	—	—	—	19
cTNT <sup>E244D</sup>	<i>In vitro</i>	—	↑	—	—	=	—	—	—	19

Mutation	Type of study	M ATPase	AM ATPase	Sys/C	Dia/R	Ca <sup>2+</sup> -sens	F <sub>avg</sub>	V <sub>max</sub>	Phenotype	Ref
cTnT <sup>R278C</sup>	<i>In vitro</i>	—	=	—	—	↑	—	—	—	19
cTnT <sup>Δ</sup>	<i>In vivo</i>	—	=	↓	↓	↑	↓	—	F,D, ↑M, ↓HW, Arr <sup>ei</sup>	17, 22-24
αTM <sup>D175N</sup>	<i>In vivo</i>	—	—	↓	↓	↑	—	—	LVH, D, F	25
cMyBPC <sup>ΔC5-C10</sup>	<i>In vivo/in vitro</i>	—	—	=	=	↑	↓	—	D	26
cMyBPC <sup>ΔC8-C10</sup>	<i>In vivo</i>	—	—	=	=	—	—	—	(MH, D, F) LVH <sup>LO</sup>	5
cMyBPC <sup>Δ10</sup>	<i>In vivo</i>	—	—	=	=	—	↓	↓	LVH	27
cMyBPC (het ko)	<i>In vivo</i>	—	—	=	=	=	—	—	—	28
cMyBPC (hom ko)	<i>In vivo</i>	—	—	↓	↓	↓	—	—	LVH, D, F	28
MLP (hom ko)	<i>In vivo</i>	—	—	↓	↓	—	—	—	DCM, CH, HF, D, F,	29

*αTM* = alpha tropomyosin; *AM ATPase* = actomyosin ATPase activity; *Arr* = arrhythmia; *Arr<sup>ei</sup>* = exercise induced arrhythmia; *Ca<sup>2+</sup>-sens* = calcium sensitivity; *CH* = concentric hypertrophy; *cMyBPC* = cardiac myosin binding protein C; *cTnT* = cardiac troponin T; *D* = disarray; *DCM* = dilated cardiomyopathy; *Dia/R* = diastolic function / relaxation; *ECG* = electrocardiographic abnormalities; *F* = fibrosis; *F<sub>avg</sub>* = average force generated; *het ko* = heterozygous knockout; *HF* = heart failure; *hom ko* = homozygous knockout; *HW* = heart weight; *LVH* = left ventricular hypertrophy; *LVH<sup>LO</sup>* = late-onset left ventricular hypertrophy; *M* = mortality; *M ATPase* = myosin ATPase activity; *MH* = myocytic hypertrophy; *MHC* = myosin heavy chain; *MLP* = muscle LIM protein; *Ref* = reference; *Sys/C* = systolic function / contractility; *V<sub>max</sub>* = maximum sliding velocity; ↑ = increase; ↓ = decrease; = = unchanged; — = not applicable/not reported; features in brackets refer to subtle variations. 1 = Marian et al., 1999; 2 = Geisterfer-Lowrance et al., 1996; 3 = Berul et al., 1997; 4 = Spindler et al., 1998; 5 = Berul et al., 2001; 6 = Georgakopoulos et al., 1999; 7 = Kim et al., 1999; 8 = Blanchard et al., 1999; 9 = Marian et al., 1995; 10 = Tyska et al., 2000; 11 = Gao et al., 1999; 12 = Sweeney et al., 1994; 13 = Sata and Ikebe, 1996; 14 = Fujita et al., 1997; 15 = Tardiff et al., 1999; 16 = Oberst et al., 1998; 17 = Montgomery et al., 2001; 18 = Marian et al., 1997; 19 = Yanaga et al., 1999; 20 = Morimoto et al., 1998; 21 = Lin et al., 1996; 22 = Tardiff et al., 1998; 23 = Frey et al., 2000; 24 = Watkins et al., 1996; 25 = Muthuchamy et al., 1999; 26 = Yang et al., 1998; 27 = Yang et al., 1999; 28 = Harris et al., 2002; 29 = Arber et al., 1997.

protein-encoding gene mutations (Maron and Ferrans, 1978; Watkins, 2003), were present in histological sections of hearts from homozygous MLP knockout mice (table I.2) (Arber et al., 1997). Homozygous MLP knockout mice also presented either with adulthood dilated cardiomyopathy (DCM), or an early phenotype characterised by concentric hypertrophy (table I.2) (Arber et al., 1997). Watkins (2003) speculated that the DCM phenotype observed in a large proportion of these mice could be the result of a rapid progression of HCM to the dilated phase, rather than of DCM *per se*. The identification of a DCM-causing mutation in MLP, shown to disrupt the interaction between MLP and telethonin (Knoll et al., 2002), however, suggests that mutations in MLP are able to cause both HCM and DCM.

The discovery of mutations in the  $\gamma_2$  subunit of AMPK, causing HCM with Wolff-Parkinson-White (WPW) syndrome (Blair et al., 2001; Gollob et al., 2001; Arad et al., 2002) has, however, broken the sarcomeric “golden thread” and led to the suggestion that mechanisms other than sarcomeric disruption may be involved in the development of HCM. AMPK has been described as the “fuel gauge”, or “low-fuel warning system” of the cell, that is switched on by depletion of adenosine triphosphate (ATP) (Hardie and Carling, 1997). AMPK is sensitive to AMP levels within the cell and is activated by a rising AMP/ATP ratio, indicative of energy depletion. In its activated state, AMPK inhibits enzymes in energy-consuming biosynthetic pathways, such as fatty-acid and sterol synthesis, increases glucose uptake and activates rate-limiting enzymes in glycolytic and fatty-acid oxidation pathways, thus reducing ATP consumption while also stimulating ATP production (figure I.1) (reviewed by Hardie and Carling, 1997; Blair et al., 2001; Tian et al., 2001; Gollob et al., 2001).

The phenotypic expression of *PRKAG2* mutations, however, differs from that classically associated with HCM caused by sarcomeric protein-encoding gene mutations. Specifically, in addition to

cardiac hypertrophy, *PRKAG2* mutation carriers also present with pre-excitation (WPW), atrial fibrillation and progressive atrioventricular conduction block (Gollob et al., 2001; Arad et al., 2002). Furthermore, Arad et al., (2002) found no evidence of myocyte disarray and fibrosis, features generally associated with HCM, while large cytosolic vacuoles, proposed to contain amylopectin, a nonsoluble product of glycogen metabolism, were present in cardiomyocytes obtained from *PRKAG2* mutation carriers. These findings prompted Arad et al., (2002) to propose that mutations in *PRKAG2* produce a novel cardiac glycogen storage disease, characterised by cardiac hypertrophy and conduction abnormalities. The classification of mutations in *PRKAG2* as causing either HCM with WPW, or a novel cardiac glycogen storage disease characterised by cardiac hypertrophy and conduction abnormalities, is largely dependent on whether or not myocytic disarray and fibrosis are regarded as pathogenic hallmarks of HCM (Maron and Ferrans, 1978; Watkins, 2003). Regardless of whether *PRKAG2* mutation carriers are classified as having atypical HCM, or a separate disease entity, the notion that mutations in non-sarcomeric proteins, result in a disease phenotype similar to HCM, may provide invaluable insights into the mechanisms involved in the development of HCM (Blair et al., 2001; Crilley et al., 2003; Watkins, 2003).

The identification of mutations in *PRKAG2* supports a hypothesis that HCM-causing mutations in sarcomeric protein-encoding genes might result in ATP wastage through inefficient chemo-mechanical force production/transduction in the sarcomere, rendering the cell vulnerable to ATP depletion during periods of increased cardiac demand (Redwood et al., 1999; Blair et al., 2001; Montgomery et al., 2001). This hypothesis is further supported by the findings that the ratio of phosphocreatine (PCr) to ATP was decreased in HCM-affected individuals, irrespective of symptomatic presentation, the presence of LVH, or the sarcomeric protein-encoding gene in which

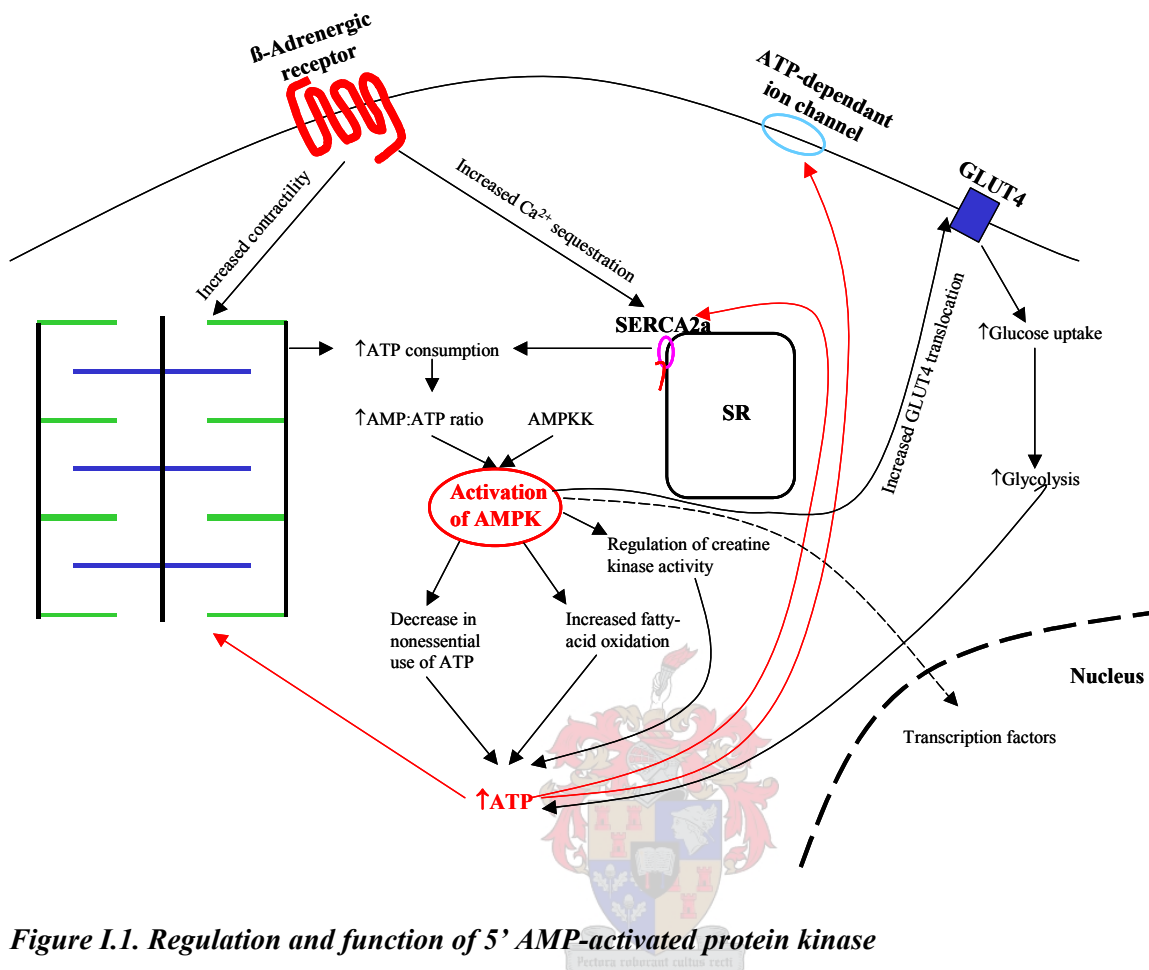


**Figure I.1. Regulation and function of 5' AMP-activated protein kinase**

In response to an elevated AMP/ATP ratio, induced by increased ATP-consumption by the contractile apparatus and  $Ca^{2+}$ -handling systems, resulting from  $\beta$ -adrenergic stimulation, AMP-activated protein kinase (AMPK) is activated through the actions of AMP-activated protein kinase kinase (AMPKK). Activation of AMPK, results in a decrease in non-essential ATP-usage, and increased ATP-production through fatty-acid oxidation, and glucose uptake. Additionally, AMPK-activation may also activate transcription factors (adapted from Gollob et al., 2001).

the mutation occurred (Jung et al., 1998; Crilley et al., 2003). A similar decrease in the PCr/ATP ratio was also noted in a mouse model heterozygous for the  $\alpha$ MHC<sup>R403Q</sup> mutation (homologue of the human  $\beta$ MHC R403Q HCM-causing mutation), in the absence of LVH (Spindler et al., 1998). Specifically, the finding that the PCr/ATP ratio was decreased in asymptomatic mutation carriers, not presenting with LVH, or ECG abnormalities, suggests that energetic abnormalities are likely to

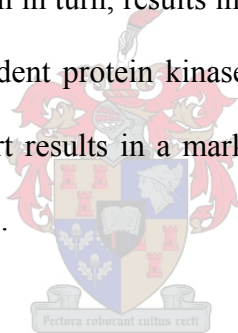
be a primary, rather than a compensatory, feature of HCM (Crilly et al., 2003). Furthermore, Tian et al., (2001) have shown that a decrease in PCr/ATP ratio in a rat model of pressure-overload hypertrophy chronically elevated AMPK-activity, resulting in increased glucose uptake and metabolism. This finding suggests that the elevated PCr/ATP ratios observed in HCM mutation carriers (Crilly et al., 2003) may act in a similar way, and that chronic AMPK-activation may be a hallmark of LVH in general.

Together, these findings strongly suggest that chronic energy depletion in the cardiomyocyte, whether resulting from inefficient chemo-mechanical force generation, caused by mutations in sarcomeric protein-encoding genes, or mutations in *PRKAG2*, could result in the development of cardiac hypertrophy. As  $\beta$ -adrenergic stimulation would result in an increase in ATP-consumption, by both the contractile apparatus and the  $\text{Ca}^{2+}$ -reuptake system, the effects of HCM-causing mutations on cellular energetics may be exacerbated by  $\beta$ -adrenergic stimulation. Support for the view that  $\beta$ -adrenergic stimulation may be detrimental to HCM-affected individuals is drawn from two lines of evidence. Firstly, high-dose  $\beta$ -blocker therapy is used in the treatment of HCM and has been shown to significantly reduce the risk of SCD (Ostman-Smith et al., 1999). Secondly, strenuous physical exercise, which may result in  $\beta$ -adrenergic stimulation of the heart, has been implicated as a risk factor for the occurrence SCD in HCM patients and an HCM animal model (Frenneaux et al., 1990; Maron et al., 1994; Geisterfer-Lowrance et al., 1996; Niimura et al., 1998; Konno et al., 2003). In the following sections, the effect of  $\beta$ -adrenergic stimulation in the heart will be discussed briefly. Specific reference will be made to the effect of  $\beta$ -adrenergic stimulation on phospholamban (PLB) and cardiac troponin I (cTNI), two proteins involved in  $\text{Ca}^{2+}$ -homeostasis and  $\text{Ca}^{2+}$ -activation of contraction respectively, functions which have previously been shown to be involved in the pathogenesis of HCM (section I.1.1.1). Particular attention will be given to the structure and

function of cMyBPC and cardiac titin. These proteins are of particular importance, as cMyBPC, the subject of the present study, and cardiac titin, a ligand of cMyBPC, are both phosphorylated as a result of  $\beta$ -adrenergic stimulation of the heart.

## **I.2. EFFECT OF $\beta$ -ADRENERGIC STIMULATION ON CARDIAC CONTRACTILITY**

Several studies, aimed at establishing the effect of  $\beta$ -adrenergic stimulation of the heart, have been carried out. The binding of noradrenalin or adrenergic agonists to the  $\beta$ -adrenergic receptor results in the activation of adenylate cyclase, which in turn, results in the elevation of intracellular cyclic AMP (cAMP) levels, activating cAMP-dependent protein kinase (PKA) (Lodish H, 1995). At the organ level, adrenergic stimulation of the heart results in a marked increase in contractile force of up to 70% (England, 1975; Solaro et al., 1976).



Although these studies have addressed the effect of  $\beta$ -adrenergic stimulation at the whole organ level, elucidating the effect thereof at the molecular level has been complicated by the presence of multiple PKA-dependent phospho-proteins within the cardiomyocyte. These include cTNI (Grand and Wilkinson, 1976; Solaro et al., 1976; Gao et al., 1994; Zhang et al., 1995), PLB (Movsesian et al., 1984; Kuschel et al., 1999; Chu et al., 2000), titin (Yamasaki et al., 2002) and cMyBPC (Hartzell and Titus, 1982; Hartzell and Sale, 1985; Gautel et al., 1995). As PKA-dependent phosphorylation of each of these four proteins plays an important role in the regulation of cardiac contractility, their structure, function and response to PKA-dependent phosphorylation will be discussed briefly in the following sections (I.4. I.5, I.6 and I.7). As both PLB and cTNI are essential components of the  $\text{Ca}^{2+}$ -

sensing/handling system,  $\text{Ca}^{2+}$ -dependent regulation of cardiac contraction will also be discussed briefly in section I.3.

### **I.3. CALCIUM-DEPENDENT REGULATION OF CARDIAC CONTRACTION**

Cardiac contraction is primarily stimulated by the release of  $\text{Ca}^{2+}$  from the sarcoplasmic reticulum (SR), stimulating actomyosin ATPase activity through thin filament activation, while relaxation is achieved through the sequestration of  $\text{Ca}^{2+}$  into the SR, resulting in deactivation of the thin filament and inhibition of actomyosin ATPase activity. The  $\text{Ca}^{2+}$ -dependent events that lead to contraction during systole and relaxation during diastole are depicted in figure I.2. Briefly, depolarisation of the sarcolemma allows the opening of sarcolemmal L-type  $\text{Ca}^{2+}$ -channels, allowing a minor  $\text{Ca}^{2+}$  influx through this channel, causing the stimulation of the ryanodine receptor (RyR) in the SR membrane. The binding of  $\text{Ca}^{2+}$  to the RyR, in turn, causes the rapid release of  $\text{Ca}^{2+}$  from the SR into the cytoplasm through the RyRs and  $\text{Ca}^{2+}$ -release channels, resulting in a rapid increase in the cytoplasmic  $\text{Ca}^{2+}$  concentration (Fabiato, 1985; Frank et al., 2003). This sudden rise in cytoplasmic  $\text{Ca}^{2+}$  concentration results in the binding of  $\text{Ca}^{2+}$  to cardiac troponin C (cTNC), which leads to a cascade of conformational changes in the troponin-tropomyosin complex. These conformational changes result in thin filament activation (section I.5), which in turn, activates actomyosin ATPase activity, constituting cardiac contraction (systole) (Zot and Potter, 1987; Spyrapoulos et al., 1997). Relaxation (diastole) is achieved through the sequestration of cytoplasmic  $\text{Ca}^{2+}$ . The main mechanism through which this is achieved, in mammalian cardiomyocytes, is through the action of SR  $\text{Ca}^{2+}$ -ATPase (SERCA2a), which pumps  $\text{Ca}^{2+}$  back into the SR, while the sarcolemmal  $\text{Na}^{2+}$ - $\text{Ca}^{2+}$  exchanger and other slower systems also play a lesser role in the sequestration of cytoplasmic  $\text{Ca}^{2+}$  (Bers et al., 1996; Frank et al., 2003). The subsequent reduction in the cytoplasmic  $\text{Ca}^{2+}$ -

concentration causes the release of  $\text{Ca}^{2+}$  from cTNC, resulting in thin filament deactivation and inhibition of actomyosin ATPase activity (Chandra et al., 1997 and references therein).

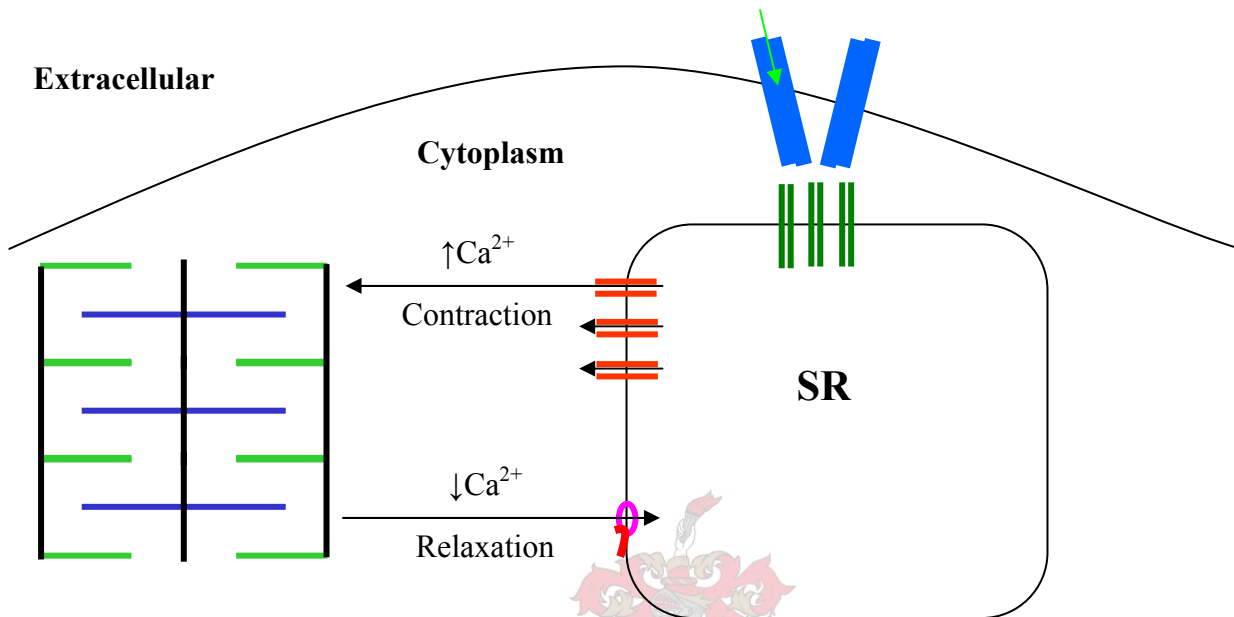


**Figure I.2.  $\text{Ca}^{2+}$ -regulation of cardiac contraction**

■ = Sarcolemmal L-type  $\text{Ca}^{2+}$  channels, ■ = phospholamban; ■ = sarcomeric thick filaments; ■ = ryanodene receptors; ■ =  $\text{Ca}^{2+}$  release channels; green arrow =  $\text{Ca}^{2+}$  flow through the sarcolemmal L-type  $\text{Ca}^{2+}$  channels following depolarisation of the sarcolemma; ■ = sarcomeric thin filaments; ○ = SERCA2a; SR = sarcoplasmic reticulum; ■ = sarcomeric M- and Z-lines; ■ = sarcolemmal and sarcoplasmic reticular membranes respectively. The black arrows indicate  $\text{Ca}^{2+}$  flux during systole and diastole respectively.

#### I.4. PHOSPHOLAMBAN

PLB, a 52 amino acid SR-membrane protein, is the primary regulator of SERCA2a activity. Under physiological conditions, about 40% of SERCA2a pumps are inhibited by the actions of PLB

(Brittsan et al., 2000). To date, three phosphorylation sites at residues 10, 16 and 17 of PLB have been identified. During  $\beta$ -adrenergic stimulation, residues 16 (serine) and 17 (threonine) are phosphorylated in a PKA-dependent fashion (Kuschel et al., 1999; Chu et al., 2000). The phosphorylation of residue 16 is the most important regulator of PLB activity, while the phosphorylation of residue 17 by either PKA or  $\text{Ca}^{2+}$ /calmodulin-dependent protein kinase II (CaMK II), and residue 10 by  $\text{Ca}^{2+}$ -activated phospholipid-dependent protein kinase (PKC), seems to also contribute, although, to a lesser extent, to PLB activity (Movsesian et al., 1984; Kuschel et al., 1999; Chu et al., 2000).

In its unphosphorylated state, PLB is associated with SERCA2a and reduces the affinity of SERCA2a for  $\text{Ca}^{2+}$ . Upon  $\beta$ -adrenergic stimulation, PLB is phosphorylated by PKA (at serine-16 and threonine-17), causing it to dissociate from SERCA2a, thereby abolishing its inhibitory effect on SERCA2a function (Luo et al., 1994; Koss and Kranias, 1996). Thus PKA-dependent phosphorylation of PLB increases the rate at which  $\text{Ca}^{2+}$  is sequestered from the cytoplasm, aiding relaxation and diastolic function (Kranias et al., 1985; Frank et al., 2003). Furthermore, the increase in  $\text{Ca}^{2+}$  sequestration from the cytoplasm, induced by the PKA-dependent phosphorylation of PLB, increases the luminal SR  $\text{Ca}^{2+}$  load, which in turn increases the sensitivity of the RyR, leading to increased  $\text{Ca}^{2+}$ -release from the SR following stimulation by  $\text{Ca}^{2+}$  influx via the L-type  $\text{Ca}^{2+}$  channels (Li et al., 2002). Dephosphorylation of PLB, associated with an increase in the affinity of PLB for SERCA2a is achieved through the action of calcineurin B (Munch et al., 2002).

## I.5. CARDIAC TROPONIN I

Troponin I (TNI), together with troponin C (TNC), troponin T (TNT) and  $\alpha$ -tropomyosin ( $\alpha$ TM), forms the troponin-tropomyosin complex (Stull and Buss, 1977; Wilkinson and Grand, 1978). Together these proteins are responsible for sensing intracellular  $\text{Ca}^{2+}$  flux and the  $\text{Ca}^{2+}$ -dependent activation/deactivation of the thin filament, resulting in actomyosin ATPase activity being either activated or inhibited (Chandra et al., 1997 and references therein). In the following sections, the structure and function of the troponin-tropomyosin complex will be discussed briefly (section I.5.1), following which the effect of PKA-dependent phosphorylation of cTNI will be discussed (section I.5.2).

### I.5.1. STRUCTURE AND FUNCTION OF THE TROPONIN-TROPOMYOSIN COMPLEX

Contraction of all vertebrate striated muscle is achieved through  $\text{Ca}^{2+}$ -activation of the troponin-tropomyosin complex. An increase in intracellular  $\text{Ca}^{2+}$  results in the binding of  $\text{Ca}^{2+}$  to the low-affinity  $\text{Ca}^{2+}$ -binding-site (regulatory binding-site), located in the N-terminal domain of cTNC (Robertson et al., 1982; Zot and Potter, 1987; Chandra et al., 1997; Spyrapoulos et al., 1997). Conformational changes in the N-terminal domain of cTNC brought about by the binding of  $\text{Ca}^{2+}$  increase its affinity for the inhibitory peptide of cTNI, resulting in an interaction between the N-terminal domain of cTNC and the inhibitory peptide of cTNI (figure I.3) (Chandra et al., 1997 and references therein). This interaction weakens the binding between cTNI and actin resulting in the movement of  $\alpha$ -TM on the thin filament, causing changes in actin structure that switch thin filaments to the “on state”, facilitating myosin ATPase activity (figure I.3) (Grand and Wilkinson, 1976; Syska et al., 1976; Wilkinson and Grand, 1978; Chandra et al., 1997).

### I.5.2. cTNI AS SUBSTRATE FOR PKA

Of the three TNI isoforms expressed in humans, namely, fast skeletal troponin I (fsTNI), slow skeletal troponin I (ssTNI) and cTNI, only the latter, which is expressed exclusively in cardiac tissue, is phosphorylated by PKA *in vivo* (Grand and Wilkinson, 1976; Saggin et al., 1989; Murphy, 2002; Westfall et al., 2002). Specifically, serine residues 23 and 24, located in the cardiac-specific 26 residue N-terminal extension, are phosphorylated by PKA (figure I.4) (Perry and Cole, 1974; Grand and Wilkinson, 1976; Solaro et al., 1976; Wilkinson and Grand, 1978; Holroyde et al., 1984; Chandra et al., 1997).

PKA-dependent phosphorylation of cTNI at these sites reduces the affinity of the N-terminal of cTNI for the C-terminal of cTNC, resulting in a conformational change in cTNC. This conformational change, in turn, results in a reduction in the affinity of the regulatory  $\text{Ca}^{2+}$ -binding-site, located in the N-terminal of cTNC for  $\text{Ca}^{2+}$  (figure I.3), causing a rightward shift in the  $[\text{Ca}^{2+}]/\text{myosin ATPase}$ -force relationship without affecting the basal, or maximal, myofibrillar ATPase activities (figure I.5a) (England, 1976; Ray and England, 1976; Solaro et al., 1976; Wyborny and Reddy, 1978; Holroyde et al., 1984; Chandra et al., 1997). The reduction in the affinity of cTNC for  $\text{Ca}^{2+}$  causes a decrease in the peak saturation of the regulatory  $\text{Ca}^{2+}$  binding-site on cTNC and an increase in the rate of  $\text{Ca}^{2+}$  dissociation from this site (Robertson et al., 1982; Chandra et al., 1997). At first glance, a rightward shift in the  $[\text{Ca}^{2+}]/\text{myosin ATPase}$  force relationship seems to be in conflict with the increase in contractility associated with  $\beta$ -adrenergic stimulation of the heart (England, 1975; Solaro et al., 1976). Holroyde et al., (1984), however, point out that the decrease in the affinity of cTNC for  $\text{Ca}^{2+}$  would aid relaxation, and thus cardiac diastolic function, during periods of  $\beta$ -adrenergic

stimulation, by reducing the amount of  $\text{Ca}^{2+}$  that has to be transported back to the SR to achieve relaxation.

Cholinergic stimulation, leading to the activation of cyclic guanine monophosphate (cGMP) mediated pathways results in the dephosphorylation of cTNI (figure I.5b) at residues 23 and 24 and the subsequent abolition of the rightward shift in  $[\text{Ca}^{2+}]$ /myosin ATPase relationship, induced by  $\beta$ -adrenergic stimulation (England, 1976; Horowitz and Winegrad, 1983). Dephosphorylation of cTNI, however, occurs at a much slower rate than dephosphorylation of proteins responsible for the increase in  $\text{Ca}^{2+}$ -activated force. This is evidenced by the finding that cTNI persists in its phosphorylated state long after the increase in  $\text{Ca}^{2+}$ -activated force, induced by  $\beta$ -adrenergic stimulation of cardiac tissue, has returned to baseline levels (Horowitz and Winegrad, 1983). This finding indicates that PKA-mediated phosphorylation of cTNI is not responsible for the increase in  $\text{Ca}^{2+}$ -activated force observed in cardiac tissue following  $\beta$ -adrenergic stimulation. Secondly, this finding indicates that the systems responsible for the dephosphorylation of cTNI differ from those responsible for the dephosphorylation of the proteins phosphorylated by PKA, which is responsible for the increase in  $\text{Ca}^{2+}$ -activated force.

Furthermore, Zakhary et al., (1999) have shown that the baseline level of phosphorylated cTNI was significantly reduced in patients with DCM, compared to normal control individuals, while the baseline level of PLB phosphorylation remained unchanged (section I.4). This finding indicates that even though both proteins are phosphorylated by PKA upon  $\beta$ -adrenergic stimulation, different mechanisms are responsible for the phosphorylation of these two proteins. This led the authors to speculate that the phosphorylation of PLB and cTNI might be catalysed by different PKA

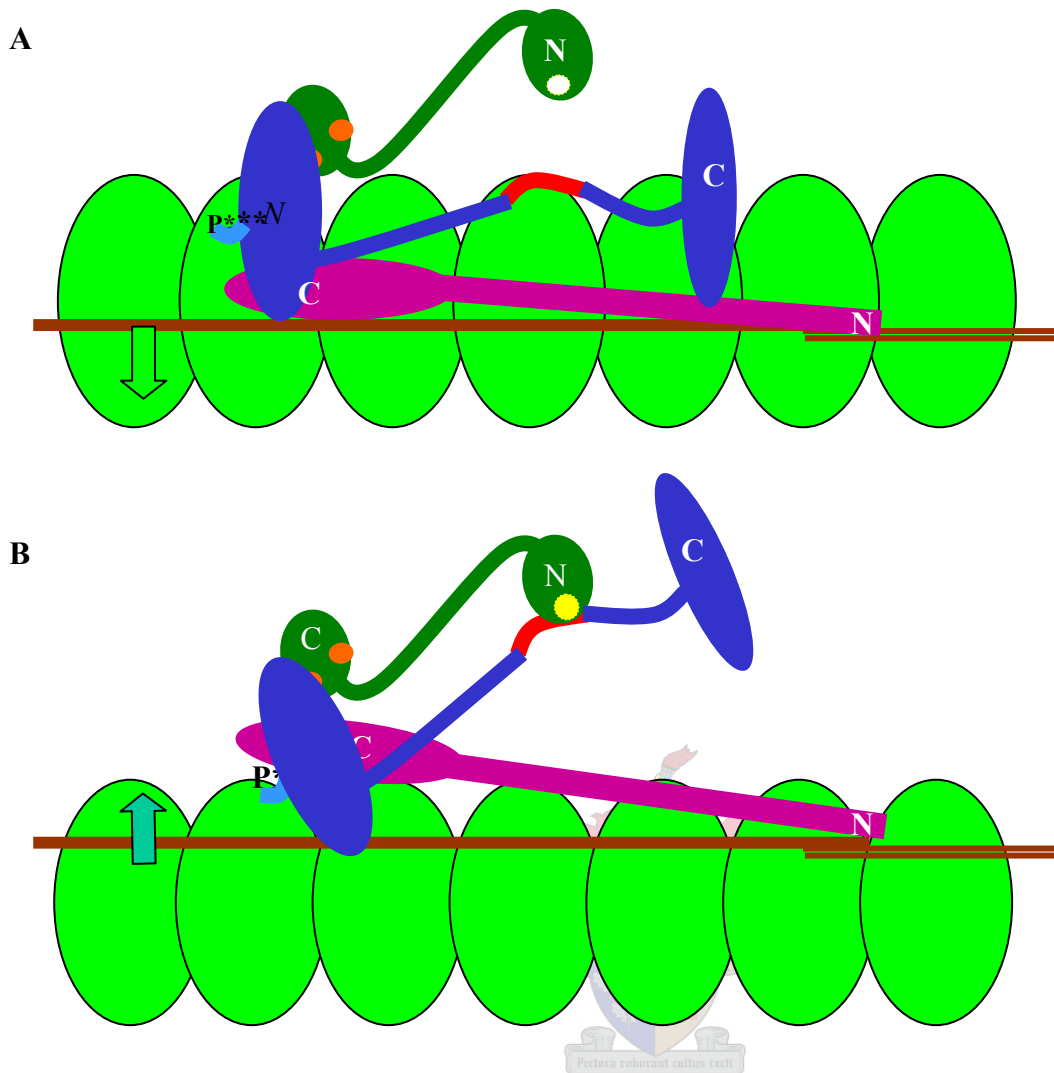


**FIGURE 1.3. Structure of troponin complex and  $\alpha$ -tropomyosin during diastole and systole**

*A. Structure of the troponin complex and  $\alpha$ -tropomyosin relative to actin during diastole. B. Structure of the troponin complex and  $\alpha$ -tropomyosin relative to actin during systole. ■ = cTNC; ● = cTNC constitutive  $\text{Ca}^{2+}/\text{Mg}^{2+}$  binding-sites; ○ = regulatory  $\text{Ca}^{2+}$  binding-site in the absence of bound  $\text{Ca}^{2+}$ ; ● = regulatory  $\text{Ca}^{2+}$  binding-site with  $\text{Ca}^{2+}$  bound; ■ = cTNI; P\* = cardiac-specific PKA phosphorylation site in cTNI; ■ = cTNT; — =  $\alpha$ -tropomyosin; ■ = actin monomers forming part of the thin filament; C = indicates the carboxy-terminals of the components of the troponin complex; N = indicates the amino-terminals of the components of the troponin complex; the arrows in A and B indicate the relative positions of the troponin complex and  $\alpha$ -tropomyosin during diastole and systole respectively (adapted from Solaro and Rarick, 1998).*

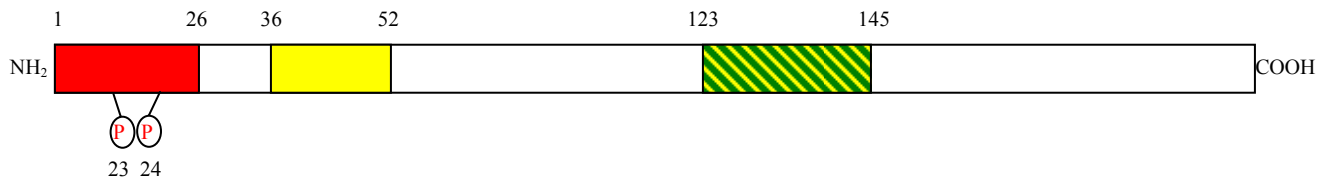


**Figure I.4. Schematic representation of cardiac troponin I**

■ = Cardiac-specific N-terminal region; ■ = major troponin C binding-site; ■ = inhibitory peptide containing actin and troponin C binding-sites; P = phosphorylation sites. The numbers at the top of the figure indicate the residue numbers which designate the start and the end of functional regions; the numbers at the bottom of the figure indicate the residue numbers of the phosphorylation sites.

isoenzymes (Zakhary et al., 1999). PKA type I, containing the RI regulatory subunit, is generally cytosolic and is, therefore, more likely to phosphorylate cTNI, while PKA type II, containing the RII subunit, tends to be compartmentalised by binding to A-kinase anchoring proteins (AKAPS), possibly in the SR-membrane, allowing it to preferentially phosphorylate PLB (Zakhary et al., 1999). This mechanism would allow for the spatial compartmentalisation of PKA within the cell, allowing the preferential phosphorylation of specific proteins under certain physiological conditions.

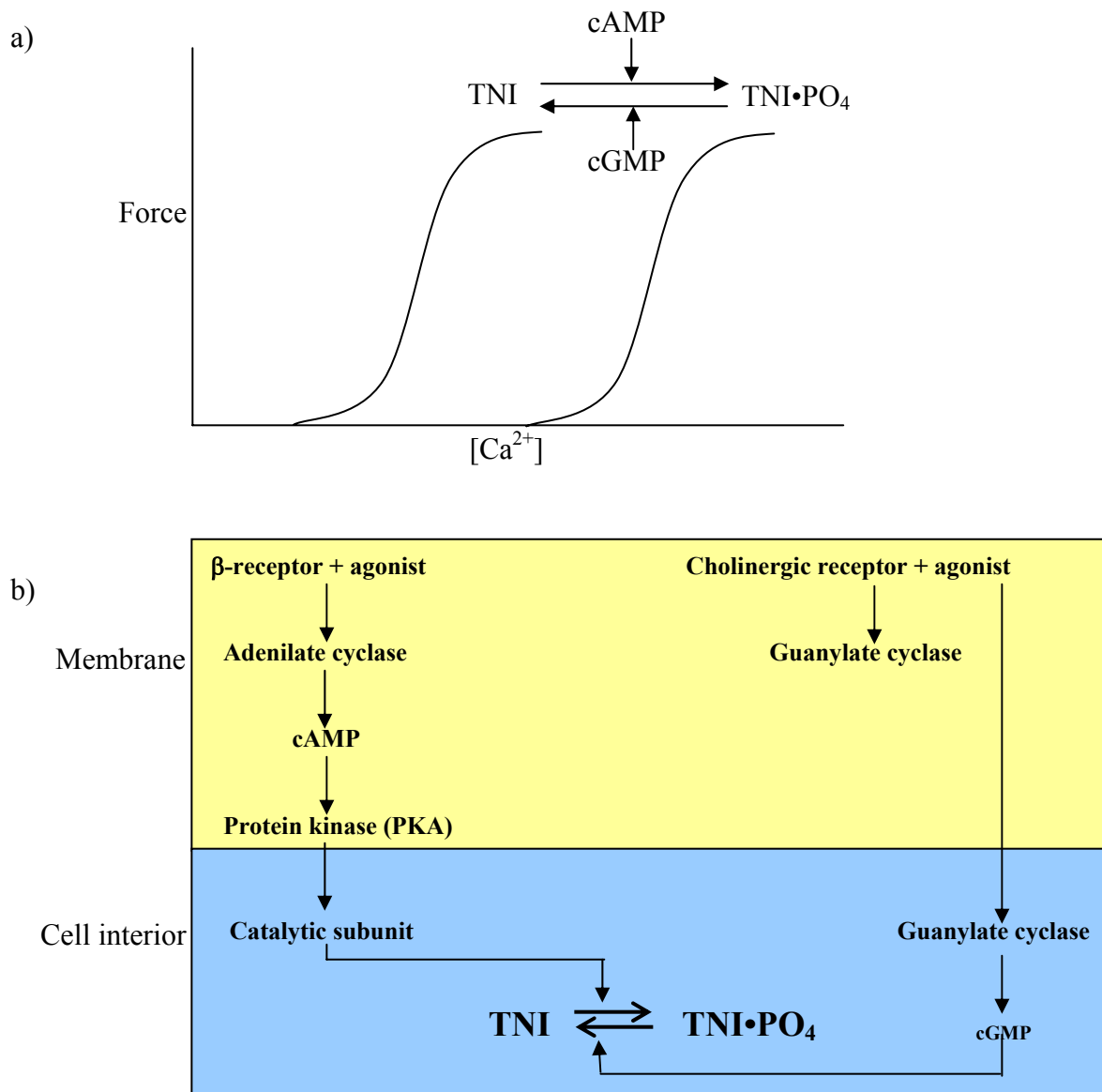


**Figure I.5. Proposed mechanisms involved in the cAMP-dependent phosphorylation and cGMP-dependent dephosphorylation of cTNI, as well as the effect thereof on  $Ca^{2+}$  sensitivity**

a) Effect of cAMP-dependant phosphorylation and cGMP-dependent dephosphorylation of cTNI on  $Ca^{2+}$  sensitivity of the contractile apparatus. b) Proposed mechanisms involved in the cAMP-dependent phosphorylation and cGMP-dependent dephosphorylation of cTNI (from Winegrad, 1984).

## I.6. TITIN

Titin is the largest protein known to be expressed in the human body and spans the length of the half sarcomere from Z-disk to M-line (Means, 1998). The functions of this protein include sarcomeric assembly during myofibrillogenesis and subsequent maintenance of sarcomeric integrity, as well as adding elasticity to the sarcomere, thereby aiding both contraction and relaxation. Based on these functions, titin has been described both as a molecular ruler (Furst et al., 1989a; Labeit et al., 1992; Gautel et al., 1993; Furst and Gautel, 1995) and a bi-directional spring (Furst et al., 1988; Linke et al., 1997; Cazorla et al., 2000; Freiburg et al., 2000).

Alternative splicing of the *TTN* transcript gives rise to various tissue-specific titin isoforms, ranging in size from 2.97MDa to 3.7MDa (Labeit et al., 1990; Freiburg et al., 2000). The variation in these titin isoforms manifests only in the I-band region, giving rise to titins with varying elastic properties (Cazorla et al., 2000; Freiburg et al., 2000).

As specifically the cardiac isoform of titin is phosphorylated by PKA, combined with the fact that this isoform interacts with cMyBPC, its structure and function will be discussed in detail in the following sections. In cases where functional or comparative studies relevant to cardiac titin were performed on skeletal isoforms, it will be indicated as such in the text.

### I.6.1. TITIN STRUCTURE

Cardiac titin is a long filamentous protein of ~850-950nm in length and ~3-4nm in diameter, consisting predominantly of immunoglobulin type C2 (IgC2) and fibronectin type 3 (Fn3) domains and has thus been classified as a member of the intracellular immunoglobulin superfamily (Nave et

al., 1989; Labeit et al., 1992; Soteriou et al., 1993; Vinkemeier et al., 1993; Labeit and Kolmerer, 1995). The N-terminal region is firmly anchored in the sarcomeric Z-disk and the protein extends all the way to the M-line, where the globular C-terminal region is firmly anchored (figure I.6) (Furst et al., 1988; Furst et al., 1989a; Nave et al., 1989; Labeit et al., 1992).

The number of titin molecules per half-sarcomere has been estimated to be between six and seven (Liversage et al., 2001), leading Liversage et al., (2001) to propose a model with six titin molecules per half-sarcomere. According to this model, titin exists as variable oligomers. The number of titin molecules involved in this oligomerisation depends on its specific sarcomeric location, *viz.*, A-band titin is found as dimers, the 22 IgC2-domain tandem repeat of I-band titin, located at the A-I junction, forms a hexamer constituting the end filament. The remainder of I-band titin is in the monomeric form, allowing individual molecules to associate with each of the thin filaments close to the Z-disk (Trinick, 1981; Linke et al., 1997; Liversage et al., 2001). The merit of this model will be discussed further in sections I.6.2-I.6.5, dealing with M-line, A-band, I-band and Z-disk titin, respectively.

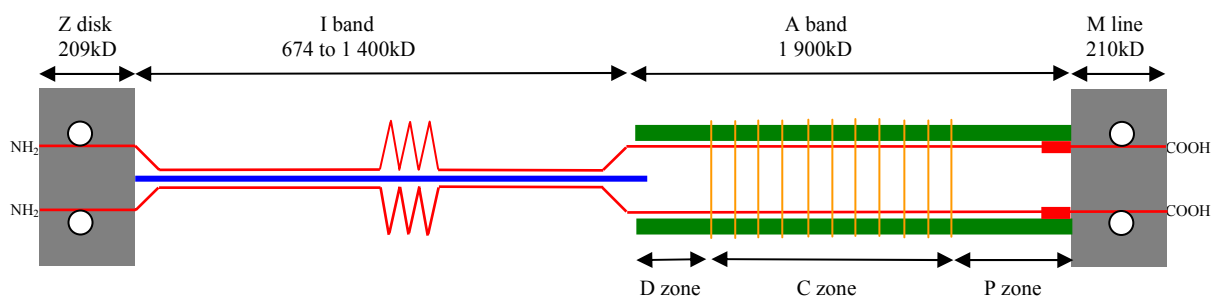


**Figure I.6. Arrangement of titin in the sarcomere**

— = Titin filaments; — = thin filament; — = thick filaments; — = myosin binding proteins; ■ = Z-disk and M-line; ○ = positions of proposed titin phosphorylation sites; ■ = positions of titin kinase domains. The position of the Z-disk, I-band, A-band and M-line, as well as the molecular weight of titin in these regions, is shown at the top of the figure, while the various zones of the A-band are indicated at the bottom of the figure (from Labeit and Kolmerer, 1995).

## I.6.2. M-LINE TITIN

M-line titin consists of 10 IgC2 domains, designated M1 to M10, separated by seven interdomain insertions designated  $is_1$  to  $is_7$ , ranging in size from 30 to 490 residues in length (figure I.7.) (Labeit et al., 1992; Gautel et al., 1993; Labeit and Kolmerer, 1995). M-line titin has been shown to interact with both M-protein and myomesin, thus anchoring the C-terminal of titin firmly in the M-line (Mayans et al., 1998; Nave et al., 1989; Vinkemeier et al., 1993). To date, however, the specific domains of M-line titin responsible for these interactions have not been identified, but are likely to involve specific IgC2 domains. Furthermore, the insertion between M5 and M6 ( $is_4$ ) contains four regions rich in lysine (K), serine (S) and proline (P) residues, designated KSP-motifs which is phosphorylated by KSP-kinase (Gautel et al., 1993). As KSP-kinase is active only in proliferating myoblasts and differentiating cells, it has been proposed that phosphorylation of the KSP-motifs may facilitate the binding of M-line titin to M-protein and myomesin during myofibrillogenesis, thus allowing incorporation of titin into the differentiating myofibril (Gautel et al., 1993; Furst and Gautel, 1995). In addition to M-line titin being bound to M-protein and myomesin, it has been proposed that M-line titin molecules from adjacent half-sarcomeres interact as antiparallel dimers (Gautel et al., 1993; Vinkemeier et al., 1993). This proposal is supported by findings that titin molecules are able to form end-on-end aggregates *in vitro* (Nave et al., 1989).

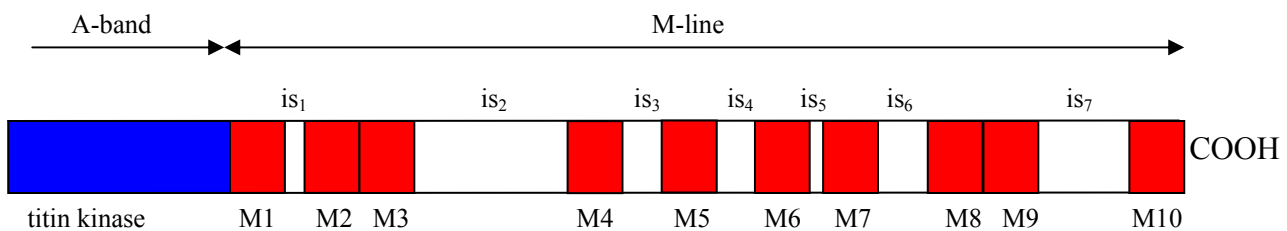


**Figure I.7. Domain organisation of C-terminal titin**

■ = IgC2 domains M1 to M10, □ = interdomain insertions  $is_1$  to  $is_7$ , ■ = titin kinase domain (adapted from Gautel et al., 1993).

### I.6.3. A-BAND TITIN

The sarcomeric A-band can be subdivided into three zones. Firstly, the D-zone, representing the portion of the thick filament closest to the Z-disk, in which no myosin binding proteins (MyBP) are associated with the thick filament. Secondly, the C-zone, representing the central region of the thick filament, in which the MyBP molecules are found, and thirdly, the P-zone, representing the portion of the thick filament between the C-zone and the M-line (figure I.6.) (Labeit and Kolmerer, 1995). It should be noted that some authors use the term C-zone when referring to the region spanning only the outer seven 43nm periods (section I.7.2), representing the positions in which myosin binding protein C (MyBPC) is always present (Sjostrom and Squire, 1977). As the distribution of MyBPC varies between various muscle types, the term of C-zone as defined by Labeit and Kolmerer (1995), encompassing all eleven 43nm periods will be used in this review.

A-band titin consists mainly of IgC2 and Fn3 domains and is found on the surface of the thick filament (Furst et al., 1988; Furst et al., 1989a; Labeit and Kolmerer, 1995), where it is constitutively bound to LMM (Furst et al., 1988; Labeit et al., 1992). It has been shown that specifically the Fn3 domains of A-band titin interact with LMM, while the presence of IgC2 domains are essential for facilitating this interaction (Labeit et al., 1992; Jin, 1995).

In addition to its interaction with LMM, A-band titin is also able to form side-by-side aggregates *in vitro* (Nave et al., 1989), lending support to the hypothesis of Liversage et al., (2001) that A-band titin molecules dimerise. This dimerisation is in all likelihood facilitated by homophilic interaction between Fn3 domains, found almost exclusively in A-band titin (Nave et al., 1989; Price and Gomer, 1993; Labeit and Kolmerer, 1995).

### I.6.3.1. D-zone titin

D-zone titin consists entirely of IgC2 and Fn3 domains. The first 13 of these domains were originally described as part of the I-band by Labeit and Kolmerer (1995), who characterised them as a region with “complex domain architecture near the junction of the I- and A-bands”, hence their numbering as part of the I-band (I42-I54 by Labeit and Kolmerer (1995) and I106-I118 by Granzier and Labeit, 2002). Trinick (1996), however, showed that these domains are in fact part of D-zone titin, rather than I-band titin, and, although this view is generally accepted, these domains are still numbered as if they were part of the I-band, rather than the A-band (Trinick, 1996).

These 13 domains are followed by a highly ordered seven-domain super-repeat (IgC2-Fn3-Fn3-IgC2-Fn3-Fn3-Fn3). This super-repeat is itself repeated six times with domains numbered A1-A42 (figure I.8.) (Labeit and Kolmerer, 1995).

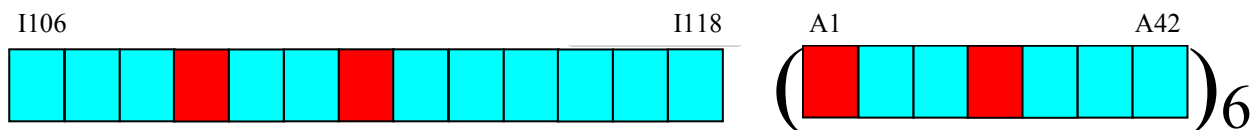


**Figure I.8. Organisation of D-zone titin**

■ = IgC2 domains, ■ = Fn3 domains. The seven domains indicated in brackets are repeated six times (adapted from Labeit and Kolmerer, 1995).

### I.6.3.2. C-zone titin

C-zone titin exhibits a regular architecture of an 11 domain super-repeat (IgC2-Fn3-Fn3-IgC2-Fn3-Fn3-Fn3-IgC2-Fn3-Fn3-Fn3), itself repeated 11 times (see figure I.9) (Labeit et al., 1992; Politou et al., 1994; Labeit and Kolmerer, 1995). The length of each of these repeats is ~43nm, which is

consistent with the spacing between the positions occupied by the MyBPs in the sarcomeric C-zone, as well as the myosin helix repeat (Labeit et al., 1992).

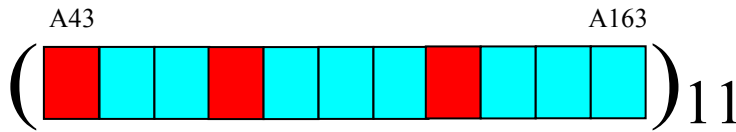


**Figure I.9. Organisation of C-zone titin**

■ = IgC2 domains, ■ = Fn3 domains. This series of 11 domains are repeated 11 times in the C-zone (from Labeit and Kolmerer, 1995).

The 11-domain super-repeat determines the distribution of MyBPC and myosin binding protein H (MyBPH) within the C-zone, at a spacing of ~43nm, thus enabling C-zone titin to function as a molecular ruler (Furst et al., 1989a; Labeit et al., 1992). The first IgC2 domain of each of the 11-domain super-repeats (A43, A54, A65, A76, A87, A98, A109, A120, A131, A142, A153) (section I.7.3.2) binds strongly to the C-terminal portion of MyBPC (Labeit et al., 1992; Labeit and Kolmerer, 1995; Freiburg and Gautel, 1996). It is interesting to note that the C-terminal region of MyBPC is also able to bind to domain A153 of titin, representing stripe 11, in which MyBPC has to date never been found in all muscle types investigated (table I.3) (for further discussion on this interaction see sections I.7.3.2 and IV.2) (Bennett et al., 1986; Labeit and Kolmerer, 1995; Freiburg and Gautel, 1996).

### **I.6.3.3. P-zone titin**

The P-zone portion of titin has a less regular domain architecture than either D- or C-zone titin and consists of four IgC2 and three Fn3 domains, designated domains A164 to A170, a short unique

sequence and a kinase domain (figure I.10.) (Labeit and Kolmerer, 1995). The kinase domain, designated titin kinase, shares significant homology with myosin-light chain kinase and has been shown to phosphorylate the Z-disk protein telethonin (Labeit and Kolmerer, 1995; Mayans et al., 1998).

Titin kinase is itself activated by phosphorylation by an as yet unidentified kinase and the binding of  $\text{Ca}^{2+}$ /calmodulin, allowing it to bind to and phosphorylate the Z-disk protein telethonin (Mayans et al., 1998). The phosphorylation of telethonin has been postulated to be involved in myofibrillogenesis (Mayans et al., 1998). It is intriguing to note that titin kinase, located close to the M-line, about  $1\mu\text{m}$  from the Z-disk in mature myofibrils, regulates Z-disk architecture. During myofibrillogenesis, however, titin is already anchored in the Z-disk at an early stage before associating with the thick filament. As the A-band and M-line portions of titin is at this stage not associated with the thick filament or M-line, it is possible for titin to fold back on itself, thereby allowing titin kinase to be transiently in close proximity to telethonin in the Z-disk (Furst et al., 1989b; Mayans et al., 1998).

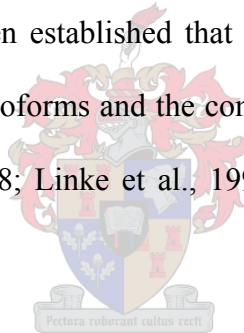


**Figure I.10. Organisation of P-zone titin**

■ = IgC2 domains; ■ = Fn3 domains; ■ = titin-kinase domain; white box = unique sequence (from Labeit and Kolmerer, 1995).

#### I.6.4. I-BAND TITIN

It is specifically in the I-band region of titin that isoform diversity, resulting from the alternative splicing of *TTN*, becomes apparent. I-band titin consists of three main components. Firstly, tandemly repeated IgC2 domains, secondly, the so-called PVEK domain, in which the amino acids P, E, K and V constitute ~70% of the domain, and, thirdly, other non-repetitive sequences of which the N2A and N2B elements are the most significant. The specific lengths of each of these segments is, however, isoform dependent (figure I.2.6.) (Labeit and Kolmerer, 1995; Freiburg et al., 2000; Granzier and Labeit, 2002). Together, these regions are responsible for the elastic properties of titin, allowing it to function as an adjustable bi-directional spring (Furst et al., 1988; Linke et al., 1997; Cazorla et al., 2000; Freiburg et al., 2000). It has been established that there is a direct correlation between the length of differentially expressed titin isoforms and the compliance/passive tension of the muscle in which it is expressed (Furst et al., 1988; Linke et al., 1997; Cazorla et al., 2000; Freiburg et al., 2000).



##### I.6.4.1. I-band titin isoform diversity

Numerous different skeletal and cardiac titin isoforms, varying specifically in their I-band regions, are generated by the alternative splicing of *TTN* (figure I.11) (Labeit and Kolmerer, 1995; Freiburg et al., 2000; Granzier and Labeit 2002). Generally, skeletal muscle titin isoforms contain more tandemly repeated IgC2 domains in the I-band region, and generally have a larger PVEK segment than cardiac titin isoforms. The main factor distinguishing the cardiac isoforms from their skeletal counterparts is, however, the presence of the N2B element (Labeit and Kolmerer, 1995; Freiburg et al., 2000; Granzier and Labeit, 2002). This element, consisting of three IgC2 domains and an unique

sequence of 572 amino acids in human titin, is constitutively found in all cardiac titin isoforms. In contrast, the N2A element, consisting of four IgC2 domains and an unique sequence of 106 amino acids in human titin, is present in all skeletal isoforms (figure I.11.) (Labeit and Kolmerer, 1995; Cazorla et al., 2000; Freiburg et al., 2000). Cardiac titin isoforms containing both the N2B and N2A elements are referred to as N2BA titin and contain a variable, but similar, number of IgC2 domains separating these elements (varying in number from 14 to 26) (figure I.11) (Labeit and Kolmerer, 1995; Cazorla et al., 2000; Freiburg et al., 2000). As this difference in the number of IgC2 domains, and the subsequent difference in elastic properties (see section I.6.4.2), is quite small, all N2BA titin isoforms have been grouped together for the purpose of this discussion.

The N2B cardiac titin isoform further differs from the larger N2BA cardiac titin isoform in that there are fewer tandemly repeated IgC2 domains separating the N2B element and the PVEK segment. Additionally, the PVEK segment found in the N2B isoform is significantly smaller than that of the N2BA isoform (figure I.11) (Labeit and Kolmerer, 1995; Cazorla et al., 2000; Freiburg et al., 2000; Granzier and Labeit, 2002).

The N2B and N2BA cardiac titin isoforms are co-expressed in cardiac muscle and it has been shown that both isoforms may also be co-expressed within a single cardiomyocyte. The specific ratios at which these isoforms are expressed in cardiac tissue are both species and location, i.e. atrial and ventricular, specific (Cazorla et al., 2000; Freiburg et al., 2000; Neagoe et al., 2002). The N2BA isoform is predominantly expressed in atrial tissue, while the expression of cardiac titin isoforms within the ventricle varies according to species. There are conflicting reports regarding the expression of these two isoforms in the human ventricular myocardium. Freiburg et al., (2000) have shown that the N2BA isoform is predominant in the human ventricular myocardium, while Neagoe

et al., (2002) found that about 70% of ventricular titin is of the N2B isoform. Cardiomyocytes in which the larger N2BA titin is the predominant isoform, are more compliant than cardiomyocytes predominantly expressing the shorter N2B isoform (Cazorla et al., 2000; Freiburg et al., 2000). Conversely, cardiomyocytes predominantly expressing the N2B isoform generate more passive tension at a given sarcomeric length than do cardiomyocytes in which N2BA titin predominates (Cazorla et al., 2000; Freiburg et al., 2000).

Additionally, a shorter titin isoform, known as novex 3 has also been described. This isoform, expressed in all striated muscle tissue (Granzier and Labeit, 2002) is made up mostly of the Z-disk portion of titin, but lacks the Z-repeats, as well as the proximal 15 IgC2 repeats of I-band titin and the so-called novex 3 element. It has been speculated that this titin isoform may be anchored in the Z-disk due to the presence of Z-disk titin IgC2 domains, while the novex 3 element may interact with either the thick filament or the end filament. This scenario is, however, highly unlikely as the Z-repeats, essential for the anchoring of titin to  $\alpha$ -actinin in the Z-disk, are absent in this isoform (Young et al., 1998). The physiological importance of this isoform, however, remains to be elucidated.

#### **I.6.4.2. I-Band titin as generator of passive tension**

In order to explain the stretch and subsequent generation of passive tension, it has been proposed that the elastic component of I-band titin, namely, the tandemly repeated IgC2 segments, the unique N2B segment and the PVEK segment, behave as a serially-linked wormlike chain (WLC) (Helmes et al., 1999). A WLC is a deformable rod whose bending rigidity is expressed in terms of its persistence length. For instance, if a peptide in a rigid WLC has a long persistence length, a relatively small

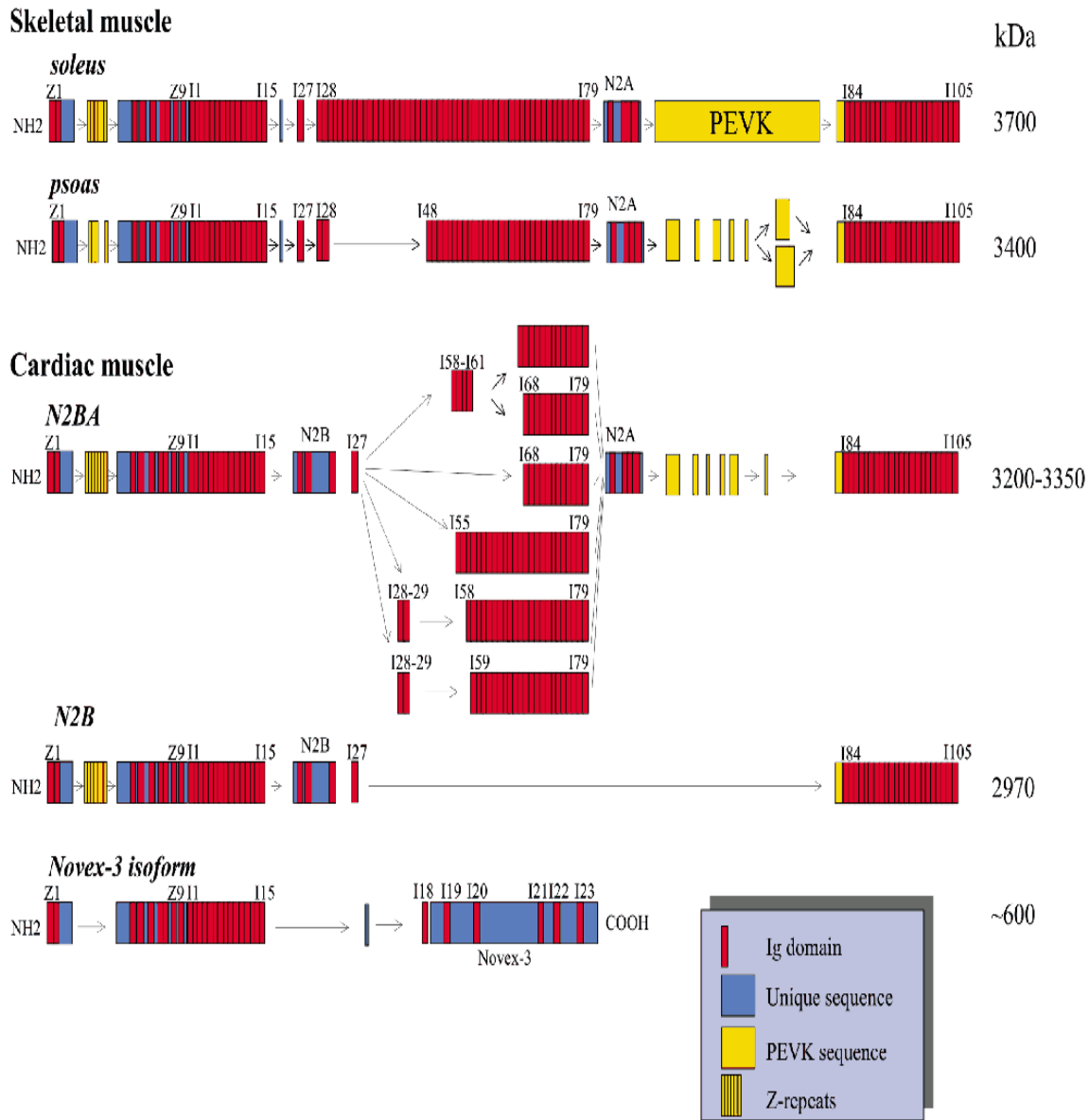


**Figure I.11. Splice isoform diversity of the I-band regions of titin**

Skeletal muscles express N2A-based titins that vary in size in different muscle types (two of many possible splice pathways are shown). Cardiac muscle express large N2BA and small N2B titins. All striated muscles express novex-3 titin (from Granzier and Labeit, 2002).

force would be required to straighten it, resulting in the generation of only a small amount of passive tension (Helmes et al., 1999). As the elastic segments of I-band titin are serially linked, and their extension is sequential, they will be discussed separately in the following sections.

#### I.6.4.2.i. Tandem IgC2 domains acting as a rigid WLC

The persistence length of the tandem IgC2-segments of I-band titin is marginally shorter than its chain length, as evidenced by its appearance as a “piled up” structure at the junction between the A- and I-bands, when the muscle is at rest (figure I.12) (Furst et al., 1988; Kellermayer et al., 1997; Tskhovrebova et al., 1997; Linke et al., 1998; Helmes et al., 1999). Helmes et al., (1999) proposed that this “piled up” conformation of the tandem IgC2-segments is energetically the most stable and is stabilised by weak non-covalent interdomain interactions (either intra-molecular or inter-molecular). Hence, force denaturation of these interactions, due to stretching of the muscle, would result in the generation of passive tension (figure I.12) (Helmes et al., 1999). Due to its relative high persistence length and rigidity, the straightening of the tandem IgC2 repeats will occur at low stretching force, with the subsequent generation of low levels of passive tension, which has been compared to the straightening of a leash (figure I.12) (Helmes et al., 1999).

#### I.6.4.2.ii. PVEK as a WLC

Although the PVEK segments of the various titin isoforms differ dramatically in size, they are all characterised by the abundance of the four amino acids P, V, E and K, which constitute about 70% of this domain (Labeit and Kolmerer, 1995; Granzier and Labeit, 2002). Additionally, the presence of clusters of negatively charged residues in the PVEK segment prevents the formation of stable tertiary structures, causing this segment of the protein to behave as an unfolded peptide, which is easily stretched (Labeit and Kolmerer, 1995; Trombitas et al., 1998; Helmes et al., 1999).

Like the tandemly repeated IgC2 domains of I-band titin, the PVEK segment also acts as a WLC, but is less rigid and has a shorter persistence length than the tandem IgC2 segments. Extension (force denaturation) of this segment requires a greater force than extension of the tandem IgC2 segments and will, therefore, only occur following complete extension of the tandem IgC2 segments. As the force that is required to cause the extension of the PVEK segment is slightly higher than predicted by the serially linked WLC model, it was proposed that weak non-covalent interactions might exist within this region when titin is “contracted” in the slack sarcomere (see figure I.12) (Helmes et al., 1999). Entropic renaturation of the PVEK segment consequently leads to a logarithmic increase in passive tension that is significantly higher than that produced by the renaturation of tandem IgC2 segments (Trombitas et al., 1998; Helmes et al., 1999). This finding prompted Helmes et al., (1999) to dub this segment the “force generator” (figure I.12).

#### I.6.4.2.iii. N2B element as an adjustable generator of passive tension

As the N2B element of cardiac titin has a shorter persistence length and lower rigidity than the tandem Ig-repeats and the PVEK segment, extension of this region only occurs following the complete extension of the tandem Ig-repeats and the PVEK segment (Helmes et al., 1999). Denaturation of the N2B element from its compact state results in a linear increase in passive tension (figure I.12) (Helmes et al., 1999). Due to the presence of more tandem Ig-domains and a longer PVEK segment in N2BA titin, denaturation of the N2B element in this isoform would occur at longer sarcomeric lengths than in the N2B isoform.

#### I.6.4.2.iv. Domain denaturation as a mechanism for generating passive tension

*In vitro* experiments have shown that titin displays step-like stress relaxation, when excessive stretching force is applied, due to the sequential denaturation of individual IgC2 domains in the

tandem Ig repeats of I-band titin (Rief et al., 1997; Tskhovrebova et al., 1997). Due to the variable stabilities of IgC2 domains in this region, the force-denaturation of these domains will occur sequentially, allowing for the elongation of I-band titin in a saw-tooth manner as increasing stretching force is applied to the sarcomere (~25nm per IgC2 domain denatured) (Rief et al., 1997; Tskhovrebova et al., 1997).

Renaturation of these domains takes place on a slower timescale (~1 second) and only occurs when tensile force is **completely** released (Kellermayer et al., 1997; Rief et al., 1997). It is, therefore, unlikely that this mechanism would contribute to the generation of passive tension, and denaturation of IgC2 domains is unlikely to happen *in vivo* under normal physiological conditions (Trombitas et al., 1998), but may be a mechanism to protect the sarcomere from permanent damage by overstretching (Rief et al., 1997).



#### **I.6.4.3. I-band titin as a generator of restoring force**

In addition to the generation of passive tension, I-band titin has also been implicated in the generation of restoring force (Helmes et al., 1996). Restoring force allows the passive re-lengthening of cardiac myocytes back to their slack length following contraction, thereby aiding ventricular filling during the early stages of diastole (Helmes et al., 1996).

The mechanism proposed for the generation of restoring force is similar to that proposed for the generation of passive tension (Labeit and Kolmerer, 1995; Helmes et al., 1999). Firstly, the tandem IgC2 repeats of I-band titin would straighten, followed by the denaturation of the PVEK region and the subsequent generation of restoring force (figure I.13) (Helmes et al., 1996; Helmes et al., 1999).

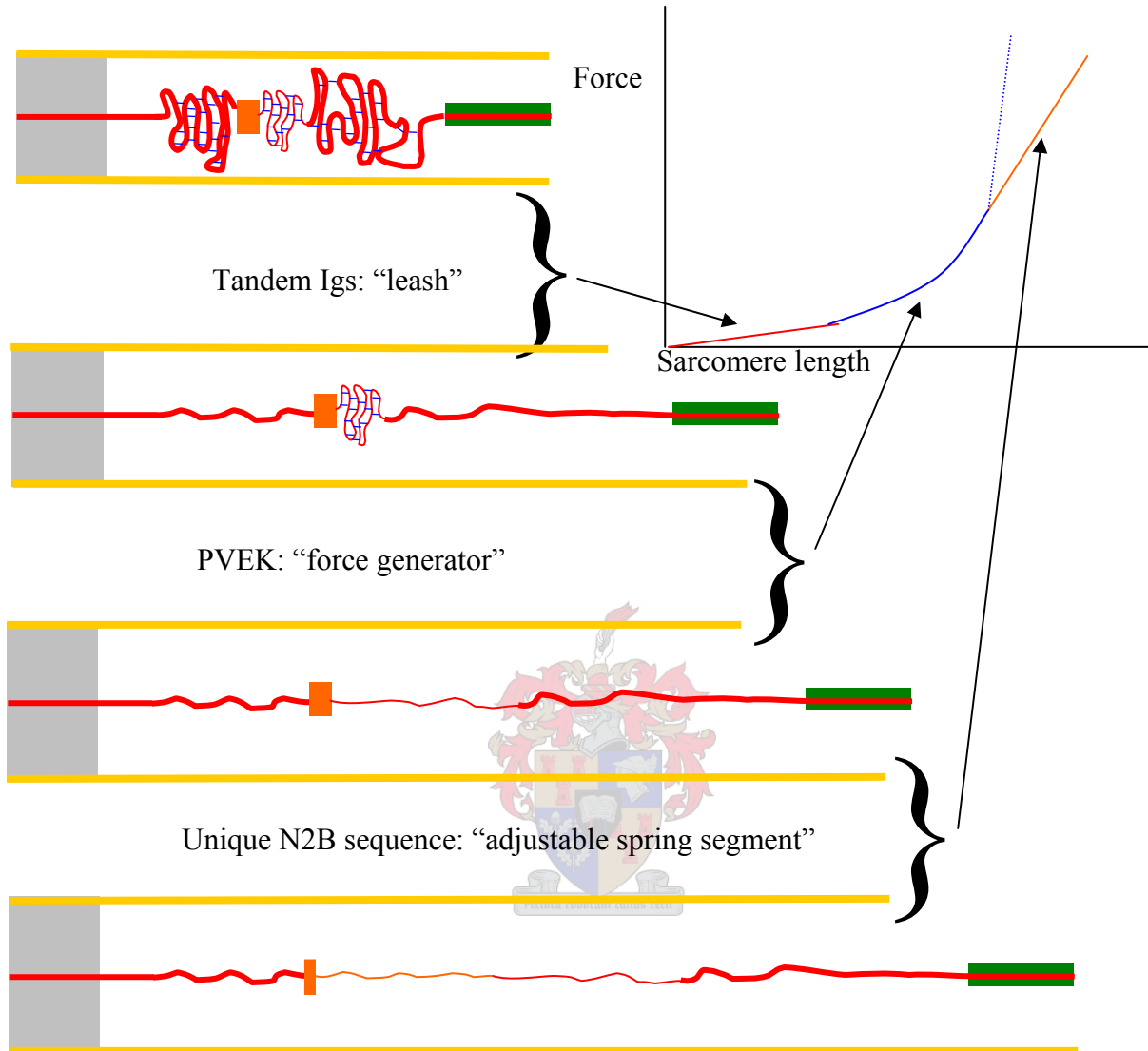


**Figure I.12. Model for passive tension development by N2B titin**

Left side: Titin's I-band segment at sarcomeric lengths from near slack (top) to highly extended (bottom). Tandem Ig segments containing folded Ig domains depicted as thick red line; folded N2B-specific segment depicted as orange square; unfolded N2B-specific segment depicted as thin orange line; PVEK segment depicted as thin red line; noncovalent interactions between Ig domains and folded PVEK segment depicted as thin blue lines. The force-sarcomeric length relationship associated with the force-denaturation of each of these segments is shown in the graph in the top right-hand corner of the figure (from Helmes et al., 1999).

In this instance, however, the force responsible for the straightening/denaturation of these segments of I-band titin would be a contractile, rather than a stretching force (Helmes et al., 1996; Helmes et al., 1999). This hypothesis, however, requires that a significant length of I-band titin has to be immobilised on the thin filament during late systole. Although I-band titin has been shown to associate with filamentous actin (F-actin), this is likely to be a relatively weak interaction that only occurs in the portion of I-band titin directly adjacent to the Z-disk (Nave et al., 1989; Jin, 1995; Linke et al., 1997).

It was, however, recently shown that the PVEK region of N2B titin is able to bind to F-actin under physiological ionic strengths, a feature specific to the cardiac N2B titin isoform (Yamasaki et al., 2001). This interaction is regulated in a  $\text{Ca}^{2+}$ -dependent manner by S100A1, a member of the S100 family of EF-hand calcium-binding proteins. At high  $\text{Ca}^{2+}$  concentrations,  $\text{Ca}^{2+}$ -S100A1 binds to the PVEK segment of the N2B titin isoform, inhibiting its interaction with F-actin (Yamasaki et al., 2001). The inhibition of this interaction by S100A1 at high  $\text{Ca}^{2+}$  concentrations suggests that the binding of the PVEK segment to F-actin would not play a major role during systole, but may be important during diastole when the cytoplasmic  $\text{Ca}^{2+}$  is low (Yamasaki et al., 2001).

The possibility that the binding of the PVEK segment to F-actin may be of importance in the generation of restoring force was, however, not considered by Yamasaki et al., (2001). Although the critical  $\text{Ca}^{2+}$  concentration at which the PVEK-F-actin interaction is inhibited is not clear from the data presented by Yamasaki et al., (2001), it may be interesting to superimpose this data onto the  $\text{Ca}^{2+}$ -activated actomyosin force curve. If this critical  $\text{Ca}^{2+}$  concentration is reached before all actomyosin activity is inhibited towards the end of systole, it could be postulated that a situation may occur where the PVEK segment of N2B titin may bind to the thin filament before all actomyosin

activity is inhibited. This would result in the straightening of I-band titin's C-terminal tandem IgC2 repeats, with the subsequent generation of restoring force (figure I.13). As the PVEK-segment of N2B titin is immobilised on the thin filament, this hypothesis would imply that the PVEK-segment and the proximal tandem Ig repeat (adjacent to the Z-line) would not participate in the generation of restoring force and that all restoring force is generated by the entropic renaturing of the distal Ig repeat (figure I.13).



**Figure I.13.** *Proposed mechanism for the generation of restoring force facilitated by an interaction between the PVEK segment of N2B titin and F-actin.*

*Tandem Ig segments containing folded Ig domains depicted as thick red line; folded N2B-specific segment depicted as orange square; PVEK segment depicted as thin red line; non-covalent interactions between Ig domains and folded PVEK segment depicted as thin blue lines; Interaction between PVEK and F-actin depicted by thick blue line. The black arrow below the figure indicates the direction force generated by  $\text{Ca}^{2+}$ -activated actomyosin activity, while the red arrow indicates the direction of restoring force generated by the straightening of the tandem IgC2 segment.*

### **I.6.5. Z-DISK TITIN**

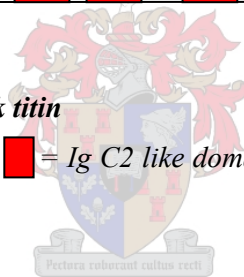
The N-terminal 209kDa of titin enters the Z-disk and contains ten IgC2 domains, numbered Z1 to Z10, which are associated with F-actin in the thin filament (figures I.14 and I.15) (Nave et al., 1989; Jin, 1995; Labeit and Kolmerer, 1995; Linke et al., 1997). In the region separating domain Z3 and Z4, a variable number of repeat sequences, unique to Z-disk titin, designated the Z-repeats, have

been identified (Gautel et al., 1996). In cardiac muscle there are five Z-repeats, designated zr1 to zr5 (figure I.14), of which zr1, zr3 and zr5 have been shown to interact with the C-terminal region of  $\alpha$ -actinin (Gautel et al., 1996; Young et al., 1998). Additionally, the unique sequence separating the Z-repeats and the Z4 IgC2 domain has also been shown to interact with the central spectrin-like repeat of  $\alpha$ -actinin (figures I.14 and I.15) (Young et al., 1998). It has been proposed that these interactions are essential for Z-disk formation, and that the titin isoform-specific number of Z-repeats determines the number of Z-filaments in the Z-disk (Gautel et al., 1996; Young et al., 1998). The proposed arrangement of titin within the Z-disk is shown in figure I.15.



**Figure I.14. Domain organisation of Z-disk titin**

 = Z-repeats zr1 to zr5, numbered 1 to 5;  = Ig C2 like domains Z1 to Z10,  = unique sequences; \* =  $\alpha$ -actinin interaction sites.



### I.6.6. PKA-MEDIATED PHOSPHORYLATION OF TITIN

It was recently shown that the cardiac-specific N2B element is mono-phosphorylated by PKA, upon  $\beta$ -adrenergic stimulation (Yamasaki et al., 2002). Previous studies have shown that  $\beta$ -adrenergic stimulation of intact cardiac myocytes led to a significant reduction in the generation of passive tension, specifically at relatively short sarcomeric lengths (Strang et al., 1994; Yamasaki et al., 2002). These findings prompted Yamasaki et al., (2002) to speculate that PKA-dependent phosphorylation of the N2B element results in the denaturation of this element. This hypothesis implies that, during periods of  $\beta$ -adrenergic stimulation of the heart, the N2B element would be in a denatured state and would extend at short sarcomeric lengths during the initial stages of sarcomeric

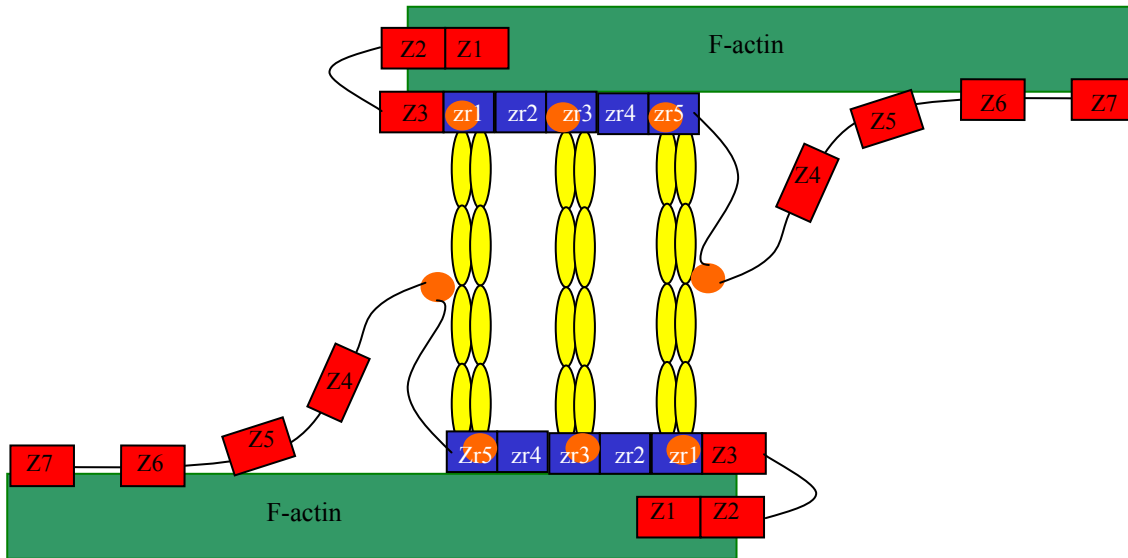


**Figure I.15. Proposed position of titin in the Z-disk**

— = non-repetitive sequences in Z-disk titin; ■ = Z-repeats of Z-disk titin; ■ = thin filament; ● = point of interaction between Z-disk titin and  $\alpha$ -actinin; ■ = IgC2 domains of Z-disk titin;  = spectrin-like domains of  $\alpha$ -actinin (from Young et al., 1998).

lengthening, with little passive tension being developed. Further stretching of the sarcomere would subsequently cause the sequential extension of the tandem IgC2 repeats and the PVEK domain, allowing the generation of passive tension comparable to that observed in the absence of adrenergic stimulation (Yamasaki et al., 2002).

This reduction in the generation of passive tension is postulated to aid ventricular filling during periods of  $\beta$ -adrenergic stimulation, associated with an increase in heart rate (Yamasaki et al., 2002). As passive tension may significantly contribute to shortening velocity at longer sarcomeric lengths (Minajeva et al., 2002), the reduction in passive tension, brought about by  $\beta$ -adrenergic stimulation, may result in a decrease, rather than an increase, in force generation. This finding suggests that the PKA-dependent phosphorylation of titin is not responsible for the increase in force generation observed following  $\beta$ -adrenergic stimulation of the heart (England, 1975; Solaro et al., 1976).

## **I.7. MYOSIN BINDING PROTEIN C**

Myosin binding protein C was first described three decades ago as a “contaminant of myosin preparations” (Offer et al., 1973). Since then, this protein has graduated from a mere contaminant to being an integral part of the thick filament with important structural and regulatory functions.

The myosin binding protein family (MyBP) consists of MyBPC and MyBPH, both of which are members of the immunoglobulin superfamily (Vaughan et al., 1993). MyBPC and MyBPH share a significant amount of amino acid sequence homology, specifically in their C-terminal regions (figure I.16) (Vaughan et al., 1993).

Three isoforms of MyBPC have been identified in striated muscle, namely, the fast skeletal (fsMyBPC), slow skeletal (ssMyBPC also previously known as MyBPX) and cardiac (cMyBPC) isoforms (Reinach et al., 1982; Yamamoto and Moos, 1983; Obinata et al., 1984). All three isoforms consist mainly of IgC2 and Fn3 domains (Einheber and Fischman, 1990; Furst et al., 1992; Vaughan et al., 1993; Weber et al., 1993). As the cardiac isoform is involved in the pathophysiology of HCM and plays an important role in the regulation of cardiac contractility, this isoform is specifically relevant to the present study. Its structure and function will, therefore, be described in detail in this section.

### **I.7.1. STRUCTURE OF THE MyBP FAMILY**

The overall structure of cMyBPC is that of an elongated protein, about 40-44nm in length and 3nm in diameter (Hartzell and Sale, 1985). The skeletal MyBPC isoforms each consists of seven IgC2

(domains C1, C2, C3, C4, C5, C8 and C10) and three Fn3 domains (domains C6, C7 and C9) (Einheber and Fischman, 1990; Furst et al., 1992; Okagaki et al., 1993; Vaughan et al., 1993; Weber et al., 1993; Gautel et al., 1995; Carrier et al., 1997; Bennett et al., 1999), while the cardiac isoform has an additional N-terminal IgC2 domain (domain C0) (Carrier et al., 1997). In addition to IgC2 and Fn3 domains, the MyBPC family is characterised by the presence of a motif specific to MyBPC located between domains C1 and C2 (MyBPC motif) and a region rich in proline and alanine residues (PA-region). In the skeletal isoforms, the PA-region is located at the N-terminal of the protein, while it separates the C0 and C1 domains in the cardiac isoform (figure I.16.) (Einheber and Fischman, 1990; Furst et al., 1992; Okagaki et al., 1993; Vaughan et al., 1993; Weber et al., 1993; Gautel et al., 1995; Carrier et al., 1997; Bennett et al., 1999). Furthermore, short interdomain linker sequences are present between domains C4 and C5, C6 and C7, C7 and C8, as well as between domains C9 and C10 in all MyBPC isoforms (figure I.16) (Okagaki et al., 1993; <http://smart.embl-heidelberg.de/smart/>). In addition to the presence of the C0 domain, the cardiac isoform further differs from the skeletal isoforms in that nine and twenty-eight amino acid residue loops are inserted into the MyBPC motif and the C5 domain, respectively (figure I.16) (Gautel et al., 1995; Yasuda et al., 1995; Freiburg and Gautel, 1996).

The second member of the MyBP family, MyBPH, consists of only two IgC2 (domains 2 and 4), and two Fn3 domains (domains 1 and 3) (Vaughan et al., 1993). Interestingly the domain distribution of MyBPH corresponds precisely with that of the final four domains of MyBPC, namely Fn3-IgC2-Fn3-IgC2. This conservation suggests a common function for MyBPH and the four C-terminal domains of MyBPC, namely binding of myosin and titin, with the major myosin binding-site located in the last IgC2 domain of both molecules (figure I.16) (Vaughan et al., 1993; Welikson and Fischman, 2002).

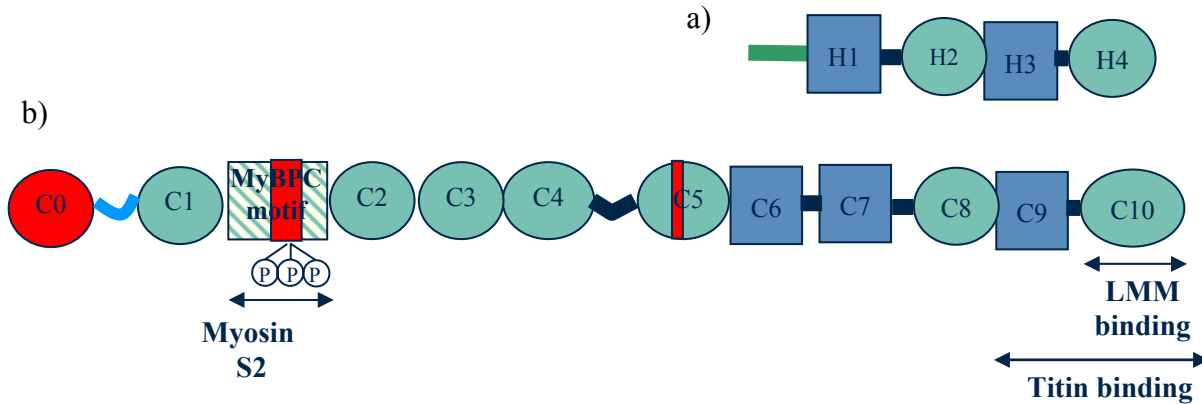


**Figure I.16. Structure of the MyBPC and MyBPH**

Structure of a) MyBPH and b) cMyBPC. Circles = immunoglobulin C2 domains; ■ = fibronectin type 3 domains; ▨ = MyBPC motif; ■ = interdomain linkers; ■ = PA-region; ■ = unique N-terminal region of MyBPH; (P) = PKA and MyBPC-associated kinase phosphorylation sites; red areas = cardiac-specific regions, absent in fsMyBPC and ss MyBPC. The arrows below the figure indicate the positions of the binding-sites for light meromyosin (LMM), myosin S2 and titin.

### I.7.2. C-ZONE LOCALISATION OF MyBPC

The myosin binding proteins (MyBPC and MyBPH) are found in 11 transverse stripes, spaced 43nm apart, in the C-zone of the sarcomere (numbered 1-11 from the Z-disk to the M-line) (figure I.17) (Offer, 1972). The distribution of MyBPC and MyBPH at these positions within the C-zone is, however, both species- and fibre-specific (table I.3) (Craig and Offer, 1976; Dennis et al., 1984; Bahler et al., 1985; Starr et al., 1985; Bennett et al., 1986; Bennett et al., 1999). The precise distribution of cMyBPC within the C-zone of the cardiac sarcomere has, however, not been reported. Incorporation of MyBPC into these specific positions in the C-zone is mediated by interactions between its C-terminal region and both LMM and C-zone titin (sections I.7.3.1 and I.7.3.2) (Okagaki et al., 1993; Labeit and Kolmerer, 1995; Freiburg and Gautel, 1996; Bennett et al., 1999; Miyamoto et al., 1999).

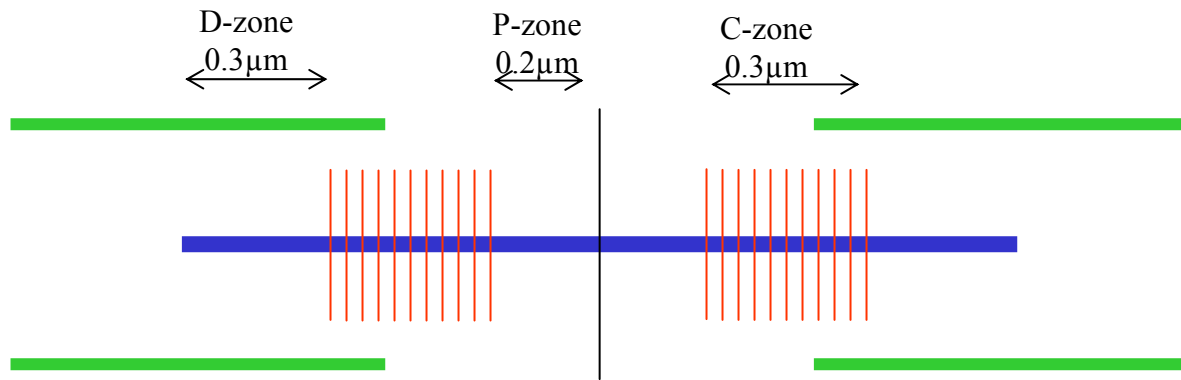


**Figure I.17. Distribution of MyBPs within the sarcomere**

— = Sarcomeric M-line, ■ = thick filament, ■ = thin filaments; — = positions of the 43nm periods in which the MyBPs are found. The arrows at the top of the figure indicated the lengths of the P-, C- and D-zones.

### I.7.3. INTERACTIONS OF MyBPC WITH OTHER SARCOMERIC COMPONENTS

#### I.7.3.1. Interactions between MyBPC and LMM

The major myosin binding-site of MyBPC is located in the C-terminal IgC2 domain (domain C10), which binds tightly to LMM (Okagaki et al., 1993). In studies in which MHC and various portions of MyBPC or MyBPH were co-transfected into COS cells, the presence of the C10 domain of MyBPC, or the co-equivalent H4 (C-terminal) domain of MyBPH, were required for MHC-MyBP co-polymer cable formation (Sebillon et al., 2001; Welikson and Fischman, 2002). Truncated MyBPC and MyBPH molecules, lacking the C10 or H4 domains respectively, co-localised with MHC within the COS cells but did not facilitate cable formation (Welikson and Fischman, 2002). These findings prompted Welikson and Fischman (2002) to speculate that the C10 domain of MyBPC and the H4 domain of MyBPH are able to associate with more than one LMM molecule, thus serving as a multivalent crosslinker, facilitating cable formation. Previously, Miyamoto et al., (1999) showed that charged residues on the surface of the C10 domain facilitate its interaction with LMM. This finding

**Table I.3. Distribution of MyBP isoforms in various skeletal muscle types**

Pattern of immuno-labeling with fast skeletal MyBPC-, slow skeletal MyBPC- and MyBPH- antibodies, in the 43nm period stripes in rabbit and chicken skeletal muscle. Data taken from Craig and Offer, 1976; Dennis et al., 1984; Bahler et al., 1985; Starr et al., 1985 and Bennett et al., 1986. Figures in brackets indicate where labeling was weak or where data suggests more than one protein occurs.

Muscle	Fibre type	fsMyBPC	ssMyBPC	MyBPH
<b>Rabbit</b>				
<i>psoas</i>	Unspecified		1-7*	
	Fast white	1-8	-	9
	Fast intermediate	1-7	8	9
	Fast red	-	1-9	-
	Slow red	-	1-9	-
<i>plantaris</i>	Fast white	1-7 (9)	8-9	-
	Fast intermediate	(1-7)	(1-7) 8-9	-
	Fast red	-	1-9	-
	Slow red	-	1-9	-
<i>solius</i>	Slow red	-	1-9	-
<b>Chicken</b>				
<i>pectoralis</i>	fast	(1-7) (9)	-	(1-7) 8-9
PLD	fast	(1-6) (9) (10)	(1-6) 7-8 (9)	?
ALD	slow	-	1-9	-

\* = MyBPC isoform not specified Craig and Offer, 1976

led the authors to propose a model in which the C10 domain is partially imbedded in a surface groove of the thick filament backbone (section IV.3) (Squire, 1973; Chew and Squire, 1995; Squire et al., 1998), allowing it to interact with three or four LMM molecules through ionic interactions, thus facilitating crosslinking of LMM molecules (figure I.18) (Miyamoto et al., 1999). The specific implications and merit of this model will be further discussed in section IV.3.1.3. In the light of these findings, it seems likely that interaction between the C10 domain of MyBPC and LMM both facilitates the anchoring of MyBPC to the thick filament backbone and plays an essential role in the regulation of thick filament formation and maintenance (Okagaki et al., 1993; Welikson and Fischman, 2002).

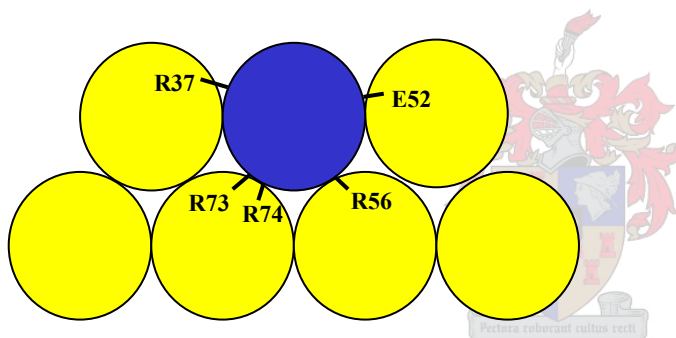


**Figure I.18. Interaction-surface model between MyBPC domain C10 and LMM**

Relative space-packing models of domain C10 of MyBPC and LMM. ● = Domain C10 of MyBPC; ● = LMM molecules; R37, R73, R74, R56 and E52 = residues which affect binding affinity when mutated (numbering according to Miyamoto et al., 1999) (from Miyamoto et al., 1999).

The finding that a truncated MyBPH construct, lacking the H4 domain, co-localised with MHC prompted Welikson and Fischman (2002) to propose that a secondary LMM binding-site is localised in the H1-H3 region of MyBPH. Based on the shared homology between the H1-H3 region of MyBPH and the C7-C9 region of MyBPC, the authors suggested that a secondary LMM binding-site might also be located in the C7-C9 region of MyBPC (Welikson and Fischman, 2002). This finding

is in step with the findings of Okagaki et al., (1993), who showed that, although the major myosin binding-site is located in the C10 domain, other regions of MyBPC were also able to interact with myosin.

Although the interaction between domain C10 and LMM is likely to be essential for the stable anchoring of MyBPC to the thick filament backbone, this interaction alone cannot explain the specific C-zone localisation of MyBPC, as LMM is not restricted to only the C-zone (Okagaki et al., 1993).

### **I.7.3.2. Interaction between MyBPC and C-zone titin**

In addition to its interaction with LMM, the C-terminal region of MyBPC also interacts with C-zone titin, and it is likely to be this interaction that specifies the C-zone localisation of MyBPC (Labeit et al., 1992; Labeit and Kolmerer, 1995; Freiburg and Gautel, 1996). The major titin binding-site has been mapped to the three C-terminal domains of MyBPC (C8, C9 and/or C10) (figure I.16) (Labeit et al., 1992; Labeit and Kolmerer, 1995; Freiburg and Gautel, 1996). Although the specific location of this binding-site within the C8-C10 region remains unclear, the data presented by Freiburg and Gautel (1996) suggests that the titin binding-site is located in the C9-C10 region of MyBPC, rather than in the C8 domain, as a MyBPC C5-C8 peptide did not interact with titin. It can, therefore, be presumed that the major titin binding-site is housed in either the C9 or C10 domain of MyBPC, or may span the C9-C10 junction, thereby requiring the presence of both these domains. In the experiments conducted by Freiburg and Gautel (1996) the C8-C10 fragment bound tightly to each of the first IgC2 domains of the eleven 11-domain super-repeats that constitute C-zone titin (A43, A54, A65, A76, A87, A98, A109, A120, A131, A142, A153) (figure I.9 and section I.6.3.2). It is interesting to note that domain A153 of titin is also able to bind to the C-terminal region of MyBPC

in these *in vitro* binding assays, although MyBPC has to date never been found in stripe eleven of the 43nm period, which corresponds to the position of this domain in the intact sarcomere (table I.3 and figure I.17) (Bennett et al., 1986; Labeit and Kolmerer, 1995; Freiburg and Gautel, 1996). Furthermore, the possibility of a secondary titin binding-site in the N-terminal or central region of MyBPC cannot be excluded by this study, as the methods employed were only able to detect relatively strong interactions in an *in vitro* environment (Freiburg and Gautel, 1996).

### **I.7.3.3. Domain C7 of MyBPC essential for correct A-band incorporation**

Although the C9 and C10 domains of MyBPC house the major thick filament anchoring LMM and titin binding-sites (sections I.7.3.1 and I.7.3.2), Gilbert et al., (1996) have shown that the whole of the C7-C10 region of MyBPC is required for correct incorporation of MyBPC into the sarcomere. Although the presence of domain C7 is not absolutely essential for the C-zone incorporation of MyBPC, the presence of this domain dramatically increases the affinity and specificity of the binding of MyBPC to this region of the thick filament (Gilbert et al., 1996; Gilbert et al., 1999). The precise nature of the involvement of the C7 domain in facilitating this interaction, however, remains unclear. It can, therefore, be postulated that this domain may be involved in an, as yet, unidentified protein:protein interaction.

### **I.7.3.4. Interaction between the MyBPC-motif and the S2 region of myosin**

In addition to interactions between the C-terminal region of MyBPC and components of the thick filament, the MyBPC-motif, located between domains C1 and C2 in the N-terminal region of MyBPC, interacts with the S2 region of myosin (figure I.16) (Moos et al., 1975; Starr and Offer, 1978; Gruen and Gautel, 1999; Gruen et al., 1999; Kunst et al., 2000). The MyBPC-motif binds to

the proximal 126 amino acid residues of myosin S2, adjacent to the MRLC binding-site, independent of MyBPC or myosin isoforms (figures I.16 and I.19) (Gruen and Gautel, 1999; Gruen et al., 1999; Kunst et al., 2000). In the skeletal MyBPC isoforms, this interaction is thought to be constitutive, while this interaction is regulated by phosphorylation of the MyBPC-motif in the cardiac isoform (Gruen et al., 1999; Kunst et al., 2000) and may, therefore, play an essential role in the cMyBPC-mediated regulation of cardiac contractility (section I.7.7).

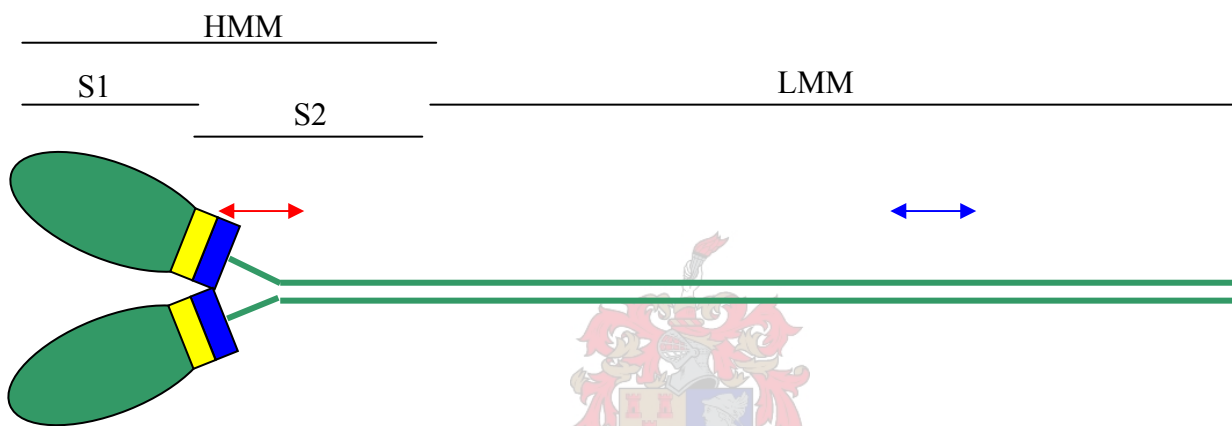


**Figure I.19. Structure of myosin II protein**

● = Myosin subfragment 1 (myosin head region); — =  $\alpha$ -helical portion of myosin II, ■ = myosin essential light chain; ■ = myosin regulatory light chain; blue arrow = MyBPC domain C10 binding-site; red arrow = MyBPC-motif binding-site; HMM = heavy meromyosin; LMM = light meromyosin; S1 = heavy meromyosin subfragment 1; S2 = heavy meromyosin subfragment 2.

### I.7.3.5. Interaction between MyBPC and F-actin

*In vitro* binding assays have shown that MyBPC is able to bind to F-actin at high ionic concentrations ( $>0.1M$ ) (Moos et al., 1978; Moos, 1981). The precise region of MyBPC involved in this interaction has, however, remained unclear, until recently when Kulikovskaya et al., (2003) proposed that the C0 domain of cMyBPC interacts with F-actin, while Squire et al., (2003) proposed that the PA-region houses the F-actin binding-site.

Kulikovskaya et al., (2003) showed that the C0 domain of cMyBPC was able to interact with F-actin *in vitro*. In order to establish whether this interaction took place *in vivo*, skinned cardiac trabeculae were soaked in a relaxing solution containing various cMyBPC fragments (Kulikovskaya et al., 2003). These experiments showed that the C0 domain of cMyBPC was able to bind to a myofibrillar protein, presumably F-actin, when endogenous cMyBPC was unphosphorylated (Kulikovskaya et al., 2003).

In contrast, the proposed presence of an F-actin binding-site in the PA-region of MyBPC (Squire et al., 2003) is based on multiple sequence alignments between this region of MyBPC and A1 MELC, which have been shown to be able to interact with F-actin (Timson et al., 1997; Timson et al., 1998; Squire et al., 2003). The presence of an interaction between the PA-region and F-actin, however, remains to be proven experimentally.



#### **I.7.4. PHOSPHORYLATION OF cMyBPC**

Phosphorylation of cMyBPC is mediated through two primary mechanisms. Firstly, an increase in intracellular  $\text{Ca}^{2+}$  concentration, below the threshold for thin filament activation (section I.2.1), results in the phosphorylation of cMyBPC to a maximum of one mol per mol cMyBPC (Schlender and Bean, 1991; Gautel et al., 1995; McClellan et al., 2001). This phosphorylation reaction is thought to be mediated by the actions of MyBPC-associated kinase, proposed to be a CaM kinase II that co-purifies with cMyBPC (Hartzell and Glass, 1984; Schlender and Bean, 1991; Gautel et al., 1995). The second mechanism responsible for the phosphorylation of cMyBPC involves the cAMP-mediated activation of PKA, upon  $\beta$ -adrenergic stimulation, resulting in cMyBPC being

phosphorylated to a maximum of three mol phosphate per mol cMyBPC (Hartzell and Titus, 1982; Hartzell and Sale, 1985; Gautel et al., 1995).

In mammalian cMyBPC, the phosphorylation sites for both MyBPC-associated kinase and PKA are located in the MyBPC-motif (figure I.16) (Gautel et al., 1995; Mohamed et al., 1998). Amino acid sequence analysis of this region revealed the presence of four putative phosphorylation sites, designated sites A to D (figure I.20) (Gautel et al., 1995). Site-directed mutagenesis of these sites showed that, specifically, site B was the substrate for MyBPC-associated kinase, sites A, B and C the substrate for PKA and that site D was not phosphorylated by either kinase (Gautel et al., 1995). Additionally, mutagenesis of site B showed phosphorylation of this site, located in the cardiac-specific LAGGRRIS insertion, was essential for the subsequent phosphorylation of sites A and C by PKA (Gautel et al., 1995). Subsequently, McClellan et al., (2001) have shown that the *in situ* PKA-dependent phosphorylation of cMyBPC is dependent on an elevation of intracellular  $\text{Ca}^{2+}$  concentration. The incubation of skinned fibres in a solution containing a low concentration of  $\text{Ca}^{2+}$  (1.25mM) and PKA did not result in the phosphorylation of cMyBPC, while control fibres incubated in a solution containing 2.5mM  $\text{Ca}^{2+}$  and PKA resulted in cMyBPC being either di- or tri-phosphorylated. Under neither of these conditions did the influx of  $\text{Ca}^{2+}$  from the bathing solution stimulate contraction, suggesting that the intracellular  $\text{Ca}^{2+}$  concentration necessary for PKA-dependent phosphorylation of cMyBPC was lower than the threshold required for thin filament activation and subsequent contraction (McClellan et al., 2001). Based on these findings, McClellan et al., (2001) proposed that phosphorylation of cMyBPC by PKA can only take place once cMyBPC has been mono-phosphorylated by MyBPC-associated kinase.

From these findings, it can be concluded that cMyBPC would be phosphorylated, at the cardiac-specific phosphorylation site in the MyBPC-motif (site B), by MyBPC-associated kinase in a  $\text{Ca}^{2+}$ -dependent fashion. In turn, mono-phosphorylation at site B would trigger a conformational change in the MyBPC-motif that would make the PKA-specific phosphorylation sites (sites A and C) accessible to PKA (Gautel et al., 1995; McClellan et al., 2001). It, however, remains unclear whether the phosphorylation/ dephosphorylation cycle of site B by MyBPC-associated kinase and MyBPC-associated phosphatase (section I.7.5) is coupled to the normal myocytic  $\text{Ca}^{2+}$  flux, caused by depolarisation of the sarcolemma, or whether a time-averaged increase in the  $\text{Ca}^{2+}$ -transient would be required for this site to be phosphorylated (McClellan et al., 2001).

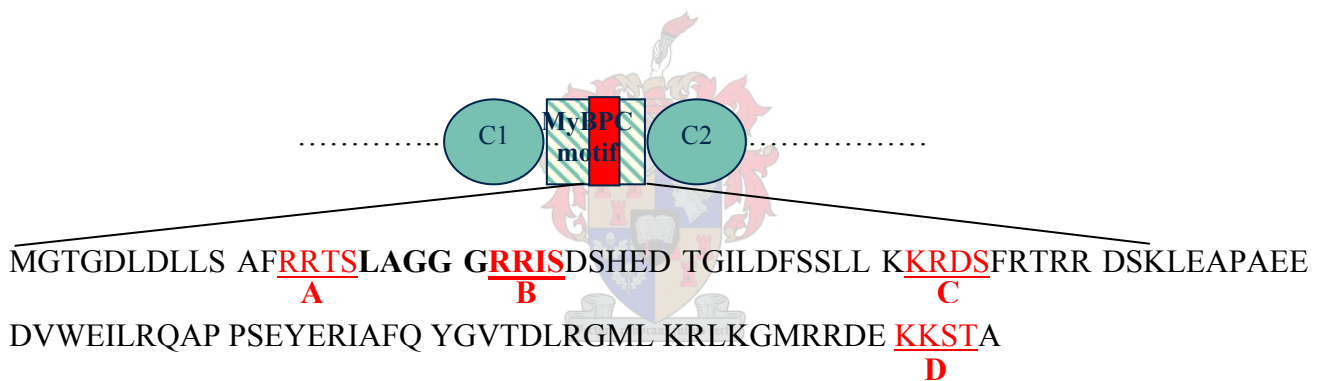


**Figure I.20. Location of phosphorylation sites in cMyBPC**

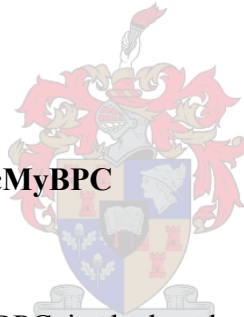
The diagram at the top of the figure shows the C1-C2 region of cMyBPC, including the MyBPC motif in which the phosphorylation sites are found. Partial amino acid sequence of the MyBPC motif is shown below the diagram. Bold lettering = cardiac-specific LAGGRRIS insertion; red, underlined lettering = putative phosphorylation sites, designated A, B, C and D (from Gautel et al., 1995).

In addition to phosphorylation by MyBPC-associated kinase and PKA, it was shown that PKC is also able to phosphorylate sites A and C in the MyBPC-motif (Venema and Kuo, 1993; Mohamed et al., 1998), while a PKC-specific phosphorylation site was also identified in the C9 domain of chicken cMyBPC (S1169 chicken cMyBPC sequence) (Mohamed et al., 1998). Multiple sequence

alignments, however, revealed that phosphorylatable amino acids were absent at this position in domain C9 of both human and mouse cMyBPC (Mohamed et al., 1998). The functional importance of PKC phosphorylation of cMyBPC *in vivo*, however, remains unclear.

The phosphorylation of cMyBPC at sites in the MyBPC-motif, by MyBPC-associated kinase and PKA, results in S2 being released from the MyBPC-motif (Gruen et al., 1999; Kunst et al., 2000; Levine et al., 2001), as well as an expansion in the thick filament backbone, thereby altering cardiac contractility (Weisberg and Winegrad, 1996; Weisberg and Winegrad, 1998; Levine et al., 2001). The proposed mechanisms through which phosphorylation of cMyBPC cause these structural changes, resulting in alterations in the contractile properties of the sarcomere, will be discussed in detail in section I.7.6.

### **I.7.5. DEPHOSPHORYLATION OF cMyBPC**



*In vitro* studies have shown that cMyBPC is dephosphorylated through the activation of cGMP dependent pathways, following cholinergic stimulation (Hartzell and Titus, 1982; Garvey et al., 1988). Additionally, it was shown that a protein co-purifying with cMyBPC had some phosphatase activity and was able to reduce the phosphorylation level of cMyBPC by about 35%. As it has previously been shown that cMyBPC is dephosphorylated by phosphatases 1 and 2A *in vitro* (Schlender et al., 1987; Schlender et al., 1989), it was speculated that this MyBPC-associated phosphatase belongs to the same family (Schlender and Bean, 1991). cMyBPC is maximally triphosphorylated by PKA and MyBPC-associated kinase (section I.4.3). It is, therefore, plausible that MyBPC-associated phosphatase is only able to dephosphorylate one of the three phosphorylation sites. As site B is phosphorylated specifically by MyBPC-associated kinase, while sites A and C are

both phosphorylated specifically by PKA, it can be speculated that MyBPC-associated phosphatase would specifically dephosphorylate site B, while sites A and C are probably dephosphorylated by cGMP dependent pathways, following cholinergic stimulation. The finding that the increase in actomyosin ATPase activity resulting from cMyBPC phosphorylation (section I.7.6) is lost even in the absence of cholinergic stimulation (England, 1976; Horowitz and Winegrad, 1983), however, suggests that cMyBPC may also be dephosphorylated through other, as yet unidentified, mechanisms *in vivo*.

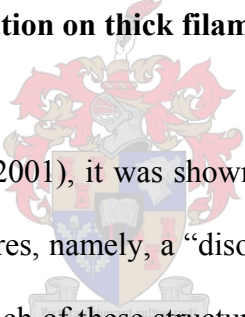
### **I.7.6. FUNCTIONS OF cMyBPC**

Several studies have implicated cMyBPC as an important regulator of both thick filament structure (Koretz, 1979; Seiler et al., 1996; Weisberg and Winegrad, 1996; Weisberg and Winegrad, 1998; Miyamoto et al., 1999; Kunst et al., 2000; Levine et al., 2001; Welikson and Fischman, 2002) and cardiac contractility (Hofmann et al., 1991; Weisberg and Winegrad, 1996; Weisberg and Winegrad, 1998; Kunst et al., 2000; Levine et al., 2001; McClellan et al., 2001). *In vitro* and *in situ* studies have shown that MyBPC is essential for the formation of normal thick filaments, and that specifically the C-terminal domain (C10) was responsible for this function (Seiler et al., 1996; Miyamoto et al., 1999; Welikson and Fischman, 2002). Harris et al., (2002), however, showed that sarcomeric assembly and maintenance was not dramatically affected by the absence of cMyBPC in homozygous cMyBPC knockout mice, even though these mice showed classical features of HCM and both systolic and diastolic function was impaired (table I.2). This finding strongly suggests that, even though MyBPC is able to modulate thick filament structure, it is not absolutely essential for thick filament assembly and that in the absence of cMyBPC other proteins, such as MyBPH, may fulfill

this function (Harris et al., 2002). The finding that contractile function, both systolic and diastolic, was impaired in these mice, however, underlines the regulatory role of cMyBPC.

Recent studies have shown that phosphorylation of cMyBPC results in alterations in the structure of both the thick filament backbone (Weisberg and Winegrad, 1998; Levine et al., 2001) and crossbridges (Weisberg and Winegrad, 1996; Weisberg and Winegrad, 1998; Kunst et al., 2000; Levine et al., 2001), and that these structural changes give rise to altered contractile properties. As these findings clearly show that the structural and regulatory functions of cMyBPC are intimately intertwined, they will be discussed together in the following sections.

#### **I.7.6.1. Effect of cMyBPC phosphorylation on thick filament structure**



In a study conducted by Levine et al., (2001), it was shown that cardiac sarcomeric thick filaments are found in one of three distinct structures, namely, a “disordered” structure, a “tight” structure and a “loose” structure. The prevalence of each of these structures was found to be directly correlated to the phosphorylation status of cMyBPC (figure I.21).

##### I.7.6.1.i. “Disordered” thick filament structure

When cMyBPC was unphosphorylated, the majority of thick filaments were found to be in the “disordered” structure (figure I.21). This structure is characterised by crossbridges extending from the thick filament backbone at varying angles (table I.4) (Levine et al., 2001). The total diameter of “disordered” thick filaments, including crossbridge extensions, varied from 24nm to 39nm (table I.4) (Levine et al., 2001). Previously, Weisberg and Winegrad (1996 and 1998) described a similar thick filament structure with a diameter of about 30 to 31nm, with crossbridges

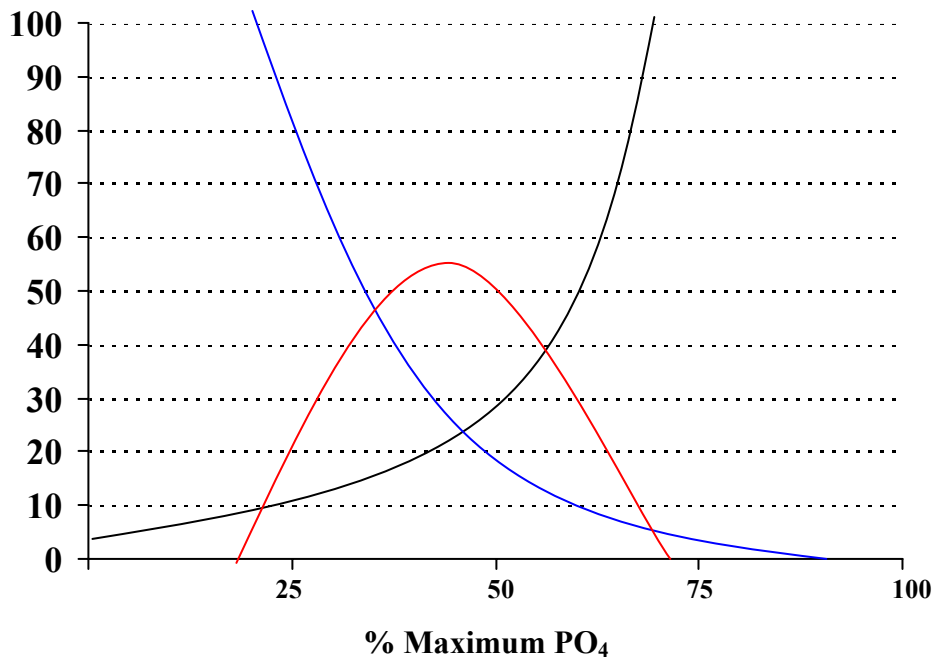


**Figure I.21. Effect of cMyBPC phosphorylation on thick filament structure**

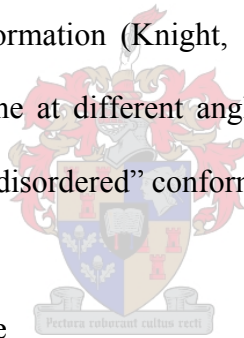
Relation between the percentage of maximum phosphorylation of cMyBPC and the relative percentage of each of the structures of the thick filament. Black line = “loose” conformation; blue line = “disordered” conformation; red line = “tight” conformation. From Levine et al., 2001.

extending about 2 to 7nm from the thick filament backbone, when cMyBPC was unphosphorylated (table I.4). In the light of the finding that the interaction between the MyBPC-motif of cMyBPC and myosin S2 is abolished by the phosphorylation of cMyBPC, it seems plausible that this interaction may alter crossbridge structure, thereby giving rise to thick filaments with a “disordered” structure (Gruen et al., 1999; Kunst et al., 2000; Levine et al., 2001), analogous to the findings of Knight (1996).

Knight (1996) showed that an antibody directed against the 25 proximal amino acids of myosin S2, housing the MyBPC-motif binding-site (Gruen and Gautel, 1999; Gruen et al., 1999), binds specifically to MHC dimers in which myosin S2 is in a random coil, rather than a coiled-coil conformation (figure I.22) (Knight, 1996). It is unclear from this study whether the binding of this antibody was dependent on the presence of S2 fragments with a random coil conformation, or

whether the binding of the antibody induced the conformational change in S2 from coiled-coil to random coil (Knight, 1996). Although Knight (1996) favoured the former scenario, it is intriguing to speculate on the possibility that the binding of a ligand, such as the MyBPC-motif, to this portion of S2 may dramatically affect the structure of S2.

If the binding of the MyBPC-motif is indeed responsible for the transition of myosin S2 from a coiled-coil to a random coil conformation, it may explain the formation of thick filaments with a “disordered” structure. In this scenario, only a specific fraction of myosin S2 molecules would be associated with a MyBPC-motif when cMyBPC is unphosphorylated, and would, therefore, be in the random coil conformation. As myosin S2 in a random coil conformation is both longer, and more flexible, than S2 in a coiled-coil conformation (Knight, 1996), it may explain why crossbridges extend from the thick filament backbone at different angles when cMyBPC is unphosphorylated, resulting in thick filaments taking on a “disordered” conformation (Levine et al., 2001).



#### I.7.6.1.ii. “Tight” thick filament structure

When cMyBPC was mono-phosphorylated, the majority of thick filaments were found to be in the “tight” conformation (Levine et al., 2001) (figure I.21). This structure is characterised by the crossbridges being ordered along the thick filament backbone. The diameter of thick filaments with a “tight” structure, including crossbridge extensions, was generally 29.8nm (table I.4.2) (Levine et al., 2001). Mono-phosphorylation of cMyBPC, at site B in the MyBPC-motif, is achieved through the actions of MyBPC-associated kinase in response to an increase in the intracellular  $\text{Ca}^{2+}$  concentration (section I.7.4) (Gautel et al., 1995; McClellan et al., 2001). Even though the precise extent of cMyBPC phosphorylation, required for the abolition of the interaction between the MyBPC-motif and myosin S2, has not been tested experimentally (Gruen et al., 1999; Kunst et al., 2000), Levine et

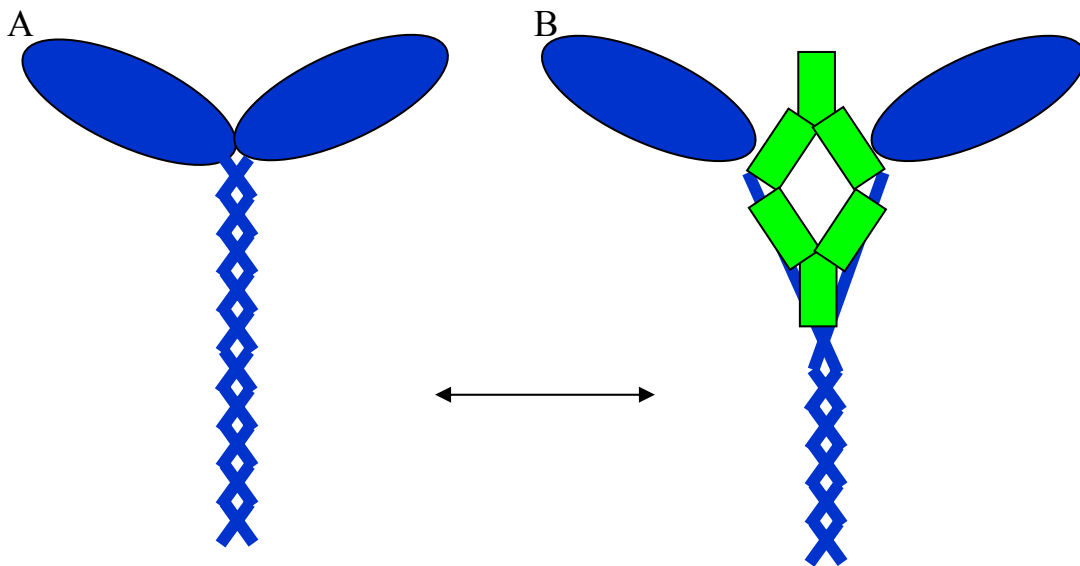


**Figure I.22. Transition of myosin S2 from a coiled-coil conformation to a random coil conformation associated with the binding of an antibody to S2**

*A = Conformation of myosin heavy chain dimers with S2 and LMM in the coiled-coil conformation; B = conformation of myosin heavy chain dimers with S2 in a random coil conformation, allowing the binding of a myosin S2 antibody. ■ = myosin heavy chain molecules; ■ = myosin S2 antibody (adapted from Knight, 1996).*

al., (2001) proposed that it is the abolition of the MyBPC-myosin S2 interaction that results in the formation of the “tight” thick filament structure seen upon cMyBPC mono-phosphorylation.

It could be proposed that the abolition of the interaction between the MyBPC-motif and myosin S2, by mono-phosphorylation of cMyBPC, would result in a conformational change in S2 from a random coil to a coiled-coil structure (Knight, 1996). This conformational change would result in a decrease in crossbridge flexibility and a subsequent increase in crossbridge order, with all crossbridges being arranged orderly along the thick filament backbone (Knight, 1996; Levine et al., 2001).

### I.7.6.1.iii. “Loose” thick filament structure

When cMyBPC was either di- or tri-phosphorylated, the majority of thick filaments were found to have a “loose” structure (figure I.21). As with thick filaments in the “tight” structure, crossbridges were highly ordered along the thick filament backbone. The diameter of thick filaments with a “loose” structure, including crossbridge extensions, was, however, significantly larger than thick filaments with a “tight” structure (34.2nm) (table I.2) (Levine et al., 2001). Previously, Weisberg and Winegrad, (1996 and 1998) described a similar thick filament structure with a diameter of about 36nm, with crossbridges extending consistently only about 2nm from the thick filament backbone, following PKA-mediated phosphorylation of cMyBPC (table I.4). It was proposed that this increase in thick filament diameter was a result of an expansion in the thick filament backbone, rather than an increase in the distance that crossbridges extend into the interfilament space (Weisberg and Winegrad, 1998; Levine et al., 2001). Following phosphorylation of site B by MyBPC-associated kinase, phosphorylation of sites A and C by PKA results in cMyBPC being di- and tri-phosphorylated. It can, therefore, be speculated that expansion in the diameter of the thick filament backbone, resulting in the formation of thick filaments with a “loose” structure, would take place in response to  $\beta$ -adrenergic stimulation (Gautel et al., 1995; Weisberg and Winegrad, 1998; Levine et al., 2001; McClellan et al., 2001). The mechanisms through which PKA-dependent phosphorylation of cMyBPC results in the expansion of the thick filament backbone have, however, remained elusive. As results obtained in this study may shed new light onto this subject, these mechanisms will be discussed in section IV.3.

**Table I.4. Effect of cMyBPC phosphorylation on thick filament structure**

<b>Muscle type</b>	<b>Species</b>	<b>MYH type</b>	<b>cMyBPC PO<sub>4</sub></b>	<b>TF (bare zone)</b>	<b>TF (A-band)</b>	<b>TF backbone (A-band)</b>	<b>Crossbridge extension</b>	<b>Ref</b>
Skeletal	Fish	N.D.	N	13-16nm	25-27nm*	13-15nm	6nm	1
Cardiac	Rat	$\alpha$ -MHC	N	20.1nm <sup>#</sup>	<b>30nm</b> /37nm <sup>#</sup>	16nm/23nm* <sup>#</sup>	ND	2
Cardiac	Rat	$\alpha$ -MHC	Y	20.1nm <sup>#</sup>	36nm <sup>#</sup>	31.6nm* <sup>#</sup>	ND	2
Cardiac	Rat	$\alpha$ -MHC	N	16nm <sup>#</sup>	<b>31nm</b> /37nm <sup>#</sup>	<b>17nm</b> /23nm* <sup>#</sup>	2-7nm	3
Cardiac	Rat	$\alpha$ -MHC	Y	16nm <sup>#</sup>	36nm <sup>#</sup>	31.6nm* <sup>#</sup>	2.2nm	3
Cardiac	Rat	$\beta$ -MHC	N	N.D.	25nm/ <b>31nm</b> <sup>#</sup>	21nm/ <b>27nm</b> * <sup>#</sup>	2nm	3
Cardiac	Rat	$\beta$ -MHC	Y	N.D.	27nm <sup>#</sup>	25.4nm* <sup>#</sup>	0.8nm	3
Cardiac	Rat	$\alpha$ -MHC	N	ND	24-39nm <sup>#</sup>	ND	“disordered”	4
Cardiac	Rat	$\alpha$ -MHC	Y (mono)	ND	29.8nm <sup>#</sup>	ND	“close”	4
Cardiac	Rat	$\alpha$ -MHC	Y (di/tri)	ND	34.2nm <sup>#</sup>	ND	“close”	4

*N = no; N.D. = not determined; Ref = reference; TF = thick filament diameter; Y = yes; \* = deduced value; <sup>#</sup> = values not corrected for metal coat thickness; 1 = Squire et al., 1998; 2 = Weisberg and Winegrad, 1996; 3 = Weisberg and Winegrad, 1998; 4 = Levine et al., 2001. In cases where there was a bimodal distribution of thick filament diameters, the diameter of the most prevalent fraction is indicated in **bold** lettering. Deduced values were normalised for the contribution of crossbridge extensions to the total thick filament diameter.*

### **I.7.7. EFFECT OF cMyBPC PHOSPHORYLATION ON CARDIAC CONTRACTILITY**

Several studies have shown that  $\beta$ -adrenergic stimulation of intact cardiac muscle results in a marked increase in contractile force, of up to 70% (England, 1975; Solaro et al., 1976). The findings that PKA-dependent phosphorylation of cTNI, PLB or titin does not result in an increase in force production (sections I.4; I.5; I.6) have resulted in a hypothesis that phosphorylation of cMyBPC is responsible for this increase in force production. This view is supported by the findings of McClellan et al., (1994) that cMyBPC is the only myofibrillar protein in which the degree of phosphorylation is consistently correlated with the level of actomyosin ATPase activity in rat ventricular tissue upon adrenergic stimulation.

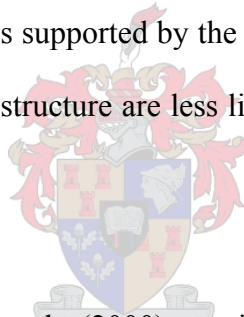
At a structural level, phosphorylation of cMyBPC results, firstly, in the abolition of the interaction between the MyBPC-motif and myosin S2 (Gruen and Gautel, 1999; Gruen et al., 1999; Kunst et al., 2000), resulting in the transition of thick filaments from the “disordered” to the “tight” structure (sections I.7.6.1.1 and I.7.6.1.2) (Levine et al., 2001). McClellan et al., (2001), however, showed that mono-phosphorylation of cMyBPC, responsible for this transition, is likely to be mediated by MyBPC-associated kinase in a  $\text{Ca}^{2+}$ -dependent fashion, rather than by PKA (Gautel et al., 1995; Levine et al., 2001; McClellan et al., 2001). Secondly, PKA specifically phosphorylates sites A and C in the MyBPC-motif, resulting in cMyBPC being di- or tri-phosphorylated, leading to an expansion of the thick filament backbone and the formation of thick filaments with a “loose” structure (section I.7.6.1.3) (Weisberg and Winegrad, 1996; Weisberg and Winegrad, 1998; Levine et al., 2001; McClellan et al., 2001). As these two mechanisms are likely to be activated by different stimuli and give rise to distinct thick filament structures, each likely to have specific contractile properties, they will be discussed separately in sections I.7.7.1 and I.7.7.2.

### I.7.7.1. Transition of thick filaments from a “disordered” to a “tight” structure

The transition of thick filaments from a “disordered” to a “tight” structure, caused by the  $\text{Ca}^{2+}$ -dependent mono-phosphorylation of cMyBPC by MyBPC-associated kinase, probably results in the abolition of the interaction between the MyBPC-motif and myosin S2 (Gautel et al., 1995; Gruen et al., 1999, Kunst et al., 2000; Levine et al., 2001; McClellan et al., 2001). Levine et al., (2001) have shown that this transition results in a small, non-significant increase in the likelihood that thick filaments will associate with thin filaments *in vitro* (table I.5). Even though this difference did not reach statistical significance, it may indicate that the degree of crossbridge order influences the ability of crossbridges to bind to thin filaments (Levine et al., 2001). It was also shown that the binding of antibodies to myosin S2 results in a decrease in  $\text{Ca}^{2+}$ -activated force, maximal sliding velocity and fibre stiffness, without affecting myosin ATPase activity (Margossian et al., 1991; Sugi et al., 1992). If it is assumed that the phosphorylation-dependent interaction between the MyBPC-motif and myosin S2 affects crossbridge structure and contractility in a similar fashion to antibodies binding to myosin S2 (section I.7.6.1.1), these findings may indicate that fewer crossbridges are formed between thick and thin filaments when cMyBPC is unphosphorylated, compared to when cMyBPC is in its phosphorylated state.

Kunst et al., (2000) showed that the transformation of unphosphorylated cMyBPC C1-C2 fragments into skinned muscle fibres resulted in a decrease in  $\text{Ca}^{2+}$ -activated force by about 50%, indicating that the interaction between the MyBPC-motif and myosin S2 may induce a similar effect to antibodies binding to S2 (Margossian et al., 1991; Sugi et al., 1992). Contrary to findings that the binding of antibodies to myosin S2 reduces muscle stiffness (Margossian et al., 1991; Sugi et al., 1992), Kunst et al., (2000) found that the interaction between the exogenous MyBPC-motif and

myosin S2 induced a significant increase in both rigour force and stiffness, without altering dynamic muscle stiffness, while also causing a slight, but significant, leftward shift in the  $\text{Ca}^{2+}$ /force relationship. These results were interpreted as suggesting that the binding of the exogenous MyBPC-motif to myosin S2 promotes the binding of crossbridges to the thin filament, while impairing movement of the myosin head-tail junction, resulting in a reduction in force generation (Kunst et al., 2000). Winegrad (2000), however, suggested that the decrease in  $\text{Ca}^{2+}$ -activated force, induced by the interaction between the MyBPC-motif and myosin S2, might be indicative of a reduction in the number of crossbridges attached to the thin filament. The increase in rigour force and rigour stiffness, observed by Kunst et al., (2000), was interpreted by Winegrad (2000) as indicative of an increase in the rate of ATP-depletion, rather than an increase in the number of crossbridges attaching to the thin filament. The latter scenario is supported by the findings of Levine et al., (2001), namely, that thick filaments with a “disordered” structure are less likely to associate with thin filaments than with those with a “tight” structure.



When interpreting the results of Kunst et al., (2000), caution should be taken that the effect of the interaction between the MyBPC-motif and myosin S2 is not overestimated, due to the fact that exogenous cMyBPC fragments were transformed into the skinned fibres. The addition of exogenous unphosphorylated cMyBPC fragments would increase the number of crossbridges affected by this interaction. The effects observed might, however, be analogous to HCM-causing truncation mutations, in which truncated cMyBPC fragments may reduce contractility through association with myosin S2.

In summary, therefore, the binding of the MyBPC-motif to myosin S2, when cMyBPC is unphosphorylated (Gruen et al., 1999; Kunst et al., 2000), may cause the S2 fragments of a

subpopulation of myosin molecules to assume a random coil, rather than a coiled-coil conformation (Knight, 1996), giving rise to the “disordered” thick filament structure. It is possible to speculate that myosin molecules in which the S2 fragments are in the random coil conformation are either not able to bind to thin filaments, or do so with a lower affinity. This would reduce the number of crossbridges bound to thin filaments, thus resulting in a reduction in  $\text{Ca}^{2+}$ -activated force and possibly actomyosin ATPase activity.

The transition of thick filaments from the “disordered” structure to the “tight” structure is achieved through the  $\text{Ca}^{2+}$ -sensitive phosphorylation of site B in the MyBPC-motif by MyBPC-associated kinase (Gautel et al., 1995; McClellan et al., 2001), abolishing the interaction between the MyBPC-motif and S2 (Gruen et al., 1999; Kunst et al., 2000). The abolition of this interaction would result in all S2 fragments assuming a coiled-coil conformation, as evidenced by the increase in crossbridge order (Levine et al., 2001). This increase in crossbridge order promotes the formation of weak interactions between thick and thin filaments, thereby, potentiating the thick filament, resulting in increased force production during systole. The physiological advantage of the “disordered” thick filament structure, however, remains unclear. One possible advantage might be that a reduction in the number of crossbridges interacting with the thin filament may aid relaxation and diastolic function, while a reduction in actomyosin ATPase activity might also reduce energy consumption.

#### **I.7.7.2. Transition of thick filaments from a “tight” to a “loose” structure**

The transition of thick filaments from the “tight” to the “loose” structure is thought to be facilitated by the PKA-dependent phosphorylation of sites A and C in the MyBPC-motif (Gautel et al., 1995; Weisberg and Winegrad, 1996; Weisberg and Winegrad, 1998; Levine et al., 2001; McClellan et al.,

2001). As described in section I.7.6.1.3, this transition is in all likelihood the result of an expansion of the thick filament backbone (Weisberg and Winegrad, 1996; Weisberg and Winegrad, 1998; Levine et al., 2001). It was postulated that the expansion of the thick filament backbone would increase the proximity of myosin S1 to the thin filaments, thus favouring the formation of weak interactions between myosin S1 and the thin filament (Weisberg and Winegrad, 1996; Weisberg and Winegrad, 1998). The formation of these weak interactions would potentiate the sarcomere for contraction when  $\text{Ca}^{2+}$  is released from the SR during early systole. As a whole, this would lead to the increase in force production, actomyosin ATPase activity and crossbridge cycling rate observed in cardiac muscle following  $\beta$ -adrenergic stimulation (Weisberg and Winegrad, 1996). This hypothesis is strongly supported by the findings of Levine et al., (2001), who showed that thick filaments in the “loose” conformation associated with thin filaments at a significantly higher frequency than those in either the “disordered” or “tight” conformation (table I.5).



**Table I.5. Frequency of interactions between thick and thin filaments**

<b>Thick filaments</b>	<b>% of the total thick filaments</b>	<b>% of parallel pairs interacting</b>
Untreated “tight”	58	29
Untreated “disordered”	12	16
Untreated “loose”	30	89*
Average of total untreated		47 <sup>#</sup>
PKA treated “loose”	84	92*

\*Significant difference ( $p < 0.05$ ) from “tight” or “disordered” filaments

<sup>#</sup> Significant difference ( $p < 0.05$ ) between averages of untreated and PKA-treated filaments

(Adapted from Levine et al., 2001)

The increase in the number of crossbridges forming weak interactions with the thin filament may, however, impair relaxation, ventricular filling and diastolic function during periods of  $\beta$ -adrenergic stimulation. The finding that PKA-dependent phosphorylation of cTNI, PLB and titin all aid diastolic function (sections I.4; I.5 and I.6) may indicate that these mechanisms are compensatory to the impairment of diastolic function caused by the PKA-dependent phosphorylation of cMyBPC.

### **I.7.7.3. Interaction between cMyBPC domain C0 and actin as a regulator of cardiac contractility**

*In vitro* functional studies in which MyBPC has been extracted from intact myocytes have shown that, although cMyBPC lacks intrinsic ATPase activity, it has the ability to modulate the actin-activated ATPase activity of myosin (Offer et al., 1973). The finding that MyBPC is able to bind to F-actin in solution and to thin filaments in skeletal muscle at high ionic strength (Moos et al., 1978; Moos, 1981) has led to the hypothesis that MyBPC may inhibit actomyosin ATPase activity by competing with myosin S1 for binding-sites on actin. In order to test this hypothesis, skinned muscle fibres and cardiac myocytes were stretched to lengths at which the individual sarcomeres would measure more than 3.2 $\mu$ m. At these sarcomeric lengths, there would be no overlap between the C-zone, in which MyBPC is found, and the thin filament, therefore, preventing these competitive interactions (Hofmann et al., 1991). Hofmann et al., (1991), however, found a similar tension-pCa relationship in both long and short sarcomeres, suggesting that the shift in the tension-pCa relationship observed after partial extraction of MyBPC was not due to competitive binding of MyBPC and myosin S1 with actin (Hofmann et al., 1991). This finding casts a doubt over whether the interaction between MyBPC and actin observed *in vitro* by Moos et al., (1978) and Moos (1981) occurs *in vivo*. Based on findings that diastolic function is impaired by the absence of cMyBPC in cMyBPC-knockout mice (Harris et al., 2002), Kulikovskaya et al., (2003) proposed that an

interaction between the C0 domain of cMyBPC and F-actin (section I.7.3.5) might act as a tether during contraction. According to this hypothesis, force generated during systole would lead to the extension of the PA-region (located between domains C0 and C1), which shares homology to the extendible PVEK region of titin (section I.6.4.2.ii). During diastole, refolding of the PA-region would, therefore, lead to the shortening of this region, resulting in the generation of passive tension, which in turn would aid relaxation and ventricular filling (Kulikovskaya et al., 2003). This scenario, however, seems highly unlikely, as the PA-region is only 50 amino acids in length. If the calculations for the maximal extended chain lengths of the PVEK region of titin used by Linke et al., (1994) and Trinick (1996) is extrapolated to calculate the maximal chain length of the PA-region of cMyBPC, the maximal chain length of the PA-region would only be about 17nm, thus, not allowing significant shortening of the sarcomere during contraction if C0 remains bound to actin.

### I.7.8. HCM-CAUSING MUTATIONS IN cMyBPC

To date, 93 HCM-causing mutations have been identified in *MYBPC3*. Unlike mutations in the other 12 genes in which HCM-causing mutations have thus far been identified (table I.1), in which most mutations are single amino acid substitutions, about two thirds of *MYBPC3* HCM-causing mutations result in the truncation of cMyBPC (figure I.23 and table I.6). Various estimates of the frequency at which HCM-causing mutations in *MYBPC3* contribute to the burden of disease have been made, e.g., about 20% (Marian and Roberts, 2001), about 42% (Richard et al., 2003) and 18.5% (Erdmann et al., 2003). Caution should, however, be observed when interpreting these mutation frequency values, as various formulae have been used to calculate these frequencies. Some authors calculate mutation frequency values by dividing the number of mutations in *MYBPC3* in their HCM-affected population by the total number of mutations found in their HCM-affected population (Richard et al., 2003), while other authors divide the number of mutations in *MYBPC3* in their HCM-affected population by

the total number of HCM-affected individuals in their study group (Erdmann et al., 2003). Furthermore, the frequency of cMyBPC-associated HCM appears to vary quite dramatically between various populations. Richard et al., (2003) and Erdmann et al., (2003) have found that mutations in *MYBPC3* are a more prevalent cause of HCM than mutations in *MYH7* in the French and German HCM-affected populations. In stark contrast to these findings, Konno et al., (2003) found only one specific *MYBPC3* HCM-causing mutation in eight probands in a panel consisting of 250 HCM-affected individuals of Japanese descent, indicating that cMyBPC-associated HCM may be rare in the Japanese population. From these findings, it can be concluded that, while in some populations mutations in *MYBPC3* may be a prevalent cause of HCM, it may be quite rare in other populations.

#### **I.7.8.1. Phenotypic expression of cMyBPC-associated HCM**

Mutations in *MYBPC3* have been associated with reduced penetrance until the fifth decade of life (Charron et al., 1998; Niimura et al., 1998; Konno et al., 2003). Furthermore, it has been reported that HCM-related deaths are less prevalent in *MYBPC3* mutation-carriers than *TNNT2* mutation-carriers, or patients in which “malignant” *MYH7* mutations (e.g., the R403Q mutation in *MYH7*) have been identified (Charron et al., 1998; Niimura et al., 1998). These findings have led to the formulation of the hypothesis that *MYBPC3* mutations cause a milder form of HCM than mutations in other sarcomeric protein-encoding genes (Niimura et al., 1998). Furthermore, mutations in *MYBPC3* also often result in progression to the “burnt out” phase HCM in elderly individuals, which may result in such individuals being diagnosed with DCM, rather than HCM (Konno et al., 2003). In order to establish whether there are differences in the phenotypic expression of missense and truncation cMyBPC mutations, cMyBPC missense and truncation mutations have been investigated separately. The data thus obtained are, however, conflicting. Niimura et al., (1998) showed that missense mutations in *MYBPC3* are associated with a higher incidence of SCD than HCM-causing

mutations resulting in the truncation of cMyBPC, while Erdmann et al., (2003) showed that *MYBPC3* truncation mutations are associated with a more severe phenotype than *MYBPC3* missense mutations. In contrast to the study by Niimura et al., (1998), SCD was a rare occurrence in the study by Erdmann et al., (2003). Furthermore, the phenotypic assessments made by Erdmann et al., (2003), were largely based on age of symptomatic presentation and the extent of LVH, which is not directly correlated to the risk of SCD (Watkins et al., 1995b; Moolman et al., 1997; Moolman-Smook et al., 2000).

Notwithstanding these studies that showed that HCM caused by mutations in *MYBPC3* is associated with later disease onset and a relatively benign phenotype, some exceptions have been noted. In the Japanese population, for instance, Doi et al., (1999) found that the  $\Delta t$  mutation in exon 19 of *MYBPC3*, resulting in the loss of part of domain C4 through to domain C10 of cMyBPC (Kimura et al., 1997), was highly penetrant, even in younger individuals (Doi et al., 1999). Additionally, Konno et al., (2003) showed that typical features of HCM were present in a 16-year-old individual carrying the *MYBPC3* R820Q mutation, generally associated with late-onset HCM, and that, even though this mutation was generally associated with a good prognosis, two incidents of SCD occurred in the same family. Taken together, these findings indicate that modulating factors, possibly more prevalent in some populations than in others, may play a role not only in the onset of HCM-associated symptoms and LVH, but also the underlying pathogenesis resulting in SCD (Charron et al., 1998; Konno et al., 2003). In the light of these findings, where variable phenotypes have been assigned to specific mutations in *MYBPC3*, and where modifying factors seem to play an important role in disease presentation, caution should be exercised not to classify all cMyBPC-associated HCM as a mere mild form of the disease.

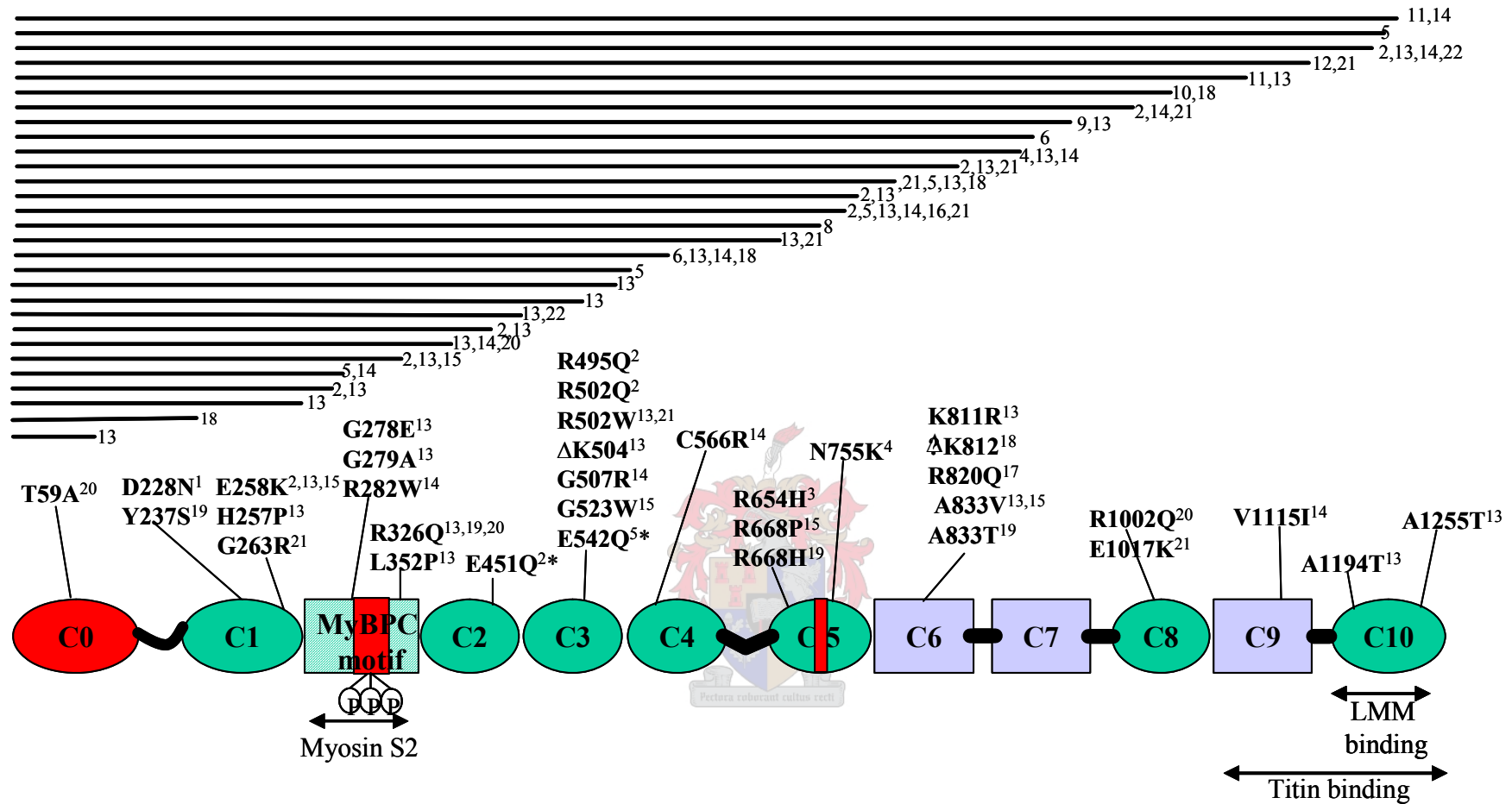


**Figure I.23. HCM-causing mutations in cMyBPC**

Circles = immunoglobulin C2 domains;  = fibronectin type 3 domains;  = MyBPC motif;  = interdomain linkers; P = PKA and MyBPC-associated kinase phosphorylation sites; red areas = cardiac-specific regions. The arrows below the figure indicate the positions of the binding-sites for light meromyosin (LMM), myosin S2 and titin respectively. The black lines above the figure indicate the respective lengths of the truncated cMyBPCs expressed as a result of HCM-causing mutations, while the positions of HCM-causing missense mutations are indicated above the diagram

of *cMyBPC*. 1 = Andersen et al., 2001; 2 = Niimura et al., 1998; 3 = Moolman-Smook et al., 1998; 4 = Yu et al., 1998; 5 = Carrier et al., 1997; 6 = Kimura et al., 1997; 8 = Bonne et al., 1995; 9 = Anan et al., 2002; 10 = Richard et al., 1999; 11 = Watkins et al., 1995a; 12 = Rottbauer et al., 1997; 13 = Richard et al., 2003; 14 = Erdmann et al., 2001; 15 = Erdmann et al., 2003; 16 = Moolman et al., 2000; 17 = Konno et al., 2003; 18 = Jaaskelainen et al., 2002; 19 = Morner et al., 2003; 20 = Niimura et al., 2002; 21 = Barr et al., unpublished data available at [http://genetics.med.harvard.edu/~seidman/cg3/muts/MYBPC3\\_mutations\\_TOC.html](http://genetics.med.harvard.edu/~seidman/cg3/muts/MYBPC3_mutations_TOC.html); 22 = Waldmuller et al., 2003.

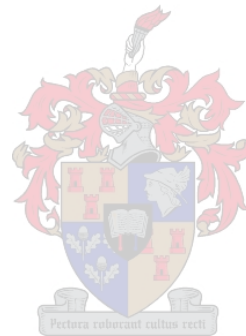


**Table I.6. HCM-causing mutations in MYBPC3**

<b>Exon/Intron</b>	<b>AA/Nt change</b>	<b>Translational change</b>	<b>Functional change</b>	<b>Reference</b>
Ex 3	Δccaagga	Frame-shift	Truncation, loss of partial C0-C10	Richard et al., 2003
Ex 3	Q76X	Nonsense	Truncation, loss of partial C0-C10	Richard et al., 2003
Ex 3	T59A	Missense	Single AA change in domain C1	Niimura et al., 2002
Int 6	IVS6-2a>c	Splicing	Truncation, loss of partial C1-C10	Jaaskelainen et al., 2002
Ex 7	D228N	Missense	Single AA change in domain C1	Andersen et al., 2001
Ex 7	Y237S	Missense	Single AA change in domain C1	Morner et al., 2003
Ex 7	H257P	Missense	Single AA change in domain C1	Richard et al., 2003
Ex 7	E258K	Missense/splicing	Single AA change in domain C1/ truncation, loss of MyBPC-motif-C10	Niimura et al., 1998; Richard et al., 2003; Erdmann et al., 2003
Int 7	IVS7+1g>a	Splicing	Truncation, loss of MyBPC-motif-C10	Erdmann et al., 2001
Int 7	IVS7-1g>a	Splicing	Truncation, loss of MyBPC-motif-C10	Carrier et al., 1997
Ex 8	G263R	Missense	Single AA change in MyBPC-motif	Barr et al., *
Int 8	IVS8+1g>a	Splicing	Truncation, loss of MyBPC-motif-C10	Niimura et al., 1998
Ex 9	G278E	Missense	Single AA change in LAGGRRIS insertion in MyBPC-motif	Richard et al., 2003
Ex 9	G279A	Missense	Single AA change in LAGGRRIS insertion in MyBPC-motif	Richard et al., 2003
Ex 9	R282W	Missense	Single AA change in LAGGRRIS insertion in MyBPC-motif	Erdmann et al., 2001
Int 12	IVS12-2a>g	Splicing	Truncation, loss of partial MyBPC-motif- C10	Niimura et al., 1998

<b>Exon/Intron</b>	<b>AA/Nt change</b>	<b>Translational change</b>	<b>Functional change</b>	<b>Reference</b>
Ex 13	$\Delta c$	Frame-shift	Truncation, loss of partial MyBPC-motif-C10	Erdmann et al., 2003
Ex 13	R326Q	Missense/splicing	Single AA change in MyBPC-motif/ Truncation, loss of partial MyBPC-motif-C10	Richard et al., 2003; Morner et al., 2003; Niimura et al., 2002
Ex 13	L352P	Missense	Single AA change in MyBPC-motif	Richard et al., 2003
Ex 14	$\Delta c$	Frame-shift	Truncation, loss of partial C2-C10	Erdmann et al., 2001
Int 14	IVS14-2a>g	Splicing	Truncation, loss of partial C2-C10	Richard et al., 2003
Int 15	IVS15-13g>a	Splicing	Truncation, loss of partial C2-C10	Jaaskelainen et al., 2002
Ex 16	Q425X	Nonsense	Truncation, loss of partial C2-C10	Niimura et al., 2002
Ex 16	$\Delta tt$	Frame-shift	Truncation, loss of partial C2-C10	Richard et al., 2003
Ex 16	$\Delta t$	Frame-shift	Truncation, loss of partial C2-C10	Richard et al., 2003
Ex 16	$\Delta c$	Frame-shift	Truncation, loss of partial C2-C10	Richard et al., 2003
Ex 16	E451Q	Missense/splicing	Single AA change in C2/ Truncation, loss of partial C2-C10	Niimura et al., 1998
Ex14	$\Delta cc$	Frame shift	Truncation, loss of partial C3-C10	Waldmuller et al., 2003
Ex 18	R495Q	Missense	Single AA change in C3	Niimura et al., 1998
Ex 18	R502Q	Missense	Single AA change in C3	Niimura et al., 1998
Ex 18	R502W	Missense	Single AA change in C3	Richard et al., 2003; Barr et al.,*
Ex 18	$\Delta K504$	1AA deletion	Single AA deletion in C3	Richard et al., 2003
Ex 18	G507R	Missense	Single AA change in C3	Erdmann et al., 2001
Ex 18	G523W	Missense	Single AA change in C3	Erdmann et al., 2003

<b>Exon/Intron</b>	<b>AA/Nt change</b>	<b>Translational change</b>	<b>Functional change</b>	<b>Reference</b>
Ex18	E542Q	Missense/splicing	Single AA change in C3/ Truncation, loss of partial C3-C10	Carrier et al., 1997
Ex 18	$\Delta$ gc	Frame-shift	Truncation, loss of partial C3-C10	Richard et al., 2003
Int 18	IVS17+2c>t	Splicing	Truncation, loss of C4-C10	Richard et al., 2003
Ex 19	K565X	Nonsense	Truncation, loss partial of C4-C10	Morner et al., 2003
Ex 19	C566R	Missense	Single AA change in C4	Erdmann et al., 2001
Ex 19	$\Delta$ t	Frame-shift	Truncation, loss of partial C4-C10	Kimura et al., 1997
Ex 20	$\Delta$ a	Frame-shift	Truncation, loss of partial C4-C10	Richard et al., 2003
Int 20	IVS20-2a>g	Splicing	Truncation, loss of partial C4-C10	Erdmann et al., 2001
Int 21	IVS21+2a>g	Splicing	Truncation, loss of C5-C10	Bonne et al., 1995
Ex 22	R654H	Missense	Single AA change in C5	Moolman-Smook et al., 1998
Ex 22	R668P	Missense	Single AA change in C5	Erdmann et al., 2003
Ex 22	R668H	Missense	Single AA change in C5	Morner et al., 2003
Ex 22	W683X	Nonsense	Truncation, loss of partial C5-C10	Richard et al., 2003
Ex 22	$\Delta$ cct ins gg	Frame-shift	Truncation, loss of partial C5-C10	Barr et al.,*
Ex 23	$\Delta$ c	Frame-shift	Truncation, loss of partial C5-C10	Niimura et al., 1998
Ex 24	22bp duplication	Frame-shift	Truncation, loss of partial C5-C10	Richard et al., 2003
Ex 24	Ins t	Frame shift	Truncation, loss of partial C5-C10	Barr et al.,*
Ex 24	N755K	Missense	Single AA change in C5	Yu et al., 1998
Int 24	IVS24+1g>a	Splicing	Truncation, loss of C6-C10	Carrier et al., 1997; Barr et al.,*
Int 24	IVS24+1g>t	Splicing	Truncation, loss of C6-C10	Niimura et al., 1998
Int 24	SBP tgat>tggt	Splicing	Truncation, loss of C6-C10	Carrier et al., 1997

<b>Exon/Intron</b>	<b>AA/Nt change</b>	<b>Translational change</b>	<b>Functional change</b>	<b>Reference</b>
Ex 25	Ins g	Frame-shift	Truncation, loss of partial C6-C10	Richard et al., 2003; Erdmann et al., 2001
Ex 25	Ins g	Splicing	Truncation, loss of partial C6-C10	Moolman et al., 2000; Barr et al.,*
Ex 26	K811R	Missense	Single AA change in C6	Richard et al., 2003
Ex 26	ΔK812	1AA deletion	Single AA deletion in C6	Jaaskelainen et al., 2002
Ex 26	R820Q	Missense	Single AA change in C6	Konno et al., 2003
Ex 26	A833V	Missense	Single AA change in C6	Richard et al., 2003; Erdmann et al., 2003
Ex 26	Δcg, ins tct	Frame-shift	Truncation, loss of partial C6-C10	Morner et al., 2003
Ex 26	A833T	Missense	Single AA change in C6	Morner et al., 2003
Ex 26	Δcgcgt	Frame-shift	Truncation, loss of partial C6-C10	Carrier et al., 1997; Richard et al., 2003
Ex 26	Δcgcgtc	Frame-shift	Truncation, loss of partial C6-C10	Richard et al., 2003
Ex 26	Δc	Frame-shift	Truncation, loss of partial C6-C10	Richard et al., 2003
Ex 27	Dup gcct	Frame shift	Truncation, loss of partial C7-C10	Barr et al.,*
Int 27	IVS27+1g>a	Splicing	Truncation, loss of partial C7-C10	Erdmann et al., 2001
Int 27	IVS27-3c>g	Splicing	Truncation, loss of partial C7-C10	Niimura et al., 2002
Ex 28	Δct	Frame-shift	Truncation, loss of partial C7-C10	Niimura et al., 1998
Ex 28	Q969X	Nonsense	Truncation, loss of partial C7-C10	Yu et al., 1998
Int 28	IVS28+1g>a	Splicing	Truncation, loss of partial C7-C10	Kimura et al., 1997
Int 28	IVS28Δ+1+2	Splicing	Truncation, loss of partial C7-C10	Richard et al., 2003
Ex 29	Δcg	Frame-shift	Truncation, loss of partial C8-C10	Anan et al., 2002
Ex 30	R1002Q	Missense	Single AA change in C8	Niimura et al., 2002

<b>Exon/Intron</b>	<b>AA/Nt change</b>	<b>Translational change</b>	<b>Functional change</b>	<b>Reference</b>
Ex 30	E1017K	Missense	Single AA change in C8	Barr et al.,*
Ex 30	Q1061X	Nonsense	Truncation, loss of partial C8-C10	Jaaskelainen et al., 2002
Ex 30	Ins aa	Frame-shift	Truncation, loss of partial C8-C10	Niimura et al., 1998; Erdmann et al., 2001
Ex 30	Δg	Frame-shift	Truncation, loss of partial C8-C10	Erdmann et al., 2001
Ex 31	Ins c	Frame-shift	Truncation, loss of C9-C10	Barr et al.,*
Ex31	E1096X	Nonsense	Truncation, loss of partial C9-C10	Richard et al., 2003
Int 31	IVS31+1g>c	Splicing	Truncation, loss of partial C9-C10	Watkins et al., 1995a
Ex 32	V1115I	Missense	Single AA change in C9	Erdmann et al., 2001
Int 32	IVS32+1g>a	Splicing	Truncation, loss of partial C9-C10	Rottbauer et al., 1997
Ex 33	A1194T	Missense	Single AA change in C10	Richard et al., 2003
Ex 33	Δc	Frame shift	Truncation, loss of partial C10	Barr et al.,*
Ex 33	Δg	Frame-shift	Truncation, loss of partial C10	Richard et al., 2003
Ex 33	A1255T	Missense	Single AA change in C10	Richard et al., 2003
Int 33	Δ 25bp	Splicing	Truncation, loss of partial C10	Waldmuller et al., 2003
Int 33	IVS33+1g>a	Splicing	Truncation, loss of partial C10	Niimura et al., 1998
Ex 34	Q1233X	Nonsense	Truncation, loss of partial C10	Erdmann et al., 2001

<b>Exon/Intron</b>	<b>AA/Nt change</b>	<b>Translational change</b>	<b>Functional change</b>	<b>Reference</b>
Ex 34	11bp ins + $\Delta$ 4bp	Frame-shift	Truncation, loss of partial C10	Carrier et al., 1997
Ex 34	18bp ins	Duplication	Duplication of 6AA in C10	Watkins et al., 1995a; Barr et al.,*
Ex 34	Ins ttca	Frame-shift	Truncation, loss of partial C10	Erdmann et al., 2001

*AA = amino acid; bp = base pair; C0, C1, C2, C3, C4, C5, C6, C7, C8, C9, C10 = domains of cMyBPC; Ex = exon; ins = insertion; Int = intron; Nt = nucleotide; SBP = splice branch point;  $\Delta$  = deletion; \* = Barr et al., unpublished data, available at [http://genetics.med.harvard.edu/~seidman/cg3/muts/MYBPC3\\_mutations\\_TOC.html](http://genetics.med.harvard.edu/~seidman/cg3/muts/MYBPC3_mutations_TOC.html).*

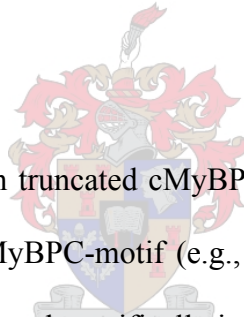


### **I.7.8.2. Pathogenesis of HCM-causing mutations resulting in the truncation of cMyBPC**

Several studies have indicated that truncated cMyBPC peptides are incorporated into the cardiac sarcomere where they are likely to act as “poison peptides” (section I.1.1). The precise mechanisms through which these truncated peptides cause HCM is, however, still unclear and is likely to vary, depending on the length of the specific peptide. It can, for instance, be speculated that longer peptides in which only a portion of the C-terminal domains, responsible for the anchoring of cMyBPC to the thick filament (sections I.7.3.1, I.7.3.2, I.7.3.3), is truncated could compete with full-length cMyBPC for LMM and titin binding-sites. Indeed, Yang et al., (1999) showed that truncated MyBPC, lacking only the C10 domain (housing the major LMM binding-site) was stably incorporated into the A-band of the sarcomeres of transgenic mice. From these findings, it seems likely that, even though the major LMM binding domain (C10) is absent, the presence of domains C8 and C9, of which at least C9 may be involved in the binding of titin (Freiburg and Gautel, 1996), and domain C7, involved in the C-zone incorporation of cMyBPC (sections I.7.3.2, I.7.3.3), is sufficient for correct A-band incorporation of truncated cMyBPC (Yang et al., 1999). Due to their ability to compete for thick filament binding-sites with full-length cMyBPC, these truncated peptides may impair the ability of full-length cMyBPC to fulfill its structural and regulatory functions.

Studies by Yang et al., (1998) and Flavigny et al., (1999) have shown that truncated cMyBPC peptides lacking the C-terminal domains, essential for association with the thick filament backbone (C7-C10) (sections I.7.3.1, I.7.3.2, I.7.3.3), are incorporated into the sarcomere, although their distribution is more diffuse. Flavigny et al., (1999) showed that truncated cMyBPC peptides lacking the C5-C10, or C3-C10 or MyBPC-motif-C10 were incorporated stably into the A-bands of about 10% of myocytes in which they were expressed, while a more diffuse pattern of distribution of the

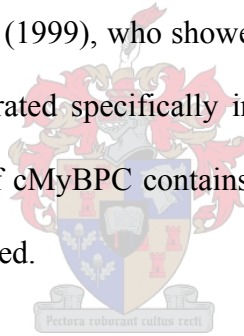
truncated peptides was observed in the remaining myocytes. Yang et al., (1999) also found A-band specific localisation of truncated cMyBPC peptides lacking the C5-C10 region, even though these peptides were also observed to be associated with the I-band and M-line, as well as being distributed diffusely throughout the cytoplasm. The A-band incorporation of truncated peptides containing the MyBPC-motif may be facilitated through interactions between this region and myosin S2 (section I.7.3.4). Interaction between truncated MyBPC peptides and S2 may result in alterations in crossbridge structure, thereby, affecting the ability of crossbridges to bind to thin filaments, resulting in alterations in the contractile properties of the sarcomere (section I.7.7.1). Additionally, this interaction between truncated cMyBPC peptides and S2 would not be restricted only to the specific positions in the A-band (C-zone) where cMyBPC is normally found, but would affect crossbridges throughout the A-band.



The specific mechanisms through which truncated cMyBPC peptides lacking the C-terminal LMM and titin binding-sites, as well as the MyBPC-motif (e.g., truncated cMyBPC peptides lacking the MyBPC-motif-C10 region), are incorporated specifically into the sarcomeric A-band (Flavigny et al., 1999), however, remain unclear. This finding, however, suggests that the C0-C1 region of cMyBPC (domains C0, PA-region and domain C1) houses an, as yet, unidentified A-band specific binding-site. Based on hydrophobic cluster analysis of the C0 domain of cMyBPC and the My1 domain (myosin binding domain) of myomesin, which showed a 22% sequence identity and 42% sequence similarity between the myosin-binding region of My1 and a portion of cMyBPC domain C0, Flavigny et al., (1999) proposed that domain C0 may contain a myosin binding-site. As the association between the My1 domain myomesin and myosin occurs in the M-band, where only the LMM portion of myosin is present, it can be assumed that this homology suggests that domain C0 would associate with LMM, rather than with HMM. Witt et al., (2001), however, proposed that the

C0 domain of cMyBPC could interact with myosin S2. Neither of these hypotheses is, however, supported by the findings of Gruen and Gautel (1999), who found no association between the C0-C1 region of cMyBPC and myosin as a whole.

Recently, however, Squire et al., (2003) and Kulikovskaya et al., (2003) proposed that the C0-C1 region of cMyBPC might be able to interact with F-actin (section I.7.3.5). An interaction between the C0-C1 region of cMyBPC and F-actin would allow truncated cMyBPC peptides to be incorporated into the sarcomeric I-band, as well as the region of overlap between thick and thin filaments. These hypotheses are, therefore, consistent with the findings of Yang et al., (1998) who showed that truncated cMyBPC peptides lacking the C5-C10 region were found in the I-band, but they are not supported by the data of Flavigny et al., (1999), who showed that the truncated cMyBPC, consisting of only the C0-C1 region, was incorporated specifically into the A-band and not the I-band. The possibility that the N-terminal region of cMyBPC contains an, as yet, unidentified A-band specific binding-site can, however, not be excluded.

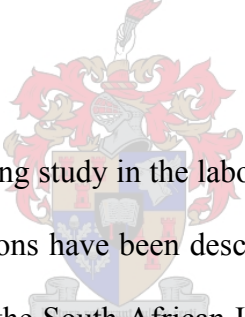


### **I.7.8.3. Pathogenesis of HCM-causing missense mutations in cMyBPC**

From the previous section it becomes apparent that HCM-causing mutations resulting in the truncation of cMyBPC are likely to act as poison peptides by being incorporated into the sarcomere, where they disrupt sarcomeric function. The mechanisms through which missense mutations in cMyBPC cause HCM are, however, largely unclear, as the functions of most of the domains in which they are found are unknown. It is plausible that the A1194T and A1255T mutations in the C10 domain of cMyBPC (Richard et al., 2003) may affect the interaction between this domain and either LMM (Okagaki et al., 1993) or titin (Freiburg and Gautel, 1996). Similarly, as the C9 domain of

cMyBPC may be involved in the interaction between cMyBPC and titin, the V1115I mutation in domain C9 (Erdmann et al., 2001) may also affect this interaction. The G278E, G279A, R282W, R326Q and L352P mutations in the MyBPC-motif may either affect the phosphorylation of cMyBPC, or the binding of the MyBPC-motif to myosin S2. As no specific functions have been assigned to the C1, C2, C3, C4, C5, C6, or C7 domains, the mechanisms through which mutations in these domains (table I.6 and figure I.23) cause HCM remain unclear. It can be speculated that these mutations may adversely affect the stability of these domains, thus destabilising the protein as a whole. Alternatively, these mutations may affect the ability of these domains to bind to, as yet, unidentified ligands.

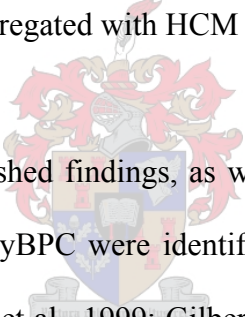
## **I.8. PRESENT STUDY**



The present study forms part of an ongoing study in the laboratory of Prof Valerie Corfield, in which all genes in which HCM-causing mutations have been described are systematically screened for the presence of HCM-causing mutations in the South African HCM-affected population. In the present, study a panel of HCM-affected individuals was screened for the presence of HCM-causing mutations in *MYBPC3* by the polymerase chain reaction (PCR) single strand conformation polymorphism (SSCP) technique, allowing the identification of both known and novel mutations and polymorphisms. Following the identification of altered mobility of single-stranded conformers, suggestive of nucleotide sequence variation, cycle sequencing was used to identify nucleotide sequence variations, which were confirmed by restriction enzyme digestion, where possible.

In cases where nucleotide sequence changes were predicted to alter either the amino acid sequence of cMyBPC, or affect the reading frame or splicing of the *MYBPC3* transcript, population-matched

control panels, consisting of at least 100 individuals, were screened for the presence of these sequence variants. Nucleotide sequence variants not found in control populations were regarded as putative HCM-causing mutations. Where putative HCM-causing mutations were predicted to alter the splicing of the *MYBPC3* transcript, reverse transcription (RT) PCR was used to establish whether these putative mutations do indeed alter splicing. Additionally, family members of individuals in which putative HCM-causing missense-, splicing- and frame-shift mutations were identified were recruited if possible, and tested for the presence of the sequence variation. All individuals in which such sequence variations were identified, were subsequently assessed clinically in order to provide evidence of co-segregation of the putative mutation and the disease. Putative HCM-causing mutations were considered disease-causing if they were not identified in relevant control panels and, when possible to establish, if they co-segregated with HCM within a particular family.



Additionally, based on previously published findings, as well as our own mutation-screening data, the C0-C1 region and C7 domain of MyBPC were identified as functionally important regions of cMyBPC (Gilbert et al., 1996; Flavigny et al., 1999; Gilbert et al., 1999; Kulikovskaya et al., 2003; Squire et al., 2003). It was, therefore, hypothesised that these regions of cMyBPC might interact with, as yet, unidentified ligands. This hypothesis was tested by screening cardiac cDNA libraries for the ligands of these regions, using the yeast two-hybrid (Y2H) method. This approach, as well as candidate-ligand Y2H-assays, led to the identification of two candidate ligands of the C7 domain, which were subsequently confirmed, using Y2H-based candidate-ligand assays (Moolman-Smook et al., 2002).

This data, in conjunction with additional Y2H and biochemical data from our group and the group of Prof Hugh Watkins (Department of Cardiovascular Medicine, University of Oxford, UK), with

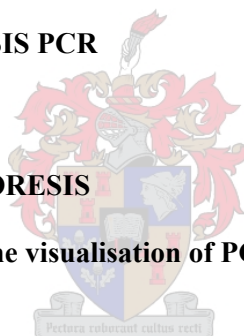
whom we collaborate, has led to the development of a novel proposed model of cMyBPC quaternary structure (Moolman-Smook et al., 2002). Based on specific domains of cMyBPC being juxtapositioned with other proteins/protein domains in this model of cMyBPC quaternary structure, putative ligands of several domains of cMyBPC were identified. Additionally, based on the findings that PKA-mediated phosphorylation of cMyBPC results in an expansion of the thick filament backbone, a model of cMyBPC quaternary structure when cMyBPC was phosphorylated was proposed. This model led to the identification of domain C10 of cMyBPC as a putative ligand of the C3 domain of cMyBPC. The interaction between these two cMyBPC domains was subsequently confirmed by Y2H-based candidate-ligand assays, supporting the model of cMyBPC quaternary structure when cMyBPC is phosphorylated by PKA.

The identification of ligands of specific regions of cMyBPC allows new insights into the mechanisms through which several HCM-causing missense mutations may have their pathogenic effect, by affecting protein:protein interactions. Additionally, the development of models of cMyBPC quaternary structure provide insights into mechanisms through which cMyBPC may regulate thick filament structure and cardiac contractility.

<b>CHAPTER II: METHODS AND MATERIALS</b>	<b>Page</b>
<b>II.1. PATIENT SELECTION</b>	<b>97</b>
<b>II.1.1. HCM-AFFECTED PANEL</b>	<b>97</b>
<b>II.1.2. CONTROL PANELS</b>	<b>97</b>
<b>II.2. CLINICAL EVALUATION</b>	<b>98</b>
<b>II.3. SAMPLE COLLECTION</b>	<b>99</b>
<b>II.4. NUCLEIC ACID EXTRACTION AND PURIFICATION</b>	<b>99</b>
<b>II.4.1. GENOMIC DNA EXTRACTION</b>	<b>99</b>
<b>II.4.1.1. Extraction of nuclei from whole blood</b>	<b>99</b>
<b>II.4.1.2. Extraction of DNA from nuclei</b>	<b>100</b>
<b>II.4.2. RNA EXTRACTION</b>	<b>101</b>
<b>II.4.2.1. Lymphocyte isolation</b>	<b>101</b>
<b>II.4.2.2. RNA Extraction from lymphocytes</b>	<b>101</b>
<b>II.4.3. DNA PRECIPITATION</b>	<b>103</b>
<b>II.4.4. WASHING OF PRECIPITATED DNA PELLETS</b>	<b>103</b>
<b>II.4.5. PHENOL CHLOROFORM DNA PURIFICATION</b>	<b>103</b>
<b>II.4.6. GEL-PURIFICATION OF PCR PRODUCTS</b>	<b>104</b>
<b>II.4.7. BACTERIAL PLASMID PURIFICATION</b>	<b>105</b>
<b>II.4.8. YEAST PLASMID PURIFICATION</b>	<b>106</b>
<b>II.5. ESTABLISHMENT OF EBV-TRANSFORMED CELL LINES</b>	<b>107</b>
<b>II.6. PCR METHODS</b>	<b>108</b>
<b>II.6.1. PRIMER DESIGN AND SYNTHESIS</b>	<b>108</b>
<b>II.6.1.1. Mutation screening primers</b>	<b>108</b>
<b>II.6.1.2. RT-PCR primers</b>	<b>109</b>



II.6.1.3. Y2H cloning primers	109
II.6.1.4. Y2H insert screening primers	112
II.6.1.5. Site-directed mutagenesis primers	115
II.6.2. ROUTINE PCR	115
II.6.3. HIGH FIDELITY PCR	116
II.6.4. RT-PCR	117
II.6.4.1. First strand cDNA synthesis	119
II.6.4.2. PCR Amplification of <i>MYBPC3</i> cDNA	120
II.6.5. BACTERIAL COLONY PCR	121
II.6.6. YEAST COLONY PCR	122
II.6.7. NESTED PCR	122
II.6.8. SITE-DIRECTED MUTAGENESIS PCR	123
II.7. GEL-ELECTROPHORESIS	125
II.7.1. AGAROSE GEL-ELECTROPHORESIS	125
II.7.1.1. Agarose gel-electrophoresis for the visualisation of PCR-amplified products	125
II.7.1.2. Agarose gel-electrophoresis for the gel-purification of PCR-amplified products	126
II.7.1.3. Agarose gel-electrophoresis for the visualisation of plasmids purified from <i>E.coli</i>	126
II.7.2. NON-DENATURING POLYACRYLAMIDE GEL-ELECTROPHORESIS	127
II.8. SINGLE-STRAND CONFORMATIONAL POLYMORPHISM (SSCP)	127
II.9. SILVER STAINING OF POLYACRYLAMIDE GELS	128
II.10. DNA SEQUENCING	129
II.10.1. MANUAL DNA SEQUENCING	129



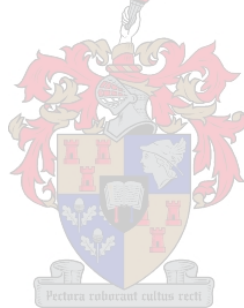
<b>II.10.2. AUTOMATED DNA SEQUENCING</b>	<b>131</b>
<b>II.10.3. DNA SEQUENCE ANALYSIS</b>	<b>131</b>
<b>II.10.3.1. Sequence analysis of specific exons of <i>MYBPC3</i></b>	<b>131</b>
<b>II.10.3.2. Sequence analysis of Y2H constructs</b>	<b>133</b>
<b>II.10.3.3. Sequence analysis of Y2H interactor prey constructs</b>	<b>133</b>
<b>II.11. RESTRICTION ENZYME DIGESTION</b>	<b>134</b>
<b>II.11.1. ALLELE-SPECIFIC RESTRICTION ENZYME DIGESTION (ASREA)</b>	<b>134</b>
<b>II.11.2. RESTRICTION ENZYME DIGESTION FOR CLONING</b>	<b>134</b>
<b>II.11.3. RESTRICTION MAPPING OF Y2H LIBRARY PREY- INSERTS</b>	<b>135</b>
<b>II.12. GENERATION OF Y2H CONSTRUCTS</b>	<b>137</b>
<b>II.12.1. Y2H BAIT- AND PREY-VECTORS</b>	<b>137</b>
<b>II.12.2. ALKALINE PHOSPHATASE TREATMENT OF VECTORS</b>	<b>137</b>
<b>II.12.3. DNA LIGATION</b>	<b>143</b>
<b>II.13. BACTERIAL AND YEAST STRAINS</b>	<b>143</b>
<b>II.13.1. BACTERIAL STRAINS</b>	<b>143</b>
<b>II.13.2. YEAST STRAINS</b>	<b>143</b>
<b>II.13.3. GENERATION OF BACTERIAL COMPETENT CELLS</b>	<b>146</b>
<b>II.14. PLASMID TRANSFORMATION</b>	<b>146</b>
<b>II.14.1. BACTERIAL PLASMID TRANSFORMATION</b>	<b>146</b>
<b>II.14.2. YEAST PLASMID TRANSFORMATION</b>	<b>147</b>
<b>II.15. QUALITY CONTROL OF Y2H CONSTRUCTS</b>	<b>148</b>
<b>II.15.1. PHENOTYPIC ASSESSMENT OF YEAST STRAINS</b>	<b>148</b>
<b>II.15.2. TOXICITY TESTS</b>	<b>149</b>
<b>II.15.3. REPORTER GENE SELF-ACTIVATION TESTS</b>	<b>150</b>

<b>II.15.4. ESTABLISHMENT OF MATING EFFICIENCY</b>	<b>150</b>
<b>II.16. Y2H INTERACTION TESTS</b>	<b>151</b>
<b>II.16.1. CANDIDATE LIGAND ASSAYS</b>	<b>151</b>
<b>II.16.2. LIBRARY-SCALE YEAST MATING</b>	<b>152</b>
<b>II.16.2.1. Cardiac cDNA library</b>	<b>152</b>
<b>II.16.2.2. Establishment of a bait culture</b>	<b>152</b>
<b>II.16.2.3. Library mating</b>	<b>154</b>
<b>II.16.2.4. Establishment of library titre</b>	<b>155</b>
<b>II.16.2.5. Control matings</b>	<b>155</b>
<b>II.16.3. DETECTION OF ACTIVATION OF NUTRITIONAL REPORTER- GENES</b>	<b>156</b>
<b>II.16.3.1. Selection of transformant yeast colonies</b>	<b>156</b>
<b>II.16.3.2. Selection of diploid yeast colonies</b>	<b>156</b>
<b>II.16.3.3. Selection of yeast colonies containing putative interactor peptides</b>	<b>157</b>
<b>II.16.4. DETECTION OF ACTIVATION OF COLOURIMETRIC REPORTER- GENES</b>	<b>158</b>
<b>II.16.4.1. X-<math>\alpha</math>-Galactosidase assays</b>	<b>158</b>
<b>II.16.4.2. <math>\beta</math>-galactosidase assays</b>	<b>159</b>
II.16.4.2.i. <u>Qualitative <math>\beta</math>-galactosidase assays</u>	<b>159</b>
II.16.4.2.ii. <u>Quantitative <math>\beta</math>-galactosidase assays</u>	<b>159</b>
<b>II.16.5. INTERACTION SPECIFICITY TESTS</b>	<b>161</b>



## CHAPTER II: METHODS AND MATERIALS

In this chapter, the methods employed and materials used will be described in detail. Basically, the present study can be subdivided into two main components. Firstly, the screening of *MYBPC3* for the presence of HCM-causing mutations, and, secondly, the identification of ligands binding to specific domains of cMyBPC, using the Y2H method. The present chapter will, however, not be subdivided along these lines, as identical, or related, methods were used in both sections of this study. To avoid repetition, related methods will, therefore, be grouped together, irrespective of their use in either mutation screening, or as part of the Y2H method. For the sake of clarity, figures II.1; II.2 and II.3, show flow diagrams of how these methods were employed to achieve the goals of this study.



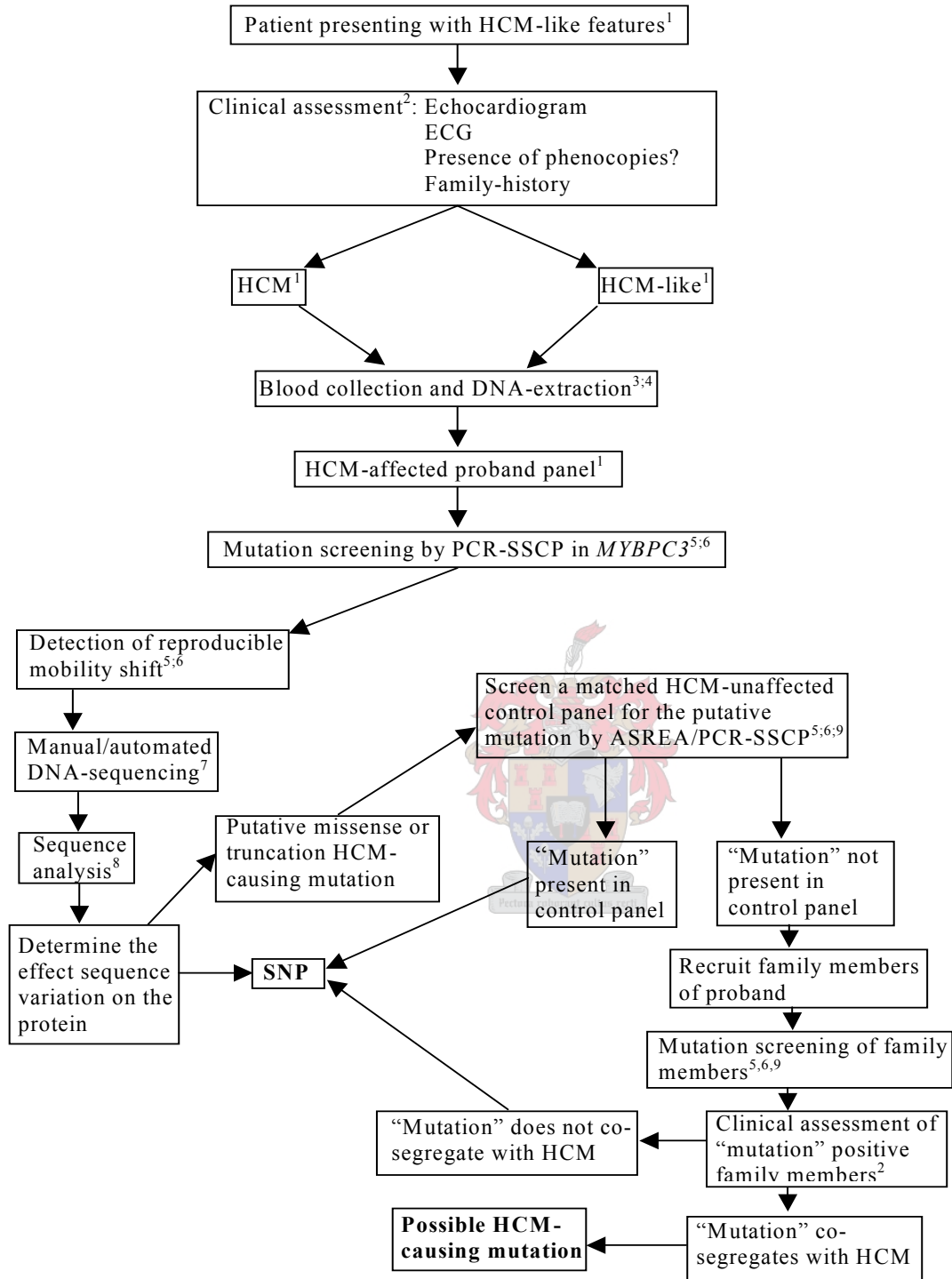


**Figure II.1. Flow-diagram depicting the mutation screening protocol followed**

1 = section II.1; 2 = section II.2; 3 = section II.3; 4 = section II.4.1; 5 = section II.6.2; 6 = section II.8; 7 = sections II.10.1 and II.10.2; 8 = section II.10.3.1; 9 = section II.11.1. ASREA = allele-specific restriction enzyme analysis; ECG = electrocardiogram; HCM = hypertrophic cardiomyopathy; PCR-SSCP = polymerase chain reaction single strand conformation polymorphism; SNP = single nucleotide polymorphism.

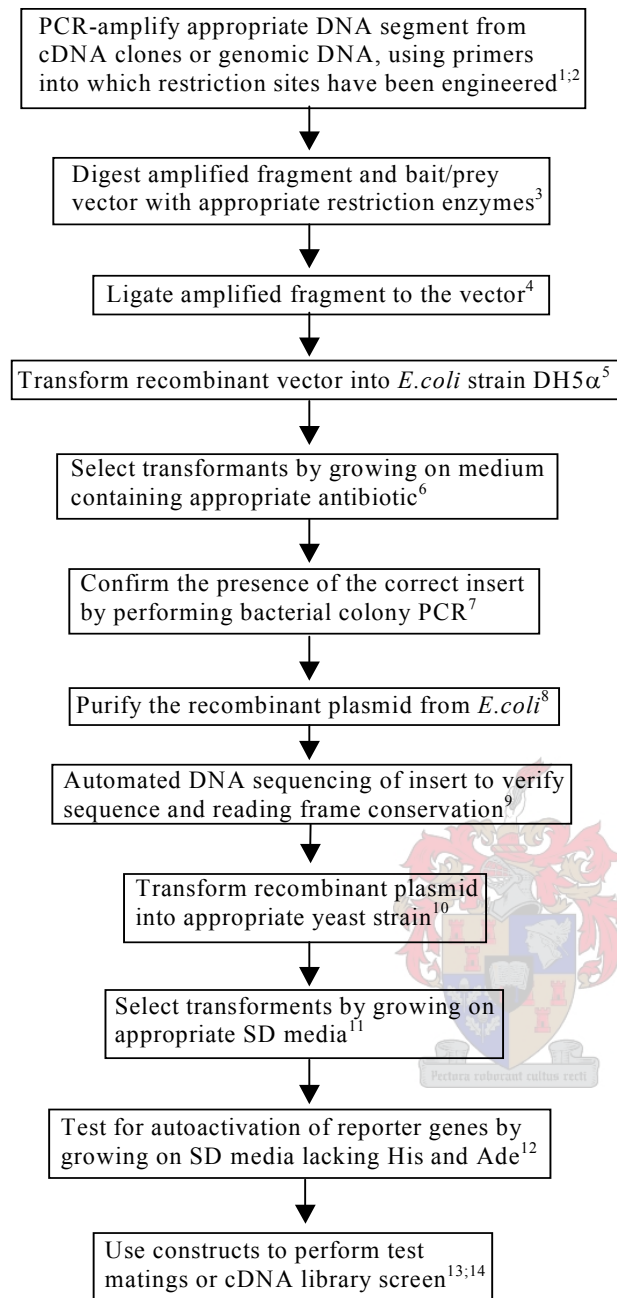


**Figure II.2. Flow-diagram depicting the procedures followed for the generation of Y2H constructs**

1 = section II.6.1.3; 2 = section II.6.3; 3 = section II.11.2; 4 = section II.12.3; 5 = section II.14.1; 6 = section II.12.1; 7 = section II.6.5; 8 = section II.4.7; 9 = section II.10.2; 10 = section II.14.2; 11 = section II.16.3.1; 12 = section II.15.3; 13 = section II.16.1; 14 = section II.16.2. cDNA = copy DNA; E.coli = Escherichia coli; PCR = polymerase chain reaction; SD = selective dropout..

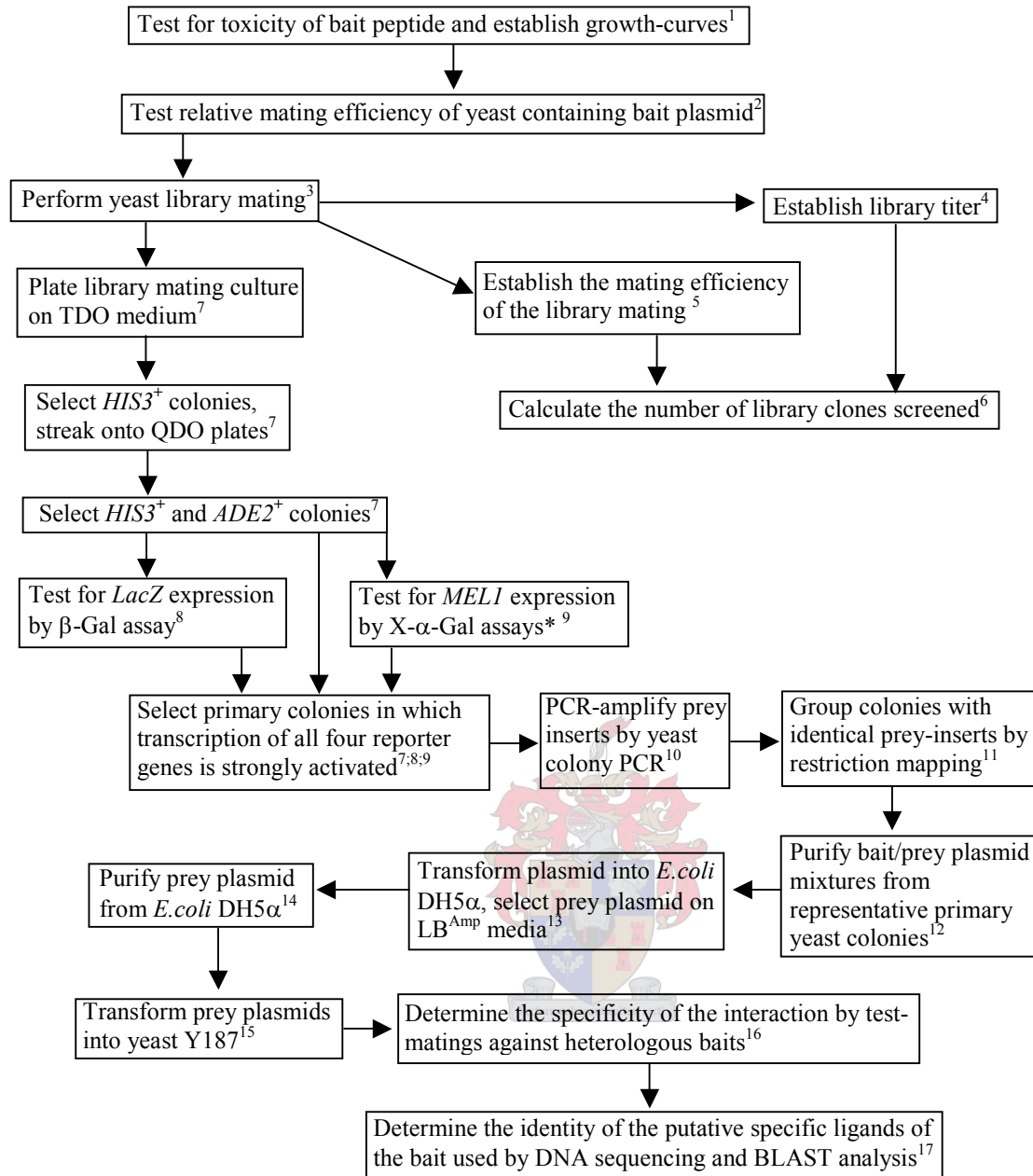


**Figure II.3. Flow-diagram depicting the procedures followed for the Y2H screening of cDNA libraries**

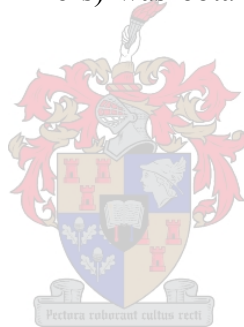
\*= Only for Matchmaker system 3; 1 = sections II.15.1 and II.15.2; 2 =section II.15.4; 3 = section II.16.2; 4 = section II.16.2.4; 5 = section II.16.2.5; 6 = appendix A; 7 = section II.16.3.3; 8 = section II.16.4.2.i; 9 = section II.16.4.1; 10 = section II.6.6; 11 = section II.11.3; 12 = section II.4.8; 13 = section II.14.1; 14 = section II.4.7; 15 = section II.14.2; 16 = section II.16.1; 17 = sections II.10.2 and II.10.3.3.  $\beta$ -Gal =  $\beta$ -galactosidase; E.coli = Escherichia coli;  $LB^{Amp}$  = Luria-Bertani media containing ampicillin; PCR = polymerase chain reaction; TDO = triple dropout medium; QDO = quadruple dropout medium; X- $\alpha$ -Gal = X- $\alpha$ -galactosidase.

## **II.1. PATIENT SELECTION**

### **II.1.1. HCM-AFFECTED PANEL**

Genomic deoxyribonucleic acid (DNA), extracted from a panel of 84 probands with HCM had previously been established in the laboratory of Prof. V.A. Corfield. This panel formed the basis of investigations into the molecular causes of HCM in this study. During the course of this study, another 89 probands have been added to the test panel.

This study was approved by the Ethics committee of the University of Stellenbosch, and informed verbal consent (parental in the case of minors) was obtained from all individuals included in the investigation.



### **II.1.2. CONTROL PANELS**

In order to establish whether putative HCM-causing mutations identified during the course of this study were present in the general population, ethnically matched control panels consisting of at least 100 individuals were screened for the presence of any particular putative mutation. The Caucasian and mixed ancestry control panels each consisted of DNA extracted from blood samples, collected from more than 100 apparently HCM-unaffected individuals. As a Xhosa control panel was not available, the panel used consisted of DNA samples obtained from non-insulin dependent diabetes mellitus (NIDDM) patients from this ethnic group. The Zulu control panel consisted of DNA samples obtained from 50 apparently HCM-unaffected individuals of Zulu descent, collected by Dr Karin Sliva at Baragwanath hospital in Gauteng South Africa.

## II.2. CLINICAL EVALUATION

Clinical evaluations included a physical examination, ECG and echocardiographic examination of patients, as well as an interview aimed at establishing whether a family history of HCM was present. These evaluations were performed either by the referring clinician, or Prof. P.A. Brink at Tygerberg Hospital.

ECG evaluation involved standard 12-lead ECG. ECG abnormalities compatible with HCM were noted for each patient. These changes included abnormal repolarisation patterns, abnormal voltages and abnormal Q-waves. LVH on ECG was calculated using the point-system of Romhilt and Estes (Romhilt and Estes, 1968).

Echocardiographic analysis was performed with an Ultramark 4 or 8 scanner using a 2.5-3.5 Mhz transducer. Cardiac dimensions were recorded with two-dimensional echocardiography according to established protocols (Maron et al., 1978). A maximal end-diastolic interventricular septal (IVS) thickness, left ventricular posterior wall (PW) thickness, as well as the location of the hypertrophy, were determined. Other echocardiographic changes compatible with HCM, such as the presence of asymmetric septal hypertrophy, systolic anterior motion of the mitral valve, and valvular abnormalities, were also recorded.

Probands were classified as “distinct HCM” if typical features of HCM, in the absence of extrinsic inciting conditions such as hypertension, or valvular stenosis, and/or when a family history of the disease, were present. Probands presenting with HCM-like hypertrophy, but where other causes of hypertrophy could not be excluded, were classified as having “HCM-like disease”. Both these groups were entered into the molecular genetic mutation screening study.

## II.3. SAMPLE COLLECTION

Peripheral blood was collected from all participating individuals, by venous puncture. Two to four 5ml ethylene-diamine-tetra-acetic acid (EDTA)-containing, and one to two heparin-containing, blood-collection tubes were drawn. These samples were subsequently used for DNA-extraction (EDTA tubes) (section II.4.1) and the establishment of Epstein-Barr virus (EBV) transformed cell lines (heparin tubes) (section II.5).

## II.4. NUCLEIC ACID EXTRACTION AND PURIFICATION

### II.4.1. GENOMIC DNA EXTRACTION

#### II.4.1.1. Extracting nuclei from whole blood



Blood was transferred from 5ml EDTA-containing collection tubes into a 50ml polypropylene tube (Greiner Labortechnik GmbH, Frickenhausen Germany) and 20ml ice-cold cell lysis buffer (appendix A) was added. After gently inverting the tube a few times, the sample was incubated on ice for 5-10min. The sample was then centrifuged at 3 000rpm for 10min at room temperature in a Beckman model TJ-6 centrifuge (Beckman Coulter, Scotland, UK). The supernatant was subsequently discarded and the pellet resuspended in 20ml ice-cold cell lysis buffer (appendix A), followed by another incubation- and centrifugation step as above. Following the second centrifugation step, the supernatant was discarded and the pellet resuspended in a mixture consisting of 900µl sodium-EDTA (appendix A) and 100µl 10% sodium dodecyl sulphate (SDS). The nuclei were immediately used for DNA extraction, or stored at -70°C.

#### II.4.1.2. Extraction of DNA from nuclei

To the freshly prepared or thawed nuclei, 100µl of proteinase K (10 µg/ml) (Roche Biochemical, Basel, Switzerland) was added. Following overnight incubation at 37°C, 2ml ddH<sub>2</sub>O, 500µl 3M sodium-acetate (appendix A) and 25µl phenol/chloroform (appendix A) was added to the sample. The tubes were subsequently inverted and mixed gently for 10min on a Voss rotator (Voss, Maldon, England) at 4°C. The sample was then transferred to a glass Corex tube, and centrifuged in a Sorvall RC-5B refrigerated super-speed centrifuge (rotor SS34, Dupont Instruments) at 8 000rpm for 10min at 4°C.

Following the transfer of the upper, DNA-containing, aqueous phase to a clean Corex tube, 25ml chloroform/octanol (appendix A) was added, after which the tube was closed with a polypropylene stopper and gently inverted for 10min on a Voss rotator (Voss, Maldon, England) at 4°C. This mixture was then centrifuged in a Sorvall RC-5B refrigerated super-speed centrifuge (rotor SS34, Dupont Instruments) at 8 000rpm for 10min at 4°C. After the transfer of the upper aqueous phase to a clean Corex tube, genomic DNA was ethanol precipitated, washed and resuspended as described in sections II.4.3 and II.4.4.

Following resuspension, the optical density (OD) of the DNA was determined in a Milton Roy series 120i spectrophotometer (Ivyland, PA, USA) at 260nm (OD<sub>260</sub>). The DNA concentration was determined by diluting 10µl DNA in 500µl 1x TE buffer (appendix A) and multiplying the OD<sub>260</sub> measurement by a factor of 2.5, estimating the DNA concentration in µg/µl. The OD<sub>260</sub> to OD<sub>280</sub> ratio was used as an estimate of DNA purity (a ratio of approximately 1.8 was taken as an indication of pure DNA).

## **II.4.2. RNA EXTRACTION**

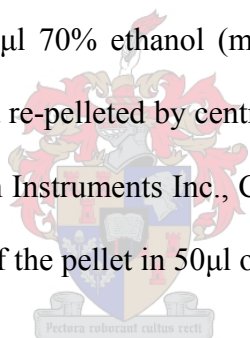
### **II.4.2.1. Lymphocyte isolation**

When fresh blood samples were available for ribonucleic acid (RNA) extraction, lymphocytes were isolated from whole blood. In short, 2ml of fresh blood was mixed with an equal volume of PBS buffer (appendix A). This mixture was carefully layered over 3ml of LSM<sup>®</sup> (Organon Teknika Corp, West Chester, NC, USA) in a 15ml polypropylene centrifuge tube (Greiner Labortechnik GmbH, Frickenhausen Germany). The mixture was then centrifuged at 6 000rpm for 30min at room temperature in a Beckman model TJ-6 centrifuge (Beckman Coulter, Scotland, UK). Following the removal of the clear supernatant layer, the mononuclear cell layer was transferred to a sterile 15ml centrifuge tube. The mononuclear cells were subsequently washed by adding an equal volume of PBS buffer (appendix A), followed by centrifugation at 3 700rpm for 10min at room temperature in a Beckman model TJ-6 centrifuge (Beckman Coulter, Scotland, UK). Following the removal of the supernatant, the cells were washed a second time in 5ml PBS buffer and precipitated by centrifugation at 3700rpm for 10min at room temperature in a Beckman model TJ-6 centrifuge (Beckman Coulter, Scotland, UK), before the supernatant was removed. These cells were then either used immediately for RNA extraction, or frozen at  $-70^{\circ}\text{C}$  for future use.

### **II.4.2.2. RNA extraction from lymphocytes**

RNA was extracted from lymphocyte cell-pellets, obtained either from freshly collected blood samples (section II.4.2.1) or from cells which had been EBV-transformed (section II.5). In short, 750 $\mu\text{l}$  RNA-denaturing solution (appendix A) was added to lymphocyte cell-pellets and the cells

homogenised by repeated pipetting. Following homogenisation, 100µl of 2M NaAc (pH 4), 1ml of ddH<sub>2</sub>O saturated phenol (Sigma, St Louis, MO, USA) and 200µl of chloroform/isoamyl-alcohol (24:1) (Sigma, St Louis, MO, USA) were added. The addition of each of these reagents was followed by thoroughly mixing the mixture through vigorous pipetting. This mixture was then incubated on ice for 15min, after which it was centrifuged at 13 000rpm for 20min at 4°C in a Beckman Microfuge Lite (Beckman Instruments Inc., CA, USA). After centrifugation, the clear RNA-containing aqueous phase was transferred to a 2ml centrifuge tube. The RNA was then precipitated by the addition of two volumes of ice-cold 100% ethanol and the mixture incubated at -20°C for 1h before centrifugation at 13 000rpm for 20min at 4°C in a Beckman Microfuge Lite (Beckman Instruments Inc., CA, USA). Following centrifugation, the supernatant was removed from the RNA pellet. The RNA was then washed twice with 500µl 70% ethanol (made up with 0.2% diethylpyrocarbonate (DEPC) treated water (appendix A)) and re-pelleted by centrifugation at 13 000rpm for 10min at 4°C in a Beckman Microfuge Lite (Beckman Instruments Inc., CA, USA). The RNA pellet was air-dried for about 10min prior to re-suspension of the pellet in 50µl of nuclease-free water.



In order to minimise ribonuclease (RNase) contamination of samples, all workbench surfaces, pipettes and apparatus used were treated with RNase Erase (ICD Biochemicals, Aurora, Ohio, USA). Furthermore, all pipette tips and centrifuge tubes used in the preparation of RNA samples were rinsed with a 0.2% DEPC (Sigma, St Louis, Missouri, USA) (appendix A) solution, prior to being autoclaved.

### **II.4.3. DNA PRECIPITATION**

Standard DNA precipitation was performed by adding two volumes of ice-cold 100% ethanol (and in some cases one tenth volume 3M NaAc) to the DNA sample. Following brief vortexing of this mixture, the DNA precipitate was either transferred to a clean 1.5ml centrifuge tube, using a sterile Pasteur pipette, or pelleted by centrifugation at 13 000rpm for 15min at room temperature in a Beckman Microfuge Lite (Beckman Instruments Inc., CA, USA) and the supernatant decanted. The DNA was subsequently washed twice with 70% ethanol (section I.4.4.).

### **I.4.4. WASHING OF PRECIPITATED DNA PELLETS**

In order to remove all excess salts and solvents, precipitated DNA pellets were washed twice with 70% ethanol. Each of these washes involved the addition of 1-2ml of 70% ethanol to the DNA pellet, followed by centrifugation at 13 000rpm for 2min at room temperature in a Beckman Microfuge Lite (Beckman Instruments Inc., CA, USA), or at 3 000rpm for 10min at 4°C in a Multex centrifuge (MSE Instruments, England). After the second wash, the supernatant was decanted and the pellet allowed to dry by inverting the tube on a section of Carlton paper towel at room temperature for approximately 30min, or until the pellet appeared dry. The pellet was then resuspended in an appropriate volume of sterile ddH<sub>2</sub>O, or 1x TE buffer (appendix A).

### **II.4.5. PHENOL-CHLOROFORM DNA PURIFICATION**

Phenol:chloroform:isoamyl alcohol (PCI) treatment of DNA was conducted by adding an equal volume of PCI solution (25:24:1) (Sigma, St Louis, MO, USA) to the sample. The sample was then

vortexed for approximately 60s, and centrifuged at 13 000rpm for 15min at room temperature in a Beckman Microfuge Lite (Beckman Instruments Inc., CA, USA). The DNA-containing aqueous layer was carefully removed and transferred into a sterile tube prior to the DNA being ethanol precipitated as described in section II.4.3.

#### **II.4.6. GEL-PURIFICATION OF PCR PRODUCTS**

Gel-purification of PCR-amplified products was routinely performed in order to obtain pure PCR-amplified products for DNA sequencing (section II.10) and cloning (section II.12). PCR products were electrophoresed in agarose gels and the appropriate band excised (II.7.1.2). This gel slice was subsequently transferred to a sterile, pre-weighed, 2ml Eppendorf microfuge tube. The gel slice was subsequently weighed and an appropriate volume of capture buffer (GFX<sup>®</sup> DNA purification kit, AmershamPharmacia Biotech, New Jersey, USA) (1 $\mu$ l/mg) added. The gel slice was then melted by incubation at 60°C for 10-15min, following which the mixture was applied to a DNA purification column (GFX<sup>®</sup> DNA purification kit, AmershamPharmacia Biotech, New Jersey, NJ, USA), that had been placed into a microfuge tube. The sample was then incubated for 1min at room temperature before being centrifuged at 13 000rpm for 30s at room temperature in a Beckman Microfuge Lite (Beckman Instruments Inc., CA, USA). Following centrifugation, the flow-through was discarded and the DNA washed by adding 500 $\mu$ l of wash buffer, supplied by the manufacturer (AmershamPharmacia Biotech, New Jersey, USA), to the column and centrifuging at 13 000rpm for 30s at room temperature in a Beckman Microfuge Lite (Beckman Instruments Inc., California, USA). After this wash step, the DNA was eluted from the column by the addition of 30-50 $\mu$ l of ddH<sub>2</sub>O to the GFX column, incubation for 1min at room temperature and centrifugation for 1min at 13 000rpm in a Beckman Microfuge Lite (Beckman Instruments Inc., California, USA).

#### II.4.7. BACTERIAL PLASMID PURIFICATION

One *Escherichia coli* (*E.coli*) colony, containing the plasmid of interest as determined by bacterial colony PCR (section II.6.5.), was picked from an appropriate selection agar plate (table II.10 and appendix A) and inoculated into 10ml of Luria-Bertani (LB)-medium (appendix A), containing the same selection antibiotic, in a 50ml polypropylene centrifuge tube. This culture was grown overnight at 37°C with shaking at 250rpm in a YIH DER model LM-530 shaking incubator (SCILAB Instrument Co Ltd., Taipei, Taiwan). The following morning, the cells were pelleted by centrifugation at 3 000rpm for 10min at room temperature in a Beckman model TJ-6 centrifuge (Beckman Coulter, Scotland, UK). The supernatant was then decanted and the pellet resuspended by gentle pipetting in 1ml of cell resuspension solution (appendix A). Two millilitres of cell lysis buffer (appendix A) was added and the contents mixed by gentle inversion, after which the mixture was incubated at room temperature for 5min. Following incubation, 2ml of neutralisation solution (appendix A) was added and the content mixed by gentle inversion, after which the mixture was incubated at room temperature for an additional 5min. Following this incubation step, 5ml of PCI (25:24:1) (Sigma, St Louis, MO, USA) was added and the content mixed by gentle inversion. In order to allow phase separation, this mixture was centrifuged at 3 000rpm for 15 min at 4°C in a Multex centrifuge (MSE Instruments, England, UK).

The clear plasmid-containing aqueous phase was removed and transferred to a new sterile 50ml polypropylene tube. To this, 0.7x volume of 100% isopropanol (Merck, Darmstadt, Germany) was added and mixed well by gentle inversion. This mixture was centrifuged at 3 000rpm for 45min at 4°C in a Multex centrifuge (MSE Instruments, England), in order to pellet the plasmid DNA. The supernatant was removed from the plasmid pellet, which was subsequently washed twice with

70% ethanol, air-dried (section II.4.4) and resuspended in 100-300 $\mu$ l H<sub>2</sub>O. An aliquot of plasmid preparation was resolved on a 1% agarose TAE gel (section II.7.1.3) to verify its integrity.

#### **II.4.8. YEAST PLASMID PURIFICATION**

Yeast cells containing the plasmid of interest were grown on appropriate agar selection plates (section II.16.3, table II.10 and appendix A) for two to five days. Following incubation, approximately 50 $\mu$ l of a yeast colony was picked and resuspended in 500 $\mu$ l of sterile ddH<sub>2</sub>O in a 1.5ml centrifuge tube, and the cells pelleted by centrifugation at 13 000rpm for 30s in a Beckman Microfuge Lite (Beckman Instruments Inc., CA, USA). After the removal of the supernatant, the cells were resuspended in 200 $\mu$ l yeast lysis buffer (appendix A). A volume representing approximately 200 $\mu$ l of sterile 425-600 $\mu$ m glass beads (Sigma, St Louis, MO, USA), and 200 $\mu$ l PCI (25:24:1) (Sigma, St Louis, MO, USA), was then added. This mixture was subsequently vortexed vigorously three times for 30s, interspersed by a 30s incubation period at room temperature. In order to achieve phase separation, the mixture was centrifuged at 13 000rpm for 1min at room temperature in a Beckman Microfuge Lite (Beckman Instruments Inc., CA, USA), before the clear aqueous phase was removed and transferred to a fresh 1.5ml centrifuge tube.

The DNA was then precipitated by adding 20 $\mu$ l of 3M NaAc (pH 6.0) (appendix A) and 500 $\mu$ l of 95% ethanol, after which the mixture was incubated at -20°C for 30min. Following incubation, the mixture was centrifuged at 13 000rpm for 15min at room temperature in a Beckman Microfuge Lite (Beckman Instruments Inc., CA, USA), the supernatant decanted and the DNA pellet washed twice with 1ml of 70% ethanol, air-dried (section II.4.4) and resuspended in an appropriate volume of sterile ddH<sub>2</sub>O.

## II.5. ESTABLISHMENT OF EBV TRANSFORMED CELL LINES

EBV transformation of lymphocytes was performed in order to establish immortal cell lines from which RNA was extracted. In short, 4-5ml of heparin containing blood was layered over 3ml Histopaque (Sigma-Aldrich, St Louis, MO, USA), preheated to 22°C. This mixture was subsequently centrifuged at 1 800rpm for 20min at room temperature in a Beckman model TJ-6 centrifuge (Beckman Coulter, Scotland, UK). Following centrifugation, the white blood cell layer was transferred to a sterile 15ml polypropylene tube to which 3ml of 1x RPMI 1640-medium (Sigma, St Louis, MO, USA), preheated to 37°C, was added. This mixture was centrifuged at 1 000rpm for 30s at room temperature in a Beckman model TJ-6 centrifuge (Beckman Coulter, Scotland, UK), the supernatant decanted and the cells washed once more with 3ml of 1x RPMI 1640-medium (Sigma, St Louis, MO, USA).

The cell-pellet was then resuspended in 1.5ml EBV-medium (appendix A) and transferred to a 25cm<sup>2</sup> cell culture flask. This culture was incubated upright for one week at 37°C with CO<sub>2</sub> at 5% and humidity at 90%. During this incubation period, 0.5ml 1x RPMI 1640-medium (Sigma, St Louis, MO, USA) was added every third day. Following incubation, this culture was transferred to a 75cm<sup>2</sup> cell culture flask, which was additionally incubated at 37°C with CO<sub>2</sub> at 5% and humidity at 90%. During this incubation period, 10ml 1x RPMI 1640-medium (Sigma, St Louis, MO, USA) was added every third day, until the volume of the culture reached 50ml, at which stage the culture was transferred to a sterile 50ml polypropylene tube. The cells were then pelleted by centrifugation at 1 000rpm for 10min at room temperature in a Beckman model TJ-6 centrifuge (Beckman Coulter, Scotland, UK). Following centrifugation, the supernatant was decanted and the pellet resuspended in 1ml 1x RPMI 1640-medium (Sigma, St Louis, MO, USA), containing 10% dimethylsulphoxide

(DMSO) (Sigma, St Louis, MO, USA), the cell-suspension transferred to a cryogenic tube, and subsequently stored in liquid N<sub>2</sub>. EBV-transformed lymphocytes were subsequently used for the extraction of RNA (section II.4.2).

## II.6. PCR METHODS

### II.6.1. PRIMER DESIGN AND SYNTHESIS

Where possible, primer sequences were obtained from published data. In cases where such data were not available, primers were designed making use of nucleotide sequence data obtained from the GenBank Database (<http://www.ncbi.nlm.nih.gov/Entrez>). Primer sequences were analysed for compatibility of melting temperatures (T<sub>m</sub>), self-complimentarity, as well as primer-primer complimentarity of primer sets, using DNAMAN version 4.0 sequence analysis software (Lynnion Biosoft Corp) prior to synthesis. All primers used in this study were either synthesised at the University of Cape Town DNA Synthesis Laboratory (University of Cape Town, CT, RSA) or at MWG-Biotech AG (Ebersberg, Germany).

#### II.6.1.1. Mutation screening primers

The sequences of all primers used for PCR-amplification of the 34 protein-encoding exons of *MYBPC3* (section II.6.2) were obtained from published data (table II.1) (Carrier et al., 1997). These primer pairs were designed in such a way that both the exon and intronic regions directly flanking the exon were amplified, allowing the detection both of missense and splicing mutations (Carrier et al., 1997). With the exception of exons 3, 15, 16, 20 and 21, all exons were amplified individually in single PCR reactions. Due to its size, however, exon 3 was amplified in two overlapping fragments, designated exon 3a and 3b. The regions encompassing exons 15 and 16 (including intron 15), as well

as exons 20 and 21 (including intron 20), were amplified in single PCR reactions, due to the close proximity and small size of these neighbouring exons (Carrier et al., 1997).

### II.6.1.2. RT-PCR primers

The sequences of primers used to amplify the *MYBPC3* messenger RNA (mRNA) transcript, by reverse transcription PCR (RT-PCR) (section II.6.4), were obtained from published primer sequences (table II.2) (Carrier et al., 1997; Watkins et al., 1995a). Primers were selected on the basis that they flanked regions of the *MYBPC3* transcript suspected of being affected by the putative HCM-causing splicing mutations.

### II.6.1.3. Y2H cloning primers

All primers used to PCR-amplify specific domains/regions of *MYBPC3* and *TTN* (section II.6.3), to be cloned into Y2H cloning vectors (section II.12), were designed as part of this study. In order to facilitate the subsequent cloning of these PCR-amplified fragments, a 5' "tag" was added to all primers. The 5' tags of forward primers always contained a restriction enzyme recognition site (*NdeI*, *NcoI* or *SmaI*) (table II.3). The 5' tags of reverse primers always contained at least one transcription termination codon, and an *EcoRI* recognition site (table II.3). The sequences used to design the target-recognition portion of these primers were obtained from GenBank, and were chosen to amplify specific domains of the *MYBPC3* and *TTN* transcripts (table II.3) (<http://www.ncbi.nlm.nih.gov/Entrez>, sequence accession numbers: NM\_000256 and AJ277892, respectively). In cases where ambiguity regarding the location of domain boundaries existed, primers were designed to co-amplify inter-domain linkers, thus ensuring the amplification of complete target domains.

**Table II.1. Primer sequences used in PCR amplification of protein-encoding exons of MYBPC3**

<b>Exon</b>	<b>Size (bp)</b>	<b>Ta (°C)</b>	<b>Forward primer sequence (5'&gt;3')</b>	<b>Reverse primer sequence (5'&gt;3')</b>
2	292	54	CATGGTGAGTGCCTGGTGTGAC	TTGGCTGTGTCCCCTCTCTGC
3a	323	54	CCTGGCTCTCCCGACTGCTA	ACTCCTGCCCCGCTCTGTCTC
3b	333	54	TTTAGCAAGAAGCCACGGTCA	CTGGATGGATGGAGAGTCGCT
4	287	54	CTTTCCTCATCCACAGCGGG	GCTTTTGAGACCTGCCCTGG
5	246	61	TGGGAGGCGGAGCTTGCAAGT	CCCCTTCCCACCCCAATGCTG
6	269	54	GCAGCAGGACACTCCCCAAG	TGTCTCCACGACCCCGGT
7	283	54	ATTACAGGCCTGAGCCACCG	AGACCAGGACCCATGGGGAG
8	271	60	TCTGAAGCCCCTTCCCCCAT	GGCTCCTGTGGGGGTTAGACT
9	252	54	CAGGGCTGGGGATGATTTGC	AGGAGCAGGATGGGAGTGGA
10	192	58	CCACTCCACTCCCATCCTGC	ACAGTGCTGGGATTTGGAGCC
11	254	58	GGTCTACCAGGTCGGCCCAA	CAGGAGAAGCCCAAGGCACA
12	267	58	GGGTGGGGTCCAGGTCTTTGA	CCCTGTCCCTCTGCCCCTTC
13	333	54	AAGGGGCAGAGGGACAGGG	TCCTGTGTAGGGAAGGGCTAGC
14	281	55	ACCTGGGCCCCAGCCACAG	GAGGCAAGGCTATGGGGGTC
15-16	384	55	CTCTCCTTTTGTCTCGGGGCT	GGGTGAGCATGAGGGTTGGC
17	263	54	CTGGGACCTGAGGATGTGGG	GGTGGGTGGGTGGCAAGTG
18	310	60	GTTCCAGAAGCACGGGGCA	GTGGGGTGGGGGCTGAGG

<b>Exon</b>	<b>Size (bp)</b>	<b>Ta (°C)</b>	<b>Forward primer sequence (5'&gt;3')</b>	<b>Reverse primer sequence (5'&gt;3')</b>
19	335	58	GGATTCACGCCACACCCACA	TCTGCCTCTCTGTCCACCTGTC
20-21	355	58	CTGGGGTATCTGGCAAGGCC	GCGGGAAAGTGAGCAGAACC
22	383	58	TGACCTGTGCTCCTCCTGGCTCT	CTCTGCTGATTCTTCCACCC
23	228	55	GGCAAGGTGGGCAGTGTGG	TGAAAGACAAACGATCCTCCTCC
24	281	54	TCCTGGGGTCTGACTTGGA	CTGAATGAGCGAACGGATG
25	227	55	GCAACGTTACTCAAGGCCCTG	CCACCTTCCCTCGGATCTGTT
26	310	56	AACAGATCCGAGGGAAGGTGG	TTTTTAACTGGGGAGGGGGC
27	310	55	GATCTCCAGCTTCCCCAGGC	GGTGTCCCTCAACTTTCGGCAA
28	300	56	ATCAGAGGAGTGGGCAGTGGG	CAAGGGCCTGGGGTGTCAAT
29	228	54	AGCTCTCTGGGCCTTGTCTCAA	TATAGCCTCTCTCCCCTGGGG
30	274	54	TGGAGTGATCCAGGTTCAGGGT	GAAACAAGGGGGCTCAAGGAG
31	274	68	TGGTTGGCAGGGGTGGGGTGG	GCCTAGGCAGGGTGCACGTGGG
32	325	56	GACCCCTCACCTCCCTCTGCTG	AGCCCTGGTTGGAAGAATGAG
33	267	59	TGGGAACAGGGAGAGGGGCC	GCTCAACGTCGGGGCCTGTG
34	345	55	GATGTGTCTCCCTGGGTCCCTG	GAGGACAACGGAGCAAAGCCC
35	237	58	TGGAGGTGCGAGGTGAGG	TGGCCATCCCCAGGAGC

*The names of the primers refer to the exon(s) of MYBPC3 that they amplify, numbering according to Niimuta et al., 1998. All primer sequences obtained from Carrier et al., (1997). Size (bp) = size of the PCR-amplified fragment produced by primer pairs in base pairs; Ta = annealing temperature used for primer pairs in PCR reactions.*

**Table II.2. MYBPC3 RT-PCR primer sequences**

Name	Sequence 5'>3'	Tm	Reference
275F	ATT GCT GGC TCC TCC AAG GTC AAG T	65°C	Watkins et al., 1995a
301F	TCG ACC TCA AGG TCA TAG AGG CAG	64°C	Watkins et al., 1995a
960R	CCC TCG GGG TCC GGA AAC TGT CTC T	70°C	Watkins et al., 1995a
985R	TCT GCT GGT GCC TCC AGC TTC GAG T	68°C	Watkins et al., 1995a
588F	CCG CCT GTG GTC AAG TGG TT	56°C	Carrier et al., 1997
648F	CAC CTG CAG CTG CAC GAC AG	57°C	Carrier et al., 1997
882R	TGA TCC GCC GAC CAC CTC C	60°C	Carrier et al., 1997
1994R	TGT CGG GCA CCA GCT CTT T	57°C	Carrier et al., 1997

Primers were named according to the number of the nucleotide at their 5'-end in GenBank (<http://www.ncbi.nlm.nih.gov/Entrez>, sequence accession number: NM\_000256). Tm = melting temperature.

#### II.6.1.4. Y2H insert screening primers

In order to facilitate the amplification of inserts cloned into Y2H cloning vectors (sections II.6.5 and II.6.6), primers were designed to vector-specific sequences flanking the multiple cloning sites (MCS) of the pGBK-T7, pGAD-T7, pAS2.1 and pACT2 Y2H cloning vectors (section II.12.1). The specific target sequences to which these primers were designed were obtained from the Clontech<sup>TM</sup> Matchmaker<sup>TM</sup> vector handbook (available at: [www.clontech.com](http://www.clontech.com)) (table II.4). As these primer sets were periodically used in bacterial and yeast colony PCR-reactions (sections II.6.5 and II.6.6), which often generate non-specific, or weak PCR-amplified products, internal (nested) primer sets were also designed in some cases, thus facilitating nested PCR reactions (section II.6.7) (table II.4).

**Table II.3. Primer sequences used in PCR amplification of target sequences encoding protein domains/regions used in Y2H assays**

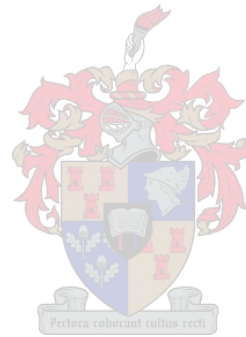
Name	Sequence 5'>3'
MyBPC C0 F <sup>NdeI</sup>	ATC GAA CAT ATG ATG CCT GAG CCG GGG AAG
MyBPC C0 R <sup>EcoRI</sup>	ACT GCA GAA TTC <u>CTA</u> GGG CTC TGC CTT CTC TGC
MyBPC C1 F <sup>NdeI</sup>	ACT GCA GAA CAT ATG CCC ATT GGC CTC TTC GTG A
MyBPC C1 R <sup>EcoRI</sup>	ACT GCA GAA TTC <u>CTA</u> CTC GTG GAC AGT GAG ATT GA
MyBPC C2 F <sup>NdeI</sup>	ACT GCA GAA CAT ATG GAT GAG AAG AAG AGC ACA GC
MyBPC C2 R <sup>EcoRI</sup>	ACT GCA GAA TTC <u>CTA</u> GGG CTC TTT CAC AAA GAG CT
MyBPC C3 F <sup>NdeI</sup>	ACT GCA GAA CAT ATG CCT GTG CTC ATC ACG CGC
MyBPC C3 R <sup>EcoRI</sup>	ACT GCA GAA TTC <u>CTA</u> CTT TTC CTG CAC AAT GAG CT
MyBPC C5 F <sup>NcoI</sup>	ACT GCA GAA CCA TGG AAC AGG AAC CTC CCA AGA TCC AC
MyBPC C5 R <sup>EcoRI</sup>	ACT GCA GAA TTC <u>CTA</u> CAC GTC GAT GAC CTT GAC TGT
MyBPC C6 F <sup>SmaI</sup>	ACT GCA GAA CCC GGG ACC AGA CGC ACC TGC GGC CCC CAA
MyBPC C6 R <sup>EcoRI</sup>	ACT GCA GAA TTC <u>CTA</u> GGG ACC GAT AGG CAT GAA GGG CTG GG
MyBPC C7 F <sup>NdeI</sup>	ACT GCA GAA CAT ATG CCC CCC AGC GAA CCC ACC CA
MyBPC C7 R <sup>EcoRI</sup>	ACT GCA GAA TTC <u>CTA</u> GGG CAG CTG AAG CCG TGG CCG GTT
MyBPC C8 F <sup>SmaI</sup>	ACT GCA GAA CCC GGG ACC CAG GCA CCT GCG CCA GAC CAT TCA G
MyBPC C8 R <sup>EcoRI</sup>	ACT GCA GAA TTC <u>CTA</u> CTT GTC AAC AAC CTG CAG CAC CAG CGT
MyBPC C9 F <sup>SmaI</sup>	ACT GCA GAA CCC GGG ACC AAG TCC TCC CCA GGA TCT CCG GG
MyBPC C10 F <sup>SmaI</sup>	ACT GCA GAA CCC GGG ACC AAG CTT CAC CCA GCC CCT GGT GAA C
MyBPC C10 R <sup>EcoRI</sup>	ACT GCA GAA TTC <u>CTA</u> CTG AGG CAC TCG CAC CTC CAG GGG
TTN A43 F <sup>NdeI</sup>	ACT GCA GAA CAT ATG CCG GAG ATT GAT TTG GAT G
TTN A43 R <sup>EcoRI</sup>	ACT GCA GAA TTC <u>CTA</u> AGT ATC TAA TAC TCT GAC ATT TAC G
TTN A109 F <sup>NdeI</sup>	ATC GCA GAA CAT ATG CCA GAA ATA GAA CTC GAT GC
TTN A109 R <sup>EcoRI</sup>	ACT GCA GAA TTC <u>TCA</u> <u>CTC</u> <u>ACT</u> CAT GAG TCA AGA ACT CTG AGC
TTN A112 F <sup>NdeI</sup>	ACT GCA GAA CAT ATG AGA CAA CTT GGA GTG CCA G
TTN A112 R <sup>EcoRI</sup>	ACT GCA GAA TTC <u>TCA</u> <u>CTC</u> <u>ACT</u> CAT CTG TCA AGG ACA ATT ATA GT
TTN A116 F <sup>NdeI</sup>	ACT GCA GAA CAT ATG GAC TCA GTT AGT GAG CCA TC
TTN A116 R <sup>EcoRI</sup>	ACT GCA GAA TTC <u>TCA</u> <u>CTC</u> <u>ACT</u> CAT GCT GGT GGA CCA GGC TAA

Blue lettering = template recognition sequences; green lettering = restriction enzyme recognition sequences; underlined lettering = stop codons.

**Table II.4. Primer sequences used in the amplification of inserts present in Y2H cloning vectors**

<b>Name</b>	<b>Ta (°C)</b>	<b>Forward primer sequence 5'&gt;3'</b>	<b>Reverse primer sequence 5'&gt;3'</b>
pGBK-T7	50	TCA TCG GAA GAG AGT AG	TCA CTT TAA AAT TTG TAT ACA
pGBK-T7 N	51	CAG TTG ACT GTA TCG CCG	AAT TAG CTT GGC TGC AAG C
pGAD-T7	61	CTA TTC GAT GAT GAA GAT ACC CCA CCA AAC C	GTG AAC TTG CGG GGT TTT TCA GTA TCT ACG AAT
pAS2.1	55	TCA TCG GAA AGT AGT AAC	CGT TTT AAA ACC TAA GAG TCA C
pACT2	68	CTA TTC GAT GAT GAA GAT ACC CCA CCA AAC	GTG AAC TTG CGG GGT TTT T CAG TAT CTA CGA
pACT2 N	68	CTG TAT GGC TTA CCC ATA CGA TGT TCC	GCG GGG TTT TTC AGT ATC TAC GAT TCA TAG

*Ta* = annealing temperature



### II.1.6.5. Site-directed mutagenesis primers

In order to facilitate the introduction of the V896M putative HCM-causing mutation into the C7 domain of cMyBPC by PCR-based site-directed mutagenesis (section II.6.8), two overlapping mutagenesis primers were designed from *MYBPC3* mRNA sequences, obtained from GenBank (<http://www.ncbi.nlm.nih.gov/Entrez>, sequence accession number: NM\_000256) (table II.5). These primers were designed to be complementary to each other and to span the mutant nucleotide (g15751a) responsible for the V896M putative HCM-causing mutation. In these primers, the wild type nucleotide (g15751) was replaced by the mutant nucleotide (a15751) (table II.5).

**Table II.5. Primer sequences of site-directed mutagenesis primers**

Name	Sequence 5'>3'	Ta (°C)
CMyBPC C7 <sup>V896M</sup> F	CCA GAG CGC ATG GGA GCA GG	50
CMyBPC C7 <sup>V896M</sup> R	CCT GCT CCC ATG CGC TCT GG	50

*Ta* = annealing temperature

### II.6.2. ROUTINE PCR

To facilitate the screening of *MYBPC3* for the presence HCM-causing mutations by PCR-SSCP and allele-specific restriction enzyme analysis (ASREA), non-radioactive PCR was performed. All 34 protein-encoding exons of *MYBPC3* (exons 2-35) were PCR-amplified using published primer sequences (section II.6.1.1 and table II.1).

In general, 200ng of human genomic DNA was aliquoted into a 0.5ml centrifuge tube (Eppendorf). To this, a cocktail consisting of the following reagents was added:- 160ng of each primer (table II.1),

1.5µl of an equimolar dNTP solution (consisting of 2.5mM each of dATP, dCTP, dTTP and dGTP), (Promega, Madison, WI, USA), 1.5µl of a 50mM MgCl<sub>2</sub> solution (Bioline Ltd, London, UK), 5µl of a 10x NH<sub>4</sub> PCR reaction buffer, supplied by the manufacturer (appendix A) (Bioline Ltd, London, UK), 0.5U BIOTAQ<sup>TM</sup> DNA polymerase (Bioline Ltd, London, UK), 2.5µl formamide (Sigma Chemical Company, St Louis, Missouri, USA) and ddH<sub>2</sub>O to a final volume of 50µl.

Thermal cycling was then performed in a GeneAmp<sup>®</sup> PCR system 9700 (PE Biosystems, Foster City, CA, USA) for 30 cycles. A typical cycling profile consisted of 30s at 94°C, to allow denaturation of the double stranded DNA, 30s at the annealing temperature (T<sub>a</sub>) of the primer pair (2-5°C below the T<sub>m</sub> of the primer with the lower T<sub>m</sub>), to allow annealing of the primers, and 30-45s at 72°C for extension. The specific annealing temperatures are listed in table II.1.

Following amplification, 5µl aliquots of each amplified sample were electrophoresed on 1.5-2% agarose gels to verify the success of the PCR (section II.7.1.1). All PCR-amplified samples were stored at room temperature until further analysis.

### II.6.3. HIGH FIDELITY PCR

High fidelity PCR was used to amplify portions of *MYBPC3* and *TTN* coding sequences. These amplified products were subsequently cloned into Y2H cloning vectors, for use in Y2H assays.

For the amplification of portions of *MYBPC3*, 50ng purified pRcCMV, containing full-length *MYBPC3* copy DNA (cDNA) (a gift from Prof Hugh Watkins, constructed by Dr Zhili Li) was used as template. For the amplification of specific domains of *TTN*, 200ng of human genomic DNA was

used as template. The above-mentioned amount of selected template was aliquoted into a 0.5ml centrifuge tube (Eppendorf). To this, a cocktail mixture consisting of the following reagents was added:- 160ng of each primer (table II.3), 4 $\mu$ l of an equimolar dNTP solution, supplied by the manufacturer (TaKaRa Shuzo Co. Ltd, Shiga, Japan) (consisting of 2.5mM each of dATP, dCTP, dTTP and dGTP), 5 $\mu$ l of 10x Ex Taq<sup>TM</sup> Mg<sup>2+</sup>-containing reaction buffer supplied by the manufacturer (TaKaRa Shuzo Co. Ltd, Shiga, Japan), 1-2.5U of Ex Taq<sup>TM</sup> (TaKaRa Shuzo Co. Ltd, Shiga, Japan) and ddH<sub>2</sub>O to a final volume of 50 $\mu$ l.

Thermal cycling was performed in a GeneAmp<sup>®</sup> PCR system 9700 (PE Biosystems, Foster City, CA, USA) for 30 cycles. A typical cycling profile consisted of 30s at 94°C, to allow denaturation of the double stranded DNA, 30s at 2-5°C below the T<sub>m</sub> of the primer with the lower T<sub>m</sub> (T<sub>a</sub>), to allow annealing of the primers, and 1-4min at 72°C for extension. Primer sequences and specific amplification conditions are listed in tables II.3 and II.6. Following amplification, 5 $\mu$ l aliquots of each amplified sample were electrophoresed on 1.0-1.5% agarose gels to verify the success of the PCR (section II.7.1.1). These PCR-amplified products were subsequently used for cloning into Y2H cloning vectors (section II.12).

#### **II.6.4. RT-PCR**

During the course of this study, several DNA sequence variations, which were postulated to alter RNA splicing, were identified (section III.1.3). In order to investigate whether these sequence variations alter splicing of the *MYBPC3* transcript, RT-PCR was performed. In these RT-PCR reactions, RNA, extracted from either lymphocytes obtained from freshly collected blood samples (section II.4) or from EBV-transformed lymphocytes (section II.5), was used as template. In order to

**Table II.6. Primer-pairs used for the amplification of bait and prey constructs used in Y2H assays**

<b>Insert</b>	<b>Type</b>	<b>Plasmid used</b>	<b>Forward primer</b>	<b>Reverse primer</b>	<b>Ta (°C)</b>
cMyBPC C0	Bait	pAS2.1	MyBPC C0 F <sup>NdeI</sup>	MyBPC C0 R <sup>EcoRI</sup>	65
cMyBPC C0	Bait	pGBKT7	MyBPC C0 F <sup>NdeI</sup>	MyBPC C0 R <sup>EcoRI</sup>	65
cMyBPC C0C1	Bait	pAS2.1	MyBPC C0 F <sup>NdeI</sup>	MyBPC C1 R <sup>EcoRI</sup>	65
cMyBPC C0C1	Bait	pGBKT7	MyBPC C0 F <sup>NdeI</sup>	MyBPC C1 R <sup>EcoRI</sup>	65
cMyBPC C0C2	Bait	pAS2.1	MyBPC C0 F <sup>NdeI</sup>	MyBPC C2 R <sup>EcoRI</sup>	55
cMyBPC C3	Bait	pGBKT7	MyBPC C3 F <sup>NdeI</sup>	MyBPC C3 R <sup>EcoRI</sup>	55
cMyBPC C7	Bait	pGBKT7	MyBPC C7 F <sup>NdeI</sup>	MyBPC C7 R <sup>EcoRI</sup>	65
cMyBPC C7 <sup>V896M</sup>	Bait	pGBKT7	pGBKT7 F	pGBKT7 R	51
TTN A43	Bait	pGBKT7	TTN A43 F <sup>NdeI</sup>	TTN A43 R <sup>EcoRI</sup>	55
cMyBPC C1	Prey	pGADT7	MyBPC C1 F <sup>NdeI</sup>	MyBPC C1 R <sup>EcoRI</sup>	55
cMyBPC C1C2	Prey	pGADT7	MyBPC C1 F <sup>NdeI</sup>	MyBPC C2 R <sup>EcoRI</sup>	55
cMyBPC C2	Prey	pGADT7	MyBPC C2 F <sup>NdeI</sup>	MyBPC C2 R <sup>EcoRI</sup>	55
cMyBPC C5	Prey	pACT2	MyBPC C5 F <sup>NcoI</sup>	MyBPC C5 R <sup>EcoRI</sup>	60
cMyBPC C6	Prey	pACT2	MyBPC C6 F <sup>SmaI</sup>	MyBPC C6 R <sup>EcoRI</sup>	65
cMyBPC C8	Prey	pACT2	MyBPC C8 F <sup>SmaI</sup>	MyBPC C8 R <sup>EcoRI</sup>	65
cMyBPC C8C10	Prey	pACT2	MyBPC C8 F <sup>SmaI</sup>	MyBPC C10 R <sup>EcoRI</sup>	65
cMyBPC C9	Prey	pACT2	MyBPC C9 F <sup>SmaI</sup>	MyBPC C9 R <sup>EcoRI</sup>	65
cMyBPC C9C10	Prey	pACT2	MyBPC C9 F <sup>SmaI</sup>	MyBPC C10 R <sup>EcoRI</sup>	65
cMyBPC C10	Prey	pACT2	MyBPC C10 F <sup>SmaI</sup>	MyBPC C10 R <sup>EcoRI</sup>	65
TTN A43	Prey	pGADT7	TTN A43 F <sup>NdeI</sup>	TTN A43 R <sup>EcoRI</sup>	55
TTN A109	Prey	pGADT7	TTN A109 F <sup>NdeI</sup>	TTN A109 R <sup>EcoRI</sup>	55
TTN A109A112	Prey	pGADT7	TTN A109 F <sup>NdeI</sup>	TTN A112 R <sup>EcoRI</sup>	55
TTN A112	Prey	pGADT7	TTN A112 F <sup>NdeI</sup>	TTN A112 R <sup>EcoRI</sup>	55
TTN A116	Prey	pGADT7	TTN A116 F <sup>NdeI</sup>	TTN A116 R <sup>EcoRI</sup>	55

*Ta* = annealing temperature; *Type* = type of Y2H construct (either bait or prey).

minimise RNase contamination of samples, all workbench surfaces, pipettes and apparatus used, were treated with RNase Erase (ICD Biochemicals, Aurora, Ohio, USA). Furthermore, all pipette tips and centrifuge tubes used in either the preparation of RNA samples, or first-strand cDNA synthesis, were rinsed with a 0.2% DEPC (Sigma, St Louis, Missouri, USA) (appendix A) solution, prior to being autoclaved.

#### **II.6.4.1. First-strand cDNA synthesis**

First-strand cDNA synthesis was performed using the Promega Reverse Transcription System (Promega, Madison, WI, USA), with minor adjustments to the manufacturer's protocol. In short, 0.5µg of random hexanucleotide primers (Promega, Madison, WI, USA) was added to 100–200ng of total RNA and the volume adjusted to 10µl by adding nuclease-free H<sub>2</sub>O. This mixture was then incubated for 5min at 70°C and snap cooled on ice for 5min. Following this incubation step, 10µl of a reaction mixture, consisting of 4µl 25mM MgCl<sub>2</sub> (Promega, Madison, WI, USA), 2µl of 10x reverse transcription buffer (Promega, Madison, WI, USA), 2µl of a 10mM dNTP mixture (Promega, Madison, WI, USA), 0.5µl recombinant RNasin<sup>®</sup> ribonuclease inhibitor (Promega, Madison, WI, USA), 15U AMV reverse transcriptase (Promega, Madison, WI, USA) and nuclease-free H<sub>2</sub>O to a final volume of 20µl, was added to the sample. This mixture was subsequently incubated for 1h at 42°C, 5min at 95°C and 5 min at 4°C. All incubations were performed in a Techne Genius PCR machine (Techne Ltd., Cambridge, UK). Aliquots of the first strand cDNA product were subsequently used for PCR amplification or frozen at -20°C for future use.

### II.6.4.2. PCR Amplification of *MYBPC3* cDNA

In order to PCR amplify specific portions of the *MYBPC3* transcript, nested PCR was performed (section II.6.7). The sequences of the primers used for these reactions, their annealing temperatures, and the combinations in which they were used, are summarised in tables II.2 and II.7.

In short, 2 $\mu$ l of first strand cDNA (section II.6.4.1) was added to 48 $\mu$ l of a reaction mixture consisting of:- 5 $\mu$ l GeneAmp<sup>®</sup> 10x PCR buffer (Perkin Elmer, manufactured by Roche Molecular Systems Inc, Branchburg, NJ, USA), 1.1 $\mu$ l of a 10mM dNTP stock solution (Promega, Madison, WI, USA), 10pmol of each primer (tables II.2 and II.7), 0.5 $\mu$ l of AmpliTaq Gold<sup>™</sup> (Perkin Elmer, manufactured by Roche Molecular Systems Inc, Branchburg, NJ, USA) and ddH<sub>2</sub>O to a final volume of 48 $\mu$ l.

Thermal cycling was performed in a Techne Genius PCR machine (Techne Ltd., Cambridge, UK) for 30 cycles. A typical cycling profile consisted of 30s at 94°C, to allow denaturation of the double stranded DNA, 30s at the *T<sub>a</sub>* of the primer set, to allow annealing of the primers, and 1-4min at 72°C for extension. Primer sequences and specific amplification conditions are listed in tables II.2 and II.7. Following amplification, 5 $\mu$ l aliquots of each RT-PCR product were electrophoresed and visualised on 1.5-2.5% agarose gels (section II.7.1.1).

**Table II.7. RT-PCR primer pairs used**

SNS investigated	Type PCR	F primer	R primer	<i>T<sub>a</sub></i> (°C)
c2646t	Outer Rn	275F	985R	60
c4154t	Nested Rn	301F	960R	62
g4177a	Outer Rn	588F	1994R	55
	Nested Rn	648F	882R	55

*Rn* = reaction; *SNS* = single nucleotide substitution; *T<sub>a</sub>* = annealing temperature

## II.6.5. BACTERIAL COLONY PCR

For rapid identification of *E.coli* colonies harbouring the desired recombinant plasmid, to be used in Y2H assays, the presence of the insert was verified by performing bacterial colony PCR.

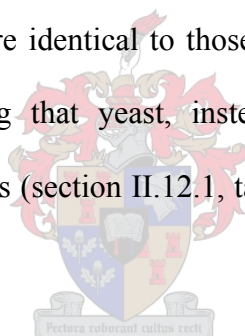
In these PCR reactions, 160ng of Y2H vector-specific primers (table II.4), was added to PCR reaction-mixtures that were identical to those used for routine PCR (section II.6.2). The DNA template, used in routine PCR was, however, substituted by individual bacterial colonies, picked directly from the LB-agar plates containing the appropriate antibiotics (section II.12 and appendix A). In each set of bacterial colony PCR reactions, a positive control, consisting of an appropriate non-recombinant plasmid, and a negative control, consisting of a water blank, were concurrently set up to correctly ascertain which colonies harboured the insert, as well as to monitor contamination.

Thermal cycling was performed in a GeneAmp<sup>®</sup> PCR system 9700 (PE Biosystems, Foster City, CA, USA). The cycling profile generally consisted of a single denaturing step of 7min at 94°C, followed by 30 cycles of a 30s denaturation step at 94°C, a 30s primer-annealing step at the  $T_a$  of the primer set (table II.4), and an extension step at 72°C. The length of the extension step was adjusted according to the expected insert size and varied between 30s and 4min (30s for fragments <1kb and up to 4min for fragments >3kb). PCR-amplified products were subsequently visualised on 1-2% agarose gels (section II.7.1.1). When colony PCR yielded weak or non-specific products, nested PCR reactions (section II.6.7) were performed, in which the nested vector-specific primers (table II.4) were used in a second round of PCR-amplification.

Following the identification of colonies harbouring the correct insert size by agarose gel-electrophoresis, the identity of the insert was confirmed by a second colony PCR reaction. The same basic protocol was followed as described above, but in these reactions, vector-specific primer sets were substituted by appropriate insert-specific primer sets and the annealing temperature adjusted accordingly (table II.6).

### **II.6.6. YEAST COLONY PCR**

In order to enable the restriction mapping of interactor prey-inserts, obtained from Y2H cDNA library-assays (section II.16.2), yeast colony PCR was performed. All reaction-mixtures, primer sets, cycling profiles and apparatus used were identical to those used for bacterial colony PCR (section II.6.5), with the only exception being that yeast, instead of bacterial colonies, picked from appropriate selective dropout (SD) plates (section II.12.1, table II.10 and appendix A), were used as template.



### **II.6.7. NESTED PCR**

Nested PCR reactions were used to increase the specificity and sensitivity of cDNA synthesis (section II.6.4.2) and bacterial/yeast colony PCR (sections II.6.5 and II.6.6). With the exception of external (outer) primers being substituted by 160ng of each internal (nested) primer, reaction mixtures used for nested PCR were identical to those used for the first round of PCR amplification (sections II.6.4.2; II.6.5; II.6.6 and tables II.2; II.4). To these reaction mixtures, 0.5µl of first round PCR products were added as template. The apparatus used, and cycling profiles of nested PCR

reactions, were identical to those used in the first round of PCR amplification, with the exception of the Ta that was adjusted according to the specific nested primer set used (tables II.2 and II.4).

#### II.6.8. SITE-DIRECTED MUTAGENESIS PCR

*In vitro* site-directed mutagenesis PCR was used to introduce the V896M putative HCM-causing mutation into the C7 domain of cMyBPC. Two complimentary mutagenesis primers, into which the g15751a mutation responsible for V896M was introduced (cMyBPC C7<sup>V896M</sup> F and cMyBPC C7<sup>V896M</sup> R) (section II.6.1.5; table II.5), were used in conjunction with the pGBKT7 R and pGBKT7 F primers (table II.4), respectively, in two separate high-fidelity PCR reactions (section II.6.3). In both these PCR-reactions, 50ng of pGBKT7-C7 bait construct was used as template (figure II.4). Thermal cycling was performed in a GeneAmp<sup>®</sup> PCR system 9700 (PE Biosystems, Foster City, CA, USA) for 30 cycles with cycling profiles consisting of 30s at 94°C, to allow denaturation of the double stranded DNA, 30s at 50°C, to allow annealing of the primers, and 1min at 72°C for extension. The two PCR-amplified products thus generated were subsequently visualised on, and excised from, a 2% agarose gel (section II.7.1.1) (figure II.4).

Following gel-purification of these PCR-amplified products (section II.4.6), a 10µl aliquot of each product was added to a reaction mixture consisting of:- 4µl of an equimolar dNTP solution (TaKaRa Shuzo Co. Ltd, Shiga, Japan) (consisting of 2.5mM each of dATP, dCTP, dTTP and dGTP), 5µl of 10x Ex Taq<sup>™</sup> Mg<sup>2+</sup>-containing reaction buffer (TaKaRa Shuzo Co. Ltd, Shiga, Japan), 2.5U of Ex Taq<sup>™</sup> (TaKaRa Shuzo Co. Ltd, Shiga, Japan) and ddH<sub>2</sub>O to a final volume of 50µl. This mixture was subjected to 10 cycles of thermal cycling identical to that described above (figure II.4). Following thermal cycling, 160ng of each of the pGBKT7 F and pGBKT7 R primers was added to

the reaction mixture, which was subjected to a further 10 cycles of thermal cycling identical to that described above (figure II.4). The full-length mutagenesis PCR product thus obtained, was subsequently gel purified from a 2% agarose gel (sections II.7.1.2 and II.4.6), prior to it being cloned into the pGBKT7 Y2H bait-vector (section II.12).

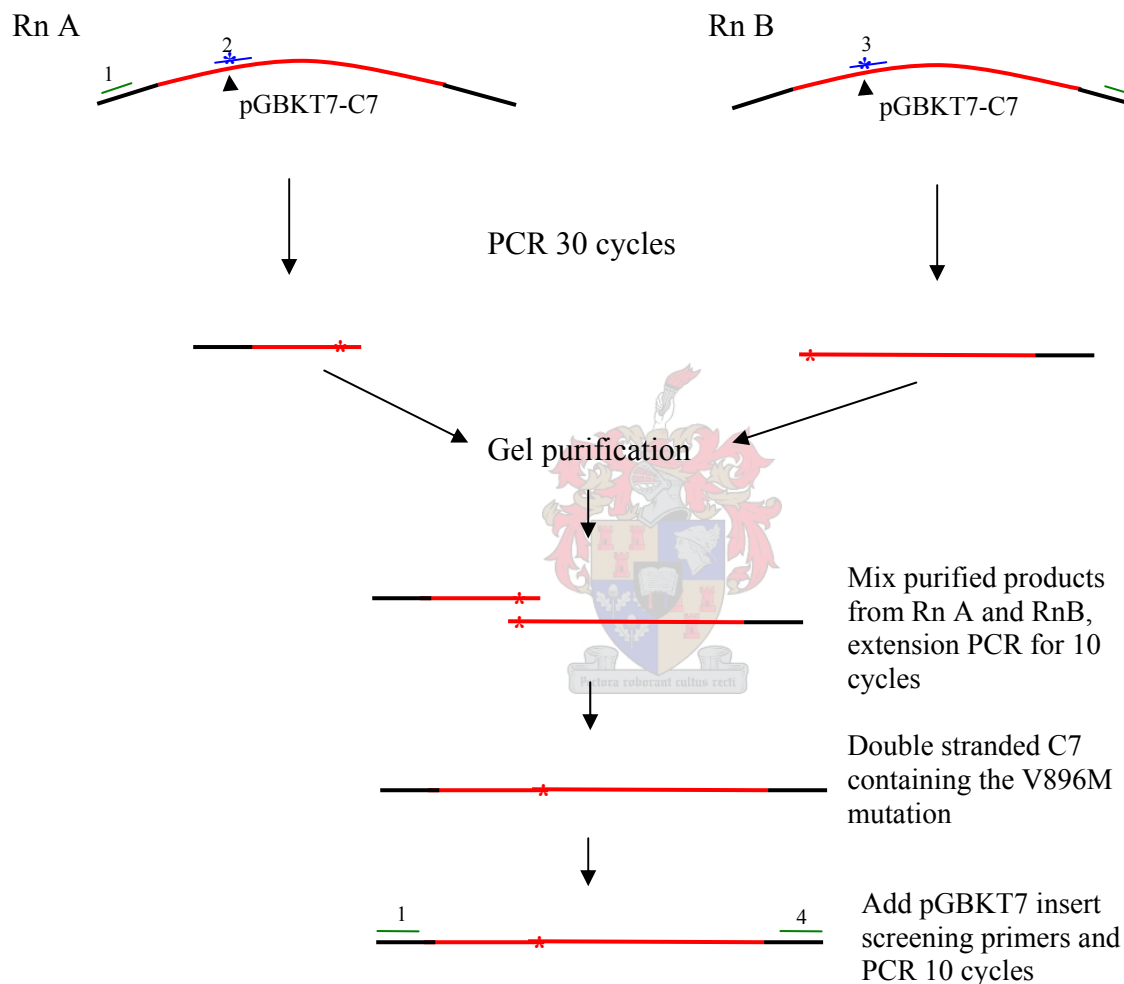


**Figure II.4. Site-directed mutagenesis PCR**

1 = pGBKT7 F primer; 2 = cMyBPC C7<sup>V896M</sup> R primer; 3 = cMyBPC C7<sup>V896M</sup> F primer; 4 = pGBKT7 R primer; Rn = reaction

## II.7. GEL-ELECTROPHORESIS

### II.7.1. AGAROSE GEL-ELECTROPHORESIS

Agarose gel-electrophoresis was used to verify the success of PCR amplification (section II.6), the gel-purification of PCR amplification products (section II.4.6) and the visualisation of plasmids purified from *E.coli* (section II.4.7).

#### II.7.1.1. Agarose gel-electrophoresis for the visualisation of PCR-amplified products

The success of PCR and RT-PCR amplifications was verified by electrophoresis as follows: 5µl of each amplification product was mixed with 1µl of bromophenol blue loading dye (appendix A). This mixture was subsequently electrophoresed in a 1.4-2% (depending on the size of the amplified fragment) horizontal agarose gel, of either 15x9x1cm or 7x9x1cm dimensions, containing 1µg/ml ethidium bromide and 1x TBE buffer (appendix A). The molecular size marker, co-electrophoresed with all PCR-amplified products, was either bacteriophage λ DNA, digested with the *Pst*I restriction enzyme (Promega, Madison, WI, USA) (λPst) (appendix A), Promega 100bp marker (Promega, Madison, WI, USA), or Roche molecular size marker VII (Roche Biochemical, Basel, Switzerland). Electrophoresis typically occurred at 10V/cm for 20min in 1x TBE running buffer (appendix A).

The DNA fragments were subsequently visualised on a long wave 3UV transilluminator (UVP, Inc. Upland, CA, USA). Photographic records were obtained using an ITC polaroid camera and Sony video-graphic printer.

### **II.7.1.2. Agarose gel-electrophoresis for the gel-purification of PCR-amplified products**

In order to facilitate the gel-purification of PCR-amplified fragments, these fragments were electrophoresed and excised from agarose gels. Agarose gels were identical to those used for the visualisation of PCR-amplified fragments (section II.7.1.1). In this case, however, 5 $\mu$ l of bromophenol blue loading dye (appendix A) was mixed with 45 $\mu$ l of PCR-amplified product. Electrophoresis typically occurred at 10V/cm for 30-60min in 1x TBE running buffer (appendix A). Following electrophoresis, PCR-amplified fragments were visualised on a long wave 3UV transilluminator (UVP, Inc. Upland, CA, USA) and the relevant DNA bands excised from the gel, using a sterile surgical blade, for subsequent gel-purification (section II.4.6).

### **II.7.1.3. Agarose gel-electrophoresis for the visualisation of plasmids purified from *E.coli***

Plasmids purified from *E.coli* were visualised by electrophoresis on agarose gels as follows: 1-5 $\mu$ l of purified plasmid was mixed with 1 $\mu$ l of bromophenol blue loading dye (appendix A). This mixture was subsequently electrophoresed in a 1% horizontal agarose gel, of 7x9x1cm dimensions, containing 1 $\mu$ g/ml ethidium bromide and 1x TAE buffer (appendix A).  $\lambda$ Pst (appendix A) was co-electrophoresed with purified plasmids as a molecular size marker. Electrophoresis typically occurred at 6V/cm for 45-60min in 1x TAE running buffer (appendix A).

The purified plasmids were subsequently visualised on a long wave 3UV transilluminator (UVP, Inc. Upland, CA, USA). Photographic records were obtained using an ITC polaroid camera and Sony video-graphic printer.

## II.7.2. NON-DENATURING POLYACRYLAMIDE GEL-ELECTROPHORESIS

Polyacrylamide gel-electrophoresis was used to visualise restriction enzyme digested PCR-amplified products (sections II.11.1 and II.11.3). Typically, 5-10 $\mu$ l of digested PCR product was mixed with 1 $\mu$ l of bromophenol blue loading dye (appendix A). This mixture was loaded into a polyacrylamide gel, of 100x80x1mm dimensions, containing 12% acrylamide and 1x TBE buffer (appendix A). In all cases either  $\lambda$ Pst marker (appendix A), or Promega 100bp marker (Promega, Madison, WI, USA), and an undigested sample were co-electrophoresed as controls. Electrophoresis was performed in 1x TBE running buffer (appendix A) at 15V/cm for 1-2 hours, following which fragments were visualised by silver staining (section II.9).

## II.8. SINGLE-STRAND CONFORMATIONAL POLYMORPHISM (SSCP)

In order to investigate specific exons of *MYBPC3* for the presence of nucleotide sequence variations, PCR-SSCP analysis was performed on PCR-amplified fragments of these exons (section II.6.2). A 5 $\mu$ l aliquot of each PCR-amplified product was mixed with an equal volume of standard SSCP-loading dye (appendix A). These mixtures were then heat-denatured at 95°C for 2min, before being loaded directly onto SSCP-gels (appendix A). Control samples that were co-electrophoresed included a non-denatured sample as control for the electrophoretic mobility of the double-stranded DNA, an amplified fragment from an unaffected individual as a negative control, and a 5 $\mu$ l aliquot of undenatured  $\lambda$ Pst (appendix A).

SSCP gels were of 400x300x1mm dimensions and were covalently bound to GelBond<sup>®</sup> PAG film during polymerisation (BMA, Rockland, ME, USA), to facilitate subsequent silver staining (section

II.9). SSCP analysis involved electrophoresis of PCR-amplified products on two gel media, namely an 8% and a 10% mildly-denaturing gel (appendix A). Electrophoresis was performed at 25W constant power for 16-18 hours at 4°C, with 0.5x TBE (appendix A) as running buffer, in all cases.

Following electrophoresis, gels were silver stained (section II.9) and air-dried for 4-6 hours, after which the gels were sealed in plastic bags and kept as permanent records. Samples in which mobility shifts were detected were re-amplified (section II.6.2), and re-analysed under similar SSCP conditions to distinguish false positives. Samples in which mobility shifts proved to be reproducible were directly sequenced (section II.10) to identify the nucleotide sequence variations.

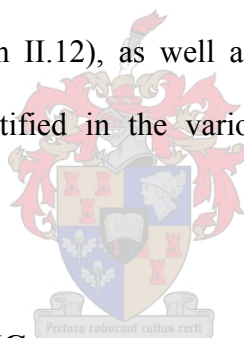
## **I.9. SILVER STAINING OF POLYACRYLAMIDE GELS**

Silver staining was used to visualise DNA fragments on polyacrylamide gels (sections II.7.2 and II.8), and was performed in a manner modified from Bassan (1991). Following the removal of polyacrylamide-gels from the glass plates, these gels were immersed in a solution of 0.1% AgNO<sub>3</sub> (appendix A) and agitated for 10min on a Labcon orbital shaker (Labcon Pty Ltd, Maraisburg, RSA). Thereafter, gels were rinsed thoroughly with ddH<sub>2</sub>O before being agitated in a developing solution (appendix A) until stained DNA bands appeared. Gels were again rinsed thoroughly in ddH<sub>2</sub>O and either air-dried or photographed to obtain permanent records.

## II.10. DNA SEQUENCING

Direct cycle sequencing of gel-purified PCR-amplified products (section II.4.6) was used to detect nucleotide sequence variations, responsible for alterations in the electrophoretic mobility of single stranded conformers detected by PCR-SSCP analysis. For the sequencing of PCR-amplified products, both manual (section II.10.1) and automated (II.10.2) DNA sequencing were used. The direct sequencing of PCR-amplified products allowed the simultaneous detection of both alleles at a locus, so that homozygosity and heterozygosity could be verified in any sample.

Automated cycle sequencing (section II.10.2) was also used to obtain the nucleotide sequence of all constructs used in Y2H assays (section II.12), as well as to obtain the nucleotide sequences of specific interactor prey-plasmids, identified in the various Y2H cDNA library-assays (section II.16.2).



### II.10.1. MANUAL DNA SEQUENCING

Two to five microlitres of gel-purified PCR product (section II.4.6) was sequenced bi-directionally using the *fmol*<sup>TM</sup> Cycle Sequencing Kit (Promega, Madison, WI, USA), with some modifications to the manufacturer's protocol. Specifically, the sequencing reaction mixture contained 2-5 $\mu$ l gel-purified PCR product as template, 5 $\mu$ l of the supplied sequencing buffer, 6pmol of the appropriate PCR amplification primer (table II.1), 0.5 $\mu$ l of [ $\alpha^{32}$ P]-dCTP (Amersham International plc, Little Chalfont, Buckinghamshire, UK), 0.8 $\mu$ l of DMSO (Sigma, St Louis, MO, USA), ddH<sub>2</sub>O to a final volume of 16 $\mu$ l and 5U of sequencing grade *Taq* polymerase (Promega, Madison, WI, USA). Four microlitres of this mixture was added to four previously prepared, prechilled 500 $\mu$ l Eppendorf tubes,

each containing 2 $\mu$ l of a cocktail comprised of all four deoxynucleotides, as well as a specific dideoxynucleotide, ddATP, ddCTP, ddTTP or ddGTP, as supplied by the manufacturer (Promega, Madison, WI, USA). Samples were subsequently overlaid with 20 $\mu$ l of mineral oil to prevent evaporation during thermal cycling.

Tubes were placed in a Techne GeneE (Techne Ltd., Cambridge, UK) thermal cycler, preheated to 94°C, in which they were incubated, at 94°C, for 5min, prior to 30 cycles of thermal cycling, using the same temperature profile as in the original PCR amplification reaction (table II.1). Following completion of thermal cycling, 4 $\mu$ l of the supplied stop solution (Promega, Madison, WI, USA) was added to each sample.

These samples were subsequently heat-denatured at 95°C for 2min, and a 4 $\mu$ l aliquot of each sample loaded on a 5% denaturing polyacrylamide gel (of 300x400x0.4mm dimensions, containing 44% (w/v) urea and 1x TBE) (appendix A) that was mounted on an electrophoresis apparatus and subjected to 1800V for about 60min prior to loading of samples (appendix A). Electrophoresis typically took place in 0.5x TBE (appendix A) running buffer at 1800V. Shorter fragments (up to 200bp in length) were electrophoresed until the bromophenol blue of the loading dye had migrated to the bottom of the gel. In order to obtain full-length nucleotide sequences of fragments larger than 200bp, electrophoresis was interrupted once the bromophenol blue loading dye had migrated to the bottom of the gel. At this time, a second set of heat-denatured 4 $\mu$ l aliquots of each sample was loaded into separate wells. Electrophoresis was then continued at 1800V till the bromophenol blue loading dye co-migrating with these newly loaded samples had reached the bottom of the gel.

After completion of electrophoresis, gels were dismantled and transferred onto Whatman™ 3MM Chromatography paper (Whatman International Ltd, Madstone, England, UK). The gels were then dried under vacuum (Slab gel drier, model SE 1160, Hoeffer Scientific Instr, San Francisco, CA, USA) for 1 hour and exposed to Cronex 4 X-ray film (Protea Medical Supplies, Cape Town, RSA) for 6 hours to overnight.

## **II.10.2. AUTOMATED DNA SEQUENCING**

Automated DNA sequencing of cloned inserts (section II.12) and PCR-amplified fragments (section II.6) was performed at the Core Sequencing Facility of the Department of Genetics, University of Stellenbosch, RSA, using either an ABI Prism™ 377 or an ABI Prism™ 3100 automated sequencer (PE Applied Biosystems, Foster City, CA, USA). The primers used in these sequencing reactions were identical to those used in the initial PCR reactions, in cases where PCR-amplified products were sequenced (table II.1), or vector specific primers, in cases where Y2H constructs were sequenced (table II.4)

## **II.10.3. DNA SEQUENCE ANALYSIS**

### **II.10.3.1. Sequence analysis of specific exons of *MYBPC3***

Sequences were either read manually, when manual cycle sequencing was performed (section II.10.1), or with the help of the Chromas 1.6 computer program (Technelysium Pty Ltd, Helensvale, Queensland, Australia), when automated DNA sequencing was performed (section II.10.2). To facilitate the detection of mutations and polymorphisms occurring in exons of *MYBPC3*, nucleotide

sequences were manually compared to the wild type *MYBPC3* sequence, obtained from the GenBank database (<http://www.ncbi.nlm.nih.gov/Entrez>, sequence accession number: Y10129). Where nucleotide sequence variations were identified, the DNAMAN version 4.0 sequence analysis program (Lynnion BioSoft Corp) was used to generate restriction enzyme maps of both the wild type and variant DNA sequences, in order to ascertain whether the sequence variants modified restriction enzyme recognition sites. If that were the case, ASREA (section II.11.1) was used to confirm sequencing results. Where nucleotide sequence variants did not alter any restriction enzyme recognition sites, these variants were to be considered confirmed only if the variant sequence was clearly visible in both sequencing directions, or was reproducible in a subsequent sequencing reaction from a fresh PCR product.

Confirmed nucleotide variants were further analysed, in order to predict whether they would affect the amino acid sequence of cMyBPC, or whether they may affect splicing of the *MYBPC3* transcript. Putative splicing mutations were identified by either comparing the nucleotide sequence surrounding the single nucleotide substitution (SNS) to splice acceptor site (SaS), splice donor site (SdS) and splice branch point (SbP) consensus sequences (Box 1), or by computational analysis performed by Dr Peter Rogan (University of Missouri-Kansas City School of Medicine, Kansas City, MO, USA). Computational analysis involved the use of the Scan, MakeWalker, DNAPlot and Lister programs (personal communication, Dr Peter Rogan, 23 December 1999; Rogan et al., 1998).

Nucleotide variations thus predicted to alter the cMyBPC protein, by either altering the amino acid sequence of cMyBPC, or predicted to result in the truncation of the protein, were classified as putative HCM-causing mutations. In these cases, ASREA- (when available) or SSCP-based tests (used in cases where nucleotide sequence variants did not alter restriction enzyme recognition sites)

were used to screen at least 100 unrelated control individuals of the same ethnicity as the proband, to ascertain whether the allele is present in the general population.

Nucleotide variations postulated to cause aberrant splicing of the *MYBPC3* transcript were further analysed by RT-PCR techniques (section II.6.4). Thus, DNA sequence variants were considered to be HCM-causing when they had an effect on the amino acid sequence of cMyBPC at conserved amino acid positions, or caused aberrant splicing of the *MYBPC3* transcript, segregated with the disease in HCM-affected individuals and their family members, and were absent from 100 control individuals. Sequence variations found, that did not meet these criteria (when ascertainable), were not pursued.

#### **II.10.3.2. Sequence analysis of Y2H constructs**

Automated DNA-sequencing was used to test the integrity of all constructs used in Y2H assays (section II.12). These sequences were read, using the Chromas 1.6 computer program (Technelysium Pty Ltd, Helensvale, Queensland, Australia), and compared to wild-type sequences obtained from the GenBank database (<http://www.ncbi.nlm.nih.gov/Entrez>), in order to establish whether both the reading-frame and the nucleotide sequence of the specific bait- and prey-inserts were maintained during the cloning process.

#### **II.10.3.3. Sequence analysis of Y2H interactor prey constructs**

The nucleotide sequences of the inserts of prey constructs found to encode peptides that interacted with baits in Y2H library-assays (interactor preys) (section II.16.2) were also determined by automated DNA-sequencing. These sequences were read using the Chromas 1.6 computer program (Technelysium Pty Ltd, Helensvale, Queensland, Australia), and the protein products which they

encode identified using the BLASTX and BLASTP algorithms available from NCBI (<http://www.ncbi.nlm.nih.gov/Blast>).

## **II.11. RESTRICTION ENZYME DIGESTION**

### **II.11.1. ALLELE-SPECIFIC RESTRICTION ENZYME ANALYSIS (ASREA)**

ASREA was used to confirm the presence of sequence variations identified by DNA sequencing (section II.10). Generally, 5 $\mu$ l of a PCR-amplified product was added to a cocktail containing 1-3U of the relevant enzyme (table II.8) in the appropriate buffer supplied by the manufacturer, in a total volume of 15 $\mu$ l. These samples were then incubated for 2h to overnight at the optimal temperature for the particular enzyme (table II.8).

Half of this reaction mixture was subsequently mixed with 1 $\mu$ l of bromophenol blue loading dye (appendix A) prior to polyacrylamide gel electrophoresis (section II.7.2). In all cases either,  $\lambda$ Pst marker (appendix A), or Promega 100bp marker (Promega, Madison, WI, USA), and an aliquot of the undigested PCR-amplified sample were co-electrophoresed as controls. Following electrophoresis, fragments were visualised by silver staining (section II.9).

### **II.11.2. RESTRICTION ENZYME DIGESTION FOR CLONING**

In order to facilitate the cloning of constructs to be used in Y2H assays, both Y2H cloning vectors and the PCR-products to be cloned were sequentially double-digested with appropriate restriction enzymes (table II.8). Generally, 30 $\mu$ l of either the PCR-amplified product to be cloned, or the specific Y2H cloning vector to be used (table II.9), were added to a cocktail containing 10-30U of the relevant restriction enzyme (table II.8), in the appropriate buffer supplied by the manufacturer, in

a total volume of 45µl. These samples were subsequently incubated for 3h at 37°C. Following this incubation period, the restriction enzyme was heat-inactivated by incubation at 60°C for 15min, after which the digested DNA was purified, by either DNA precipitation (section II.4.3) or gel-purification (section II.4.6), prior to digestion with the second restriction enzyme, which was performed as described above. The double-digested DNA samples were then once again purified by either DNA precipitation (section II.4.3), or gel-purification (section II.4.6). Double-digested Y2H cloning vectors were subsequently treated with calf intestinal alkaline phosphatase (CIP) (section II.12.2) and purified by DNA precipitation (section II.4.3), prior to being used in ligation reactions, while double-digested PCR-amplified products were used directly in ligation reactions (section II.12.3).

### II.11.3. RESTRICTION MAPPING OF Y2H LIBRARY PREY-INSERTS

In order to allow the grouping of identical prey-plasmids, identified by Y2H library-assays as interacting with a specific bait, prey-inserts of interactor colonies were PCR-amplified by yeast colony PCR (section II.6.6) and the PCR-products digested with *HaeIII* restriction enzyme (Promega, Madison, WI, USA). Generally, 5µl of the yeast colony PCR-amplified product was added to a cocktail containing 1-3U of *HaeIII* (Promega, Madison, WI, USA) in the appropriate buffer supplied by the manufacturer, in a total volume of 15µl. These samples were then incubated for 3h at 37°C. Following digestion, polyacrylamide gel-electrophoresis and silver staining were used to visualise restriction enzyme digested PCR-amplified products (sections II.7.2 and II.9). Prey-inserts displaying identical *HaeIII* digestion patterns were additionally digested with *RsaI* (Promega, Madison, WI, USA) in a separate reaction, as described above. Prey-inserts displaying identical *HaeIII* and *RsaI* restriction patterns, were considered to be identical and only a representative prey clone used in subsequent Y2H assays (section II.16).

**Table II.8. Restriction enzymes used**

<b>RE</b>	<b>Application</b>	<b>Substrate</b>	<b>Supplier</b>
<i>AvaI</i>	ASREA of c8612t	PCR-amplified product	Roche Applied Science, Roche Biochemical, Basel, Switzerland
<i>AluI</i>	ASREA of a18443g and g19706a	PCR-amplified product	Promega, Madison, WI, USA
<i>BstEII</i>	Verification of aberrant splicing	RT-PCR-amplified product	Promega, Madison, WI, USA
<i>EcoRI</i>	Cloning	PCR-amplified product and Y2H bait- and prey-plasmids	Promega, Madison, WI, USA
<i>HaeIII</i>	Restriction mapping of interactor prey-inserts	Yeast colony PCR-amplified product	Promega, Madison, WI, USA
<i>HhaI</i>	ASREA of g2785a	PCR-amplified product	Amersham, Little Chalfont, Buckinghamshire, UK
<i>HphI</i>	ASREA of t2510c and c2646t	PCR-amplified product	New England Biolabs, Beverly, MA, USA
<i>MnII</i>	ASREA of g5047a	PCR-amplified product	New England Biolabs, Beverly, MA, USA
<i>NcoI</i>	Cloning	PCR-amplified product and Y2H bait-plasmids	Promega, Madison, WI, USA
<i>NdeI</i>	Cloning	PCR-amplified product and Y2H bait-plasmids	Promega, Madison, WI, USA
<i>NlaIII</i>	ASREA of g2626a, g15751a and c19731t	PCR-amplified product	New England Biolabs, Beverly, MA, USA
<i>NlaIV</i>	ASREA of c4825t and c13314g	PCR-amplified product	New England Biolabs, Beverly, MA, USA
<i>RsaI</i>	Restriction mapping of interactor prey-inserts	Yeast colony PCR-amplified product	Promega, Madison, WI, USA
<i>SmaI</i>	Cloning	PCR-amplified product and Y2H bait-plasmids	Promega, Madison, WI, USA

*ASREA* = allele-specific restriction enzyme analysis; *RE* = restriction enzyme; *RT-PCR* = reverse transcription PCR; *Y2H* = yeast two-hybrid.

## **II.12. GENERATION OF Y2H CONSTRUCTS**

### **II.12.1. Y2H BAIT- AND PREY-VECTORS**

Y2H bait constructs were cloned into either the pAS2.1 (figure II.5) or pGBKT7 (figure II.6) Y2H bait-vectors, while Y2H prey constructs were cloned into either the pACT2 (figure II.7) or pGADT7 (figure II.8) Y2H prey-vectors (BD Biosciences, Clontech, Palo Alto, CA, USA).

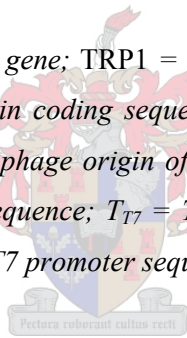
### **II.12.2. ALKALINE PHOSPHATASE TREATMENT OF VECTORS**

Double digested Y2H cloning vectors were CIP-treated to remove the phosphate end groups, thereby reducing the chances of self-ligation of the vector. To achieve this, a 50 $\mu$ l aliquot of double-digested vector was incubated with 1 $\mu$ l of CIP (1U/ $\mu$ l) (Promega, Madison, WI, USA) at 37°C for 15min in the buffer supplied by the manufacturer, after which another 1 $\mu$ l of CIP (Promega, Madison, WI, USA) was added to the sample prior to incubation at 37°C for a further 15min. Following incubation, 0.02x volume of 0.5M EDTA was added and the sample incubated at 65°C for 20min, in order to inactivate the enzyme. The vector was subsequently purified by PCI treatment (section II.4.5).

**Table II.9. Characteristics of Y2H cloning plasmids**

Plasmid	<i>Amp<sup>r</sup></i>	<i>Kan<sup>r</sup></i>	<i>TRP1</i>	<i>LEU2</i>	<i>CYN2</i>	GAL4- BD	GAL4- AD	<i>O</i> <sub>2μ</sub>	<i>O</i> <sub>f1</sub>	<i>O</i> <sub>pUC</sub>	<i>O</i> <sub>pBR322</sub>	<i>T</i> <sub>ADH1</sub>	<i>T</i> <sub>T7</sub>	<i>T</i> <sub>CYC1</sub>	<i>P</i> <sub>ADH1</sub>	<i>P</i> <sub>T7</sub>	cMyc	HA
pAS2.1	+	-	+	-	+	+	-	+	+	+	-	+	-	+	+	-	-	-
pGBKT7	-	+	+	-	-	+	-	+	+	+	-	+	+	-	-	+	+	-
pACT2	+	-	-	+	-	-	+	+	-	-	+	+	-	-	+	-	-	+
pGADT7	+	-	-	+	-	-	+	+	-	+	-	+	-	-	+	+	-	+

*Amp<sup>r</sup>* = ampicillin resistance gene; *Kan<sup>r</sup>* = kanamycin resistance gene; *TRP1* = *TRP1* coding sequence; *LEU2* = *LEU2* coding sequence; *CYN2* = *CYN2* coding sequence; *GAL4-BD* = *GAL4* DNA-binding domain coding sequence; *GAL4-AD* = *GAL4* transcriptional activation domain coding sequence, *O*<sub>2μ</sub> = yeast 2μ origin of replication; *O*<sub>f1</sub> = *f1* bacteriophage origin of replication; *O*<sub>pUC</sub> = pUC origin of replication; *O*<sub>pBR322</sub> = pBR322 origin of replication; *T*<sub>ADH1</sub> = *ADH1* transcription termination sequence; *T*<sub>T7</sub> = *T7* transcription termination sequence, *T*<sub>CYC1</sub> = *CYC1* transcription termination sequence; *P*<sub>ADH1</sub> = *ADH1* promoter sequence; *P*<sub>T7</sub> = *T7* promoter sequence; cMyc = c-Myc epitope tag; HA = hemagglutinin epitope tag.



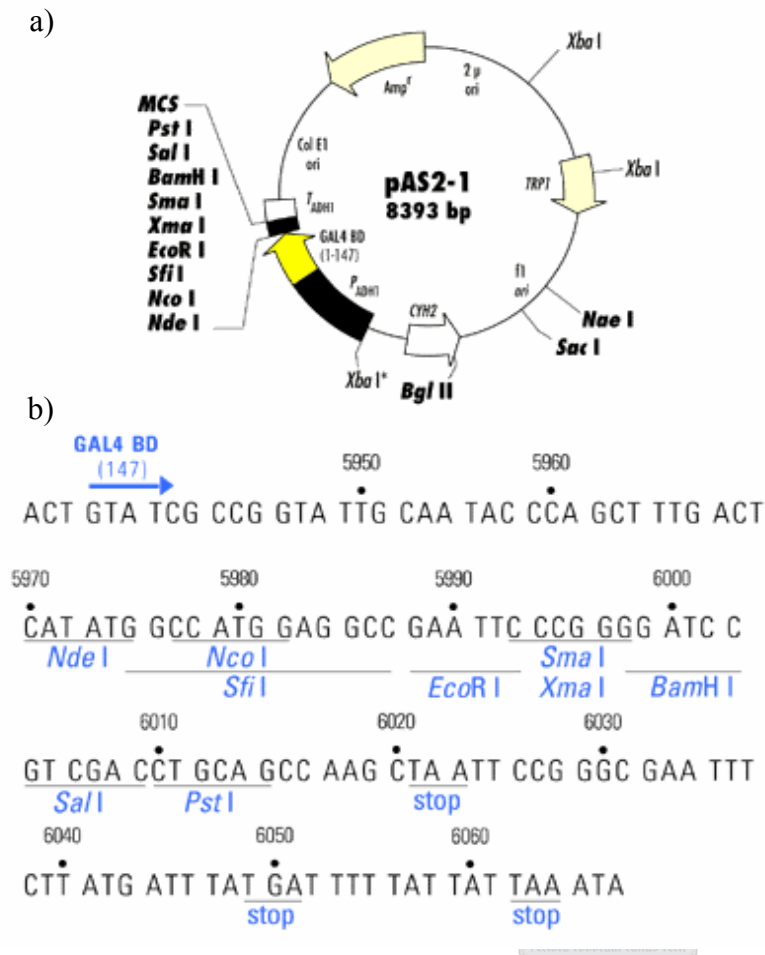


**Figure II.5. Restriction map and multiple cloning site of pAS2.1**

a) Restriction map of the pAS2.1 Y2H bait-vector. The positions of unique restriction sites are indicated in bold. The positions of the ampicillin resistance- ( $Amp^r$ ), TRP1-, CYH2- and GAL4-BD coding sequences, the  $2\mu$  yeast-, f1 bacteriophage- and pUC plasmid origins of replication, the *S.cerevisiae* ADH1 promoter sequence, the CYC1 and *S.cerevisiae* ADH1 termination signal sequences and the position of the multiple cloning site (MCS) are indicated on the map.

b) Nucleotide sequence of the pAS2.1 MCS. The positions of all unique restriction enzyme recognition sequences, stop codons and the final codon (147) of the GAL4-BD coding sequence are indicated on the map (from Clontech MATCHMAKER vectors handbook).

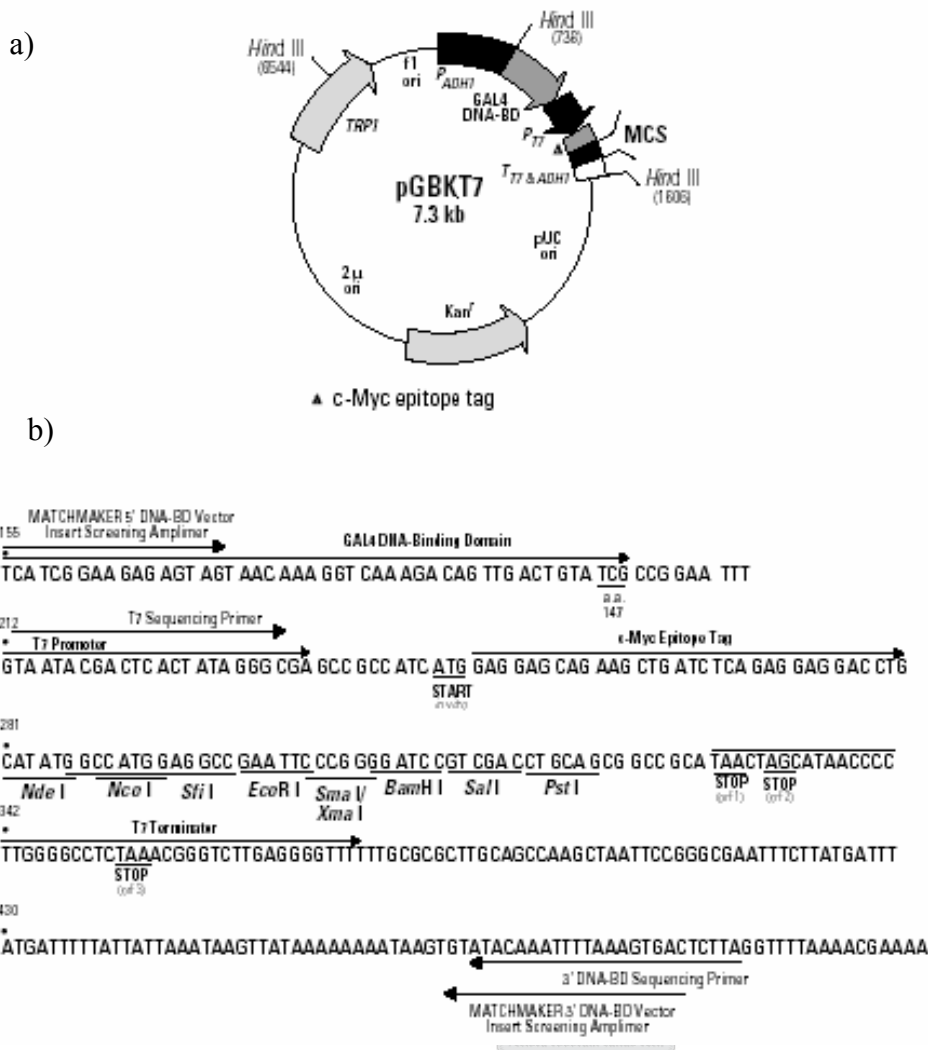
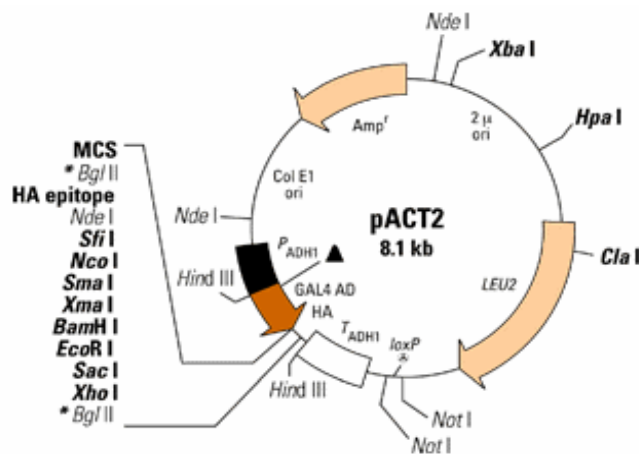


**Figure II.6. Restriction map and multiple cloning site of pGBKT7**

a) Restriction map of the pGBKT7 Y2H bait-vector. The positions of the kanamycin resistance- ( $Kan^r$ ), TRP1- and GAL4-BD coding sequences, the  $2\mu$  yeast-, f1 bacteriophage- and pUC plasmid origins of replication, the truncated *S.cerevisiae* ADH1 promoter sequence ( $P_{ADH1}$ ), the T7 RNA polymerase promoter, the T7 and *S.cerevisiae* ADH1 termination signal sequences, the position of the multiple cloning site (MCS) and the c-Myc epitope tag, are indicated on the map.

b) Nucleotide sequence of the pGBKT7 MCS. The positions of all unique restriction enzyme recognition sequences, stop codons in the T7 terminator sequence, the GAL4-BD coding sequence, the T7 promoter sequence, c-Myc epitope tag and the positions of various insert screening and sequencing primers are indicated on the map (from Clontech MATCHMAKER vectors handbook).

a)



b)

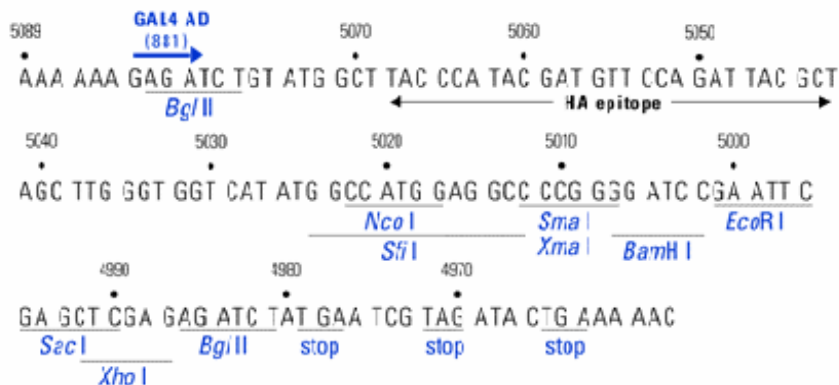


**Figure II.7. Restriction map and multiple cloning site of pACT2**

a) Restriction map of the pACT2 Y2H prey-vector. The positions of unique restriction sites are indicated in bold. The positions of the ampicillin resistance- ( $Amp^r$ ), LEU2- and GAL4-AD coding sequences, the  $2\mu$  yeast-, and pBR322 plasmid origins of replication, the *S.cerevisiae* ADH1 promoter sequence, the *S.cerevisiae* ADH1 termination signal sequences, *Lox* sites (*Lox1* and *Lox2*), the Hemagglutinin (HA) epitope tag and the multiple cloning site (MCS) are indicated on the map.

b) Nucleotide sequence of the pACT2 MCS. The positions of all unique restriction enzyme recognition sequences, stop codons, the position of the final codon (881) of the GAL4-AD coding sequence, and the HA epitope tag are indicated on the map (from Clontech MATCHMAKER vectors handbook).

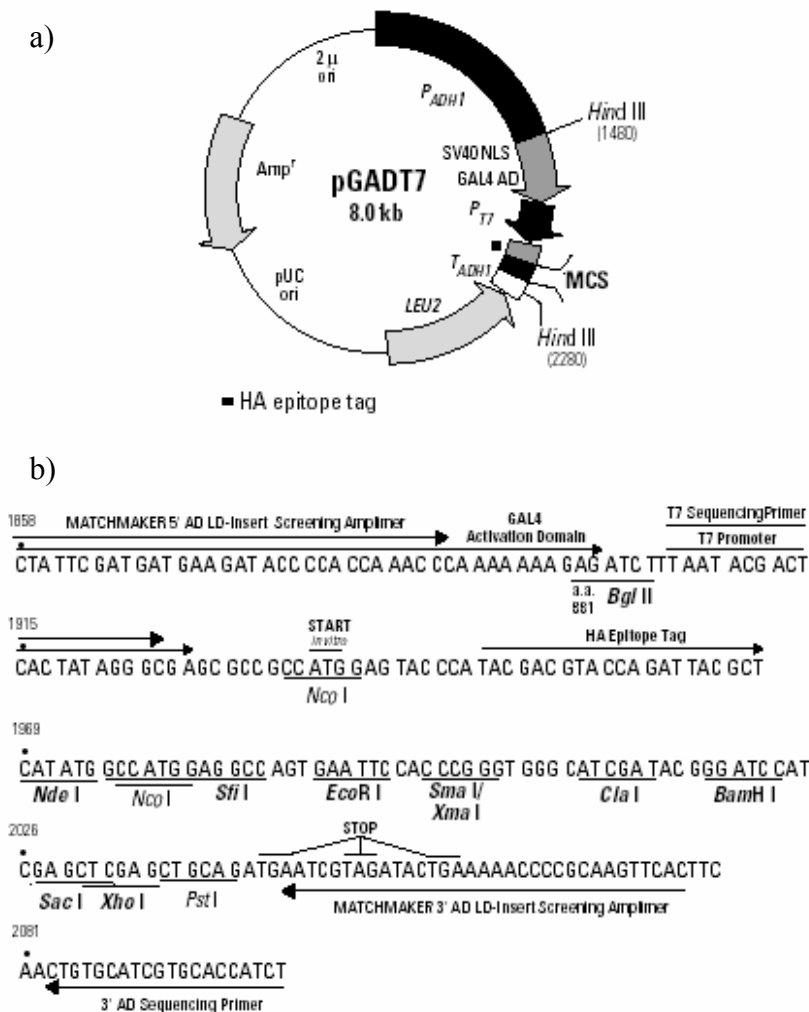


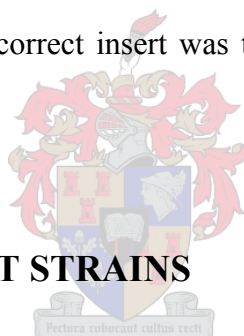
**Figure II.8. Restriction map and multiple cloning site of pGADT7**

a) Restriction map of the pGADT7 Y2H prey-vector. The positions of the ampicillin resistance- ( $Amp^r$ ), LEU2- and GAL4-AD coding sequences, the  $2\mu$  yeast- and pUC plasmid origins of replication, the *S.cerevisiae* ADH1 promoter sequence ( $P_{ADH1}$ ), the T7 RNA polymerase promoter, the *S.cerevisiae* ADH1 termination signal sequences ( $T_{ADH1}$ ), the position of the multiple cloning site (MCS) and the HA epitope tag are indicated on the map.

b) Nucleotide sequence of the pGADT7 MCS. The positions of all unique restriction enzyme recognition sequences, the T7 promoter sequence, the GAL4-AD coding sequence, the HA epitope tag, stop codons and the positions of various insert screening and sequencing primers are indicated on the map (from Clontech MATCHMAKER vectors handbook).

### II.12.3. DNA LIGATION

DNA ligations were performed to effect the generation of constructs used in Y2H-assays. Generally, 2-7 $\mu$ l of purified double-digested PCR-product (sections II.6.3 and II.11.2) was added to 1 $\mu$ l of the appropriate double-digested, CIP-treated (section II.12.2), Y2H cloning vector. To this mixture, 1 $\mu$ l of 10x T4 DNA ligase buffer (Promega, Madison, WI, USA), 5U of T4 DNA ligase (Promega, Madison, WI, USA) and ddH<sub>2</sub>O to a final volume of 10 $\mu$ l were added. This mixture was subsequently incubated at 16°C for 14-16h. Following incubation, a 5 $\mu$ l aliquot of the ligation reaction mixture was transformed into *E.coli* strain DH5 $\alpha$  (appendix B), and transformed bacterial colonies selected by growing them on LB-agar plates containing appropriate antibiotic (table II.10 and appendix A). The presence of the correct insert was then confirmed by bacterial colony PCR (section II.6.5).



## II.13. BACTERIAL AND YEAST STRAINS

### II.13.1. BACTERIAL STRAINS

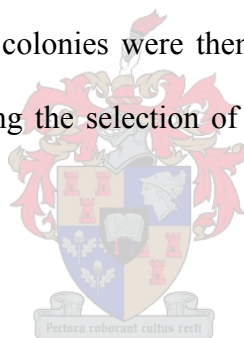
In order to facilitate the selection and purification of Y2H constructs, ligation reaction mixtures (section II.12.3) were transformed (section II.14.1) into *E.coli* strain DH5 $\alpha$  (appendix B). Transformed bacterial colonies were selected, based on their ability to grow on LB plates containing either ampicillin (when selecting pAS2.1-, pACT2- and pGADT7- based constructs), or kanamycin (when selecting pGBKT7- based constructs) (table II.10) (appendix A).

Table II.10. Generation of Y2H-constructs

Construct name	Insert	Type	Plasmid used	Restriction enzyme		Selection media	
				5'	3'	Bacterial	Yeast
pAS2.1-C0	cMyBPC C0	Bait	pAS2.1	<i>NdeI</i>	<i>EcoRI</i>	LB <sup>Amp</sup>	SD <sup>-W</sup>
pGBKT7-C0	cMyBPC C0	Bait	pGBKT7	<i>NdeI</i>	<i>EcoRI</i>	LB <sup>Kan</sup>	SD <sup>-W</sup>
pAS2.1-C0C1	cMyBPC C0C1	Bait	pAS2.1	<i>NdeI</i>	<i>EcoRI</i>	LB <sup>Amp</sup>	SD <sup>-W</sup>
pGBKT7-C0C1	cMyBPC C0C1	Bait	pGBKT7	<i>NdeI</i>	<i>EcoRI</i>	LB <sup>Kan</sup>	SD <sup>-W</sup>
pAS2.1-C0C2	cMyBPC C0C2	Bait	pAS2.1	<i>NdeI</i>	<i>EcoRI</i>	LB <sup>Amp</sup>	SD <sup>-W</sup>
pGBKT7-C3	cMyBPC C3	Bait	pGBKT7	<i>NdeI</i>	<i>EcoRI</i>	LB <sup>Kan</sup>	SD <sup>-W</sup>
pGBKT7-C7	cMyBPC C7	Bait	pGBKT7	<i>NdeI</i>	<i>EcoRI</i>	LB <sup>Kan</sup>	SD <sup>-W</sup>
pGBKT7-C7 <sup>V896M</sup>	cMyBPC C7 <sup>V896M</sup>	Bait	pGBKT7	<i>NdeI</i>	<i>EcoRI</i>	LB <sup>Kan</sup>	SD <sup>-W</sup>
pGBKT7-A43	TTN A43	Bait	pGBKT7	<i>NdeI</i>	<i>EcoRI</i>	LB <sup>Kan</sup>	SD <sup>-W</sup>
pGADT7-C1	cMyBPC C1	Prey	pGADT7	<i>NdeI</i>	<i>EcoRI</i>	LB <sup>Amp</sup>	SD <sup>-L</sup>
pGADT7-C1C2	cMyBPC C1C2	Prey	pGADT7	<i>NdeI</i>	<i>EcoRI</i>	LB <sup>Amp</sup>	SD <sup>-L</sup>
pGADT7-C2	cMyBPC C2	Prey	pGADT7	<i>NdeI</i>	<i>EcoRI</i>	LB <sup>Amp</sup>	SD <sup>-L</sup>
pACT2-C5	cMyBPC C5	Prey	pACT2	<i>NcoI</i>	<i>EcoRI</i>	LB <sup>Amp</sup>	SD <sup>-L</sup>
pACT2-C6	cMyBPC C6	Prey	pACT2	<i>SmaI</i>	<i>EcoRI</i>	LB <sup>Amp</sup>	SD <sup>-L</sup>
pACT2-C8	cMyBPC C8	Prey	pACT2	<i>SmaI</i>	<i>EcoRI</i>	LB <sup>Amp</sup>	SD <sup>-L</sup>
pACT2-C8C10	cMyBPC C8C10	Prey	pACT2	<i>SmaI</i>	<i>EcoRI</i>	LB <sup>Amp</sup>	SD <sup>-L</sup>
pACT2-C9	cMyBPC C9	Prey	pACT2	<i>SmaI</i>	<i>EcoRI</i>	LB <sup>Amp</sup>	SD <sup>-L</sup>
pACT2-C9C10	cMyBPC C9C10	Prey	pACT2	<i>SmaI</i>	<i>EcoRI</i>	LB <sup>Amp</sup>	SD <sup>-L</sup>
pACT2-C10	cMyBPC C10	Prey	pACT2	<i>SmaI</i>	<i>EcoRI</i>	LB <sup>Amp</sup>	SD <sup>-L</sup>
pGADT7-A109	TTN A109	Prey	pGADT7	<i>NdeI</i>	<i>EcoRI</i>	LB <sup>Amp</sup>	SD <sup>-L</sup>
pGADT7-A109A112	TTN A109A112	Prey	pGADT7	<i>NdeI</i>	<i>EcoRI</i>	LB <sup>Amp</sup>	SD <sup>-L</sup>
pGADT7-A112	TTN A112	Prey	pGADT7	<i>NdeI</i>	<i>EcoRI</i>	LB <sup>Amp</sup>	SD <sup>-L</sup>
pGADT7-A116	TTN A116	Prey	pGADT7	<i>NdeI</i>	<i>EcoRI</i>	LB <sup>Amp</sup>	SD <sup>-L</sup>

LB<sup>Amp</sup> = Luria-Bertani media containing ampicillin; LB<sup>Kan</sup> = Luria-Bertani media containing kanamycin; SD<sup>-L</sup> = selective dropout media lacking leucine; SD<sup>-W</sup> = selective dropout media lacking tryptophan.

Where pGBKT7-based bait constructs were used to screen cardiac cDNA libraries (pGBKT7-C0, pGBKT7-C0C1(2) and pGBKT7-C7), prey-plasmids were selected in a similar fashion, by transforming plasmids purified from diploid yeast cells (containing both bait- and prey constructs) into *E.coli* strain DH5 $\alpha$  and selecting transformant colonies containing the prey-vector, by growing them on LB plates containing ampicillin (appendix A). In one cardiac cDNA library screen, however, pAS2.1-C0C1(1) was used as bait. In this case, selection of prey-plasmids was hampered by the fact that both the pAS2.1 bait-vector and the pACT2 prey-vector contained the ampicillin resistance gene. Plasmids purified from diploid yeast cells (containing both bait and prey constructs) were, therefore, transformed into *E.coli* strain KC8 (appendix B) and transformant colonies, each containing either a bait- or prey-plasmid, selected by growing them on LB plates containing ampicillin (appendix A). Transformant colonies were then replicated onto M9 agar plates lacking leucine (appendix A), therefore, allowing the selection of only transformant colonies in which the prey-plasmid was present.



### **II.13.2. YEAST STRAINS**

All pAS2.1-based Y2H bait constructs (table II.10) were transformed into yeast strain PJ69-2A (appendix B), while pGBKT7-based Y2H bait constructs (table II.10) were transformed into yeast strain AH109 (appendix B). All prey constructs used during the course of this study, whether they be pACT2- or pGADT7- based (table II.10), were transformed into yeast strain Y187 (appendix B).

### II.13.3. GENERATION OF BACTERIAL COMPETENT CELLS

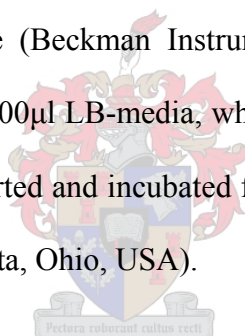
A scrape of either DH5 $\alpha$  or KC8 (section II.13.1) strains of *E.coli* (appendix B) frozen glycerol stocks (stored at  $-70^{\circ}\text{C}$ ) were inoculated into 10ml LB-media. This culture was then incubated overnight at  $37^{\circ}\text{C}$  with shaking at 200rpm in a YIH DER model LM-530 shaking incubator (SCILAB Instrument Co Ltd., Taipei, Taiwan). Following incubation, a 1ml aliquot of this culture was inoculated into a 2l Erlenmeyer flask containing 200ml of freshly autoclaved LB-media (appendix A). This culture was then incubated at room temperature with shaking at 200rpm to mid log-phase on a Labcon orbital shaker (about 16 to 20 hours) (Labcon Pty Ltd, Maraisburg, RSA) (an OD<sub>600</sub> of approximately 0.6), at which stage the culture was decanted into four 50ml polypropylene tubes and centrifuged at 3 000rpm for 15min at  $4^{\circ}\text{C}$  in a Multex centrifuge (MSE Instruments, England). The supernatant was subsequently discarded and the pellet resuspended in 8ml of ice-cold CAP buffer (appendix A). The cells were then re-pelleted by centrifugation at 3 000rpm for 15min at  $4^{\circ}\text{C}$  in a Multex centrifuge (MSE Instruments, England, UK). The supernatant was discarded and the pellet once again resuspended in 4ml of ice-cold CAP buffer (appendix A). The suspended cells were subsequently aliquoted as 0.5ml aliquots into 2ml Eppendorf tubes, which were submersed in liquid nitrogen and stored at  $-70^{\circ}\text{C}$  until further use.

## II.14. PLASMID TRANSFORMATION

### II.14.1. BACTERIAL PLASMID TRANSFORMATION

For bacterial transformations, competent cells of bacterial strains KC8 and DH5 $\alpha$  (appendix B) were generated as described in section II.13.3. Prior to transformation, an aliquot of the appropriate strain

was allowed to thaw on ice for 20-30min. Following this period, 1µl of yeast plasmid preparation, or 5µl of a ligation reaction mixture (section II.12.3) was added to the competent cells and mixed gently by flicking the tube. This mixture was incubated on ice for an additional 20-30min, after which it was incubated at 42°C for 45s in a Lasec model 102 circulating waterbath (Lasec Laboratory and Scientific Company (Pty) Ltd., Cape Town, RSA). The transformation mixture was then incubated at room temperature for an additional 2min before adding 1ml of LB-media (appendix A) before being incubated at 37°C for 1h with shaking at 200rpm in a YIH DER model LM-530 shaking incubator (SCILAB Instrument Co Ltd., Taipei, Taiwan). Following this incubation period, 200µl of the transformation reaction mixture was plated out on LB-agar plates containing an appropriate selection antibiotic (table II.10). The remainder of the transformation mixture was centrifuged at 13 000rpm for 30s in a Beckman Microfuge Lite (Beckman Instruments Inc., CA, USA), the supernatant discarded and the cells resuspended in 200µl LB-media, which was also plated onto appropriate LB-agar plates. These plates were then inverted and incubated for 16h at 37°C in a model 329 stationary CO<sub>2</sub> incubator (Forma Scientific, Marietta, Ohio, USA).



### **II.13.2. YEAST PLASMID TRANSFORMATION**

Yeast from the appropriate strain to be transformed was plated out onto YPDA agar plates (table II.10 and appendix A). These plates were subsequently incubated at 30°C for two to three days in a Sanyo MIR262 stationary ventilated incubator (Sanyo, Electronic Company Ltd, Ora-Gun, Japan). Following incubation, a volume representing 20-50µl of yeast cells was picked and resuspended in 1ml of sterile ddH<sub>2</sub>O in a sterile 2ml Eppendorf tube. The cells were then re-pelleted by centrifugation at 13 000rpm for 30s in a Beckman Microfuge Lite (Beckman Instruments Inc., CA, USA). Following the removal of the supernatant, the cell-pellet was resuspended in 1ml 100mM

lithium acetate (LiAc), and incubated for 5min at 30°C in a Sanyo MIR262 stationary ventilated incubator (Sanyo, Electronic Company Ltd, Ora-Gun, Japan). After incubation, the cells were re-pelleted by centrifugation at 13 000rpm for 20s in a Beckman Microfuge Lite (Beckman Instruments Inc., CA, USA). The LiAc was removed from the cell-pellet and the following reagents were added in this specific order:- 240µl 50% polyethylene glycol (PEG), 36µl 1M LiAc, 25µl 2mg/ml sonicated, heat-denatured, herring sperm DNA (Promega, Madison, WI, USA), 50ng plasmid preparation and finally sterile ddH<sub>2</sub>O to a final volume of 350µl. The cell-pellet was then resuspended by vigorous vortexing for at least 1min, after which the transformation mixture was incubated at 42°C for 25min in a Lasec model 102 circulating waterbath (Lasec Laboratory and Scientific Company (Pty) Ltd., Cape Town, RSA). Following this incubation period, the cells were pelleted by centrifugation at 13 000rpm for 30s in a Beckman Microfuge Lite (Beckman Instruments Inc., CA, USA), after which the supernatant was removed from the pellet. The cells were resuspended in 250µl sterile ddH<sub>2</sub>O, of which 150µl was plated out on appropriate selection plates (table II.10 and appendix A). These plates were incubated for two to five days at 30°C in a Sanyo MIR262 stationary ventilated incubator (Sanyo, Electronic Company Ltd, Ora-Gun, Japan)

## **II.15. QUALITY CONTROL OF Y2H CONSTRUCTS**

### **II.15.1. PHENOTYPIC ASSESSMENT OF YEAST STRAINS**

The phenotypes of all yeast host strains used in Y2H-assays were assessed prior to them being transformed with the various Y2H constructs. In all cases, non-transformed yeast host strains (Y187, PJ69-2A and AH109 (appendix B)) were plated onto SD<sup>-Ade</sup>, SD<sup>-His</sup>, SD<sup>-L</sup>, SD<sup>-W</sup> and SD<sup>-Ura</sup> agar plates (appendix A). Only non-transformed yeast that were unable to grow on SD<sup>-Ade</sup>, SD<sup>-His</sup>, SD<sup>-L</sup>

and SD<sup>-W</sup> media, but that were able to grow on SD<sup>-Ura</sup> medium, were selected for transformation and subsequent Y2H-assays.

## II.15.2. TOXICITY TESTS

In order to establish whether any bait-peptides, used in Y2H library-assays, were toxic to the specific yeast host strain, growth-curves of yeast bait host strains transformed with the respective Y2H bait constructs (pGBKT7-C0, pGBKT7-C0C1, pGBKT7-C7 and pAS2.1-C0 transformed into yeast strains AH109 or PJ69-2A) were generated. These growth-curves were subsequently compared to growth-curves of identical yeast strains transformed with non-recombinant plasmids (AH109 transformed with pGBKT7 or PJ69-2A transformed with pAS2.1) generated in concurrent experiments.



Growth-curves were generated by growing transformed yeast strains to stationary phase in liquid SD<sup>-W</sup>-medium (appendix A) at 30°C with shaking at 200rpm (for 24-36h) in a YIH DER model LM-510R shaking incubator (SCILAB Instrument Co Ltd., Taipei, Taiwan). Following this incubation period, a 1:10 dilution of this primary culture was made in liquid SD<sup>-W</sup>-medium. This culture was then incubated at 30°C for an additional 8-12h with shaking at 200rpm in a YIH DER model LM-510R shaking incubator (SCILAB Instrument Co Ltd., Taipei, Taiwan). One millilitre aliquots of this culture were taken at hourly intervals, and the OD<sub>600</sub> measurements of these aliquots plotted against time. These curves were also linearised by drawing a graph of the log of the OD<sub>600</sub> measurements against time, and the slopes of these lines compared. Statistical analyses on the slopes of the linearised growth-curves were performed, using GraphPad Prism version 4.00 for Windows (GraphPad Software, San Diego CA, USA).

### II.15.3. REPORTER GENE SELF-ACTIVATION TESTS

In order to establish whether bait-GAL4BD or prey-GAL4AD fusion-proteins were able to autonomously activate transcription of reporter genes, yeast transformed with these constructs were grown on specific selection media (table II.10 and appendix A). Bait construct-containing yeast (strain AH109 or PJ69-2A) were plated out onto selective dropout media lacking tryptophan and histidine ( $SD^{-W-H}$ ), as well as selective dropout media lacking tryptophan, histidine and adenosine ( $SD^{-W-H-Ade}$ ) (Appendix A). Prey construct-containing yeast (strain Y187) were plated out onto selective dropout media lacking leucine and histidine ( $SD^{-L-H}$ ), as well as selective dropout media lacking leucine, histidine and adenosine ( $SD^{-L-H-Ade}$ ) (appendix A). Following incubation of these plates at 30°C for four days, the growth of yeast on these media was assessed. Clones that were unable to grow on these media were deemed suitable for Y2H assays.

### II.15.4. ESTABLISHMENT OF MATING EFFICIENCY

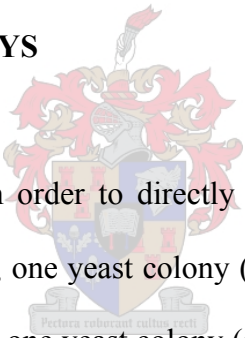


In order to establish whether bait-peptides, to be used in Y2H library-assays, affected the mating efficiency of the yeast strain in which they were expressed, small-scale yeast matings were performed (section II.16.1). In these experiments, the appropriate transformed bait host strain (PJ69-2A or AH109) was mated with prey host strain Y187 transformed with the non-recombinant pACT2 Y2H prey-vector. Concurrent to these experiments, control matings were also performed. In control matings, the appropriate bait host strain, transformed with either the appropriate non-recombinant bait-vector (PJ69-2A transformed with pAS2.1, or AH109 transformed with pGBKT7), or a control bait-vector supplied by the manufacturer (PJ69-2A transformed with pVA3.1 or AH109 transformed with pGBKT7-53) (BD Biosciences, Clontech, Palo Alto, CA, USA), was mated with Y2H prey host

strain Y187, either transformed with the non-recombinant pACT2 Y2H prey-vector, or a control prey-vector supplied by the manufacturer (pTD1.1 or pGADT7-T) (BD Biosciences, Clontech, Palo Alto, CA, USA). Following overnight incubation, serial dilutions of the mating cultures were plated out onto SD<sup>-L</sup>, SD<sup>-W</sup> and SD<sup>-L-W</sup> plates, which were incubated for four days at 30°C in a Sanyo MIR262 stationary ventilated incubator (Sanyo, Electronic Company Ltd, Ora-Gun, Japan). Following incubation, colony counts from these plates were used to calculate mating efficiency (appendix C).

## II.16. Y2H INTERACTION TESTS

### II.16.1. CANDIDATE LIGAND ASSAYS



Small-scale yeast matings were used in order to directly test specific protein:protein interactions between bait and prey peptides. In short, one yeast colony (strain AH109 or PJ69-2A), into which a bait construct had been transformed, and one yeast colony (strain Y187), into which a prey construct had been transformed, were both inoculated into 1ml of YPDA media (appendix A) in a 2ml centrifuge tube (Eppendorf). These mating cultures were subsequently incubated overnight at 30°C with shaking at 200rpm in a YIH DER model LM-510R shaking incubator (SCILAB Instrument Co Ltd., Taipei, Taiwan). Following incubation, a 150ul aliquot of the mating culture was plated out onto SD<sup>-L-W</sup> plates (appendix A), and the plates incubated at 30°C for 2-5 days in a Sanyo MIR262 stationary ventilated incubator (Sanyo, Electronic Company Ltd, Ora-Gun, Japan), thereby selecting diploid yeast colonies in which bait and prey fusion-peptides were co-expressed.

## II.16.2. LIBRARY-SCALE YEAST MATING

Library-scale yeast matings were performed to identify unknown ligands of specific domains of cMyBPC (domains C0, C7 and the C0 to C1 region), from a cardiac cDNA library.

### II.16.2.1. Cardiac cDNA library

A pre-transformed MATCHMAKER library (BD Biosciences, Clontech, Palo Alto, CA, USA), consisting of *S.cerevisiae* strain Y187 transformed with a cardiac cDNA library constructed in pACT2, was used in all Y2H library-assays. A limitation of the MATCHMAKER pre-transformed library used in this study was that cDNA was generated from mRNA by oligo(dT) priming. This implies that only the 3' ends of large transcripts would be represented in these libraries, as the insert size in the libraries used was estimated to be between 0.4 and 4kb (pretransformed human heart MATCHMAKER cDNA library product analysis certificate, BD Biosciences, Clontech, Palo Alto, CA, USA). Interactions between the baits and the N-terminal regions of large proteins would, therefore, remain undetectable in Y2H library-assays.

### II.16.2.2. Establishment of a bait culture

Four yeast colonies (strain AH109 or PJ69-2A), transformed with the bait construct of interest, were inoculated into four separate 500ml Erlenmeyer flasks, each containing 50ml SD<sup>W</sup>-media. The rationale for generating multiple bait cultures was to facilitate pooling of initial bait cultures, allowing the generation of a final bait culture with a titre of at least  $1 \times 10^{10}$ . These cultures were incubated for 24h at 30°C with shaking at 200rpm in a YIH DER model LM-510R shaking incubator

(SCILAB Instrument Co Ltd., Taipei, Taiwan), after which the cultures were transferred to 50ml polypropylene tubes, and the cells pelleted by centrifugation at 3 000rpm for 10min at room temperature in a Beckman model TJ-6 centrifuge (Beckman Scotland, UK). Following centrifugation, the supernatants were discarded and the cells resuspended in 50ml SD<sup>-W</sup> (appendix A), after which the suspensions were transferred to sterile 500ml Erlenmeyer flasks, and the cultures incubated for a further 16-24h at 30°C with shaking at 200rpm in a YIH DER model LM-510R shaking incubator (SCILAB Instrument Co Ltd., Taipei, Taiwan). Following incubation, the titre of the bait culture was estimated by measuring the OD<sub>600</sub> of a 1ml aliquot. The titre of the bait culture was then confirmed by means of a haemocytometer cell count. In cases where the titre of none of the individual bait cultures reached the threshold of at least  $1 \times 10^{10}$ , an appropriate number of bait cultures (which when combined would represent  $>1 \times 10^{10}$  cells) were transferred to 50ml polypropylene tubes (Greiner Labortechnik GmbH, Frickenhausen Germany) and the cells pelleted by centrifugation at 3 000rpm for 10min at room temperature in a Beckman model TJ-6 centrifuge (Beckman Coulter, Scotland, UK). After centrifugation, the supernatants were removed, the cell-pellets resuspended in 10ml SD<sup>-W</sup> medium (appendix A), and the cultures combined in a single 50ml polypropylene tube.

This entire bait culture was subsequently centrifuged at 3 000rpm for 10min at room temperature in a Beckman model TJ-6 centrifuge (Beckman Coulter, Scotland, UK). Following centrifugation, the supernatant was decanted and the cell-pellet resuspended in 5ml SD<sup>-W</sup> medium (appendix A). An appropriate number of 10µl aliquots of this culture was made, and subsequently used to perform control matings (section II.16.2.5).

### II.16.2.3. Library mating

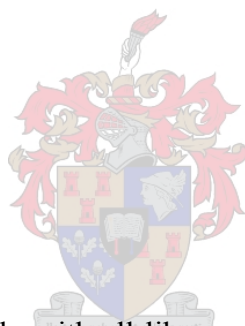
A 1ml cardiac cDNA library yeast culture (BD Biosciences, Clontech, Palo Alto, CA, USA) was removed from storage at  $-70^{\circ}\text{C}$  and thawed at  $20^{\circ}\text{C}$  for 20min. The library culture was then mixed by gentle vortexing and a 10ul aliquot set aside on ice for subsequent library titering (section II.16.2.4). The entire bait culture (section II.16.2.2) was subsequently added to 45ml of 2x YPDA media (appendix A), containing  $10\mu\text{g/ml}$  kanamycin (Kan), in a 2l Erlenmeyer flask, to which the entire 1ml library culture was added. This mating culture was incubated at  $30^{\circ}\text{C}$  for 24h with shaking at 30rpm in a YIH DER model LM-510R shaking incubator (SCILAB Instrument Co Ltd., Taipei, Taiwan).

Following incubation, the entire mating culture was transferred to a 50ml polypropylene tube and centrifuged at 3 000rpm for 10min at room temperature in a Beckman model TJ-6 centrifuge (Beckman Coulter, Scotland, UK). After removing the supernatant, the Erlenmeyer flask in which the library mating was performed, was rinsed twice with 40ml 2x YPDA medium containing  $10\mu\text{g/ml}$  Kan. Each time, the 2x YPDA medium used to rinse the flask was used to resuspend the cell-pellet, and the cells re-pelleted by centrifugation at 3 000rpm for 10min at room temperature in a Beckman model TJ-6 centrifuge (Beckman Coulter, Scotland, UK). Following the final centrifugation step, the supernatant was removed and the cell-pellet resuspended by gentle vortexing in 10ml of 0.5x YPDA, containing  $10\mu\text{g/ml}$  Kan (appendix A). Serial dilutions of a 100ul aliquot of this cell-suspension were subsequently plated out onto 90mm  $\text{SD}^{\text{L}}$ ,  $\text{SD}^{\text{W}}$  and  $\text{SD}^{\text{L-W}}$  plates (appendix A), while the remainder of the cell-suspension was plated out onto 50-60 150mm TDO plates (200ul per plate) (appendix A). TDO plates were incubated at  $30^{\circ}\text{C}$  for up to 14 days in a Sanyo MIR262 stationary ventilated incubator (Sanyo, Electronic Company Ltd, Ora-Gun, Japan),

while colony counts were performed on the  $SD^{-L}$ ,  $SD^{-W}$  and  $SD^{-L-W}$  plates after four days, thereby allowing the calculation of the mating-efficiency of the library mating (appendix C), and the number of library plasmids screened (appendix C).

#### **II.16.2.4. Establishment of library titre**

Serial dilutions of the 10 $\mu$ l library culture aliquot (section II.16.2.3) were made with 0.5x YPDA containing 10 $\mu$ g/ml Kan (appendix A). These dilutions were subsequently plated onto  $SD^{-L}$  plates (appendix A) and incubated at 30°C for four days in a Sanyo MIR262 stationary ventilated incubator (Sanyo, Electronic Company Ltd, Ora-Gun, Japan), after which colonies were counted in order to calculate the library titre (appendix C).



#### **II.16.2.5. Control matings**

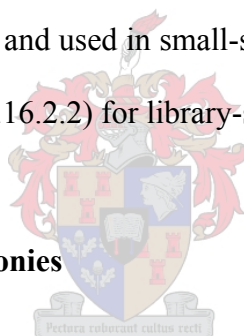
Control matings were set up concurrently with all library-scale matings. In short, a 10 $\mu$ l aliquot of the bait culture (section II.16.2.2) and a single test prey colony (of at least 1mm in diameter) were co-inoculated in 1ml of 2x YPDA, containing 10 $\mu$ g/ml Kan (appendix A), in a 2ml centrifuge tube (Eppendorf). These cultures were subsequently incubated for 24h at 30°C with shaking at 30rpm in a YIH DER model LM-510R shaking incubator (SCILAB Instrument Co Ltd., Taipei, Taiwan). Following incubation, serial dilutions of these cultures were plated out onto  $SD^{-L}$ ,  $SD^{-W}$  and  $SD^{-L-W}$  plates (appendix A), which were incubated at 30°C for four days in a Sanyo MIR262 stationary ventilated incubator (Sanyo, Electronic Company Ltd, Ora-Gun, Japan), after which colony counts were performed and mating efficiency calculated (appendix C). Control preys included non-

recombinant prey-vector (pACT2), transformed into yeast strain Y187, and either the pTD1.1 or pGADT7-T control vectors (supplied by the manufacturer), transformed into yeast strain Y187.

### **II.16.3. DETECTION OF ACTIVATION OF NUTRITIONAL REPORTER GENES**

#### **II.16.3.1. Selection of transformant yeast colonies**

Yeast transformed with either bait- or prey-plasmids was plated out onto SD<sup>W</sup> and SD<sup>L</sup> plates, respectively (appendix A). Following incubation of these plates at 30°C for 4-6 days in a Sanyo MIR262 stationary ventilated incubator (Sanyo, Electronic Company Ltd, Ora-Gun, Japan), transformant yeast colonies were picked and used in small-scale yeast matings (section II.16.1), or to grow large-scale bait cultures (section II.16.2.2) for library-scale yeast matings (section II.16.2).



#### **II.16.3.2. Selection of diploid yeast colonies**

Following small-scale yeast mating (section II.16.1), diploid yeast colonies, expressing both bait- and prey fusion-peptides, were selected by plating mating cultures onto SD<sup>L-W</sup> plates (appendix A). These plates were subsequently incubated at 30°C for 4-6 days in a Sanyo MIR262 stationary ventilated incubator (Sanyo, Electronic Company Ltd, Ora-Gun, Japan), following which activation of transcription of nutritional reporter genes were tested as described below.

### II.16.3.3. Selection of yeast colonies containing putative interactor peptides

In order to select diploid yeast colonies in which an interaction occurred between the bait- and prey-peptides, yeast were grown on TDO plates (appendix A), as well as solid phase SD media lacking leucine, tryptophan, histidine and adenine hemisulphate (Ade) (QDO plates) (appendix A). Growth of yeast colonies on TDO plates indicated transcriptional activation of the *HIS3* nutritional reporter gene, while growth on QDO plates was indicative of transcriptional activation of both the *HIS3* and *ADE2* nutritional reporter genes, caused by an interaction between the bait- and prey-peptides.

When the small-scale yeast mating protocol was used (section II.16.1), diploid yeast colonies were transferred directly from SD<sup>-L-W</sup> plates onto both TDO and QDO plates (appendix A). These plates were then incubated for 4-6 days at 30°C in a Sanyo MIR262 stationary ventilated incubator (Sanyo, Electronic Company Ltd, Ora-Gun, Japan), following which growth of yeast colonies on the respective media was assessed. In cases where growth were observed on TDO plates, but not on QDO plates, yeast were picked from the TDO plates and re-streaked onto QDO plates, following which these plates were incubated at 30°C for an additional 4-6 days in a Sanyo MIR262 stationary ventilated incubator (Sanyo, Electronic Company Ltd, Ora-Gun, Japan), prior to growth being assessed.

When library-scale matings were performed (section II.16.2.3), the mating culture was plated directly onto 50-60 150mm TDO plates. These were subsequently incubated for up to 14 days at 30°C in a Sanyo MIR262 stationary ventilated incubator (Sanyo, Electronic Company Ltd, Ora-Gun, Japan). The growth of yeast colonies, in which transcription of the *HIS3* reporter gene was activated, was assessed at two-day intervals, at which time colonies were picked and re-streaked onto TDO-

and QDO plates. These plates were then incubated for 4-6 days at 30°C in a Sanyo MIR262 stationary ventilated incubator (Sanyo, Electronic Company Ltd, Ora-Gun, Japan), prior to phenotypic assessment of yeast colonies.

Specific incubation periods were dependent on the bait-plasmid used. Where pGBKT7-based constructs, transformed into yeast strain AH109, were used, plates were assessed after four days, while yeast strain PJ69-2A, transformed with pAS2.1-based constructs, were incubated for six days prior to phenotypic assessment. Phenotypic assessment of yeast colonies on TDO and QDO plates took into account the size and robustness of yeast colonies on the selection medium, as well as the colour of the yeast colonies.

#### II.16.4. DETECTION OF ACTIVATION OF COLOURIMETRIC REPORTER GENES



##### II.16.4.1. X- $\alpha$ -Galactosidase assays

X- $\alpha$ -Galactosidase assays were performed in order to establish whether transcription of the *MEL1* reporter gene had been activated by interaction between specific bait- and prey-peptides. These assays were only performed in Y2H experiments where the AH109 bait host strain was used. In short, yeast colonies, in which transcription of the *HIS3* and *ADE2* reporter genes was activated, were replicated from QDO plates onto a Hybond N<sup>+</sup> nylon membrane. This membrane was subsequently placed colony-side up on a QDO-plate, onto which 200 $\mu$ l of a 20mg/ml X- $\alpha$ -Gal solution (BD Biosciences, Clontech, Palo Alto, CA, USA) had been spread just prior to use. These plates were then incubated for 16-48h at 30°C in a Sanyo MIR262 stationary ventilated incubator

(Sanyo, Electronic Company Ltd, Ora-Gun, Japan), following which blue colour development produced by the yeast colonies was assessed.

#### **II.16.4.2. $\beta$ -Galactosidase assays**

##### II.16.4.2.i. Qualitative $\beta$ -galactosidase assays

Filter-lift  $\beta$ -galactosidase assays were performed in order to establish whether transcription of the *lacZ* reporter gene had been activated by interaction between bait- and prey-peptides. In short, yeast colonies in which transcription of the *HIS3* and *ADE2* reporter genes was activated were lifted from QDO plates using a Hybond N<sup>+</sup> nylon membrane (Amersham Pharmacia Biotech, Little Chalfont, Buckinghamshire, UK). This membrane was subsequently submersed, colony-side up, in liquid N<sub>2</sub> for 10s, after which the membrane was placed colony-side up on a Whatman #5 filter (Whatman International Ltd., Maidstone, England, UK) and incubated at room temperature for 20-30min, allowing the cells to thaw. This freeze-thaw cycle was subsequently repeated once more. The membrane was then placed colony-side up on a Whatman #5 filter (Whatman International Ltd., Maidstone, England) which had been presoaked in Z-buffer/X-gal solution (appendix A), and incubated at 30°C for 30min to 8h, following which the speed and intensity of blue colour development was assessed.

##### II.16.4.2.ii. Quantitative $\beta$ -galactosidase assays

Quantitative  $\beta$ -galactosidase assays were performed, in order to quantify the relative strength of interactions between specific bait and prey fusion-peptides. In order to achieve this, diploid yeast colonies were picked from appropriate SD agar plates (table II.10 and appendix A) and inoculated into 5ml of appropriate liquid SD-medium (table II.10 and appendix A) in 50ml polypropylene tubes.

These cultures were subsequently incubated at 30°C with shaking at 250rpm in a YIH DER model LM-510R shaking incubator (SCILAB Instrument Co Ltd., Taipei, Taiwan), until stationary phase was reached (typically 24-30h). After incubation, the cultures were mixed well by vortexing, and the OD<sub>600</sub> of a 1ml aliquot recorded. These primary cultures were subsequently diluted with YPDA-medium, in order to obtain an OD<sub>600</sub> of 0.2-0.3, in a total volume of 10ml. These cultures were then incubated for an additional 4-5h at 30°C with shaking at 250rpm in a YIH DER model LM-510R shaking incubator (SCILAB Instrument Co Ltd. Taipei, Taiwan). Following this incubation period, the cultures were mixed by vortexing and the OD<sub>600</sub> of 1ml aliquots of each of the cultures recorded.

Three 1.5ml aliquots of each culture were transferred to sterile 1.5ml centrifuge tubes (Eppendorf). These aliquots were then centrifuged at 13 000rpm for 30s at room temperature in a Beckman Microfuge Lite (Beckman Instruments Inc., CA, USA), the supernatant decanted, 1.5ml Z-buffer (appendix A) added to each tube and the cell-pellets resuspended by vortexing. The cells were subsequently pelleted once more by centrifugation at 13 000rpm for 30s at room temperature in a Beckman Microfuge Lite (Beckman Instruments Inc., CA, USA), the supernatants removed, and the cells resuspended in 300µl of Z-buffer (appendix A). One hundred microlitres of each of these cell resuspensions was subsequently transferred to fresh 1.5ml centrifuge tubes (Eppendorf), and the lids of these tubes punctured, using a sterile syringe needle. These tubes were then subjected to three freeze-thaw cycles, each consisting of immersing the tubes in liquid N<sub>2</sub> for 60s, followed by 60s of incubation at 37°C. Following the freeze-thaw cycles, 700µl of freshly made Z-buffer/β-mercaptoethanol (appendix A) was added to each tube, as well as to an additional tube containing 100µl of Z-buffer (appendix A), which was subsequently used as a negative control. To each of these tubes, including the negative control, 160µl of ONPG/Z-buffer (appendix A) was added, at which time a

timer was started. These tubes were subsequently incubated at 30°C until a yellow colour had developed, at which point the elapsed time was noted and 400µl of 1M Na<sub>2</sub>CO<sub>3</sub> added to each yellowed tube to quench the reaction. The cellular debris was subsequently pelleted by centrifugation at 13 000rpm for 10min at room temperature in a Beckman Microfuge Lite (Beckman Instruments Inc., CA, USA) and the OD<sub>420</sub> measurements of the supernatants taken. These OD<sub>420</sub> measurements, the time to colour development and the cellular concentration of the YPDA cultures were used to calculate the β-gal unit measurement (appendix C). In order to establish whether differences in β-gal unit measurements were statistically significant, standard t-tests were performed using GraphPad Prism version 4.00 for Windows (GraphPad Software, San Diego CA, USA).

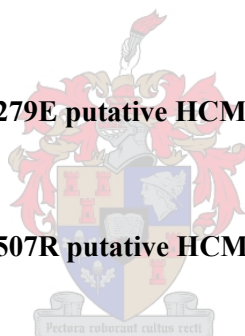
#### **II.16.5. INTERACTION SPECIFICITY TESTS**

Interaction specificity tests were used to establish whether interactions detected by Y2H assays, as evidenced by activation of reporter genes, were specific interactions between the particular bait- and prey-peptides. In short, yeast strain Y187 expressing specific prey-peptides was mated with the relevant bait host strain (strain PJ69-2A, or AH109), transformed with either non-recombinant bait-plasmid (pAS2.1, or pGBKT7), or a control bait-plasmid supplied by the manufacturer (pVA3.1 or pGBKT7-53) (BD Biosciences, Clontech, Palo Alto, CA, USA). Following the selection of diploid clones (section II.16.3.2), these clones were streaked on TDO- and QDO-selection media (appendix A), thereby testing whether prey-peptides were able to interact with these heterologous bait-peptides.

# CHAPTER III: RESULTS

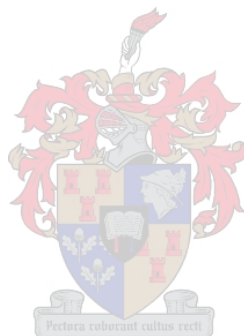
Page

<b>III.1. MUTATION SCREENING OF <i>MYBPC3</i></b>	<b>165</b>
<b>III.1.1. IDENTIFICATION OF POLYMORPHISMS AND SVS IN <i>MYBPC3</i></b>	<b>165</b>
<b>III.1.2. PUTATIVE MISSENSE MUTATIONS IN <i>MYBPC3</i></b>	<b>183</b>
<b>III.1.2.1. Identification of the <i>MYBPC3</i> V158M putative HCM-causing missense mutation</b>	<b>183</b>
<b>III.1.2.2. Identification of the <i>MYBPC3</i> A181T putative HCM-causing missense mutation</b>	<b>185</b>
<b>III.1.2.3. Identification of the <i>MYBPC3</i> R177H putative HCM-causing missense mutation</b>	<b>187</b>
<b>III.1.2.4. Identification of the <i>MYBPC3</i> G279E putative HCM-causing missense mutation</b>	<b>189</b>
<b>III.1.2.5. Identification of the <i>MYBPC3</i> G507R putative HCM-causing missense mutation</b>	<b>191</b>
<b>III.1.2.6. Identification of the <i>MYBPC3</i> V896M putative HCM-causing missense mutation</b>	<b>193</b>
<b>III.1.3. IDENTIFICATION OF PUTATIVE SPLICING MUTATIONS IN <i>MYBPC3</i></b>	<b>195</b>
<b>III.1.3.1. Identification of the exon 5 SdS -13 c&gt;t putative splicing mutation</b>	<b>196</b>
<b>III.1.3.2. Identification of the exon 7 SaS+1 g&gt;a putative splicing mutation</b>	<b>199</b>
<b>III.1.3.3. Identification of the intron 6 SbP +1 c&gt;t putative splicing mutation</b>	<b>202</b>
<b>III.1.4. IDENTIFICATION OF THE NOVEL <math>\Delta</math>C 13255 FRAME-SHIFT HCM-CAUSING MUTATION IN EXON 24 OF <i>MYBPC3</i></b>	<b>205</b>
<b>III.2. GENOTYPE:PHENOTYPE ASSOCIATION STUDIES</b>	<b>205</b>



<b>III.2.1. GENOTYPE:PHENOTYPE ASSOCIATION OF THE</b>	<b>207</b>
<b><i>MYBPC3</i> V896M MUTATION</b>	
<b>III.2.2. PHENOTYPIC EXPRESSION OF THE <i>MYBPC3</i> EXON 7</b>	<b>210</b>
<b>SaS +1 g&gt;a PUTATIVE HCM-CAUSING SPLICING</b>	
<b>MUTATION, IN A COMPOUND HETEROZYGOTE</b>	
<b>III.2.3. PHENOTYPIC EXPRESSION OF THE <i>MYBPC3</i> G507R</b>	<b>213</b>
<b>PUTATIVE HCM-CAUSING MUTATION</b>	
<b>III.3. YEAST TWO-HYBRID ASSAYS</b>	<b>213</b>
<b>III.3.1. QUALITY CONTROL OF Y2H CONSTRUCTS</b>	<b>213</b>
<b>III.3.1.1. Sequence analysis of Y2H constructs</b>	<b>213</b>
<b>III.3.1.2. Toxicity tests of Y2H constructs</b>	<b>214</b>
<b>III.3.1.3. Reporter gene self-activation tests</b>	<b>214</b>
<b>III.3.1.4. Effect of bait-peptides on mating efficiency</b>	<b>217</b>
<b>III.3.2. YEAST TWO-HYBRID LIBRARY-ASSAYS</b>	<b>218</b>
<b>III.3.2.1. cMyBPC C0C1 Y2H library-assay (1)</b>	<b>218</b>
<b>III.3.2.2. cMyBPC C0C1 Y2H library-assay (2)</b>	<b>221</b>
<b>III.3.2.3. cMyBPC C0 Y2H library-assay</b>	<b>229</b>
<b>III.3.2.4. cMyBPC C7 Y2H library-assay</b>	<b>234</b>
<b>III.3.3. MULTIPLE SEQUENCE ALIGNMENT ANALYSIS OF TITIN</b>	<b>242</b>
<b>INTERACTOR PREY CLONES AND TITIN</b>	
<b>III.3.4. CANDIDATE LIGAND Y2H-ASSAYS</b>	<b>246</b>
<b>III.3.4.1. Identification of cMyBPC domain C10 as a ligand of the cMyBPC</b>	<b>246</b>
<b>domain C7</b>	
<b>III.3.4.2. Identification of specific IgC2 domains of C-zone titin as ligands of</b>	<b>247</b>
<b>the cMyBPC domain C7</b>	

<b>III.3.4.3. Establishment of the effect of the V896M putative HCM-causing mutation in cMyBPC domain C7 on its interaction with cMyBPC domain C10 and titin domain A43</b>	<b>251</b>
<b>III.3.4.4. Identification of specific IgC2 domains of C-zone titin as putative ligands of the C0C1 region of cMyBPC</b>	<b>253</b>
<b>III.3.4.5. Identification of an interaction between the C3 and C10 domains of cMyBPC</b>	<b>254</b>
<b>III.3.4.6. N-terminal cMyBPC domains as candidate ligands of the cMyBPC C0C1 region</b>	<b>254</b>
<b>III.3.4.7. Cardiac actin as a candidate ligand of the C0C1 region of cMyBPC</b>	<b>257</b>



## CHAPTER III: RESULTS

### III.1. MUTATION SCREENING OF *MYBPC3*

Screening of the HCM-affected panel of probands (section II.1) for known and novel HCM-causing mutations in all 34 protein-encoding exons of *MYBPC3* (exons 2-35) by SSCP analysis (section II.8) resulted in the detection of several mobility shifts. DNA sequencing (section II.10) of samples, in which reproducible mobility shifts were detected, led to the identification of several SNS. Subsequent DNA sequence analysis (section II.10.3.1) facilitated the classification of these SNSs as silent polymorphisms, silent site sequence variations (ssSVs) (section III.1.1), putative HCM-causing missense mutations (section III.1.2), or putative splice site mutations (section III.1.3) (all of which are listed in table III.1).



#### III.1.1. IDENTIFICATION OF SILENT POLYMORPHISMS AND ssSVs IN *MYBPC3*

SNSs not predicted to alter the amino acid sequence of cMyBPC, or to alter the splicing of the *MYBPC3* transcript, were classified as polymorphisms (SNSs with an allele a frequency of 1% or more in the HCM-affected panel), ssSVs (SNSs with an allele a frequency lower than 1% in the HCM-affected panel). During the course of this study, several such non-deleterious polymorphisms and ssSVs were identified (table III.1 and figures III.1-III.15).

**Table III.1. Sequence variations identified in MYBPC3**

Ex/Int	Sequence	Position	Codon	AA	Type	RE site	#Heterozygotes	Status	Figure
Int 4	t2510c	Ex5 SaS -51bp	N.A.	N.A.	Polym	<i>HphI</i>	Het. = 8%	Novel	III.1
Ex 5	g2626a	Ex5 CS	gtg>atg	V158M	pMSM	<i>NlaIII</i>	1	Novel	III.16
Ex 5	c2646t	Ex5 CS	ggc>ggt	G164G	pSSM	<i>HphI</i>	Het = 8%	Novel	III.28 & III.29
Int 5	ins/del c2735	Ex6 SaS -13bp	N.A.	N.A.	Polym	-	Het = 34%	Novel	III.2
Ex 6	g2774a	Ex6 CS	cgc>cac	R177H	pMSM	-	5	Novel	III.20
Ex 6	g2785a	Ex6 CS	gcc>acc	A181T	pMSM	<i>HhaI</i>	2	Novel	III.18
Int 6	c4154t	Int6 SbP +1bp	N.A.	N.A.	pSSM	-	2	Novel	III.32 & III.33
Int 6	g4177a	Ex7 SaS +1bp	N.A.	N.A.	pSSM	-	1	Novel	III.30 & III.31
Ex 8	c4825t	Ex8 CS	acc>act	T262T	Polym	<i>NlaIV</i>	Het = 18%	Novel	III.11
Int 8	a4962g	Ex9 SaS -74bp	N.A.	N.A.	ssSV	-	1	Novel	III.3
Ex 9	g5047a	Ex9 CS	gga>gaa	G278E	pMSM	<i>MnII</i>	1	Known	III.22
Int 12	c6114a	Ex12 SdS +25bp	N.A.	N.A.	Polym	-	2	Novel	III.4
Int 13	g8168a	Ex14 SaS -31bp	N.A.	N.A.	Polym	-	Het. = 17%	Novel	III.5
Int 15	c8612t	Ex16 SaS -66bp	N.A.	N.A.	Polym	<i>AvaI</i>	2	Novel	III.6
Ex 18	g9140a	Ex18 CS	ggg>agg	G507R	pMSM	-	1	Known	III.24
Ex 18	g9187a	Ex18 CS	gcg>gca	A522A	ssSV	-	1	Novel	III.12
Ex 23	c12474t	Ex 23 CS	agc>agt	S708S	Polym	-	Het = 5%	Novel	III.13
Ex 24	Δc 13255	Ex 24 CS	F.S. 756>	F.S. 756>	pFSM	-	1	Novel	III.34

Ex/Int	$\Delta$ Sequence	Position	Codon	$\Delta$ AA	Type	RE site	#Probands	Status	Figure
Ex 24	g13199a	Ex 24 CS	acg>aca	T737T	ssSV	-	1	Novel	III.14
Int 24	c13314g	Ex24 SdS +18bp	N.A.	N.A.	Polym	<i>NlaIV</i>	Het = 6%	Novel	III.7
Ex 27	g15751a	Ex27 CS	ctg>atg	V896M	pMSM	<i>NlaIII</i>	1	Novel	III.26
Ex 31	a18443g	Ex 31 CS	gaa>gag	E1096E	Polym	<i>AluI</i>	Het = 41%	Novel	III.15
Int 33	g19143a	Ex33 SdS +30bp	N.A.	N.A.	Polym	-	2	Novel	III.8
Int 34	c19731t	Ex35 SaS -66bp	N.A.	N.A.	Polym	<i>NlaIII</i>	Het = 59%	Novel	III.9
Int 34	g19706a	Ex35 SaS -91bp	N.A.	N.A.	ssSV	<i>AluI</i>	1	Novel	III.10

$\Delta$  = deletion; AA = amino acid; CS = coding sequence; Ex = exon; F.S. = frame shift; Het = observed heterozygosity; Int = intron; N.A. = not applicable; pFSM = putative frame shift mutation; pMSM = putative HCM-causing missense mutation; pSSM = putative HCM-causing splicing mutation; Polym = polymorphism; RE = restriction enzyme used in ASREA to confirm the presence of the sequence variant; SaS = splice acceptor site; SdS = splice donor site. Positions of intronic SNPs relative to SaS and SdS are indicated as the number of nucleotides that the SNP is removed from the nearest intron/exon boundary (box 1). Nucleotide sequence numbers according to GenBank database (<http://www.ncbi.nlm.nih.gov/Entrez>) accession #: Y10129. Substituted nucleotides are underlined; status refers to whether a sequence variant is novel, or has been described elsewhere (Known). #Probands refers to the number of probands in the HCM-affected control panel, or the observed heterozygosity of the sequence variant in the HCM-affected panel.

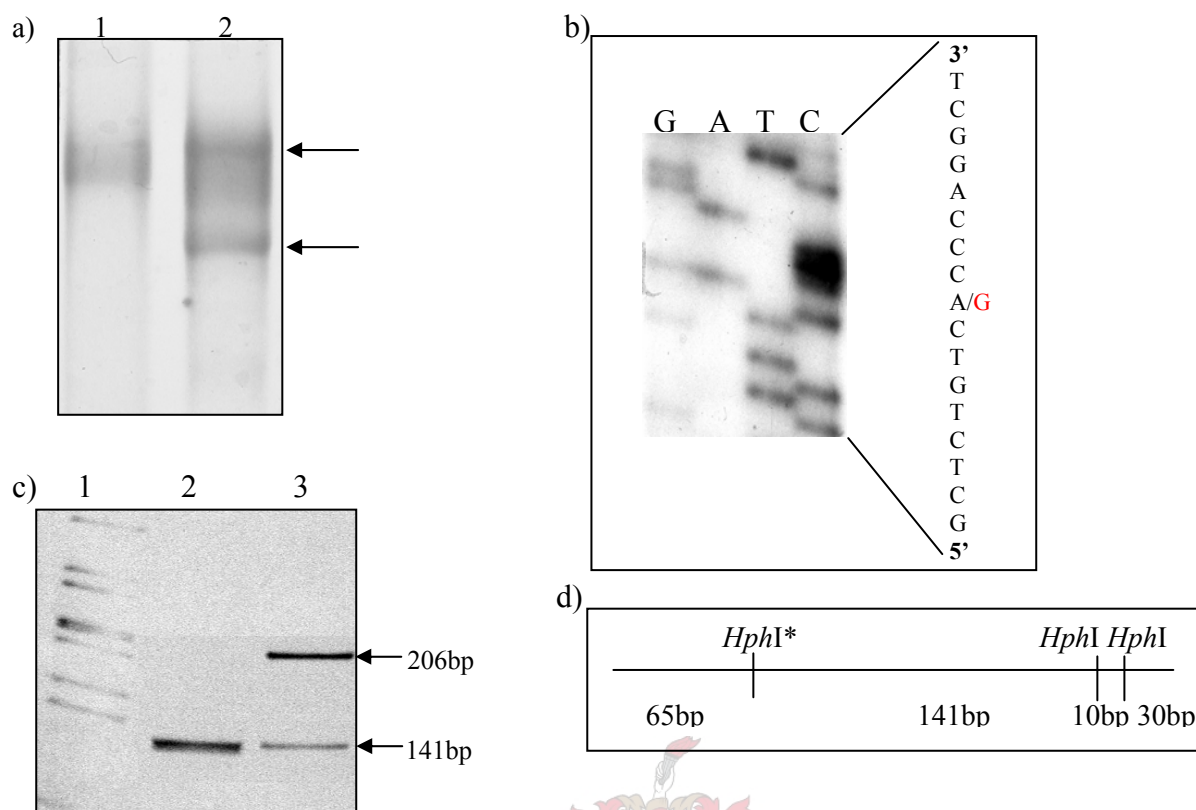


**Figure III.1. Identification of the novel *t2510c* polymorphism in intron 4 of MYBPC3**

a) PCR-SSCP analysis of the MYBPC3 exon 5 PCR-amplified product on a 10% MD-SSCP gel. Lane 1 = individual homozygous for the *t* allele (*t/t*); lane 2 = heterozygous individual (*t/c*). The arrows indicate the mobility shift caused by the *t/c* polymorphism at nucleotide 2510 in a heterozygous individual.

b) Partial sequence of the minus-strand of intron 4 of MYBPC3 in an individual heterozygous for the *t2510c* polymorphism, showing the *a/g* substitution on the minus-strand.

c) Genotyping of the MYBPC3 *t2510c* polymorphism by ASREA. Products of the *HphI* restriction enzyme digestion of the 246bp PCR-amplified product of exon 5 were electrophoresed on a 12% polyacrylamide gel. The internal *HphI* sites generate 10bp, 30bp, 65bp and 141bp fragments in *t/t* homozygotes, while the *t2510c* polymorphism abolishes an *HphI* restriction site, resulting in an additional 206bp fragment in *t/c* heterozygotes. The 10bp and 30bp restriction fragments could not be resolved under these electrophoretic conditions, while the 65bp fragment is not shown. Lane 1 =  $\lambda$ Pst marker; lane 2 = individual homozygous for the *t* allele (*t/t*); lane 3 = heterozygous individual (*t/c*).

d) Schematic representation of the exon 5 PCR-amplified product, indicating the position of the *HphI* sites. \* = variable restriction enzyme site.

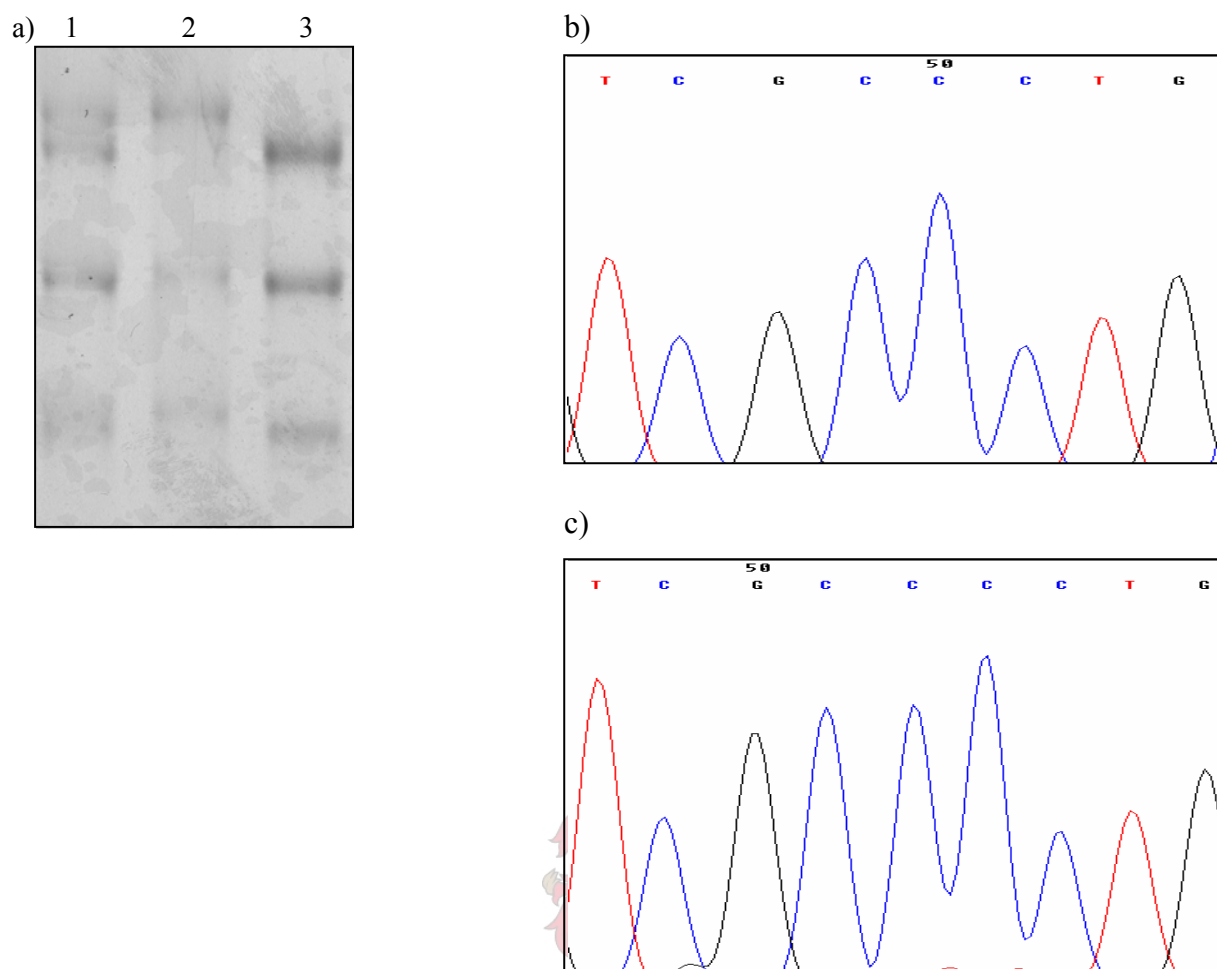


**Figure III.2. Identification of the novel ins/del c2735 polymorphism in intron 5 of MYBPC3**

a) PCR-SSCP analysis of the MYBPC3 exon 6 PCR-amplified product on a 10% MD-SSCP gel. Lane 1 = heterozygous individual; lane 2 = individual homozygous for the c deletion allele; lane 3 = individual homozygous for the c insertion allele.

b) Partial sequence of the plus-strand of intron 5 of MYBPC3 in an individual homozygous for the c 2735 deletion allele.

c) Partial sequence of the plus-strand of intron 5 of MYBPC3 in an individual homozygous for the c 2735 insertion allele.

This polymorphism did not alter a restriction enzyme recognition site and could, therefore, not be confirmed by ASREA.

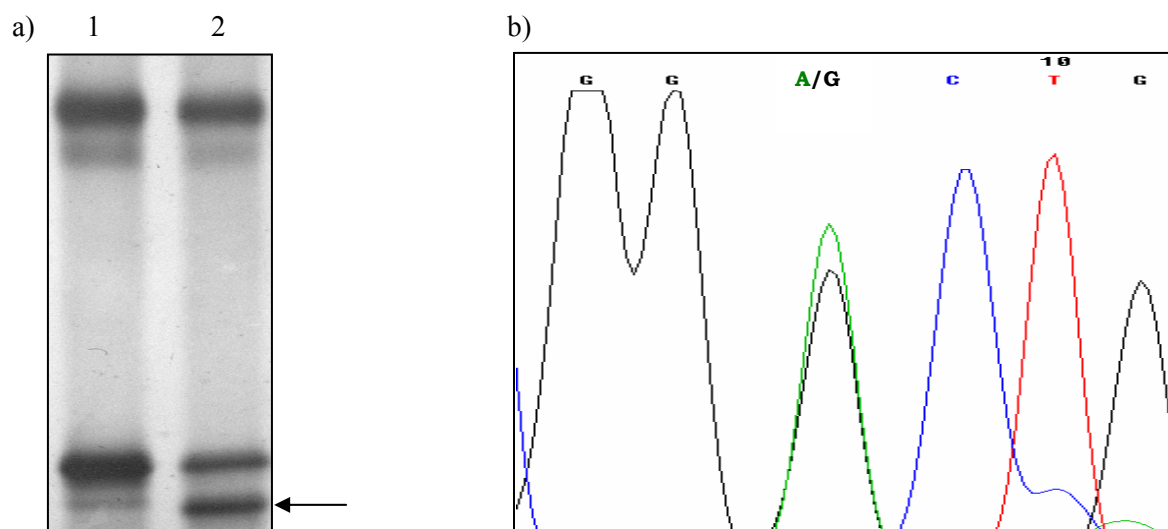
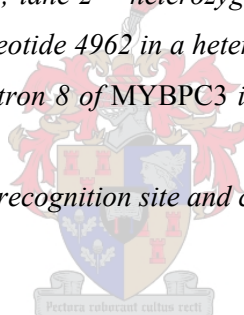


**Figure III.3. Identification of the novel a4962g ssSV in intron 8 of MYBPC3**

a) PCR-SSCP analysis of the MYBPC3 exon 9 PCR-amplified product on an 8% MD-SSCP gel. Lane 1 = individual homozygous for the a allele (a/a); lane 2 = heterozygous individual (a/g). The arrow indicates the mobility shift caused by the a/g ssSV at nucleotide 4962 in a heterozygous individual.

b) Partial sequence of the plus-strand of intron 8 of MYBPC3 in an individual heterozygous for the a4962g ssSV, showing the **a/g** substitution.

This ssSV did not alter a restriction enzyme recognition site and could, therefore, not be confirmed by ASREA.



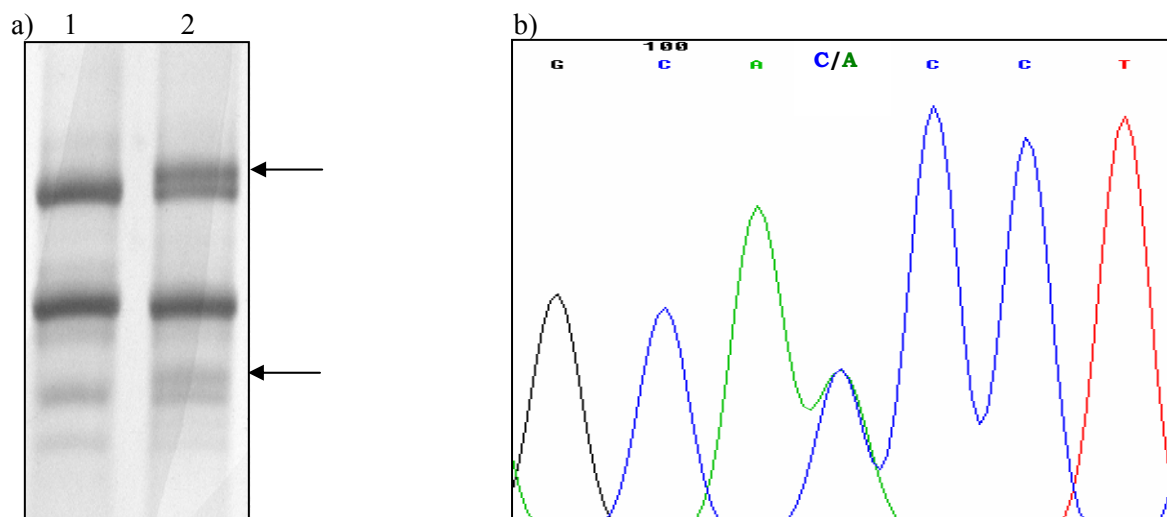


**Figure III.4. Identification of the novel c6114a polymorphism in intron 12 of MYBPC3**

a) PCR-SSCP analysis of the MYBPC3 exon 12 PCR-amplified product on a 10% MD-SSCP gel. Lane 1 = individual homozygous for the c allele (c/c); lane 2 = heterozygous individual (c/a). The arrows indicate the mobility shift caused by the c/a polymorphism at nucleotide 6114 in a heterozygous individual.

b) Partial sequence of the plus-strand of intron 12 of MYBPC3 in an individual heterozygous for the c6114a polymorphism, showing the c/a substitution.

This polymorphism did not alter a restriction enzyme recognition site and could, therefore, not be confirmed by ASREA.



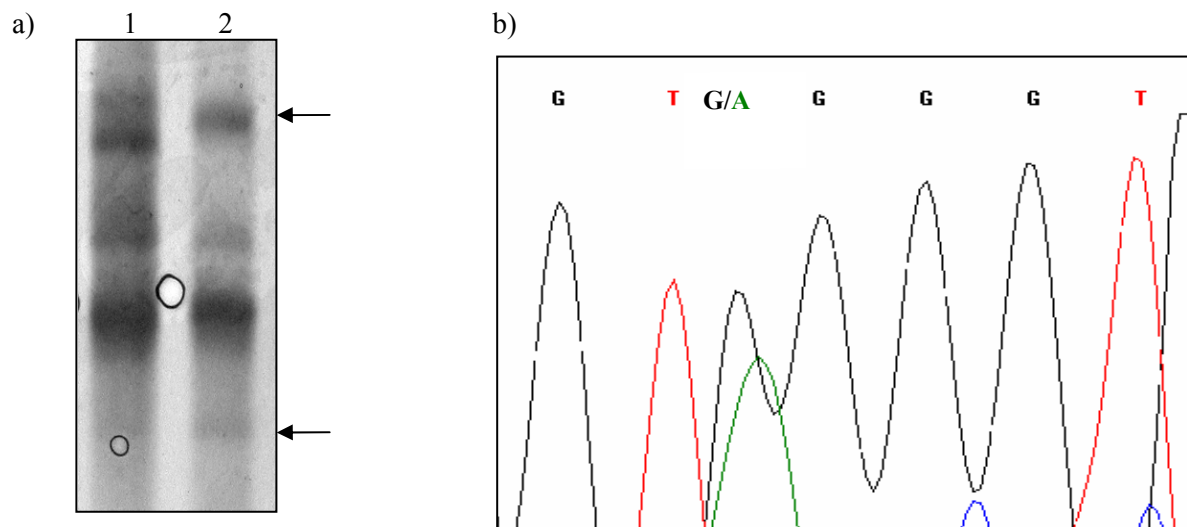
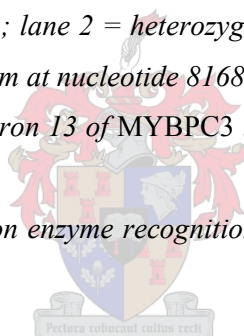


**Figure III.5. Identification of the novel g8168a polymorphism in intron13 of MYBPC3**

a) PCR-SSCP analysis of the MYBPC3 exon 14 PCR-amplified product on a 10% MD-SSCP gel. Lane 1 = individual homozygous for the g allele (g/g); lane 2 = heterozygous individual (g/a). The arrows indicate the mobility shift caused by the g/a polymorphism at nucleotide 8168 in a heterozygous individual.

b) Partial sequence of the plus-strand of intron 13 of MYBPC3 in an individual heterozygous for the g8168a polymorphism, showing the g/a substitution.

This polymorphism did not alter a restriction enzyme recognition site and could, therefore, not be confirmed by ASREA.



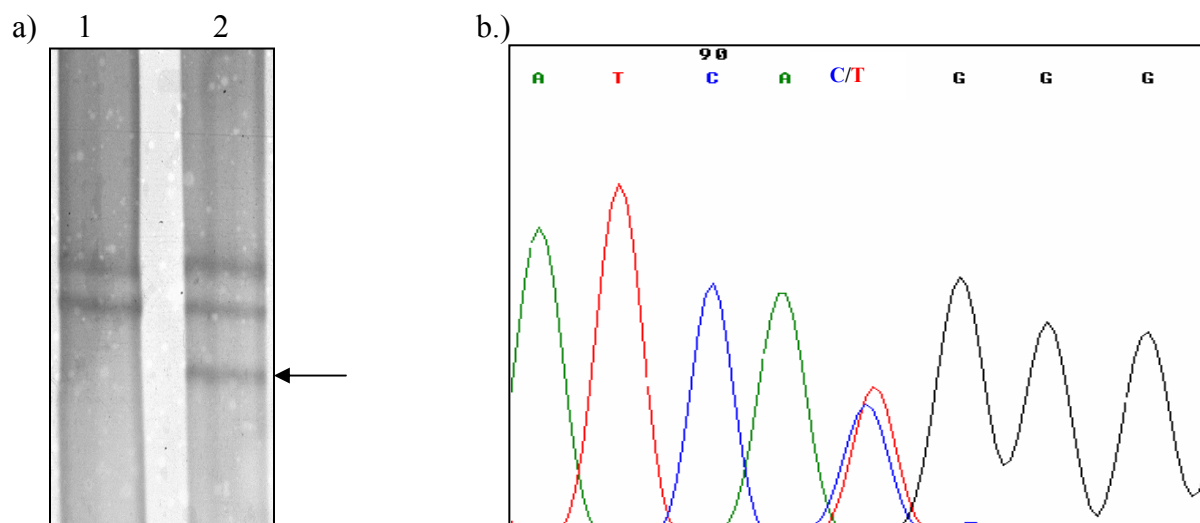


**Figure III.6. Identification of the novel c8612t polymorphism in intron 15 of MYBPC3**

a) PCR-SSCP analysis of the MYBPC3 exon 15 and 16 PCR-amplified product on an 8% MD-SSCP gel. Lane 1 = individual homozygous for the c allele (c/c); lane 2 = heterozygous individual (c/t). The arrow indicates the mobility shift caused by the c8612t polymorphism in a heterozygous individual.

b) Partial sequence of the plus-strand of intron 15 of MYBPC3 in an individual heterozygous for the c8612t polymorphism, showing the c/t substitution.

This polymorphism did not alter a restriction enzyme recognition site and could, therefore, not be confirmed by ASREA.



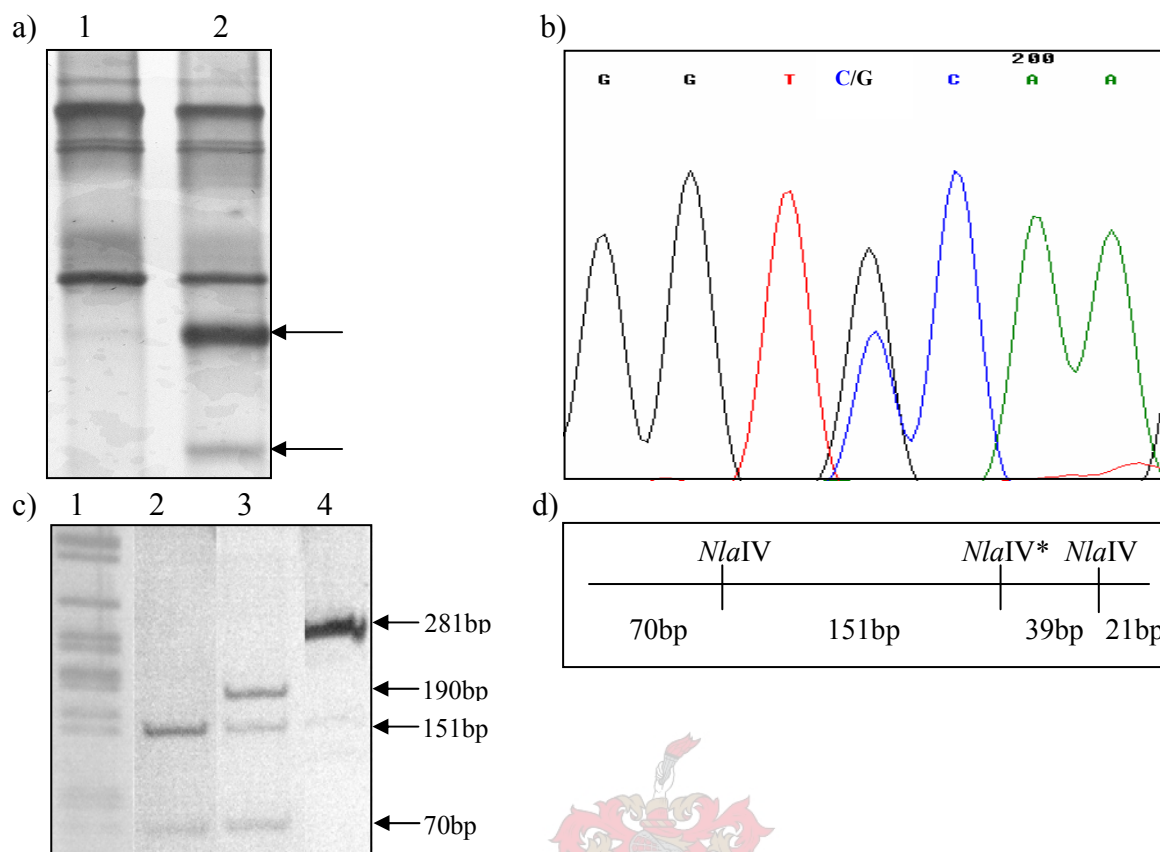


**Figure III.7. Identification of the novel c13314g polymorphism in intron 24 of MYBPC3**

a) PCR-SSCP analysis of the MYBPC3 exon 24 PCR-amplified product on a 10% MD-SSCP gel. Lane 1 = individual homozygous for the c allele (c/c); lane 2 = heterozygous individual (c/g). The arrows indicate the mobility shift caused by the c/g polymorphism at nucleotide 13314 in a heterozygous individual.

b) Partial sequence of the plus-strand of intron 24 of MYBPC3 in an individual heterozygous for the c13314g polymorphism, showing the c/g substitution.

c) Genotyping of the MYBPC3 c13314g polymorphism by ASREA. Products of the NlaIV restriction enzyme digestion of the 281bp PCR-amplified product of exon 24 were electrophoresed on a 12% polyacrylamide gel. The internal NlaIV sites generate 21bp, 39bp, 70bp and 151bp fragments in c/c homozygotes, while the presence of the g allele abolishes an NlaIV site, resulting in an additional 190bp fragment in c/g heterozygotes. The 21bp and 39bp restriction fragments could, however, not be resolved under these electrophoretic conditions. Lane 1 =  $\lambda$ Pst marker; lane 2 = individual homozygous for the c allele (c/c); lane 3 = heterozygous individual (c/g); lane 4 = undigested exon 24 PCR-amplified product.

d) Schematic representation of the PCR-amplified product, indicating the position of the NlaIV sites. \* = variable restriction enzyme site.

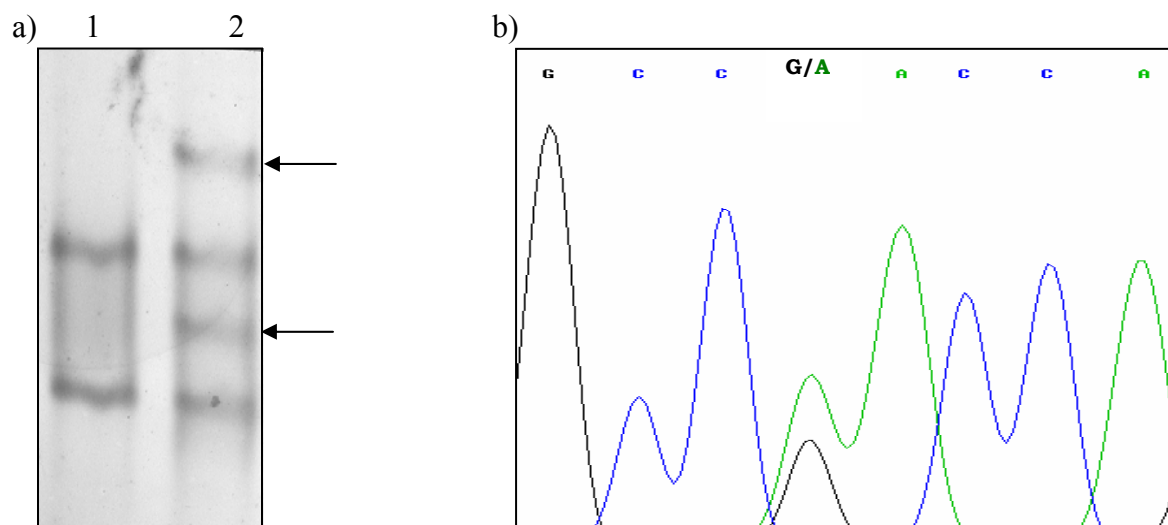
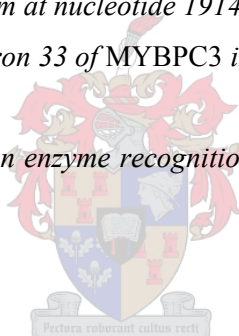


**Figure III.8. Identification of the novel g19143a polymorphism in intron 33 of MYBPC3**

a) PCR-SSCP analysis of the MYBPC3 exon 33 PCR-amplified product on a 10% MD-SSCP gel. Lane 1 = individual homozygous for the g allele (g/g); lane 2 = heterozygous individual (g/a). The arrows indicate the mobility shift caused by the g/a polymorphism at nucleotide 19143 in a heterozygous individual.

b) Partial sequence of the plus-strand of intron 33 of MYBPC3 in an individual heterozygous for the g19143a polymorphism, showing the **g/a** substitution.

This polymorphism did not alter a restriction enzyme recognition site and could, therefore, not be confirmed by ASREA.



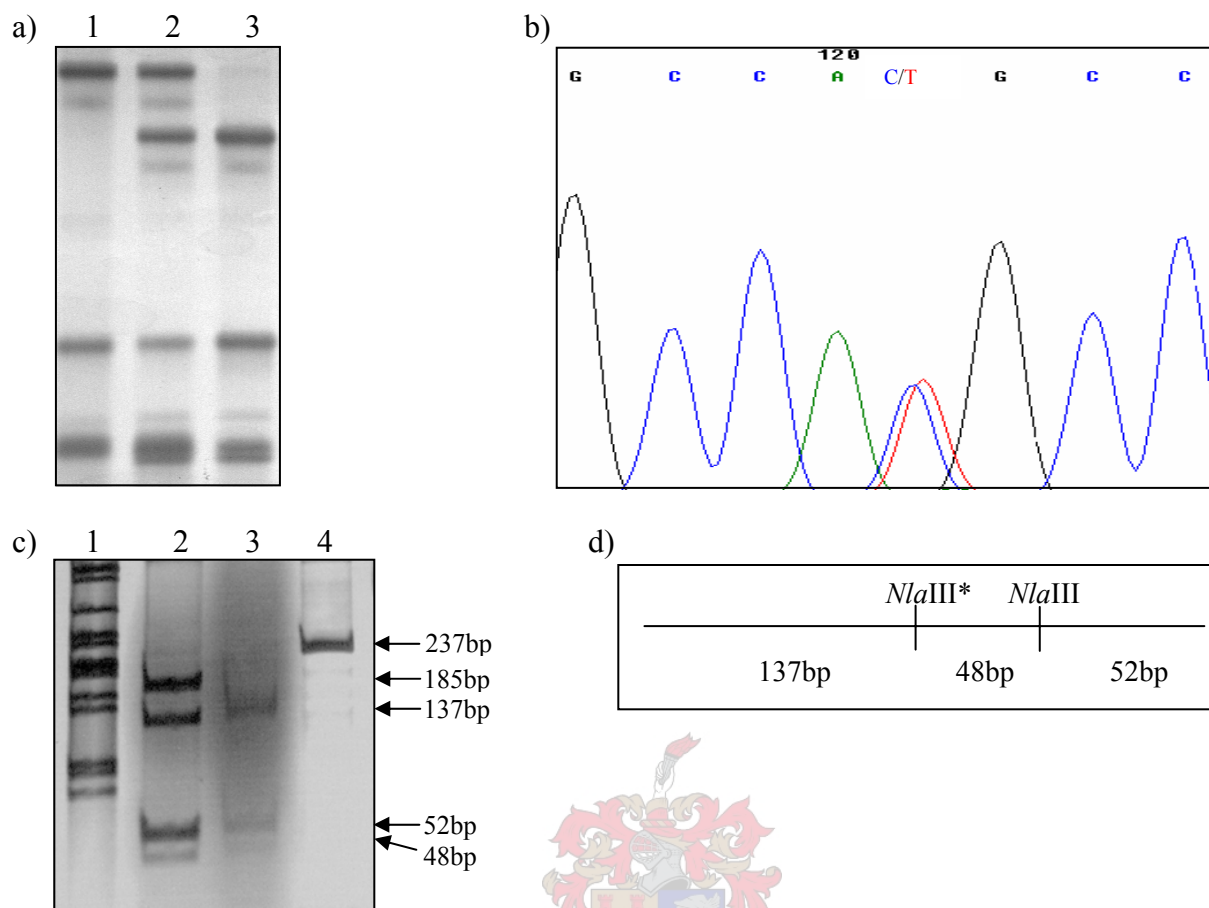


**Figure III.9. Identification of the novel *c19731t* polymorphism in intron 34 of MYBPC3**

a) PCR-SSCP analysis of the MYBPC3 exon 35 PCR-amplified product on a 10% MD-SSCP gel. Lane 1 = individual homozygous for the *c* allele (*c/c*); lane 2 = heterozygous individual (*c/t*); lane 3 = individual homozygous for the *t* allele (*t/t*).

b) Partial sequence of the plus-strand of intron 35 of MYBPC3 in an individual heterozygous for the *c19731t* polymorphism, showing the *c/t* substitution.

c) Genotyping of the MYBPC3 *c19731t* polymorphism by ASREA. Products of the *Nla*III restriction enzyme digestion of the 237bp PCR-amplified product of exon 35 were electrophoresed on a 12% polyacrylamide gel. The internal *Nla*III site generates 185bp and 52bp fragments in *c/c* homozygotes, while the presence of the *t* allele generates an additional *Nla*III site, resulting in additional 137bp and 48bp fragments in *c/t* heterozygotes. Lane 1 =  $\lambda$ Pst marker; lane 2 = heterozygous individual (*c/t*); lane 3 = individual homozygous for the *t* allele (*t/t*); lane 4 = undigested 237bp exon 35 PCR-amplified fragment..

d) Schematic representation of the PCR-amplified product, indicating the position of the *Nla*III sites. \* = variable restriction enzyme site.

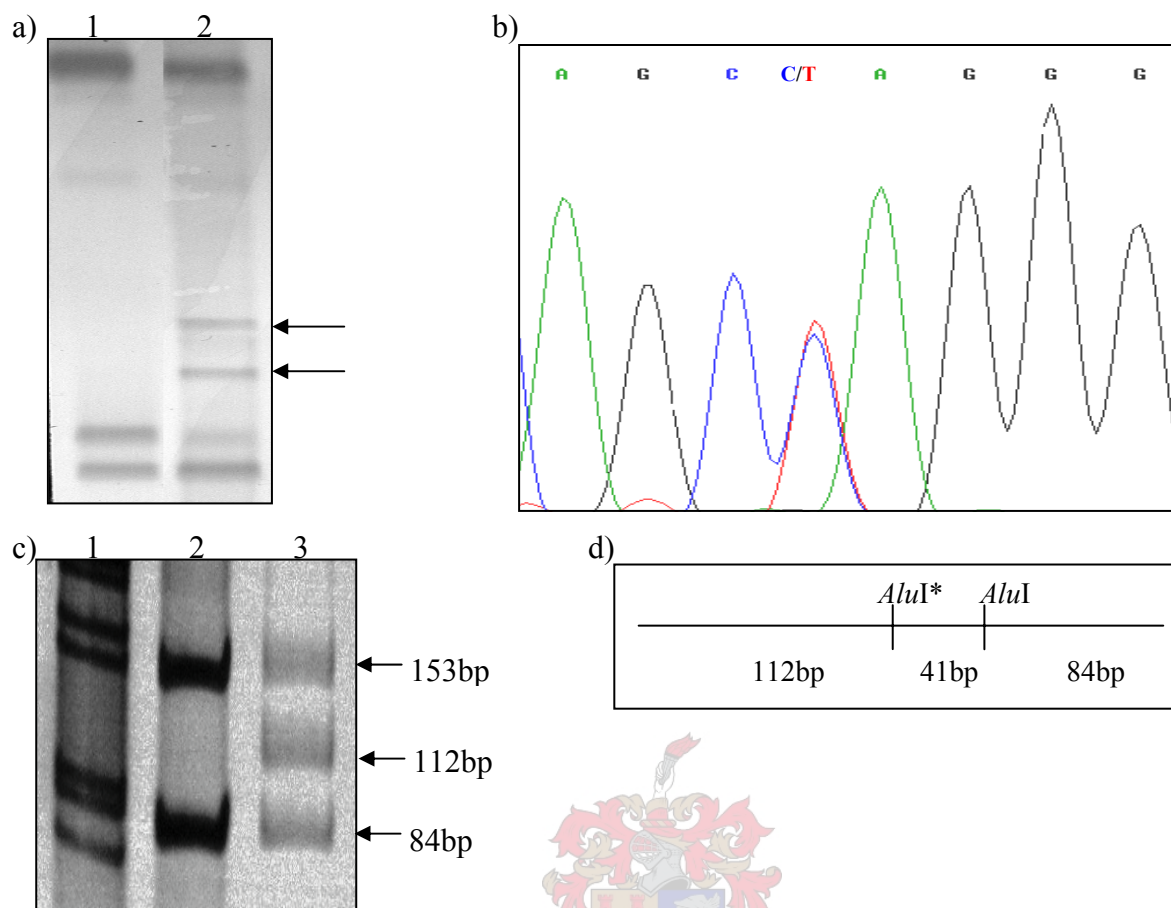


**Figure III.10. Identification of the novel g19706a ssSV in intron 34 of MYBPC3**

a) PCR-SSCP analysis of the MYBPC3 exon 35 PCR-amplified product on a 10% MD-SSCP gel. Lane 1 = individual homozygous for the g allele (g/g); lane 2 = heterozygous individual (g/a). The arrows indicate the mobility shift caused by the g/a polymorphism at nucleotide 19706 in a heterozygous individual.

b) Partial sequence of the minus-strand of exon 35 of MYBPC3 in an individual heterozygous for the g19706a polymorphism, showing the c/t substitution on the minus-strand.

c) Genotyping of the MYBPC3 g19706a polymorphism by ASREA. Products of the AluI restriction enzyme digestion of the 237bp PCR-amplified product of exon 35 were electrophoresed on a 12% polyacrylamide gel. The internal AluI site generates 153bp and 84bp fragments in g/g homozygotes, while the presence of the a allele generates an additional AluI site, resulting in additional 112bp and 41bp fragments in g/a heterozygotes. The 41bp fragment could not be resolved under these electrophoretic conditions. Lane 1 =  $\lambda$ Pst marker; lane 2 = individual homozygous for the g allele (g/g); lane 3 = heterozygous individual (g/a).

d) Schematic representation of the amplified product, indicating the position of the AluI sites. \* = variable restriction enzyme site.

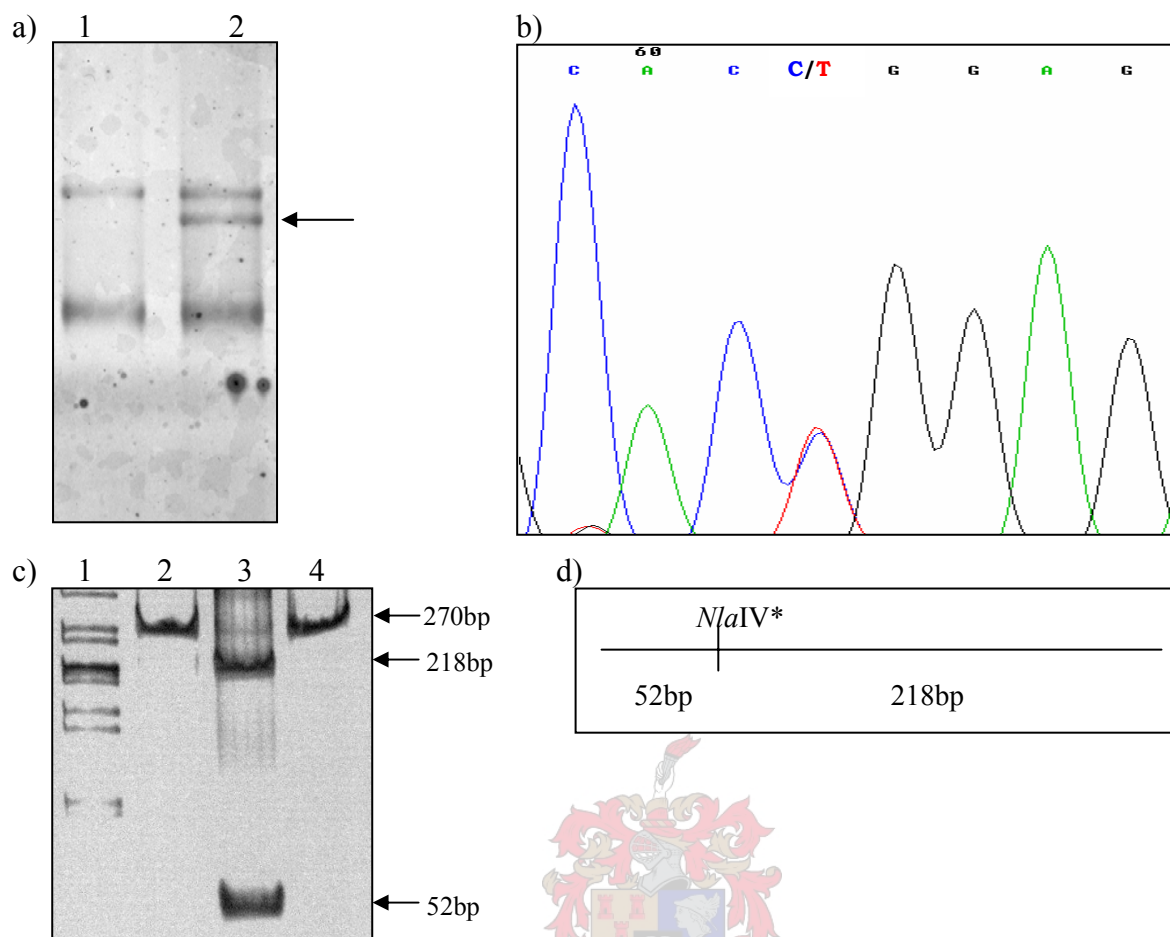


**Figure III.11. Identification of the novel T262T polymorphism in exon 8 of MYBPC3**

a) PCR-SSCP analysis of the MYBPC3 exon 8 PCR-amplified product on a 10% MD-SSCP gel. Lane 1 = individual homozygous for the *c* allele (*c/c*); lane 2 = heterozygous individual (*c/t*). The arrow indicates the mobility shift caused by the *c/t* polymorphism at nucleotide 4825 in a heterozygous individual.

b) Partial sequence of the coding strand of exon 8 of MYBPC3 in an individual heterozygous for the *c4825t* polymorphism, showing the *c/t* substitution.

c) Genotyping of the MYBPC3 *c4825t* polymorphism by ASREA. Products of the *NlaIV* restriction enzyme digestion of the 270bp PCR-amplified product of exon 8 were electrophoresed on a 12% polyacrylamide gel. The presence of the *t* allele generates an *NlaIV* site, resulting in the generation of 218bp and 52bp fragments in *c/t* heterozygotes. Lane 1 =  $\lambda$ Pst marker; lane 2 = individual homozygous for the *c* allele (*c/c*); lane 3 = heterozygous individual (*c/t*); lane 4 = undigested 270bp exon 8 PCR-amplified fragment.

d) Schematic representation of the PCR-amplified product, indicating the position of the *NlaIV* sites. \* = variable restriction enzyme site.

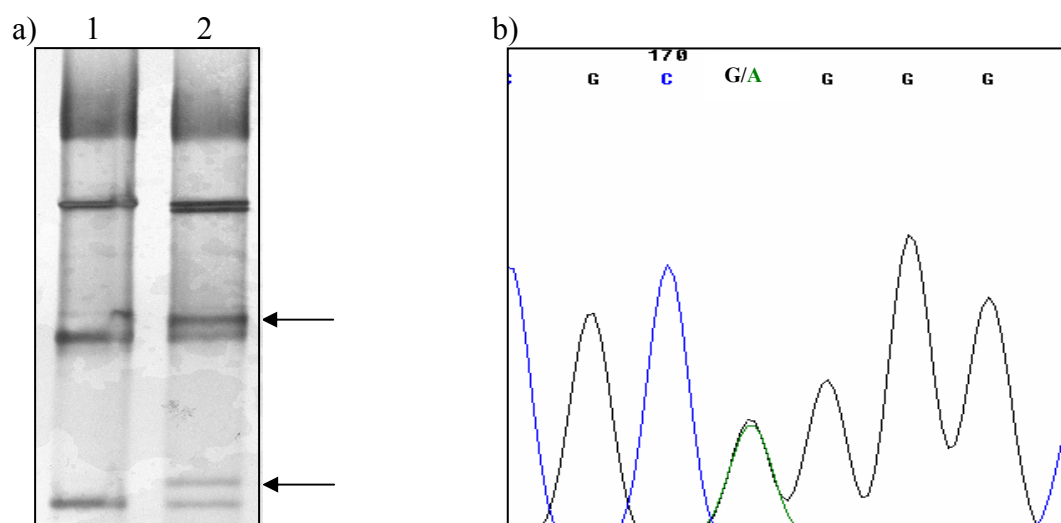
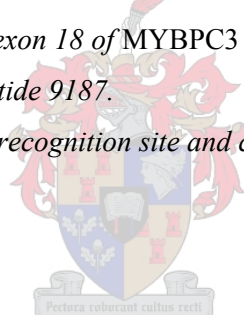


**Figure III.12. Identification of the novel A522A ssSV in MYBPC3 exon 18**

a) PCR-SSCP analysis of the MYBPC3 exon 18 PCR-amplified product on a 10% MD-SSCP gel. Lane 1 = individual homozygous for the g allele (g/g); lane 2 = heterozygous individual (g/a). The arrows indicate the mobility shift caused by the g/a polymorphism at nucleotide 9187 in a heterozygous individual.

b) Partial sequence of the coding strand of exon 18 of MYBPC3 in an individual heterozygous for the g9187a sSSV, showing the g/a substitution at nucleotide 9187.

This ssSV did not alter a restriction enzyme recognition site and could, therefore, not be confirmed by ASREA.



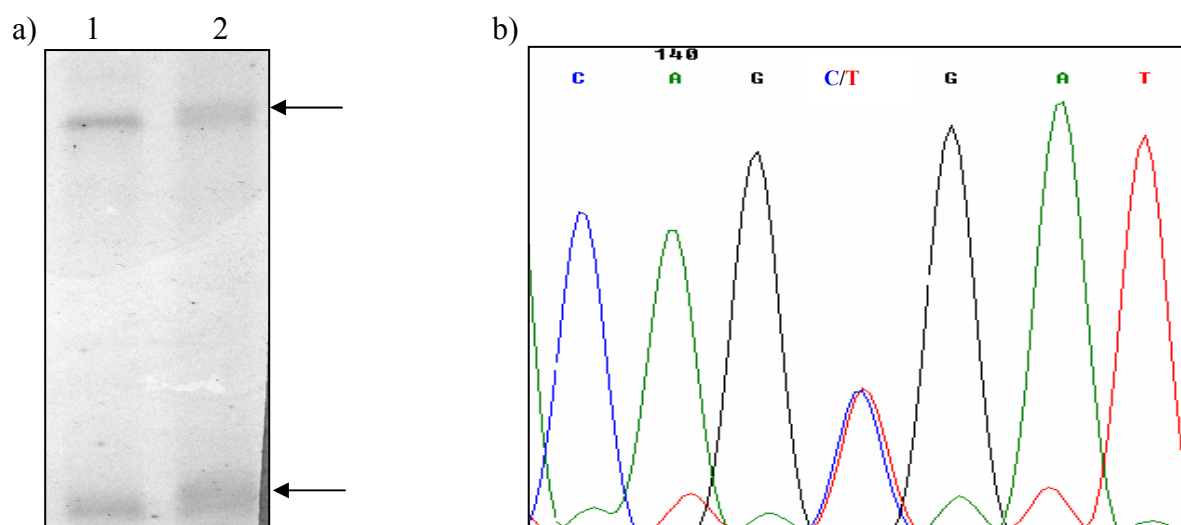


**Figure III.13. Identification of the novel S708S polymorphism in MYBPC3 exon 23**

a) PCR-SSCP analysis of the MYBPC3 exon 23 PCR-amplified product on a 10% MD-SSCP gel. Lane 1 = individual homozygous for the c allele (c/c); lane 2 = heterozygous individual (c/t). The arrows indicate the mobility shift caused by the c/t polymorphism at nucleotide 12474 in a heterozygous individual.

b) Partial sequence of the coding strand of exon 23 of MYBPC3 in an individual heterozygous for the c12474t polymorphism, showing the c/t substitution.

This polymorphism did not alter a restriction enzyme recognition site and could, therefore, not be confirmed by ASREA.



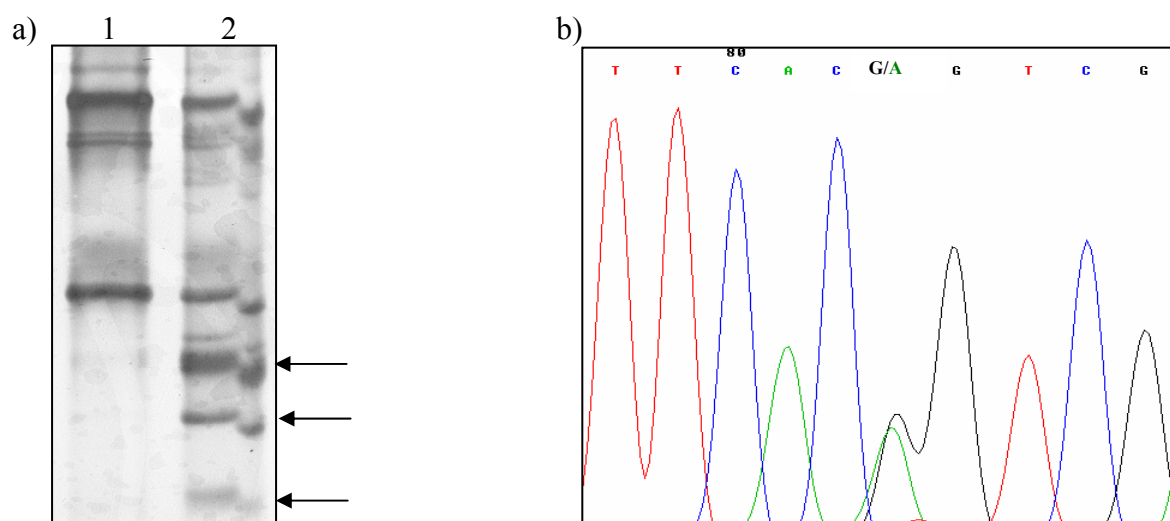


**Figure III.14. Identification of the novel T737T ssSV in exon 24 of MYBPC3**

a) PCR-SSCP analysis of the MYBPC3 exon 24 PCR-amplified product on a 10% MD-SSCP gel. Lane 1 = individual homozygous for the g allele (g/g); lane 2 = heterozygous individual (g/a). The arrows indicate the mobility shift caused by the g/a polymorphism at nucleotide 13199 in a heterozygous individual.

b) Partial sequence of the coding strand of exon 24 of MYBPC3 in an individual heterozygous for the g13199a SsSV, showing the **g/a** substitution.

This ssSV did not alter a restriction enzyme recognition site and could, therefore, not be confirmed by ASREA.



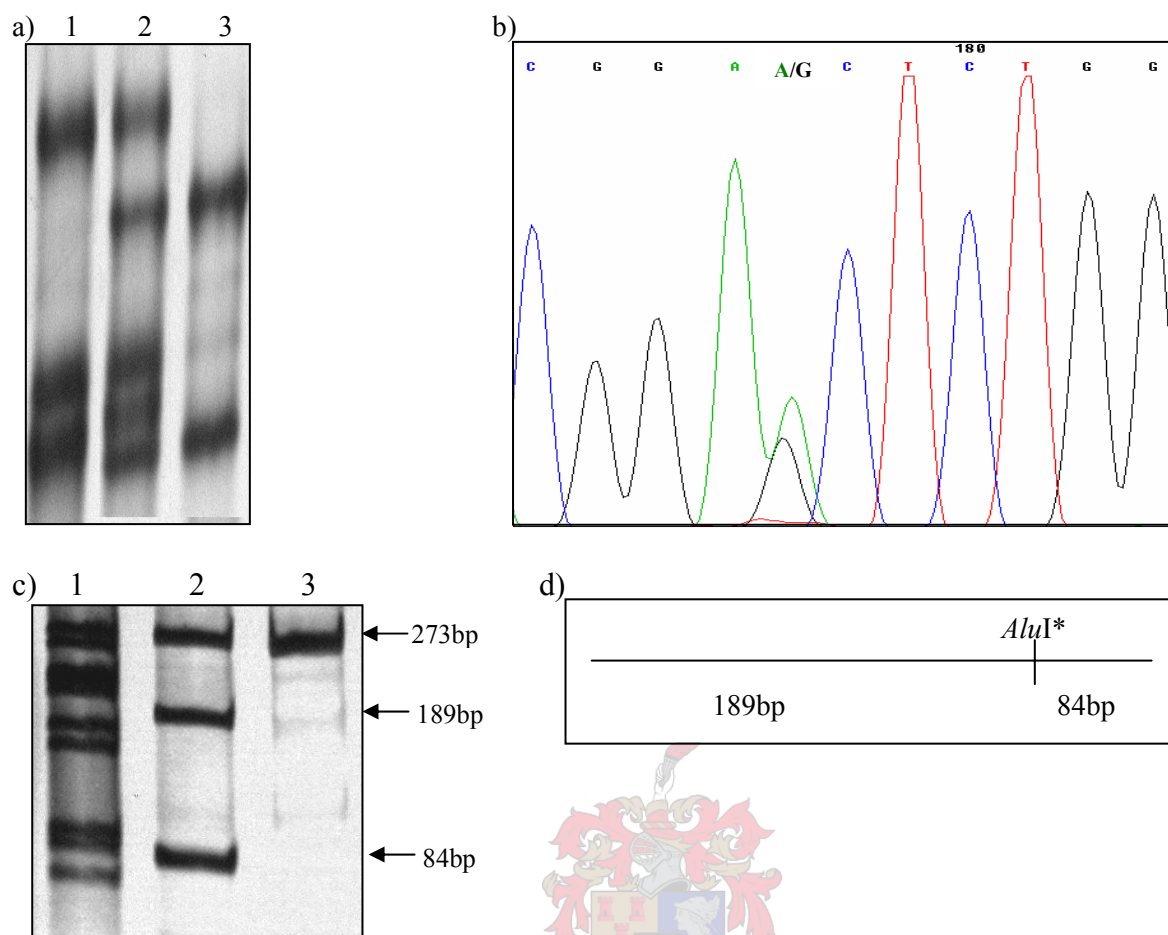


**Figure III.15. Identification of the novel E1096E polymorphism in exon 31 of MYBPC3**

a) PCR-SSCP analysis of the MYBPC3 exon 31 PCR-amplified product on a 10% MD-SSCP gel. Lane 1 = individual homozygous for the a allele (a/a); lane 2 = heterozygous individual (a/g); lane 3 = individual homozygous for the g allele (g/g).

b) Partial sequence of the coding strand of exon 31 of MYBPC3 in an individual heterozygous for the a18443g polymorphism, showing the a/g substitution.

c) Genotyping of the a18443g polymorphism by ASREA. Products of the AluI restriction enzyme digestion of the 273bp PCR-amplified product of exon 31 were electrophoresed on a 12% polyacrylamide gel. The g allele creates an AluI site, resulting in the generation of additional 189bp and 84bp fragments. Lane 1 =  $\lambda$ Pst marker; lane 2 = heterozygous individual (a/g); lane 3 = individual homozygous for the a allele (a/a).

d) Schematic representation of the amplified product, indicating the position of the induced AluI site. \* = variable restriction enzyme site.

### **III.1.2. PUTATIVE MISSENSE MUTATIONS IN *MYBPC3***

During the course of this study, several non-synonymous SNSs were identified within the coding sequence of *MYBPC3* (exons), and classified as putative HCM-causing missense mutations (table III.1). In order to establish whether these SNSs are indeed disease-causing, ethnically-matched control panels were screened for the presence of these SNSs (section II.1.2). Additionally, multiple sequence alignments were performed in order to establish whether amino acid substitutions occurred at conserved residues.

#### **III.1.2.1. Identification of the *MYBPC3* V158M putative HCM-causing missense mutation**

The V158M putative HCM-causing missense mutation was detected in one individual, of Caucasian descent, in the HCM-affected panel. This putative disease-causing mutation, caused by the g2626a SNS in exon 5 of *MYBPC3* (figure III.16), occurs at a conserved residue in the C1 domain of cMyBPC (figure III.17). Following the screening of a control panel, consisting of 110 individuals of Caucasian descent, this SNS was detected in three individuals.

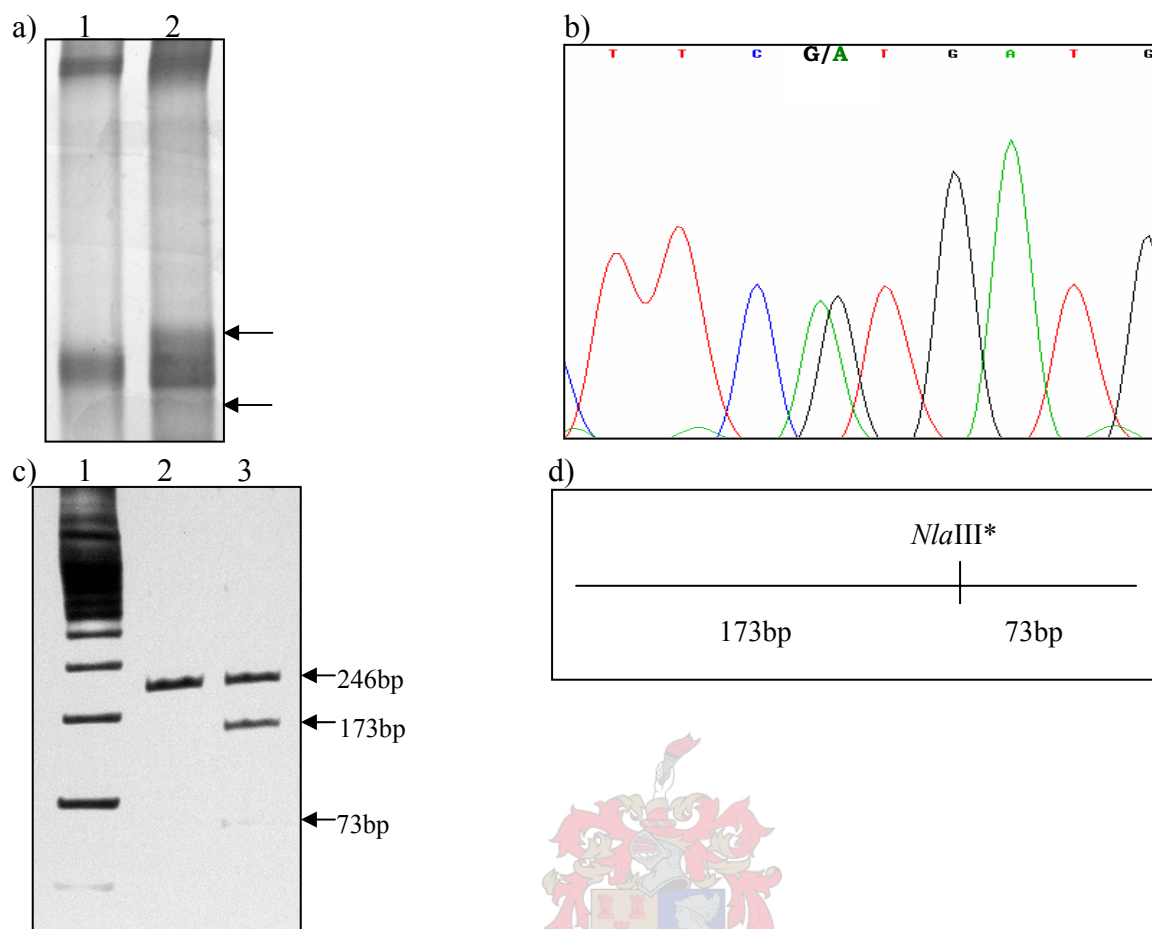


**Figure III.16. Identification of the novel V158M putative HCM-causing missense mutation in exon 5 of MYBPC3**

a) PCR-SSCP analysis of the MYBPC3 exon 5 PCR-amplified product on a 10% MD-SSCP gel. Lane 1 = individual homozygous for the g allele (g/g); lane 2 = heterozygous individual (g/a). The arrows indicate the mobility shift caused by the g2626a SNS in a heterozygous individual.

b) Partial sequence of the coding strand of exon 5 of MYBPC3 in a heterozygous individual, showing the g/a substitution.

c) Genotyping of the MYBPC3 V158M putative HCM-causing mutation by ASREA. Products of the NlaIII restriction enzyme digestion of the 246bp PCR-amplified product of exon 5 were electrophoresed on a 12% polyacrylamide gel. The NlaIII site is absent in the g/g homozygote, indicated by the presence of only the 246bp product, while the presence of the a allele creates an NlaIII site, resulting in the generation of 173bp and 73bp fragments. Lane 1 =  $\lambda$ Pst marker; lane 2 = individual homozygous for the g allele (g/g); lane 3 = heterozygous individual (g/a).

d) Schematic representation of the PCR-amplified product, indicating the position of the induced NlaIII site. \* = variable restriction enzyme site.

↓

Human cMyBPC	TPGAPDDP IGLFVMRPQDGEVTVGGSIT
Mouse cMyBPC	HQGAPDDP IGLFLMRPQDGEVTVGGSIV
Chicken cMyBPC	QPEEPVDF IGLFVTRPQDGEVTVGGNIT
Frog cMyBPC	QPEPPKDE IGLFLERPQDGEITVGTNIK
Human fsMyBPC	QSPTAEPTGVFLKKPDSVSVETGKDAV
Mouse fsMyBPC	QSPTAEPTGIFLKKPDSVSVETGKDAV
Human ssMyBPC	KONANSQLSILFIEKPQGGTVKVGEDIT
	:    :* :    :* :    :    . *    .

**Figure III.17. Cross-species/isoform multiple sequence alignment of a portion of the C1 domain of MyBPC**  
 Chicken cMyBPC = chicken cardiac myosin binding protein C; frog cMyBPC = frog cardiac myosin binding protein C; human cMyBPC = human cardiac myosin binding protein C; human fsMyBPC = human fast skeletal myosin binding protein C; human ssMyBPC = human slow skeletal myosin binding protein C; mouse cMyBPC = mouse cardiac myosin binding protein C; mouse fsMyBPC = mouse fast skeletal myosin binding protein C; \* = absolute conservation of amino acid residue; : = charge of amino acid residue conserved; . = conserved as a hydrophobic or hydrophilic amino acid residue. The arrow at the top of the figure indicates the position of cardiac myosin binding protein C residue 158 which is affected by the V158M putative HCM-causing mutation (multiple sequence alignment performed using ClustalW, available at <http://www.ebi.ac.uk/service/ncbi/blast/>).

### III.1.2.2. Identification of the MYBPC3 A181T putative HCM-causing missense mutation

The A181T putative HCM-causing missense mutation was detected in two individuals, both of mixed ancestry, in the HCM-affected panel. This putative disease-causing mutation, caused by the g2785a SNS in exon 6 of MYBPC3 (figure III.18), occurs at a non-conserved residue in the C1 domain of cMyBPC (figure III.19). Following the screening of a control panel, consisting of 105 individuals of mixed ancestry, this SNS was detected in two individuals.

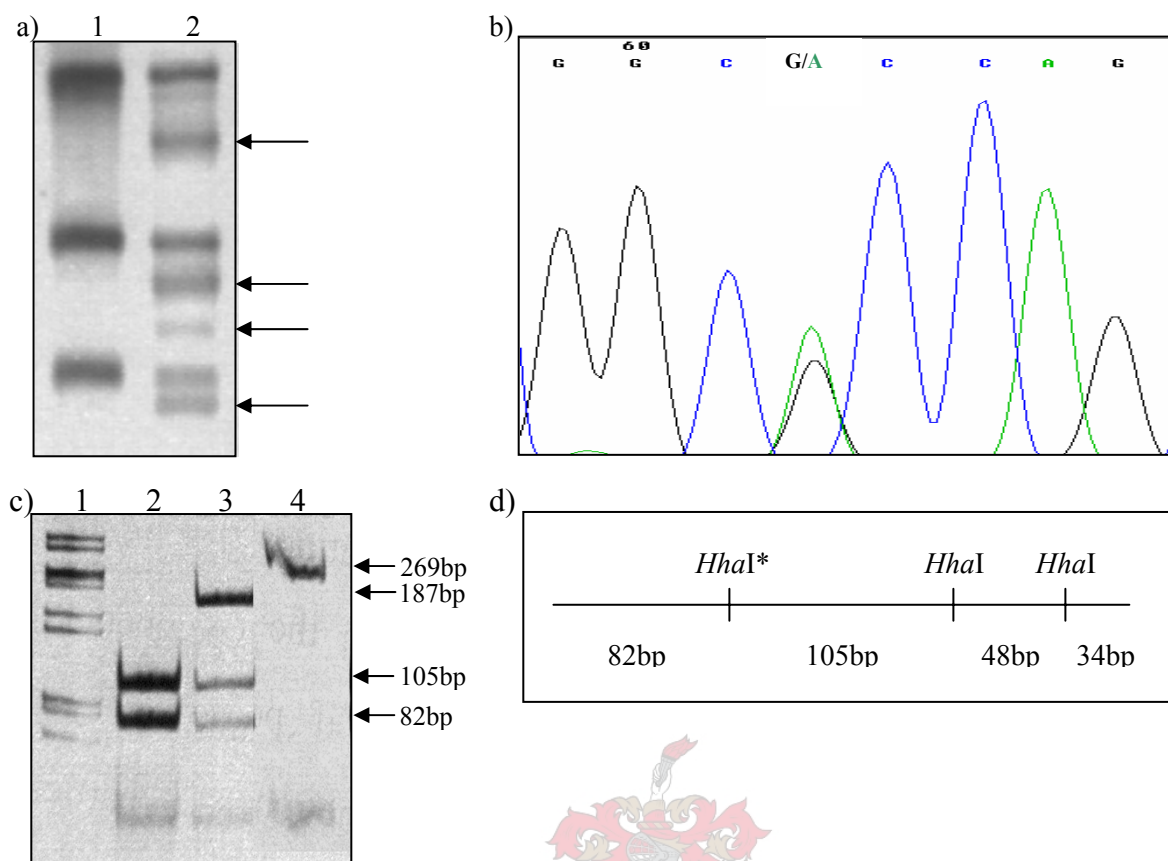


**Figure III.18. Identification of the novel A181T putative HCM-causing mutation in exon 6 of MYBPC3**

a) PCR-SSCP analysis of the MYBPC3 exon 6 PCR-amplified product on a 10% MD-SSCP gel. Lane 1 = individual homozygous for the g allele (g/g); lane 2 = heterozygous individual (g/a). The arrows indicate the mobility shift caused by the g2785a SNS in a heterozygous individual.

b) Partial sequence of the coding strand of exon 6 of MYBPC3 in a heterozygous individual, showing the g/a substitution.

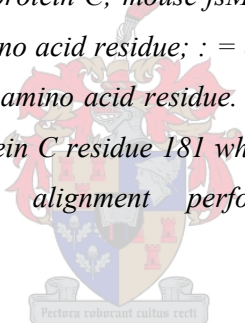
c) Genotyping of the MYBPC3 A181T putative HCM-causing mutation by ASREA. Products of the HhaI restriction enzyme digestion of the 269bp PCR-amplified product of exon 5 were electrophoresed on a 12% polyacrylamide gel. The internal HhaI sites generate 34bp, 48bp, 82bp and 105bp fragments in g/g homozygotes, while the presence of the a allele abolishes an HhaI site, resulting in an additional 187bp fragment in g/a heterozygotes. The 34bp and 48bp fragments could, however, not be resolved under these electrophoretic conditions. Lane 1 =  $\lambda$ Pst marker; lane 2 = individual homozygous for the g allele (g/g); lane 3 = heterozygous individual (g/a); lane 4 = undigested exon 6 PCR-amplified fragment.

d) Schematic representation of the PCR-amplified product, indicating the position of the HhaI sites. \* = variable restriction enzyme site.

↓

Human cMyBPC	FSARVAGASLLKPPVVKWFKGKWVDLSSK
Mouse cMyBPC	FSARVAGASLLKPPVVKWFKGKWVDLSSK
Chicken cMyBPC	FTAKVAGESLLKKPSVKWFKGKWMDLASK
Frog cMyBPC	FTARIAGANLIKKPVVKWFKGKWMDLTSK
Human fsMyBPC	VVAKVNGKELPKPTIKWFKGKWLELGSK
Mouse fsMyBPC	ILAKVNGKELPGKPTIKWFKGKWQELGSK
Human ssMyBPC	FIAKVKAEDLLRKPTIKWFKGKWMDLASK
	. *:: . .* * :***** :* **

**Figure III.19. Cross-species/isoform multiple sequence alignment of a portion of the C1 domain of MyBPC**  
 Chicken cMyBPC = chicken cardiac myosin binding protein C; frog cMyBPC = frog cardiac myosin binding protein C; human cMyBPC = human cardiac myosin binding protein C; human fsMyBPC = human fast skeletal myosin binding protein C; human ssMyBPC = human slow skeletal myosin binding protein C; mouse cMyBPC = mouse cardiac myosin binding protein C; mouse fsMyBPC = mouse fast skeletal myosin binding protein C; \* = absolute conservation of amino acid residue; : = charge of amino acid residue conserved; . = conserved as a hydrophobic or hydrophilic amino acid residue. The arrow at the top of the figure indicates the position of cardiac myosin binding protein C residue 181 which is affected by the A181T putative HCM-causing mutation (multiple sequence alignment performed using ClustalW, available at <http://www.ebi.ac.uk/servicestmp/clustalw>).



### III.1.2.3. Identification of the *MYBPC3* R177H putative HCM-causing missense mutation

The R177H putative HCM-causing missense mutation was detected in five individuals in the HCM-affected panel. Two of these individuals were of mixed ancestry, two were of Caucasian descent and one individual was of Xhosa descent. This putative disease-causing mutation, caused by the g2774a SNS in exon 6 of *MYBPC3* (figure III.20), occurs at a conserved residue in the C1 domain of cMyBPC (figure III.21). Following the screening of a control panel, consisting of 235 individuals of Xhosa descent (n = 137) and mixed ancestry (n = 105), this SNS was detected in six individuals, all of Xhosa descent.

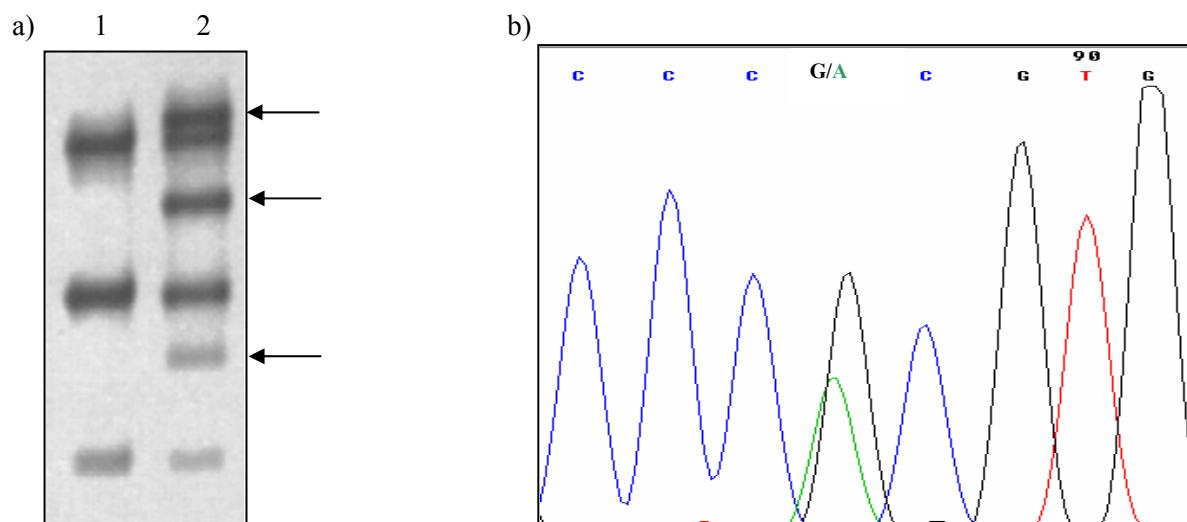
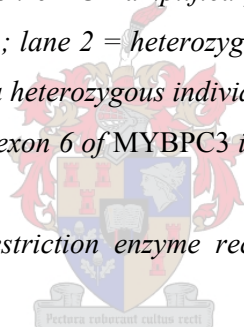


**Figure III.20. Identification of the novel R177H putative HCM-causing mutation in exon 6 of MYBPC3**

a) PCR-SSCP analysis of the MYBPC3 exon 6 PCR-amplified product on a 10% MD-SSCP gel. Lane 1 = individual homozygous for the g allele (g/g); lane 2 = heterozygous individual (g/a). The arrows indicate the mobility shift caused by the g2774a SNS in a heterozygous individual.

b) Partial sequence of the coding strand of exon 6 of MYBPC3 in a heterozygous individual, showing the g/a substitution.

This putative mutation did not alter a restriction enzyme recognition site and could, therefore, not be confirmed by ASREA.



```

      ↓
Human cMyBPC   FSARVAGASLLKPPVVKWFKGKWVDLSSK
Mouse cMyBPC   FSARVAGASLLKPPVVKWFKGKWVDLSSK
Chicken cMyBPC FTAKVAGESLLKKPSVKWFKGKWMDLASK
Frog cMyBPC    FTARIAGANLIKPPVVKWFKGKWMDLTSK
Human fsMyBPC  VVAKVNGKELPDKPTIKWFKGKWLELGSK
Mouse fsMyBPC  ILAKVNGKELPGKPTIKWFKGKWQELGSK
Human ssMyBPC  FIAKVKAEDLLRKPTIKWFKGKWMDLASK
               . * : : . . *   * :***** : * **

```

**Figure III.21. Cross-species/isoform multiple sequence alignment of a portion of the C1 domain of MyBPC**  
 Chicken cMyBPC = chicken cardiac myosin binding protein C; frog cMyBPC = frog cardiac myosin binding protein C; human cMyBPC = human cardiac myosin binding protein C; human fsMyBPC = human fast skeletal myosin binding protein C; human ssMyBPC = human slow skeletal myosin binding protein C; mouse cMyBPC = mouse cardiac myosin binding protein C; mouse fsMyBPC = mouse fast skeletal myosin binding protein C; \* = absolute conservation of amino acid residue; : = charge of amino acid residue conserved; . = conserved as a hydrophobic or hydrophilic amino acid residue. The arrow at the top of the figure indicates the position of cardiac myosin binding protein C residue 177 which is affected by the R177H putative HCM-causing mutation (multiple sequence alignment performed using ClustalW, available at <http://www.ebi.ac.uk/services/mp/clustalw>).

#### III.1.2.4. Identification of the MYBPC3 G278E putative HCM-causing missense mutation

The G278E putative HCM-causing missense mutation was detected in one individual, of mixed ancestry, in the HCM-affected panel. This putative disease-causing mutation, caused by the g5047a SNS in exon 9 of MYBPC3 (figure III.22), occurs at a conserved residue in the cardiac-specific LAGGGRIS insertion in the MyBPC-motif (figure III.23). Following the screening of a control panel, consisting of 104 HCM-unaffected individuals of mixed ancestry, this SNS was detected in five individuals.

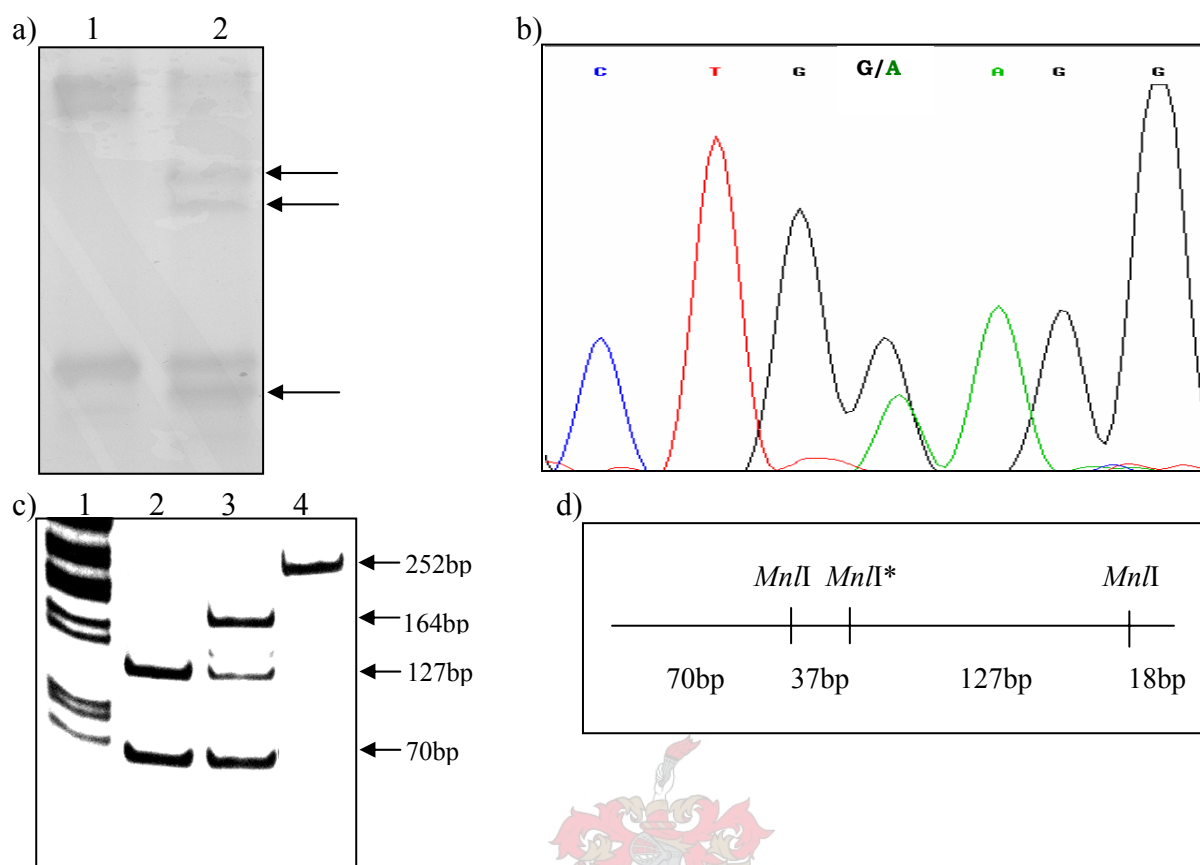


**Figure III.22. Identification of the G278E polymorphism in exon 9 of MYBPC3**

a) PCR-SSCP analysis of the MYBPC3 exon 9 PCR-amplified product on a 10% MD-SSCP gel. Lane 1 = individual homozygous for the g allele (g/g); lane 2 = heterozygous individual (g/a). The arrows indicate the mobility shift caused by the g5047a SNS in a heterozygous individual.

b) Partial sequence of the coding strand of exon 9 of MYBPC3 in a heterozygous individual, showing the g/a substitution.

c) Genotyping of the MYBPC3 G278E putative HCM-causing missense mutation by ASREA. Products of the MnlI restriction enzyme digestion of the 252bp PCR-amplified product of exon 9 were electrophoresed on a 12% polyacrylamide gel. The internal MnlI sites generate 18bp, 37bp, 70bp and 127bp fragments in g/g homozygotes, while the presence of the a allele abolishes an MnlI site, resulting in an additional 164bp fragment in g/a heterozygotes. The 18bp and 37bp fragments could, however, not be resolved under these electrophoretic conditions. Lane 1 =  $\lambda$ Pst marker; lane 2 = individual homozygous for the g allele (g/g); lane 3 = heterozygous individual (g/a); lane 4 = undigested exon 9 PCR-amplified fragment.

d) Schematic representation of the PCR-amplified product, indicating the position of the MnlI sites. \* = variable restriction enzyme site.

```

Human cMyBPC      DLDLLSAFRRTSLAGGRRIS-----DS
Mouse cMyBPC      DLDLRSAFRRTSLAGAGRRTS-----DS
Chicken cMyBPC    EMDIRAAFRTSLAGGRRMTSAFLSTEG
Frog cMyBPC       EVDIRAAFRTSLVGAAKRRVSIAFSGDG
Human fsMyBPC     SGQSLESFKRTSEKKS-----
Mouse fsMyBPC     SGQSLESFKRSGDGKS-----
Human ssMyBPC     NIDIRSAFKRSG-----EG
. :   :*:*:.

```

**Figure III.23. Cross-species/isoform multiple sequence alignment of a portion of the MyBPC-motif of MyBPC**

Chicken cMyBPC = chicken cardiac myosin binding protein C; frog cMyBPC = frog cardiac myosin binding protein C; human cMyBPC = human cardiac myosin binding protein C; human fsMyBPC = human fast skeletal myosin binding protein C; human ssMyBPC = human slow skeletal myosin binding protein C; mouse cMyBPC = mouse cardiac myosin binding protein C; mouse fsMyBPC = mouse fast skeletal myosin binding protein C; \* = absolute conservation of amino acid residue; : = charge of amino acid residue conserved; . = conserved as a hydrophobic or hydrophilic amino acid residue. The arrow at the top of the figure indicates the position of cardiac myosin binding protein C residue 278 which is affected by the G278E putative HCM-causing mutation (multiple sequence alignment performed using ClustalW, available at <http://www.ebi.ac.uk/servecstmp/clustalw>).



### III.1.2.5. Identification of the MYBPC3 G507R putative HCM-causing missense mutation

The G507R putative HCM-causing missense mutation was detected in one individual, of Zulu descent, in the HCM-affected panel. This putative disease-causing mutation, caused by the g9140a SNS in exon 18 of MYBPC3 (figure III.24), occurs at a highly conserved residue in the C3 domain of cMyBPC (figure III.25). This SNS was not present in a control panel consisting of 50 individuals of Zulu descent and 50 individuals of Xhosa descent.

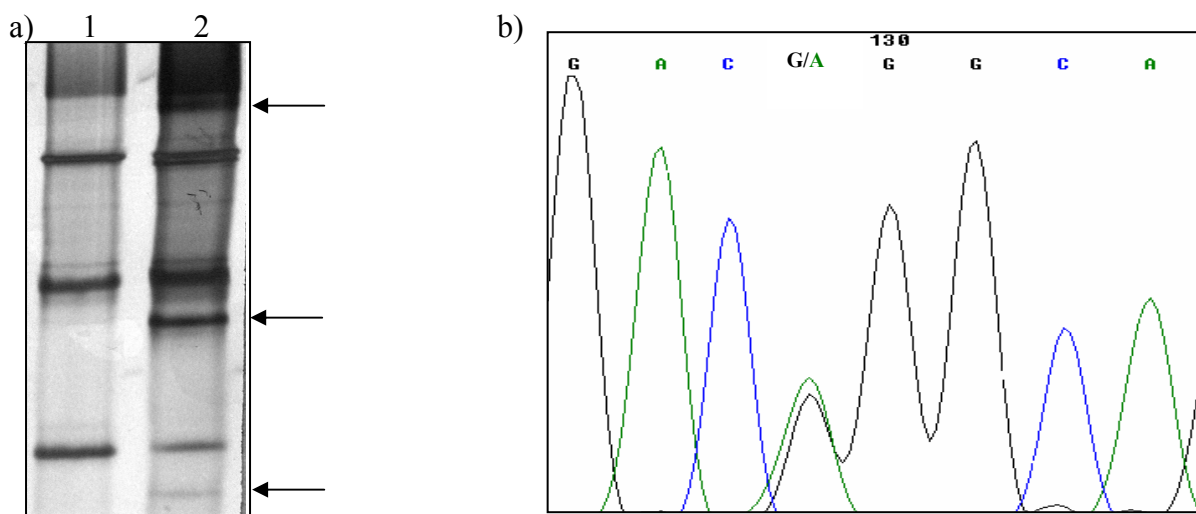
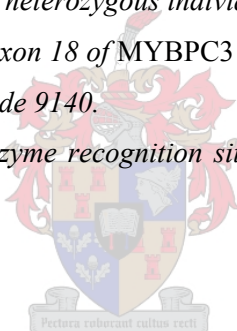


**Figure III.24. Identification of the G507R putative HCM-causing mutation in exon 18 of MYBPC3**

a) PCR-SSCP analysis of the MYBPC3 exon 18 PCR-amplified product on a 10% MD-SSCP gel. Lane 1 = individual homozygous for the g allele (g/g); lane 2 = heterozygous individual (g/a). The arrows indicate the mobility shift caused by the g9140a SNS in a heterozygous individual.

b) Partial sequence of the coding strand of exon 18 of MYBPC3 in an individual heterozygous for the g9140a SNS, showing the **g/a** substitution at nucleotide 9140.

This mutation did not alter a restriction enzyme recognition site and could, therefore, not be confirmed by ASREA.



```

      ↓
Human cMyBPC -YRFKKDGQRHHL I INE AMLE
Mouse cMyBPC -YRFKKDGRKHHL I INE ATLE
Chicken cMyBPC -YRFKKDGKKQYL I INESTKE
Frog cMyBPC -YRFKKDGKKHYL I INETTVE
Human fsMyBPC ǂYRFKKDGKRHIL I FSDVVQE
Mouse fsMyBPC ǂYRFKKDGKRHIL I YSDVAQE
Human ssMyBPC -YRIRVEGKKHIL I IEGATKA
      **:: :*::: ** .

```

**Figure III.25. Cross-species/isoform multiple sequence alignment of a portion of the C3 domain of MyBPC**  
*Chicken cMyBPC = chicken cardiac myosin binding protein C; frog cMyBPC = frog cardiac myosin binding protein C; human cMyBPC = human cardiac myosin binding protein C; human fsMyBPC = human fast skeletal myosin binding protein C; human ssMyBPC = human slow skeletal myosin binding protein C; mouse cMyBPC = mouse cardiac myosin binding protein C; mouse fsMyBPC = mouse fast skeletal myosin binding protein C; \* = absolute conservation of amino acid residue; : = charge of amino acid residue conserved; . = conserved as a hydrophobic or hydrophilic amino acid residue. The arrow at the top of the figure indicates the position of cardiac myosin binding protein C residue 507 which is affected by the G507R putative HCM-causing mutation (multiple sequence alignment performed using ClustalW, available at <http://www.ebi.ac.uk/service/seq/seq.cgi>).*

### III.1.2.6. Identification of the *MYBPC3* V896M putative HCM-causing missense mutation



The V896M putative HCM-causing missense mutation was detected in one individual, of Caucasian descent, in the HCM-affected panel. This putative disease-causing mutation, caused by the g15751a SNS in exon 27 of *MYBPC3* (figure III.26), occurs at a conserved residue in the C7 domain of cMyBPC (figure III.27). The g15751a SNS was not detected in a control panel consisting of 102 individuals of Caucasian descent.

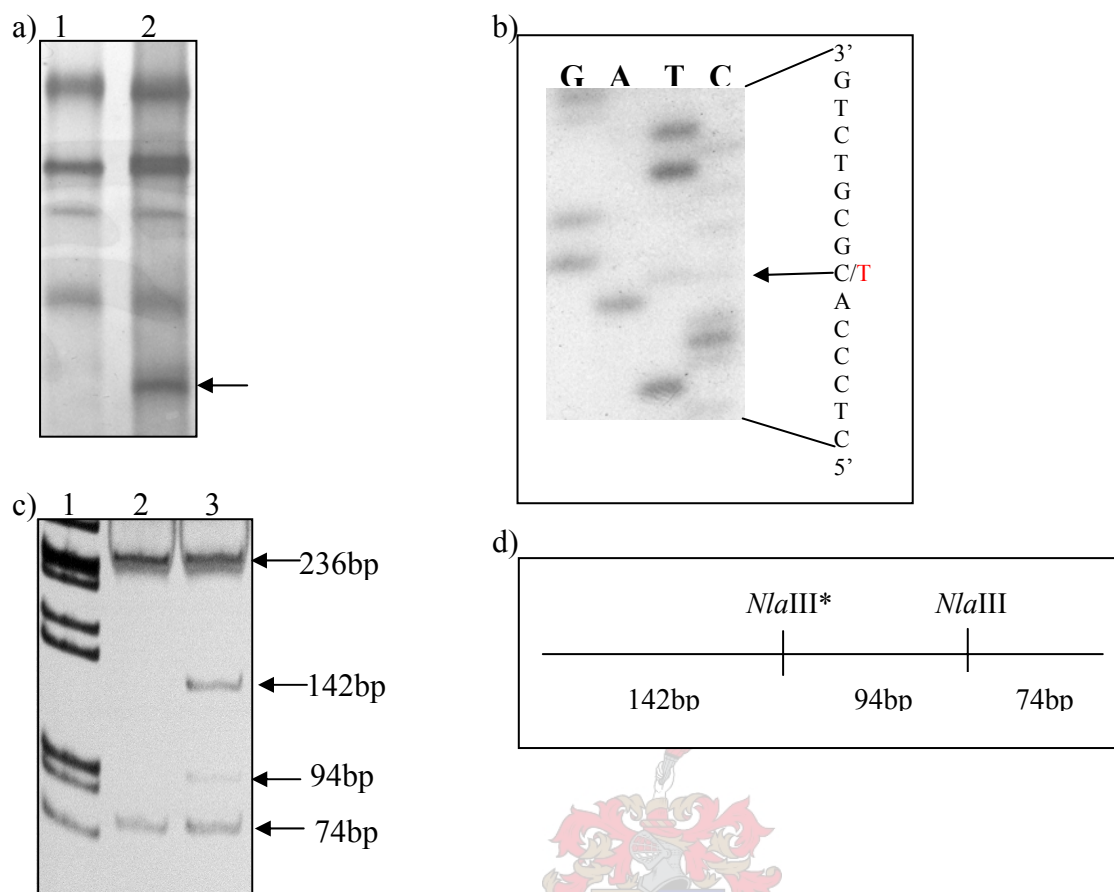


**Figure III.26. Identification of the novel V896M putative HCM-causing mutation in exon 27 of MYBPC3**

a) PCR-SSCP analysis of the MYBPC3 exon 27 PCR-amplified product on an 8% MD-SSCP gel. Lane 1 = individual homozygous for the g allele; lane 2 = heterozygous individual (g/a). The arrow indicates the mobility shift caused by the g15751a SNS in a heterozygous individual.

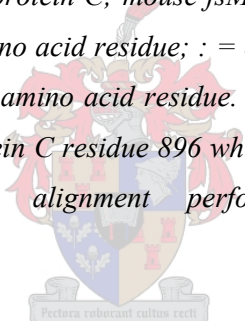
b) Partial sequence of the non-coding strand of exon 27 of MYBPC3 in an individual heterozygous for the g15751a SNS, showing the c/t substitution on the non-coding strand.

c) Genotyping of the MYBPC3 V896M putative HCM-causing missense mutation by ASREA. Products of the NlaIII restriction enzyme digestion of the 310bp PCR-amplified product of exon 27 were electrophoresed on a 12% polyacrylamide gel. The internal NlaIII site generates 236bp and 74bp fragments in g/g homozygotes, while the presence of the a allele creates an additional NlaIII site, resulting in additional 142bp and 94bp fragments in g/a heterozygotes. Lane 1 =  $\lambda$ Pst marker; lane 2 = individual homozygous for the g allele (g/g); lane 3 = heterozygous individual (g/a).

d) Schematic representation of the PCR-amplified product, indicating the position of the NlaIII sites. \* = variable restriction enzyme site.

	↓
Human cMyBPC	DTTVSLKWRPPERVGAGGLDGYSV
Mouse cMyBPC	DTTVSLKWRPPERVGAGGLDGYSV
Chicken cMyBPC	DTTVALKWRPPERIGAGGLDGYIV
Frog cMyBPC	DTSISLKWRPPERIGAGGLDGYTV
Human fsMyBPC	DTTTTLKWRPPNRIGAGGIDGYLV
Mouse fsMyBPC	DTTTTLKWRPPDRIGAGGIDGYLV
Human ssMyBPC	DTTVTMRWRPPDHIGAAGLDGYVL
	** : : : * * * * : : : * * . * : * * * :

**Figure III.27. Cross-species/isoform multiple sequence alignment of a portion of the C7 domain of MyBPC**  
*Chicken cMyBPC = chicken cardiac myosin binding protein C; frog cMyBPC = frog cardiac myosin binding protein C; human cMyBPC = human cardiac myosin binding protein C; human fsMyBPC = human fast skeletal myosin binding protein C; human ssMyBPC = human slow skeletal myosin binding protein C; mouse cMyBPC = mouse cardiac myosin binding protein C; mouse fsMyBPC = mouse fast skeletal myosin binding protein C; \* = absolute conservation of amino acid residue; : = charge of amino acid residue conserved; . = conserved as a hydrophobic or hydrophilic amino acid residue. The arrow at the top of the figure indicates the position of cardiac myosin binding protein C residue 896 which is affected by the V896M putative HCM-causing mutation (multiple sequence alignment performed using ClustalW, available at <http://www.ebi.ac.uk/servecstmp/clustalw>).*



### III.1.3. IDENTIFICATION OF PUTATIVE SPLICING MUTATIONS IN *MYBPC3*

Several SNSs identified during the course of this study (table III.1) were predicted to alter the splicing of the *MYBPC3* transcript. These SNSs, occurring in both the exonic and intronic regions of *MYBPC3*, were, therefore, deemed to be putative splicing HCM-causing mutations.

### III.1.3.1. Identification of the exon 5 SdS -13 c>t putative splicing mutation

The c2646t SNS, occurring in the coding sequence of exon 5 (table III.1 and figure III.28), was detected in eight probands in the HCM-affected panel. This SNS causes codon 164 to change from *ggc* to *ggt*, both encoding glycine (G) (G164G). Computational analysis, however, revealed that this SNS creates a cryptic SdS 15bp upstream of, and approximately of the same strength as, the natural exon 5 SdS, as described by Carrier et al., (1997) (figure III.29). It was, therefore, hypothesised that this cryptic SdS may be utilised preferentially, due to the processivity of splicing (personal communication, Dr Peter Rogan, 23 December 1999), and that this SNS may act as an HCM-causing splicing mutation (figure III.29).

RT-PCR analysis (section II.6.4 and table II.7) was, however, hampered by the fact that the RT-PCR product resulting in the normal splicing of the *MYBPC3* transcript, and that produced by the putative aberrantly spliced transcript, were similar in size (659bp and 644bp, respectively) (figure III.29). The possibility that this small size difference would not be detectable by agarose gel electrophoresis was resolved by digestion of RT-PCR products with *BstEII*, as this site would be absent from the aberrantly spliced transcript. Following digestion of the RT-PCR product with *BstEII*, only the digested 435bp and 224bp fragments were detected (figure III.29), indicating that the c2646t SNS does not affect splicing of the *MYBPC3*.

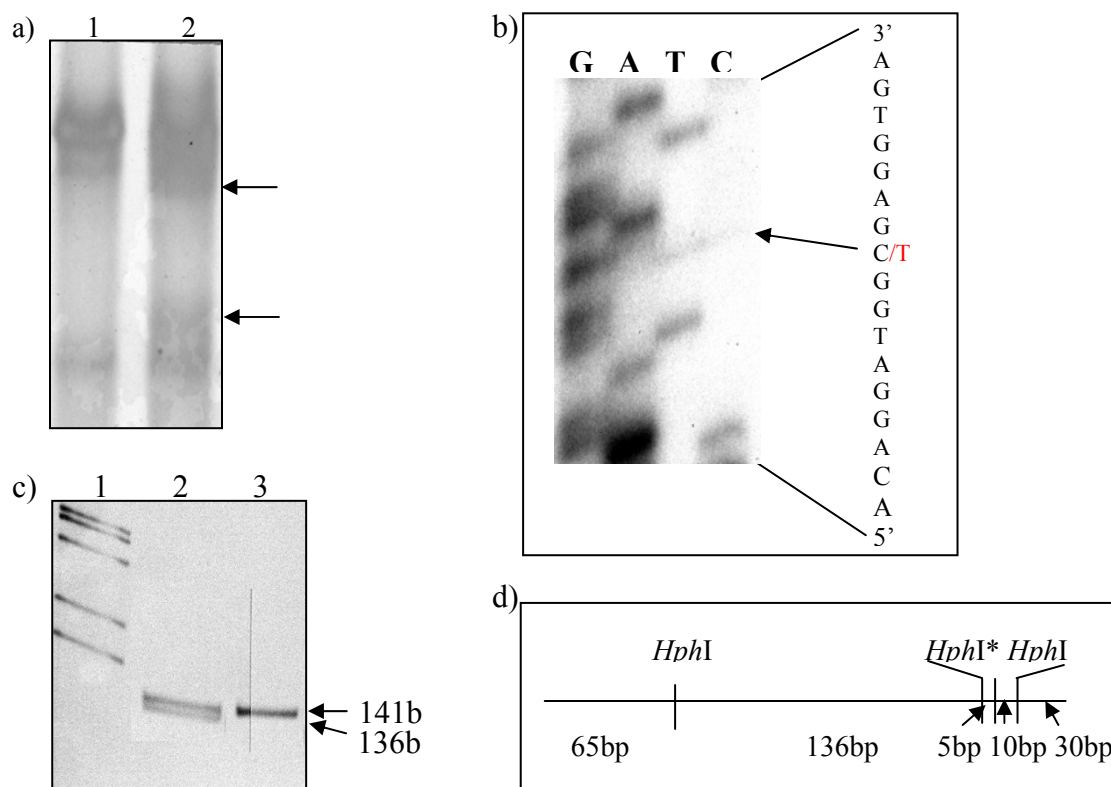


**Figure III.28. Identification of the exon 5 SdS-13 c>t putative HCM-causing splicing mutation**

a) PCR-SSCP analysis of the MYBPC3 exon 5 PCR-amplified product on a 10% MD-SSCP gel. Lane 1 = individual homozygous for the c allele (c/c); lane 2 = heterozygous individual (c/t). The arrows indicate the mobility shift caused by the c2646t SNS in a heterozygous individual.

b) Partial sequence of the coding strand of exon 5 of MYBPC3 in an individual heterozygous for the c2646t SNS, showing the c/t substitution.

c) Genotyping of the MYBPC3 c2646t putative HCM-causing splicing mutation by ASREA. Products of the HphI restriction enzyme digestion of the 246bp PCR-amplified product of exon 5 were electrophoresed on a 12% polyacrylamide gel. The internal HphI sites generate 10bp, 30bp, 65bp and 141bp fragments in c/c homozygotes, while the presence of the t allele creates an additional HphI site, resulting in additional 136bp and 5bp fragments in c/t heterozygotes. The 5bp, 10bp and 30bp fragments could, however, not be resolved under these gel conditions. Lane 1 =  $\lambda$ Pst marker; lane 2 = heterozygous individual (c/t); lane 3 = individual homozygous for the c allele (c/c).

d) Schematic representation of the PCR-amplified product, indicating the position of the HphI sites. \* = variable restriction enzyme site.

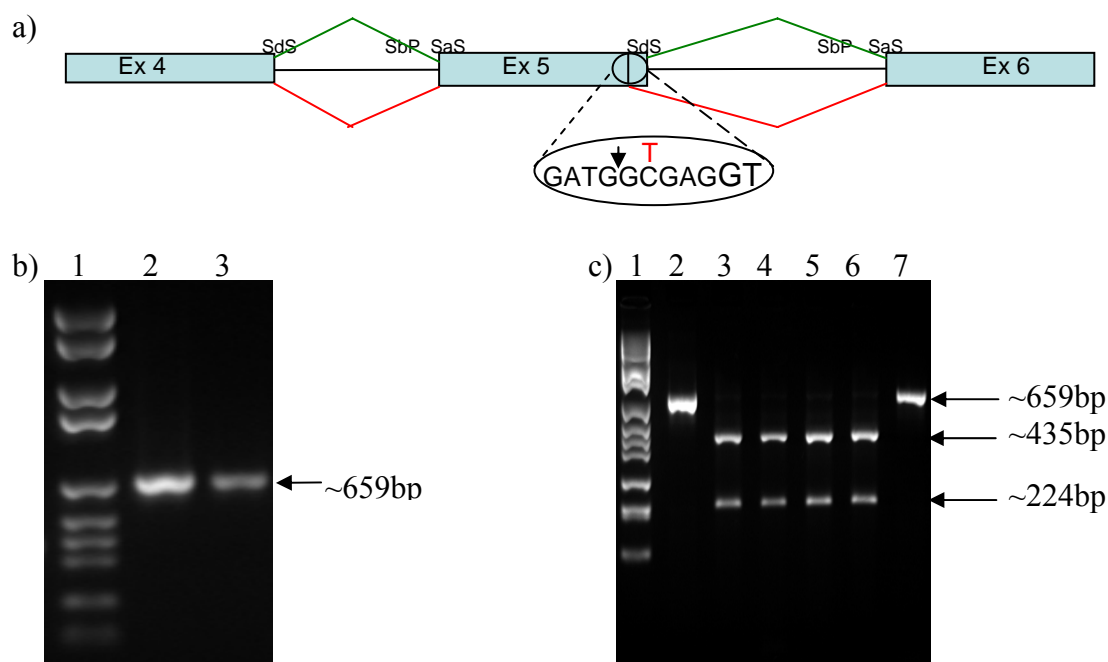


**Figure III.29. RT-PCR analysis of the exon 5 Sds -13 c>t putative HCM-causing splicing mutation**

a) Diagrammatic representation of the MyBPC3 splice pathway in the exon 4-6 region. The sequence of the cryptic splice donor site generated by the c2646t SNS, is indicated in the oval at the bottom of the figure.

— = Intronic sequence;  = exons; Ex = exon; — = normal splicing pattern; — = postulated aberrant splicing pattern caused by the c2646t SNS; SaS = splice acceptor site; SbP = splice branch point; SdS = splice donor site.

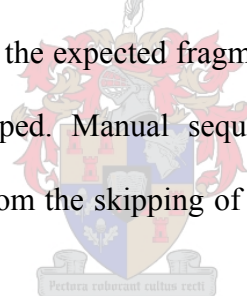
b) RT-PCR products electrophoresed on a 2% agarose gel. The normal splicing pattern would result in the generation of a 659bp fragment, while the RT-PCR product resulting from an aberrantly spliced transcript would result in the generation of a 644bp fragment. Lane 1 = Roche molecular size marker VII; lane 2 = individual homozygous for the c allele (c/c); lane 3 = heterozygous individual (c/t).

c) Products of the BstEII restriction enzyme digestion of the ~659bp RT-PCR product, electrophoresed on a 2% agarose gel. The internal BstEII site generates 435bp and 224bp fragments in the RT-PCR product generated from the normally spliced transcript, while this BstEII site would be abolished in RT-PCR products generated from the aberrantly spliced transcript, resulting in the generation of an additional 644bp fragments. Lane 1 = Roche molecular size marker VII, lane 2 = undigested sample from an individual homozygous for the c allele (cc), lane 3 = sample from an individual homozygous for the c allele (cc) digested with BstEII, lanes 4, 5 and 6 = samples from a heterozygous individual (c/t) digested with BstEII, lane 7 = undigested sample from a heterozygous individual (c/t).

### III.1.3.2. Identification of the exon 7 SaS +1 g>a putative splicing mutation

The g4177a SNS, occurring at position +1 of the exon 7 SaS (box 1, table III.1, figures III.30 and III.31), was detected in one proband, of mixed ancestry, in the HCM-affected panel. The g4177a SNS was not detected in a control panel consisting of 107 individuals of mixed ancestry. Computational analysis revealed that this SNS may inactivate the natural exon 7 SaS, as described by Carrier et al., (1997). It was hypothesised that the g4177a SNS would cause the skipping of *MYBPC3* exon 7 (personal communication, Dr Peter Rogan, 23 December 1999) (figure III.31).

RT-PCR analysis revealed the presence of a ~225bp fragment, resulting from the amplification of the normally spliced transcript, as well as an additional ~107bp fragment (figure III.31). The size of the additional fragment was consistent with the expected fragment size resulting from amplification of a transcript in which exon 7 was skipped. Manual sequencing of the 107bp RT-PCR product confirmed that this fragment resulted from the skipping of exon 7 in the *MYBPC3* transcript (figure III.31).



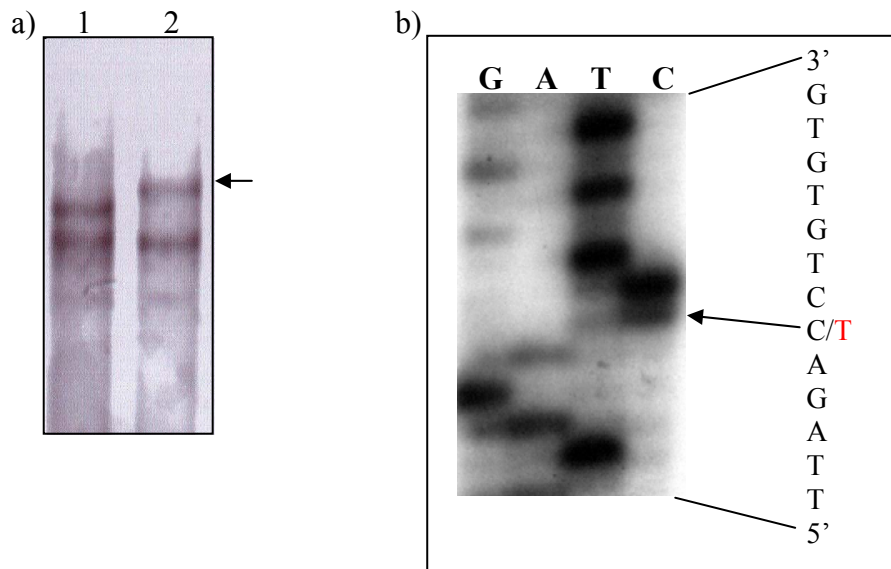


**Figure III.30. Identification of the exon 7 SaS +1 g>a putative HCM-causing splicing mutation**

a) PCR-SSCP analysis of the MYBPC3 exon 7 PCR-amplified region on a 10% MD-SSCP gel. Lane 1 = individual homozygous for the g allele (g/g); lane 2 = heterozygous individual (g/a). The arrow indicates the mobility shift caused by the g4177a SNS in a heterozygous individual.

b) Partial sequence of the minus-strand at the MYBPC3 intron 6 - exon 7 boundary in an individual heterozygous for the g4177a SNS, showing the c/t substitution on the minus-strand.

The g4177a SNS did not affect any restriction enzyme recognition sites and could, therefore, not be confirmed by ASREA.



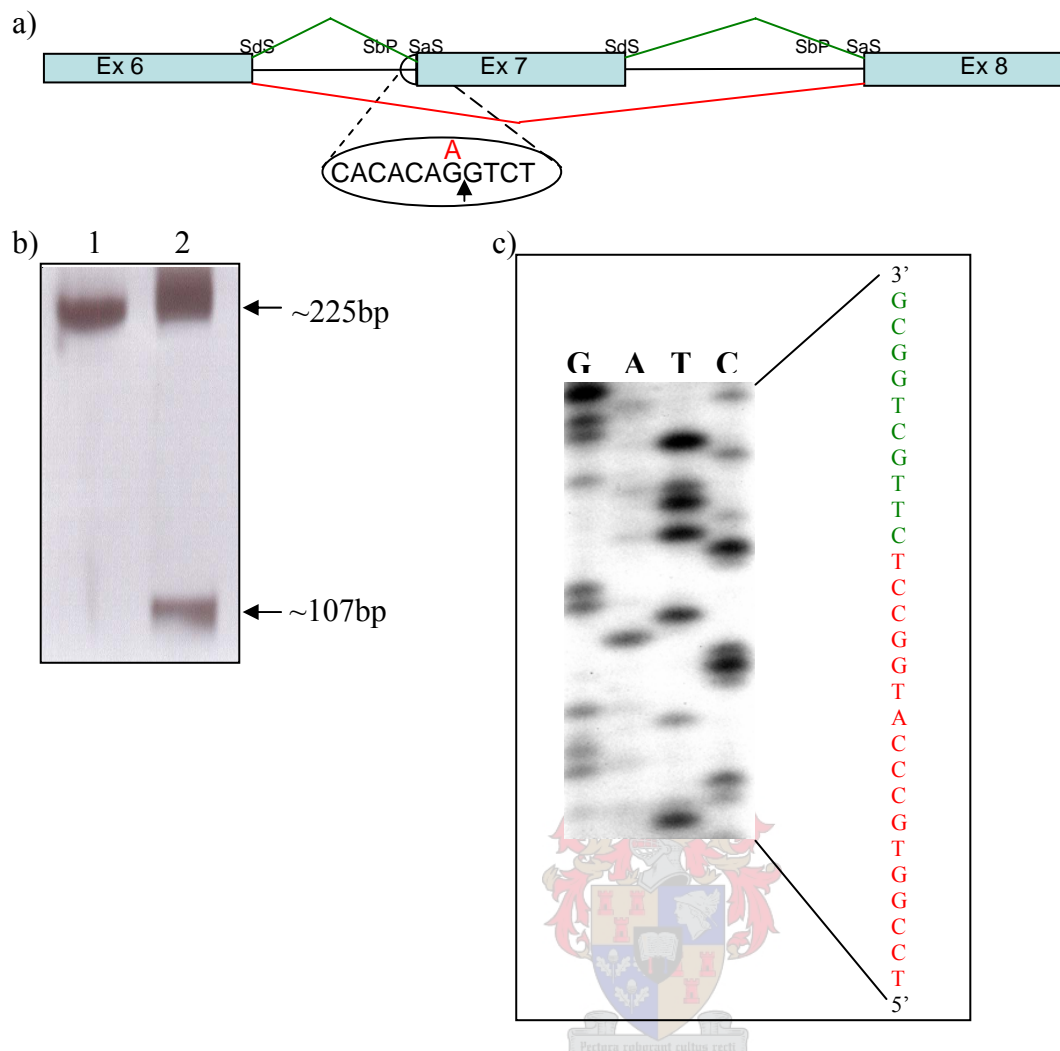


**Figure III.31. RT-PCR analysis of the exon 7 SaS +1 g>a putative HCM-causing splicing mutation**

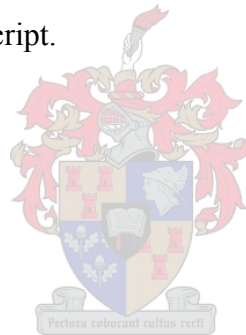
a) Diagrammatic representation of the MyBPC3 splice pathway in the exon 6-8 region. The sequence of the exon 7 SaS affected by the g4177a SNS is indicated in the oval at the bottom of the figure. — = Intronic sequence;  = exons; Ex = exon; — = normal splicing pattern; — = postulated aberrant splicing pattern caused by the g4177a SNS; SaS = splice acceptor site; SbP = splice branch point; SdS = splice donor site.

b) RT-PCR products electrophoresed on a 12% polyacrylamide gel. The normal splicing pattern would result in the generation of a 225bp fragment, while the RT-PCR product resulting from an aberrantly spliced transcript would result in the generation of a 107bp fragment. Lane 1 = individual homozygous for the g allele (g/g); lane 2 = heterozygous individual (g/a).

c) Partial sequence of the non-coding strand of the ~107bp fragment. Exon 6 sequence indicated in green lettering, exon 8 sequence indicated in red lettering.

### III.1.3.3. Identification of the intron 6 SbP +1 c>t putative splicing mutation

The c4154t SNS, occurring in intron 6 (table III.1 and figure III.32), was detected in two probands, both of mixed ancestry, in the HCM-affected panel. This SNS occurs 24bp upstream of the exon 7 SaS and at position +1 of the intron 6 SbP (figure III.33). Computational analysis revealed that this SNS slightly weakens the exon 7 SaS, and would probably not affect the splicing of the *MYBPC3* transcript. The possibility that this SNS might inactivate the exon 7 SaS, resulting in the skipping of *MYBPC3* exon 7, could, however, not be excluded (personal communication, Dr Peter Rogan, 23 December 1999). RT-PCR analysis revealed the presence of only a ~659bp fragment (figure III.33), resulting from the amplification of the normally spliced transcript, suggesting that this SNS does not affect the splicing of the *MYBPC3* transcript.



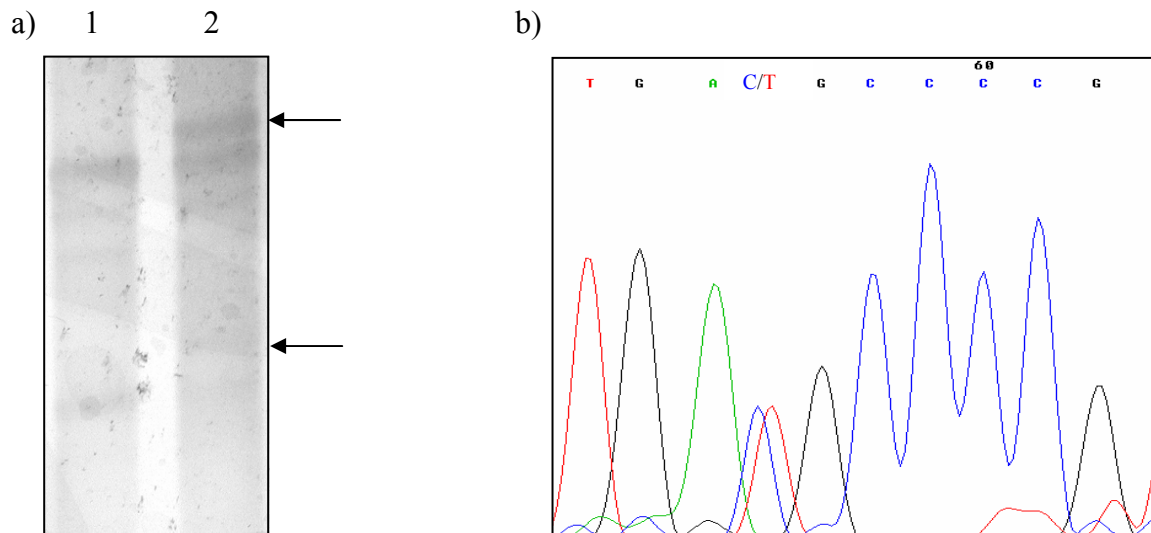
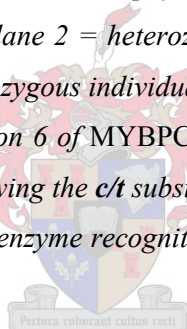


**Figure III.32. Identification of the novel intron 6 S<sub>b</sub>P +1 c>t putative HCM-causing mutation**

a) PCR-SSCP analysis of the MYBPC3 exon 7 PCR-amplified product on a 10% MD-SSCP gel. Lane 1 = individual homozygous for the c allele (c/c); lane 2 = heterozygous individual (c/t). The arrows indicate the mobility shift caused by the c4154a in a heterozygous individual.

b) Partial sequence of the plus-strand of intron 6 of MYBPC3 in an individual heterozygous for the c4154t putative HCM-causing splicing mutation, showing the c/t substitution.

The c4154t SNS did not affect any restriction enzyme recognition sites and could, therefore, not be confirmed by ASREA.



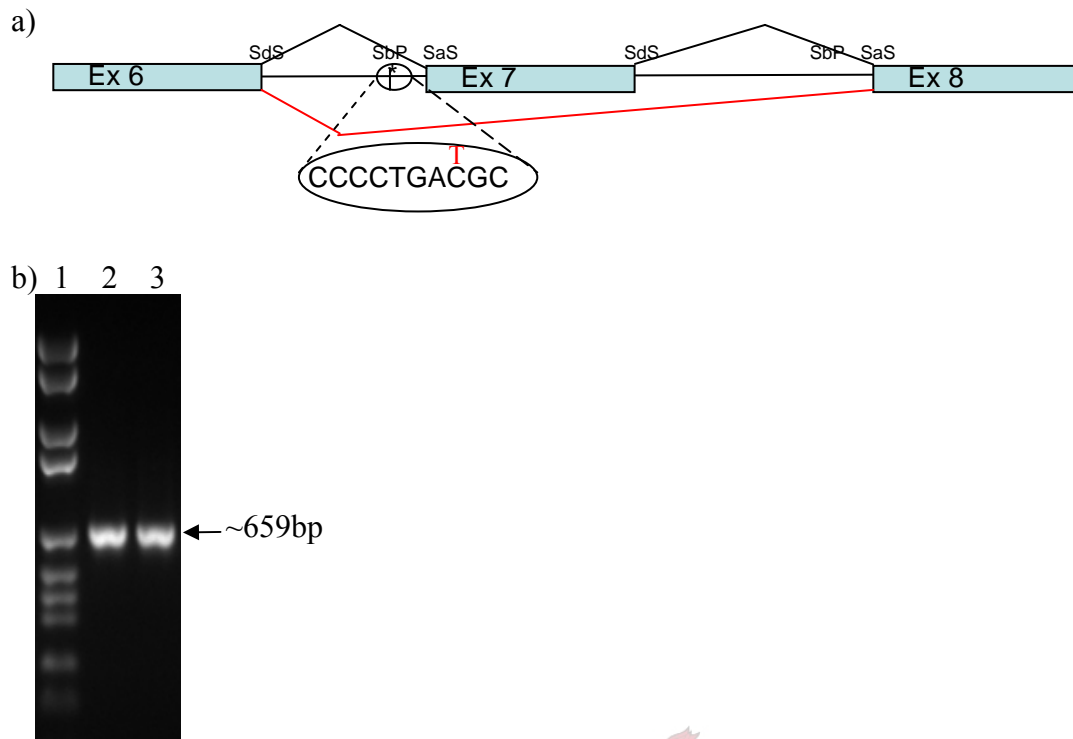


**Figure III.33. RT-PCR analysis of the intron 6 SbP +1 c>t putative HCM-causing splicing mutation**

a) Diagrammatic representation of the MyBPC3 splice pathway in the exon 6-8 region. The sequence surrounding the intron 6 SbP affected by the c4154t SNS, is indicated in the oval at the bottom of the figure.

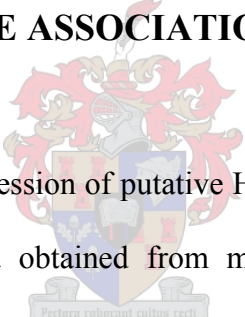
— = intronic sequence;  = exons; Ex = exon; — = normal splicing pattern; — = postulated aberrant splicing pattern caused by the c4154t SNS; SaS = splice acceptor site; SbP = splice branch point; SdS = splice donor site.

b) RT-PCR products electrophoresed on a 2% agarose gel. The normal splicing pattern would result in the generation of a 659bp fragment, while the RT-PCR product, resulting from an aberrantly spliced transcript, would result in the generation of a 541bp fragment. Lane 1 = Roche molecular size marker 7; lane 2 = individual homozygous for the c allele (c/c); lane 3 = heterozygous individual (c/t).

### **III.1.4. IDENTIFICATION OF THE NOVEL $\Delta$ c13255 FRAME-SHIFT HCM-CAUSING MUTATION IN EXON 24 OF *MYBPC3***

The deletion of a cytosine residue in exon 24 of *MYBPC3* at position 13255 ( $\Delta$ c13255) (table III.1 and figure III.34) was detected in one individual, of mixed ancestry, in the HCM-affected panel. This mutation is predicted to cause a frame-shift, resulting in the addition of 65 novel amino acids, prior to the generation of a stop codon and the truncation of the protein. The truncated protein thus generated, would consist of domains C0-C5. This mutation was not found in 100 control individuals of mixed ancestry.

### **III.2. GENOTYPE:PHENOTYPE ASSOCIATION STUDIES**



In order to establish the phenotypic expression of putative HCM-causing mutations identified during the course of this study, clinical data obtained from mutation carriers were used to conduct genotype:phenotype association studies (sections III.2.1 and III.2.2). As families of probands identified as carrying the G507R and  $\Delta$ c13255 putative HCM-causing mutations could not be traced, comprehensive genotype:phenotype association studies could not be performed. The phenotypic presentation of the proband carrying the G507R mutation is, therefore, given in section III.2.3.

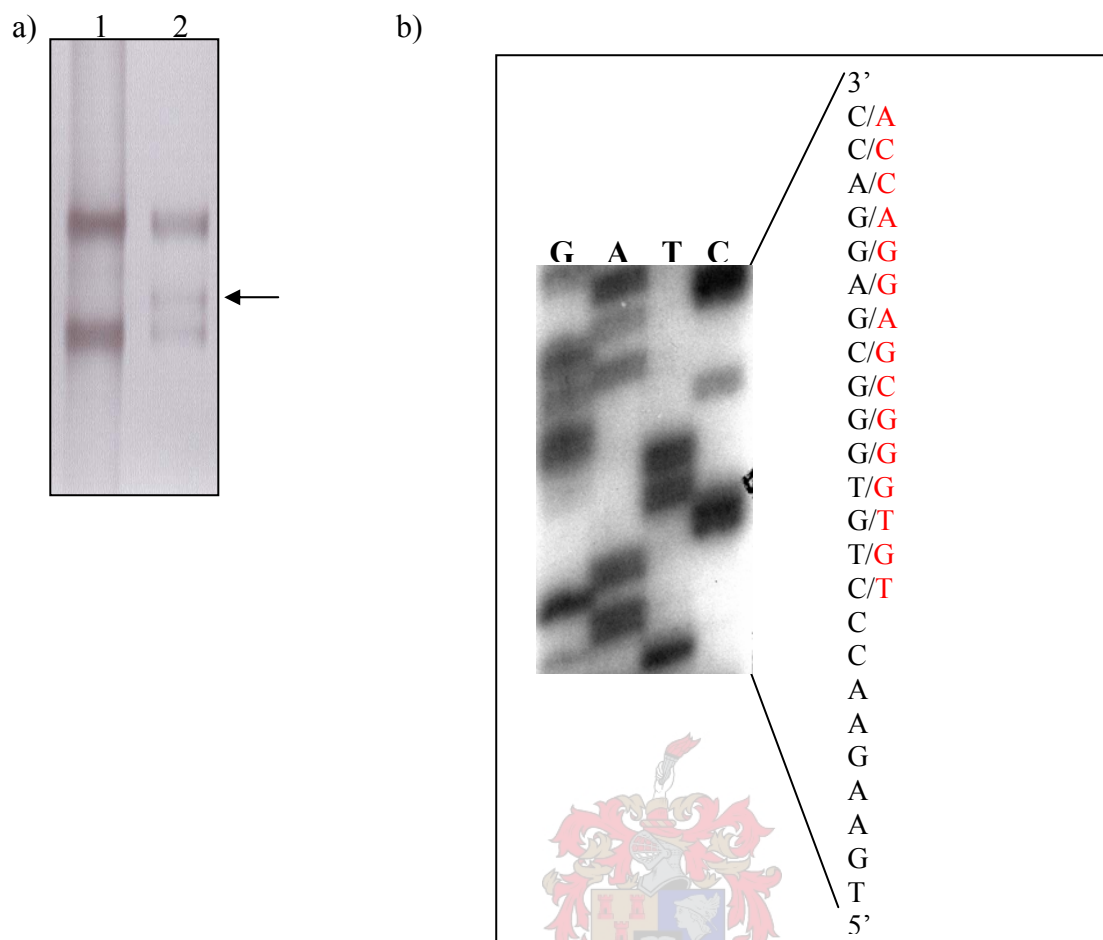


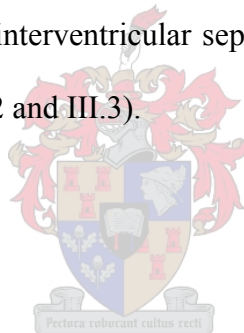
**Figure III.34. Identification of the novel  $\Delta c$  13255 HCM-causing mutation in exon 24 of MYBPC3**

a) PCR-SSCP analysis of the MYBPC3 exon 24 PCR-amplified product on a 10% MD-SSCP gel. Lane 1 = individual homozygous for the wild type allele; lane 2 = individual heterozygous for the  $\Delta c$  allele. The arrow indicates the mobility shift caused by the  $\Delta c$ 13255 putative HCM-causing mutation, in a heterozygous individual.

b) Partial sequence of the coding strand of exon 24 of MYBPC3 in an individual heterozygous for the  $\Delta c$ 13255 HCM-causing mutation, showing the deletion of nucleotide 13255 ( $\Delta c$ ).

### III.2.1. GENOTYPE:PHENOTYPE ASSOCIATION OF THE *MYBPC3* V896M PUTATIVE HCM-CAUSING MUTATION

Six individuals of pedigree 120 (figure III.35) were genotyped for the presence of the V896M putative HCM-causing mutation. Of the individuals genotyped, four tested positive for the V896M mutation. Clinical assessment of mutation carriers revealed that only the proband (individual II.2) fulfilled the echocardiographic criteria for the diagnosis of HCM (table III.3). Both individuals II.1 and II.2 presented with angina, while individual I.2 had dyspnoea and palpitations, and was diagnosed with congestive heart failure due to DCM at the age of 75 years (table III.2). Although no symptoms of HCM, or ECG-abnormalities associated with HCM were present in individual III.1, echocardiographic measurement of the interventricular septum (IVS) was at the upper limits of the normal range at age 19 years (tables III.2 and III.3).



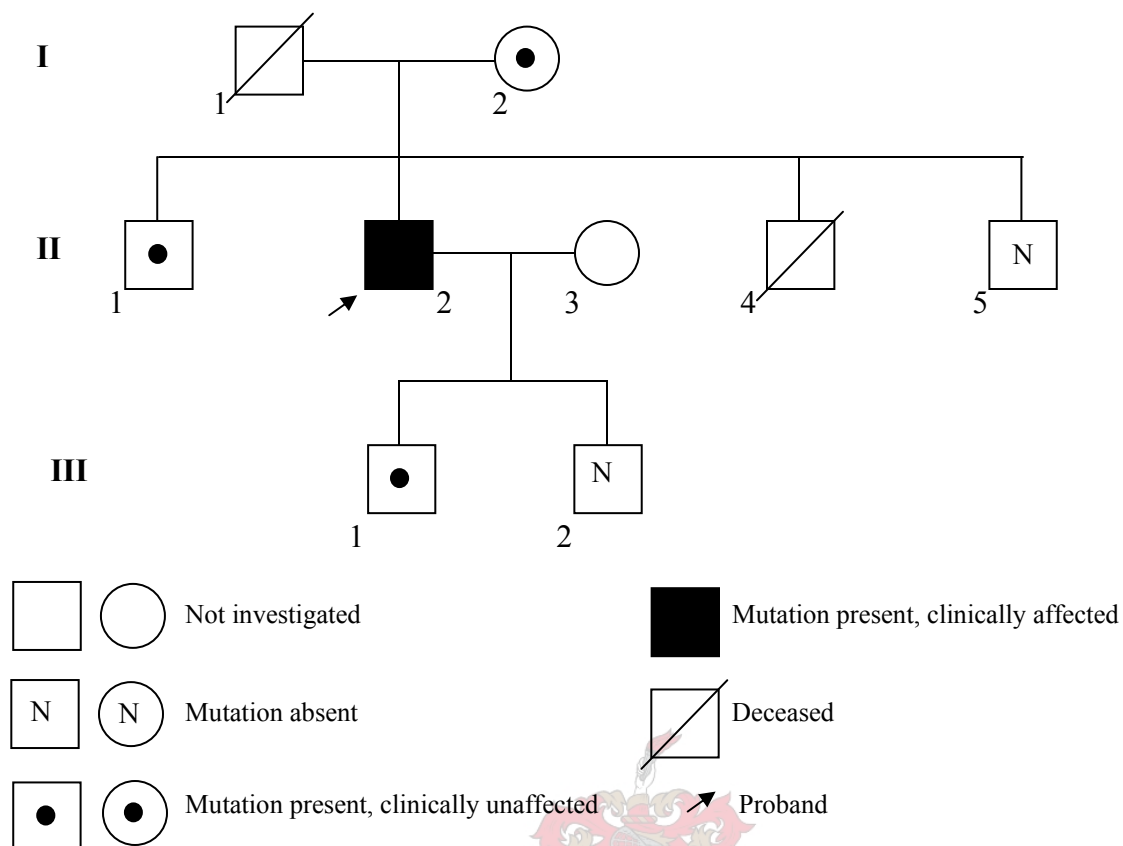


**Figure III.35. Pedigree 120 in which the MYBPC3 V896M putative HCM-causing mutation segregates**  
 Clinically affected individuals were diagnosed with HCM on at least the strictest echocardiographic criterion of a maximal left ventricular wall thickness of 13mm or more, or the electrocardiographic criterion of left ventricular hypertrophy, based on the points system of Romhilt and Estes.

**Table III.2. Symptoms present in individuals carrying the V896M putative HCM-causing mutation**

Ind no	Sex/Age at diagnosis (yrs)	Syncope/ Presyncope	Dyspnoea	Palpitations	Angina	Cardiac failure
I.2	F/75	-	y	y	-	y
II.1	M/54	-	-	-	y	-
II.2	M/50	-	-	-	y	-
III.1	M/27	-	-	-	-	-

*F = female; Ind no = individual identity number (figure III.35), M = male; y = feature present; yrs = years; - feature absent.*

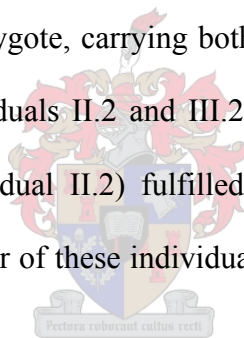
**Table III.3. Echocardiographic and electrocardiographic features present in individuals with the V896M putative HCM-causing mutation**

Ind no	Sex/ Age (yrs)	Echocardiographic features						ECG features				
		IVS (mm)	PW (mm)	Area of Hypert	ASH	SAM	Valve	Ab Rep	Inc V	Ab Qs	↑A	R&E LVH
I.2	F/75	8	10	N.A.	-	-	-	-	-	-	-	-
II.1	M/54	11	11	N.A.	-	-	-	-	-	y	-	-
II.2	M/50	17	14	IVS	y	y	-	-	-	y	-	-
III.1	M/27	11	11	N.A.	-	-	-	-	-	-	-	-

*Ab Qs = abnormal Q-waves; Ab Rep = abnormal repolarisation; ASH = asymmetrical hypertrophy; F = female; Hypert = hypertrophy; Inc V = increased voltages; Ind no = individual identity number (figure III.35); IVS = inter-ventricular septum; M = male; N.A. = not assessed; PW= posterior left ventricular free wall; R&E LVH = left ventricular hypertrophy by Romhilt and Estes criteria; SAM= systolic anterior motion of the mitral valve; y = feature present; yrs = years; ↑A = atrial hypertrophy; - = feature absent.*

### III.2.2. PHENOTYPIC EFFECT OF THE *MYBPC3* EXON 7 SaS +1 g>a PUTATIVE HCM-CAUSING SPLICING MUTATION, IN A COMPOUND HETEROZYGOTE

The exon 7 SaS +1 g>a putative HCM-causing splicing mutation was identified in only one proband in the HCM-affected panel, in which the *TNNT2* R92W HCM-causing mutation had previously been described (Moolman et al., 1997; Moolman-Smook et al., 1999) (figure III.36). Three individuals of pedigree 137 (figure III.36) were genotyped for the presence of the *TNNT2* R92W HCM-causing and *MYBPC3* exon 7 SaS +1 g>a putative HCM-causing splicing mutations. Of the individuals genotyped, two carried the previously identified *TNNT2* R92W HCM-causing mutation, while the *MYBPC3* exon 7 SaS +1 g>a putative HCM-causing splicing mutation was found only in the proband, who was a compound heterozygote, carrying both these mutations (figure III.31). Clinical assessment of mutation carriers (individuals II.2 and III.2; figure III.36 and tables III.4 and III.5) revealed that only the proband (individual II.2) fulfilled the Romhilt and Estes criteria for the diagnosis of LVH on ECG, while neither of these individuals fulfilled the echocardiographic criteria for the diagnosis of HCM (table III.3).



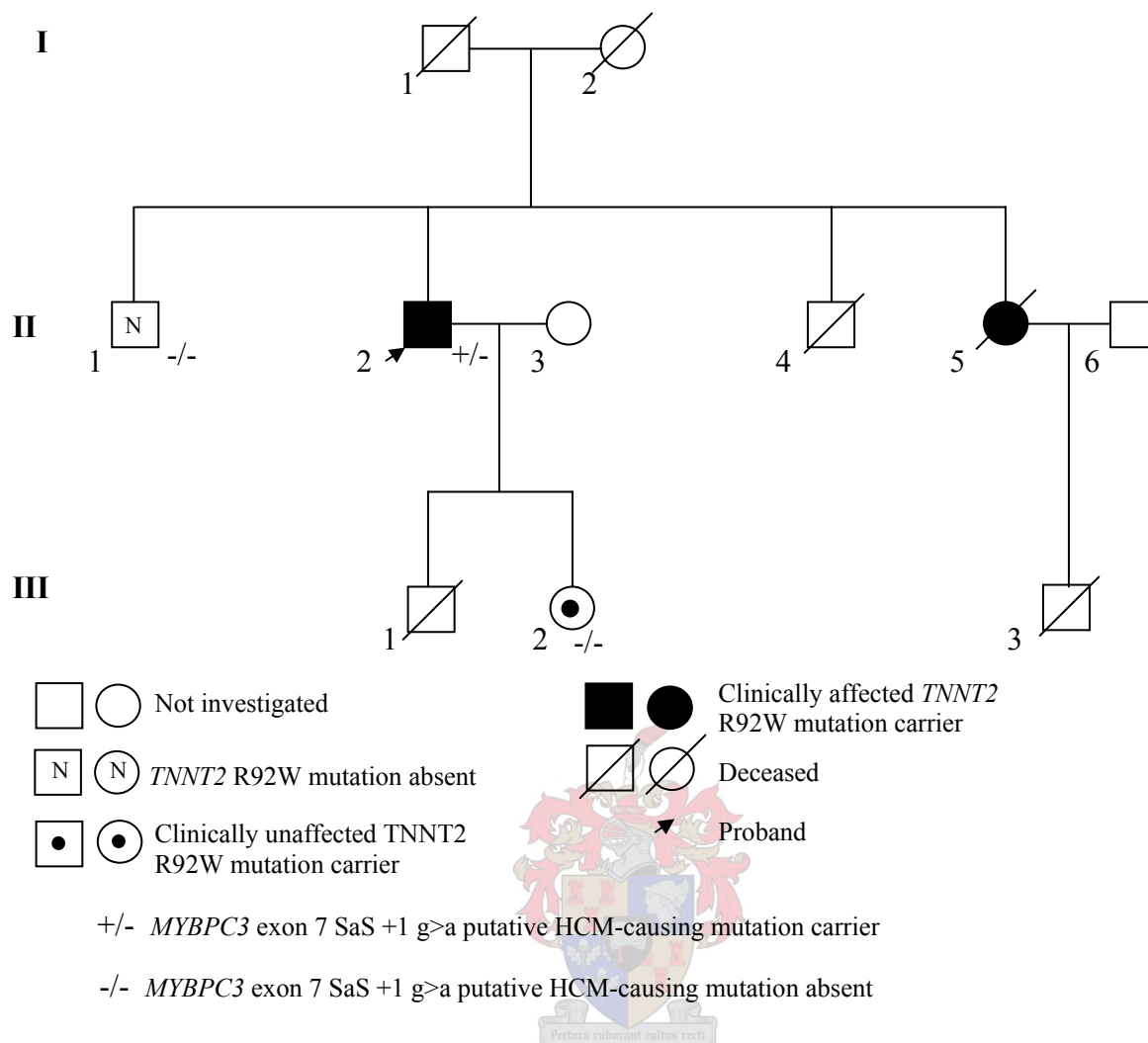


**Figure III.36. Pedigree 137 in which both the *TNNT2* R92W HCM-causing mutation and *MYBPC3* exon 7 SaS +1 g>a putative HCM-causing splicing mutation were identified**

Clinically affected individuals were diagnosed with HCM on at least the strictest echocardiographic criterion of a maximal left ventricular wall thickness of 13mm or more, or the electrocardiographic criterion of left ventricular hypertrophy, based on the points system of Romhilt and Estes.

**Table III.4. Symptoms present in individuals from pedigree 137 carrying the TNNT2 R92W HCM-causing mutation**

Ind no	Sex/Age at diagnosis (yrs)	Syncope/ Presyncope	Dyspnoea	Palpitations	Angina	Cardiac failure
II.2*	M/49	-	-	-	-	-
III.2	F/21	-	-	-	-	-

*F = female; Ind no = individual identity number (figure III.36), M = male; y = feature present; yrs = years; - = feature absent; \* = compound heterozygote for the TNNT2 R92W HCM-causing mutation and the MYBPC3 exon 7 splice acceptor site putative HCM-causing mutation.*

**Table III.5. Echocardiographic and electrocardiographic features present in individuals from pedigree 137 with the TNNT2 R92W HCM-causing mutation**

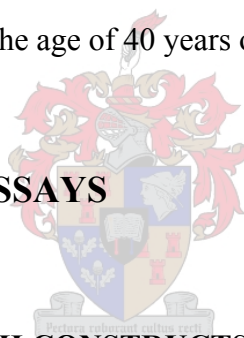
Ind no	Sex/ Age (yrs)	Echocardiographic features						ECG features				
		IVS (mm)	PW (mm)	Area of Hypert	ASH	SAM	Valve	Ab Rep	Inc V	Ab Qs	↑A	R&E LVH
II.2*	M/49	9.0	9.0	n.a.	-	-	-	y	y	-	y	y
III.2	F/21	8.0	7.0	n.a.	-	-	-	-	-	-	-	n

*Ab Qs = abnormal Q-waves; Ab Rep = abnormal repolarisation; ASH = asymmetrical hypertrophy; F = female; Hypert = hypertrophy; Inc V = increased voltages; Ind no = individual identity number (figure III.36); IVS = inter-ventricular septum; M = male; n = no; n.a. = not applicable; PW= posterior left ventricular free wall; R&E LVH = left ventricular hypertrophy by Romhilt and Estes criteria; SAM= systolic anterior motion of the mitral valve; y = feature present; yrs = years; ↑A = atrial hypertrophy; - = feature absent; \* = compound heterozygote for the TNNT2 R92W HCM-causing mutation and the MYBPC3 exon 7 SaS +1 g>a putative HCM-causing mutation.*

### **III.2.3. PHENOTYPIC EXPRESSION OF THE *MYBPC3* G507R PUTATIVE HCM-CAUSING MUTATION**

As the family of the proband carrying the G507R putative HCM-causing mutation could not be traced, a detailed genotype:phenotype correlation study could not be done, nor could it be shown that this putative HCM-causing mutation segregates with HCM in this family. The proband, a 50 year old woman of Zulu descent, presented with dyspnoea, palpitations and angina. ECG-analysis revealed increased voltages, abnormal repolarisation and fulfilled the Romhilt and Estes criteria for the diagnosis of HCM, while echocardiographic evaluation revealed severe LVH with a maximal wall thickness of 25mm (IVS) as well as systolic anterior motion of the mitral valve. Additionally, the mother of the proband died suddenly at the age of 40 years of unknown, but non-violent, causes.

### **III.3. YEAST TWO-HYBRID ASSAYS**



#### **III.3.1. QUALITY CONTROL OF Y2H CONSTRUCTS**

##### **III.3.1.1. Sequence analysis of Y2H constructs**

Sequence analysis of constructs used in Y2H-assays (section II.10 and table II.9) revealed that the reading-frame of all inserts was maintained. Furthermore, BLASTX analysis (<http://www.ncbi.nlm.nih.gov/Blast>) of insert sequences revealed that the deduced amino acid sequences of all bait- and prey-peptides, used in Y2H-assays, were identical to relevant amino acid sequences in the GenBank database (<http://www.ncbi.nlm.nih.gov/Entrez>).

### III.3.1.2. Toxicity tests of Y2H constructs

All yeast transformed with bait- or prey- constructs were able to grow on appropriate selection media (table II.10 and appendix A), indicating that none of the bait- or prey-peptides used in Y2H-assays were toxic to the yeast and that the phenotypes of the yeast strains were retained. Additionally, growth-curves were constructed for yeast strains transformed with all bait constructs used in Y2H library-assays (section II.16.1; figures III.37 and III.38). There was never any significant difference between the slopes of the Linearised growth-curves of yeast transformed with bait constructs, and yeast transformed with the relevant non-recombinant bait-vector (figures III.37 and III.38). It was, therefore, concluded that none of the peptides encoded by bait constructs used in Y2H library-assays were toxic to, or significantly affected growth of, the yeast strains in which they were expressed.

### III.3.1.3. Reporter gene self-activation tests

None of the yeast strains transformed with any bait- or prey-constructs, used in Y2H-assays, were able to grow on relevant selection media (section II.15.3, tables II.10, III.6 and appendix A). It was, therefore, concluded that none of the peptides encoded by these constructs were able to independently activate transcription of either the *HIS3* or *ADE2* reporter genes.

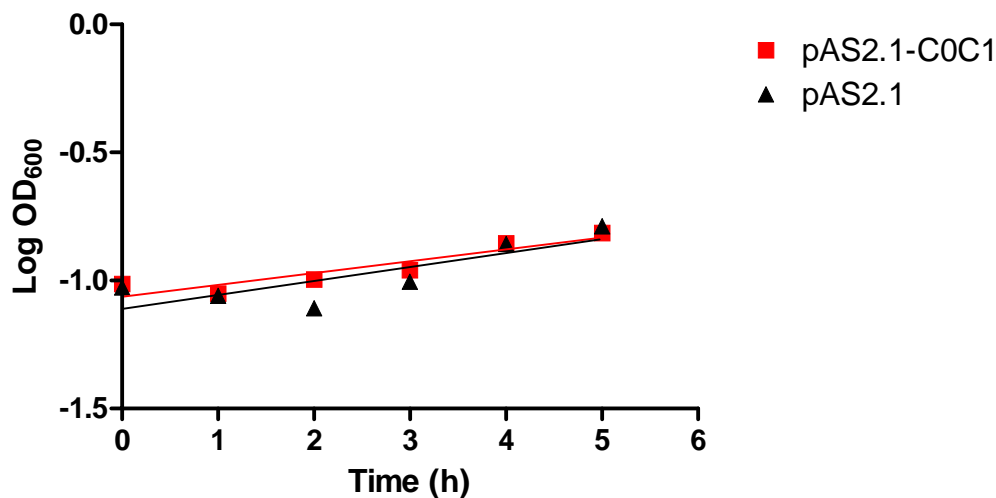


**Figure III.37. Linearised growth-curve of yeast strain PJ69-2A transformed with pAS2.1-based Y2H bait-vectors**

Linearised growth-curves (log OD<sub>600</sub> plotted against time) of yeast strain PJ69-2A transformed with pAS2.1-C0C1 bait-plasmid or pAS2.1 non-recombinant plasmid.

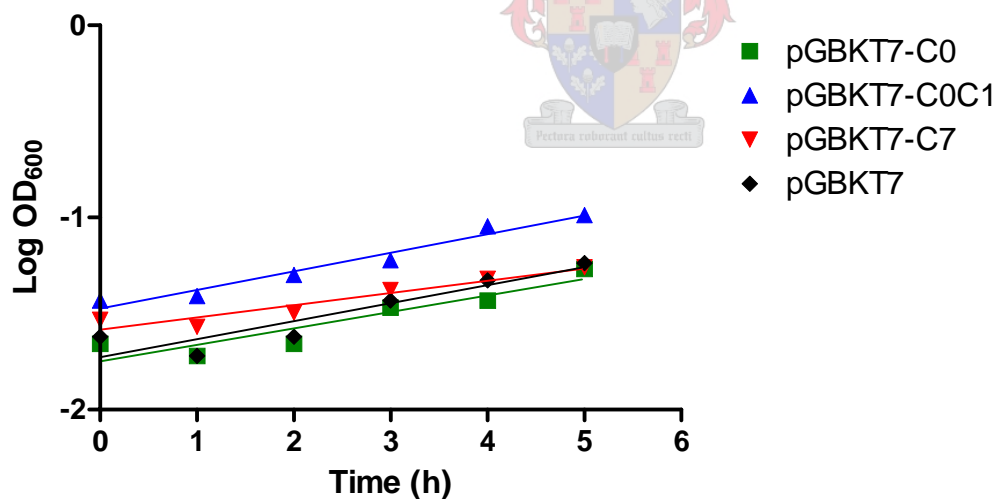


**Figure III.38. Linearised growth-curves of yeast strain AH109 transformed with pGBKT7-based Y2H bait-vectors**

Linearised growth-curves (log OD<sub>600</sub> plotted against time) of yeast strain AH109 transformed with pGBKT7-C0 bait-plasmid, pGBKT7-C0C1 bait-plasmid, pGBKT7-C7 bait-plasmid or pGBKT7 non-recombinant plasmid.

**Table III.6. Reporter gene self-activation tests of Y2H constructs**

Construct name	Type	Yeast selection medium			
		SD <sup>-W-H</sup>	SD <sup>-W-H-Ade</sup>	SD <sup>-L-H</sup>	SD <sup>-L-H-Ade</sup>
pAS2.1-C0	Bait	X	X	N.A.	N.A.
pGBKT7-C0	Bait	X	X	N.A.	N.A.
pAS2.1-C0C1	Bait	X	X	N.A.	N.A.
pGBKT7-C0C1	Bait	X	X	N.A.	N.A.
pAS2.1-C0C2	Bait	X	X	N.A.	N.A.
pGBKT7-C7	Bait	X	X	N.A.	N.A.
pGBKT7-C7 <sup>V896M</sup>	Bait	X	X	N.A.	N.A.
pGBKT7-A43	Bait	X	X	N.A.	N.A.
pGADT7-C1	Prey	N.A.	N.A.	X	X
pGADT7-C1C2	Prey	N.A.	N.A.	X	X
pGADT7-C2	Prey	N.A.	N.A.	X	X
pACT2-C5	Prey	N.A.	N.A.	X	X
pACT2-C6	Prey	N.A.	N.A.	X	X
pACT2-C8	Prey	N.A.	N.A.	X	X
pACT2-C8C10	Prey	N.A.	N.A.	X	X
pACT2-C9	Prey	N.A.	N.A.	X	X
pACT2-C9C10	Prey	N.A.	N.A.	X	X
pACT2-C10	Prey	N.A.	N.A.	X	X
pGADT7-A109	Prey	N.A.	N.A.	X	X
pGADT7-A109A112	Prey	N.A.	N.A.	X	X
pGADT7-A112	Prey	N.A.	N.A.	X	X
pGADT7-A116	Prey	N.A.	N.A.	X	X

$SD^{-L-H}$  = selective dropout yeast media lacking leucine and histidine;  $SD^{-L-H-Ade}$  = selective dropout yeast media lacking leucine, histidine and adenosine;  $SD^{-W-H}$  = selective dropout yeast media lacking tryptophan and histidine;  $SD^{-W-H-Ade}$  = selective dropout yeast media lacking tryptophan, histidine and adenosine; N.A. = not applicable; X = no growth observed.

*Table III.7. Effect of bait-peptides on yeast mating efficiency*

<b>Mating</b>	<b>Mating efficiency (%)</b>
<i>pAS2.1 (PJ69-2A) x pACT2 (Y187)</i>	<i>1.1%</i>
<i>pVA3.1 (PJ69-2A) x pTD1.1 (Y187)</i>	<i>1.0%</i>
<b>pAS2.1-C0C1 (PJ69-2A) x pACT2 (Y187)</b>	<b>0.4%</b>
<i>pGBKT7 (AH109) x pACT2 (Y187)</i>	<i>4.2%</i>
<i>pGBKT7-53 (AH109) x pGADT7-T (Y187)</i>	<i>38.1%</i>
<b>pGBKT7-C0C1 (AH109) x pACT2 (Y187)</b>	<b>0.8%</b>
<b>pGBKT7-C0 (AH109) x pACT2 (Y187)</b>	<b>3.7%</b>
<b>pGBKT7-C7 (AH109) x pACT2 (Y187)</b>	<b>1.1%</b>

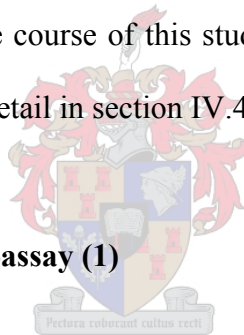
*Bait- and prey- host strains in brackets; control matings in italics; test matings of bait constructs in bold.*

#### **III.3.1.4. Effect of bait-peptides on mating efficiency**

In order to establish whether any of the bait-peptides used in Y2H library-assays affected the mating ability of the bait host strain, small-scale yeast matings were performed and mating efficiencies calculated (section II.16.3). Although results of such experiments showed a great deal of inter-experimental variation, bait constructs generally inferred a slight mating disadvantage (table III.7). In order to reduce the possibility that this reduction in mating efficiency might adversely affect the number of library clones screened during subsequent Y2H library-assays, bait cultures used in these assays (section II.17.2.2) were grown to a titre of  $>1 \times 10^{10}$ /ml, one order higher than that suggested by the manufacturer of the MATCHMAKER Y2H systems (BD Biosciences, Clontech, Palo Alto, CA, USA), and two orders of magnitude greater than the titre of the yeast library to be screened.

### III.3.2. YEAST TWO-HYBRID LIBRARY-ASSAYS

During the course of this study, four Y2H cardiac cDNA library-screening assays were performed. In two of these assays, the C0C1 region of cMyBPC was used as bait, while the C0 and C7 domains of cMyBPC were used as bait in each of the two remaining Y2H library-assays. One of the library-assays, in which the C0C1 region of cMyBPC was used as bait, was performed in the MATCHMAKER GAL4 Two-Hybrid System 2 (cMyBPC C0C1 (1)), while the other, as well as library-assays in which the C0 and C7 domains of cMyBPC were used as bait, were all performed in the MATCHMAKER GAL4 Two-Hybrid System 3 (cMyBPC C0C1 (2), cMyBPC C0 and cMyBPC C7). The rationale for preferentially using the MATCHMAKER GAL4 Two-Hybrid System 3, which only became available during the course of this study, as well as for repeating the cMyBPC C0C1 (1) library-assay, is discussed in detail in section IV.4.1.



#### III.3.2.1. cMyBPC C0C1 Y2H library-assay (1)

The pAS2.1-C0C1 bait construct (table II.10), transformed into *S. cerevisiae* strain PJ69-2A, was used to screen a pACT2-based cardiac cDNA library, pre-transformed into *S. cerevisiae* strain Y187 (BD Biosciences, Clontech, Palo Alto, CA, USA) (section II.17.2.2). The screening of an estimated  $1.04 \times 10^6$  library clones yielded 77 clones in which transcription of the *HIS3* reporter gene was activated, as evidenced by their ability to grow on TDO-selection medium. Of these 77 clones, only six were able to grow on QDO-selection medium, indicating additional activation of transcription of the *ADE2* reporter gene. Filter  $\beta$ -galactosidase assays showed that transcription of the *LacZ* reporter gene was activated in all six clones (table III.8). Interaction-specificity tests (section II.17.7) showed that three of these clones contained prey-peptides which activated transcription of the *HIS3* and

*ADE2* reporter genes in the presence of heterologous baits, and were, therefore, discarded as non-specific interactor clones (table III.8). The remaining three clones were classified as putative true interactor clones. Following DNA sequencing of the cDNA inserts contained in these clones, BLAST-analysis was used to identify interactor peptides (table III.9). Two of these peptides were identified as human Jun coactivator (COP9) subunit 5, while the other peptide was identified as the human homeobox protein MOX-1. As both these proteins have a nuclear localisation, they were not deemed plausible ligands of cMyBPC (section IV.4.1).

**Table III.8 cMyBPC C0C1 (1) putative interactor clones**

Clone #	Colony phenotype (after 6 days)		Specificity tests (after 6 days)			
	QDO		β-galactosidase assay		x pAS2.1	x pTD1.1
	R&S	Colour	Time	Colour	QDO	QDO
1	✓ ✓	LP	2 hours	+++	✓ ✓	X
3	✓ ✓ ✓	LP	2 hours	+++	✓ ✓	✓ ✓ ✓
7	✓ ✓	P	2 hours	++	✓ ✓	X
9	✓	P	2 hours	++	✓ ✓ ✓	✓ ✓ ✓
34	✓ ✓	LP	2 hours	+++	✓ ✓	✓ ✓ ✓
77	✓	P	3 hours	+	✓	X

*LP = light pink; P = pink; QDO = solid medium lacking lacking Leu, Trp, His and Ade; R&S = robustness and size of colony; Time = time to blue colour development; ✓ = weak; ✓ ✓ = intermediate; ✓ ✓ ✓ = strong; + = light blue; ++ = blue; +++ = dark blue; X = no growth observed.*

**Table III.9. Identification of cMyBPC C0C1 (1) primary putative interactor clones**

Clone #	Genomic hit		In-frame ORF protein hit		Length (AA)	E-value	Cellular localisation
	Identity	Accession #	Identity	Accession #			
1	<i>H.s.</i> Jun activation domain	U65928	<i>H.s.</i> Jun coactivator; COP9 (constitutive photomorphogenic), subunit 5	AAP36860	152	$9 \times 10^{-62}$	Nuclear
7	<i>H.s.</i> Jun activation domain	U65928	<i>H.s.</i> Jun coactivator; COP9 (constitutive photomorphogenic), subunit 5	AAP36860	160	$4 \times 10^{-77}$	Nuclear
77	<i>H.s.</i> mesenchyme homeo box 1 ( <i>MEOX1</i> )	XM_008351	<i>H.s.</i> Homeobox protein MOX-1	NP_004518	168	$3 \times 10^{-70}$	Nuclear

*AA* = amino acids; *Hs* = Homo sapiens; *ORF* = open reading frame

### III.3.2.2. cMyBPC C0C1 Y2H library-assay (2)

The pGBKT7-C0C1 bait construct (table II.10), transformed into *S. cerevisiae* strain AH109, was used to screen a pACT2-based cardiac cDNA library, pre-transformed into *S. cerevisiae* strain Y187 (BD Biosciences, Clontech, Palo Alto, CA, USA) (section II.17.2.2). The screening of an estimated  $1.4 \times 10^6$  library clones yielded 324 clones in which transcription of the *HIS3* reporter gene was activated. Of these clones, 265 were able to grow on QDO-selection medium, indicating additional activation of transcription of the *ADE2* reporter gene. Filter  $\beta$ -galactosidase assays and X- $\alpha$ -galactosidase assays allowed elimination of an additional 60 of the 265 clones, due to their inability to activate transcription of the *LacZ* and *MEL1* reporter genes (table III.10). The remaining 205 clones were classified as either primary or secondary interactor clones, based on the size, robustness and colour of the colony, as well as their respective  $\beta$ -galactosidase and X- $\alpha$ -galactosidase phenotypes (time to, and intensity of, colour development). In total, 111 primary and 94 secondary interactor clones were identified.



Restriction mapping of the prey-inserts (section II.11.3) of all primary and secondary interactor clones revealed the presence of eight groups of identical clones, as well as 70 unique clones (table III.10). Each of these groups was subsequently represented by a single clone in interaction-specificity tests, reducing the number of primary interactor clones to 78. Interaction-specificity tests (section II.17.7) were performed on 76 primary interactor clones and four secondary interactor clones, each representing a group of identical secondary interactor clones. These tests showed that only ten clones (all primary interactor clones) contained prey peptides that did either not activate transcription of the *HIS3* and *ADE2* reporter genes in the presence of heterologous

baits, or activated transcription of these genes very weakly, and were, therefore, considered to be specific interactor clones (table III.10). These specific interactor clones, as well as two additional primary interactor clones, from which the prey-plasmid could not be purified, and could thus not be used in interaction-specificity tests, were subsequently sequenced.

Six of the total number of putative interactor clones were identified by BLAST analysis as encoding a portion of M-line titin and two as encoding human multiple PDZ-domain protein (table III.11). The remaining preys identified were deemed to be implausible binding partners of the C0C1 domain of cMyBPC, due to their cellular location, or because they encoded very short peptides with no significant protein database matches (table III.11 and section IV.4.1).

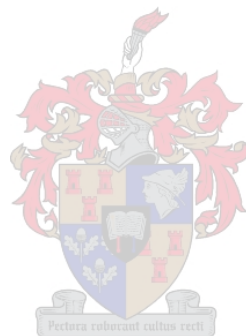


Table III.10. Putative interactor clones from the Y2H library screen with the C0C1 (2) region of cMyBPC

Clone #	# Clones represented	Colony phenotype (QDO) (after 4 days)		X- $\alpha$ -galactosidase assay			Specificity tests (after 4 days)		Sel seq (Y/N)
		R&S	Colour	Time	Colour	Classification	x pGBKT7 (QDO)	x pGBKT7-53 (QDO)	
1	1	✓ ✓ ✓	W	16 hours	+++	1 <sup>?</sup>	✓ ✓ ✓	✓ ✓ ✓	N
4	1	✓ ✓ ✓	W	16 hours	+++	1 <sup>?</sup>	✓ ✓ ✓	✓ ✓ ✓	N
6	1	✓ ✓ ✓	LP	16 hours	++	1 <sup>?</sup>	✓	✓ ✓ ✓	N
12	1	✓ ✓ ✓	W	16 hours	++	1 <sup>?</sup>	✓ ✓	✓	N
13	1	✓ ✓ ✓	LP	16 hours	++	1 <sup>?</sup>	✓ ✓ ✓	✓ ✓ ✓	N
14	1	✓ ✓ ✓	LP	16 hours	+++	1 <sup>?</sup>	✓ ✓	✓	Y
16	1	✓ ✓ ✓	LP	16 hours	++	1 <sup>?</sup>	✓ ✓ ✓	✓ ✓ ✓	N
17	1	✓ ✓ ✓	LP	16 hours	++	1 <sup>?</sup>	✓ ✓	✓ ✓ ✓	N
18	1	✓ ✓ ✓	LP	16 hours	++	1 <sup>?</sup>	✓ ✓	✓ ✓ ✓	N
19	1	✓ ✓	P	16 hours	+++	1 <sup>?</sup>	X	✓ ✓	Y
20	1	✓ ✓ ✓	LP	16 hours	+++	1 <sup>?</sup>	✓ ✓ ✓	✓ ✓ ✓	N
26	1	✓ ✓ ✓	W	16 hours	++	1 <sup>?</sup>	✓ ✓ ✓	✓ ✓ ✓	N
31	1	✓ ✓ ✓	LP	16 hours	+++	1 <sup>?</sup>	✓ ✓ ✓	✓ ✓ ✓	N
32	1	✓ ✓ ✓	W	16 hours	+++	1 <sup>?</sup>	X	X	Y
35	1	✓ ✓ ✓	W	16 hours	++	1 <sup>?</sup>	✓ ✓	✓	N
38	1	✓ ✓ ✓	W	16 hours	+++	1 <sup>?</sup>	✓ ✓ ✓	✓ ✓ ✓	N
43	21	✓ ✓ ✓	W	16 hours	++	1 <sup>?</sup>	X	✓	Y
46	1	✓ ✓ ✓	W	16 hours	+++	1 <sup>?</sup>	✓ ✓	✓ ✓	N
48	2	✓ ✓	LP	16 hours	+	2 <sup>?</sup>	✓ ✓	✓ ✓ ✓	N
51	1	✓ ✓ ✓	W	16 hours	+++	1 <sup>?</sup>	✓ ✓	✓ ✓ ✓	N
54	1	✓ ✓ ✓	LP	16 hours	+++	1 <sup>?</sup>	✓ ✓ ✓	✓ ✓ ✓	N
66	2	✓ ✓	P	16 hours	++	2 <sup>?</sup>	✓ ✓	✓ ✓	N

Clone #	# Clones represented	Colony phenotype (QDO) (after 4 days)			X- $\alpha$ -galactosidase assay		Specificity tests (after 4 days)		Sel seq (Y/N)
		R&S	Colour	Time	Colour	Classification	x pGBKT7 (QDO)	x pGBKT7-53 (QDO)	
68	1	✓ ✓ ✓	W	16 hours	+++	1 <sup>?</sup>	✓ ✓ ✓	✓ ✓ ✓	N
83	2	✓	P	16 hours	+++	2 <sup>?</sup>	✓ ✓ ✓	✓ ✓ ✓	N
85	1	✓ ✓	W	16 hours	+++	1 <sup>?</sup>	✓ ✓ ✓	✓ ✓ ✓	N
88	1	✓ ✓ ✓	W	16 hours	+++	1 <sup>?</sup>	✓ ✓ ✓	✓ ✓ ✓	N
89	1	✓ ✓ ✓	LP	16 hours	++	1 <sup>?</sup>	✓	✓ ✓ ✓	N
96	1	✓ ✓ ✓	LP	16 hours	++	1 <sup>?</sup>	✓ ✓	✓ ✓ ✓	N
100	2	✓ ✓	W	16 hours	+	2 <sup>?</sup>	✓ ✓	✓ ✓	N
105	1	✓ ✓	LP	16 hours	++	1 <sup>?</sup>	✓ ✓	✓ ✓ ✓	N
124	1	✓ ✓ ✓	W	16 hours	++	1 <sup>?</sup>	✓ ✓ ✓	✓ ✓ ✓	N
126	1	✓ ✓ ✓	W	16 hours	++	1 <sup>?</sup>	✓ ✓ ✓	✓ ✓ ✓	N
127	1	✓ ✓ ✓	LP	16 hours	++	1 <sup>?</sup>	✓ ✓ ✓	✓ ✓ ✓	N
128	1	✓ ✓ ✓	W	16 hours	+++	1 <sup>?</sup>	✓ ✓ ✓	✓ ✓ ✓	N
129	1	✓ ✓ ✓	W	16 hours	+++	1 <sup>?</sup>	✓ ✓ ✓	✓ ✓ ✓	N
140	1	✓ ✓	W	16 hours	++	1 <sup>?</sup>	✓ ✓	✓ ✓	N
141	1	✓ ✓ ✓	W	16 hours	++	1 <sup>?</sup>	✓ ✓ ✓	✓ ✓ ✓	N
142	1	✓ ✓ ✓	W	16 hours	++	1 <sup>?</sup>	✓ ✓ ✓	✓ ✓ ✓	N
143	1	✓ ✓ ✓	LP	16 hours	+++	1 <sup>?</sup>	✓ ✓ ✓	✓ ✓	N
144	1	✓ ✓	LP	16 hours	+++	1 <sup>?</sup>	✓	✓ ✓	N
145	1	✓ ✓ ✓	LP	16 hours	+++	1 <sup>?</sup>	✓ ✓ ✓	✓ ✓ ✓	N
147	1	✓ ✓	W	16 hours	++	1 <sup>?</sup>	✓ ✓ ✓	✓ ✓ ✓	N
160	1	✓ ✓	LP	16 hours	++	1 <sup>?</sup>	✓ ✓	✓ ✓ ✓	N
164	1	✓ ✓ ✓	W	16 hours	++	1 <sup>?</sup>	✓ ✓ ✓	✓ ✓ ✓	N
170	1	✓ ✓	W	16 hours	+++	1 <sup>?</sup>	✓ ✓ ✓	✓ ✓ ✓	N
171	1	✓ ✓ ✓	W	16 hours	+++	1 <sup>?</sup>	NT	NT	Y
184	1	✓ ✓ ✓	LP	16 hours	+++	1 <sup>?</sup>	✓ ✓ ✓	✓ ✓ ✓	N

Clone #	# Clones represented	Colony phenotype (QDO) (after 4 days)			X- $\alpha$ -galactosidase assay		Specificity tests (after 4 days)		Sel seq (Y/N)
		R&S	Colour	Time	Colour	Classification	x pGBKT7 (QDO)	x pGBKT7-53 (QDO)	
186	1	✓ ✓ ✓	W	16 hours	++	1 <sup>?</sup>	✓ ✓	✓ ✓ ✓	N
189	1	✓ ✓ ✓	LP	16 hours	++	1 <sup>?</sup>	✓	✓ ✓	N
196	1	✓ ✓	LP	16 hours	+++	1 <sup>?</sup>	X	✓ ✓ ✓	N
198	1	✓ ✓	LP	16 hours	+++	1 <sup>?</sup>	✓	✓ ✓	N
213	1	✓ ✓	LP	16 hours	+++	1 <sup>?</sup>	X	✓ ✓	N
214	1	✓ ✓	W	16 hours	+++	1 <sup>?</sup>	✓	✓	Y
215	1	✓ ✓ ✓	W	16 hours	+++	1 <sup>?</sup>	✓ ✓	✓ ✓	N
216	1	✓ ✓ ✓	W	16 hours	+++	1 <sup>?</sup>	✓ ✓ ✓	✓ ✓ ✓	N
222	2	✓ ✓ ✓	W	16 hours	++	1 <sup>?</sup>	✓ ✓ ✓	✓ ✓ ✓	N
226	1	✓ ✓ ✓	W	16 hours	+++	1 <sup>?</sup>	✓ ✓ ✓	✓ ✓	N
227	2	✓ ✓	LP	16 hours	+++	1 <sup>?</sup>	✓	✓ ✓ ✓	N
228	1	✓ ✓	W	16 hours	+++	1 <sup>?</sup>	✓	✓ ✓	N
230	1	✓ ✓ ✓	LP	16 hours	+++	1 <sup>?</sup>	NT	NT	Y
231	1	✓ ✓ ✓	LP	16 hours	++	1 <sup>?</sup>	✓ ✓	✓ ✓ ✓	N
235	1	✓ ✓ ✓	LP	16 hours	+++	1 <sup>?</sup>	✓ ✓ ✓	✓ ✓ ✓	N
239	1	✓ ✓ ✓	W	16 hours	+++	1 <sup>?</sup>	✓ ✓	✓ ✓ ✓	N
242	1	✓ ✓ ✓	W	16 hours	+++	1 <sup>?</sup>	✓ ✓ ✓	✓ ✓	N
245	1	✓ ✓ ✓	LP	16 hours	++	1 <sup>?</sup>	✓ ✓ ✓	✓ ✓ ✓	N
247	1	✓ ✓	LP	16 hours	++	1 <sup>?</sup>	X	✓ ✓	Y
251	1	✓ ✓	LP	16 hours	+++	1 <sup>?</sup>	✓ ✓ ✓	✓ ✓ ✓	N
252	1	✓ ✓	LP	16 hours	+++	1 <sup>?</sup>	✓	✓ ✓ ✓	N
255	1	✓ ✓ ✓	LP	16 hours	+++	1 <sup>?</sup>	✓ ✓ ✓	✓ ✓ ✓	N
256	1	✓ ✓	LP	16 hours	++	1 <sup>?</sup>	✓ ✓	✓ ✓	N
258	1	✓ ✓	LP	16 hours	++	1 <sup>?</sup>	✓ ✓	✓ ✓ ✓	N
259	1	✓ ✓ ✓	LP	16 hours	++	1 <sup>?</sup>	✓	✓	Y

Clone #	# Clones represented	Colony phenotype (QDO) (after 4 days)		X- $\alpha$ -galactosidase assay			Specificity tests (after 4 days)		Sel seq (Y/N)
		R&S	Colour	Time	Colour	Classification	x pGBKT7 (QDO)	x pGBKT7-53 (QDO)	
262	1	✓ ✓	LP	16 hours	+++	1 <sup>?</sup>	X	✓ ✓	Y
263	3	✓ ✓ ✓	W	16 hours	++	1 <sup>?</sup>	✓ ✓	✓ ✓ ✓	N
264	1	✓ ✓ ✓	LP	16 hours	++	1 <sup>?</sup>	✓ ✓	✓ ✓	N
266	1	✓ ✓	LP	16 hours	+++	1 <sup>?</sup>	✓ ✓ ✓	✓ ✓	N
267	1	✓ ✓	LP	16 hours	+++	1 <sup>?</sup>	✓ ✓ ✓	✓ ✓ ✓	N
268	1	✓ ✓ ✓	LP	16 hours	+++	1 <sup>?</sup>	✓	✓	Y
275	1	✓ ✓ ✓	LP	16 hours	++	1 <sup>?</sup>	✓ ✓ ✓	✓ ✓ ✓	N
277	1	✓ ✓ ✓	W	16 hours	+++	1 <sup>?</sup>	✓ ✓ ✓	✓ ✓ ✓	N
278	1	✓ ✓	LP	16 hours	++	1 <sup>?</sup>	✓ ✓ ✓	✓ ✓ ✓	N
280	1	✓ ✓	LP	16 hours	+++	1 <sup>?</sup>	✓ ✓	✓ ✓	N
281	1	✓ ✓ ✓	LP	16 hours	+++	1 <sup>?</sup>	✓ ✓ ✓	✓ ✓	N
282	1	✓ ✓ ✓	LP	16 hours	++	1 <sup>?</sup>	✓ ✓	✓ ✓	N
286	1	✓ ✓ ✓	LP	16 hours	+++	1 <sup>?</sup>	✓ ✓	✓	N
294	1	✓ ✓ ✓	W	16 hours	++	1 <sup>?</sup>	X	✓ ✓	Y
297	1	✓ ✓ ✓	LP	16 hours	+++	1 <sup>?</sup>	✓ ✓ ✓	✓	N
298	1	✓ ✓ ✓	LP	16 hours	+++	1 <sup>?</sup>	✓ ✓ ✓	✓ ✓ ✓	N
306	1	✓ ✓ ✓	W	16 hours	++	1 <sup>?</sup>	✓	✓	Y
316	1	✓ ✓ ✓	LP	16 hours	+++	1 <sup>?</sup>	✓ ✓	✓ ✓ ✓	N
324	1	✓ ✓ ✓	LP	16 hours	+++	1 <sup>?</sup>	✓ ✓ ✓	✓ ✓ ✓	N

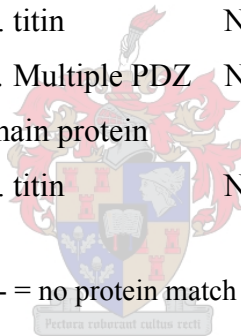
LP = light pink; N = no; NT = not tested; P = pink; R&S = robustness and size of colony; Sel seq = selected for sequencing; Time = time to blue colour development; W = white; X = no growth; ✓ = weak; ✓ ✓ = intermediate; ✓ ✓ ✓ = strong; + = light blue; ++ = blue; +++ = dark blue; 1<sup>?</sup> = primary colony; 2<sup>?</sup> = secondary colony.

**Table III.11. Identification of primary putative interactor clones from the Y2H library screen (2) with the C0C1 region of cMyBPC**

Clone#	Genomic hit		In-frame ORF protein hit				Cellular localisation
	Identity	Accession #	Identity	Accession #	Length (AA)	E-value	
14	<i>H.s.</i> titin ( <i>TTN</i> )	<a href="#">XM_038279</a>	<i>H.s.</i> titin	NP_003310	69	2x10 <sup>-33</sup>	Sarcomeric
19	<i>H.s.</i> multiple PDZ domain protein ( <i>MPDZ</i> )	NM_003829	<i>H.s.</i> Multiple PDZ domain protein	NP_003820	667	4x10 <sup>-13</sup>	Cytoplasmic/ cytoskeletal
43	<i>H.s.</i> Isolate F192 (PL56) mitochondrion, complete genome	<a href="#">AY339593</a>	<i>H.s.</i> Cytochrome c oxidase subunit I	AAK17768	165	7x10 <sup>-83</sup>	Mitochondrial inner membrane
171	<i>H.s.</i> BAC clone RP11-809N18 (E = 0.0)	<a href="#">AC058822</a>	-	N.A.	N.A.	N.A.	N.A.
214	<i>H.s.</i> Isolate F192 (PL56) mitochondrion, complete genome	<a href="#">AY339593</a>	<i>H.s.</i> Cytochrome c oxidase subunit I	AAK17768	165	7x10 <sup>-83</sup>	Mitochondrial inner membrane
230	<i>H.s.</i> titin ( <i>TTN</i> )	<a href="#">XM_038279</a>	<i>H.s.</i> titin	NP_003310	58	1x10 <sup>-11</sup>	Sarcomeric

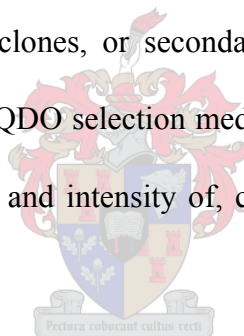
Clone#	Genomic hit		In-frame ORF protein hit				Cellular localisation
	Identity	Accession #	Identity	Accession #	Length (AA)	E-value	
247	<i>H.s.</i> Isolate F192 (PL56) mitochondrion, complete genome	<a href="#">AY339593</a>	<i>H.s.</i> Cytochrome c oxidase subunit I	AAK17768	190	$2 \times 10^{-82}$	Mitochondrial inner membrane
259	<i>H.s.</i> titin ( <i>TTN</i> )	<a href="#">XM_038279</a>	<i>H.s.</i> titin	NP_003310	56	$2 \times 10^{-22}$	Sarcomeric
262	<i>H.s.</i> titin ( <i>TTN</i> )	<a href="#">XM_038279</a>	<i>H.s.</i> titin	NP_003310	56	$5 \times 10^{-22}$	Sarcomeric
268	<i>H.s.</i> titin ( <i>TTN</i> )	<a href="#">XM_038279</a>	<i>H.s.</i> titin	NP_003310	56	$5 \times 10^{-22}$	Sarcomeric
294	<i>H.s.</i> Multiple PDZ domain protein (MPDZ)	<a href="#">NM_003829</a>	<i>H.s.</i> Multiple PDZ domain protein	NP_003820	37	$4 \times 10^{-13}$	Cytoplasmic/cytoskeletal
306	<i>H.s.</i> titin ( <i>TTN</i> )	<a href="#">XM_038279</a>	<i>H.s.</i> titin	NP_003310	34	$2 \times 10^{-4}$	Sarcomeric

AA = amino acids; H.s. = Homo sapiens; N.A. = not applicable; - = no protein match found



### III.3.2.3. cMyBPC C0 Y2H library-assay

The pGBKT7-C0 bait construct (table II.10), transformed into *S. cerevisiae* strain AH109, was used to screen a pACT2-based cardiac cDNA library, pre-transformed into *S. cerevisiae* strain Y187 (BD Biosciences, Clontech, Palo Alto, CA, USA) (section II.17.2.2). The screening of an estimated  $1.1 \times 10^6$  library clones yielded 69 clones in which transcription of the *HIS3* reporter gene was activated. Of these clones, 40 were able to grow on QDO-selection medium, indicating activation of transcription of the *ADE2* reporter gene. Filter  $\beta$ -galactosidase assays and X- $\alpha$ -galactosidase assays allowed the elimination of an additional 14 of the 40 clones, based on their inability to activate transcription of the *LacZ* and *MEL1* reporter genes (table III.12). The remaining 26 clones were classified as either primary interactor clones, or secondary interactor clones, based on the size, robustness and colour of the colony on QDO selection medium, as well as their  $\beta$ -galactosidase and X- $\alpha$ -galactosidase phenotypes (time to, and intensity of, colour development). In total 16 primary and 10 secondary clones were identified.



Restriction mapping of the library inserts (section II.11.3) of all primary and secondary clones revealed the presence of five groups of identical clones (table III.12), as well as eight unique primary clones, that were each represented by a single clone in subsequent Y2H assays. The 13 primary interactor clones thus identified (table III.12) were subsequently sequenced and the prey inserts identified by BLAST-analysis. Two of the prey inserts encoded RAN binding protein 9, one encoded sarcoglycan delta subunit, one encoded tousel-like kinase 1 and one encoded an ATPase Na<sup>+</sup>/K<sup>+</sup> exchanger, while the remaining preys were identified as portions of a human genomic DNA clone RP4-614C10 (table III.13 and section IV.4.1). BLASTX and BLASTP analysis of clones containing portions of human genomic DNA clone DJ0614C10, as well as the portion of clone DJ0614C10 with

which they shared homology, revealed the absence of any known genes, or open reading frames (ORFs) of any significant length, as determined by BLASTX analysis. The peptides encoded by these clones were, therefore, deemed to be implausible binding partners of the C0 domain of cMyBPC.

Interaction-specificity tests (section II.11) performed on clones 1, 3, 6 and 16, encoding sarcoglycan delta subunit, touselled-like kinase 1, ATPase Na<sup>+</sup>/K<sup>+</sup> exchanger and RAN binding protein 9, respectively, showed that these prey peptides activated transcription of the *HIS3* and *ADE2* reporter genes in the presence of heterologous baits (table III.13) and were, therefore, not considered to be specific ligands of the C0 domain of cMyBPC (section IV.4.1).

**Table III.12. Putative interactor clones from the Y2H library screen with the C0 domain of cMyBPC**

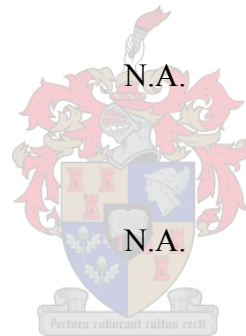
Clone #	# Clones represented	Colony phenotype (QDO)		X- $\alpha$ -galactosidase assay			Sel seq (Y/N)
		R&S	Colour	Time	Colour	Clasn	
1	1	✓ ✓ ✓	W	16 hours	+++	1'	Y
3	1	✓ ✓ ✓	LP	24 hours	++	1'	Y
6	1	✓ ✓ ✓	W	16 hours	+++	1'	Y
9	1	✓ ✓ ✓	W	16 hours	+++	1'	Y
16	1	✓ ✓ ✓	W	16 hours	+++	1'	Y
22	1	✓ ✓ ✓	LP	16 hours	++	1'	Y
31	1	✓ ✓ ✓	W	16 hours	++	1'	Y
38	1	✓ ✓ ✓	W	16 hours	+++	1'	Y
43	2	✓ ✓ ✓	W	16 hours	+++	1'	Y
44	1	✓ ✓	LP	16 hours	++	1'	Y
47	1	✓ ✓ ✓	LP	16 hours	+++	1'	Y
48	2	✓ ✓ ✓	W	16 hours	+	1'	Y
57	2	✓ ✓ ✓	LP	16 hours	+	1'	Y

*Clasn* = classification; *LP* = light pink; *N* = no; *NT* = not tested; *R&S* = robustness and size of colony; *Sel seq* = selected for sequencing; *Time* = time to blue colour development; *W* = white; *X* = no growth; *Y* = yes; ✓ = weak; ✓ ✓ = intermediate; ✓ ✓ ✓ = strong; + = light blue; ++ = blue; +++ = dark blue; 1' = primary colony; - = discarded.

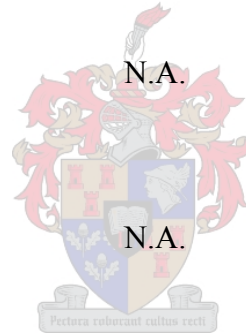
**Table III.13. Identification of primary putative interactor clones from the Y2H library screen with the C0 domain of cMyBPC**

Clone#	Genomic hit		In-frame ORF protein hit			Length (AA)	Cellular location	Specific interaction (Y/N)
	Identity	Accession #	Identity	Accession #	E-value			
1	<i>H.s.</i> Sarcoglycan, delta subunit	<a href="#">XM_003929</a>	<i>H.s.</i> Delta- sarcoglycan (35 kDa dystrophin-associated glycoprotein)	Q92629	$1 \times 10^{-37}$	90	Cytoskeletal (dystrophin- associated)	N
3	<i>H.s.</i> Tousled-like kinase 1 ( <i>TLK1</i> )	<a href="#">AF162666</a>	<i>H.s.</i> Tousled-like kinase 1 (aca PKU)	NP_036422	$1 \times 10^{-48}$	150	Nuclear	N
6	<i>H.s.</i> ATPase, Na <sup>+</sup> /K <sup>+</sup> transporter	XM_001571	<i>H.s.</i> Na <sup>+</sup> /K <sup>+</sup> - transporting ATPase beta-1 chain	P06583	$5 \times 10^{-22}$	61	Sarcolemmal	N
9	<i>H.s.</i> clone RP4- 614C10 (chr 2) (E = 0.0)	<a href="#">AC006453</a>	-	N.A.	N.A.	N.A.	N.A.	NT

Clone#	Genomic hit		In-frame ORF protein hit			Length (AA)	Cellular location	Specific interaction (Y/N)
	Identity	Accession #	Identity	Accession #	E-value			
16	<i>H.s.</i> Ran binding protein 9	<a href="#">NM_005493</a>	<i>H.s.</i> Ran binding protein 9	XP_344581	$2 \times 10^{-92}$	702	Centrosomal	N
22	<i>H.s.</i> clone RP4-614C10 (chr 2) (E = 0.0)	<a href="#">AC006453</a>	-	N.A.	N.A.	N.A.	N.A.	NT
31	<i>H.s.</i> clone RP4-614C10 (chr 2) (E = 0.0)	<a href="#">AC006453</a>	-	N.A.	N.A.	N.A.	N.A.	NT
38	<i>H.s.</i> clone RP4-614C10 (chr 2) (E = 0.0)	<a href="#">AC006453</a>	-	N.A.	N.A.	N.A.	N.A.	NT
43	<i>H.s.</i> clone RP4-614C10 (chr 2) (E = 0.0)	<a href="#">AC006453</a>	-	N.A.	N.A.	N.A.	N.A.	NT



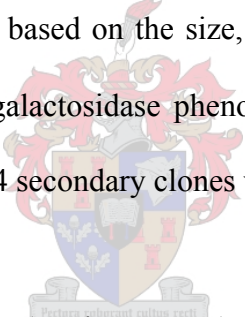
Clone#	Genomic hit		In-frame ORF protein hit				Cellular location	Specific interaction (Y/N)
	Identity	Accession #	Identity	Accession #	E-value	Length (AA)		
44	<i>H.s.</i> clone RP4-614C10 (chr 2) (E = 0.0)	<a href="#">AC006453</a>	-	N.A.	N.A.	N.A.	N.A.	NT
47	<i>H.s.</i> Ran binding protein 9	<a href="#">NM_005493</a>	<i>H.s.</i> Ran binding protein 9	AAH52781	1x10 <sup>-84</sup>	702	Centrosomal	NT
48	<i>H.s.</i> clone RP4-614C10 (chr 2) (E = 0.0)	<a href="#">AC006453</a>	-	N.A.	N.A.	N.A.	N.A.	NT
57	<i>H.s.</i> clone RP4-614C10 (chr 2) (E = 0.0)	<a href="#">AC006453</a>	-	N.A.	N.A.	N.A.	N.A.	NT



*AA* = amino acid; *chr* = chromosome; *H.s.* = Homo sapiens, *N* = no; *N.A.* = not applicable; *NT* = Not tested; *Y* = yes; - = no protein match found

#### III.3.2.4. cMyBPC C7 Y2H library-assay

The pGBKT7-C7 bait construct (table II.10), transformed into *S. cerevisiae* strain AH109, was used to screen a pACT2-based cardiac cDNA library, pre-transformed into *S. cerevisiae* strain Y187 (BD Biosciences, Clontech, Palo Alto, CA, USA) (section II.17.2.2). The screening of an estimated  $1.2 \times 10^6$  clones yielded 124 clones in which transcription of the *HIS3* reporter gene was activated. Of these clones, 101 were able to grow on QDO-selection medium, indicating activation of transcription of the *ADE2* reporter gene. Filter  $\beta$ -galactosidase assays and X- $\alpha$ -galactosidase assays led to the elimination of an additional 19 of the 101 clones, based on their inability to activate transcription of the *LacZ* and *MEL1* reporter genes (table III.14). The remaining 82 clones were classified as either primary, or secondary interactor clones, based on the size, robustness and colour of the colony, as well as their  $\beta$ -galactosidase and X- $\alpha$ -galactosidase phenotypes (time to, and intensity of, colour development). In total, 28 primary and 54 secondary clones were identified.



Restriction mapping of the library inserts (section II.11.3) of all primary- and secondary- interactor clones revealed the presence of two groups of identical clones, as well as some unique clones (table III.14). Each group was subsequently represented by a single clone, used for DNA sequencing. The nucleotide sequences of the cDNA inserts contained in all 24 representative primary clones, as well as one secondary clone, that represented a group of eight clones, were subsequently used for BLAST-analyses, allowing the identification of interactor peptides (table III.15). Nineteen of the prey-peptides identified were deemed to be implausible binding partners of the C7 domain of cMyBPC, due to either their cellular localisation, or the fact that they encoded very short peptides with no significant protein database matches (table III.15). One of the prey inserts was identified as

encoding a partial cMyBPC domain C10, one as encoding myomesin 2 (M-protein), and three as encoding M-line titin. The identification of a clone encoding a partial C10 peptide confirmed the presence of an interaction between the C7 and C10 domains of cMyBPC, previously identified in candidate-ligand Y2H assays. Additionally, the titin and M-protein peptides were regarded as informative ligands, based on the fact that they are members of the intracellular immunoglobulin superfamily, notwithstanding their M-line localisation (section IV.2).

Interaction specificity tests (section II.17.7) were performed on clones expressing partial cMyBPC, M-line titin and M-protein peptides. These tests showed that the M-line titin and cMyBPC peptides interacted specifically with domain C7 of cMyBPC, while the M-protein interaction was found to be non-specific, as evidenced by its ability to activate transcription of the *HIS3* and *ADE2* reporter genes in the presence of heterologous baits (table III.15 and section IV.2).

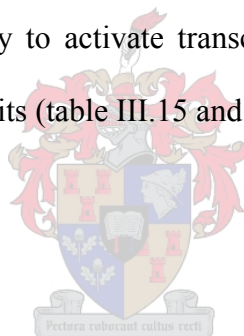


Table III.14. Putative interactor clones identified in the cMyBPC domain C7 Y2H library-assay

Clone #	# Clones represented	Colony phenotype (QDO)		X- $\alpha$ -galactosidase assay		Clasn	Sel seq (Y/N)
		R&S	Colour	Time	Colour		
2	1	✓ ✓	LP	16 hours	+++	1'	Y
3	1	✓ ✓	W	16 hours	+++	1'	Y
4	1	✓ ✓ ✓	LP	16 hours	+++	1'	Y
5	1	✓ ✓ ✓	W	16 hours	+++	1'	Y
7	1	✓ ✓	LP	16 hours	+++	1'	Y
9	1	✓ ✓	LP	16 hours	++	1'	Y
10	8	✓	P	16 hours	++	2'	Y
12	1	✓ ✓	P	16 hours	+++*	1'	Y
16	1	✓ ✓	W	16 hours	+++	1'	Y
20	1	✓ ✓	LP	16 hours	+++	1'	Y
24	1	✓ ✓	LP	16 hours	++	1'	Y
27	1	✓ ✓ ✓	W	16 hours	++	1'	Y
30	1	✓ ✓	LP	16 hours	+++	1'	Y
31	1	✓ ✓	LP	16 hours	+++	1'	Y
33	1	✓ ✓	LP	16 hours	++	1'	Y
35	1	✓ ✓	LP	16 hours	++	1'	Y
40	1	✓ ✓ ✓	W	16 hours	++	1'	Y
46	1	✓ ✓	W	16 hours	++	1'	Y
48	1	✓ ✓	LP	16 hours	+++	1'	Y
53	1	✓ ✓ ✓	W	16 hours	+++	1'	Y
67	1	✓ ✓ ✓	LP	16 hours	+++	1'	Y
72	1	✓ ✓	P	16 hours	+++*	1'	Y
84	1	✓ ✓ ✓	LP	16 hours	++	1'	Y
99	5	✓ ✓	LP	16 hours	+++	1'	Y
119	1	✓ ✓	LP	16 hours	++	1'	Y

Clasn = classification; LP = light pink; N = no; NT = not tested; P = pink; R&S = robustness and size of colony; Sel seq = selected for sequencing; Time = time to blue colour development; W = white; X = no growth; Y = yes; ✓ = weak; ✓ ✓ = intermediate; ✓ ✓ ✓ = strong; + = light blue; ++ = blue; +++ = dark blue; 1' = primary colony; 2' = secondary colony; \* selected as primary colony based on strong  $\beta$ -galactosidase phenotype.

Table III.15. Identification of primary interactor clones selected in the cMyBPC domain C7 Y2H library-assay

Clone#	Genomic hit		In-frame ORF protein hit				Cellular location	Specific interaction (Y/N)
	Identity	Accession #	Identity	Accession #	Length (AA)	E-value		
2	<i>H.s.</i> Mitochondrial genome	<a href="#">AF347015</a>	<i>H.s.</i> cytochrome c oxidase subunit II	AAP90859	89	$1 \times 10^{-24}$	Mitochondrial inner membrane	NT
3	<i>H.s.</i> ATP synthase, H <sup>+</sup> transporting, mitochondrial F1 complex, alpha subunit, isoform 1	<a href="#">BT007209</a>	<i>H.s.</i> ATP synthase, H <sup>+</sup> transporting, mitochondrial F1 complex, alpha subunit, isoform 1	AAP36942	471	$1 \times 10^{-81}$	Mitochondrial	NT
4	<i>H.s.</i> ATPase, H <sup>+</sup> transporting, lysosomal 13kDa, V1 subunit G isoform 1 ( <i>ATP6V1G1</i> ) (E = $1 \times 10^{-101}$ )	<a href="#">NM_004888</a>	-	N.A.	N.A.	N.A.	N.A.	NT
5	<i>H.s.</i> Titin ( <i>TTN</i> )	<a href="#">XM_038279</a>	<i>H.s.</i> titin	NP_003310	595	$1 \times 10^{-73}$	Sarcomeric	Y

Clone#	Genomic hit		In-frame ORF protein hit				Cellular location	Specific interaction (Y/N)
	Identity	Accession #	Identity	Accession #	Length (AA)	E-value		
7	<i>H.s.</i> PAC clone RP5-997N5 (E = 0.0)	<a href="#">AC004945</a>	-	N.A.	N.A.	N.A.	N.A.	NT
9	<i>H.s.</i> Platelet-activating factor acetylhydrogenase $\alpha$ -subunit ( <i>PAFAH1B1</i> ) (E = $1 \times 10^{-48}$ )	<a href="#">NM_000430</a>	-	N.A.	N.A.	N.A.	N.A.	NT
10	<i>H.s.</i> Mitochondrial genome	<a href="#">AF347015</a>	<i>M.a.</i> cytochrome oxidase chain I	AAB82423	36	$6 \times 10^{-12}$	Mitochondrial inner membrane	NT
12	<i>H.s.</i> Collagen type I, $\alpha 2$ subunit ( <i>COL1A2</i> )	<a href="#">XM_029246</a>	<i>H.s.</i> Alpha2(I) collagen	AAB69977	76	$6 \times 10^{-32}$	Extacellular matrix	NT
16	<i>H.s.</i> Cardiac myosin binding protein C (MYBPC3)	<a href="#">X84075</a>	<i>H.s.</i> Cardiac myosin binding protein C	NP_000247	39	$8 \times 10^{-16}$	Sarcomeric	Y

Clone#	Genomic hit		In-frame ORF protein hit				Cellular location	Specific interaction (Y/N)
	Identity	Accession #	Identity	Accession #	Length (AA)	E-value		
20	<i>H.s.</i> Titin ( <i>TTN</i> )	<a href="#">XM_038279</a>	<i>H.s.</i> titin	NP_003310	35	2x10 <sup>-13</sup>	Sarcomeric	Y
24	<i>H.s.</i> Titin ( <i>TTN</i> )	<a href="#">XM_038279</a>	<i>H.s.</i> titin	NP_003310	35	2x10 <sup>-13</sup>	Sarcomeric	Y
27	<i>H.s.</i> phosphoglucomutase 1	BT006961	<i>H.s.</i> phosphoglucomutase 1	XP_001442	54	5x10 <sup>-6</sup>	Cytoplasmic	NT
30	<i>H.s.</i> Mitochondrial genome	<a href="#">AF347015</a>	<i>H.s.</i> NADH dehydrogenase subunit 2	AA088476	89	3x10 <sup>-10</sup>	Mitochondrial	NT
31	<i>H.s.</i> Mitochondrial genome	<a href="#">AF347015</a>	<i>H.s.</i> NADH dehydrogenase subunit 1	AAK17324	62	4x10 <sup>-43</sup>	Mitochondrial	NT
33	<i>H.s.</i> Genomic clone RP5-1137017 (E = 0.0)	<a href="#">AL133295</a>	-	N.A.	N.A.	N.A.	N.A.	NT
35	<i>H.s.</i> Mitochondrial genome	<a href="#">AF347015</a>	<i>H.s.</i> Quinoline phosphotransferase	AAP36539	63	2x10 <sup>-28</sup>	Mitochondrial	NT

Clone#	Genomic hit		In-frame ORF protein hit				Cellular location	Specific interaction (Y/N)
	Identity	Accession #	Identity	Accession #	Length (AA)	E-value		
40	<i>H.s.</i> Mitochondrial genome	<a href="#">AF347015</a>	<i>H.s.</i> Cytochrome oxidase subunit III	AA066832	152	1x10 <sup>-47</sup>	Mitochondrial inner membrane	NT
46	<i>H.s.</i> Mitochondrial genome	<a href="#">AF347015</a>	<i>H.s.</i> Cytochrome c oxidase subunit 1	AAK17768	150	3x10 <sup>-57</sup>	Mitochondrial inner membrane	NT
48	<i>H.s.</i> Mitochondrial genome	<a href="#">AF347015</a>	<i>H.s.</i> NADH dehydrogenase subunit 1	AAK17324	87	9x10 <sup>-26</sup>	Mitochondrial	NT
53	<i>H.s.</i> Myomesin 2 (M-protein) ( <i>MYOM2</i> )	<a href="#">XM_005198</a>	<i>H.s.</i> Myomesin 2 (M-protein)	NP_003961	62	2x10 <sup>-40</sup>	Sarcomeric	N
67	<i>H.s.</i> Mitochondrial genome	<a href="#">AF347015</a>	<i>H.s.</i> NADH dehydrogenase	AAP90895	103	5x10 <sup>-10</sup>	Mitochondrial inner membrane	NT
72	<i>H.s.</i> Mitochondrial genome	<a href="#">AF347015</a>	<i>M.a.</i> cytochrome oxidase chain I	AAB82423	40	9x10 <sup>-28</sup>	Mitochondrial inner membrane	NT

Clone#	Genomic hit		In-frame ORF protein hit				Cellular location	Specific interaction (Y/N)
	Identity	Accession #	Identity	Accession #	Length (AA)	E-value		
84	<i>H.s.</i> chemokine-like factor super family 6 ( <i>CKLFSF6</i> ) (321bp E = 1x10 <sup>-178</sup> )	<a href="#">AF479261</a>	-	N.A.	N.A.	N.A.	N.A.	NT
46	<i>H.s.</i> Mitochondrial genome	<a href="#">AF347015</a>	<i>H.s.</i> Cytochrome c oxidase subunit 1	AAK17768	150	3x10 <sup>-57</sup>	Mitochondrial inner membrane	NT
99	<i>H.s.</i> Mitochondrial genome	<a href="#">AF347015</a>	<i>H.s.</i> NADH dehydrogenase subunit 1	AAK17324	62	3x10 <sup>-7</sup>	Mitochondrial	NT
119	<i>H.s.</i> Mitochondrial genome	<a href="#">AF347015</a>	<i>H.s.</i> ATP synthase F0 subunit 6	AAP89457	120	1x10 <sup>-62</sup>	Mitochondrial	NT

*AA* = amino acid; *H.s.* = Homo sapiens; *M.a.* = Mesocricetus auratus; N = no; NT = not tested; Y = yes; - = no protein match found

### III.3.3. MULTIPLE SEQUENCE ALIGNMENT ANALYSIS OF TITIN INTERACTOR PREY CLONES AND TITIN

The titin interactor clones identified as putative ligands of the C7 domain of cMyBPC and the C0C1 region of cMyBPC encoded portions of M-line titin, varying in length between 34 and 595 amino acids. As these clones all encoded portions of titin embedded in the M-line and, as cMyBPC is found in the C-zone, interactions between this region of titin and cMyBPC were deemed implausible.

BLASTP (<http://www.ncbi.nlm.nih.gov/Blast>) analysis of these clones, however, revealed that the shorter titin interactor peptides shared a high degree of homology with several other domains of titin. In order to identify which domains of titin shared the highest homology with these short M-line titin peptides, sequential ClustalW (<http://www.ebi.ac.uk/service/seq/seq.cgi>) two-sequence alignments were performed, using the 35 amino acid titin interactor peptide (clones 20 and 24, table III.15) and the full-length titin amino acid sequence (<http://www.ncbi.nlm.nih.gov/Entrez> accession number NP\_003310). These alignments revealed that the 35 amino acid M-line titin peptide shared highest homology with each of the eleven domains of C-zone titin, previously reported to interact with the C9C10 region of MyBPC (Labeit and Kolmerer, 1995) (section I.7.3.2; table III.15 and figures III.39 and III.40).

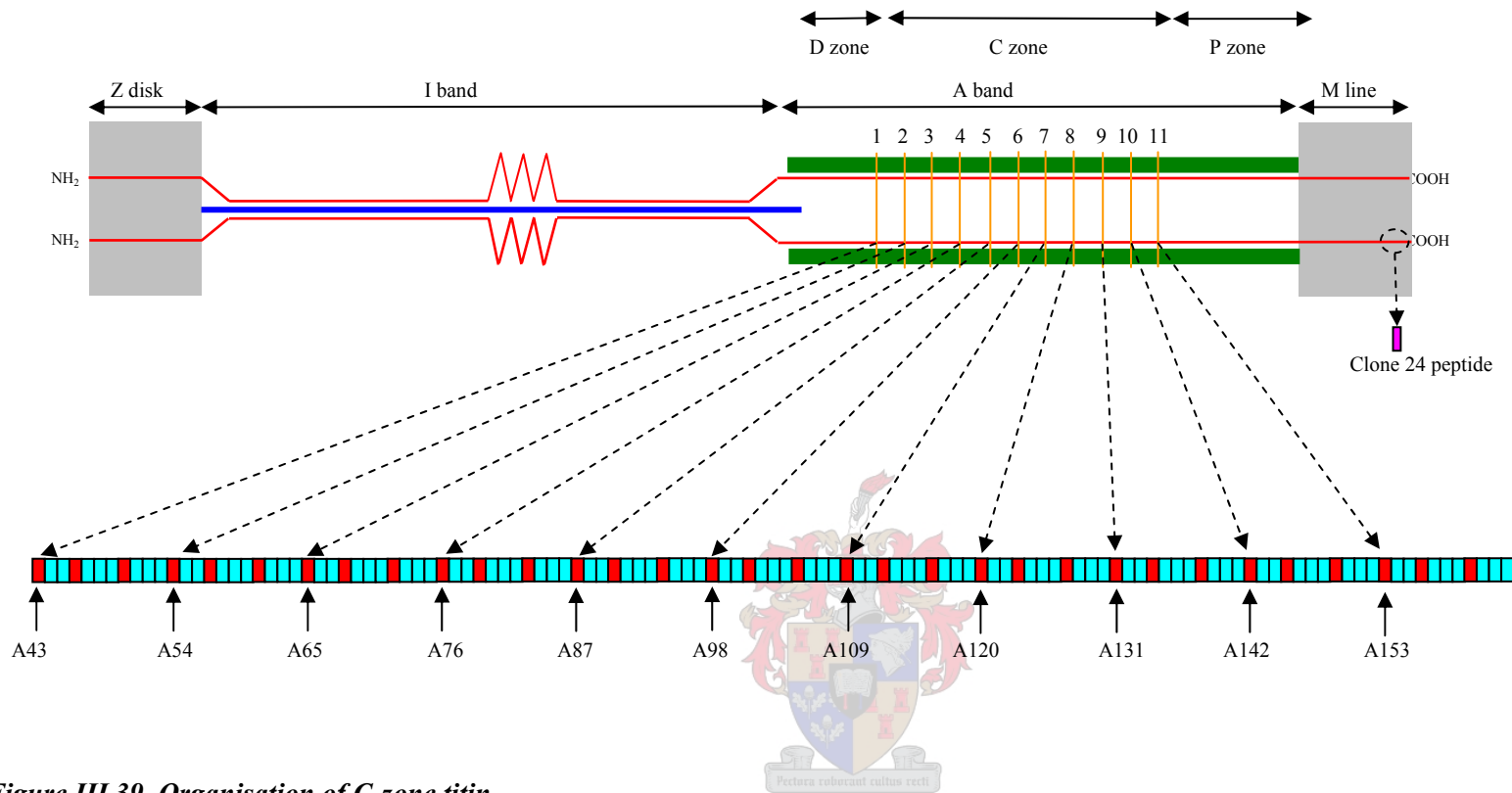
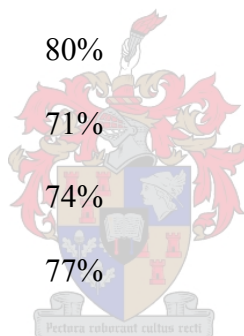


**Figure III.39. Organisation of C-zone titin**

The position of titin within the half sarcomere is shown at the top of the figure (see figure I.6). The domain organisation of C-zone titin is shown at the bottom of the figure, with the domain numbers of the first IgC2 of each eleven domain super-repeat indicated. The position of the clone 24 M-line titin peptide is indicated by the purple box at the right of the figure and the numbers of the eleven stripes in which the MyBPs are found are shown above each stripe. ■ = IgC2 domains; ■ = Fn3 domains.

**Table III.16. Amino acid homology shared between the 35 amino acid M-line titin peptide and specific C-zone titin domains**

<b>C-zone titin domain</b>	<b>Identity (%)</b>	<b>Similarity (%)</b>
A43	29%	71%
A54	34%	77%
A65	26%	69%
A76	37%	74%
A87	40%	86%
A98	34%	74%
A109	49%	80%
A120	26%	80%
A131	31%	71%
A142	29%	74%
A153	37%	77%



Clone_24	.....	0
A43	..VIVRAGCP <del>IRLFAIVRGR</del> PAPKVTWRKVGIDNVVRKGQ	38
A54	KTLILRAGV <del>TMRLYV</del> VKGRPPPKITWSKPNVNLDRIGL	40
A65	RTL <del>VVRAGL</del> SIRIFVPIKGRPAPEVTWTKDNINLKNRAN.	39
A76	.....TLR <del>LFVPIKGR</del> PAPEV <del>KWARDHGESL</del> ..DKA	29
A87	.....RAG <del>SLR</del> LFVPIKGRPTPEVKWGKVDGEIR..DAA	33
A98	..IVVRAGGSAR <del>IHIPFKGR</del> PTPEITWSREEG.EFT.DKV	36
A109	KVVVLRASATL <del>R</del> LFV <del>TIKGR</del> PEPEVKWEKAEG.ILT.DRA	38
A120	KTLIVKAGAS <del>F</del> TMIVPFRGRPV <del>PNV</del> LWSKPD <del>TDLR</del> TRA..	38
A131	.SVIAKAGEDVQV <del>LIPFKGR</del> PPPTVTWRKDEKNLGS <del>DARY</del>	39
A142	QTHVVRAGAS <del>IRLF</del> IAYQGRPTPTAVWSK <del>PDSNLS</del> RA..	38
A153	KTVTIRAGAS <del>LRLM</del> SVSGRPPPVITWSKQ <del>GIDL</del> ASRA..	38
Consensus	rag s rlfvp kgrp p vtw k l r	
Clone_24	.....IIMDVQKQD <del>GG</del> LYTL <del>SLG</del> NEFGS.DSATV	28
A43	.VDLVD <del>TMAFLV</del> IPNSTRDD <del>SCKY</del> SLTLVNPAGE.KAVFV	76
A54	DIKSTDFD <del>TFLRCEN</del> VNKYDACKYIL <del>TLEN</del> SCGK.KEYTI	79
A65	.IENTES <del>SFTLLLI</del> IPECNRYD <del>ICKF</del> VMTIENPAGK.KSGFV	77
A76	SIESTSSY <del>TLLIVGN</del> VNRFD <del>SCKY</del> IL <del>TVEN</del> SSGS.KSAFV	68
A87	IIDVTSS <del>FTSLVLD</del> NVNR <del>YD</del> SCKY <del>TLTLEN</del> SSGT.KSAFV	72
A98	QIEKGVNY <del>TQLSID</del> NCD <del>RND</del> ACKYIL <del>KLEN</del> SSGS.KSAFV	75
A109	QIEVTSS <del>F</del> TMLVIDNVTRFD <del>SCRYN</del> L <del>TLEN</del> SSGS.KTAFV	77
A120	YVD <del>TIDS</del> R <del>TS</del> LT <del>TIEN</del> ANRND <del>SCKY</del> TL <del>TIQ</del> NVLSA.ASLTL	77
A131	SIENTD <del>SSSLLT</del> IPQVTRND <del>ICKY</del> IL <del>TIEN</del> GVGEPK <del>SSTV</del>	79
A142	DIHT <del>TDS</del> F <del>STL</del> TVENCNRND <del>ACKY</del> TL <del>TVEN</del> SSGS.KSITF	77
A153	IID <del>TTE</del> SYSLLIVDKVNR <del>YD</del> ACKY <del>TIEAEN</del> QSGK.KSATV	77
Consensus	i t s t l i nvr d gky ltlen sg ksafv	
Clone_24	NIHIRS	34
A43	NVRVL	81
A54	VVKVL	84
A65	NVRVL	82
A76	NVRVL	73
A87	TVRVL	77
A98	TVKVL	80
A109	NVRVL	82
A120	VVKVL	82
A131	SVKVL	84
A142	TVKVL	82
A153	LVKVY	82
Consensus	vkvl	



**Figure III.40. Multiple sequence alignment of cMyBPC domain C7 ligand 24 and C-zone domains of titin**  
 Multiple sequence alignment of the 35 amino acid titin clone identified from the cMyBPC domain C7 library screen (clones 20 and 24, table III.12.) and the first Ig-domain of each of the 11, C-zone titin eleven-domain super-repeats. Titin domains, numbered according to Labeit and Kolmerer (1995). Conserved residues highlighted by gray shading with degrees of shading indicating the degree of conservation.

### III.3.4. CANDIDATE LIGAND Y2H-ASSAYS

Small-scale yeast matings (section II.17.1) were used to facilitate the detection of interactions between specific domains of cMyBPC and specific candidate ligands. Candidate ligands were chosen based either on their position within the sarcomere, rendering them capable of interacting with cMyBPC, or them previously having been reported to interact with cMyBPC, or plausible ligands of cMyBPC that share significant homology with implausible sarcomeric ligands, found to spuriously interact with specific domains of cMyBPC in Y2H library-assays.

#### III.3.4.1. Identification of cMyBPC domain C10 as a ligand of the cMyBPC domain C7

Based on the identification of an interaction between the C5 and C8 domains of cMyBPC (Moolman-smook et al., 2002), the C6 and C10 domains of cMyBPC were identified as candidate ligands of the C7 domain (section IV.2). In order to test whether either of these domains interacted with domain C7, small-scale yeast matings were used to co-express domain C7 bait fusion-peptides with cMyBPC domains C6- and C10- prey fusion-peptides, in diploid yeast cells. As additional controls, C5- and C8- prey fusion-peptides were also co-expressed with C7 bait fusion peptides. These experiments showed that only yeast cells co-expressing the C7 bait and C10 prey fusion-peptides activated transcription of the *HIS3* and *ADE2* nutritional reporter genes, thus allowing them to grow on QDO selection plates, indicating that only domain C10 of cMyBPC specifically interacts with domain C7 (figure III.41 and section IV.2.1).

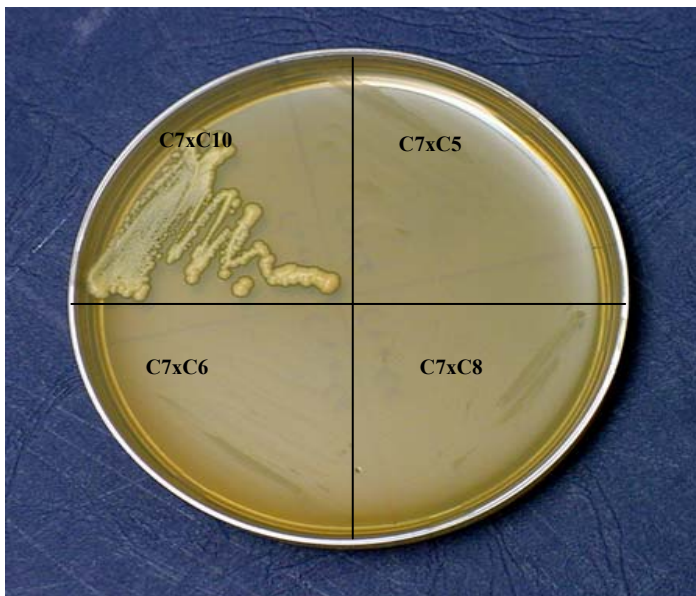


**Figure III.41. Identification of cMyBPC domain C10 as the ligand of the cMyBPC domain C7**

Growth of diploid yeast on QDO medium indicates interaction between respective bait and prey fusion-peptides, leading to activation of transcription of the HIS3 and ADE2 nutritional reporter genes. C7 = yeast strain AH109 transformed with pGBKT7-C7 bait construct; C5 = yeast strain Y187 transformed with pACT2-C5 prey construct; C6 = yeast strain Y187 transformed with pACT2-C6 prey construct; C8 = yeast strain Y187 transformed with pACT2-C8 prey construct; C10 = yeast strain Y187 transformed with pACT2-C10 prey construct; x = mated to in small-scale yeast mating.



### III.3.4.2. Identification of specific IgC2 domains of C-zone titin as ligands of the cMyBPC domain C7

Based on the amino acid sequence conservation shared by specific C-zone titin domains with the M-line titin peptide identified as a ligand of cMyBPC domain C7 in the Y2H library-assay (section III.3.2.4, tables III.15, III.16, figures III.39; III.40), these domains were considered plausible ligands of cMyBPC domain C7. In order to test this hypothesis, cMyBPC domain C7 bait fusion-peptides were co-expressed with titin domain A43, A109, A112, A116 and A109-A112 prey fusion-peptides

(figure III.39). These experiments showed that only yeast cells co-expressing the C7 bait fusion peptide and either the titin domain A43, A109, or A109-A112 prey fusion-peptide, activated transcription of the *HIS3* and *ADE2* nutritional reporter genes, thus allowing them to grow on QDO selection plates (figure III.42 and table III.17). In order to establish whether these interactions were specific, a cMyBPC domain C2 bait fusion-peptide was co-expressed with titin domains A43- and A109- prey-peptides, but no growth was observed on QDO selection plates, indicating that domain C2 of cMyBPC does not interact with either of these titin domains (figure III.42).

Phenotypic differences between diploid yeast cells co-expressing domain C7 of cMyBPC and domain A43 of titin, and those co-expressing domain C7 of cMyBPC and either domain A109 or the A109-A112 region of titin, suggested that domain C7 of cMyBPC interacted more strongly with domain A43 of titin than with domain A109 of titin. These phenotypic differences included: the ability of yeast co-expressing domain C7 of cMyBPC and domain A43 of titin to grow on highly stringent QDO media directly from rich mating media, while yeast co-expressing domain C7 of cMyBPC, and either domain A109 or the A109-A112 region of titin, required passage via TDO media. Secondly, yeast colonies in which the C7 and A43 domains were co-expressed, were larger and lighter coloured than yeast colonies co-expressing C7 and either domain A109 or the A109-A112 region of titin (figure III.42, table III.17 and section IV.2.2).

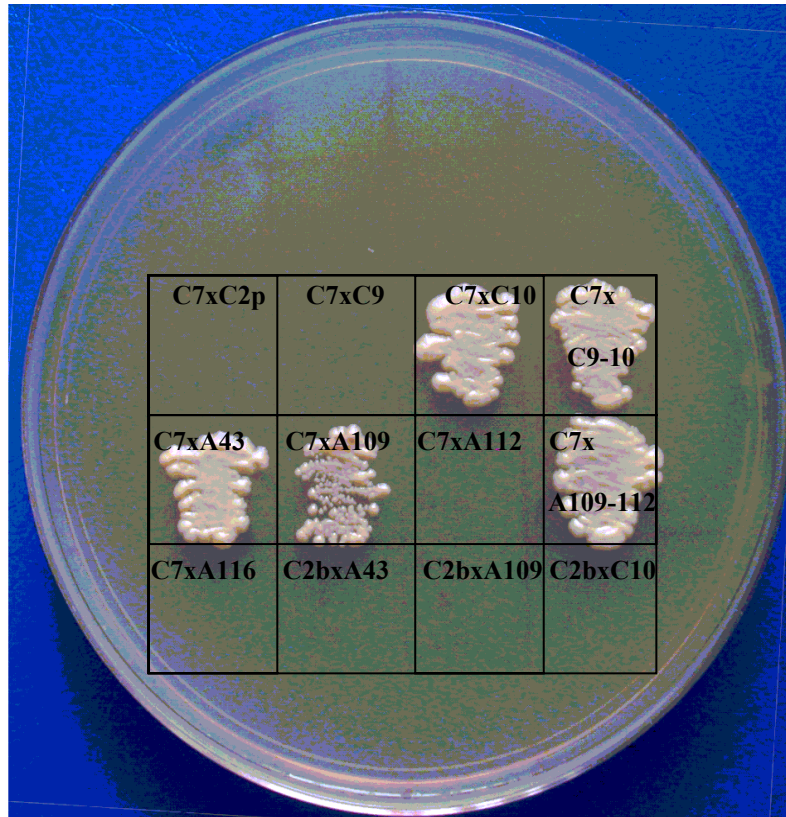


**Figure III.42. Detection of an interaction between domain C7 of cMyBPC and C-zone titin**

Growth of diploid yeast on QDO medium indicates interaction between respective bait and prey fusion-peptides, leading to activation of transcription of the *HIS3* and *ADE2* nutritional reporter genes. C7 = yeast strain AH109 transformed with pGBKT7-C7 bait construct, C2b = yeast strain AH109 transformed with pGBKT7-C2 bait construct; C2p = yeast strain Y187 transformed with pGADT7-C2 prey construct; C9 = yeast strain Y187 transformed with pACT2-C9 prey construct; C10 = yeast strain Y187 transformed with pACT2-C10 prey construct; C9-C10 = yeast strain Y187 transformed with pACT2-C9C10 prey construct; A43 = yeast strain Y187 transformed with pGADT7-A43 prey construct; A109 = yeast strain Y187 transformed with pGADT7-A109 prey construct; A112 = yeast strain Y187 transformed with pGADT7-A112 prey construct; A109-A112 = yeast strain Y187 transformed with pGADT7-A109A112 prey construct; A116 = yeast strain Y187 transformed with pGADT7-A116 prey construct; x = mated to in small-scale yeast mating.

**Table III.17. Assessment of interactions between domain C7 of cMyBPC and C-zone titin**

<b>Mating</b>	<b>TDO (LW)</b>	<b>QDO (LW)</b>	<b>QDO (TDO)</b>
C7 x A43	✓ ✓	✓ ✓	✓ ✓ ✓
C7 x A109	✓ ✓ ✓	X	✓ ✓
C7 x A109-A112	✓ ✓	X	✓ ✓ ✓
C7 x A112	✓	X	X
C7 x A116	X	X	NT
C2 x A43	X	X	NT
C2 x A109	X	X	NT
C2 x C10	X	X	NT

*C7 = yeast strain AH109 transformed with pGBKT7-C7 bait construct, C2 = yeast strain AH109 transformed with pGBKT7-C2 bait construct; A43 = yeast strain Y187 transformed with pGADT7-A43 prey construct; A109 = yeast strain Y187 transformed with pGADT7-A109 prey construct; A112 = yeast strain Y187 transformed with pGADT7-A112 prey construct; A109-A112 = yeast strain Y187 transformed with pGADT7-A109A112 prey construct; A116 = yeast strain Y187 transformed with pGADT7-A116 prey construct; x = mated to in small-scale yeast mating; TDO = TDO selection medium; QDO = QDO selection medium, (LW) = yeast transferred from SD<sup>L-W</sup> medium; (TDO) = yeast transferred from TDO selection medium; NT = not tested; X = no growth observed; ✓ = weak growth; ✓ ✓ = intermediate growth; ✓ ✓ ✓ = robust growth.*

### **III.3.4.3. Establishment of the effect of the V896M putative HCM-causing mutation in cMyBPC domain C7 on its interaction with cMyBPC domain C10 and titin domain A43**

In order to establish whether the V896M mutation in domain C7 of cMyBPC abolishes its interaction with either cMyBPC domain C10 or titin domain A43, these domains were co-expressed as prey fusion-peptides with a domain C7 bait fusion-peptide into which V896M was engineered (section II.6.8). Yeast co-expressing either the wild-type, or C7<sup>V896M</sup> bait fusion-peptides and either the cMyBPC domain C10, or titin domain A43 prey fusion-peptides, were able to grow on QDO selection media, indicating that the V896M mutation did not abolish either of these interactions.

Quantitative ONPG  $\beta$ -galactosidase assays (section II.17.6) were subsequently performed, in order to establish whether the presence of the V896M putative HCM-causing mutation in cMyBPC domain C7 affected the strength of its interaction with either cMyBPC domain C10 or titin domain A43. These assays, performed in triplicate, showed that the presence of V896M in domain C7 of cMyBPC significantly strengthened its interaction with the C10 domain of cMyBPC ( $p = 0.0047$ ) (figure III.43). However, V896M did not affect the interaction between cMyBPC domain C7 and titin domain A43 (figure III.43). These assays were subsequently repeated twice, and although absolute  $\beta$ -galactosidase unit values differed, the relative strength of interactions, as well as the significance of the strengthening of the C7:C10 interaction by the presence of the V896M in cMyBPC domain C7, remained constant (data not shown) (section IV.5).

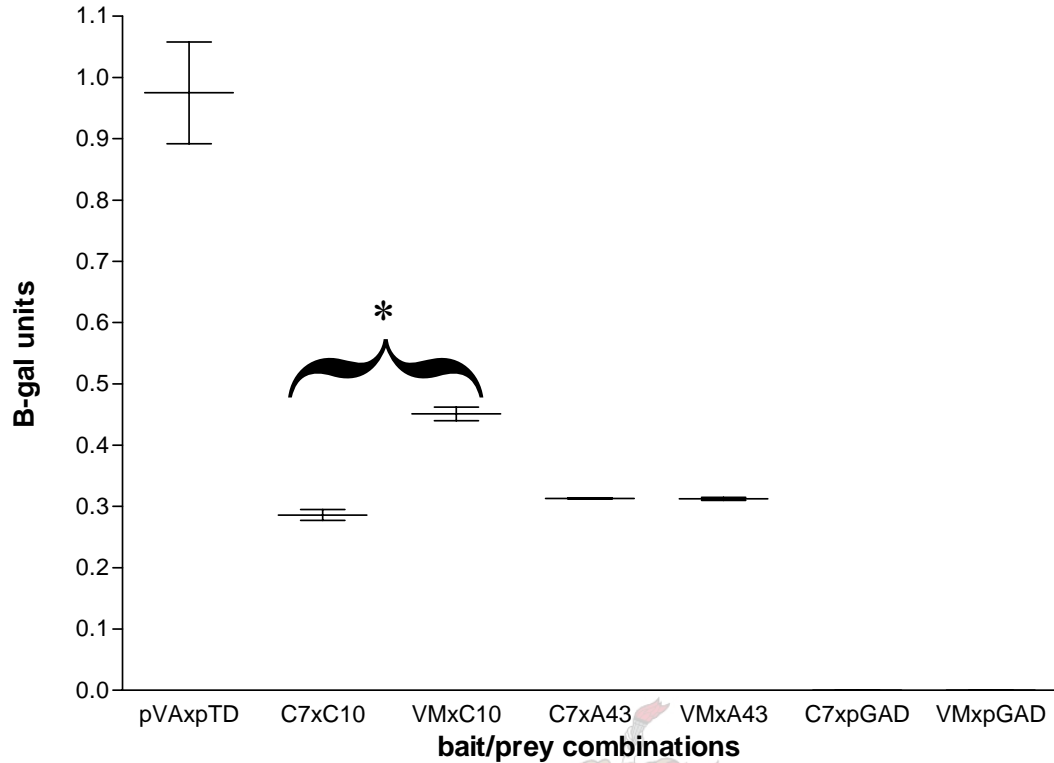


**Figure III.43. Quantitative ONPG  $\beta$ -galactosidase assays performed to establish the effect of the V896M mutation in domain C7 of cMyBPC**

B-gal units =  $\beta$ -galactosidase units; pVAxpTD = yeast strain AH109 transformed with pVA.3.1, mated with yeast strain Y187 transformed with pTD1.1; C7xC10 = yeast strain AH109 transformed with pGBKT7-C7, mated with yeast strain Y187 transformed with pACT2-C10; VMxC10 = yeast strain AH109 transformed with pGBKT7-C7<sup>V896M</sup>, mated with yeast strain Y187 transformed with pACT2-C10; C7xA43 = yeast strain AH109 transformed with pGBKT7-C7, mated with yeast strain Y187 transformed with pGADT7-A43. VMxA43 = yeast strain AH109 transformed with pGBKT7-C7<sup>V896M</sup>, mated with yeast strain Y187 transformed with pGADT7-A43; C7xpGAD = yeast strain AH109 transformed with pGBKT7-C7, mated with yeast strain Y187 transformed with non-recombinant pGADT7; VMxpGAD = yeast strain AH109 transformed with pGBKT7-C7<sup>V896M</sup>, mated with yeast strain Y187 transformed with non-recombinant pGADT7, \* = statistically significant variation in strength of interaction ( $p = 0.0047$ )

### III.3.4.4. Identification of specific IgC2 domains of C-zone titin as putative ligands of the C0C1 region of cMyBPC

Based on the amino acid sequence conservation shared by specific C-zone titin domains and the M-line titin peptide identified as a ligand of the C0C1 region of cMyBPC in Y2H library-assays (sections III.3.2.2.; III.3.2.4.; tables III.10.; III.16 and figures III.39; III.40), these domains were considered plausible ligands of the C0C1 region of cMyBPC. In order to test this hypothesis, cMyBPC C0C1 bait fusion-peptides were co-expressed with titin domain A43, A109, A112, A116 and A109-A112 prey fusion-peptides (figure III.39). Transcription of the *HIS3* and *ADE2* nutritional reporter genes were not activated in any of these yeast cells, as evidenced by their inability to grow on QDO selection plates (table III.18 and section IV.4.3.2).

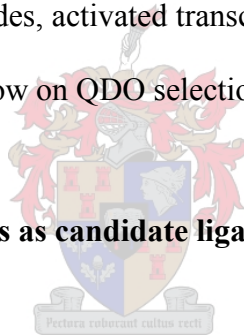
**Table III.18. Assessment of interactions between the C0C1 region of cMyBPC and C-zone titin**

Mating	TDO (LW)	QDO (LW)	QDO (TDO)
C0C1 x A43	✓	X	X
C0C1 x A109	✓ ✓	X	X
C0C1 x A112	✓ ✓ ✓	X	X
C0C1 x A109A112	✓ ✓	X	X
C0C1 x A116	X	X	NT

*Assessment of growth of diploid yeast on TDO and QDO selection media to allow detection of interaction between respective bait and prey fusion-peptides, leading to activation of transcription of the HIS3 and ADE2 nutritional reporter genes. C0C1 = yeast strain AH109 transformed with pGBKT7-C0C1 bait construct; A109 = yeast strain Y187 transformed with pGADT7-A109 prey construct, A112 = yeast strain Y187 transformed with pGADT7-A112 prey construct; A109A112 = yeast strain Y187 transformed with pGADT7-A109A112 prey construct; A116 = yeast strain Y187 transformed with pGADT7-A116 prey construct; x = co-expression of bait and prey fusion-peptides encoded by the respective constructs in diploid yeast cells, subsequent to small-scale yeast mating; TDO = TDO selection medium; QDO = QDO selection medium, (LW) = yeast transferred from SD<sup>-L-W</sup> medium; (TDO) = yeast transferred from TDO selection medium; NT = not tested; X = no growth observed; ✓ = weak growth; ✓ ✓ = intermediate growth; ✓ ✓ ✓ = robust growth.*

### III.3.4.5. Identification of an interaction between the C3 and C10 domains of cMyBPC

Based on our model of cMyBPC quaternary structure (Moolman-Smook et al., 2002 and section IV.3), combined with findings that phosphorylation of cMyBPC results in an expansion of the thick filament backbone, as well as the dimensions of the “expanded” thick filament backbone (sections I.4.6.1.3 and IV.3.2), the C-terminal domains of cMyBPC and specific IgC2 domains of C-zone titin were considered as plausible ligands of the C3 domain of cMyBPC. In order to test this hypothesis, cMyBPC domain C3 bait fusion-peptides were co-expressed with cMyBPC domain C2, C5; C9, C10 and C9-C10, as well as titin domain A43, A109, A112 and A109-A112, prey fusion-peptides. These experiments showed that only yeast cells co-expressing the C3 bait fusion-peptide, and either the C10, C9-C10 or A109 prey fusion-peptides, activated transcription of the *HIS3* and *ADE2* nutritional reporter genes, thus allowing them to grow on QDO selection plates (figure III.44).



### III.3.4.6. N-terminal cMyBPC domains as candidate ligands of the cMyBPC C0C1 region

In order to establish whether the C0C1 region of cMyBPC interacts with specific N-terminal domains of cMyBPC, candidate-ligand Y2H-assays were performed. In these experiments, yeast strain PJ69-2A transformed with either pAS2.1-C0, pAS2.1-C0C1 or pAS2.1-C0C2 (table II.10) was mated with yeast strain Y187 transformed with pACT2-C1, pACT2-C1C2, pACT2-C2, or non-recombinant pACT2 prey-vector. Although weak growth on QDO selection media was observed in some cases, these results could not be reproduced consistently (table III.19).

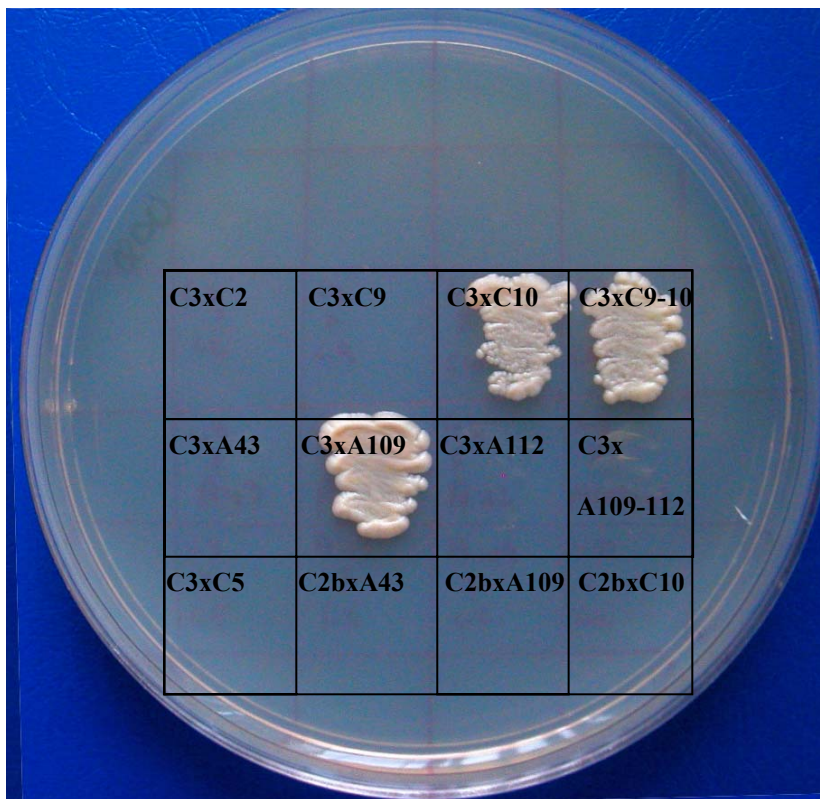


**Figure III.44. Detection of an interaction between domains C3 and C10 of cMyBPC**

Growth of diploid yeast on QDO medium indicates interaction between respective bait and prey fusion-peptides, leading to activation of transcription of the *HIS3* and *ADE2* nutritional reporter genes. C3 = yeast strain AH109 transformed with pGBKT7-C3 bait construct, C2b = yeast strain AH109 transformed with pGBKT7-C2 bait construct; C2p = yeast strain Y187 transformed with pGADT7-C2 prey construct; C5 = yeast strain Y187 transformed with pACT2-C5 prey construct; C9 = yeast strain Y187 transformed with pACT2-C9 prey construct; C10 = yeast strain Y187 transformed with pACT2-C10 prey construct; C9-C10 = yeast strain Y187 transformed with pACT2-C9C10 prey construct; A43 = yeast strain Y187 transformed with pGADT7-A43 prey construct; A109 = yeast strain Y187 transformed with pGADT7-A109 prey construct; A112 = yeast strain Y187 transformed with pGADT7-A112 prey construct; A109-A112 = yeast strain Y187 transformed with pGADT7-A109A112 prey construct; x = mated to in small-scale yeast mating.

**Table III.19. N-terminal domains of cMyBPC as candidate ligands of the C0C1 region of cMyBPC**

<b>Mating</b>	<b>TDO (LW)</b>	<b>QDO (LW)</b>	<b>QDO (TDO)</b>
C0 X C1	✓ ✓	X	X
C0 X C1C2	✓ ✓	X	X
C0 X C2	✓ ✓	X	✓
C0 X pACT2	X	X	NT
C0C1 x C1	✓ ✓	✓	✓
C0C1 x C1C2	✓ ✓	X	X
C0C1 x C2	✓	X	✓
C0C1 x pACT2	✓	✓	X
C0C2 x C1	✓	X	✓
C0C2 x C1C2	✓	X	X
C0C2 x C2	X	X	NT
C0C2 x pACT2	X	X	NT

*Assessment of growth of diploid yeast on TDO and QDO media, enabling the detection of interaction between respective bait and prey fusion-peptides. C0 = yeast strain PJ69-2A transformed with pAS2.1-C0 bait construct, C0C1 = yeast strain PJ69-2A transformed with pAS2.1-C0C1 bait construct; C0C2 = yeast strain PJ69-2A transformed with pAS2.1-C0C2 bait construct; C1 = yeast strain Y187 transformed with pACT2-C1 prey construct C1C2 = yeast strain Y187 transformed with pACT2-C1C2 prey construct; C2 = yeast strain Y187 transformed with pACT2-C2 prey construct; pACT2 = yeast strain Y187 transformed with non-recombinant pACT2 prey-plasmid; x = prey construct co-expression of bait and prey fusion-peptides encoded by the respective constructs in diploid yeast cells, subsequent to small-scale yeast mating; TDO = TDO selection medium; QDO = QDO selection medium, (LW) = yeast transferred from SD<sup>L-W</sup> medium; (TDO) = yeast transferred from TDO selection medium; NT = not tested; X = no growth observed; ✓ = weak growth; ✓ ✓ = intermediate growth; ✓ ✓ ✓ = robust growth.*

### III.3.4.7. Cardiac actin as a candidate ligand of the C0C1 region of cMyBPC

Recently, Kulikovskaya et al., (2003) showed that the C0 domain of cMyBPC was able to interact with cardiac actin monomers in *in vitro* binding-assays, while Squire et al., (2003) proposed that the PA-region of cMyBPC may interact with F-actin. In the light of these findings, cardiac actin was considered a candidate ligand of the C0C1 region of cMyBPC.

In order to test this hypothesis, candidate-ligand Y2H-assays were performed. In these experiments, yeast strain AH109 transformed with either pGBKT7-C0, or pGBKT7-C0C1 (table II.10), was mated with yeast strain Y187 transformed with pACT2-CI182, pACT2-CI268, pACT2-CI286, or non-recombinant pACT2 prey-vector. The pACT2-CI182, pACT2-CI268 and pACT2-CI286 are preys that were previously identified as candidate ligands of the C1C2 region of cMyBPC in a Y2H library-assay by Dr Hanlie Moolman-Smook, and encoded the C-terminal 211, 288 and 176 amino acid residues of cardiac actin (377 amino acid residues), respectively. No growth was, however, observed on either TDO or QDO selection media when these preys were co-expressed with either the C0 or C0C1 bait fusion-peptides (table III.20), indicating the absence of an interaction between cardiac actin and the N-C0C1 region of cMyBPC.

**Table III.20. Cardiac actin as a candidate ligand of the C0C1 region of cMyBPC**

<b>Mating</b>	<b>TDO (LW)</b>	<b>QDO (LW)</b>
C0 x C1182	X	X
C0 x C1268	X	X
C0 x C1286	X	X
C0 x pACT2	X	X
C0C1 x C1182	X	X
C0C1 x C1267	X	X
C0C1 x C1286	X	X
C0C1 x pACT2	X	X

*Assessment of growth of diploid yeast on TDO and QDO media, enabling the detection of interaction between respective bait and prey fusion-peptides. C0 = yeast strain AH109 transformed with pGBKT7-C0 bait construct, C0C1 = yeast strain AH109 transformed with pGBKT7-C0C1 bait construct; C1182 = yeast strain Y187 transformed with pACT2-C1182 prey construct; C1268 = yeast strain Y187 transformed with pACT2-C1268 prey construct; C1286 = yeast strain Y187 transformed with pACT2-C1286 prey construct; pACT2 = yeast strain Y187 transformed with non-recombinant pACT2 prey-plasmid; x = prey construct co-expression of bait and prey fusion-peptides encoded by the respective constructs in diploid yeast cells, subsequent to small-scale yeast mating; TDO = TDO selection medium; QDO = QDO selection medium, (LW) = yeast transferred from SD<sup>-L-W</sup> medium; X = no growth observed.*

<b>CHAPTER IV: DISCUSSION</b>	<b>Page</b>
<b>IV.1. PUTATIVE HCM-CAUSING MUTATIONS IN cMyBPC</b>	<b>262</b>
<b>IV.1.1. PUTATIVE HCM-CAUSING MISSENSE MUTATIONS IN cMyBPC</b>	<b>262</b>
<b>IV.1.1.1. V158M putative HCM-causing missense mutation in cMyBPC</b>	<b>262</b>
<b>IV.1.1.2. A181T putative HCM-causing missense mutation in cMyBPC</b>	<b>263</b>
<b>IV.1.1.3. R177H putative HCM-causing missense mutation in cMyBPC</b>	<b>263</b>
<b>IV.1.1.4. G278E putative HCM-causing missense mutation in cMyBPC</b>	<b>264</b>
<b>IV.1.1.5. G507R putative HCM-causing missense mutation in cMyBPC</b>	<b>265</b>
<b>IV.1.1.6. V896M putative HCM-causing missense mutation in cMyBPC</b>	<b>268</b>
<b>IV.1.2. PUTATIVE HCM-CAUSING SPLICING MUTATIONS IN <i>MYBPC3</i></b>	<b>270</b>
<b>IV.1.2.1. Exon 5 SdS -13 c&gt;t putative HCM-causing splicing mutation in <i>MYBPC3</i></b>	<b>270</b>
<b>IV.1.2.2. Exon 7 SaS +1 g&gt;a putative HCM-causing splicing mutation in <i>MYBPC3</i></b>	<b>271</b>
<b>IV.1.2.3. Intron 6 SbP +1 g&gt;a putative HCM-causing splicing mutation in <i>MYBPC3</i></b>	<b>273</b>
<b>IV.1.3. PUTATIVE HCM-CAUSING FRAME-SHIFT MUTATION IN <i>MYBPC3</i></b>	<b>273</b>
<b>IV.1.3.1. Δc 13255 Frame-shift putative HCM-causing mutation</b>	<b>273</b>
<b>IV.2. PROPOSED MODEL OF cMyBPC QUATERNARY STRUCTURE</b>	<b>274</b>
<b>IV.2.1. cMyBPC DOMAIN C7 LIBRARY-ASSAY</b>	<b>279</b>
<b>IV.2.2. IDENTIFICATION OF A SPECIFIC INTERACTION BETWEEN THE C7 DOMAIN OF cMyBPC AND C-ZONE TITIN</b>	<b>282</b>
<b>IV.3. QUATERNARY STRUCTURE OF THE A-BAND THICK FILAMENT BACKBONE</b>	<b>284</b>
<b>IV.3.1. QUATERNARY STRUCTURE OF THE DISORDERED/"TIGHT" A-BAND THICK FILAMENT BACKBONE</b>	<b>285</b>
<b>IV.3.1.1. LMM thick filament backbone structure</b>	<b>285</b>
<b>IV.3.1.2. Incorporation of A-band titin into the model of the thick filament</b>	<b>288</b>

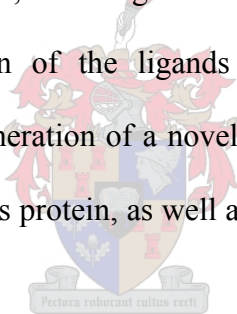
backbone	
<b>IV.3.1.3. Incorporation of cMyBPC into the model of the thick filament backbone</b>	<b>291</b>
<b>IV.3.2. EFFECT OF cMyBPC PHOSPHORYLATION ON THICK FILAMENT BACKBONE STRUCTURE</b>	<b>297</b>
<b>IV.3.2.1. Proposed structure of LMM dimers in the “expanded” thick filament backbone</b>	<b>300</b>
<b>IV.3.2.2. Position of titin dimers on the “expanded” thick filament backbone</b>	<b>302</b>
<b>IV.3.2.2. Position of cMyBPC on the “expanded” thick filament backbone</b>	<b>304</b>
<b>IV.3.3. PHYSIOLOGICAL EFFECT OF cMyBPC MEDIATED EXPANSION OF THE THICK FILAMENT BACKBONE</b>	<b>307</b>
<b>IV.4. Y2H-ANALYSIS OF THE N-TERMINAL REGION OF cMyBPC</b>	<b>309</b>
<b>IV.4.1. Y2H LIBRARY-ASSAYS IN WHICH THE C0C1 REGION OF cMyBPC WERE USED AS BAIT</b>	<b>309</b>
<b>IV.4.2. Y2H LIBRARY-ASSAY IN WHICH THE C0 DOMAIN OF cMyBPC WAS USED AS BAIT</b>	<b>311</b>
<b>IV.4.3. Y2H CANDIDATE-LIGAND ASSAYS IN WHICH THE N-TERMINAL DOMAINS OF cMyBPC WAS USED AS BAIT</b>	<b>312</b>
<b>IV.4.3.1. C-zone titin as a candidate-ligand of the N-terminal region of cMyBPC</b>	<b>312</b>
<b>IV.4.3.2. N-terminal domains of cMyBPC as a candidate-ligands of the N-terminal region of cMyBPC</b>	<b>314</b>
<b>IV.4.3.3. Cardiac actin as a candidate-ligand of the N-terminal region of cMyBPC</b>	<b>316</b>

<b>IV.5. EFFECT OF HCM-CAUSING <i>MYBPC3</i> MUTATIONS ON cMyBPC QUATERNARY STRUCTURE</b>	<b>320</b>
<b>IV.5.1. POSITION OF HCM-CAUSING MISSENSE MUTATIONS IN THE C3 DOMAIN OF cMyBPC</b>	<b>327</b>
<b>IV.5.2. POSITION OF HCM-CAUSING MISSENSE MUTATIONS IN THE C5 DOMAIN OF cMyBPC</b>	<b>329</b>
<b>IV.5.3. POSITION OF HCM-CAUSING MISSENSE MUTATIONS IN THE C6 DOMAIN OF cMyBPC</b>	<b>333</b>
<b>IV.5.4 POSITION OF THE V896M PUTATIVE DISEASE-MODIFYING FACTOR IN THE C7 DOMAIN OF cMyBPC</b>	<b>334</b>
<b>IV.5.5 POSITION OF HCM-CAUSING MISSENSE MUTATIONS IN THE C8 DOMAIN OF cMyBPC</b>	<b>336</b>
<b>IV.5.6 POSITION OF THE V1115I HCM-CAUSING MISSENSE MUTATION IN THE C9 DOMAIN OF cMyBPC</b>	<b>337</b>
<b>IV.5.7 POSITION OF HCM-CAUSING MISSENSE MUTATIONS IN THE C10 DOMAIN OF cMyBPC</b>	<b>340</b>
<b>IV.6. CONCLUDING REMARKS</b>	<b>341</b>



## CHAPTER IV: DISCUSSION

During the course of this study, the screening of *MYBPC3* for HCM-causing mutations has led to the identification of several novel putative HCM-causing mutations. The identification of these putative disease-causing mutations in specific domains of cMyBPC indicates that these domains/regions are of functional importance, as these “experiments of nature” are likely to have a deleterious effect. As cMyBPC has no enzymatic activity, it was postulated that these domains/regions are involved in, as yet, unidentified protein:protein interactions. In order to test this hypothesis, specific domains/regions of cMyBPC, affected by putative HCM-causing mutations identified in this and other studies, were used in Y2H-assays, allowing the identification of ligands binding to these domains. The subsequent identification of the ligands of specific domains of cMyBPC has significantly contributed towards the generation of a novel model of cMyBPC quaternary structure, shedding new light on the function of this protein, as well as providing insights into the pathogenesis of MyBPC-associated HCM.



### IV.1. PUTATIVE HCM-CAUSING MUTATIONS IN cMyBPC

#### IV.1.1. PUTATIVE HCM-CAUSING MISSENSE MUTATIONS IN cMyBPC

##### IV.1.1.1. V158M putative HCM-causing missense mutation in cMyBPC

The V158M putative HCM-causing missense mutation, caused by the g2626a (GenBank sequence accession number: Y10129, available at: <http://www.ncbi.nlm.nih.gov/Entrez>) SNS in exon 5 of *MYBPC3* (figure III.16), was detected in one individual, of Caucasian descent, in the HCM-affected panel (section III.1.2.1). The V158M putative HCM-causing mutation occurs at a residue in the C1

domain of cMyBPC that is conserved as an aliphatic residue (V, L or I), as assessed by cross-species and cross-isoform multiple sequence comparisons (figure III.17), and results in this residue being replaced by a sulphur-containing M residue. As the V158M putative HCM-causing mutation was also detected in three individuals in a control panel consisting of 110 individuals of Caucasian descent, this variant was considered to be a polymorphism, rather than an HCM-causing mutation, and was, therefore, not pursued further.

#### **IV.1.1.2. A181T putative HCM-causing missense mutation in cMyBPC**

The A181T putative HCM-causing missense mutation, caused by the g2785a SNS in exon 6 of *MYBPC3* (figure III.18), was detected in two individuals, both of mixed ancestry, in the HCM-affected panel (section III.1.2.2). The A181T putative HCM-causing mutation occurs at a residue in the C1 domain of cMyBPC that is not conserved in cross-species and cross-isoform multiple sequence comparisons (figure III.19). The A181T putative HCM-causing mutation results in this hydrophobic aliphatic residue being replaced by a hydrophilic hydroxyl-containing residue. As the A181T putative HCM-causing mutation was also detected in two individuals in a control panel consisting of 105 individuals of mixed ancestry, this variant was considered to be a polymorphism, rather than an HCM-causing mutation, and was, therefore, not pursued further.

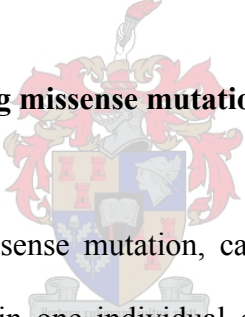
#### **IV.1.1.3. R177H putative HCM-causing missense mutation in cMyBPC**

The R177H putative HCM-causing missense mutation, caused by the g2774a SNS in exon 6 of *MYBPC3* (figure III.20), was detected in two individuals in the HCM-affected panel (section

III.1.2.3). One of the individuals carrying this putative HCM-causing mutation was of Caucasian descent, while the other was of Xhosa descent.

The R177H putative HCM-causing mutation occurs at a residue in the C1 domain of cMyBPC that is conserved as a basic, hydrophilic residue in cross-species and cross-isoform multiple sequence comparisons (either R or K) (figure III.21). The R177H putative HCM-causing mutation results in a conservative substitution of an R residue at position 177 by a hydrophilic basic H residue. As the R177H putative HCM-causing mutation was also detected in six individuals in a control panel consisting of 137 individuals of Xhosa descent, this variant was considered to be a polymorphism, rather than an HCM-causing mutation, and was, therefore, not pursued further.

#### **IV.1.1.4. G278E putative HCM-causing missense mutation in cMyBPC**



The G278E putative HCM-causing missense mutation, caused by the g5047a SNS in exon 9 of *MYBPC3* (figure III.22), was detected in one individual of mixed ancestry in the HCM-affected panel (section III.1.2.4). The G278E putative HCM-causing mutation occurs at a residue that is conserved as an aliphatic residue (either a G or an A) in the cardiac-specific LAGGRRIS insertion in the MyBPC-motif (figure III.23). The G278E putative HCM-causing mutation results in the substitution of a hydrophobic aliphatic G residue with a hydrophilic E residue. As this substitution results in the introduction of a negative charge in the LAGGRRIS insertion, G278E was considered to be a strong candidate for being a disease-causing mutation. The G278E putative HCM-causing mutation was, however, detected in five individuals in a control panel consisting of 104 individuals of mixed ancestry, and was considered a polymorphism, rather than an HCM-causing mutation.

Recently, however, Richard et al., (2003) described G278E in an HCM-affected individual and assigned disease-causing status to this “mutation”, based on the sequence conservation of this residue and its absence in 100 control individuals. Based on the finding that this “mutation” is reasonably prevalent in the control population screened in the present study, combined with the fact that Richard et al., (2003) did not show segregation of G278E with HCM in a family, it is proposed that G278E is not a main-locus HCM-causing mutation. The possibility that G278E may have a more subtle functional effect and may, in combination with an HCM-causing main-locus mutation or even with other non-pathogenic polymorphisms with subtle functional effects, play a role in the pathogenesis of HCM, cannot be excluded.

#### **IV.1.1.5. G507R putative HCM-causing missense mutation in cMyBPC**

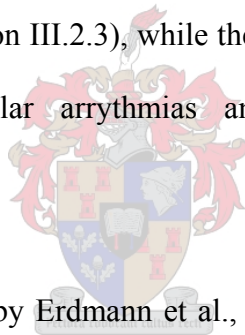
The G507R putative HCM-causing missense mutation, caused by the g9140a SNS in exon 18 of *MYBPC3* (figure III.24) was detected in one individual of Zulu descent in the HCM-affected panel (section III.1.2.5). As the Zulu control panel at our disposal only consisted of 50 individuals, this panel, as well as a Xhosa control panel, consisting of an additional 50 individuals, were screened for the presence of the G507R putative HCM-causing mutation (section II.2). As the Xhosa and Zulu ethnic groups both belong to the Nguni family of tribes, that split about 600 years ago to give rise to the Xhosa, Zulu, Swazi and Ndebele tribes, it can be presumed that these two ethnic groups are genetically closely related (information obtained from: 1Up Info - Country Study & Country Guide - South Africa, available at <http://www.1upinfo.com/country-guide-study/south-africa/south-africa51.html>). The G507R putative HCM-causing mutation was not present in either of these control panels, suggesting that it might be an HCM-causing mutation.

This putative HCM-causing mutation occurs at a residue in the C3 domain of cMyBPC that is highly conserved as a G residue in cross-species and cross-isoform multiple sequence comparisons (figure III.25). The G507R putative HCM-causing mutation results in this uncharged, hydrophilic, aliphatic G residue being replaced by a basic hydrophilic R residue. Based on the conservation of this residue and its absence in a control population, it was considered to be a possible disease-causing mutation. As DNA samples and clinical records of family members of the proband carrying the G507R putative HCM-causing mutation were not available, it was impossible to establish whether G507R segregated with HCM in the family of the proband.

Recently, Erdmann et al., (2001) also described G507R in an HCM-affected individual and described it as an HCM-causing mutation, on the basis that it caused a charge change at a conserved residue and was not present in 50 control individuals. As Erdmann et al., (2001) were unable to establish whether this mutation segregated with HCM in a family setting, and they only screened 50 control individuals, the possibility that G507R is a rare non-disease-causing polymorphism could not be ruled out by this study. Although, segregation of G507R with HCM could not be shown in either the present study, or that by Erdmann et al., (2001), this mutation was present in two distinct HCM-affected populations and absent in matched control populations (totalling 150 individuals). This finding, combined with the fact that this mutation results in a charge change at a highly conserved residue, provides strong evidence that G507R is an HCM-causing mutation rather than a naturally occurring polymorphism.

Furthermore, there are striking similarities between the phenotypic presentation of the probands identified as carrying the G507R mutation in the present study and in that of Erdmann et al., (2001). The proband in the present study, a female of Zulu descent, was diagnosed with HCM at the age of

50 years and presented with dyspnoea, palpitations and angina (section III.2.3), while the proband in the study by Erdmann et al., (2001), a male of Caucasian descent, presented with dyspnoea and palpitations at age 30 years. Furthermore, echocardiography revealed that both these probands had severe LVH of, primarily, the interventricular septum (IVS). The proband in this study had a maximal left ventricular wall thickness of 25mm (IVS) (section III.2.3), while the proband in the study of Erdmann et al., (2001) had a maximal left ventricular wall thickness of 30mm (IVS) and required sinoatrial ablation. The proband in the present study, however, also had systolic anterior motion of the mitral valve (section III.2.3), while this feature was absent in the proband carrying the G507R mutation in the study by Erdmann et al., (2001). ECG-analysis of the proband in the present study revealed increased voltages, abnormal repolarisation and fulfilled the Romhilt and Estes criteria for the diagnosis of HCM (section III.2.3), while the proband in the study by Erdmann et al., (2001) presented with supraventricular arrhythmias and repeated monomorphic ventricular tachycardia.

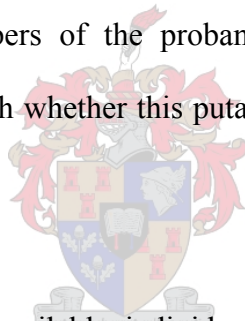


Additionally, the proband in the study by Erdmann et al., (2001) presented with recurrent syncope and required implantation of an implantable cardiac defibrillator, suggesting that this proband was at risk of SCD. As the mother of the proband in the present study died suddenly at the age of 40 years of unknown, non-violent, causes (section III.2.3), it seems possible that a high risk of SCD may also be associated with the G507R mutation in this family.

These phenotypic similarities between carriers of this mutation suggest that G507R is indeed an HCM-causing mutation. From the findings of the present study, and that of Erdmann et al., (2001), it can be suggested that the G507R HCM-causing mutation in the C3 domain of cMyBPC results in HCM characterised by pronounced LVH, ECG abnormalities and an increased risk of SCD. The putative functional effect of the G507R is discussed in section IV.5.1.

#### IV.1.1.6. V896M putative HCM-causing missense mutation in cMyBPC

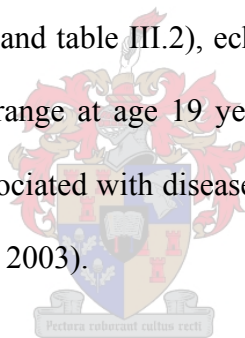
The V896M putative HCM-causing missense mutation, caused by the g15751a SNS in exon 27 of *MYBPC3* (figure III.26) was detected in one individual of Caucasian descent in the HCM-affected panel (section III.1.2.6). The V896M putative HCM-causing mutation occurs at a residue in the C7 Fn3 domain of cMyBPC that is conserved as an aliphatic uncharged hydrophobic residue in cross-species and cross-isoform multiple sequence comparisons (V or I) (figure III.27). The V896M putative HCM-causing mutation results in this residue being replaced by a sulphur-containing hydrophobic M residue. As the V896M putative HCM-causing mutation was not detected in a control panel consisting of 102 individuals of Caucasian descent, it was considered likely to be an HCM-causing mutation. Family members of the proband were, therefore, investigated for the presence of V896M, in order to establish whether this putative disease-causing mutation segregated with HCM in this family.



Following the genotyping of the six available individuals in pedigree 120 for the presence of V896M, four individuals were found to carry this putative HCM-causing mutation (individuals I.2, II.1, II.2 and III.1; figure III.35 and tables III.2 and III.3) (section III.2.1). Clinical assessment of these four individuals revealed that only the proband (individual II.2; figure III.35 and tables III.2 and III.3) fulfilled the echocardiographic criteria for the diagnosis of HCM (table II.3) of a maximal left ventricular wall thickness of more than 13mm. Both the proband (individual II.2; figure III.35) and his eldest brother (individual II.1; figure III.35) presented with angina (table III.2), while the only ECG abnormality in either of these individuals were abnormal Q-waves (table III.3). These findings, combined with the echocardiographic finding that individual II.1 (figure III.35) has a maximal left ventricular wall thickness of 11mm (table III.3), which is at the upper limit of

normality, suggest that, even though this individual does not fulfill the echocardiographic, or the Romhilt and Estes criteria for diagnosis of HCM, he may be affected by HCM.

Additionally, the mother of the proband (individual I.2; figure III.35) presented with dyspnoea and palpitations and was diagnosed with congestive heart failure (table III.2) due to DCM at the age of 75 years. Although there is no ECG evidence of HCM in this patient, ECG-features generally associated with HCM, may have been lost due to congestive heart failure. It is plausible that the diagnosis of DCM may be indicative of dilatation due to end-stage HCM (“burnt out HCM”), which was previously shown to be common in elderly individuals with MyBPC-associated HCM (Konno et al., 2003). Although no symptoms of HCM, or ECG-abnormalities associated with HCM, were present in individual III.1 (figure III.35 and table III.2), echocardiographic measurement of the IVS was at the upper limits of the normal range at age 19 years. This may be indicative of MyBPC-associated HCM, which is generally associated with disease presentation later in life (Charron et al., 1998; Niimura et al., 1998; Konno et al., 2003).

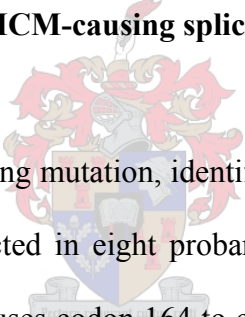


The younger brother of the proband (individual II.4; figure III.35) died suddenly at the age of 28 years while running, and, although no clinical, molecular, or postmortem data were available for this individual, it seems plausible that his death might have been due to HCM-associated SCD. These data suggest that the V896M putative HCM-causing mutation may segregate with HCM in pedigree 120, and that V896M is indeed an HCM-causing mutation. From this data, it was concluded that V896M is associated with reduced penetrance, with late-onset mild LVH, progressing to congestive heart failure at an advanced age, while an increased risk of SCD cannot be excluded.

Subsequent to this mutation being published as an HCM-causing mutation (Moolman-Smook et al., 1999), however, Jaaskelainen et al., (2002), Richard et al., (2003) and Morner et al., (2003) identified V896M in both HCM-affected individuals and HCM-unaffected control populations. These findings prompted Jaaskelainen et al., (2002) and Morner et al., (2003) to describe V896M as a naturally occurring polymorphism, while Richard et al., (2003) proposed that V896M may act as a modifying factor. The functional effect of V896M was further investigated and is discussed in sections IV.5 and IV.5.4.

## **IV.1.2. PUTATIVE HCM-CAUSING SPLICING MUTATIONS IN *MYBPC3***

### **IV.1.2.1. Exon 5 SdS -13 c>t putative HCM-causing splicing mutation in *MYBPC3***



The c2646t putative HCM-causing splicing mutation, identified in the exon 5 coding sequence, 13bp upstream of the exon 5 SdS, was detected in eight probands in the HCM-affected panel (section III.1.3.1 and figure III.28). This SNS causes codon 164 to change from ggc to ggt, both encoding G (G164G). Computational analysis, performed by Dr Peter Rogan (University of Missouri-Kansas City School of Medicine, Kansas City, Missouri, USA), showed that this SNS creates a cryptic SdS 15bp upstream of the natural exon 5 SdS, as described by Carrier et al., (1997). As the cryptic SdS created by the c2646t SNS was predicted to be approximately the same strength as the natural exon 5 SdS, it was hypothesised that this cryptic SdS may be utilised preferentially, due to the processivity of splicing (personal communication, Dr Peter Rogan, 23 December 1999). If indeed the cryptic SdS generated by the c2646t SNS was utilised preferentially to the natural exon 5 SdS, it was predicted that this would lead to the deletion of five amino acid residues in the C1 domain of cMyBPC, and could, therefore, act as an HCM-causing mutation. RT-PCR analysis, however, revealed that this

SNS does not affect the splicing of the *MYBPC3* transcript (section III.1.3.1 and figure III.29) and is, therefore, likely to be a naturally occurring polymorphism, rather than an HCM-causing mutation.

#### IV.1.2.2. Exon 7 SaS +1 g>a putative HCM-causing splicing mutation in *MYBPC3*

The g4177a SNS, occurring at position +1 of the exon 7 SaS (ex7 SaS+1 g>a) (table III.1, section III.1.3.2 and figure III.30), was detected in one proband, of mixed ancestry, in the HCM-affected panel. Computational analysis, performed by Dr Peter Rogan (University of Missouri-Kansas City School of Medicine, Kansas City, Missouri, USA), revealed that this SNS may inactivate the natural exon 7 SaS, as described by Carrier et al., (1997). It was hypothesised that the g4177a SNS would cause the skipping of *MYBPC3* exon 7 (personal communication, Dr Peter Rogan, 23 December 1999).

RT-PCR analysis revealed that this SNS did affect the splicing of the *MYBPC3* transcript, resulting in the skipping of exon 7 (section III.1.3.2 and figure III.31). It is predicted that the skipping of exon 7 would result in a frame-shift in the C1 domain of cMyBPC following amino acid residue 168, the addition of 90 novel amino acids, and the subsequent truncation of the protein, resulting in the loss of the C-terminal portion of the C1 domain through the C10 region of the protein (figure IV.1).

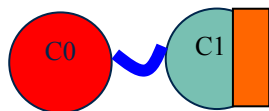


**Figure IV.1. Structure of the truncated cMyBPC protein predicted to be created by the exon 7 SaS+1 g>a putative HCM-causing splicing mutation**

Circles = immunoglobulin C2 domains; ■ = PA-region; ■ = novel amino acids; red area = cardiac-specific C0 domain.

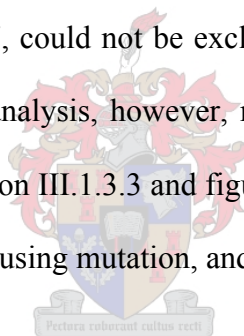
Following the genotyping of the two available family members of the proband (pedigree 137), it was found that only the proband in this pedigree (individual II.2; figure III.36) carries the *MYBPC3* g4177a putative HCM-causing splicing mutation. Additionally, the *TNNT2* R92W HCM-causing founder mutation was previously shown to segregate with the disease in pedigree 137 (Moolman et al., 1997; Moolman-Smook et al., 1999), with the proband being a compound heterozygote for the *TNNT2* R92W HCM-causing and the *MYBPC3* g4177a putative HCM-causing splicing mutations. In the light of these findings, it was impossible to show segregation between the *MYBPC3* g4177a putative HCM-causing splicing mutation and HCM in this pedigree. The finding that the g4177a SNS was not detected in a control panel consisting of 107 individuals of mixed ancestry is, however, suggestive that g4177a may be a disease-causing mutation in its own right. Additional support that g4177a may be an HCM-causing mutation comes from the studies by Erdmann et al., (2001) and Carrier et al., (1997) who have shown that two distinct splicing mutations occurring in intron 7 of *MYBPC3*, both resulting in the skipping of exon 8, cause HCM. Both these mutations would result in the generation of truncated cMyBPC that would be only marginally longer than that caused by the g4177a putative HCM-causing splicing mutation (218 amino acid residues, compared to 168 amino acid residues). In the light of these findings, it seems likely that g4177a is an HCM-causing mutation, rather than a naturally occurring polymorphism.

Due to the fact that only the proband in pedigree 137, a compound heterozygote, carries g4177a, it is impossible to assign a phenotype to this putative HCM-causing mutation. It is, however, intriguing to note that, notwithstanding the high incidence of SCD in individuals in this family (figure III.36), which is generally a feature of the *TNNT2* R92W HCM-causing mutation (Moolman et al., 1997; Moolman-Smook et al., 1999), the proband who carries both this mutation and the *MYBPC3* g4177a putative splicing mutation, has escaped SCD till the age of 49 years. It can, therefore, be speculated

that in a *TNNT2* R92W background, the *MYBPC3* g4177a splicing mutation does not convey an increased risk of SCD, and may in fact reduce the risk of SCD.

#### **IV.1.2.3. Intron 6 SbP +1 g>a putative HCM-causing splicing mutation in *MYBPC3***

The c4154t SNS, occurring 1bp downstream of the intron 6 SbP, was identified in two probands in the HCM-affected panel, who were both of mixed ancestry (section III.1.3.3 and figure III.32). Computational analysis, performed by Dr Peter Rogan (University of Missouri-Kansas City School of Medicine, Kansas City, Missouri, USA), revealed that this SNS slightly weakens the exon 7 SaS, and even though it was predicted to be unlikely, the possibility that it might inactivate the exon 7 SaS, resulting in the skipping of exon 7, could not be excluded (personal communication, Dr Peter Rogan, 23 December 1999). RT-PCR analysis, however, revealed that this SNS did not affect the splicing of the *MYBPC3* transcript (section III.1.3.3 and figure III.33) and was, therefore, likely to be a polymorphism, rather than an HCM-causing mutation, and was, therefore, not pursued further.



#### **IV.1.3. PUTATIVE HCM-CAUSING FRAME-SHIFT MUTATION IN *MYBPC3***

##### **IV.1.3.1. $\Delta$ c 13255 Frame-shift putative HCM-causing mutation**

The  $\Delta$ c13255 frame-shift putative HCM-causing mutation was identified in one individual of mixed ancestry in the HCM-affected panel. As this putative HCM-causing mutation was not identified in 100 control individuals of mixed ancestry, it was postulated that  $\Delta$ c13255 was likely to be an HCM-causing mutation. This mutation results in a frame-shift after amino acid residue 754 in the C5

domain of cMyBPC and is predicted to result in the addition of 65 novel amino acids, prior to the generation of a stop codon and the truncation of the protein (figure IV.2).

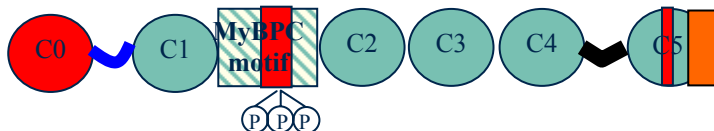


**Figure IV.2. Structure of the truncated cMyBPC protein predicted to be created by the  $\Delta c13255$  frame-shift putative HCM-causing mutation**

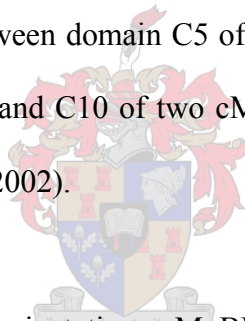
Circles = immunoglobulin C2 domains;  = MyBPC motif;  = interdomain linker;  = PA-region;  = novel amino acids;  = PKA and MyBPC-associated kinase phosphorylation sites; red areas = cardiac-specific regions.

As this mutation was only detected in only one individual, whose family could not be traced, it was impossible to establish whether this mutation segregated with HCM within a family setting, nor was it possible to accurately establish the phenotype associated with this mutation. On the basis that several other previously described mutations also result in the generation of truncated cMyBPC in which a similar portion of cMyBPC is truncated (partial C5 through to C10) (table I.6; Niimura et al., 1998; Richard et al., 2003), combined with the fact that  $\Delta c13255$  was not found in a matched control panel,  $\Delta c13255$  was described as an HCM-causing mutation (Moolman-Smook et al., 1999).

## IV.2. PROPOSED MODEL OF cMyBPC QUATERNARY STRUCTURE

The discovery of an interaction between the C5 and C8 domains of cMyBPC, by Dr Hanlie Moolman-Smook from our laboratory, indicated that cMyBPC was able to dimerise. This finding was in agreement with findings that MyBPC molecules are able to dimerise and possibly to form higher aggregates (Offer et al., 1973; Hartzell and Sale, 1985; Welikson and Fischman, 2002). Additionally, the finding that cMyBPC molecules purify as v-shaped particles with arm lengths of

about 22.1nm ( $\pm 4.5$ nm) (Hartzell and Sale, 1985), suggests that the hinge in the v-shape is likely to be located in the interdomain linker region separating the C4 and C5 domains of cMyBPC (Okagaki et al., 1993; <http://smart.embl-heidelberg.de/smart/>). As both domains C5 and C8 are located on the same (C-terminal) arm of the v-shape, it was considered likely that the interaction between the C5 and C8 domains of cMyBPC would be inter-, rather than intra-molecular (Moolman-Smook et al., 2002). If indeed the C5:C8 interaction is inter-molecular, it was considered that cMyBPC molecules would be able to interact in either a parallel, or antiparallel orientation. In an antiparallel arrangement, it would be possible that domains C5 and C8 of one cMyBPC molecule would interact with domains C8 and C5 of another cMyBPC molecule. In this orientation, domain C7 of one cMyBPC molecule would be juxtapositioned with domain C6 of another (figure IV.3a). In a parallel orientation, however, an interaction between domain C5 of one cMyBPC molecule with domain C8 of another would result in domains C7 and C10 of two cMyBPC molecules being juxtapositioned (figure IV.3b) (Moolman-Smook et al., 2002).



In order to establish in which of these orientations cMyBPC molecules dimerise, domains C6 and C10 were considered candidate ligands of the C7 domain of cMyBPC. Candidate-ligand Y2H-assays revealed the presence of a specific interaction between the C7 and C10 domains of cMyBPC, while domain C7 was unable to interact with domain C6 (section III.3.4.1 and figure III.41) (Moolman-Smook et al., 2002). The existence of an interaction between these domains of cMyBPC is supported by the findings of Welikson and Fischman (2002), who have shown that C7-C10 MyBPC fragments, transfected into COS cells, were able to aggregate, while C8-C10 fragments did not. Additionally, this interaction may also explain why the C7 domain of cMyBPC is essential for correct C-zone incorporation of cMyBPC into the sarcomere (Gilbert et al., 1996; Gilbert et al., 1999). The presence

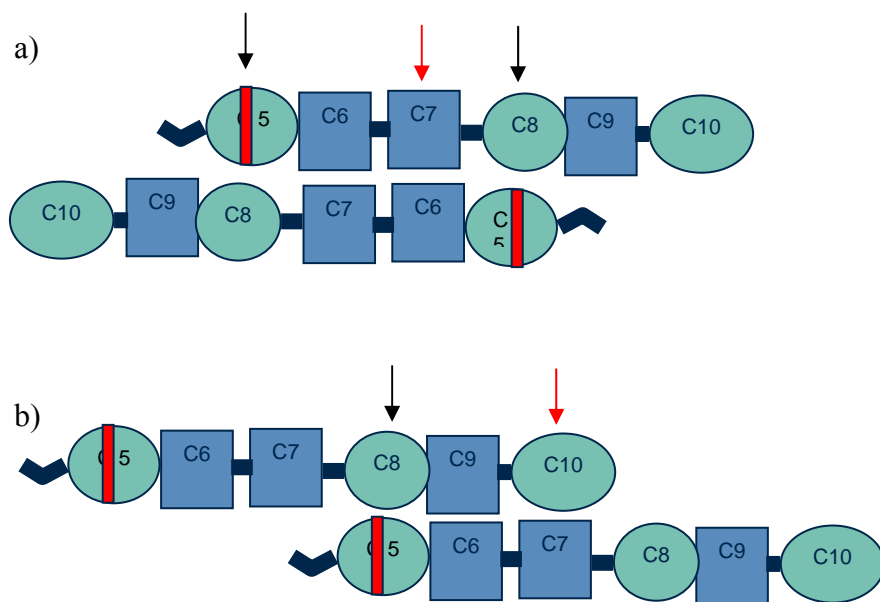


**Figure IV.3. C5:C8 mediated dimerisation of cMyBPC molecules in an antiparallel and parallel fashion**

a) cMyBPC molecules dimerising in an antiparallel orientation, stabilised by interactions between domains C5 and C8; b) cMyBPC molecules dimerising in a parallel orientation, stabilised by interactions between domains C5 and C8; ↓ = positions of interactions between C5 and C8 domains; ■ = interdomain linkers; boxes = fibronectin type 3 domains; ovals = immunoglobulin C2 domains; ↓ = positions of C7 domains, indicating the juxtapositioning of these domains with the C6 and C10 domains when cMyBPC molecules dimerise in the antiparallel and parallel orientations, respectively; red area = cardiac-specific insertion in the C5 domain. In the interest of clarity, only the six C-terminal domains of cMyBPC, constituting the one “arm of the v-shape” of cMyBPC, are shown.

of an interaction between the C7 and C10 domains of cMyBPC was subsequently confirmed in co-immunoprecipitation (CoIP) analyses (personal communication Dr Hanlie Moolman-Smook, 12 September 2003).

The identification of this interaction indicates that cMyBPC molecules are likely to dimerise in a parallel, rather than an antiparallel, orientation, with interactions between domains C5 and C7 of one cMyBPC molecule interacting with domains C8 and C10 of another (Moolman-Smook et al., 2002). Together, this data was used to develop a novel model of cMyBPC quaternary structure (Moolman-Smook et al., 2002). In this model, cMyBPC homo-trimerises to form a “tight collar” around the thick filament backbone, with domains C5-C7 of one cMyBPC molecule overlapping with domains

C8-C10 of the following cMyBPC molecule (figure IV.4) (Moolman-Smook et al., 2002). It was postulated that this trimeric “tight collar” structure would be stabilised by the interaction between domains C5 and C8, as well as between domains C7 and C10 (figure IV.4) (Moolman-Smook et al., 2003).

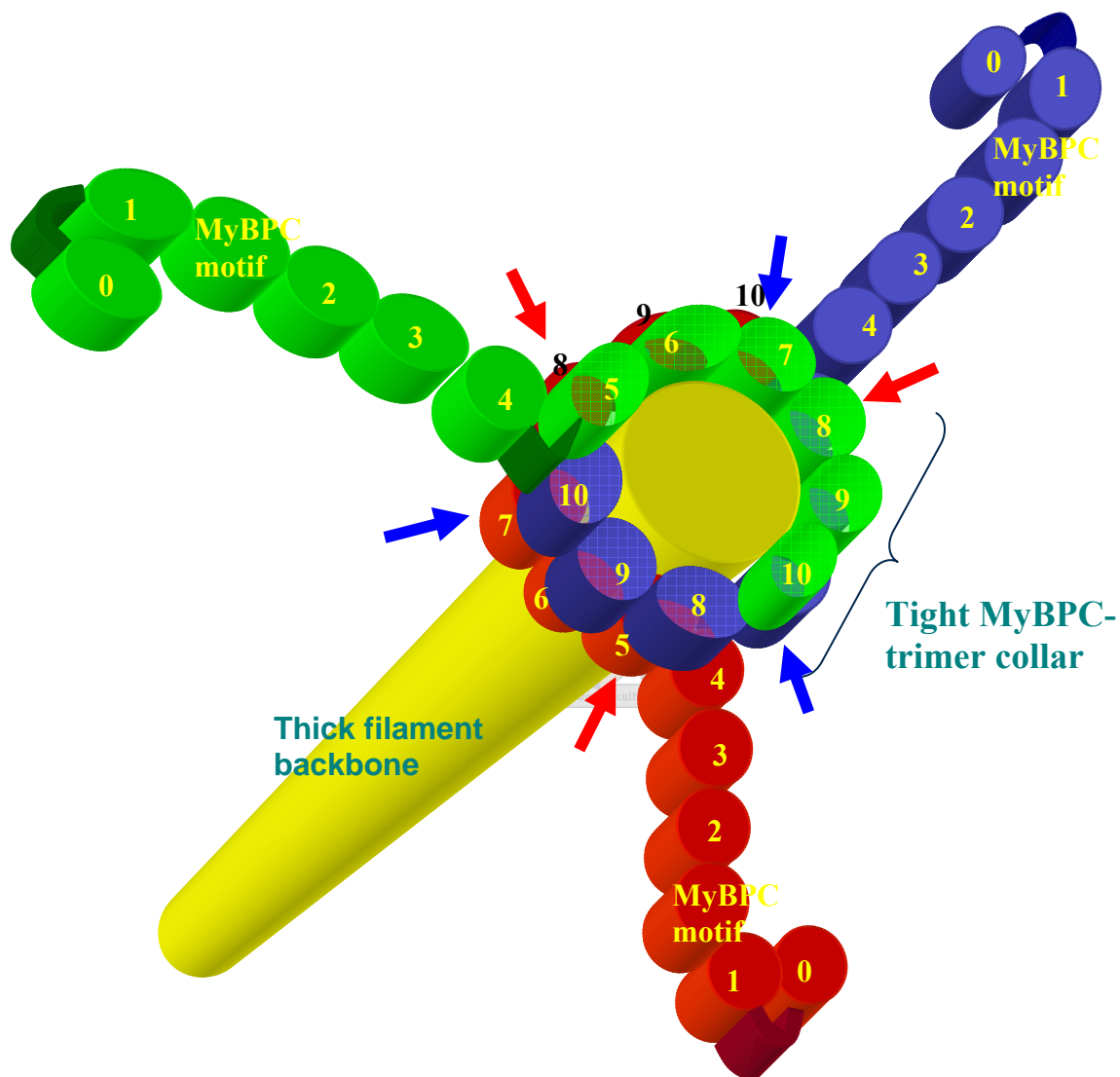


**Figure IV.4 Proposed model of cMyBPC quaternary structure**

Blue arrows = positions of interactions between C7 and C10 domains of two consecutive cMyBPC molecules; blue, green and red molecules = three consecutive cMyBPC molecules trimerised to form a “tight collar” around the thick filament backbone; red arrows = positions of interactions between C5 and C8 domains of two consecutive cMyBPC molecules; yellow cylinder = thick filament backbone (consisting of light meromyosin and titin molecules) (from Moolman-Smook et al., 2002).

In addition to this model being in agreement with the position of the bend in cMyBPC molecules and the finding that MyBPC molecules are able to dimerise or form higher aggregates, as stated previously, this model is also supported by the findings of several other studies. Firstly, MyBPC is located on the surface of the thick filament backbone, as was shown by immunochemical studies (Offer et al., 1973). Secondly, the trimeric structure of MyBPC is in agreement with findings that two to four (most likely three) MyBPC molecules are found at each 43nm period in the sarcomeric C-zone (Offer et al., 1973; Morimoto and Harrington, 1974; Bennett et al., 1986). Thirdly, previous studies have shown the axial extent of MyBPC on the thick filament backbone to be about 7nm (Craig and Offer, 1976), which is roughly the width of two IgC2 or Fn3 domains lying side-by side (Nave et al., 1989; Labeit et al., 1992; Soteriou et al., 1993; Vinkemeier et al., 1993), which is in agreement with the double layered cMyBPC collar proposed by Moolman-Smook et al., (2002).

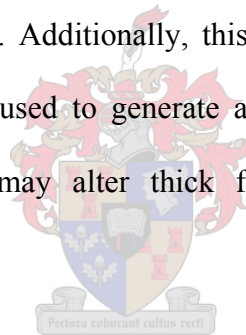


Additionally, in the model proposed by Moolman-Smook et al., (2002), domains C5-C10 of cMyBPC are associated with the thick filament backbone, while domains C0-C4 extend into the interfilament space, with a bend in the molecule occurring between domains C4 and C5. This arrangement is supported by the findings that the C-terminal domains of MyBPC bind to LMM and titin in the thick filament backbone (Okagaki et al., 1993; Freiburg and Gautel, 1996; Welikson and Fischman, 2002), while the N-terminal portion of MyBPC extends away from the thick filament backbone, allowing it to interact with myosin S2 and possibly actin (Hartzell and Sale, 1985; Gruen and Gautel, 1999; Gruen et al., 1999; Kunst et al., 2000; Kulikovskaya et al., 2003; Squire et al., 2003).

This model also for the first time, assigns a function to the C7 domain of cMyBPC. Previous studies have shown that the C7-C10 region of cMyBPC was necessary for correct A-band incorporation of

cMyBPC into the sarcomere, indicating that the C7 domain is of specific functional significance (section I.7.3.3) (Gilbert et al., 1996; Gilbert et al., 1999). In the model of cMyBPC quaternary structure proposed by Moolman-Smook et al., (2002), the C7 to C10 region of cMyBPC would be the minimal C-terminal portion of the protein required to form a collar around the thick filament backbone (figure IV.4).

One shortcoming of the model proposed by Moolman-Smook et al., (2002) is, however, that it did not take into account the quaternary structure of the thick filament backbone, that is in all likelihood not a simple cylindrical structure as portrayed in figure IV.4. In section IV.3, the currently accepted model of thick filament backbone structure will be discussed and the cMyBPC “tight collar” arrangement integrated into this model. Additionally, this integrated model of thick filament and cMyBPC quaternary structure will be used to generate a hypothesis of the mechanisms through which phosphorylation of cMyBPC may alter thick filament structure and regulate cardiac contractility (section IV.3).



#### **IV.2.1. cMyBPC DOMAIN C7 LIBRARY-ASSAY**

In order to confirm the presence of an interaction between the C7 and C10 domains of cMyBPC, as well as to establish whether the C7 domain interact with any other ligands, domain C7 of cMyBPC was used as bait in a Y2H library assay. In this assay, the MATCHMAKER GAL4 Two-Hybrid System 3 (BD Biosciences, Clontech, Palo Alto, CA, USA) was used to screen a pre-transformed cardiac cDNA library. This assay allowed the identification of human cytochrome c oxidase (subunits I [four independent clones], II [one clone] and III [one clone]), human ATP synthase (H<sup>+</sup> transporting, mitochondrial F1 complex, alpha subunit, isoform 1 [one clone] and the F0 subunit

[one clone]), NADH dehydrogenase (subunits 1 [four independent clones] and 2 [one clone]), human quinolinate phosphorybosyltransferase (one clone), human  $\alpha 2(I)$  collagen (one clone), human phosphoglucomutase 1 (one clone), human myomesin 2 (M-protein) (one clone), human titin (three independent clones) and human cMyBPC (one clone) as putative ligands of the C7 domain of cMyBPC (section III.3.2.4 and table III.15).

Cytochrome c oxidase (subunits I, II and III), ATP synthase ( $H^+$  transporting, mitochondrial F1 complex, alpha subunit, isoform 1 and the F0 subunit), NADH dehydrogenase (subunits 1 and 2) and quinolinate phosphorybosyltransferase were not considered plausible ligands of cMyBPC, based on their localisation in the mitochondrion. Similarly, based on its extracellular localisation,  $\alpha 2(I)$  collagen was not considered a plausible ligand of the C7 domain of cMyBPC. Additionally, as phosphoglucomutase 1 has not been localised specifically to the sarcomeric A-band, interaction between this protein and the C7 domain of cMyBPC was not considered to be of specific significance to this study, but may require further investigation in future studies (table III.15). Notwithstanding its sarcomeric localisation, M-protein was also not considered to be a plausible ligand of the C7 domain of cMyBPC for several reasons. Firstly, the interaction between domain C7 and M-protein was found to be non-specific in interaction-specificity tests (table III.13). Secondly, similar spurious interactions between M-protein peptides and other regions of cMyBPC (the C5 domain and C1C2 region of cMyBPC) were previously detected in Y2H library-assays (personal communication Dr Hanlie Moolman-Smook). Finally, as M-protein is localised in the sarcomeric M-line, while cMyBPC is found in the C-zone, an interaction between these proteins was deemed highly unlikely.

The cMyBPC clone identified as a putative ligand of the C7 domain of cMyBPC encoded only the C-terminal 39 amino acids of cMyBPC (sections III.3.2.4 and table III.15), constituting a partial C10 domain. Interaction specificity tests showed that the interaction between domain C7 and this partial C10 peptide was indeed specific (table III.15). In order to gain insight into the specific region of the C10 domain of cMyBPC involved in the interaction with the C7 domain, the relative positions of the C-terminal 39 amino acids of this domain, shown to interact with domain C7 (sections III.3.2.4, IV.2 and table III.13), were mapped to the three-dimensional structure of telokin (chain A) (three-dimensional model of an IgC2 domain) (figure IV.21). This analysis revealed that the C-terminal 39 amino acids of cMyBPC constituted  $\beta$ -strands E, F and G of the C10 domain of cMyBPC. In complete IgC2 domains,  $\beta$ -strands A, B, D and E form a four-stranded  $\beta$ -sheet (ABDE), while  $\beta$ -strands C, F and G form a three-stranded  $\beta$ -sheet (CFG), with each of these two  $\beta$ -sheets forming a distinct ligand-binding surface. These two  $\beta$ -sheets associate to form a  $\beta$ -sandwich (Idowu et al., 2003; <http://pfam.wustl.edu/>). It is postulated that in the 39 amino acid C10 peptide,  $\beta$ -strands F and G may form a partial  $\beta$ -sheet, the tertiary structure of which is stabilised by the presence of  $\beta$ -strand E (figure IV.3). In the light of this finding, it is likely that the C7 binding-site is located on the three-stranded (CFG), rather than the four-stranded (ABDE),  $\beta$ -sheet of the C10 domain of cMyBPC.

Additionally, the interaction between domain C7 of cMyBPC and putative interactor clones encoding titin was also found to be specific in interaction specificity tests (section III.3.2.4 and table III.15). In the light of this finding, combined with the sarcomeric localisation of titin, Y2H candidate-ligand assays were used to further investigate the possibility of an interaction between domain C7 of cMyBPC and titin (section IV.2.2).

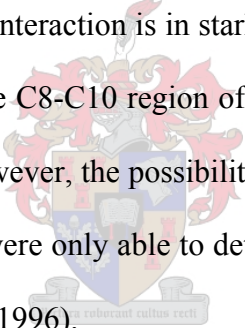
#### **IV.2.2. IDENTIFICATION OF A SPECIFIC INTERACTION BETWEEN THE C7 DOMAIN OF cMyBPC AND C-ZONE TITIN**

Three of the interactor clones identified in the C7 Y2H library-assay encoded portions of the C-terminal region of titin, which varied in size from 35 to 595 amino acids in length (sections III.3.2.4, IV.2 and table III.15). As the region of titin encoded by these clones would be embedded in the M-line in the intact sarcomere, while cMyBPC is found in the C-zone, the region encoded by these clones was not considered to be a plausible ligand of cMyBPC (section III.3.2.4 and table III.15). BLAST-P and multiple sequence alignment analyses, however, revealed that the minimal titin clone identified as interacting with domain C7 (a 35 amino acid peptide encoding the partial M10 IgC2 domain of titin) (sections III.3.2.4, IV.2 and table III.15), shared highest homology with the first IgC2 domain of each of the eleven-domain super-repeats constituting C-zone titin (sections I.6.3.2, III.3.3; figures I.9, III.39, III.40 and table III.16). These domains shared between 26% and 49% amino acid sequence identity with the 35 amino acid C-terminal titin peptide, while the sequence similarity varied between 69% and 86% (table III.16 and figure III.40). This is considerably higher than the average sequence identity and sequence similarity shared by IgC2 domains of the intracellular immunoglobulin superfamily, which was estimated to be about 20-30% and 40-45%, respectively (Politou et al., 1994; Vinkemeier et al., 1993). Based on this finding, the first IgC2 domain of each of the eleven-domain super-repeats, previously shown to interact with the C-terminal region of cMyBPC (Freiburg and Gautel, 1996), were considered plausible ligands of the C7 domain of cMyBPC.

As C-zone titin was not expected to be represented in the cardiac cDNA library that was screened, due to the gigantic size of the titin transcript (>27kb) (section II.16.2.1), Y2H candidate-ligand

assays were performed to test whether the C7 domain of cMyBPC did indeed interact with these IgC2 domains of C-zone titin. In these assays, the first IgC2 domain of the first and the seventh eleven-domain super-repeat of A-band titin (domains A43 and A109 of titin) were used as candidate preys in Y2H candidate-ligand assays (figure III.39). These assays clearly showed that domain C7 of cMyBPC interacts specifically with these two domains, while it did not interact with either the second or the third IgC2 domain of the seventh eleven-domain super-repeat (domains A112 and A116, respectively) (section III.3.4.2; figures III.39 and III.42). The interaction between domain C7 of cMyBPC and the A43 and A109 IgC2 domains of C-zone titin was subsequently confirmed by CoIP analysis (personal communication Dr Hanlie Moolman-Smook, 12 September 2003).

At first glance, the identification of this interaction is in stark contrast to the findings of Freiburg and Gautel (1996), who showed that only the C8-C10 region of cMyBPC interacted with titin. From the study of Freiburg and Gautel (1996), however, the possibility of a secondary titin binding-site cannot be excluded, as the methods employed were only able to detect relatively strong interactions in an *in vitro* environment (Freiburg and Gautel, 1996).

A faint watermark of a university crest is visible in the center of the page. The crest features a shield with various symbols, topped by a crown and surrounded by decorative flourishes. Below the shield is a banner with the Latin motto "a roborant cultus recti".

### **IV.3. QUATERNARY STRUCTURE OF THE A-BAND THICK FILAMENT BACKBONE**

One shortcoming of the model of cMyBPC quaternary structure proposed by Moolman-Smook et al., (2002) is that it did not address the quaternary structure of the A-band thick filament backbone, of which it forms part. Furthermore, as it has been shown that PKA-mediated phosphorylation of cMyBPC results in an expansion of the thick filament backbone in  $\alpha$ MHC-containing thick filaments (Weisberg and Winegrad, 1996; Weisberg and Winegrad, 1998; Levine et al., 2001), the dimensions of the model of cMyBPC quaternary structure proposed by Moolman-Smook et al., (2002) would only be applicable when cMyBPC is either un- or mono-phosphorylated (“disordered” and “tight” thick filament structures) (section I.7.6). As an adjunct to the present study it was undertaken to incorporate the model of cMyBPC quaternary structure proposed by Moolman-Smook et al., (2002) into the quaternary structure of the thick filament backbone. Additionally, data generated in the present study was used to devise a novel model of thick filament quaternary structure following PKA-mediated phosphorylation of cMyBPC (“loose” thick filament structure). In order to allow the generation of these models, data regarding the quaternary structure of the A-band thick filament backbone, consisting of LMM, titin and cMyBPC, had to be considered.

### **IV.3.1. QUATERNARY STRUCTURE OF THE “DISORDERED”/”TIGHT” A-BAND THICK FILAMENT BACKBONE**

#### **IV.3.1.1. LMM thick filament backbone structure**

The thick filament is composed mainly of three elements, namely, myosin molecules (each consisting of two myosin heavy chain monomers, two MELCs and two MRLCs (Widnell, 1990) (figure I.22), titin and the MyBPs. Each myosin heavy chain monomer can be further subdivided into the LMM portion, also referred to as the myosin rod section, and the HMM portion, which can be further subdivided into an S1 (also referred to as the myosin head) and S2 subfragments (figure I.19) (Widnell and Pfenninger, 1990). The thick filament backbone consists mainly of LMM, while HMM extends away from the thick filament backbone, where it is arranged in a three-stranded 9/1 helix of pitch  $9 \times 14.3\text{nm}$  and a repeat of  $3 \times 14.3\text{nm}$ , with the two heads of one myosin molecule on each lattice site on the helix (figure IV.5) (reviewed by Chew and Squire, 1995). As LMM is the major component of the thick filament backbone, as opposed to HMM which forms the crossbridges that extend from the backbone towards the thin filament (figure I.22) (Widnell and Pfenninger, 1990), only the structure of LMM will be discussed in detail in this section.

Each LMM monomer consists entirely of an  $\alpha$ -helix, and dimerises with another LMM monomer through the formation of a coiled-coil (figures I.22 and IV.5) (Knight, 1996). The way in which these LMM dimers associate to form the thick filament backbone has, however, remained a contentious issue and several models for the arrangement of LMM within the thick filament backbone have been proposed (Squire, 1973; Squire, 1979; Stewart et al., 1981; reviewed by Chew and Squire, 1995). Subsequent measurements of the fish skeletal muscle A-band thick filament backbone (outer radius,

including MyBPs and titin, = 6.5-7.5nm; hollow inner core radius = 1.5-2nm; radial packing thickness = 4-5nm) made by Squire et al., (1998) have, however, excluded most of these models and favour the curved crystalline layer model proposed by Squire (1973). This model predicted that the thick filament backbone (composed of only LMM) has an outer radius of ~7nm, a hollow inner core of ~1.5-2nm, with the LMM dimers separated by ~0.2nm, and aligned nearly parallel to the long axis of the thick filament (figure IV.5) (Squire, 1973; Chew and Squire, 1995; Squire et al., 1998).

The curved crystalline layer model (Squire, 1973) is compatible with the empiric measurements of the thick filament backbone and also allows for the arrangement of crossbridges in a three-stranded 9/1 helix conformation (Chew and Squire, 1995, Squire et al., 1998). A shortcoming of this model is, however, that it only accounts for the positioning of LMM within the thick filament backbone, and does not take accessory proteins into account. Furthermore, the dimensions predicted by this model for a thick filament backbone composed entirely of LMM is greater than that of the measured values of the A-band fish skeletal muscle thick filament backbone that include the accessory proteins (Squire et al., 1998). It should, therefore, be considered that the dimensions predicted by the curved crystalline layer model may not be absolutely accurate.

The following sections describe how previously reported data, as well as data generated in the present study regarding the structure, position and interaction of titin and cMyBPC, were used to obtain an integrated model of the A-band thick filament backbone quaternary structure that takes into account the three main components of the thick filament backbone: LMM, titin and MyBPC.

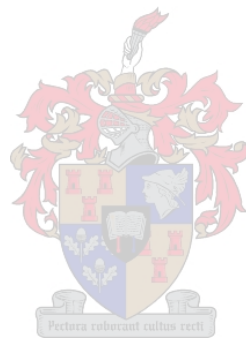
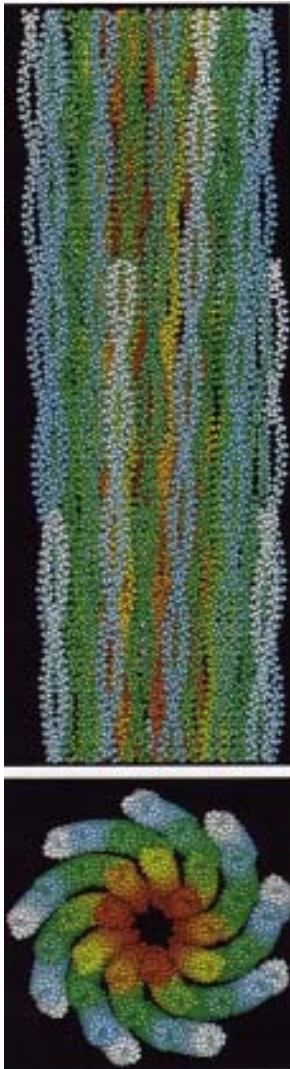


**Figure IV.5. Colour representation of a 42.9nm segment of the curved crystalline layer model of a vertebrate striated myosin muscle filament**

*The top and bottom panels show stereo pairs of the structure viewed from the axial and transverse directions, respectively. The colour codes indicate the relative positions of the amino acids along the sequence with increasing distance from the C-terminus indicated by red, yellow, green, blue, and finally white where the myosin heads originate (Chew and Squire, 1995).*

#### **IV.3.1.2. Incorporation of A-band titin into the curved crystalline layer model of the thick filament backbone**

Liversage et al., (2001) proposed a model in which six titin molecules are found in each half-sarcomere, with A-band titin being in a dimeric form (section I.6.3). These titin dimers are located on the surface of the thick filament (Furst et al., 1988; Labeit et al., 1992; Jin, 1995; Labeit and Kolmerer, 1995) where they are constitutively bound to LMM (section I.6.3) (Furst et al., 1988; Labeit et al., 1992), and are arranged parallel to the long axis of the thick filament (Squire et al., 1998; Liversage et al., 2001).

As the arrangement of LMM within the thick filament backbone, according to the curved crystalline layer model, results in the formation of nine major surface grooves (Squire, 1973; Chew and Squire, 1995, Squire et al., 1998), it was considered likely that the titin dimers would be partially imbedded in three of these surface grooves (figures IV.5 and IV.6). Even though these surface grooves do not run absolutely parallel to the axis of the thick filament, they are arranged in an open-angled zigzag pattern on the surface of the thick filament (figure IV.5) (Chew and Squire, 1995, Squire et al., 1998). It is possible that titin may be found in these surface grooves, thus allowing the overall orientation of titin to be parallel to the long axis of the thick filament, as proposed by Liversage et al., (2001) (figure IV.6a).

In order to establish the contribution made by these titin dimers to the total diameter of the thick filament backbone, as well as to establish an accurate diameter for this structure

in the absence of titin dimers, the curved crystalline model of the myosin backbone was used as a basis for producing detailed scale drawings of the A-band thick filament backbone in the presence of titin dimers (figure IV.6). In the construction of these scale drawings, several assumptions were made. Aside from assuming that LMM dimers are arranged in the thick filament backbone according to the curved crystalline layer model proposed by Squire (1973), it was assumed that A-band titin is found in the dimeric form and is aligned parallel to the long axis of the thick filament (Liversage et al., 2001), and, finally, that the IgC2 and Fn3 domains, constituting A-band titin, have a diameter of about 2.5nm (Nave et al., 1989; Labeit et al., 1992; Soteriou et al., 1993; Vinkemeier et al., 1993).

Thus, three titin dimers were positioned in three of the surface grooves in the LMM thick filament backbone, with the diameter of the titin representations determined relative to the scale of an LMM dimer in the curved crystalline layer model. Thereafter, the scale of these drawings was reset with the outer diameter of the thick filament backbone, containing titin dimers, fixed at 13.0nm and this scale used for subsequent calculations in the present study (figure IV.6a). This value of 13nm was derived from the measurements of the native fish skeletal muscle A-band thick filament backbone, made by Squire et al., (1998) as being between 13 and 15nm. These empirically derived measurements were specifically chosen because they were corrected for the thickness of the metal coat used in electron microscopy studies, and also included the contribution made by the accessory thick filament proteins, titin and MyBPC. Specifically, the minimal value of 13nm was

chosen as titin would be expected to be present, and contribute to the diameter of the thick filament backbone, throughout the A-band, while MyBPC would only contribute to the diameter of the thick filament backbone at seven to nine specific locations, where it is present.

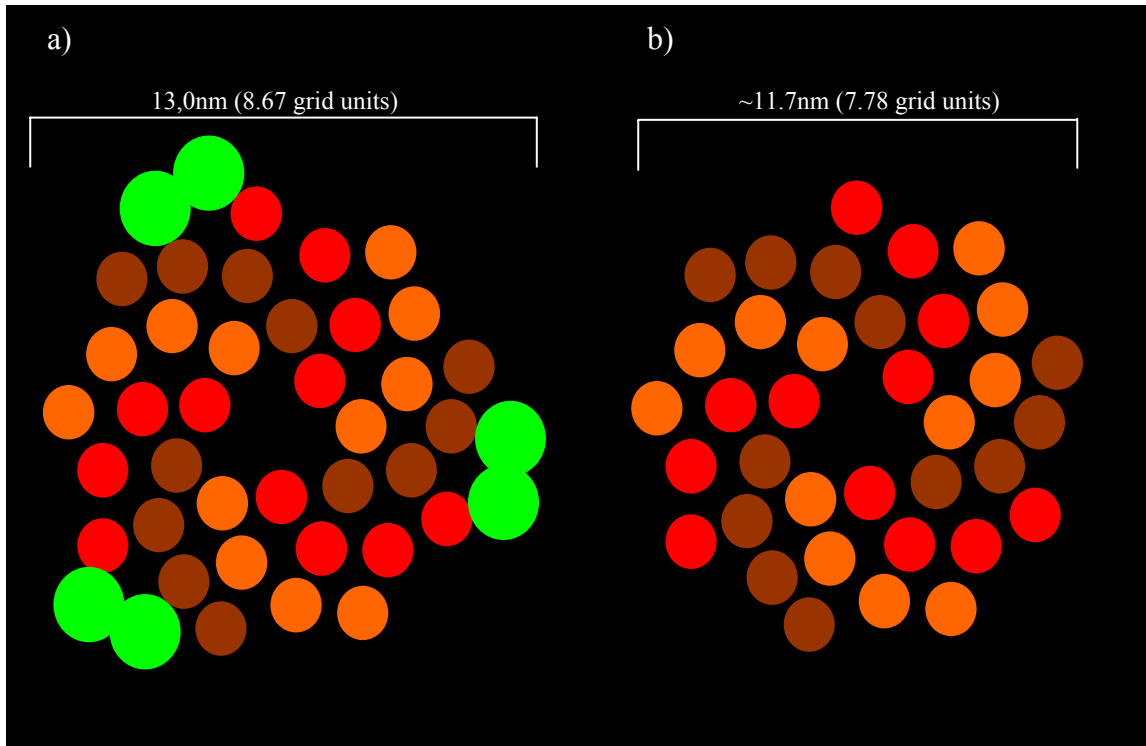


**Figure IV.6. Incorporation of A-band titin into the thick filament backbone**

Diagrammatic representation of transverse sections of the thick filament backbone, showing the arrangement of LMM and titin dimers within the thick filament backbone that was drawn to scale. a) Arrangement of LMM in the thick filament backbone according to the curved crystalline layer model, also showing the proposed position of titin dimers within the surface grooves; b) arrangement of only LMM in the thick filament backbone according to the curved crystalline layer model. ●; ●; ● = LMM dimers from different layers; ● = titin molecules (modified from Chew and Squire, 1995).

From the grid of these scale drawings, it was then possible to deduce the specific diameter of the thick filament in the absence of “accessory proteins,” which was estimated at being ~11.7nm (figure IV.6b). This value is slightly less than, but reconcilable with, the diameter of LMM thick filaments, according to the curved crystalline layer model proposed by Squire (1973).

#### **IV.3.1.3. Incorporation of cMyBPC into the curved crystalline model of the thick filament backbone**

Following the incorporation of titin dimers into the curved crystalline model of A-band thick filament quaternary structure, the quaternary structure, position and interactions of cMyBPC at its seven to nine specific positions within the A-band was considered. Several features of cMyBPC had to be taken into account, to achieve this. Firstly, the C10 domain of cMyBPC interacts with more than one LMM molecule (Okagaki et al., 1993; Miyamoto et al., 1999; Welikson and Fischman, 2002), and it has been proposed that this domain of cMyBPC is partially imbedded in a surface groove of the thick filament backbone (Chew and Squire, 1995; Miyamoto et al., 1999). The specific orientation of the C10 domain in a surface groove as proposed by Miyamoto et al., (1999) (figure I.18) was, however, not considered essential, as this arrangement requires a deep groove on the surface of the thick filament formed by four LMM dimers (figure I.18), a feature absent from the curved crystalline layer model of Squire (1973) (figure IV.5), on which it was reportedly based. The data presented by Miyamoto et al., (1999) and Welikson and Fischman (2002), however, provide compelling evidence that the C10 domain interacts with more than one LMM dimer, thereby crosslinking LMM dimers. It was, therefore, considered essential that the C10 domain should be able to interact with at least two LMM dimers, preferably from two different layers of the curved crystalline layer model.

Secondly, the C9 and/or C10 domain(s) of cMyBPC is/are known to interact with C-zone titin (Labeit et al., 1992; Labeit and Kolmerer, 1995; Freiburg and Gautel, 1996). Additionally, the dimensions of the thick filament backbone, including the “accessory proteins” titin and MyBPC, as measured by Squire et al., (1998), as well as the dimensions of cMyBPC (Hartzell and Sale, 1985) and individual IgC2, Fn3 domains, and the positions of interdomain linkers in cMyBPC (Nave et al., 1989; Labeit et al., 1992; Okagaki et al., 1993; Soteriou et al., 1993; Vinkemeier et al., 1993), had to be taken into account.

Based on the interactions between the C5 and C8 and between the C7 and C10 domains of cMyBPC (Moolman-Smook et al., 2002), and the rationale supporting the collar model of cMyBPC quaternary structure (section IV.2) (Moolman-Smook et al., 2002), this model was assumed to be essentially correct. The basis of this model, *viz.*, three cMyBPC molecules trimerising and forming a “tight collar” around the thick filament backbone, with overlap between the C5-C7 domains of one cMyBPC molecule with domains C8-C10 of another, was, therefore, kept. Moreover, based on the interaction between the C7 domain of cMyBPC and C-zone titin identified in this study (sections III.3.2.4, III.3.4.2 and IV.2.2), the C7 domain also had to be juxtapositioned with C-zone titin.

Thus, the trimeric tight cMyBPC collar (Moolman-Smook et al., 2002) was incorporated into the curved crystalline layer model (Squire, 1973; Chew and Squire, 1995; Squire et al., 1998) into which the postulated positions of titin dimers had been integrated (section IV.6.1.2 and figure IV.6). From these detailed scale drawings, it appeared that two arrangements of the cMyBPC trimeric “tight collar” were possible, both of which fulfill all the requirements stated above (figures IV.7a and IV.7b).

The major differences between these two arrangements are, firstly, that, in the arrangement proposed in figure IV.7a, both domains C9 and C10 of cMyBPC would be able to interact with titin, while in the arrangement proposed in figure IV.7b, the C9 domain of cMyBPC would not be able to interact with titin. Previously, Freiburg and Gautel (1996) have implicated the C9 and C10 domains of cMyBPC in the binding of titin. From the data presented by Freiburg and Gautel (1996) it is, however, unclear whether both of these domains are involved in this interaction, or whether the major titin binding-site may, in fact, be located entirely on the C10 domain. Secondly, in figure IV.7a, the interdomain linker between the C9 and C10 domains, as well as the interdomain linker between the C6 and C7 domains of cMyBPC (Okagaki et al., 1993; <http://smart.embl-heidelberg.de/smart/>), bridges the titin dimers in the major surface grooves. In the arrangement proposed in figure IV.7b, titin is bridged only by the interdomain linker between domains C7 and C8.

In order to establish which of these two cMyBPC arrangements is more likely, the respective lengths of these interdomain linkers were obtained from Genbank (<http://www.ncbi.nlm.nih.gov/entrez/>; sequence accession [NP\\_000247](http://www.ncbi.nlm.nih.gov/entrez/)) and analysed using SMART and Pfam protein sequence analysis software (available at: <http://smart.embl-heidelberg.de/smart/> and <http://www.sanger.ac.uk/Software/Pfam/>, respectively). The lengths of these interdomain linkers were found to be 15, 34 and 40 amino acid residues for the C6-C7, C7-C8 and C9-C10 linkers, respectively. The formula for calculating maximum chain length of peptides, used by Rief et al., (1997) and Tskhovrebova et al., (1997) to calculate the maximum chain length of extended IgC2 domains in I-band titin (section I.6.4.2.iv), was used to calculate the respective maximal chain lengths of these interdomain linker peptides in this study. The maximum chain lengths of the C6-C7,

C7-C8 and C9-C10 interdomain linkers are calculated to be 3.75, 8.5 and 10nm, respectively (a value of  $\sim 0.25$ nm per amino acid residue).

From the scale drawings of the curved crystalline layer model in which titin dimers were included (figure IV.6), it was estimated that the minimal linker length necessary to bridge titin dimers was about 2.8nm. It is, therefore, possible that any of these three interdomain linkers would be able to bridge titin dimers. The C6-C7 interdomain linker (15 amino acid residues) would, however, need to be extended to a length of close to its maximum chain length in order to do so, thus allowing for very little secondary structure of this linker, while the C7-C8 and C9-C10 linkers are of sufficient length to bridge titin, even if they took on a more compact secondary structure. Additionally, the interdomain linker separating the C7 and C8 domains, which spans the titin dimers in the arrangement depicted in figure 7b, was predicted to contain “regions of low compositional complexity”, while the other two linkers did not contain such regions. “Regions of low compositional complexity are regions of biased composition that are often mosaics of a small number of amino acids and have been shown to be functionally important in some proteins, but they are generally not very well understood” (data obtained from: <http://www.sanger.ac.uk/Software/Pfam/>).

Recently Idowu et al., (2003) showed that about ten amino acid residues, previously predicted to be part of the interdomain linker separating the C4 and C5 domains of cMyBPC, by SMART and Pfam protein sequence analysis software, actually formed part of the C5 domain of cMyBPC. The possibility that predicted interdomain linkers separating domains C6 and C7, as well as between C9 and C10, may also form part of the IgC2 and Fn3 domains by which they are flanked can, therefore, not be excluded. The finding that the interdomain linker between the C7 and C8 domains of

cMyBPC contains “regions of low compositional complexity,” however, suggests that this region would indeed be an interdomain linker, rather than forming part of either the C7 or C8 domain of cMyBPC.

Furthermore, the dimensions of the thick filament backbone, including both titin and cMyBPC, were deduced from these scale drawings (figure IV.7a and b) and compared to the maximal diameter of the A-band native fish skeletal muscle thick filament backbone of 15nm (Squire et al., 1998). This value of 15nm was specifically chosen based on the fact that cMyBPC would only be present at, and contribute to the diameter of thick filaments in, seven to nine specific positions in the C-zone. The deduced diameters of thick filaments, in which the cMyBPC “tight collar” was arranged in the two possible fashions, were 15.60 and 15.35nm for the arrangements depicted in figures IV.7a and IV.7b, respectively. As both these values are in good agreement with the maximal measured diameter of A-band native fish skeletal muscle thick filament of 15nm (Squire et al., 1998), neither of these arrangements could be excluded on this basis. The finding that the linker between the C6 and C7 domains of cMyBPC may be too short to bridge titin, combined with the finding that the dimensions obtained from the scale drawing of the conformation depicted in figure IV.7b is closer to the measured values of Squire et al., (1998), has led to the arrangement depicted in figure IV.7b being favoured by this author. Future candidate-ligand assays may help distinguish between the two models.

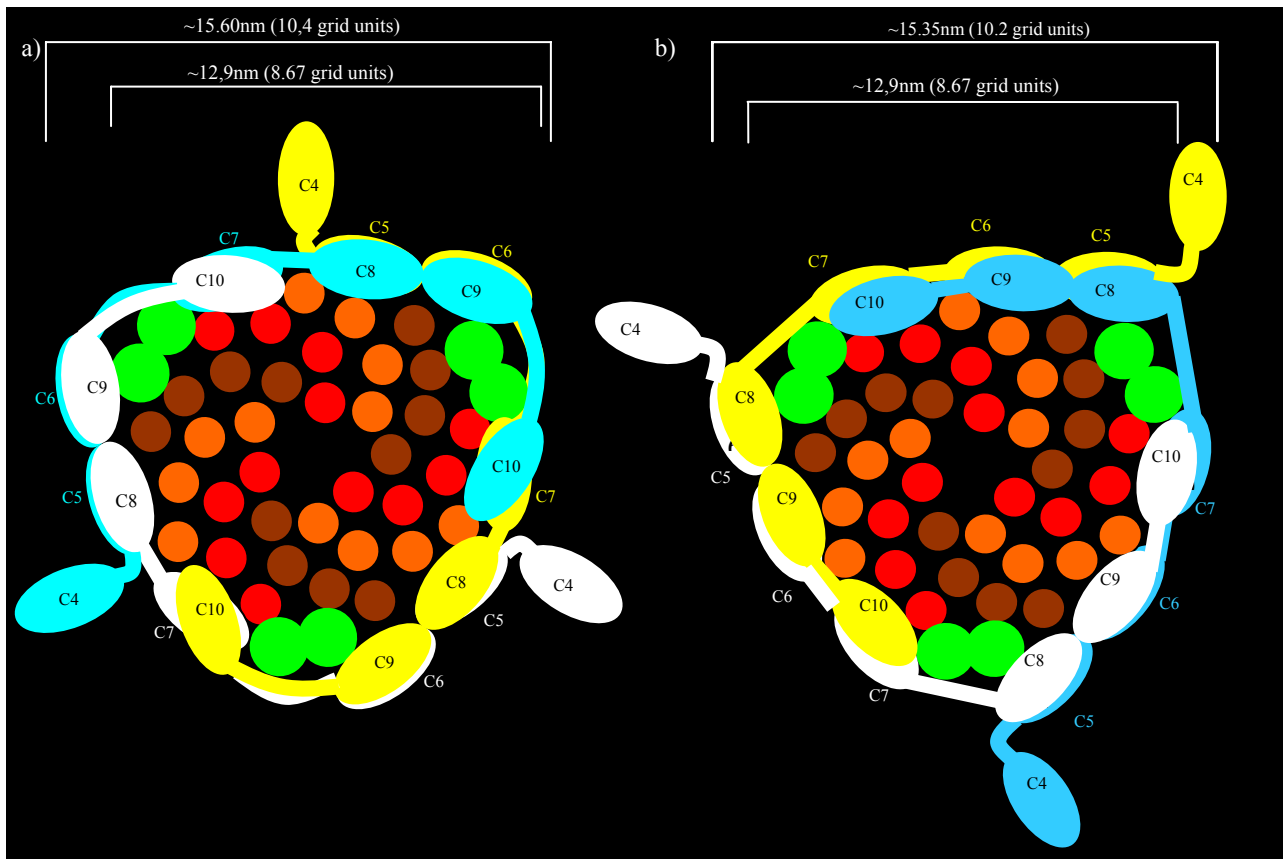


**Figure IV.7 Incorporation of cMyBPC into the thick filament backbone**

Diagrammatic representation of transverse sections of the thick filament backbone, showing the proposed arrangement of LMM and titin dimers, as well as cMyBPC molecules within the thick filament backbone, that was drawn to scale. Two possible arrangements of the cMyBPC trimeric “tight collar” are depicted in a) and b), respectively. ●; ○; ● molecules = three consecutive partial cMyBPC molecules trimerising to form a “tight collar” around the thick filament backbone; ●; ●; ● = LMM dimers from different layers; ● = titin molecules. The N-terminal regions of cMyBPC molecules (domains C0 to C3) are not indicated in the figure and are expected to extend into the interfilament space (modified from Chew and Squire, 1995).

### IV.3.2. EFFECT OF cMyBPC PHOSPHORYLATION ON THICK FILAMENT BACKBONE STRUCTURE

Several studies have shown that phosphorylation of cMyBPC results in an expansion in the thick filament diameter in  $\alpha$ MHC-containing thick filaments, which encompasses changes both in thick filament backbone and crossbridge structure (Weisberg and Winegrad, 1996; Weisberg and Winegrad, 1998; Levine et al., 2001). As discussed in sections I.7.6 and I.7.7, it is likely that this expansion in the thick filament backbone would be the result of cMyBPC being either di- or tri-phosphorylated by PKA, following  $\beta$ -adrenergic stimulation, thus giving rise to the “loose” thick filament structure (Gautel et al., 1995; Weisberg and Winegrad, 1996; Weisberg and Winegrad, 1998; Levine et al., 2001). The effect of this phosphorylation event on the quaternary structure of the A-band thick filament backbone has, however, not been studied in detail to date.

In particular, the studies of Weisberg and Winegrad (1996 and 1998) and Levine et al., (2001) merely measured the increase in total thick filament dimensions upon cMyBPC phosphorylation and did not consider how much of this increase in diameter was due to expansion of the thick filament backbone itself (figure IV.8 and box 2). Moreover, as the measurements made by Weisberg and Winegrad (1996 and 1998) and Levine et al., (2001) were not corrected for the thickness of the metal coat used in electron microscopy, absolute values of thick filament diameter could not be used directly in conjunction with Squire’s values.

The data from the Winegrad laboratory were, therefore, used in the present study to calculate the relative magnitude of thick filament backbone expansion, and this value added to the measurements of the A-band fish skeletal muscle thick filament backbone made by Squire et al., (1998). These calculations were done by, firstly, calculating the diameter of the A-band thick filament backbone by

subtracting the distance that the crossbridges extend into the interfilament space from the total diameter of the thick filaments in which cMyBPC was either unphosphorylated, or fully phosphorylated, by PKA. The magnitude of the expansion of the thick filament backbone was then calculated by deducting the backbone diameter when cMyBPC was phosphorylated from its diameter when cMyBPC was unphosphorylated (box 2). From these calculations, the diameter of the thick filament backbone was calculated to increase by between 14.6nm (deduced from data presented by Weisberg and Winegrad, 1998) and 15.6nm (deduced from data presented by Weisberg and Winegrad, 1996) following phosphorylation of cMyBPC by PKA (calculations shown in box 2). Consequently, when these values were added to the diameter of the A-band fish skeletal muscle thick filament backbone previously reported by Squire et al., (1998), it was estimated that the diameter of the thick filament backbone itself would increase to about 29.6 to 30.6nm, following cMyBPC phosphorylation.

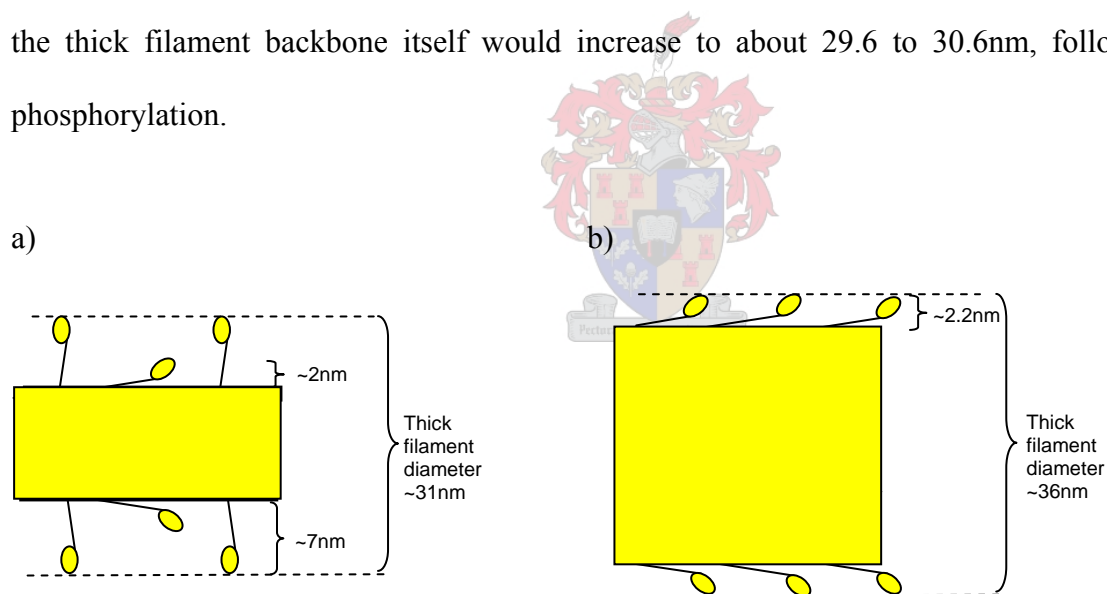


**Figure IV.8. Dimensions of  $\alpha$ -myosin “tight” and “loose” heavy chain containing cardiac thick filaments**  
 Measurements of the cardiac muscle A-band thick filament when a) cMyBPC is unphosphorylated (thick filaments with a “tight” structure) and b) cMyBPC is triphosphorylated by PKA (thick filaments with a “loose” structure).  $\square$  = thick filament backbone;  $\circ$  = crossbridge extensions. The total dimensions of the thick filament, as well as the extent of crossbridge extension, as measured Weisberg and Winegrad (1998) is shown in a) and b) when cMyBPC was unphosphorylated and triphosphorylated, respectively.

**BOX 2****FORMULAE**

TF backbone diameter = Total maximal TF diameter – 2(Maximal crossbridge extension)

TF backbone diameter expansion = Maximal TF backbone diameter cMyBPC-PO<sub>4</sub> – Maximal TF backbone diameter cMyBPC

$$\begin{aligned} \text{TF backbone diameter cMyBPC}^* &= 30\text{nm}^* - 2(7\text{nm}^\#) \\ &= 16\text{nm} \end{aligned}$$

\*Values obtained from Weisberg and Winegrad, 1996

^\#Values obtained from Weisberg and Winegrad, 1998

$$\begin{aligned} \text{TF backbone diameter cMyBPC-PO}_4^* &= 36\text{nm}^* - 2(2.2\text{nm}^\#) \\ &= 31.6\text{nm} \end{aligned}$$

$$\begin{aligned} \text{TF backbone diameter expansion}^* &= 31.6\text{nm} - 16\text{nm} \\ &= 15.6\text{nm} \end{aligned}$$

$$\begin{aligned} \text{TF backbone diameter cMyBPC}^\# &= 31\text{nm}^\# - 2(7\text{nm}^\#) \\ &= 17\text{nm} \end{aligned}$$

$$\begin{aligned} \text{TF backbone diameter cMyBPC-PO}_4^\# &= 36\text{nm}^\# - 2(2.2\text{nm}^\#) \\ &= 31.6\text{nm} \end{aligned}$$

$$\begin{aligned} \text{TF backbone diameter expansion}^\# &= 31.6\text{nm} - 17\text{nm} \\ &= 14.6\text{nm} \end{aligned}$$

As the distances that crossbridges extend into the interfilament space was not given in the study by Weisberg and Winegrad (1996), values of 7nm when cMyBPC was unphosphorylated and 2.2nm when cMyBPC was phosphorylated, measured by Weisberg and Winegrad (1998) were used when calculating thick filament backbone diameters.

None of the measurements obtained from these studies were corrected for the thickness of the metal coat applied to thick filaments prior to X-ray diffraction.

Specific values given in table I.4

*TF = thick filament*

It is plausible that this expansion of the thick filament is facilitated by, or at least necessitates, the abolition of interactions between the C5 and C8 domains, the C7 and C10 domains, as well as the interaction between the C7 domain of cMyBPC and titin, following PKA-dependent phosphorylation of cMyBPC. The mechanisms through which the PKA-dependent phosphorylation of sites in the MyBPC-motif, located in the N-terminal region of the protein, results in the abolition of these interactions between domains located in the central to C-terminal region of cMyBPC are, however, still unclear. The long distance effects of PKA-dependent phosphorylation of sarcomeric components are, however, not unprecedented. It was, for instance, shown that PKA-dependent phosphorylation of residues in the N-terminal region of cTNI causes conformational changes in cTNC, resulting in a significant reduction in the affinity of cTNC for  $\text{Ca}^{2+}$  (Chandra et al., 1997).

#### **IV.3.2.1. Proposed structure of LMM dimers in the “expanded” thick filament backbone**

In order to gain an understanding of how LMM dimers, arranged in the curved crystalline layer model, may be rearranged to give rise to an “expanded” thick filament structure, another series of scale drawings was made in the present study (figure IV.9). In these scale drawings, it was assumed that the different layers of LMM dimers in the curved crystalline layer model would slide across each other, thus allowing all 36 LMM dimers to be arranged in a circular structure (figure IV.9). Furthermore, it was assumed that the inter-molecular spacing between LMM dimers of about 0.2nm, predicted in the curved crystalline layer model (Squire, 1973), would be retained following expansion of the thick filament backbone.

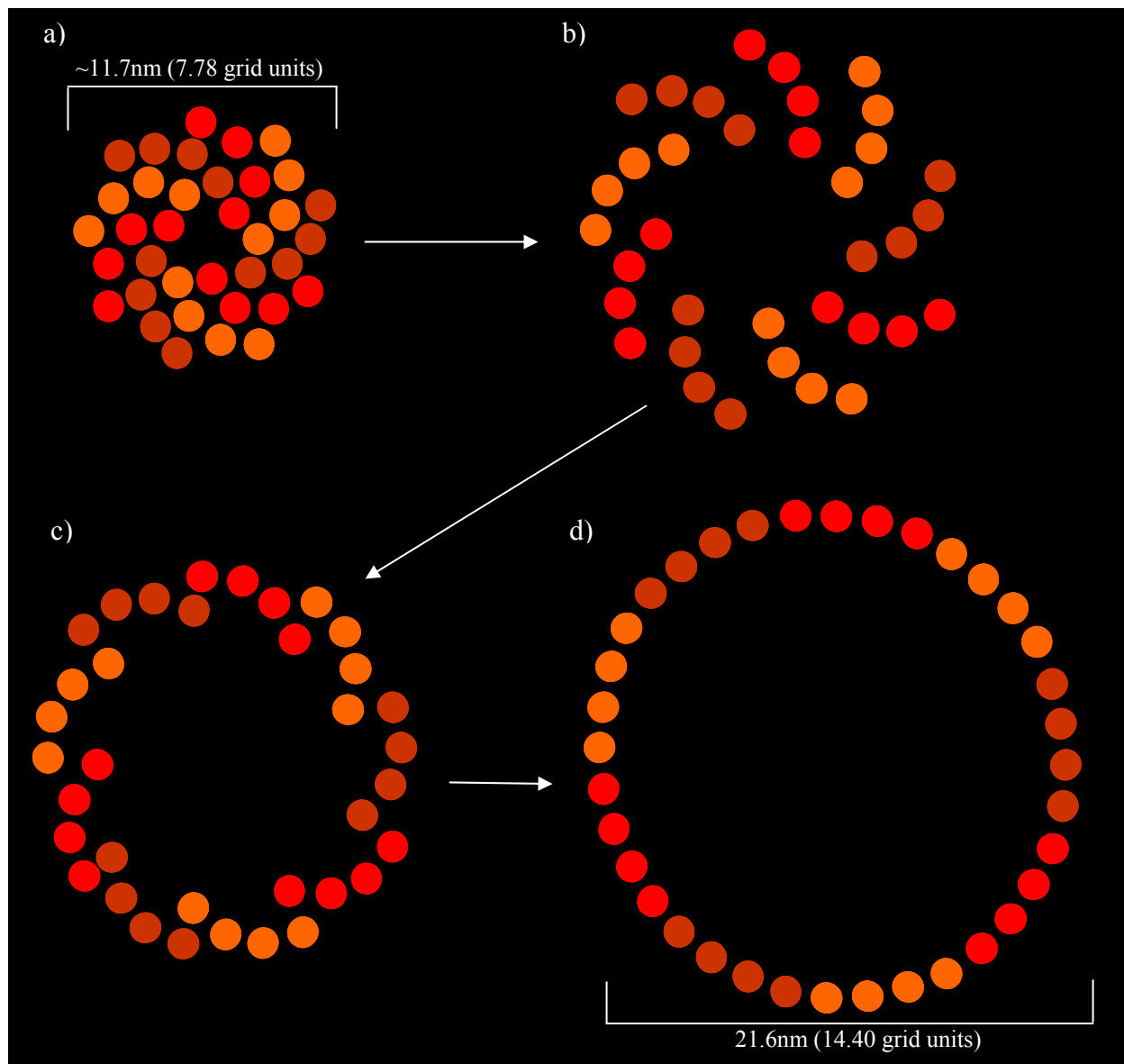


**Figure IV.9. Proposed mechanism of LMM thick filament expansion**

Scale drawings of the arrangement LMM dimers in the thick filament backbone. a) Arrangement of LMM molecules in the thick filament backbone according to the curved crystalline layer model of Squire, (1973) (“compact” arrangement); d) proposed arrangement of LMM dimers in the “expanded” thick filament following phosphorylation of cMyBPC; b) and c) show possible intermediate arrangements of LMM dimers, showing how the various layers of LMM dimers might shift across each other to form the circular “expanded” arrangement depicted in d). The estimated diameters of the “compact” and “expanded” arrangements are indicated in a) and d), respectively. ● ○ ● = LMM dimers from different layers in the curved crystalline layer model.

From these scale drawings, the maximal diameter of thick filaments consisting of only LMM dimers was estimated as being about 21.6nm (figure IV.9). The possibility that expansion of the thick filament backbone may also result in an increase in the inter-molecular spacing of LMM dimers, thus resulting in the generation of a thick filament with a larger diameter, cannot be dismissed.

#### **IV.3.2.2. Position of titin dimers on the “expanded” thick filament backbone**

Following the construction of these scale drawings of “expanded” thick filaments consisting entirely of LMM dimers, the positions of titin dimers in the thick filament backbone were considered. Firstly, it was assumed that titin dimers would remain on the surface of the thick filament, where they would retain interaction with LMM dimers. When positioning titin dimers on the “expanded” LMM backbone, it was considered that titin dimers would, in all likelihood, remain in contact with the same LMM dimers as in the “compact” thick filament conformation (figures IV.6 and IV.7). In the “compact” thick filament conformation, however, titin dimers interacted with LMM dimers from different layers, thus indicating that at least one of the titin:LMM interactions would have to be abolished during the expansion of the thick filament backbone. Depending on the specific interaction abolished, it is possible that titin dimers could be positioned at two different positions on the LMM backbone (figures IV.9b and IV.9c). From scale drawings to which titin dimers were added in the two possible positions depicted in figures IV.9b and IV.9c, the diameter of the “expanded” thick filament, including titin, was deduced to be about 23.1nm, irrespective of whether titin dimers were positioned as depicted in either figure IV.10b or IV.10c.

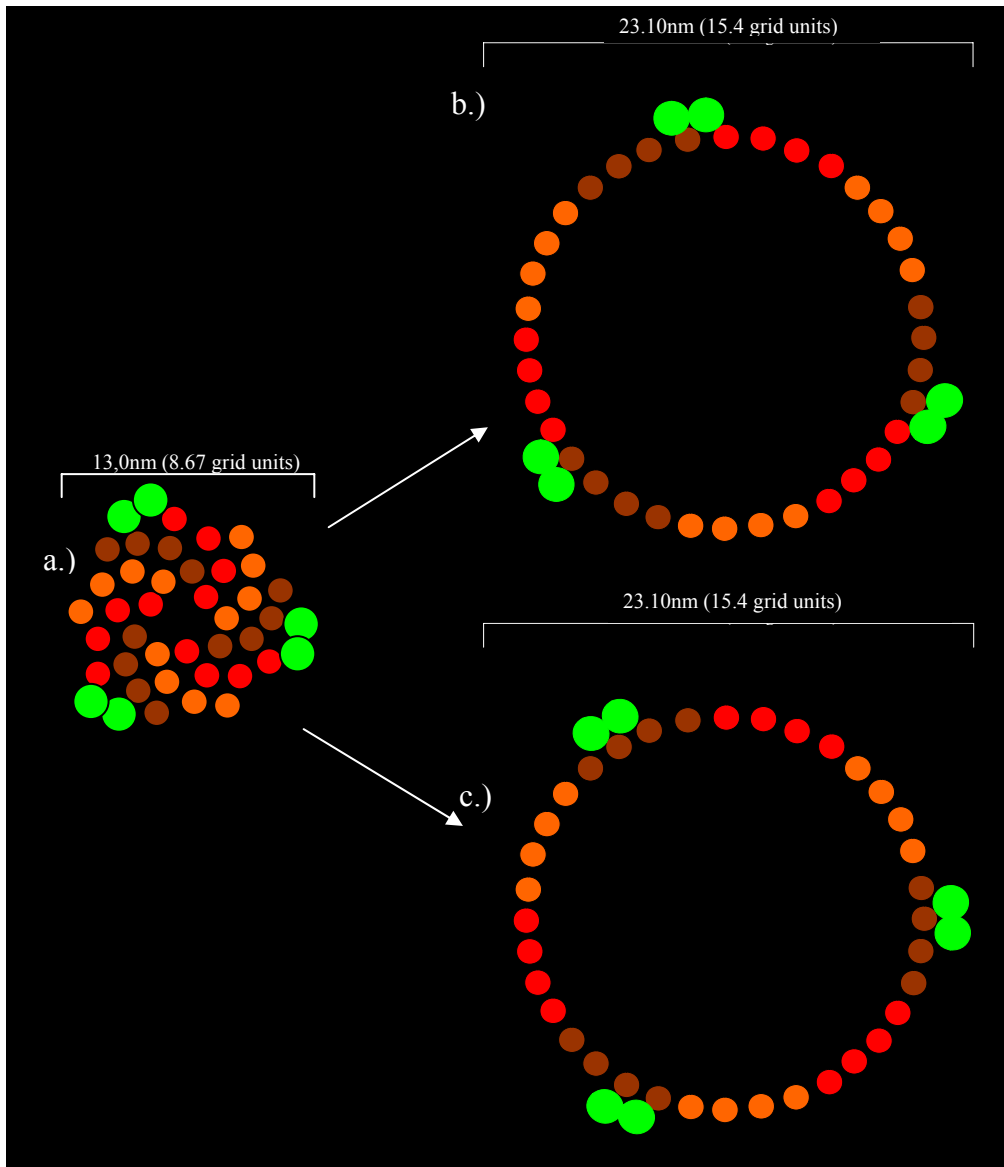


**Figure IV.10. Proposed positions of titin dimers on the “expanded” LMM thick filament backbone**  
*a) Position of LMM dimers on the “compact” thick filament backbone, b) and c) two possible positions of titin dimers on the thick filament backbone following expansion thereof. ● ● ● = LMM dimers from different layers; ● = titin molecules.*

### IV.3.2.2. Position of cMyBPC on the “expanded” thick filament backbone

Following the addition of titin dimers to the proposed model of the quaternary structure of the “expanded” thick filament backbone, cMyBPC was integrated into this model. In order to allow the positioning of cMyBPC on the “expanded” thick filament backbone, several factors had to be taken into account. The interactions between the C10 domain of cMyBPC and LMM (Okagaki et al., 1993; Miyamoto et al., 1999; Welikson and Fischman, 2002), as well as that between the C9 and/or C10 domain(s) of cMyBPC and titin (Freiburg and Gautel, 1996), were considered to be constitutive, irrespective of the phosphorylation state of cMyBPC, as these interactions are responsible for the C-zone localisation and anchoring of cMyBPC (section IV.7). If the “tight collar” arrangement of cMyBPC, depicted in figure IV.7b, is accepted to be correct, it would allow the positioning of the C10 domain on the “expanded” thick filament backbone in such a way that it would retain interaction with the same two LMM dimers as in the “compact” conformation (figure IV.11). Additionally, if titin dimers are arranged on the “expanded” thick filament backbone, as depicted in figure IV.10b, the C10:titin interaction would be retained (figure IV.11).

Following the expansion of the thick filament backbone, the portion of the cMyBPC N-terminal of the C10 domain could assume two possible conformations. Firstly, it is possible that the collar would be completely abrogated and that cMyBPC would extend into the interfilament space, where its N-terminal portion could interact with other sarcomeric components. Alternatively, the trimeric collar conformation of cMyBPC might not be lost, but may assume a looser conformation. To investigate the latter scenario, scale drawings were constructed in which cMyBPC would form a trimeric, predominantly single layer, “loose collar” around the thick filament backbone (figure IV.11b). From these scale drawings, the diameter of the thick filament backbone, including both titin and cMyBPC, was estimated at being about 27.9nm, a value that is compatible with the values calculated for the

diameter of the “expanded” thick filament backbone of about 29.6nm to 30.6nm (box 2) (Weisberg and Winegrad, 1996; Weisberg and Winegrad, 1998).

It appeared from these scale drawings that, in this model of the “expanded” thick filament, the C10 domain of cMyBPC would be juxtaposed to the C3 domain in the “loose collar” conformation. It was, therefore, postulated that if the cMyBPC trimeric single layer “loose collar” could form around the thick filament backbone (figure IV.11b), it may be stabilised by an interaction between these two cMyBPC domains. In order to test this proposal, Y2H candidate-ligand assays were performed. These assays clearly showed that the C3 domain of cMyBPC specifically interacted with the C10 domain of cMyBPC, whereas domains C2 and C5 did not (figure III.44 and section III.3.4.5)\*. This finding, combined with the fact the arrangement of cMyBPC depicted in figure IV.11b produces an “expanded” thick filament with a diameter that is in step with the measurements of Weisberg and Winegrad (1996 and 1998), suggests that cMyBPC is likely to form a trimeric single layer “loose collar” around the “expanded thick” filament backbone. However, the possibility that the cMyBPC collar conformation may be completely abrogated under certain circumstances cannot be excluded by this study.

---

\* Subsequent experiments showed that a frame-shift mutation occurred in the pGBKT7-C3 bait construct used in these experiments. These results should, therefore, be considered preliminary until tested.

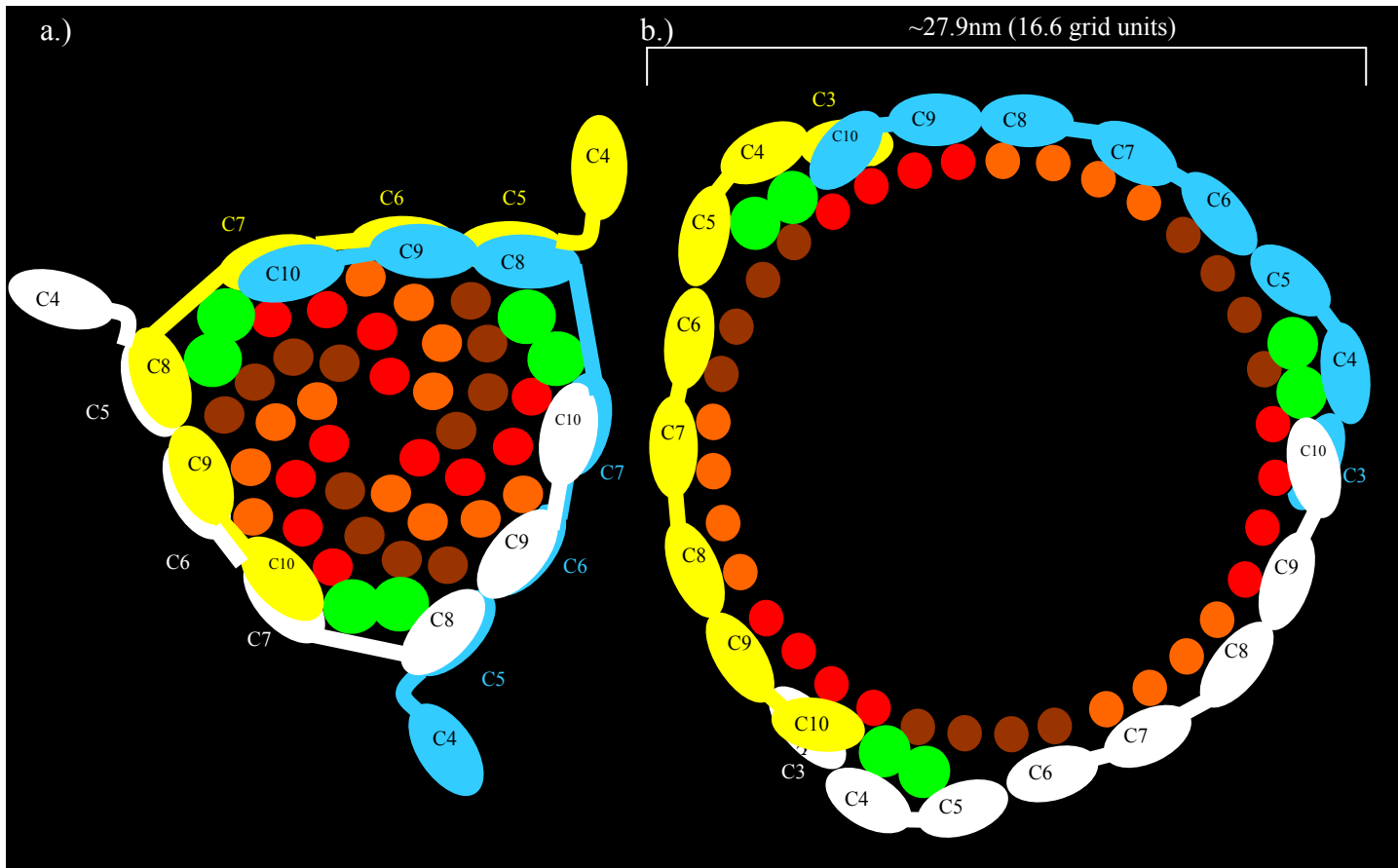


**Figure IV.11. Proposed arrangement of cMyBPC “loose collar” around the “expanded” thick filament backbone**

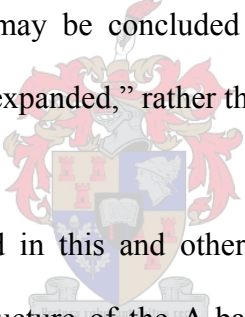
Scale drawings depicting transverse sections of the thick filament backbone in its a) “compact” and b) “expanded” state, showing the arrangement of LMM and titin dimers, as well as cMyBPC, within the thick filament backbone. ● ○ ● molecules = three consecutive partial cMyBPC molecules trimerising to form a) a “tight”, double layer and b) a loose, predominantly single layer, collar around the thick filament backbone; ● ● ● = LMM dimers from different layers; ● = titin molecules. The N-terminal regions of cMyBPC molecules (domains C0 to C3 in a) and domains C0 to C2 in b)) are not indicated in the figure and are predicted to extend into the interfilament space.

### **IV.3.3. PHYSIOLOGICAL EFFECT(S) OF cMyBPC MEDIATED EXPANSION OF THE THICK FILAMENT BACKBONE**

Expansion of the thick filament backbone (transition of thick filaments from a “tight” to a “loose” structure), following the PKA-dependent phosphorylation of cMyBPC, results in crossbridges being brought into closer proximity to the thin filament, thereby favouring the formation of weak interactions between thick and thin filaments (Weisberg and Winegrad, 1996; Weisberg and Winegrad, 1998; Levine et al., 2001). The formation of these weak interactions potentiates the contractile apparatus, resulting in an increase in force production, in actomyosin ATPase activity and in crossbridge cycling rates during systole (Weisberg and Winegrad, 1996; Weisberg and Winegrad, 1998; Levine et al., 2001). This view is in step with the findings of England (1975) and Solaro et al., (1976), who showed that  $\beta$ -adrenergic stimulation of intact cardiac muscle results in a marked increase in contractile force, of up to 70%, which is likely to be the result of the PKA-dependent phosphorylation of cMyBPC (sections I.4, I.5, I.6 and I.7.7) (McClellan et al., 1994). The increase in the number of crossbridges forming weak interactions with the thin filament may, however, impair relaxation, ventricular filling and diastolic function during periods of  $\beta$ -adrenergic stimulation.

The models of thick filament and cMyBPC quaternary structure in its “compact” and “expanded” state have important implications concerning the regulatory functions of cMyBPC, by suggesting a mechanism through which cMyBPC might regulate the dimensions of the thick filament backbone (Weisberg and Winegrad, 1996; Weisberg and Winegrad, 1998; Levine et al., 2001). Offer et al., (1973) found that the addition of purified skeletal MyBPC reduced actomyosin ATPase activity of isolated myosin and F-actin by about 50% in a  $\text{Ca}^{2+}$ -independent fashion, indicating that MyBPC plays an inhibitory, rather than an activatory, role (Offer et al., 1973). In the light of this finding, it is

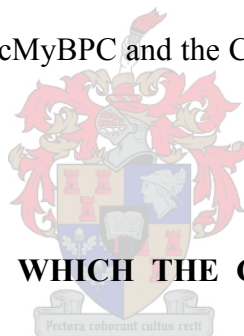
likely that the increase in actomyosin activity, observed following the phosphorylation of cMyBPC, may abolish the inhibitory effect of MyBPC on actomyosin activity. The phosphorylation-dependent abolition of this inhibitory effect of cMyBPC is likely to happen in two stages. Firstly, the release of myosin S2 from the MyBPC-motif, following phosphorylation of site B in the MyBPC-motif by MyBPC-associated kinase, results in alterations in crossbridge structure (Gruen et al., 1999; Kunst et al., 2000), leading to an increase in actomyosin ATPase activity. Secondly, the PKA-dependent phosphorylation of sites A and C in the MyBPC-motif would result in the release of the cMyBPC “tight collar”, causing expansion of the thick filament backbone to a diameter of about 28nm, thereby bringing crossbridges into closer proximity to thin filaments, resulting in an increase in actomyosin ATPase activity (Weisberg and Winegrad, 1996; Weisberg and Winegrad, 1998; Levine et al., 2001). From these findings, it may be concluded that, in the absence of MyBPC, thick filaments are more likely to take on an “expanded,” rather than a “tight”, conformation.



In conclusion, therefore, data generated in this and other studies was used to construct detailed integrated models of the quaternary structure of the A-band thick filament backbone both in the presence, and absence, of phosphorylation of cMyBPC by PKA. These models provide new insights into the mechanisms through which phosphorylation of cMyBPC by PKA results in increased actomyosin ATPase activity. Furthermore, these models have assigned either experimental or putative functions to several domains of cMyBPC to which no function was previously ascribed. As HCM-causing missense mutations are found in several of these domains, the models proposed in this study may be invaluable in gaining an understanding of how these mutations may have their pathogenic effect (section IV.5).

## IV.4. Y2H-ANALYSIS OF THE N-TERMINAL REGION OF cMyBPC

The exon 7 SaS +1 g>a splicing mutation is postulated to result in the generation of a truncated peptide consisting of only the C0 domain, the PA-region, a partial C1 domain and 90 novel amino acids (section IV.1.2.2). Based on the hypothesis that truncated cMyBPC peptides are likely to act as “poison peptides”, rather than through haploinsufficiency (sections I.1.1.1 and I.7.8.2), it was proposed that this region of the protein (C0C1) contained, as yet, unidentified protein binding-site(s), allowing this peptide to be incorporated into the sarcomeric A-band. This hypothesis is supported by the finding that C0C1 is incorporated specifically into the sarcomeric A-band (Flavigny et al., 1999), suggesting that the C0C1 region of cMyBPC contains an A-band specific binding-site. In order to test this hypothesis, the C0C1 region of cMyBPC and the C0 domain of cMyBPC were used in Y2H library-assays.



### IV.4.1. Y2H LIBRARY-ASSAYS IN WHICH THE C0C1 REGION OF cMyBPC WERE USED AS BAIT

In the first of these assays, the C0C1 region of cMyBPC was used to screen a cardiac cDNA library, using the MATCHMAKER GAL4 Two-Hybrid System 2 (BD Biosciences, Clontech, Palo Alto, CA, USA) (cMyBPC C0C1 Y2H library-assay (1)). This assay allowed the identification of human Jun coactivator (COP9 subunit 5) (two independent clones) and human homeobox protein MOX-1 (one clone) as putative ligands of the C0C1 region of cMyBPC. Neither of these proteins was, however, considered a plausible ligand of cMyBPC, as they both are reported to have a nuclear localisation. As this library-assay failed to identify any plausible ligands of the C0C1 region of cMyBPC, this library screen was subsequently repeated using the MATCHMAKER GAL4 Two-

Hybrid System 3 (BD Biosciences, Clontech, Palo Alto, CA, USA), that only became available during this study.

The MATCHMAKER GAL4 Two-Hybrid System 3 (hereafter referred to as system 3), was used in this and other Y2H library-assays, as it had several advantages over the MATCHMAKER GAL4 Two-Hybrid System 2 (hereafter referred to as system 2). Firstly, in addition to the *HIS3*, *ADE2* and *lacZ* reporter genes provided by yeast strain PJ69 2A used in system 2, yeast strain AH109, used in system 3, also provides the *MEL1* reporter gene, thus allowing further elimination of false positive interactions by means of X- $\alpha$ -gal assays (MATCHMAKER GAL4 Two-Hybrid System 3 & libraries user manual, BD Biosciences, Clontech, Palo Alto, CA, USA). Secondly, in the bait-vector used in system 3 (pGBKT7), the *T7* RNA polymerase promoter, rather than the *ADHI* promoter sequence contained in the bait-vector used in system 2 (pAS2.1), facilitates high-level bait fusion-protein expression, thus allowing the detection of weak interactions (MATCHMAKER GAL4 Two-Hybrid System 3 & libraries user manual, BD Biosciences, Clontech, Palo Alto, CA, USA). Thirdly, as the bait and prey-vectors used in system 3 contain different antibiotic resistance genes (kanamycin and ampicillin, respectively) (a feature not present in system 2), the isolation and purification of prey-vectors encoding putative interactor peptides was greatly simplified (MATCHMAKER GAL4 Two-Hybrid System 3 & libraries user manual, BD Biosciences, Clontech, Palo Alto, CA, USA). Finally, bait and prey fusion-proteins, expressed by vectors used in system 3, contained different epitope tags (c-Myc and hemagglutinin, respectively), allowing the isolation and use of fusion-peptides in CoIP assays (MATCHMAKER GAL4 Two-Hybrid System 3 & libraries user manual, BD Biosciences, Clontech, Palo Alto, CA, USA).

The second Y2H library-assay (cMyBPC C0C1 Y2H library-assay (2)) identified the C-terminal region of human titin (six independent clones), human multiple PDZ domain protein (two independent clones) and human cytochrome c oxidase subunit I (three independent clones) as putative ligands of the C0C1 region of cMyBPC. Based on its cellular localisation in the mitochondrial inner membrane, cytochrome c oxidase subunit I was not considered a plausible ligand of cMyBPC.

Additionally, as multiple PDZ domain protein, a “scaffolding” protein, is predominantly a nuclear protein, it was not considered to be of specific significance to the present study. However, as minor fractions of this protein are found in the cytoplasm and cytoskeletal lattice (localisation according to PSORT II, available at: <http://psort.ims.u-tokyo.ac.jp/cgi-bin/runpsort.pl>), it is possible that multiple PDZ domain protein may facilitate the crosslinking of the N-terminal region of cMyBPC and other ligands, and may, therefore, require further investigation. Based on its sarcomeric localisation, titin was, however, considered a plausible ligand of cMyBPC and was, therefore, investigated further in Y2H candidate-ligand assays (section IV.4.3.1).

#### **IV.4.2. Y2H LIBRARY-ASSAY IN WHICH THE C0 DOMAIN OF cMyBPC WAS USED AS BAIT**

The Y2H library-assay in which the C0 domain of cMyBPC was used as bait was performed using Y2H system 3 (BD Biosciences, Clontech, Palo Alto, CA, USA). This assay identified human sarcoglycan (delta subunit) (one clone), human tousel-like kinase 1 (also known as protein kinase U) (one clone), the beta-1 chain of human sodium/potassium-transporting ATPase (one clone) and human Ran binding protein 9 (two independent clones) as putative ligands of the C0 domain of

cMyBPC. Interaction-specificity tests, however, showed that the sarcoglycan delta subunit, tousel-like kinase 1, the sodium/potassium-transporting ATPase and RAN binding protein 9 all led to activation of reporter gene transcription in the presence of heterologous baits (table III.13). These proteins were, therefore, not considered to be specific ligands of the C0 domain of cMyBPC.

Additionally, eight putative interactor clones contained portions of human clone RP4-614C10 from chromosome 2. Analysis of the sequences contained in these clones, as well as the specific portion, and the region 5', of human clone RP4-614C10 to which they mapped, revealed the absence of any known genes, or any open reading frames of any significant length. Based on this finding, it was concluded that these clones do not encode plausible binding partners of the C0 domain of cMyBPC.

It is interesting to note that there was no overlap between putative interactor clones identified in the C0 and C0C1 library screens. One possible explanation for this apparent discrepancy is that the tertiary/quaternary structure of the C0C1 region may sterically hinder the association between the C0 domain and peptides identified as spuriously interacting with it in the C0 library-assay.

#### **IV.4.3. Y2H CANDIDATE-LIGAND ASSAYS IN WHICH THE N-TERMINAL DOMAINS OF cMyBPC WERE USED AS BAIT**

##### **IV.4.3.1. C-zone titin as a candidate-ligand of the N-terminal region of cMyBPC**

Six of the interactor clones identified in the cMyBPC C0C1 Y2H library-assay (2) encoded portions of the C-terminal region of titin, which varied in size from 34 to 69 amino acids in length (sections III.2.2, IV.4.1 and table III.9). As the region of titin encoded by these clones would be embedded in

the M-line in the intact sarcomere, while cMyBPC is found in the C-zone, the region encoded by these clones was not considered to be a plausible ligand of cMyBPC (figure III.39). The shortest of these peptides were, however, virtually identical to the 35 amino acid peptide that was identified as an informative ligand in the C7 Y2H library-assay. As this 35 amino acid peptide was shown to share the highest homology to the first IgC2 domain of each of the eleven-domain super-repeats of C-zone titin (sections I.6.3.2, III.3.3; figures I.9, III.39, III.40 and table III.16), these titin domains were considered plausible ligands of the C0C1 region of cMyBPC.

The candidacy of C-zone titin as a ligand of the C0C1 region of MyBPC is supported by the findings of Flavigny et al., (1999), who showed that truncated cMyBPC peptides consisting only of the C0C1 region, were incorporated specifically into the sarcomeric A-band. Bennett et al., (1986 and 1999), however, showed that antibodies directed against either the N- or C-terminal regions of MyBPC labelled two distinct lines about 15-20nm apart. This finding largely excluded the possibility that the C0C1 region of cMyBPC would interact with the first IgC2 domain of the eleven-domain super-repeat of C-zone titin, as the C-terminal region of cMyBPC would be bound to these domains. Based on this finding, combined with the fact that the C0C1 region of cMyBPC is able to interact with a partial IgC2 domain (domain M10 of titin) (sections III.2.2 and IV.4.1), it was postulated that the C0C1 region may interact with IgC2 domains in C-zone titin, other than the first domain of the eleven-domain super-repeat.

As the N-terminal region of cMyBPC was shown to be located about 15-20nm closer to the Z-disk than the C-terminal of cMyBPC, it was postulated that the C0C1 (N-terminal) region of cMyBPC may interact with the third IgC2 domain of the previous eleven-domain super-repeat of C-zone titin (figures III.39 and IV.11). If this were so, it would be expected that the N- and C-termini of cMyBPC would be separated by about 12 to 14nm. This predicted distance is slightly less than, but compatible

with, the measurements of Bennett et al., (1986 and 1999). Furthermore, it was postulated that the presence of an interaction between the N-terminal region of cMyBPC and C-zone titin may also allow the formation of thick filaments with a “disordered” structure observed when cMyBPC is unphosphorylated (Weisberg and Winegrad, 1996; Weisberg and Winegrad, 1998; Levine et al., 2001), as some crossbridges may be pulled towards the thick filament backbone (figure IV.12).

As C-zone titin was not expected to be represented in the cardiac cDNA library that was screened, due to the gigantic size of titin transcript (>27kb) (section II.16.2.1), Y2H candidate-ligand assays were performed to test whether the C0C1 region of cMyBPC did indeed interact with IgC2 domains of C-zone titin. In these assays, the third IgC2 domain of the seventh eleven-domain super-repeat of A-band titin (domain A116 of titin) was used as candidate prey in Y2H candidate-ligand assays (figure III.39). Additionally, other constructs, representing the first (domain A43 and A109 of titin) and second (domain A112 of titin) IgC2 domains of the first and seventh eleven-domain super-repeat, as well as a construct representing the first four domains of the seventh eleven-domain super-repeat of titin, were used as candidate-ligands in Y2H candidate-ligand assays (figure III.39). These assays, however, showed that the C0C1 region of cMyBPC did not interact with any of the IgC2 domains of C-zone titin, indicating that the orientation of the N-terminal region of cMyBPC depicted in figure IV.12 is unlikely.

#### **IV.4.3.2. N-terminal domains of cMyBPC as candidate-ligands of the N-terminal region of cMyBPC**

Based on the findings of Flavigny et al., (1999), which showed that truncated cMyBPC peptides, consisting only of the C0C1 region, were incorporated specifically into the sarcomeric A-band, it was postulated that the C0C1 region of cMyBPC interacts with an A-band specific ligand. In the light of this finding, it was postulated that this region of cMyBPC may be able to interact with other

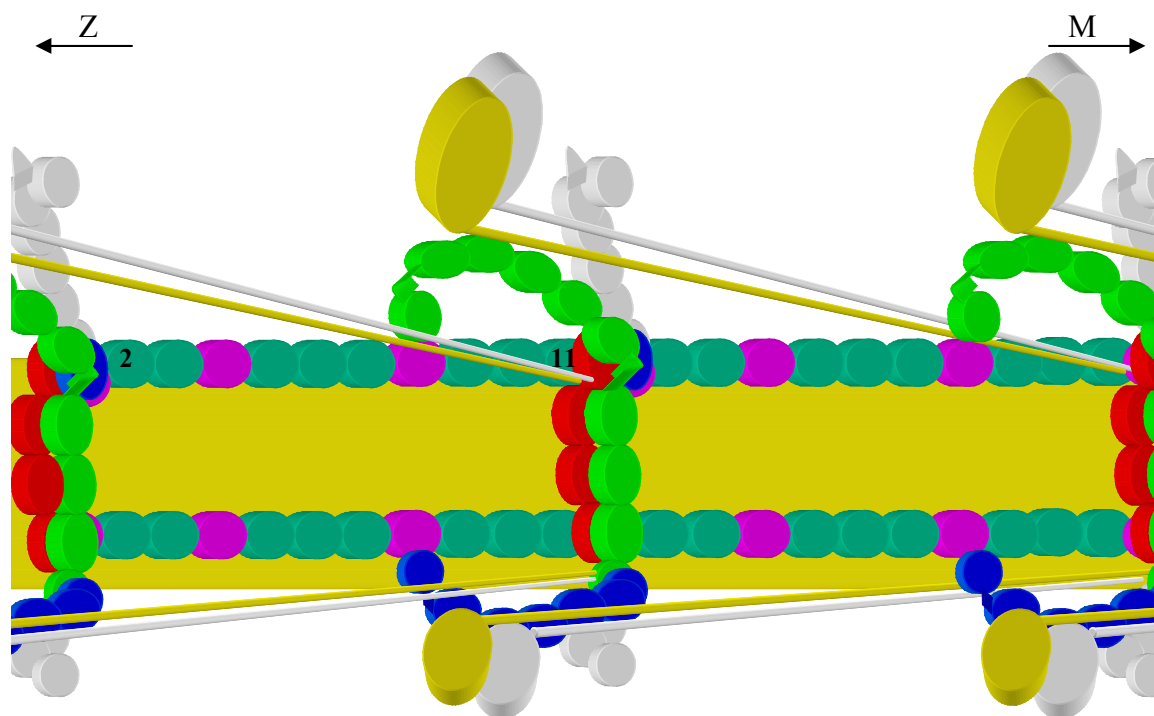


**Figure IV.12. Proposed orientation of the N-terminal portion of cMyBPC**

Side-on view of the “compact” thick filament in the C-zone, depicting the positions of crossbridges, cMyBPC and titin. cMyBPC is depicted in its unphosphorylated state in which the C-terminal domains trimerise to form a “tight collar” around the thick filament backbone, the MyBPC-motif interacting with myosin S2 and the C0C1 (N-terminal) region interacting with the third IgC2 domain of the previous eleven-domain super-repeat of C-zone titin (adjacent eleven-domain super-repeat towards the Z-disk). The relative positions of the N-terminal region of cMyBPC and crossbridges in the absence of an interaction between the C0C1 region of cMyBPC and C-zone titin are also depicted as shaded white structures. In the interest of clarity, only crossbridges from every third crown are shown. ● ● ● molecules = cMyBPC molecules; ● = Fn3 domains of C-zone titin; ● = IgC2 domains of C-zone titin; ● structures = myosin molecules, of which LMM forms the body of the thick filament backbone. The second (fn3) and eleventh (IgC2) domains of one of the C-zone titin eleven-domain super-repeat is labeled in the figure, while the arrows labeled M and Z indicate the directions in which the M-line and Z-disk is located, respectively.

N-terminal domains of cMyBPC itself. As the N-terminal region of cMyBPC was not expected to be represented in the cardiac cDNA libraries that were screened, due to the size of cMyBPC transcript (>4.1kb) (section II.16.2.1), Y2H candidate-ligand assays were performed to test whether the C0C1 region of cMyBPC did indeed interact with other domains/regions in the N-terminal region of cMyBPC. In these assays, the C0, C0C1 and C0C2 domains/regions of cMyBPC were used as baits, while the C1, C2 and C1C2 domains/regions of cMyBPC were used as preys. No interactions between any of these domains/regions were detected in these assays, indicating the absence of any inter-molecular or intra-molecular interactions between domains/regions in the N-terminal portion of cMyBPC.

#### **IV.4.3.3. Cardiac actin as a candidate-ligand of the N-terminal region of cMyBPC**

As the C0 domain of cMyBPC was shown to interact with cardiac actin monomers in *in vitro* binding-assays (Kulikovskaya et al., 2003), combined with the proposal by Squire et al., (2003) that the PA-region of cMyBPC may interact with cardiac F-actin (sections I.7.3.5 and I.7.7.3), cardiac actin was considered a candidate ligand of the C0C1 region of cMyBPC. Cardiac actin was, however, not identified as a candidate ligand of this region of cMyBPC in the cMyBPC C0 Y2H library-assay (sections III.3.2.3 and IV.4.2) or either the Y2H library-assays in which the C0C1 region of cMyBPC was used as bait (sections III.3.2.1, III.3.2.2 and IV.4.1). This finding was surprising due to the fact that, firstly, a high level of cardiac actin expression is expected in cardiac tissue, indicating that multiple cardiac actin clones should be present in the cardiac cDNA libraries screened. Secondly, due to the relatively small size of the cardiac actin transcript (1.5kb), it was anticipated that full-length cardiac actin clones would be present in the cardiac cDNA libraries screened.

The presence of cardiac actin clones in the cardiac cDNA libraries that were screened in this study was subsequently confirmed when cardiac actin was identified as a putative ligand of the tri-phosphomimic C1C2 region of cMyBPC in a Y2H library-assay in which an identical cardiac cDNA library was used (personal communication Dr Hanlie Moolman-Smook, 10 April 2003). In addition to the Y2H library-assays in which the C0 and C0C1 regions of cMyBPC were used as bait, these regions were also used as bait in candidate-ligand Y2H-assays in which cardiac actin clones, identified as putative ligands of the C1C2 region, were used as preys. These candidate-ligand Y2H assays, however, failed to show any interaction between this region of cMyBPC and cardiac actin.

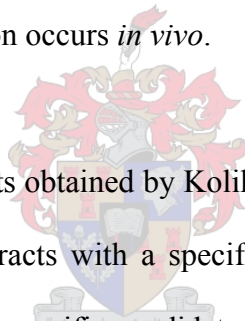
There may be several explanations as to why the interaction between the C0C1 region of cMyBPC and cardiac actin remained undetected in Y2H assays. Firstly, it is possible that the N-terminal region of cardiac actin, absent from the clones used as prey in the candidate-ligand-assays, is essential for its interaction with the N-terminal region of cMyBPC. However, full-length cardiac actin transcripts are expected to have been in abundance in the cardiac cDNA libraries screened, using the N-terminal region of cMyBPC as bait. Secondly, it is possible that the position of the GAL4-AD that is part of the actin prey fusion-peptide may sterically hinder the binding of the cardiac actin fusion-peptide to the C0C1 region of cMyBPC. If this is the case, it would be impossible to detect an interaction between cardiac actin and the C0C1 region of cMyBPC using Y2H-assays. However, the GAL4-AD did not hinder the interaction between actin clones and the C1C2 region of cMyBPC in a Y2H library-assay. Thirdly, it is possible that, even though Kulikovskaya et al., (2003) showed binding between the C0 domain of cMyBPC and cardiac actin *in vitro*, such an interaction does not occur in an *in situ* environment. In order to establish whether the latter scenario is plausible, the results obtained by Kulikovskaya et al., (2003) in *in situ* experiments were re-interpreted.

In these experiments by Kulikovskaya et al., (2003), skinned cardiac trabeculae were soaked in a relaxing solution containing low concentrations of either C0C1, C1C2, or C0C2 cMyBPC fragments. It was shown that in trabeculae in which cMyBPC was predominantly unphosphorylated, C1C2 cMyBPC fragments were not bound to the trabeculae, but that C0C1 and C0C2 cMyBPC fragments did bind to the trabeculae. The authors interpreted these results as suggesting that all cMyBPC binding-sites on myosin S2 are occupied by endogenous cMyBPC (through the MyBPC-motif), thus not allowing the binding of exogenous C1C2 cMyBPC fragments. The fact that C0C1 and C0C2 cMyBPC fragments were bound to these trabeculae was interpreted as suggesting that cMyBPC binding-sites on F-actin would be free of endogenous cMyBPC, therefore, allowing interaction with exogenous C0C1 and C0C2 cMyBPC fragments. Conversely, in trabeculae with a high degree of phosphorylation, C0C1 cMyBPC fragments were not bound to the trabeculae, while C1C2 and C0C2 cMyBPC fragments did bind to the trabeculae (Kolikovskaya et al., 2003).



These results suggested that, in cases where MyBPC were predominantly phosphorylated, and the MyBPC-motif was not bound to myosin S2 (Gruen et al., 1999; Kunst et al., 2000), the cMyBPC binding-sites on F-actin would be occupied by endogenous cMyBPC, thus not allowing exogenous C0-containing cMyBPC fragments to bind to actin. Exogenous cMyBPC fragments in which the MyBPC-motif was present (C0C2 and C1C2) would, however, be able to bind to trabeculae through interaction with myosin S2 (Kolikovskaya et al., 2003). It was, therefore, suggested that these interactions of the N-terminal region of cMyBPC were competitive and that the phosphorylation status of cMyBPC would determine whether the MyBPC-motif would interact with myosin S2 (Kunst et al., 2000), or the C0 domain would interact with F-actin (Kolikovskaya et al., 2003).

This hypothesis is, however, implausible due to the fact that myosin S2 is not restricted to the C-zone, and, even in the C-zone, the molar ratio of cMyBPC to myosin S2 is 1:3, suggesting that sufficient S2 binding-sites would remain available for exogenous C1C2 fragments independent of the endogenous cMyBPC phosphorylation status in these trabeculae. Furthermore, it can be assumed that each actin monomer in F-actin, of which only a small fraction would interact with the endogenous cMyBPC, would contain a cMyBPC C0 binding-site, and would, therefore, be able to interact with exogenous C0-containing cMyBPC fragments, irrespective of the phosphorylation status of endogenous cMyBPC. Additionally, the interaction originally described by Moos and coworkers, was between skeletal MyBPC and F-actin (Moos et al., 1978; Moos, 1981). As the skeletal MyBPC isoforms lack the C0 domain (Carrier et al., 1997), the F-actin binding-site cannot be located in this domain only, if indeed such an interaction occurs *in vivo*.



An alternative interpretation of the results obtained by Kolikovskaya et al. (2003) may be that the C0 domain of cMyBPC competitively interacts with a specific, as yet unidentified, ligand, restricted only to positions in the C-zone. C-zone specific candidate ligands include domains of cMyBPC, or C-zone specific domains of titin. This interpretation would explain why exogenous C0C1 cMyBPC fragments were able to bind to trabeculae with a low degree of endogenous cMyBPC phosphorylation, but not to trabeculae with a high degree of cMyBPC phosphorylation. The reason why C1C2 cMyBPC fragments were not able to bind to trabeculae with a low degree of endogenous cMyBPC phosphorylation, however, remains inexplicable.

In summary, therefore, even though the *in vitro* binding assays performed by Kolikovskaya et al., (2003) provide compelling evidence that the C0 domain of cMyBPC can interact with F-actin *in vitro*, the evidence provided for this interaction taking place *in situ* and *in vivo* seems less convincing. The data obtained from skinned trabeculae studies performed by Kolikovskaya et al.,

(2003), however, provides new insights into the functioning of the N-terminal region of cMyBPC, and suggests that the C0 domain interacts with an, as yet, unidentified C-zone specific ligand, when cMyBPC is phosphorylated.

#### **IV.5. EFFECT OF HCM-CAUSING *MYBPC3* MUTATIONS ON cMyBPC QUATERNARY STRUCTURE**

The identification of ligands of specific domains of cMyBPC, during the course of this study, has led to the assignment of novel function to the C3, C7 and C10 domains of cMyBPC (sections III.3.2.4, III.3.4.1, III.3.4.2, III.3.4.5, IV.2.1 and IV.2.2). Additionally, the identification the C8 domain of cMyBPC as the ligand of the C5 domain (Moolman-Smook et al., 2002) has led to novel functions being assigned to these two domains of cMyBPC (table IV.1). In conjunction, this data was used in the establishment of models of cMyBPC quaternary structure in both the “compact” and “expanded” thick filaments. As the C6 and C9 domains of cMyBPC are juxtapositioned in the cMyBPC “tight collar” model (cMyBPC unphosphorylated, thick filaments in the “compact” conformation) (section IV.6.1.3 and figure IV.7), it is possible that these domains could also interact, thus assigning putative function to these two domains (table IV.1). The presence of an interaction between the C6 and C9 domains (both Fn3 domains) of cMyBPC was, however, not tested experimentally in this study, as Fn3 domains are known to be inherently “sticky” molecules that often form homophilic interaction with other Fn3 domains (Nave et al., 1989; Price and Gomers, 1993; Labeit and Kolmerer, 1995).

As the cMyBPC trimeric “tight collar” is proposed to be stabilised by the C5:C8 interaction, the C7:C10 interaction, the C7:titin interaction, and possibly also the C6:C9 interaction (section IV.6.1.3, figure IV.7 and table IV.4), it was postulated that HCM-causing missense mutations in these domains may be pathogenic by adversely affecting these interactions. In a study by Moolman-

**Table IV.1. Functions assigned to specific domains/regions of cMyBPC**

<b>cMyBPC domain/region</b>	<b>Known function</b>	<b>Novel function</b>	<b>Status</b>	<b>Ref</b>
C0	Interaction with F-actin	-	Exp	1-3
PA-region	Interaction with F-actin	-	Put	4
C1	-	-	-	-
MyBPC-motif	Contains phosphorylation sites	-	Exp	5
	Interaction with myosin S2	-	Exp	6-8
C2	-	-	-	-
C3	-	Interaction with C10 domain of cMyBPC	Exp	9
C4	-	-	-	-
C5	Interaction with C8 domain of cMyBPC	-	Exp	10
C6	-	Interaction with C9 domain of cMyBPC	Put	9,10
C7	-	Interactions with C10 domain of cMyBPC, and with C-zone titin	Exp	9
C8	Interaction with C5 domain of cMyBPC	-	Exp	10

<b>cMyBPC domain/region</b>	<b>Known function</b>	<b>Novel function</b>	<b>Status</b>	<b>Ref</b>
C9	Interaction with C-zone titin		Exp*	11
		Interaction with C6 domain of cMyBPC	Put	9-10
C10	Interaction with LMM		Exp	12,13
	Interaction with C-zone titin		Exp*	11
		Interactions with C7 domain of cMyBPC in the “compact” thick filament	Exp	9
		Interactions with C3 domain of cMyBPC in the “expanded” thick filament	Exp	9

*Status refers to whether the function assigned to a specific cMyBPC domain or region has been shown experimentally or is a proposed/putative function. Exp = shown experimentally; Known function = functions previously reported; Novel function = function assigned in the present study; Put = proposed/putative function that has not been confirmed by experimental data; Ref = reference; 1 = Moos et al., 1978; 2 = Moos, 1981; 3 = Kulikovskaya et al., 2003; 4 = Squire et al., 2003; 5 = Gautel et al., 1995; 6 = Gruen and Gautel, 1999; 7 = Gruen et al., 1999; 8 = Kunst et al., 2000; 9 = present study; 10 = Moolman-Smook et al., 2002; 11 = Freiburg and Gautel, 1996; 12 = Okagaki et al., 1993; 13 = Welikson and Fischman, 2002; \* = binding-site located in the C9 and/or C10 domain(s); - = no known/putative function assigned to a particular domain.*

Smook et al., (2002), it was shown that the R654H and N755K HCM-causing missense mutations in the C5 domain of cMyBPC (Moolman-Smook et al., 1998; Yu et al., 1998) both significantly decrease the affinity of the C5 domain for the C8 domain of cMyBPC (Moolman-Smook et al., 2002). These findings indicate that these HCM-causing missense mutations in the C5 domain may result in a destabilisation of the cMyBPC “tight collar” conformation, and may allow expansion of the thick filament backbone in the absence of PKA-mediated phosphorylation of cMyBPC.

In order to establish whether V896M, which was until recently considered to be an HCM-causing mutation (Moolman-Smook et al., 1999), acts in a similar fashion by destabilising the cMyBPC trimeric “tight collar”, as a result of a weakening of either the C7:10 or C7:titin interactions, quantitative  $\beta$ -galactosidase Y2H-assays were performed. These assays indicated that V896M significantly strengthened the C7:C10 interaction, without having any effect on the C7:titin interaction (section III.3.4.3 and figure III.43). This result was surprising, as it suggested that V896M would result in a strengthening, rather than a weakening, of the cMyBPC “tight collar” and might prevent the expansion of the thick filament backbone following PKA-mediated phosphorylation of cMyBPC, while HCM-causing missense mutations in the C5 domain had the opposite effect. Subsequently, however, CoIP studies have shown that the presence of V896M in the C7 domain decreases the strength of both the C7:C10 and C7:titin interactions (personal communication Dr Hanlie Moolman-Smook, 12 September 2003), suggesting that V896M may indeed act similarly to mutations in the C5 domain by destabilising the cMyBPC “tight collar”.

The discrepancy in the findings of CoIP analysis and quantitative  $\beta$ -galactosidase Y2H-assays, however, casts doubt over the accuracy and usefulness of quantitative  $\beta$ -galactosidase Y2H-assays. Similar discrepancies were also found when the effect of the R654H and N755K HCM-causing

missense mutations on the C5:C8 interaction was assessed by quantitative  $\beta$ -galactosidase Y2H-assays and BIAcore experiments. Both these mutations were shown to significantly strengthen the C5:C8 interaction as assessed by quantitative  $\beta$ -galactosidase Y2H-assays, while BIAcore experiments showed that these mutations significantly weakened this interaction (personal communication Dr Hanlie Moolman-Smook, 20 January 2002; Moolman-Smook et al., 2002). It can, therefore, be concluded that quantitative data obtained from  $\beta$ -galactosidase Y2H-assays should be treated with some suspicion, and that results obtained from these assays should be confirmed by at least one independent biochemical assay such as CoIP or BIAcore.

Subsequent to V896M being described as an HCM-causing mutation (Moolman-Smook et al., 1999), V896M was also described in HCM-affected populations in several other studies (Jaaskelainen et al., 2002; Morner et al., 2003; Richard et al., 2003). In these studies, however, V896M was described as either a polymorphism (Jaaskelainen et al., 2002; Morner et al., 2003), or a disease-modifying factor (Richard et al., 2003), based on the finding that it was also present in HCM-unaffected control populations. The finding that V896M results in a weakening in the strength of the C7:C10 and C7:titin interactions, both of which are predicted to destabilise the cMyBPC trimeric “tight collar”, suggests that V896M may indeed be of functional, if not pathological, relevance. V896M may result in the formation of thick filaments with a “loose” structure being favoured in the absence of PKA-mediated phosphorylation of cMyBPC. As this effect is similar to the proposed pathogenic effect of the R654H and N755K HCM-causing missense mutations in the C5 domain of cMyBPC, it is plausible that V896M may act as a disease-modifying factor in individuals carrying other HCM-causing mutations.

As the R654H and N755K HCM-causing missense mutations and the V896M putative disease-modifying factor were all found to weaken interactions stabilising the cMyBPC trimeric “tight collar” conformation, it could be postulated that other HCM-causing missense mutations may act in a similar fashion. A destabilisation of the cMyBPC trimeric “tight collar” would favour the formation of thick filaments with a “loose” structure in the absence of PKA-mediated phosphorylation of cMyBPC. As domains C5, C6, C7, C8 and C9 are all involved in interdomain interactions that stabilise the cMyBPC “tight collar” conformation (C5:C8, C6:C9, C7:C10 and C7:titin interactions) (section IV.3), it can be proposed that missense mutations in any of these domains would weaken these stabilising interdomain interactions. Conversely, as the interaction between the C3 and C10 domain of cMyBPC is likely to stabilise the cMyBPC “loose collar” conformation, it is possible that missense mutations in the C3 domain of cMyBPC would lead to a strengthening of this interaction, thus also favouring the formation of thick filaments with a “loose” conformation. According to this hypothesis, missense mutations in the C10 domain of cMyBPC could either lead to a strengthening of the C3:C10, interaction or a weakening of the C7:C10 interaction. Missense mutations in these domains may affect these interactions by either altering specific binding surfaces on a domain, or by destabilising the structure of the domain as a whole. The possibility that some missense mutations may cause a strengthening of interactions stabilising the cMyBPC “tight collar” conformation can, however, not be excluded by this study. The former scenario, in which missense mutations in cMyBPC favours the formation of thick filaments with a “loose” structure is, however, favoured by this author as it would provide a unifying mechanism through which HCM-causing missense mutations cause disease.

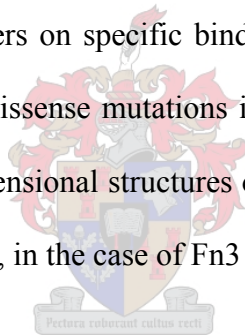
Additionally, it is plausible that HCM-causing mutations, resulting in the truncation of cMyBPC, may also favour the formation of thick filaments with a “loose” conformation, irrespective of

whether they function through a mechanism of haploinsufficiency, or act as “poison peptides” (sections I.1.1.1 and I.7.8.2). If *MYBPC3* truncation mutations act through a mechanism of haploinsufficiency, it is likely that this would prevent the formation of the cMyBPC trimeric “tight” and “loose collar” structures, due to a stoichiometric deficiency in cMyBPC, resulting in the loss of regulation of thick filament structure by cMyBPC. The subsequent loss of the cMyBPC trimeric “tight collar” may result in thick filaments taking on a “loose”, rather than a “tight”, conformation (section IV.3.3). Similarly, if truncated MyBPC peptides act as “poison peptides,” (sections I.1.1.1 and I.7.8.2), these truncated peptides may be incorporated into the sarcomere, where they would compete with full length cMyBPC for the respective sarcomeric binding-sites. As these truncated cMyBPC peptides lack varying portions of their C-terminal regions (figure I.23 and table I.6), necessary for forming the cMyBPC “tight collar”, it is likely that the presence of these truncated peptides in the A-band would prevent the formation of the cMyBPC “tight collar” conformation, resulting in the formation of thick filaments with a “loose” conformation (section IV.3.3).

The hypothesis that HCM-causing missense mutations in the C3, C5, C6, C7, C8, C9 and C10 domains of cMyBPC, and cMyBPC truncation mutations, may share a common disease pathogenesis by favouring the formation of thick filaments with a “loose” structure has several important implications. Firstly, as thick filaments in the “loose” conformation are more likely to form weak interactions with thin filaments, it is possible that the relaxation of cardiac muscle may be impaired, leading to diastolic dysfunction, a feature commonly caused by HCM-causing mutations (section I.1.1.1, table I.2 and references therein). Secondly, the formation of a larger number of weak interactions between thick and thin filaments, resulting from thick filaments being in the “loose” conformation, would potentiate the contractile apparatus, resulting in an increase in actomyosin ATPase activity. This increase in actomyosin ATPase activity would result in increased ATP usage,

which may lead to ATP depletion, specifically during periods of  $\beta$ -adrenergic stimulation, or during strenuous exercise when ATP demand is increased. The finding that ATP depletion may be a hallmark of all HCM-causing mutations (section I.1.1.2 and references therein) supports this hypothesis. Additionally, ATP depletion, in turn, may impair the function of SERCA2a, thus resulting in alterations in  $\text{Ca}^{2+}$  homeostasis in the cardiomyocyte, which has been associated with HCM (section I.1.1.1, table I.2 and references therein).

If indeed destabilisation of the trimeric cMyBPC “tight collar” conformation, or a strengthening of the “loose” cMyBPC collar conformation, is a hallmark of cMyBPC HCM-causing missense mutations, it would be possible that HCM-causing missense mutations in domains stabilising these conformations would be found in clusters on specific binding surfaces. In order to investigate this possibility, the positions of cMyBPC missense mutations in the C3, C5, C6, C7\*, C8, C9 and C10 domains were mapped on the three-dimensional structures of chain A of telokin, in the case of IgC2 domains, or the Fn3 consensus sequence, in the case of Fn3 domains (figures IV.12 to IV.20).



#### **IV.5.1. POSITION OF HCM-CAUSING MISSENSE MUTATIONS IN THE C3 DOMAIN OF cMyBPC**

The identification of an interaction between the C3 and C10 domains of cMyBPC has led to the hypothesis that HCM-causing missense mutations in the C3 domain of cMyBPC may strengthen this interaction (section IV.5 and table IV.1). It was, therefore, postulated that missense mutations in the C3 domain may be clustered on a specific  $\beta$ -sheet of this domain, indicative of the position of the binding surface.

---

\* V896M putative disease-modifying factor.

The mapping of the positions of HCM-causing missense mutations in the C3 domain of cMyBPC revealed that the R502Q, R502W and  $\Delta$ K504 HCM-causing missense mutations (Niimura et al., 1998; Richard et al., 2003) all occur in  $\beta$ -strand D of this IgC2 domain, while the G507R HCM-causing mutation (sections III.1.2.5 and IV.1.5) (Erdmann et al., 2001) occurs in  $\beta$ -strand E of this domain (figure IV.13). As these four mutations all cluster in a small portion of the four-stranded  $\beta$ -sheet, consisting of  $\beta$ -strands A, B, D and E (ABDE- $\beta$ -sheet), it can be assumed that these four mutations may affect the same binding surface, which may be involved in the C3:C10 interaction.

The G523W and E542Q HCM-causing mutations (Carrier et al., 1997; Erdmann et al., 2003) were, however, found to be located in the F and G  $\beta$ -strands, respectively (figure IV.13). As the F and G  $\beta$ -strands, together with the  $\beta$ -strand C, form the three-stranded  $\beta$ -sheet (CFG- $\beta$ -sheet) in IgC2 domains, it is unlikely that the G523W and E542Q HCM-causing mutations would affect the same protein binding-site as the R502Q, R502W,  $\Delta$ K504 and G507R mutations (figure IV.13). As the G523W and E542Q mutations are also in close proximity to each other, the possibility that the C10 binding-site is located on the CFG- $\beta$ -sheet cannot be excluded.

The R495Q HCM-causing missense mutation (Niimura et al., 1998) was found to be located in the loop region that separates the C and D  $\beta$ -strands and is unlikely to directly affect protein binding-sites. This mutation may, however, have its pathogenic effect by disrupting the overall structure of the C3 IgC2 domain.

In summary, therefore, most of the missense mutations in the C3 domain of cMyBPC were found in one of two clusters on the ABDE- and CFG- $\beta$ -sheets, indicating that both these  $\beta$ -sheets may be involved in protein:protein interactions. In this study, the C10 domain of cMyBPC was identified as

a ligand of the C3 domain in candidate-ligand Y2H-assays, while the identity of a putative second ligand, binding to the second binding-site, was not determined. It is also not possible to predict which of the two  $\beta$ -sheets contains the C10 binding-site.

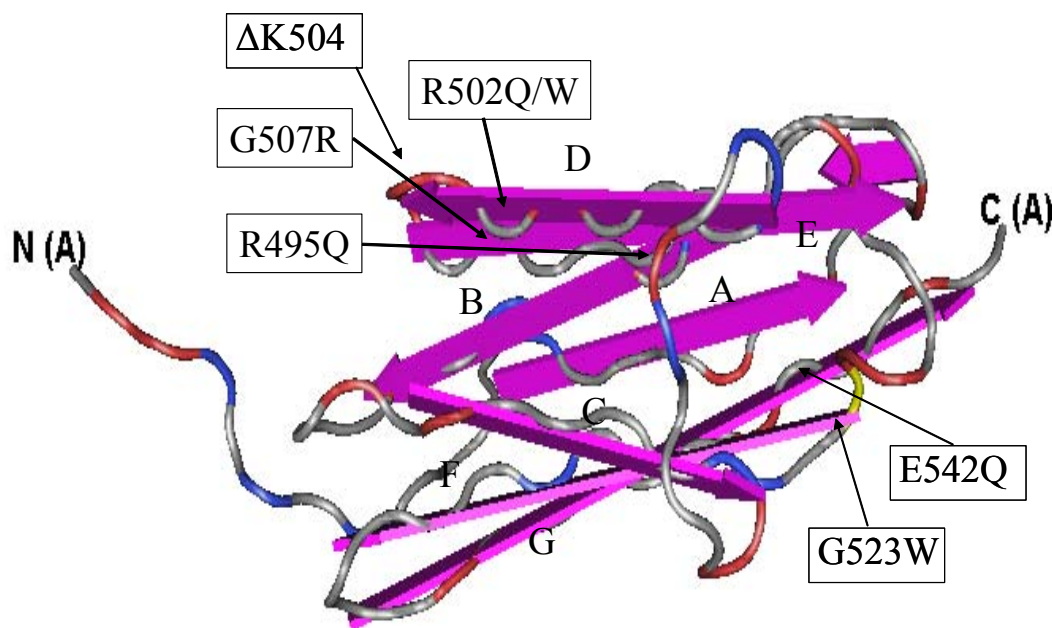


**Figure IV.13. Relative positions of HCM-causing missense mutations in the C3 IgC2 domain of cMyBPC**  
Structure of chain A of telokin, on which the positions corresponding to the positions of HCM-causing missense mutations occurring in the C3 domain of cMyBPC have been indicated. The seven  $\beta$ -strands (indicated as broad purple arrows) constituting an IgC2 domain are labeled A to G, and the N- and C-termini of the domain indicated by N(A) and C(A), respectively (three-dimensional modeling performed using Cn3D version 4.1, available at <http://www.ncbi.nih.gov>).

#### IV.5.2. POSITION OF HCM-CAUSING MISSENSE MUTATIONS IN THE C5 DOMAIN OF cMyBPC

Moolman-Smook et al., (2002) have shown an interaction between the C5 and C8 domains of cMyBPC, which is affected by the presence of the R654H and N755K HCM-causing mutations in the C5 domain (section IV.5 and table IV.1). It was, therefore, postulated that missense mutations in

the C5 domain may be clustered on a specific  $\beta$ -sheet of this domain, indicative of the position of the binding surface.

The mapping of the positions of HCM-causing missense mutations in the C5 domain of cMyBPC revealed that the R668P, and R668H HCM-causing missense mutations (Erdmann et al., 2003; Morner et al., 2003) occur in  $\beta$ -strand B of this IgC2 domain, while the R654H HCM-causing mutation (Moolman-Smook et al., 1998) occurs in  $\beta$ -strand A of this domain (figure IV.14). As these three mutations all cluster in the four-stranded  $\beta$ -sheet, consisting of  $\beta$ -strands A, B, D and E (ABDE- $\beta$ -sheet) (figure IV.14) (three-dimensional modeling performed using Cn3D version 4.1, available at: <http://www.ncbi.nih.gov>), it can be speculated that this  $\beta$ -sheet contains the binding surface for the C8 domain of cMyBPC, as the R654H HCM-causing mutation was shown to decrease the affinity of the C5 domain for the C8 domain (Moolman-Smook et al., 2002). The N755K HCM-causing missense mutation (Yu et al., 1998), which was shown to have an even more pronounced effect on the C5:C8 interaction (Moolman-Smook et al., 2002), was, however, found to be located in  $\beta$ -strand F, which together with  $\beta$ -strands C and G form the three-stranded  $\beta$ -sheet (CFG- $\beta$ -sheet) (figures IV.13 and IV.14b).

Structural NMR spectroscopical analysis of the C5 domain of cMyBPC by Idowu et al., (2003), however, indicated that in this domain of cMyBPC, the A  $\beta$ -strand that was predicted to form part of the ABDE- $\beta$ -sheet may, in fact, be shorter than predicted by Cn3D version 4.1 (figure IV.15). Additionally, Idowu et al., (2003) predicted that  $\beta$ -strand A may, in fact, together with  $\beta$ -strands C, F and G, form a  $\beta$ -sheet (ACFG- $\beta$ -sheet), while  $\beta$ -strands B, D and E would form a three-stranded  $\beta$ -sheet (BDE- $\beta$ -sheet) that would form the opposite surface of the domain (figure IV.14).

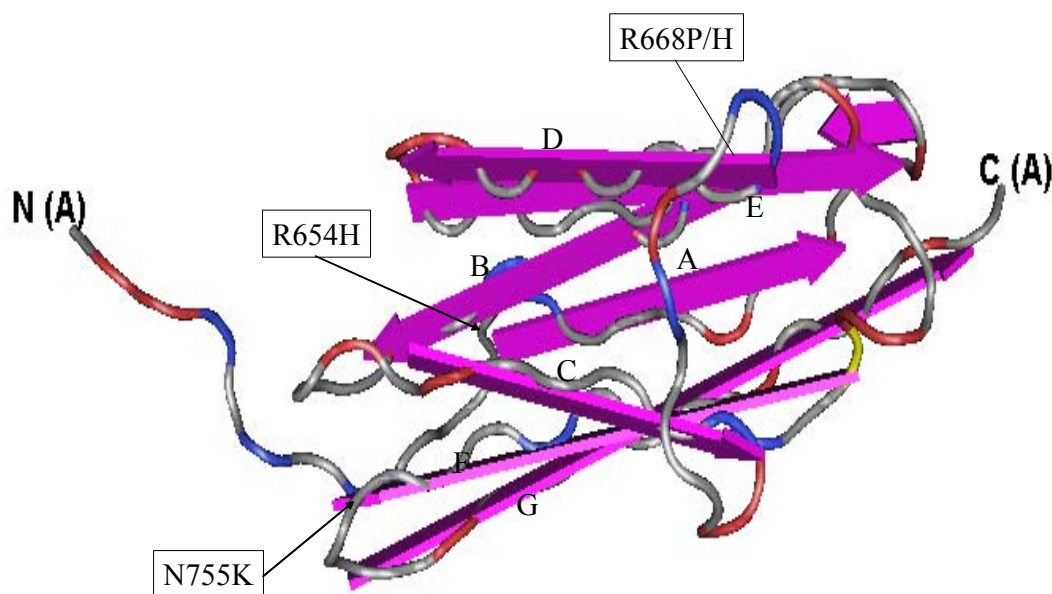


**Figure IV.14. Relative positions of HCM-causing missense mutations in the C5 IgC2 domain of cMyBPC**  
 Structure of chain A of telokin, on which the positions corresponding to the positions of HCM-causing missense mutations occurring in the C5 domain of cMyBPC have been indicated. The seven  $\beta$ -strands (indicated as broad purple arrows) constituting an IgC2 domain are labeled A to G, and the N- and C-termini of the domain indicated by N(A) and C(A), respectively (three-dimensional modeling performed using Cn3D version 4.1, available at <http://www.ncbi.nih.gov>).

In this conformation of the C5 domain, the R654H HCM-causing missense mutation would be located in the region N-terminal of  $\beta$ -strand A, on, or near to, the ACFG- $\beta$ -sheet (figure IV.15a) (Idowu et al., 2003). In this arrangement, the R654H and N755K HCM-causing missense mutations would both be located on the ACFG- $\beta$ -sheet, while the R668P and R668H mutations would be on the BDE- $\beta$ -sheet, indicating two possible binding surfaces of the C8 domain (figure IV.15a).

Idowu et al., (2003), however, also showed that the N755K HCM-causing missense mutation results in a total destabilisation of the C5 domain, indicating that this mutation may have a deleterious

effect, without directly affecting the C8 binding-surface. It is intriguing to note that if, indeed, the three-dimensional structure of the C5 domain as predicted using Cn3D version 4.1, rather than that predicted by Idowu et al., (2003), is correct, the R668P, R668H and R654H HCM-causing missense mutations would all be located on the surface of the ABDE- $\beta$ -sheet, which may contain the C8 binding-site (figures IV.13 and IV.14b). This scenario would provide an elegant mechanism through which missense mutations in domain C5 could affect the binding of the C8 domain, as R668P, R668H and R654H could all directly alter the C8 binding-surface, while the N755K mutation could affect the C5:C8 interaction by destabilising the C5 domain.

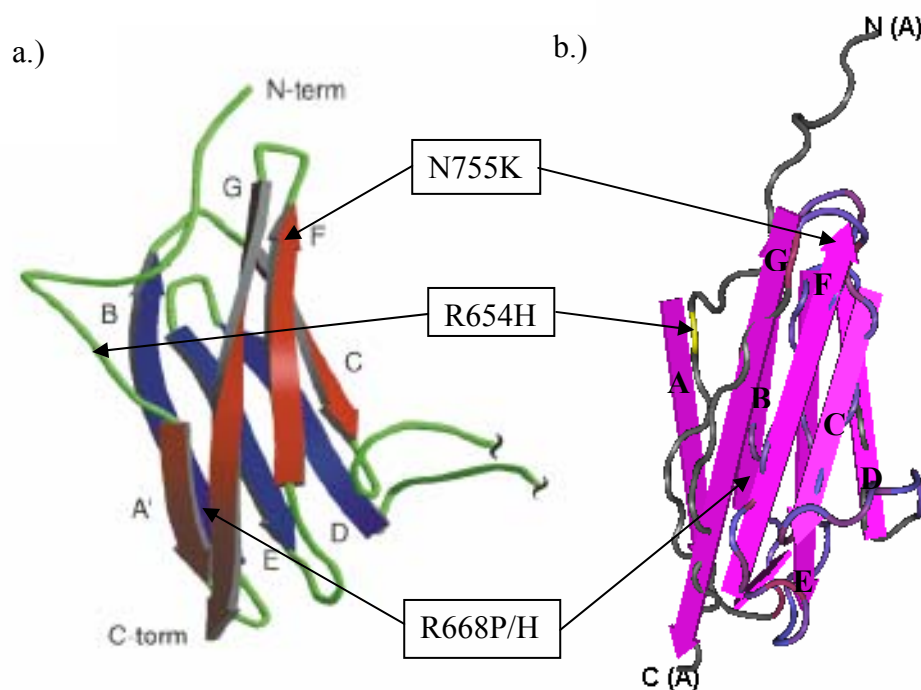


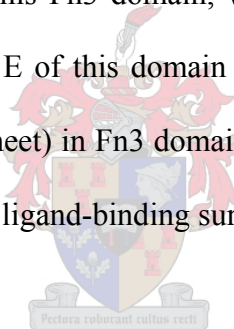
**Figure IV.15. Proposed three-dimensional structures of domain C5 of cMyBPC**

a) Three-dimensional structure of the C5 domain of cMyBPC as predicted by Idowu et al., (2003); b) three-dimensional structure of the C5 domain of cMyBPC based on the structure of chain A of telokin by Cn3D version 4.1. The relative positions of HCM-causing missense mutations in the C5 domain of cMyBPC are shown in both figures. Broad arrows =  $\beta$ -strands; a) from Idowu et al., 2003); b) three-dimensional modeling performed using Cn3D version 4.1, available at <http://www.ncbi.nih.gov>.

### IV.5.3. POSITION OF HCM-CAUSING MISSENSE MUTATIONS IN THE C6 DOMAIN OF cMyBPC

Based on the cMyBPC trimeric “tight collar” model, it was speculated that the C6 domain of cMyBPC may interact with the C9 domain of cMyBPC (section IV.5 and table IV.1). Furthermore, it was postulated that missense mutations in the C6 domain may be clustered on a specific  $\beta$ -sheet of this domain, which may be indicative of the position of the binding surface.

The mapping of the positions of HCM-causing missense mutations in the C6 domain of cMyBPC revealed that the R811K and  $\Delta$ K812 HCM-causing mutations (Jaaskelainen et al., 2002; Richard et al., 2003) both occur in  $\beta$ -strand D of this Fn3 domain, while the R820Q HCM-causing mutation (Konno et al., 2003) occurs in  $\beta$ -strand E of this domain (figure IV.16). As  $\beta$ -strands D, E and G form a three-stranded  $\beta$ -sheet (DEG- $\beta$ -sheet) in Fn3 domains, it is possible that these mutations may share a pathological effect by affecting a ligand-binding surface located on this  $\beta$ -sheet.



The A833V and A833T HCM-causing missense mutations (Richard et al., 2003; Erdmann et al., 2003; Morner et al., 2003) are located in  $\beta$ -strand F, which together with  $\beta$ -strands B and C, form the second three-stranded  $\beta$ -sheet (BCF) in Fn3 domains (figure IV.16). It is, therefore, also possible that the BCF- $\beta$ -sheet may contain a protein binding surface. As the mutations in the C6 domain do not cluster in one specific  $\beta$ -sheet which may constitute a binding surface, it is not possible to speculate which of these two  $\beta$ -sheets contain the putative C9-binding surface.

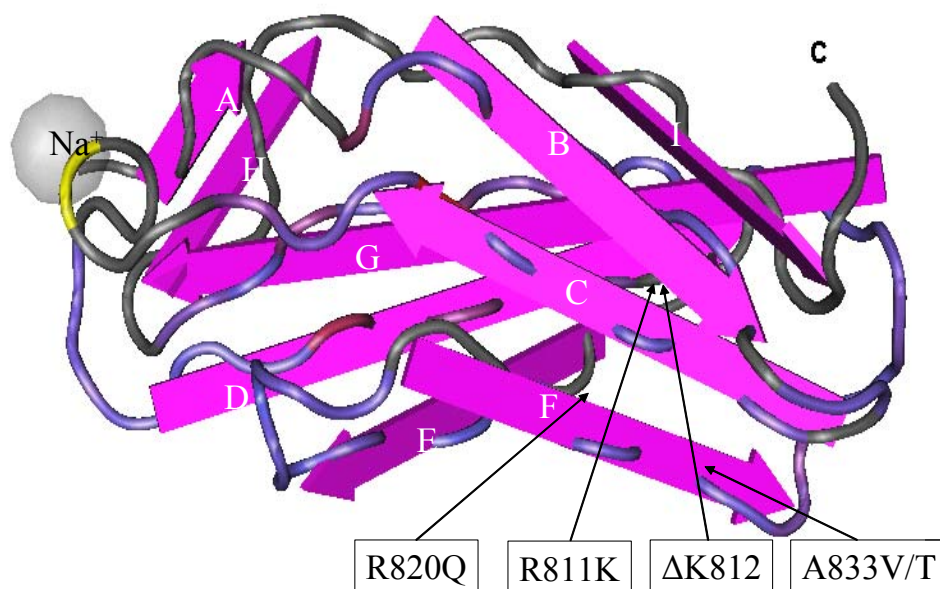


**Figure IV.16. Relative positions of HCM-causing missense mutations in the C6 Fn3 domain of cMyBPC**

Structure of the consensus sequence of Fn3 domains, on which the positions corresponding to the positions of HCM-causing missense mutations occurring in the C6 domain of cMyBPC have been indicated. The nine  $\beta$ -strands (indicated as broad purple arrows) constituting a Fn3 domain are labeled A to H, and the C-terminus of the domain indicated by C (three-dimensional modeling performed using Cn3D version 4.1, available at <http://www.ncbi.nih.gov>).

#### **IV.5.4 POSITION OF THE V896M PUTATIVE DISEASE-MODIFYING FACTOR IN THE C7 DOMAIN OF cMyBPC**

Based on the finding that the V896M putative disease-modifying factor affects the C7:C10 and C7:titin interactions, it was postulated that the position of this mutation may facilitate the identification of the binding surfaces of these two ligands of the C7 domain (sections III.3.4.3, IV.5 and figure III.43).

The V896M putative disease-modifying factor (Moolman-Smook et al., 1999; Jaaskelainen et al., 2002; Morner et al., 2003; Richard et al., 2003) was, however, found to be located in the loop

separating the C and D  $\beta$ -strands in the C7 Fn3 domain (figure IV.17). It is, therefore, postulated that V896M would affect the overall structure of this domain, thereby altering its interaction with both C10 and titin, rather than affecting a specific binding surface, a finding that is supported by CoIP analysis that showed that the presence of V896M in the C7 domain significantly weakens its interactions with both C10 and titin.

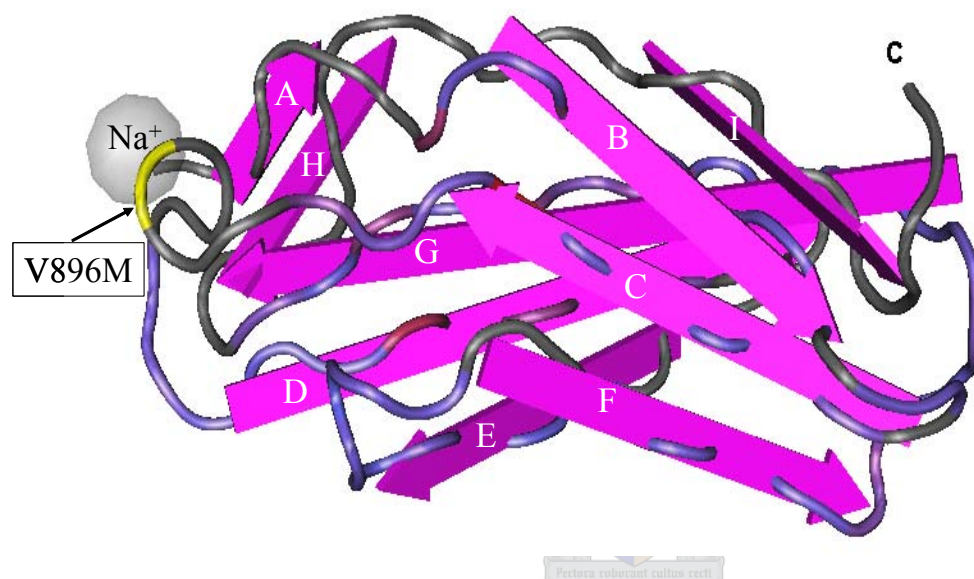


**Figure IV.17. Relative positions of the V896M putative disease-modifying factor in the C7 Fn3 domain of cMyBPC**

Structure of the consensus sequence of Fn3 domains, on which the position corresponding to position 896 in domain C7 of cMyBPC, affected by the V896M putative disease-modifying factor, has been indicated. The nine  $\beta$ -strands (indicated as broad purple arrows) constituting a Fn3 domain are labeled A to H, and the C-terminus of the domain indicated by C (three-dimensional modeling performed using Cn3D version 4.1, available at <http://www.ncbi.nih.gov>).

#### **IV.5.5 POSITION OF HCM-CAUSING MISSENSE MUTATIONS IN THE C8 DOMAIN OF cMyBPC**

Moolman-Smook et al., (2002) have shown an interaction between the C5 and C8 domains of cMyBPC, which was affected by the presence of the R654H and N755K HCM-causing mutations in the C5 domain (section IV.5 and table IV.1). It was, therefore, postulated that missense mutations in the C8 domain may be clustered on a specific  $\beta$ -sheet of this domain, indicative of the position of the C5 domain binding surface.

The mapping of the positions of HCM-causing missense mutations in the C8 domain of cMyBPC revealed that the R1002Q and E1017K HCM-causing mutations (Niimura et al., 2002; Barr et al., unpublished data available at: [http://genetics.med.harvard.edu/~seidman/cg3/muts/MYBPC3\\_mutations\\_TOC.html](http://genetics.med.harvard.edu/~seidman/cg3/muts/MYBPC3_mutations_TOC.html)) occur in the loops connecting  $\beta$ -strands B and C, and  $\beta$ -strands C and D, respectively (figure IV.18). As neither of these mutations occur in either the three- or four-stranded  $\beta$ -sheets, it is likely that they would affect the overall structure of the C8 IgC2 domain, rather than specifically affecting the C5 binding surface.

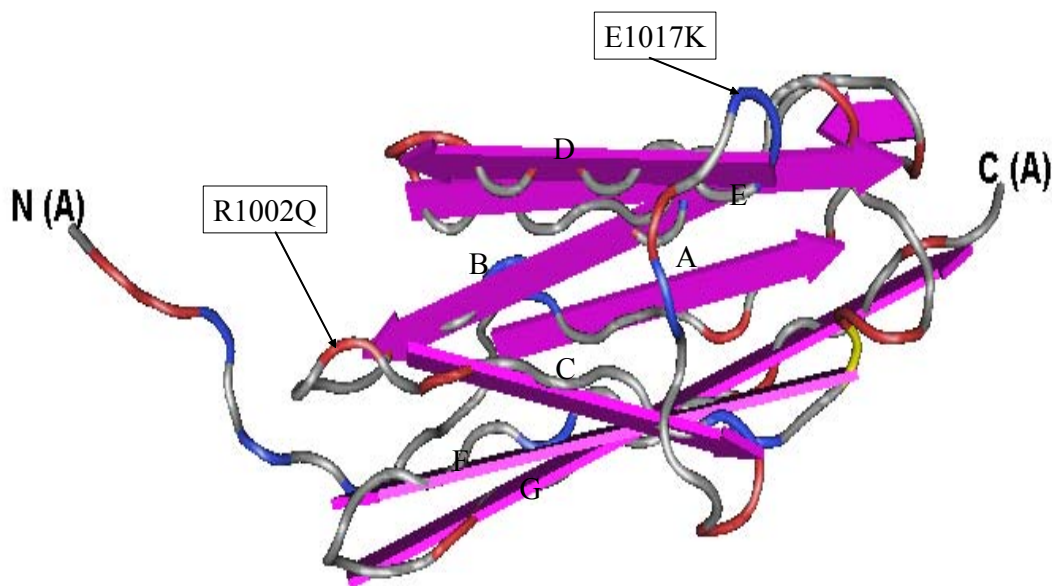


**Figure IV.18. Relative positions of HCM-causing missense mutations in the C8 IgC2 domain of cMyBPC**  
 Structure of chain A of telokin, on which the positions corresponding to the positions of HCM-causing missense mutations occurring in the C8 domain of cMyBPC have been indicated. The seven  $\beta$ -strands (indicated as broad purple arrows) constituting an IgC2 domain are labeled A to G, and the N- and C-termini of the domain indicated by N(A) and C(A), respectively (three-dimensional modeling performed using Cn3D version 4.1, available at <http://www.ncbi.nih.gov>).

#### **IV.5.6 POSITION OF THE V1115I HCM-CAUSING MISSENSE MUTATION IN THE C9 DOMAIN OF cMyBPC**

Based on the cMyBPC trimeric “tight collar” model, it was speculated that the C6 domain of cMyBPC may interact with the C9 domain of cMyBPC (section IV.5 and table IV.1). Furthermore, it was postulated that the position of the V1115I (Erdmann et al., 2001) HCM-causing missense mutation in the C9 domain may be indicative of the position of the C6 binding-site.

The mapping of the position of the V1115H HCM-causing missense mutation (Erdmann et al., 2001) in the C9 domain of cMyBPC revealed that this mutation was located in  $\beta$ -strand E, which, together

with  $\beta$ -strands D and G, forms the three-stranded EDG- $\beta$ -sheets of Fn3 domains (figure IV.19). Even though it is tempting to speculate that this finding may be indicative of the position of the C6 binding-site on the EDG  $\beta$ -sheet, caution should be taken, as this assumption is made based solely on the position of a single HCM-causing missense mutation.

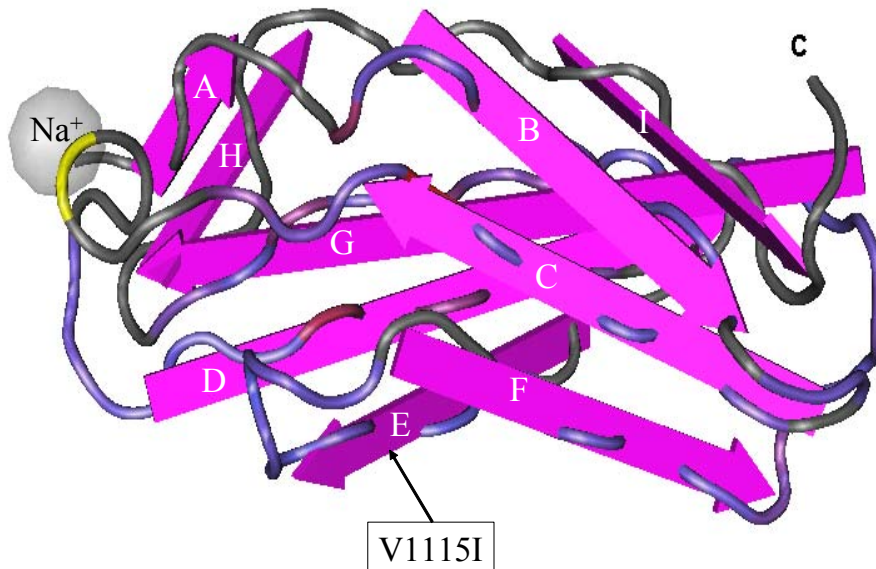


**Figure IV.19. Relative position of the V1115I HCM-causing missense mutation in the C9 Fn3 domain of cMyBPC**

Structure of the consensus sequence of Fn3 domains, on which the position corresponding to position 1115 in the C9 Fn3 domain of cMyBPC, at which the V1115I HCM-causing missense mutation occurs, has been indicated. The nine  $\beta$ -strands (indicated as broad purple arrows) constituting a Fn3 domain are labeled A to H, and the C-terminus of the domain indicated by C (three-dimensional modeling performed using Cn3D version 4.1, available at <http://www.ncbi.nih.gov>).

#### IV.5.7 POSITION OF HCM-CAUSING MISSENSE MUTATIONS IN THE C10 DOMAIN OF cMyBPC

Previous studies have shown that the C10 domain of cMyBPC interacts with LMM (Okagaki et al., 1993; Miyamoto et al., 1999; Welikson and Fischman, 2002) and it has also been implicated in the binding of C-zone titin (Freiburg and Gautel, 1996).

Additionally, it was found that this domain of cMyBPC is also able to interact with the C7 domain in the cMyBPC “tight collar” conformation and with domain C3 in the cMyBPC “loose” collar conformation. It was postulated that the positions of HCM-causing missense mutations in this domain may allow insights into the positions of the binding-sites of these ligands on the C10 domain, as they may disrupt ligand-binding.

The mapping of the positions of HCM-causing missense mutations in the C10 domain of cMyBPC revealed that the A1194T HCM-causing missense mutation (Richard et al., 2003) is located in the loop connecting  $\beta$ -strands A and B (figure IV.20). The A1255T HCM-causing missense mutation (Richard et al., 2003) was found to be located in  $\beta$ -strand F, which, together with  $\beta$ -strands C and G, form the three-stranded CFG- $\beta$ -sheet in IgC2 domains (figure IV.20).

As A1194T is located in a loop connecting  $\beta$ -strands A and B, both of which form part of the four-stranded ABDE- $\beta$ -sheet in IgC2 domains, it is possible that this mutation could alter the structure of this  $\beta$ -sheet, thus disrupting the binding-site of one of the ligands of the C10 domain which may be located on this  $\beta$ -sheet. The finding that the A1255T mutation is located in the three-stranded CFG- $\beta$ -sheet may indicate that this  $\beta$ -sheet may also be involved in ligand-binding.

In order to establish which of the  $\beta$ -sheets of the C10 domain is most likely to contain the binding-site of the C7 domain, the relative position of the 39 amino acid residue partial C10 peptide, identified as the ligand of the C7 domain of cMyBPC in the C7 Y2H library-assay (sections III.3.2.4 and IV.2), was mapped on the three-dimensional structure of chain A of telokin (figure IV.21). This revealed that the partial C10 peptide which was found to interact with domain C7, consisted of  $\beta$ -strands E, F and G.  $\beta$ -strands F and G, together with  $\beta$ -strand C, constitute the three-stranded CFG- $\beta$ -

sheet, while  $\beta$ -strand E forms part of the four-stranded ABDE- $\beta$ -sheet in IgC2 domains. As two strands (F and G) of the three-stranded CFG- $\beta$ -sheet were present in the partial C10 peptide, combined with the fact that its tertiary structure may be stabilised by the presence of  $\beta$ -strand E, it was postulated that the C7 binding-site was likely to be located on the three-stranded CFG- $\beta$ -sheet (figures IV.19 and IV.20). It is, therefore, possible that the A1255T mutation in  $\beta$ -strand F may adversely affect the C7:C10 interaction.

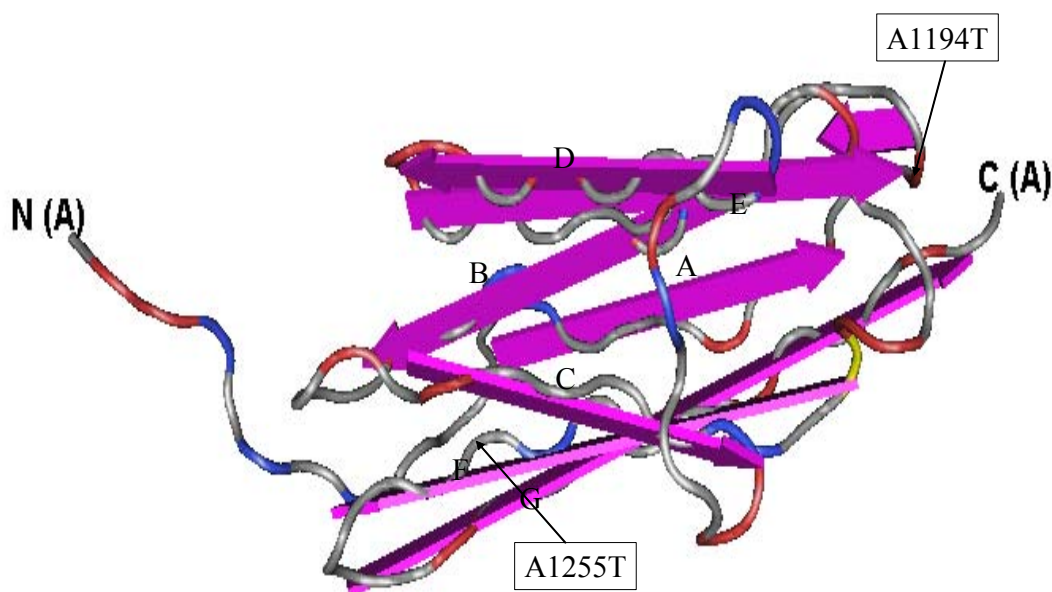


**Figure IV.20. Relative positions of HCM-causing missense mutations in the C10 IgC2 domain of cMyBPC**  
Structure of chain A of telokin, on which the positions corresponding to the positions of HCM-causing missense mutations occurring in the C10 domain of cMyBPC have been indicated. The seven  $\beta$ -strands (indicated as broad purple arrows) constituting an IgC2 domain are labeled A to G, and the N- and C-termini of the domain indicated by N(A) and C(A), respectively (three-dimensional modeling performed using Cn3D version 4.1, available at <http://www.ncbi.nih.gov>).

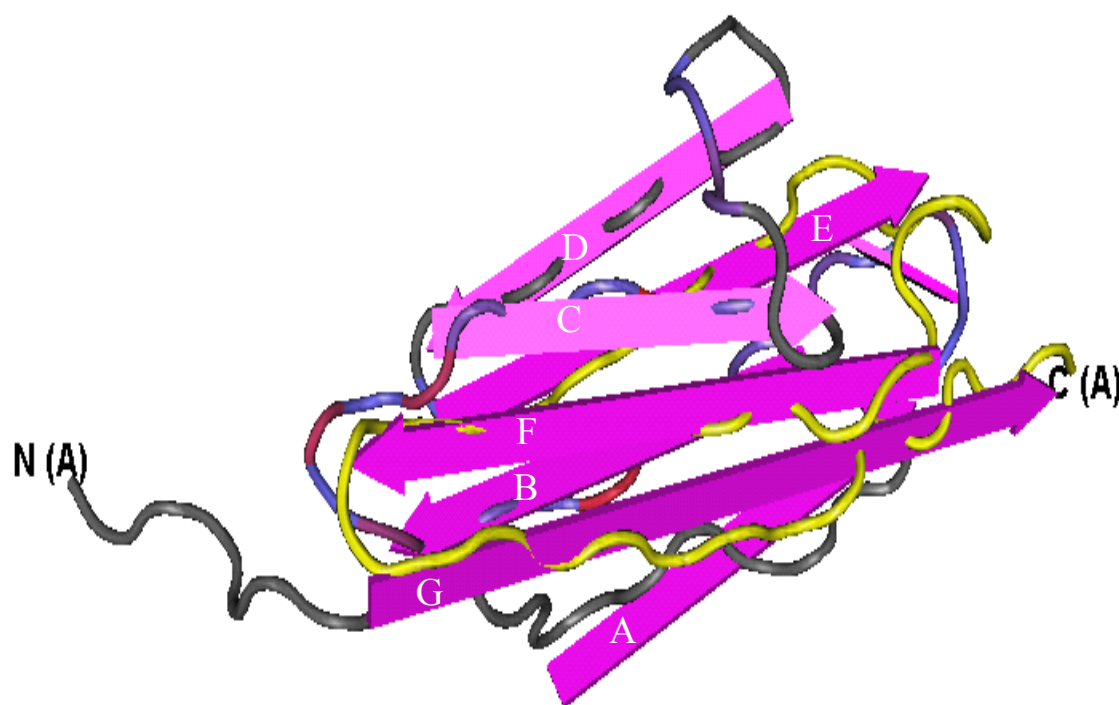


**Figure IV.21. Proposed structure of the partial C10 domain identified as the ligand of the C7 domain**

Structure of chain A of telokin, on which the position corresponding to the 39 amino acid residue partial C10 peptide, identified as the ligand of the C7 domain of cMyBPC in the C7 Y2H library-assay, has been highlighted in yellow. The seven  $\beta$ -strands (indicated as broad purple arrows) constituting an IgC2 domain are labeled A to G, and the N- and C-termini of the domain indicated by N(A) and C(A), respectively (three-dimensional modeling performed using Cn3D version 4.1, available at <http://www.ncbi.nih.gov>).

## IV.6. CONCLUDING REMARKS

The screening of *MYBPC3* in a South African HCM-affected population led to the identification of two novel putative disease-causing mutations that result in the truncation of cMyBPC ( $\Delta$ c13255 and ex7 SaS+1 g>a), as well as two missense mutations, previously described as being HCM-causing (G278E and G507R) (Erdmann et al., 2001; Richard et al., 2003). The data generated in the present study, in combination with that presented by Erdmann et al., (2001), suggests that G507R is indeed an HCM-causing mutation, and that this mutation may be associated with early-onset HCM,

pronounced LVH and an increased risk of SCD. The finding that G278E occurred at a significant frequency in a control population, however, suggests that it is, in all likelihood, a disease-modifying factor, rather than a main-locus HCM-causing mutation. Similarly, V896M, which was described as a putative HCM-causing mutation in the present study (Moolman-Smook et al., 1999), was subsequently found in control populations in other studies (Jaaskelainen et al., 2002; Morner et al., 2003; Richard et al., 2003), indicating that V896M may also be either a polymorphism or a disease-modifying factor, rather than a main-locus HCM-causing mutation.

Based on the identification of V896M in the C7 domain of cMyBPC, combined with the fact that previous studies have implicated this domain as being functionally important (section I.7.3.3), it was postulated that this domain of cMyBPC may be involved in, as yet unidentified, protein:protein interactions. Subsequent Y2H-assays allowed the identification of the C10 domain of cMyBPC and specific domains of C-zone titin as ligands of this domain. This finding, in combination with Y2H results generated by Dr Hanlie Moolman-Smook in our laboratory, allowed the development of a novel model of cMyBPC quaternary structure in which cMyBPC trimerises to form a “tight collar” around the thick filament backbone, when cMyBPC is in its unphosphorylated state. This model has allowed new insights into the functioning of this protein in both in health and disease (Moolman-Smook et al., 2002). This model was subsequently refined to include not only the quaternary structure of cMyBPC, but an integrated model of thick filament quaternary structure based on the curved crystalline layer model of the myosin filament.

Additionally, the identification of the G507R putative HCM-causing mutation in the C3 domain of cMyBPC indicated that this domain, to which no function had previously been ascribed, may also be of functional importance. The subsequent identification of the C10 domain of cMyBPC as a ligand of

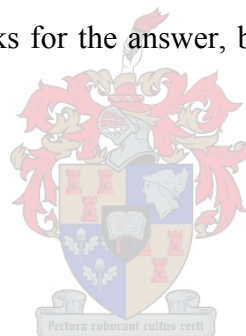
the C3 domain in Y2H-assays allowed the development of a novel integrated model of cMyBPC and thick filament quaternary structure. In this model, cMyBPC forms a trimeric “loose collar” around the thick filament backbone following PKA-dependent phosphorylation of cMyBPC.

Together, the development of these models of cMyBPC quaternary structures has allowed new insights into the mechanisms through which cMyBPC regulates thick filament structure and cardiac contractility, following  $\beta$ -adrenergic stimulation. Additionally, it was found that HCM-causing mutations in the C5 domain of cMyBPC (Moolman-Smook et al., 2002), and the V896M putative disease-modifying factor in the C7 domain, weaken interactions that are thought to stabilise the cMyBPC trimeric “tight collar” conformation. These findings have led to the development of a unifying hypothesis, namely, that cMyBPC HCM-causing mutations and disease-modifying factors, whether missense or truncation, result in the destabilisation of the cMyBPC “tight collar” conformation, thus favouring the formation of “expanded” thick filaments in the absence of  $\beta$ -adrenergic stimulation. The preferential formation of “expanded” thick filaments in cMyBPC mutation carriers, in turn, may result in altered cardiac contractility, impaired diastolic function, ATP wastage and altered  $\text{Ca}^{2+}$  homeostasis, features which are all associated with HCM.

In order to test this hypothesis, future biochemical studies are required to establish the effect of HCM-causing mutations on interactions that are postulated to stabilise the cMyBPC “tight” and “loose collar” conformations.

**“I was grading exams, and a student referred to the components of a two hybrid screen as  
“bait” and “pray”.” David Stillman**

Having worked with the yeast two-hybrid system for the last four years, it is my opinion that not only does this student deserve full marks for the answer, but deserves bonus marks for insights far beyond his/her experience!



# APPENDIX A

## 1. DNA EXTRACTION SOLUTIONS

### Cell lysis buffer

Sucrose (Merck)	0.32M
Triton X-100 (Merck)	1%
MgCl <sub>2</sub> (Merck)	5mM
Tris-HCl pH 8.0 (Biorad)	10mM
ddH <sub>2</sub> O to 1 litre	

### 3M NaAc

NaAc.3H <sub>2</sub> O (Merck)	40.81g
ddH <sub>2</sub> O	50ml

Adjust pH to 5.2 with glacial acetic acid (Merck) and adjust volume to 100ml with ddH<sub>2</sub>O.

### Na-EDTA solution

NaCl (Merck)	18.75ml of 4M stock solution
EDTA (B&M Scientific)	250ml of a 100mM stock solution
Mix well.	



### Phenol/Chloroform

Phenol (saturated with 1x TE) (Merck)	50ml
Chloroform (Merck)	48ml
8-Hydroxiquinoline (Merck)	2ml
Mix well, store at 4°C.	

### Chloroform/octanol (24:1)

Chloroform (Merck)	96ml
Octanol (Merck)	4ml
Mix well, store at 4°C.	

10x TE stock solution

Tris-HCl (Biorad)	0.1M (pH 8.0)
EDTA (Biorad)	0.01M (pH 8.0)

**2. RNA EXTRACTION SOLUTIONS**0.2% DEPC water (RNase treatment of surfaces and equipment)

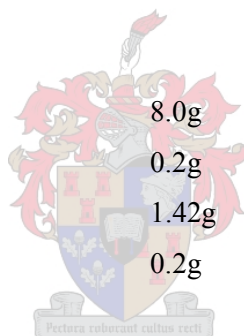
Diethylpyrocarbonate (DEPC)	2ml
ddH <sub>2</sub> O to a final volume of 1 litre	

0.2% DEPC water (reaction use)

Diethylpyrocarbonate (DEPC)	2ml
ddH <sub>2</sub> O to a final volume of 1 litre	
Autoclave to inactivate DEPC	

PBS buffer

NaCl	8.0g
KCl	0.2g
Na <sub>2</sub> HPO <sub>4</sub> ·2H <sub>2</sub> O	1.42g
KH <sub>2</sub> PO <sub>4</sub>	0.2g
ddH <sub>2</sub> O to a final volume of 1 litre	

RNA-Denaturing Solution

Guanidinium Thiocyanate	250g
ddH <sub>2</sub> O	293ml
0.75M Sodium Citrate	17.6ml
10% Sodium Sarcosyl	26.4ml

This stock solution was stored in the dark for up to three months, 360 µl β-mercaptoethanol per 50ml stock solution should be added just prior to use

**3. BACTERIAL PLASMID PURIFICATION SOLUTIONS:**Cell Resuspension Solution:

50mM Tris-HCL, pH 7.5	2.5ml 1M Tris
10mM EDTA	1ml 0.5M EDTA
ddH <sub>2</sub> O to a final volume of 50ml	

Cell Lysis solution:

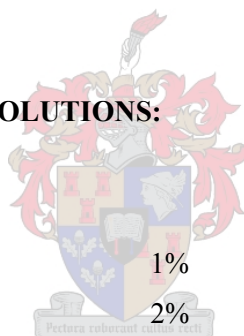
0.2M NaOH	2.5ml 4M NaOH
1% SDS	5ml
ddH <sub>2</sub> O to a final volume of 50ml	

Neutralization solution

1.32M KOAc, pH 4.8	13.2ml 5M KOAc
ddH <sub>2</sub> O to a final volume of 50ml	

**4. YEAST PLASMID PURIFICATION SOLUTIONS:**Yeast lysis buffer

SDS	1%
Triton X-100	2%
NaCl	100mM
Tris (pH 8)	10mM
EDTA (pH 8)	1mM

**5. ELECTROPHORESIS STOCK SOLUTIONS**10% Ammonium persulphate

Ammonium persulphate (Merck)	10g
ddH <sub>2</sub> O	10ml
Mix well and store at 4°C	

10x TBE stock solution

Tris base (Biorad)	108g
Boric Acid (Merck)	58g
Na <sub>2</sub> EDTA (Merck)	9.3g
ddH <sub>2</sub> O to a final volume of 1 litre	

50x TAE stock solution

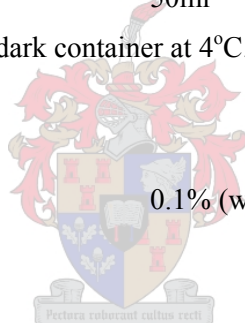
Tris base	242g
Acetic acid (glacial)	57.1ml
Na <sub>2</sub> EDTA	37.2g
ddH <sub>2</sub> O to a final volume of 1 litre	

Ethidium bromide

Ethidium bromide (Sigma)	500mg
ddH <sub>2</sub> O	50ml
Stir well on magnetic stirrer for 4h, store in dark container at 4°C.	

Bromophenol blue loading dye

Bromophenol blue	0.1% (w/v)
ddH <sub>2</sub> O to a final volume of 100ml	
store in dark at 4°C	

SSCP loading dye

Bromophenol blue	0.1% (w/v)
Xylene cyanol	0.1% (w/v)
Formamide	95% (v/v)
NaOH	10mM (w/v)
EDTA	20mM (w/v)
ddH <sub>2</sub> O to a final volume of 100ml	
store in dark at 4°C	

## 6. MOLECULAR SIZE MARKERS

### $\lambda$ Pst molecular size marker

Bacteriophage Lambda genomic DNA	200 $\mu$ l
<i>Pst</i> I Restriction enzyme	3 $\mu$ l (30U)
Promega buffer H	30 $\mu$ l
ddH <sub>2</sub> O to a final volume of 300 $\mu$ l	

Incubate at 37°C for 3h, heat inactivate enzyme at 65°C for 10min. Use 1 $\mu$ l of digestion product on polyacrylamide gels, or 3 $\mu$ l on ethidium bromide stained agarose gels.

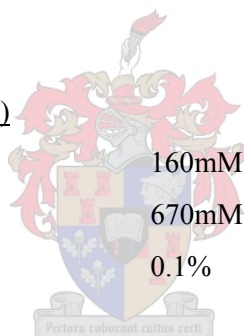
Fragment Sizes:

11497bp, 5077bp, 4507bp, 2838bp, 2560bp, 2459bp, 2443bp, 2140bp, 1986bp, 1700bp, 1159bp, 1093bp, 805bp, 514bp, 468bp, 448bp, 339bp, 264bp, 247bp, 211bp, 200bp, 164bp, 150bp, 94bp, 87bp, 72bp

## 7. PCR BUFFER

### 10x NH<sub>4</sub> PCR Reaction Buffer (Bioline, UK)

(NH <sub>4</sub> ) <sub>2</sub> SO <sub>4</sub>	160mM
Tris-HCl	670mM pH 8.8(25°C),
Tween 20	0.1%



## 7. SILVER STAINING SOLUTIONS

### 0.1% AgNO<sub>3</sub>

AgNO <sub>3</sub>	1g
ddH <sub>2</sub> O to a final volume of 1 litre	

### Developing solution

BaBH <sub>4</sub>	0.1g
NaOH	15g
Formaldehyde	4ml
ddH <sub>2</sub> O to a final volume of 1 litre	

## 8. SOLUTIONS USED FOR THE ESTABLISHMENT OF EBV TRANSFORMED CELL LINES

### EBV-medium

RPMI 1640

FCS 15%

## 9. SOLUTIONS USED FOR THE ESTABLISHMENT BACTERIAL COMPETENT CELLS

### CAP-buffer

CaCl<sub>2</sub> 2.21g

Glycerol 37.5ml

PIPES 0.76g

ddH<sub>2</sub>O to a final volume of 250ml

Adjust pH to 7.0, store at 4°C

## 10. SSCP SOLUTIONS AND METHODOLOGY

### *Solutions*

#### 8% Mildly denaturing SSCP gel

40% Acrylamide-bisacrylamide (37.5:1) stock solution 32ml [8% (v/v)]

Urea 24g [15% (w/v)]

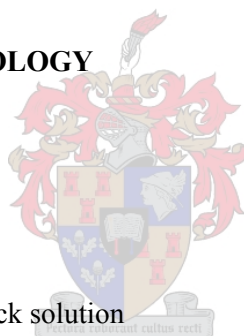
Glycerol 8ml [5% (v/v)]

10xTBE buffer stock solution 8ml [1x (v/v)]

ddH<sub>2</sub>O 92ml

Ammonium persulphate 1.6ml [0.1% (w/v)]

TEMED 160µl [0.01% (v/v)]



10% Mildly denaturing SSCP gel

40% Acrylamide-bisacrylamide (37.5:1) stock solution	40ml [8% (v/v)]
Urea	24g [15% (w/v)]
Glycerol	8ml [5% (v/v)]
10xTBE buffer stock solution	8ml [1x (v/v)]
ddH <sub>2</sub> O	81ml
Ammonium persulphate	1.6ml [0.1% (w/v)]
TEMED	160µl [0.01% (v/v)]

***Methodology***

Glass plates were prepared by carefully and meticulously washing both plates with detergent. Any traces of detergent were subsequently removed by wiping the plates with 70% ethanol, and drying them thoroughly. The notched plate was then silanised with Wynn's C-thru windshield rain dispersant (Wynn Oil S.A. Ptd Ltd, SA) to allow the gel to remain stuck to the large plate upon dismantling after electrophoresis. More 70% ethanol was then sprayed on the inner surface of the large glass plate. A sheet of Gelbond™ (BMA, Rockland, ME, USA), cut to the same size as the large glass plate, was placed, hydrophobic side down, on this plate, taking care not to remove the protective sheet of paper from the hydrophilic side of the Gelbond™ membrane (BMA, Rockland, ME, USA). Air bubbles trapped between the Gelbond™ and the glass were removed by careful rubbing over the protective sheet of paper with a piece of paper towel. Subsequently this sheet of paper was removed from the Gelbond™ membrane and spacers of 1mm thickness were placed lengthwise at the edges of the large plate, and the notched plate placed silanised side-down on top of the spacers. This assembly was subsequently sealed with the use of a rubber boot (S2 casting boot, Life™ Technologies) and gel poured with the glass assembly slanted at a slight angle. The glass assembly was subsequently layed down horizontally and a square-tooth well-forming comb inserted. The gel was allowed to set for 1-2 hours.

## 11. POLYACRYLAMIDE SEQUENCING GELS SOLUTIONS AND METHODOLOGY

### *Solutions*

#### 5% Denaturing polyacrylamide gel solution

30% Acrylamide stock solution	8.1ml
10x TBE stock solution	6ml
Urea	26.64g
H <sub>2</sub> O	15.45ml

Stir well with a magnetic stirrer until all the urea is dissolved, prior to the addition of:

10% ammonium persulphate	500µl
TEMED	50µl

### *Methodology*

Glass plates were prepared by carefully and meticulously washing both plates with detergent. Any traces of detergent was subsequently removed by wiping the plates with 70% ethanol, and drying them thoroughly. The notched plate was then silanised with Wynn's C-thru windshield rain dispersant (Wynn Oil S.A. Ptd Ltd, SA) to allow the gel to remain stuck to the large plate upon dismantling after electrophoresis. Spacers of 0.4mm thickness were placed lengthwise at the edges of the large plate, and the notched plate placed silanised side-down on top of the spacers. This assembly was subsequently sealed with the use of a rubber boot (S2 casting boot, Life™ Technologies) and gel poured with the glass assembly slanted at a slight angle. The glass assembly was subsequently layed down horizontally and the loading front formed with a top spacer of identical thickness to the lengthwise spacers. The gel was allowed to set for 1-2 hours, whereupon the top spacer was removed and replaced by a sharktooth comb to separate wells for loading samples.

## 12. BACTERIAL MEDIA

### LB-media

Bacto tryptone	5g
Yeast extract	2.5g
NaCl	5g

ddH<sub>2</sub>O to a final volume of 500ml

Autoclave and add appropriate antibiotic to media when a temperature of >55°C is reached (Amp 25mg/l or Kan 5mg/l).

LB-agar plates

Bacto tryptone	5g
Yeast extract	2.5g
NaCl	5g
Bacto agar	8g

ddH<sub>2</sub>O to a final volume of 500ml

Autoclave and add appropriate antibiotic to media when a temperature of >55°C is reached (Amp 25mg/l or Kan 5mg/l), prior to pouring ~20, 90mm plates. These plates were subsequently allowed to set for 2-5h and stored at room temperature for up to three weeks.

M9 agar plates

5x M9 salts	200ml
20% glucose	20ml
Bacto agar	8g
SD <sup>-L</sup> amino acid supplement	0.67g

ddH<sub>2</sub>O to a final volume of 1 litre

Autoclave and add Amp 25mg to media when a temperature of >55°C is reached, prior to pouring ~20, 90mm plates. These plates were subsequently allowed to set for 2-5h and stored at room temperature for up to three weeks.

5x M9 salt solution

Na <sub>2</sub> HPO <sub>4</sub> ·7H <sub>2</sub> O	64g
KH <sub>2</sub> PO <sub>4</sub>	15g
NaCl	2.5g
NH <sub>4</sub> Cl	5g

ddH<sub>2</sub>O to a final volume of 1 litre

**13. YEAST MEDIA**YPDA media

Difco peptone	10g
Yeast extract	10g
Glucose	10g
L-adenine hemisulphate (0.2% stock solution)	7.5ml

ddH<sub>2</sub>O to a final volume of 500ml

Adjust pH to 5.8 and autoclave at 121°C for 15min.

YPDA agar plates

Difco peptone	10g
Yeast extract	10g
Glucose	10g
Bacto agar	10g
L-adenine hemisulfate (0.2% stock solution)	7.5ml

ddH<sub>2</sub>O to a final volume of 500ml

Adjust pH to 5.8, autoclave at 121°C for 15min and allow to cool to a temperature of ~55°C is reached, prior to pouring ~20, 90mm plates. These plates were subsequently allowed to set for 2-5h and stored at room temperature for up to three weeks.

SD<sup>W</sup> media

Glucose	12g
Yeast nitrogen base without amino acids	4g
SD <sup>W</sup> amino acid supplement	0.4g
0.2% adenine hemisulfate	9ml

ddH<sub>2</sub>O to a final volume of 600ml

Adjust pH to 5.8 and autoclave at 121°C for 15min.

SD<sup>W</sup> agar plates

Glucose	12g
Yeast nitrogen base without amino acids	4g
SD <sup>W</sup> amino acid supplement	0.4g
Bacto agar	12g
0.2% adenine hemisulfate	9ml

ddH<sub>2</sub>O to a final volume of 600ml

Adjust pH to 5.8, autoclave at 121°C for 15min and allow to cool to a temperature of ~55°C is reached, prior to pouring ~20, 90mm plates. These plates were subsequently allowed to set for 2-5h and stored at room temperature for up to three weeks.

SD<sup>-L</sup> media

Glucose	12g
Yeast nitrogen base without amino acids	4g
SD <sup>-L</sup> amino acid supplement	0.4g
0.2% adenine hemisulfate	9ml

ddH<sub>2</sub>O to a final volume of 600ml

Adjust pH to 5.8 and autoclave at 121°C for 15min.

SD<sup>-L</sup> agar plates

Glucose	12g
Yeast nitrogen base without amino acids	4g
SD <sup>-L</sup> amino acid supplement	0.4g
Bacto agar	12g
0.2% adenine hemisulfate	9ml

ddH<sub>2</sub>O to a final volume of 600ml

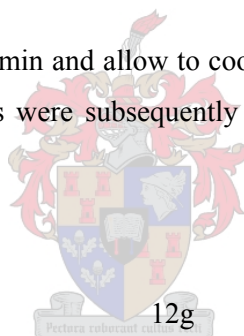
Adjust pH to 5.8, autoclave at 121°C for 15min and allow to cool to a temperature of ~55°C is reached, prior to pouring ~20, 90mm plates. These plates were subsequently allowed to set for 2-5h and stored at room temperature for up to three weeks.

SD<sup>-L-W</sup> media

Glucose	12g
Yeast nitrogen base without amino acids	4g
SD <sup>-L-W</sup> amino acid supplement	0.4g
0.2% adenine hemisulfate	9ml

ddH<sub>2</sub>O to a final volume of 600ml

Adjust pH to 5.8 and autoclave at 121°C for 15min.



SD<sup>-L-W</sup> agar plates

Glucose	12g
Yeast nitrogen base without amino acids	4g
SD <sup>-L-W</sup> amino acid supplement	0.4g
Bacto agar	12g
0.2% adenine hemisulfate	9ml

ddH<sub>2</sub>O to a final volume of 600ml

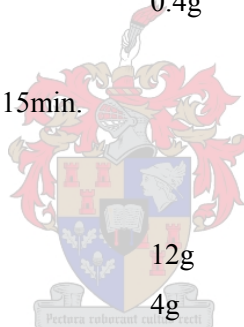
Adjust pH to 5.8, autoclave at 121°C for 15min and allow to cool to a temperature of ~55°C is reached, prior to pouring ~20, 90mm plates. These plates were subsequently allowed to set for 2-5h and stored at room temperature for up to three weeks.

TDO media

Glucose	12g
Yeast nitrogen base without amino acids	4g
SD <sup>-L-W-H</sup> amino acid supplement	0.4g

ddH<sub>2</sub>O to a final volume of 600ml

Adjust pH to 5.8 and autoclave at 121°C for 15min.

TDO agar plates

Glucose	12g
Yeast nitrogen base without amino acids	4g
SD <sup>-L-W-H</sup> amino acid supplement	0.4g
Bacto agar	12g

ddH<sub>2</sub>O to a final volume of 600ml

Adjust pH to 5.8, autoclave at 121°C for 15min and allow to cool to a temperature of ~55°C is reached, prior to pouring ~20, 90mm plates or ~5, 150mm plates. These plates were subsequently allowed to set for 2-5h and stored at room temperature for up to three weeks.

QDO media

Glucose	12g
Yeast nitrogen base without amino acids	4g
SD <sup>-L-W-H-Ad<sup>e</sup></sup> amino acid supplement	0.4g

ddH<sub>2</sub>O to a final volume of 600ml

Adjust pH to 5.8 and autoclave at 121°C for 15min.

QDO agar plates

Glucose	12g
Yeast nitrogen base without amino acids	4g
SD <sup>-L-W-H-Ad<sup>e</sup></sup> amino acid supplement	0.4g
Bacto agar	12g

ddH<sub>2</sub>O to a final volume of 600ml

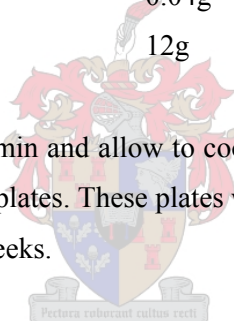
Adjust pH to 5.8, autoclave at 121°C for 15min, allow to cool to a temperature of ~55°C is reached, prior to pouring ~20, 90mm plates. These plates were subsequently allowed to set for 2-5h and stored at room temperature for up to three weeks.

SD<sup>-H-W</sup> agar plates

Glucose	12g
Yeast nitrogen base without amino acids	4g
SD <sup>-L-W-H</sup> amino acid supplement	0.4g
Leucine supplement	0.04g
Bacto agar	12g

ddH<sub>2</sub>O to a final volume of 600ml

Adjust pH to 5.8, autoclave at 121°C for 15min and allow to cool to a temperature of ~55°C is reached, prior to pouring ~20, 90mm plates or ~5, 150mm plates. These plates were subsequently allowed to set for 2-5h and stored at room temperature for up to three weeks.

SD<sup>-L-H</sup> agar plates

Glucose	12g
Yeast nitrogen base without amino acids	4g
SD <sup>-L-W-H</sup> amino acid supplement	0.4g
Tryptophan supplement	0.04g
Bacto agar	12g

ddH<sub>2</sub>O to a final volume of 600ml

Adjust pH to 5.8, autoclave at 121°C for 15min and allow to cool to a temperature of ~55°C is reached, prior to pouring ~20, 90mm plates or ~5, 150mm plates. These plates were subsequently allowed to set for 2-5h and stored at room temperature for up to three weeks.

SD<sup>-W-H-Ade</sup> agar plates

Glucose	12g
Yeast nitrogen base without amino acids	4g
SD <sup>-L-W-H-Ade</sup> amino acid supplement	0.4g
Leucine supplement	0.04g
Bacto agar	12g

ddH<sub>2</sub>O to a final volume of 600ml

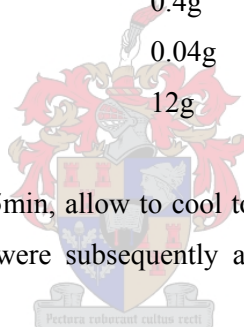
Adjust pH to 5.8, autoclave at 121°C for 15min, allow to cool to a temperature of ~55°C is reached, prior to pouring ~20, 90mm plates. These plates were subsequently allowed to set for 2-5h and stored at room temperature for up to three weeks.

SD<sup>-L-H-Ade</sup> agar plates

Glucose	12g
Yeast nitrogen base without amino acids	4g
SD <sup>-L-W-H-Ade</sup> amino acid supplement	0.4g
Tryptophan supplement	0.04g
Bacto agar	12g

ddH<sub>2</sub>O to a final volume of 600ml

Adjust pH to 5.8, autoclave at 121°C for 15min, allow to cool to a temperature of ~55°C is reached, prior to pouring ~20, 90mm plates. These plates were subsequently allowed to set for 2-5h and stored at room temperature for up to three weeks.

**14. ONPG QUANTITATIVE  $\beta$ -GALACTOSIDASE ASSAY SOLUTIONS:**Z-buffer

Na <sub>2</sub> HPO <sub>4</sub> ·7H <sub>2</sub> O	16.1g
NaH <sub>2</sub> PO <sub>4</sub> ·H <sub>2</sub> O	5.5g
KCl	0.75g
MgSO <sub>4</sub> ·7H <sub>2</sub> O	0.246g

ddH<sub>2</sub>O to a final volume of 50ml

Adjust to pH 7.0, autoclave and store at room temperature.

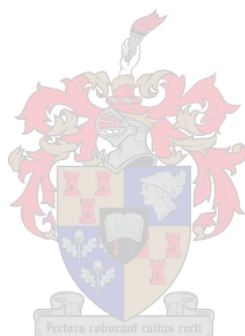
Z-buffer/ $\beta$ -mercapto-ethanol

Add 0.27ml  $\beta$ -mercapto-ethanol per 100ml of Z-buffer

ONPG/Z-buffer

Add 4mg o-nitrophenyl  $\beta$ -D-galactopyranoside (ONPG) per 1ml of Z-buffer.

Adjust pH to 7 and mix well.



## APPENDIX B

### BACTERIAL STRAIN PHENOTYPES

#### *E. coli* strain DH5 $\alpha$

$\phi$  80d *lacZ* $\Delta$ M15 *recA1 endA1 gyrA96 thi-1 hsdR17 supE44 relA1 deoR  $\Delta$ (*lacZYA-argF*)U169*

#### *E. coli* strain KC8

*hsdR, leuB600, trpC9830, pyrF::Tn5, hisB463, lacDX74, strA, galU, K (3)*

### YEAST STRAIN PHENOTYPES

#### Yeast strain PJ69-2A

*MATa, trp1-901, leu2-3, 112, ura3-52, his3-200, gal4 $\Delta$ , gal80 $\Delta$ , LYS2::GAL1<sub>UAS</sub>-GAL1<sub>TATA</sub>-HIS3, GAL2<sub>UAS</sub>-GAL2<sub>TATA</sub>-ADE2*

(James et al., 1996)

#### Yeast strain AH109

*MATa, trp1-901, leu2-3, 112, ura3-52, his3-200, gal4 $\Delta$ , gal80 $\Delta$ , LYS2::GAL1<sub>UAS</sub>-GAL1<sub>TATA</sub>-HIS3, GAL2<sub>UAS</sub>-GAL2<sub>TATA</sub>-ADE2, URA3::MEL1<sub>UAS</sub>-MEL1<sub>TATA</sub>-lacZ*

(James et al., 1996)

#### Yeast strain Y187

*MAT $\alpha$ , ura3-52, his3-200, ade2-101, trp1-901, leu2-3, 112, gal4 $\Delta$ , met<sup>-</sup>, gal80 $\Delta$ , URA3::GAL1<sub>UAS</sub>-GAL1<sub>TATA</sub>-lacZ*

(Harper et al., 1993)

# APPENDIX C

## CALCULATIONS

### Mating efficiencies

Count # of colonies on all plates with 30-300 colonies after 4 days.

$$\#cfu/ml = \frac{cfux\ 1000ul/ml}{\text{volume plated (ul)} \times \text{dilution factor}}$$

1. #cfu/ml on SD-Leu plates = viability of prey partner
2. #cfu/ml on SD-Trp plates = viability of bait partner
3. #cfu/ml on SD -L-W plates = viability of diploids
4. Lowest #cfu/ml of SD-Leu or SD-Trp indicate limiting partner.
5. Mating efficiency =  $\frac{\#cfu/ml\ \text{of diploids} \times 100}{\#cfu/ml\ \text{of limiting partner}}$

### Library titre

Count # of colonies on all plates with 30-300 colonies after 4 days

$$\#cfu/ml = \frac{\# \text{ colonies}}{\text{plating volume (ml)} \times \text{dilution factor}}$$

### Number of clones screened

# cfu/ml of diploids x final resuspension volume

### Calculation of $\beta$ -gal units

$$\beta\text{-gal units} = 1\ 000 \times OD420 / (t \times V \times OD600)$$

where

t = elapsed time for colour to develop

V = 0.1ml x concentration factor (i.e. 100ul x 5 in this case)

OD600 = either the absorption at A600 for 1ml taken from the post-5hr YPDA culture

## REFERENCES

**Anan, R., Niimura, H., Minagoe, S. and Tei, C.** (2002). A novel deletion mutation in the cardiac myosin-binding protein C gene as a cause of Maron's type IV hypertrophic cardiomyopathy. *Am.J.Cardiol.* **89**:487-488.

**Andersen, P. S., Havndrup, O., Bundgaard, H., Moolman-Smook, J. C., Larsen, L. A., Mogensen, J., Brink, P. A., Borglum, A. D., Corfield, V. A., Kjeldsen, K., Vuust, J. and Christiansen, M.** (2001). Myosin light chain mutations in familial hypertrophic cardiomyopathy: phenotypic presentation and frequency in Danish and South African populations. *J Med.Genet.* **38**:E43.

**Arad, M., Benson, D. W., Perez-Atayde, A. R., McKenna, W. J., Sparks, E. A., Kanter, R. J., McGarry, K., Seidman, J. G. and Seidman, C. E.** (2002). Constitutively active AMP kinase mutations cause glycogen storage disease mimicking hypertrophic cardiomyopathy. *J.Clin.Invest* **109**:357-362.

**Arber, S., Halder, G. and Caroni, P.** (1994). Muscle LIM protein, a novel essential regulator of myogenesis, promotes myogenic differentiation. *Cell* **79**:221-231.

**Arber, S., Hunter, J. J., Ross, J., Jr., Hongo, M., Sansig, G., Borg, J., Perriard, J. C., Chien, K. R. and Caroni, P.** (1997). MLP-deficient mice exhibit a disruption of cardiac cytoarchitectural organization, dilated cardiomyopathy, and heart failure. *Cell* **88**:393-403.

**Bahler, M., Eppenberger, H. M. and Wallimann, T.** (1985). Novel thick filament protein of chicken pectoralis muscle: the 86 kd protein. II. Distribution and localization. *J.Mol.Biol.* **186**:393-401.

**Bassan, B.J., Caetano-Anolles, G., Greshoff, D.M.** (1991) Fast and sensitive silver staining of DNA in polyacrylamide gels. *Anal Biochem* **196**:80-83.

**Bennett, P., Craig, R., Starr, R. and Offer, G.** (1986). The ultrastructural location of C-protein, X-protein and H-protein in rabbit muscle. *J.Muscle Res.Cell Motil.* **7**:550-567.

**Bennett, P. M., Furst, D. O. and Gautel, M.** (1999). The C-protein (myosin binding protein C) family: regulators of contraction and sarcomere formation? *Rev.Physiol Biochem.Pharmacol.* **138**:203-234.



**Bers, D. M., Bassani, J. W. and Bassani, R. A.** (1996). Na-Ca exchange and Ca fluxes during contraction and relaxation in mammalian ventricular muscle. *Ann.N.Y.Acad.Sci.* **779**:430-442.

**Berul, C. I., Christe, M. E., Aronovitz, M. J., Seidman, C. E., Seidman, J. G. and Mendelsohn, M. E.** (1997). Electrophysiological abnormalities and arrhythmias in alpha MHC mutant familial hypertrophic cardiomyopathy mice. *J.Clin.Invest* **99**:570-576.

**Berul, C. I., McConnell, B. K., Wakimoto, H., Moskowitz, I. P., Maguire, C. T., Semsarian, C., Vargas, M. M., Gehrmann, J., Seidman, C. E. and Seidman, J. G.** (2001). Ventricular arrhythmia vulnerability in cardiomyopathic mice with homozygous mutant Myosin-binding protein C gene. *Circulation* **104**:2734-2739.

**Blair, E., Redwood, C., Ashrafian, H., Oliveira, M., Broxholme, J., Kerr, B., Salmon, A., Ostman-Smith, I. and Watkins, H.** (2001). Mutations in the gamma(2) subunit of AMP-activated protein kinase cause familial hypertrophic cardiomyopathy: evidence for the central role of energy compromise in disease pathogenesis. *Hum.Mol.Genet.* **10**:1215-1220.

**Blair, E., Redwood, C., de Jesus, O. M., Moolman-Smook, J. C., Brink, P., Corfield, V. A., Ostman-Smith, I. and Watkins, H.** (2002). Mutations of the light meromyosin domain of the beta-myosin heavy chain rod in hypertrophic cardiomyopathy. *Circ.Res.* **90**:263-269.

**Blanchard, E., Seidman, C., Seidman, J. G., LeWinter, M. and Maughan, D.** (1999). Altered crossbridge kinetics in the alphaMHC403/+ mouse model of familial hypertrophic cardiomyopathy. *Circ.Res.* **84**:475-483.

**Bonne, G., Carrier, L., Bercovici, J., Cruaud, C., Richard, P., Hainque, B., Gautel, M., Labeit, S., James, M., Beckmann, J. and .** (1995). Cardiac myosin binding protein-C gene splice acceptor site mutation is associated with familial hypertrophic cardiomyopathy. *Nat.Genet.* **11**:438-440.

**Brittsan, A. G., Carr, A. N., Schmidt, A. G. and Kranias, E. G.** (2000). Maximal inhibition of SERCA2 Ca(2+) affinity by phospholamban in transgenic hearts overexpressing a non-phosphorylatable form of phospholamban. *J.Biol.Chem.* **275**:12129-12135.

**Carrier, L., Bonne, G., Bahrend, E., Yu, B., Richard, P., Niel, F., Hainque, B., Cruaud, C., Gary, F., Labeit, S., Bouhour, J. B., Dubourg, O., Desnos, M., Hagege, A. A., Trent, R. J., Komajda, M., Fiszman, M. and Schwartz, K. (1997).** Organization and sequence of human cardiac myosin binding protein C gene (MYBPC3) and identification of mutations predicted to produce truncated proteins in familial hypertrophic cardiomyopathy. *Circ.Res.* **80**:427-434.

**Cazorla, O., Freiburg, A., Helmes, M., Centner, T., McNabb, M., Wu, Y., Trombitas, K., Labeit, S. and Granzier, H. (2000).** Differential expression of cardiac titin isoforms and modulation of cellular stiffness. *Circ.Res.* **86**:59-67.

**Chandra, M., Dong, W. J., Pan, B. S., Cheung, H. C. and Solaro, R. J. (1997).** Effects of protein kinase A phosphorylation on signaling between cardiac troponin I and the N-terminal domain of cardiac troponin C. *Biochemistry* **36**:13305-13311.

**Charron, P., Dubourg, O., Desnos, M., Bennaceur, M., Carrier, L., Camproux, A. C., Isnard, R., Hagege, A., Langlard, J. M., Bonne, G., Richard, P., Hainque, B., Bouhour, J. B., Schwartz, K. and Komajda, M. (1998).** Clinical features and prognostic implications of familial hypertrophic cardiomyopathy related to the cardiac myosin-binding protein C gene. *Circulation* **97**:2230-2236.

**Chew, M. W. and Squire, J. M. (1995).** Packing of alpha-helical coiled-coil myosin rods in vertebrate muscle thick filaments. *J.Struct.Biol.* **115**:233-249.

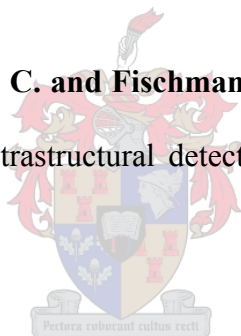
**Chu, G., Lester, J. W., Young, K. B., Luo, W., Zhai, J. and Kranias, E. G. (2000).** A single site (Ser16) phosphorylation in phospholamban is sufficient in mediating its maximal cardiac responses to beta -agonists. *J.Biol.Chem.* **275**:38938-38943.

**Craig, R. and Offer, G.** (1976). The location of C-protein in rabbit skeletal muscle. *Proc.R.Soc.Lond B Biol.Sci.* **192**:451-461.

**Crilley, J .G., Boehm, E. A., Blair, E., Rajagopalan, B., Blamire, A. M., Styles, P., McKenna, W. J., Ostman-Smith, I., Clarke, K. and Watkins, H.** (2003). Hypertrophic cardiomyopathy due to sarcomeric gene mutations is characterized by impaired energy metabolism irrespective of the degree of hypertrophy. *J.Am.Coll.Cardiol.* **41**:1776-1782.

**Davies, M. J. and McKenna, W. J.** (1995). Hypertrophic cardiomyopathy--pathology and pathogenesis. *Histopathology* **26**:493-500.

**Dennis, J. E., Shimizu, T., Reinach, F. C. and Fischman, D. A.** (1984). Localization of C-protein isoforms in chicken skeletal muscle: ultrastructural detection using monoclonal antibodies. *J.Cell Biol.* **98**:1514-1522.



**Doi, Y. L., Kitaoka, H., Hitomi, N., Satoh, M. and Kimura, A.** (1999). Clinical expression in patients with hypertrophic cardiomyopathy caused by cardiac myosin-binding protein C gene mutation. *Circulation* **100**:448-449.

**Einheber, S. and Fischman, D. A.** (1990). Isolation and characterization of a cDNA clone encoding avian skeletal muscle C-protein: an intracellular member of the immunoglobulin superfamily. *Proc.Natl.Acad.Sci.U.S.A* **87**:2157-2161.

**England, P. J.** (1975). Correlation between contraction and phosphorylation of the inhibitory subunit of troponin in perfused rat heart. *FEBS Lett.* **50**:57-60.

**England, P. J.** (1976). Studies on the phosphorylation of the inhibitory subunit of troponin during modification of contraction in perfused rat heart. *Biochem.J.* **160**:295-304.

**Erdmann, J., Daehmlow, S., Wischke, S., Senyuva, M., Werner, U., Raible, J., Tanis, N., Dyachenko, S., Hummel, M., Hetzer, R. and Regitz-Zagrosek, V.** (2003). Mutation spectrum in a large cohort of unrelated consecutive patients with hypertrophic cardiomyopathy. *Clin.Genet.* **64**:339-349.

**Erdmann, J., Raible, J., Maki-Abadi, J., Hummel, M., Hammann, J., Wollnik, B., Frantz, E., Fleck, E., Hetzer, R. and Regitz-Zagrosek, V.** (2001). Spectrum of clinical phenotypes and gene variants in cardiac myosin-binding protein C mutation carriers with hypertrophic cardiomyopathy. *J.Am.Coll.Cardiol.* **38**:322-330.

**Fabiato, A.** (1985). Simulated calcium current can both cause calcium loading in and trigger calcium release from the sarcoplasmic reticulum of a skinned canine cardiac Purkinje cell. *J.Gen.Physiol* **85**:291-320.

**Fananapazir, L., Chang, A. C., Epstein, S. E. and McAreavey, D.** (1992). Prognostic determinants in hypertrophic cardiomyopathy. Prospective evaluation of a therapeutic strategy based on clinical, Holter, hemodynamic, and electrophysiological findings. *Circulation* **86**:730-740.

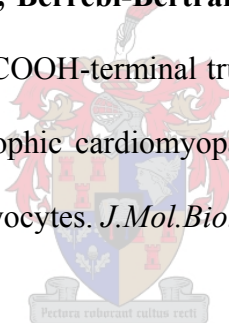
**Fananapazir, L. and Epstein, N. D.** (1994). Genotype-phenotype correlations in hypertrophic cardiomyopathy. Insights provided by comparisons of kindreds with distinct and identical beta-myosin heavy chain gene mutations. *Circulation* **89**:22-32.

**Fananapazir, L. and Epstein, S. E.** (1989). VT and sudden death in HCM patients. *Circulation* **80**:1923.

**Fananapazir, L. and Epstein, S. E.** (1991). Value of electrophysiologic studies in hypertrophic cardiomyopathy treated with amiodarone. *Am.J.Cardiol.* **67**:175-182.

**Fananapazir, L., Tracy, C. M., Leon, M. B., Winkler, J. B., Cannon, R. O., III, Bonow, R. O., Maron, B. J. and Epstein, S. E.** (1989). Electrophysiologic abnormalities in patients with hypertrophic cardiomyopathy. A consecutive analysis in 155 patients. *Circulation* **80**:1259-1268.

**Flavigny, J., Souchet, M., Sebillon, P., Berrebi-Bertrand, I., Hainque, B., Mallet, A., Bril, A., Schwartz, K. and Carrier, L.** (1999). COOH-terminal truncated cardiac myosin-binding protein C mutants resulting from familial hypertrophic cardiomyopathy mutations exhibit altered expression and/or incorporation in fetal rat cardiomyocytes. *J.Mol.Biol.* **294**:443-456.



**Flick, M. J. and Konieczny, S. F.** (2000). The muscle regulatory and structural protein MLP is a cytoskeletal binding partner of beta1-spectrin. *J.Cell Sci.* **113 ( Pt 9)**:1553-1564.

**Frank, K. F., Bolck, B., Erdmann, E. and Schwinger, R. H.** (2003). Sarcoplasmic reticulum Ca<sup>2+</sup>-ATPase modulates cardiac contraction and relaxation. *Cardiovasc.Res.* **57**:20-27.

**Freiburg, A. and Gautel, M.** (1996). A molecular map of the interactions between titin and myosin-binding protein C. Implications for sarcomeric assembly in familial hypertrophic cardiomyopathy. *Eur.J.Biochem.* **235**:317-323.

**Freiburg, A., Trombitas, K., Hell, W., Cazorla, O., Fougerousse, F., Centner, T., Kolmerer, B., Witt, C., Beckmann, J. S., Gregorio, C. C., Granzier, H. and Labeit, S. (2000).** Series of exon-skipping events in the elastic spring region of titin as the structural basis for myofibrillar elastic diversity. *Circ.Res.* **86**:1114-1121.

**Frenneaux, M. P., Counihan, P. J., Caforio, A. L., Chikamori, T. and McKenna, W. J. (1990).** Abnormal blood pressure response during exercise in hypertrophic cardiomyopathy. *Circulation* **82**:1995-2002.

**Frey, N., Franz, W. M., Gloeckner, K., Degenhardt, M., Muller, M., Muller, O., Merz, H. and Katus, H. A. (2000).** Transgenic rat hearts expressing a human cardiac troponin T deletion reveal diastolic dysfunction and ventricular arrhythmias. *Cardiovasc.Res.* **47**:254-264.

**Fujita, H., Sugiura, S., Momomura, S., Omata, M., Sugi, H. and Sutoh, K. (1997).** Characterization of mutant myosins of *Dictyostelium discoideum* equivalent to human familial hypertrophic cardiomyopathy mutants. Molecular force level of mutant myosins may have a prognostic implication. *J.Clin.Invest* **99**:1010-1015.

**Furst, D. O. and Gautel, M. (1995).** The anatomy of a molecular giant: how the sarcomere cytoskeleton is assembled from immunoglobulin superfamily molecules. *J.Mol.Cell Cardiol.* **27**:951-959.

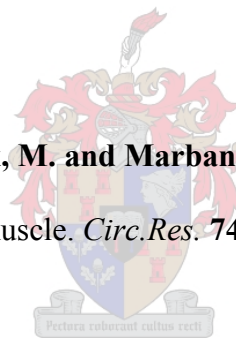
**Furst, D. O., Nave, R., Osborn, M. and Weber, K. (1989a).** Repetitive titin epitopes with a 42 nm spacing coincide in relative position with known A band striations also identified by major myosin-associated proteins. An immunoelectron-microscopical study on myofibrils. *J.Cell Sci.* **94**:119-125.

**Furst, D. O., Osborn, M., Nave, R. and Weber, K.** (1988). The organization of titin filaments in the half-sarcomere revealed by monoclonal antibodies in immunoelectron microscopy: a map of ten nonrepetitive epitopes starting at the Z line extends close to the M line. *J.Cell Biol.* **106**:1563-1572.

**Furst, D. O., Osborn, M. and Weber, K.** (1989b). Myogenesis in the mouse embryo: differential onset of expression of myogenic proteins and the involvement of titin in myofibril assembly. *J.Cell Biol.* **109**:517-527.

**Furst, D. O., Vinkemeier, U. and Weber, K.** (1992). Mammalian skeletal muscle C-protein: purification from bovine muscle, binding to titin and the characterization of a full-length human cDNA. *J.Cell Sci.* **102 ( Pt 4)**:769-778.

**Gao, W. D., Backx, P. H., Azan-Backx, M. and Marban, E.** (1994). Myofilament Ca<sup>2+</sup> sensitivity in intact versus skinned rat ventricular muscle. *Circ.Res.* **74**:408-415.



**Gao, W. D., Perez, N. G., Seidman, C. E., Seidman, J. G. and Marban, E.** (1999). Altered cardiac excitation-contraction coupling in mutant mice with familial hypertrophic cardiomyopathy. *J.Clin.Invest* **103**:661-666.

**Garvey, J. L., Kranias, E. G. and Solaro, R. J.** (1988). Phosphorylation of C-protein, troponin I and phospholamban in isolated rabbit hearts. *Biochem.J.* **249**:709-714.

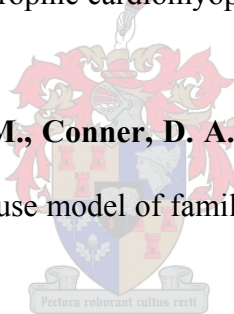
**Gautel, M., Goulding, D., Bullard, B., Weber, K. and Furst, D. O.** (1996). The central Z-disk region of titin is assembled from a novel repeat in variable copy numbers. *J.Cell Sci.* **109**:2747-2754.

**Gautel, M., Leonard, K. and Labeit, S.** (1993). Phosphorylation of KSP motifs in the C-terminal region of titin in differentiating myoblasts. *EMBO J.* **12**:3827-3834.

**Gautel, M., Zuffardi, O., Freiburg, A. and Labeit, S.** (1995). Phosphorylation switches specific for the cardiac isoform of myosin binding protein-C: a modulator of cardiac contraction? *EMBO J.* **14**:1952-1960.

**Geier, C., Perrot, A., Ozcelik, C., Binner, P., Counsell, D., Hoffmann, K., Pilz, B., Martiniak, Y., Gehmlich, K., van der Ven, P. F., Furst, D. O., Vornwald, A., von Hodenberg, E., Nurnberg, P., Scheffold, T., Dietz, R. and Osterziel, K. J.** (2003). Mutations in the human muscle LIM protein gene in families with hypertrophic cardiomyopathy. *Circulation* **107**:1390-1395.

**Geisterfer-Lowrance, A. A., Christe, M., Conner, D. A., Ingwall, J. S., Schoen, F. J., Seidman, C. E. and Seidman, J. G.** (1996). A mouse model of familial hypertrophic cardiomyopathy. *Science* **272**:731-734.



**Geisterfer-Lowrance, A. A., Kass, S., Tanigawa, G., Vosberg, H. P., McKenna, W., Seidman, C. E. and Seidman, J. G.** (1990). A molecular basis for familial hypertrophic cardiomyopathy: a beta cardiac myosin heavy chain gene missense mutation. *Cell* **62**:999-1006.

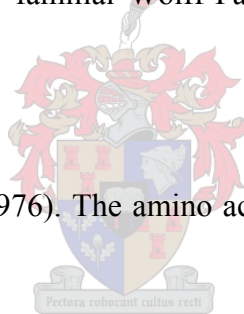
**Georgakopoulos, D., Christe, M. E., Giewat, M., Seidman, C. M., Seidman, J. G. and Kass, D. A.** (1999). The pathogenesis of familial hypertrophic cardiomyopathy: early and evolving effects from an alpha-cardiac myosin heavy chain missense mutation. *Nat.Med.* **5**:327-330.

**Gilbert, R., Cohen, J. A., Pardo, S., Basu, A. and Fischman, D. A.** (1999). Identification of the A-band localization domain of myosin binding proteins C and H (MyBP-C, MyBP-H) in skeletal muscle. *J.Cell Sci.* **112**:69-79.

**Gilbert, R., Kelly, M. G., Mikawa, T. and Fischman, D. A.** (1996). The carboxyl terminus of myosin binding protein C (MyBP-C, C-protein) specifies incorporation into the A-band of striated muscle. *J.Cell Sci.* **109**:101-111.

**Gollob, M. H., Green, M. S., Tang, A. S., Gollob, T., Karibe, A., Ali Hassan, A. S., Ahmad, F., Lozado, R., Shah, G., Fananapazir, L., Bachinski, L. L., Roberts, R. and Hassan, A. S.** (2001). Identification of a gene responsible for familial Wolff-Parkinson-White syndrome. *N.Engl.J.Med.* **344**:1823-1831.

**Grand, R. J. and Wilkinson, J. M.** (1976). The amino acid sequence of rabbit cardiac troponin I. *Biochem.J.* **159**:633-641.



**Granzier, H. and Labeit, S.** (2002). Cardiac titin: an adjustable multi-functional spring. *J.Physiol* **541**:335-342.

**Gruen, M. and Gautel, M.** (1999). Mutations in beta-myosin S2 that cause familial hypertrophic cardiomyopathy (FHC) abolish the interaction with the regulatory domain of myosin-binding protein-C. *J.Mol.Biol.* **286**:933-949.

**Gruen, M., Prinz, H. and Gautel, M.** (1999). cAPK-phosphorylation controls the interaction of the regulatory domain of cardiac myosin binding protein C with myosin-S2 in an on-off fashion. *FEBS Lett.* **453**:254-259.

**Hardie, D. G. and Carling, D.** (1997). The AMP-activated protein kinase--fuel gauge of the mammalian cell? *Eur.J Biochem* **246**:259-273.

**Harper, J. W., Adami, G. R., Wei, N., Keyomarsi, K. and Elledge, S. J.** (1993). The p21 Cdk-interacting protein Cip1 is a potent inhibitor of G1 cyclin-dependent kinases. *Cell* **75**:805-816.

**Harris, S. P., Bartley, C. R., Hacker, T. A., McDonald, K. S., Douglas, P. S., Greaser, M. L., Powers, P. A. and Moss, R. L.** (2002). Hypertrophic cardiomyopathy in cardiac myosin binding protein-C knockout mice. *Circ.Res.* **90**:594-601.

**Hartzell, H. C. and Glass, D. B.** (1984). Phosphorylation of purified cardiac muscle C-protein by purified cAMP- dependent and endogenous Ca<sup>2+</sup>-calmodulin-dependent protein kinases. *J Biol Chem* **259**:15587-15596.

**Hartzell, H.C. and Sale, W. S.** (1985). Structure of C protein purified from cardiac muscle. *J Cell Biol* **100**:208-215.

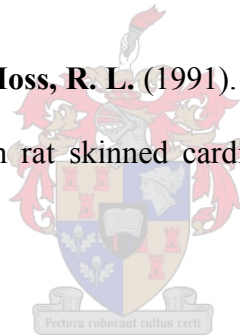
**Hartzell, H. C. and Titus, L.** (1982). Effects of cholinergic and adrenergic agonists on phosphorylation of a 165,000-dalton myofibrillar protein in intact cardiac muscle. *J Biol Chem* **257**:2111-2120.

**Helmes, M., Trombitas, K., Centner, T., Kellermayer, M., Labeit, S., Linke, W. A. and Granzier, H.** (1999). Mechanically driven contour-length adjustment in rat cardiac titin's unique N2B sequence: titin is an adjustable spring. *Circ.Res.* **84**:1339-1352.

**Helmes, M., Trombitas, K. and Granzier, H.** (1996). Titin develops restoring force in rat cardiac myocytes. *Circ.Res.* **79**:619-626.

**Hoffmann, B., Schmidt-Traub, H., Perrot, A., Osterziel, K. J. and Gessner, R.** (2001). First mutation in cardiac troponin C, L29Q, in a patient with hypertrophic cardiomyopathy. *Hum.Mutat.* **17**:524.

**Hofmann, P. A., Hartzell, H. C. and Moss, R. L.** (1991). Alterations in Ca<sup>2+</sup> sensitive tension due to partial extraction of C- protein from rat skinned cardiac myocytes and rabbit skeletal muscle fibers. *J Gen.Physiol* **97**:1141-1163.



**Holroyde, M, J., Howe, E., Solaro, R, J.,** (1984) Modifications of calcium requirements for activation of cardiac myofibrillar ATPase by cyclic AMP dependant phosphorylation. *Biochim Biophys Acta* **586**:63-69

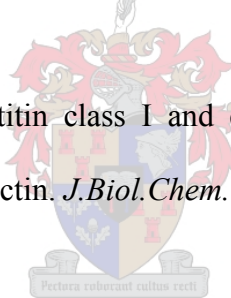
**Horowitz, R. and Winegrad, S.** (1983). Cholinergic regulation of calcium sensitivity in cardiac muscle. *J.Mol.Cell Cardiol.* **15**:277-280.

**Idowu, S. M., Gautel, M., Perkins, S. J. and Pfuhl, M.** (2003). Structure, stability and dynamics of the central domain of cardiac myosin binding protein C (MyBP-C): implications for multidomain assembly and causes for cardiomyopathy. *J.Mol.Biol.* **329**:745-761.

**Jaaskelainen, P., Kuusisto, J., Miettinen, R., Karkkainen, P., Karkkainen, S., Heikkinen, S., Peltola, P., Pihlajamaki, J., Vauhkonen, I. and Laakso, M.** (2002). Mutations in the cardiac myosin-binding protein C gene are the predominant cause of familial hypertrophic cardiomyopathy in eastern Finland. *J.Mol.Med.* **80**:412-422.

**James, P., Halladay, J. and Craig, E. A.** (1996). Genomic libraries and a host strain designed for highly efficient two-hybrid selection in yeast. *Genetics* **144**:1425-1436.

**Jin, J. P.** (1995). Cloned rat cardiac titin class I and class II motifs. Expression, purification, characterization, and interaction with F-actin. *J.Biol.Chem.* **270**:6908-6916.



**Jung, W. I., Sieverding, L., Breuer, J., Hoess, T., Widmaier, S., Schmidt, O., Bunse, M., van Erckelens, F., Apitz, J., Lutz, O. and Dietze, G. J.** (1998). <sup>31</sup>P NMR spectroscopy detects metabolic abnormalities in asymptomatic patients with hypertrophic cardiomyopathy. *Circulation* **97**:2536-2542.

**Kellermayer, M.S., Smith, S. B., Granzier, H. L. and Bustamante, C.** (1997). Folding-unfolding transitions in single titin molecules characterized with laser tweezers. *Science* **276**:1112-1116.

**Kim, S. J., Iizuka, K., Kelly, R. A., Geng, Y. J., Bishop, S. P., Yang, G., Kudej, A., McConnell, B. K., Seidman, C. E., Seidman, J. G. and Vatner, S. F. (1999).** An alpha-cardiac myosin heavy chain gene mutation impairs contraction and relaxation function of cardiac myocytes. *Am.J.Physiol* **276**:H1780-H1787.

**Kimura, A., Harada, H., Park, J. E., Nishi, H., Satoh, M., Takahashi, M., Hiroi, S., Sasaoka, T., Ohbuchi, N., Nakamura, T., Koyanagi, T., Hwang, T. H., Choo, J. A., Chung, K. S., Hasegawa, A., Nagai, R., Okazaki, O., Nakamura, H., Matsuzaki, M., Sakamoto, T., Toshima, H., Koga, Y., Imaizumi, T. and Sasazuki, T. (1997).** Mutations in the cardiac troponin I gene associated with hypertrophic cardiomyopathy. *Nat.Genet* **16**:379-382.

**Knight, P. J. (1996).** Dynamic behaviour of the head-tail junction of myosin. *J.Mol.Biol.* **255**:269-274.



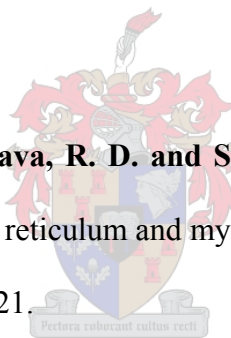
**Knoll, R., Hoshijima, M., Hoffman, H.M., Person, V., Lorenzen-Schmidt, I., Bang, M.L., Hayashi, T., Shiga, N., Yasukawa, H., Schaper, W., McKenna, W., Yokoyama, M., Schork, N.J., Omens, J.H., McCulloch, A.D., Kimura, A., Gregorio, C.C., Poller, W., Schaper, J., Schultheiss, H.P. and Chien, K.R. (2002).** The cardiac mechanical stretch sensor machinery involves a Z disc complex that is defective in a subset of human dilated cardiomyopathy. *Cell* **111**:943-955.

**Konno, T., Shimizu, M., Ino, H., Matsuyama, T., Yamaguchi, M., Terai, H., Hayashi, K., Mabuchi, T., Kiyama, M., Sakata, K., Hayashi, T., Inoue, M., Kaneda, T. and Mabuchi, H.** (2003). A novel missense mutation in the myosin binding protein-C gene is responsible for hypertrophic cardiomyopathy with left ventricular dysfunction and dilation in elderly patients. *J.Am.Coll.Cardiol.* **41**:781-786.

**Koretz, J. F.** (1979). Effects of C-protein on synthetic myosin filament structure. *Biophys.J.* **27**:433-446.

**Koss, K. L. and Kranias, E. G.** (1996). Phospholamban: a prominent regulator of myocardial contractility. *Circ.Res.* **79**:1059-1063.

**Kranias, E. G., Garvey, J. L., Srivastava, R. D. and Solaro, R. J.** (1985). Phosphorylation and functional modifications of sarcoplasmic reticulum and myofibrils in isolated rabbit hearts stimulated with isoprenaline. *Biochem.J.* **226**:113-121.



**Kulikovskaya, I., McClellan, G., Levine, R. and Winegrad, S.** (2003). Effect of extraction of myosin binding protein C on contractility of rat heart. *Am.J.Physiol Heart Circ.Physiol* **285**:H857-H865.

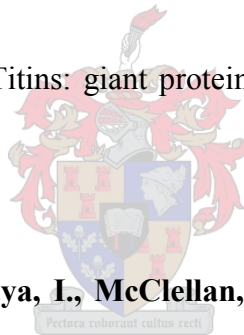
**Kunst, G., Kress, K. R., Gruen, M., Uttenweiler, D., Gautel, M. and Fink, R. H.** (2000). Myosin binding protein C, a phosphorylation-dependent force regulator in muscle that controls the attachment of myosin heads by its interaction with myosin S2. *Circ.Res.* **86**:51-58.

**Kuschel, M., Karczewski, P., Hempel, P., Schlegel, W. P., Krause, E. G. and Bartel, S. (1999).** Ser16 prevails over Thr17 phospholamban phosphorylation in the beta-adrenergic regulation of cardiac relaxation. *Am.J.Physiol* **276**:H1625-H1633.

**Labeit, S., Barlow, D. P., Gautel, M., Gibson, T., Holt, J., Hsieh, C. L., Francke, U., Leonard, K., Wardale, J., Whiting, A. and . (1990).** A regular pattern of two types of 100-residue motif in the sequence of titin. *Nature* **345**:273-276.

**Labeit, S., Gautel, M., Lakey, A. and Trinick, J. (1992).** Towards a molecular understanding of titin. *EMBO J.* **11**:1711-1716.

**Labeit, S. and Kolmerer, B. (1995).** Titins: giant proteins in charge of muscle ultrastructure and elasticity. *Science* **270**:293-296.



**Levine, R., Weisberg, A., Kulikovskaya, I., McClellan, G. and Winegrad, S. (2001).** Multiple structures of thick filaments in resting cardiac muscle and their influence on cross-bridge interactions. *Biophys.J.* **81**:1070-1082.

**Li, Y., Kranias, E. G., Mignery, G. A. and Bers, D. M. (2002).** Protein kinase A phosphorylation of the ryanodine receptor does not affect calcium sparks in mouse ventricular myocytes. *Circ.Res.* **90**:309-316.

**Lin, D., Bobkova, A., Homsher, E. and Tobacman, L. S. (1996).** Altered cardiac troponin T in vitro function in the presence of a mutation implicated in familial hypertrophic cardiomyopathy. *J.Clin.Invest* **97**:2842-2848.

**Linke, W. A., Ivemeyer, M., Labeit, S., Hinssen, H., Ruegg, J. C. and Gautel, M. (1997).** Actin-titin interaction in cardiac myofibrils: probing a physiological role. *Biophys.J.* **73**:905-919.

**Linke, W. A., Stockmeier, M. R., Ivemeyer, M., Hosser, H. and Mundel, P. (1998).** Characterizing titin's I-band Ig domain region as an entropic spring. *J.Cell Sci.* **111**:1567-1574.

**Liversage, A. D., Holmes, D., Knight, P. J., Tskhovrebova, L. and Trinick, J. (2001).** Titin and the sarcomere symmetry paradox. *J Mol.Biol* **305**:401-409.

**Lodish H, Baltimore D, Berk A, Zipursky SL, Matsudaira P, Darnell J. (1995)** Molecular cell biology. *Third edition* W.H. Freeman and Co: New York

**Luo, W., Grupp, I. L., Harrer, J., Ponniah, S., Grupp, G., Duffy, J. J., Doetschman, T. and Kranias, E. G. (1994).** Targeted ablation of the phospholamban gene is associated with markedly enhanced myocardial contractility and loss of beta-agonist stimulation. *Circ.Res.* **75**:401-409.

**Margossian, S. S., Krueger, J. W., Sellers, J. R., Cuda, G., Caulfield, J. B., Norton, P. and Slayter, H. S. (1991).** Influence of the cardiac myosin hinge region on contractile activity. *Proc.Natl.Acad.Sci.U.S.A* **88**:4941-4945.

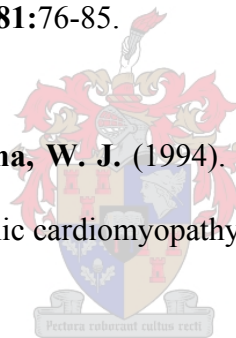
**Marian, A. J. and Roberts, R. (2001).** The molecular genetic basis for hypertrophic cardiomyopathy. *J.Mol.Cell Cardiol.* **33**:655-670.

**Marian, A. J., Wu, Y., Lim, D. S., McCluggage, M., Youker, K., Yu, Q. T., Brugada, R., DeMayo, F., Quinones, M. and Roberts, R. (1999).** A transgenic rabbit model for human hypertrophic cardiomyopathy. *J.Clin.Invest* **104**:1683-1692.

**Marian, A. J., Yu, Q. T., Mann, D. L., Graham, F. L. and Roberts, R. (1995).** Expression of a mutation causing hypertrophic cardiomyopathy disrupts sarcomere assembly in adult feline cardiac myocytes. *Circ.Res.* **77**:98-106.

**Marian, A. J., Zhao, G., Seta, Y., Roberts, R. and Yu, Q. T. (1997).** Expression of a mutant (Arg92Gln) human cardiac troponin T, known to cause hypertrophic cardiomyopathy, impairs adult cardiac myocyte contractility. *Circ.Res.* **81**:76-85.

**Maron, B. J., Cecchi, F. and McKenna, W. J. (1994).** Risk factors and stratification for sudden cardiac death in patients with hypertrophic cardiomyopathy. *Br.Heart J.* **72**:S13-S18.



**Maron, B. J. and Fananapazir, L. (1992).** Sudden cardiac death in hypertrophic cardiomyopathy. *Circulation* **85**:I57-I63.

**Maron, B. J. and Ferrans, V. J. (1978).** Ultrastructural features of hypertrophied human ventricular myocardium. *Prog.Cardiovasc.Dis.* **21**:207-238.

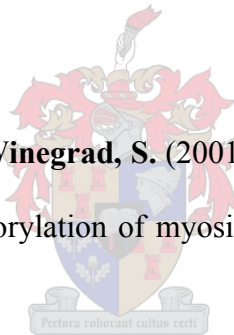
**Maron, B. J., Gardin, J. M., Flack, J. M., Gidding, S. S., Kurosaki, T. T. and Bild, D. E. (1995).** Prevalence of hypertrophic cardiomyopathy in a general population of young adults. Echocardiographic analysis of 4111 subjects in the CARDIA Study. Coronary Artery Risk Development in (Young) Adults. *Circulation* **92**:785-789.

**Maron, B. J., Lipson, L. C., Roberts, W. C., Savage, D. D. and Epstein, S. E. (1978).** "Malignant" hypertrophic cardiomyopathy: identification of a subgroup of families with unusually frequent premature death. *Am.J.Cardiol.* **41**:1133-1140.

**Maron, B. J., Nichols, P. F., III, Pickle, L. W., Wesley, Y. E. and Mulvihill, J. J. (1984).** Patterns of inheritance in hypertrophic cardiomyopathy: assessment by M- mode and two-dimensional echocardiography. *Am.J.Cardiol.* **53**:1087-1094.

**Mayans, O., van der Ven, P. F., Wilm, M., Mues, A., Young, P., Furst, D. O., Wilmanns, M. and Gautel, M. (1998).** Structural basis for activation of the titin kinase domain during myofibrillogenesis. *Nature* **395**:863-869.

**McClellan, G., Kulikovskaya, I. and Winegrad, S. (2001).** Changes in cardiac contractility related to calcium-mediated changes in phosphorylation of myosin-binding protein C. *Biophys.J.* **81**:1083-1092.



**McClellan, G., Weisberg, A. and Winegrad, S. (1994).** cAMP can raise or lower cardiac actomyosin ATPase activity depending on alpha-adrenergic activity. *Am.J.Physiol* **267**:H431-H442.

**Means, A. R. (1998).** The clash in titin. *Nature* **395**:846-847.

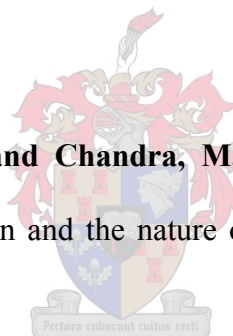
**Minajeva, A., Neagoe, C., Kulke, M. and Linke, W. A. (2002).** Titin-based contribution to shortening velocity of rabbit skeletal myofibrils. *J.Physiol* **540**:177-188.

**Miyamoto, C. A., Fischman, D. A. and Reinach, F. C.** (1999). The interface between MyBP-C and myosin: site-directed mutagenesis of the CX myosin-binding domain of MyBP-C. *J.Muscle Res.Cell Motil.* **20**:703-715.

**Mogensen, J., Klausen, I. C., Pedersen, A. K., Egeblad, H., Bross, P., Kruse, T. A., Gregersen, N., Hansen, P. S., Baandrup, U. and Borglum, A. D.** (1999). Alpha-cardiac actin is a novel disease gene in familial hypertrophic cardiomyopathy. *J.Clin.Invest* **103**:R39-R43.

**Mohamed, A. S., Dignam, J. D. and Schlender, K. K.** (1998). Cardiac myosin-binding protein C (MyBP-C): identification of protein kinase A and protein kinase C phosphorylation sites. *Arch.Biochem.Biophys.* **358**:313-319.

**Montgomery, D. E., Tardiff, J. C. and Chandra, M.** (2001). Cardiac troponin T mutations: correlation between the type of mutation and the nature of myofilament dysfunction in transgenic mice. *J Physiol* **536**:583-592.



**Moolman, J. A., Reith, S., Uhl, K., Bailey, S., Gautel, M., Jeschke, B., Fischer, C., Ochs, J., McKenna, W. J., Klues, H. and Vosberg, H. P.** (2000). A newly created splice donor site in exon 25 of the MyBP-C gene is responsible for inherited hypertrophic cardiomyopathy with incomplete disease penetrance. *Circulation* **101**:1396-1402.

**Moolman, J. C., Corfield, V. A., Posen, B., Ngumbela, K., Seidman, C., Brink, P. A. and Watkins, H.** (1997). Sudden death due to troponin T mutations. *J Am.Coll.Cardiol.* **29**:549-555.

**Moolman-Smook, J. C., de Lange, W. J., Corfield, V. A. and Brink, P. A.** (2000). Expression of HCM-causing mutations: lessons learnt from genotype:phenotype studies of the S.A. founder MYH7 A797T mutation. *J Med Genet* **37**:951-956.

**Moolman-Smook, J., Flashman, E., de Lange, W., Li, Z., Corfield, V., Redwood, C. and Watkins, H.** (2002). Identification of novel interactions between domains of Myosin binding protein-C that are modulated by hypertrophic cardiomyopathy missense mutations. *Circ.Res.* **91**:704-711.

**Moolman-Smook, J. C., De Lange, W. J., Bruwer, E. C., Brink, P. A. and Corfield, V. A.** (1999). The origins of hypertrophic cardiomyopathy-causing mutations in two South African subpopulations: a unique profile of both independent and founder events. *Am.J Hum.Genet.* **65**:1308-1320.

**Moolman-Smook, J. C., Mayosi, B., Brink, P. and Corfield, V. A.** (1998). Identification of a new missense mutation in MyBP-C associated with hypertrophic cardiomyopathy. *J.Med.Genet.* **35**:253-254.

**Moos, C.** (1981). Fluorescence microscope study of the binding of added C protein to skeletal muscle myofibrils. *J.Cell Biol.* **90**:25-31.

**Moos, C., Mason, C. M., Besterman, J. M., Feng, I. N. and Dubin, J. H.** (1978). The binding of skeletal muscle C-protein to F-actin, and its relation to the interaction of actin with myosin subfragment-1. *J.Mol.Biol.* **124**:571-586.

**Moos, C., Offer, G., Starr, R. and Bennett, P.** (1975). Interaction of C-protein with myosin, myosin rod and light meromyosin. *J Mol.Biol* **97**:1-9.

**Morimoto, K. and Harrington, W. F.** (1974). Substructure of the thick filament of vertebrate striated muscle. *J.Mol.Biol.* **83**:83-97.

**Morimoto, S., Yanaga, F., Minakami, R. and Ohtsuki, I.** (1998). Ca<sup>2+</sup>-sensitizing effects of the mutations at Ile-79 and Arg-92 of troponin T in hypertrophic cardiomyopathy. *Am.J.Physiol* **275**:C200-C207.

**Morner, S., Richard, P., Kazzam, E., Hellman, U., Hainque, B., Schwartz, K. and Waldenstrom, A.** (2003). Identification of the genotypes causing hypertrophic cardiomyopathy in northern Sweden. *J.Mol.Cell Cardiol.* **35**:841-849.

**Movsesian, M. A., Nishikawa, M. and Adelstein, R. S.** (1984). Phosphorylation of phospholamban by calcium-activated, phospholipid-dependent protein kinase. Stimulation of cardiac sarcoplasmic reticulum calcium uptake. *J.Biol.Chem.* **259**:8029-8032.

**Munch, G., Bolck, B., Karczewski, P. and Schwinger, R. H.** (2002). Evidence for calcineurin-mediated regulation of SERCA 2a activity in human myocardium. *J.Mol.Cell Cardiol.* **34**:321-334.

**Murphy, A. M.** (2002). Troponin I: in sickness and in health-and normal development. *Circ.Res.* **91**:449-450.

**Muthuchamy, M., Pieples, K., Rethinasamy, P., Hoit, B., Grupp, I. L., Boivin, G. P., Wolska, B., Evans, C., Solaro, R. J. and Wieczorek, D. F.** (1999). Mouse model of a familial hypertrophic cardiomyopathy mutation in alpha-tropomyosin manifests cardiac dysfunction. *Circ.Res.* **85**:47-56.

**Nave, R., Furst, D. O. and Weber, K.** (1989). Visualization of the polarity of isolated titin molecules: a single globular head on a long thin rod as the M band anchoring domain? *J.Cell Biol.* **109**:2177-2187.

**Neagoe, C., Kulke, M., del Monte, F., Gwathmey, J. K., De Tombe, P. P., Hajjar, R. J. and Linke, W. A.** (2002). Titin isoform switch in ischemic human heart disease. *Circulation* **106**:1333-1341.

**Niimura, H., Bachinski, L. L., Sangwatanaroj, S., Watkins, H., Chudley, A. E., McKenna, W., Kristinsson, A., Roberts, R., Sole, M., Maron, B. J., Seidman, J. G. and Seidman, C. E.** (1998). Mutations in the gene for cardiac myosin-binding protein C and late-onset familial hypertrophic cardiomyopathy. *N.Engl.J.Med.* **338**:1248-1257.

**Niimura, H., Patton, K. K., McKenna, W. J., Soultis, J., Maron, B. J., Seidman, J. G. and Seidman, C. E.** (2002). Sarcomere protein gene mutations in hypertrophic cardiomyopathy of the elderly. *Circulation* **105**:446-451.

**Oberst, L., Zhao, G., Park, J. T., Brugada, R., Michael, L. H., Entman, M. L., Roberts, R. and Marian, A. J.** (1998). Dominant-negative effect of a mutant cardiac troponin T on cardiac structure and function in transgenic mice. *J.Clin.Invest* **102**:1498-1505.

- Obinata, T., Reinach, F. C., Bader, D. M., Masaki, T., Kitani, S. and Fischman, D. A.** (1984). Immunochemical analysis of C-protein isoform transitions during the development of chicken skeletal muscle. *Dev.Biol.* **101**:116-124.
- Offer, G.** (1972) C-protein and the periodicity in the thick filaments of vertebrate skeletal muscle. *Cold Spring Harbour Symposia Quantitative Biology* **37**:87-95.
- Offer, G., Moos, C. and Starr, R.** (1973). A new protein of the thick filaments of vertebrate skeletal myofibrils. Extractions, purification and characterization. *J Mol.Biol* **74**:653-676.
- Okagaki, T., Weber, F. E., Fischman, D. A., Vaughan, K. T., Mikawa, T. and Reinach, F. C.** (1993). The major myosin-binding domain of skeletal muscle MyBP-C (C protein) resides in the COOH-terminal, immunoglobulin C2 motif. *J.Cell Biol.* **123**:619-626.
- Ostman-Smith, I., Wettrell, G. and Riesenfeld, T.** (1999). A cohort study of childhood hypertrophic cardiomyopathy: improved survival following high-dose beta-adrenoceptor antagonist treatment. *J.Am.Coll.Cardiol.* **34**:1813-1822.
- Perry, S. V. and Cole, H. A.** (1974). Phosphorylation of troponin and the effects of interactions between the components of the complex. *Biochem.J.* **141**:733-743.
- Poetter, K., Jiang, H., Hassanzadeh, S., Master, S. R., Chang, A., Dalakas, M. C., Rayment, I., Sellers, J. R., Fananapazir, L. and Epstein, N. D.** (1996). Mutations in either the essential or regulatory light chains of myosin are associated with a rare myopathy in human heart and skeletal muscle. *Nat.Genet* **13**:63-69.

**Politou, A. S., Gautel, M., Pfuhl, M., Labeit, S. and Pastore, A.** (1994). Immunoglobulin-type domains of titin: same fold, different stability? *Biochemistry* **33**:4730-4737.

**Price, M. G. and Gomer, R. H.** (1993). Skelemin, a cytoskeletal M-disc periphery protein, contains motifs of adhesion/recognition and intermediate filament proteins. *J.Biol.Chem.* **268**:21800-21810.

**Ray, K. P. and England, P. J.** (1976). Phosphorylation of the inhibitory subunit of troponin and its effect on the calcium dependence of cardiac myofibril adenosine triphosphatase. *FEBS Lett.* **70**:11-16.

**Redwood, C. S., Moolman-Smook, J.C. and Watkins, H.** (1999) Properties of mutant contractile proteins that cause hypertrophic cardiomyopathy. *Cardiovasc Res.* **4**:20-36.

**Reinach, F. C., Masaki, T., Shafiq, S., Obinata, T. and Fischman, D. A.** (1982). Isoforms of C-protein in adult chicken skeletal muscle: detection with monoclonal antibodies. *J.Cell Biol.* **95**:78-84.

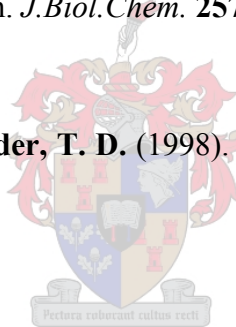
**Richard, P., Charron, P., Carrier, L., Ledeuil, C., Cheav, T., Pichereau, C., Benaiche, A., Isnard, R., Dubourg, O., Burban, M., Gueffet, J. P., Millaire, A., Desnos, M., Schwartz, K., Hainque, B. and Komajda, M.** (2003). Hypertrophic cardiomyopathy: distribution of disease genes, spectrum of mutations, and implications for a molecular diagnosis strategy. *Circulation* **107**:2227-2232.

**Richard, P., Isnard, R., Carrier, L., Dubourg, O., Donatien, Y., Mathieu, B., Bonne, G., Gary, F., Charron, P., Hagege, M., Komajda, M., Schwartz, K. and Hainque, B.** (1999). Double heterozygosity for mutations in the beta-myosin heavy chain and in the cardiac myosin binding protein C genes in a family with hypertrophic cardiomyopathy. *J.Med.Genet.* **36**:542-545.

**Rief, M., Gautel, M., Oesterhelt, F., Fernandez, J. M. and Gaub, H. E.** (1997). Reversible unfolding of individual titin immunoglobulin domains by AFM. *Science* **276**:1109-1112.

**Robertson, S. P., Johnson, J. D., Holroyde, M. J., Kranias, E. G., Potter, J. D. and Solaro, R. J.** (1982). The effect of troponin I phosphorylation on the Ca<sup>2+</sup>-binding properties of the Ca<sup>2+</sup>-regulatory site of bovine cardiac troponin. *J.Biol.Chem.* **257**:260-263.

**Rogan, P. K., Faux, B. M. and Schneider, T. D.** (1998). Information analysis of human splice site mutations. *Hum.Mutat.* **12**:153-171.



**Romhilt, D. W. and Estes, E. H.** (1968). A point-score system for the ECG diagnosis of left ventricular hypertrophy. *Am.Heart J.* **75**:752-758.

**Rottbauer, W., Gautel, M., Zehelein, J., Labeit, S., Franz, W. M., Fischer, C., Vollrath, B., Mall, G., Dietz, R., Kubler, W. and Katus, H. A.** (1997). Novel splice donor site mutation in the cardiac myosin-binding protein- C gene in familial hypertrophic cardiomyopathy. Characterization Of cardiac transcript and protein. *J.Clin.Invest* **100**:475-482.

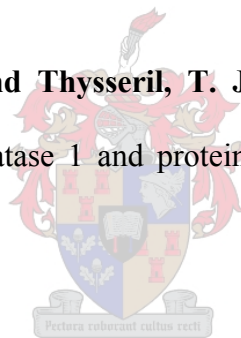
**Saggin, L., Gorza, L., Ausoni, S. and Schiaffino, S.** (1989). Troponin I switching in the developing heart. *J.Biol.Chem.* **264**:16299-16302.

**Sata, M. and Ikebe, M.** (1996). Functional analysis of the mutations in the human cardiac beta-myosin that are responsible for familial hypertrophic cardiomyopathy. Implication for the clinical outcome. *J.Clin.Invest* **98**:2866-2873.

**Satoh, M., Takahashi, M., Sakamoto, T., Hiroe, M., Marumo, F. and Kimura, A.** (1999). Structural analysis of the titin gene in hypertrophic cardiomyopathy: identification of a novel disease gene. *Biochem Biophys.Res.Commun.* **262**:411-417.

**Schlender, K. K. and Bean, L. J.** (1991). Phosphorylation of chicken cardiac C-protein by calcium/calmodulin- dependent protein kinase II. *J.Biol.Chem.* **266**:2811-2817.

**Schlender, K. K., Hegazy, M. G. and Thysseril, T. J.** (1987). Dephosphorylation of cardiac myofibril C-protein by protein phosphatase 1 and protein phosphatase 2A. *Biochim.Biophys.Acta* **928**:312-319.



**Schlender, K. K., Wang, W. and Wilson, S. E.** (1989). Evidence for a latent form of protein phosphatase 1 associated with cardiac myofibrils. *Biochem.Biophys.Res.Commun.* **159**:72-78.

**Sebillon, P., Bonne, G., Flavigny, J., Venin, S., Rouche, A., Fiszman, M., Vikstrom, K., Leinwand, L., Carrier, L. and Schwartz, K.** (2001). COOH-terminal truncated human cardiac MyBP-C alters myosin filament organization. *C.R.Acad.Sci.III* **324**:251-260.

**Seidman, J. G. and Seidman, C.** (2001). The genetic basis for cardiomyopathy: from mutation identification to mechanistic paradigms. *Cell* **104**:557-567.

**Seidman, J. G. and Seidman, C.** (2002). Transcription factor haploinsufficiency: when half a loaf is not enough. *J.Clin.Invest* **109**:451-455.

**Seiler, S. H., Fischman, D. A. and Leinwand, L. A.** (1996). Modulation of myosin filament organization by C-protein family members. *Mol.Biol.Cell* **7**:113-127.

**Sjostrom, M. and Squire, J. M.** (1977). Fine structure of the A-band in cryo-sections. The structure of the A-band of human skeletal muscle fibres from ultra-thin cryo-sections negatively stained. *J.Mol.Biol.* **109**:49-68.

**Solaro, R. J., Moir, A. J. and Perry, S. V.** (1976). Phosphorylation of troponin I and the inotropic effect of adrenaline in the perfused rabbit heart. *Nature* **262**:615-617.

**Solaro, R. J. and Rarick, H. M.** (1998). Troponin and tropomyosin: proteins that switch on and tune in the activity of cardiac myofilaments. *Circ.Res.* **83**:471-480.

**Soteriou, A., Gamage, M. and Trinick, J.** (1993). A survey of interactions made by the giant protein titin. *J.Cell Sci.* **104**:119-123.

**Spindler, M., Saupe, K. W., Christe, M. E., Sweeney, H. L., Seidman, C. E., Seidman, J. G. and Ingwall, J. S.** (1998). Diastolic dysfunction and altered energetics in the alphaMHC403/+ mouse model of familial hypertrophic cardiomyopathy. *J Clin.Invest* **101**:1775-1783.

**Spirito, P., Seidman, C. E., McKenna, W. J. and Maron, B. J.** (1997). The management of hypertrophic cardiomyopathy. *N.Engl.J.Med.* **336**:775-785.

**Spyracopoulos, L., Li, M. X., Sia, S. K., Gagne, S. M., Chandra, M., Solaro, R. J. and Sykes, B. D.** (1997). Calcium-induced structural transition in the regulatory domain of human cardiac troponin C. *Biochemistry* **36**:12138-12146.

**Squire J. M.** (1979). Organisation of myosin in thick filaments of muscles. In '*Fibrous Proteins: Scientific, Industrial and Medical Aspects*'. (Ed. Parry DAD and Creamer LK (Eds.) pp. 27-70. (Academic Press: London.)

**Squire, J., Cantino, M., Chew, M., Denny, R., Harford, J., Hudson, L. and Luther, P.** (1998). Myosin rod-packing schemes in vertebrate muscle thick filaments. *J.Struct.Biol.* **122**:128-138.

**Squire, J. M.** (1973). General model of myosin filament structure. 3. Molecular packing arrangements in myosin filaments. *J.Mol.Biol.* **77**:291-323.

**Squire, J. M., Luther, P. K. and Knupp, C.** (2003). Structural evidence for the interaction of C-protein (MyBP-C) with actin and sequence identification of a possible actin-binding domain. *J.Mol.Biol.* **331**:713-724.

**Starr, R., Almond, R. and Offer, G.** (1985). Location of C-protein, H-protein and X-protein in rabbit skeletal muscle fibre types. *J.Muscle Res.Cell Motil.* **6**:227-256.

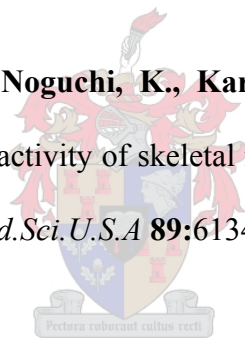
**Starr, R. and Offer, G.** (1978). The interaction of C-protein with heavy meromyosin and subfragment-2. *Biochem.J.* **171**:813-816.

**Stewart, M., Ashton, F. T., Lieberson, R. and Pepe, F. A.** (1981). The myosin filament. IX. Determination of subfilament positions by computer processing of electron micrographs. *J.Mol.Biol.* **153**:381-392.

**Strang, K. T., Sweitzer, N. K., Greaser, M. L. and Moss, R. L.** (1994). Beta-adrenergic receptor stimulation increases unloaded shortening velocity of skinned single ventricular myocytes from rats. *Circ.Res.* **74**:542-549.

**Stull, J. T. and Buss, J. E.** (1977). Phosphorylation of cardiac troponin by cyclic adenosine 3':5'-monophosphate-dependent protein kinase. *J.Biol.Chem.* **252**:851-857.

**Sugi, H., Kobayashi, T., Gross, T., Noguchi, K., Karr, T. and Harrington, W. F.** (1992). Contraction characteristics and ATPase activity of skeletal muscle fibers in the presence of antibody to myosin subfragment 2. *Proc.Natl.Acad.Sci.U.S.A* **89**:6134-6137.



**Sweeney, H. L., Straceski, A. J., Leinwand, L. A., Tikunov, B. A. and Faust, L.** (1994). Heterologous expression of a cardiomyopathic myosin that is defective in its actin interaction. *J.Biol.Chem.* **269**:1603-1605.

**Syska, H., Wilkinson, J. M., Grand, R. J. and Perry, S. V.** (1976). The relationship between biological activity and primary structure of troponin I from white skeletal muscle of the rabbit. *Biochem.J.* **153**:375-387.

**Tardiff, J. C., Factor, S. M., Tompkins, B. D., Hewett, T. E., Palmer, B. M., Moore, R. L., Schwartz, S., Robbins, J. and Leinwand, L. A.** (1998). A truncated cardiac troponin T molecule in transgenic mice suggests multiple cellular mechanisms for familial hypertrophic cardiomyopathy. *J.Clin.Invest* **101**:2800-2811.

**Tardiff, J. C., Hewett, T. E., Palmer, B. M., Olsson, C., Factor, S. M., Moore, R. L., Robbins, J. and Leinwand, L. A.** (1999). Cardiac troponin T mutations result in allele-specific phenotypes in a mouse model for hypertrophic cardiomyopathy. *J.Clin.Invest* **104**:469-481.

**Thierfelder, L., Watkins, H., MacRae, C., Lamas, R., McKenna, W., Vosberg, H. P., Seidman, J. G. and Seidman, C. E.** (1994). Alpha-tropomyosin and cardiac troponin T mutations cause familial hypertrophic cardiomyopathy: a disease of the sarcomere. *Cell* **77**:701-712.

**Tian, R., Musi, N., D'Agostino, J., Hirshman, M. F. and Goodyear, L. J.** (2001). Increased adenosine monophosphate-activated protein kinase activity in rat hearts with pressure-overload hypertrophy. *Circulation* **104**:1664-1669.

**Timson, D. J., Trayer, H.R., and Trayer, I.P.** (1998) The N-terminus of A1-type myosin essential light chains binds actin and modulates myosin motor function. *Eur J Biochem.* **255**:654-662.

**Timson, D. J., and Trayer, I.P.**(1997) The role of the proline-rich region in A1-type myosin essential light chains: implications for information transmission in the actomyosin complex. *FEBS Lett.* **400**:31-36

**Trinick, J.** (1996). Titin as a scaffold and spring. Cytoskeleton. *Curr.Biol.* **6**:258-260.

**Trinick, J. A.** (1981). End-filaments: a new structural element of vertebrate skeletal muscle thick filaments. *J.Mol.Biol.* **151**:309-314.

**Trombitas, K., Greaser, M., Labeit, S., Jin, J. P., Kellermayer, M., Helmes, M. and Granzier, H.** (1998). Titin extensibility in situ: entropic elasticity of permanently folded and permanently unfolded molecular segments. *J.Cell Biol.* **140**:853-859.

**Tskhovrebova, L., Trinick, J., Sleep, J. A. and Simmons, R. M.** (1997). Elasticity and unfolding of single molecules of the giant muscle protein titin. *Nature* **387**:308-312.

**Tyska, M. J., Hayes, E., Giewat, M., Seidman, C. E., Seidman, J. G. and Warshaw, D. M.** (2000). Single-molecule mechanics of R403Q cardiac myosin isolated from the mouse model of familial hypertrophic cardiomyopathy. *Circ.Res.* **86**:737-744.

**Vaughan, K. T., Weber, F. E., Einheber, S. and Fischman, D. A.** (1993). Molecular cloning of chicken myosin-binding protein (MyBP) H (86-kDa protein) reveals extensive homology with MyBP-C (C-protein) with conserved immunoglobulin C2 and fibronectin type III motifs. *J.Biol.Chem.* **268**:3670-3676.

**Venema, R. C. and Kuo, J. F.** (1993). Protein kinase C-mediated phosphorylation of troponin I and C-protein in isolated myocardial cells is associated with inhibition of myofibrillar actomyosin MgATPase. *J.Biol.Chem.* **268**:2705-2711.

**Vinkemeier, U., Obermann, W., Weber, K. and Furst, D. O.** (1993). The globular head domain of titin extends into the center of the sarcomeric M band. cDNA cloning, epitope mapping and immunoelectron microscopy of two titin-associated proteins. *J.Cell Sci.* **106**:319-330.

**Waldmuller, S., Sakthivel, S., Saadi, A. V., Selignow, C., Rakesh, P. G., Golubenko, M., Joseph, P. K., Padmakumar, R., Richard, P., Schwartz, K., Tharakan, J. M., Rajamanickam, C. and Vosberg, H. P.** (2003). Novel deletions in MYH7 and MYBPC3 identified in Indian families with familial hypertrophic cardiomyopathy. *J.Mol.Cell Cardiol.* **35**:623-636.

**Watkins, H.** (2003). Genetic clues to disease pathways in hypertrophic and dilated cardiomyopathies. *Circulation* **107**:1344-1346.

**Watkins, H., Conner, D., Thierfelder, L., Jarcho, J. A., MacRae, C., McKenna, W. J., Maron, B. J., Seidman, J. G. and Seidman, C. E.** (1995a). Mutations in the cardiac myosin binding protein-C gene on chromosome 11 cause familial hypertrophic cardiomyopathy. *Nat.Genet.* **11**:434-437.

**Watkins, H., McKenna, W. J., Thierfelder, L., Suk, H. J., Anan, R., O'Donoghue, A., Spirito, P., Matsumori, A., Moravec, C. S., Seidman, J. G. and .** (1995b). Mutations in the genes for cardiac troponin T and alpha-tropomyosin in hypertrophic cardiomyopathy. *N.Engl.J.Med.* **332**:1058-1064.

**Watkins, H., Seidman, C. E., Seidman, J. G., Feng, H. S. and Sweeney, H. L.** (1996). Expression and functional assessment of a truncated cardiac troponin T that causes hypertrophic cardiomyopathy. Evidence for a dominant negative action. *J.Clin.Invest* **98**:2456-2461.

- Watkins, H., Seidman, J. G. and Seidman, C. E.** (1995c). Familial hypertrophic cardiomyopathy: a genetic model of cardiac hypertrophy. *Hum.Mol.Genet.* **4**:1721-1727.
- Weber, F. E., Vaughan, K. T., Reinach, F. C. and Fischman, D. A.** (1993). Complete sequence of human fast-type and slow-type muscle myosin- binding-protein C (MyBP-C). Differential expression, conserved domain structure and chromosome assignment. *Eur.J.Biochem.* **216**:661-669.
- Weisberg, A. and Winegrad, S.** (1996). Alteration of myosin cross bridges by phosphorylation of myosin-binding protein C in cardiac muscle. *Proc.Natl.Acad.Sci.U.S.A* **93**:8999-9003.
- Weisberg, A. and Winegrad, S.** (1998). Relation between crossbridge structure and actomyosin ATPase activity in rat heart. *Circ.Res.* **83**:60-72.
- Welikson, R. E. and Fischman, D. A.** (2002). The C-terminal IgI domains of myosin-binding proteins C and H (MyBP-C and MyBP-H) are both necessary and sufficient for the intracellular crosslinking of sarcomeric myosin in transfected non-muscle cells. *J.Cell Sci.* **115**:3517-3526.
- Westfall, M. V., Borton, A. R., Albayya, F. P. and Metzger, J. M.** (2002). Myofilament calcium sensitivity and cardiac disease: insights from troponin I isoforms and mutants. *Circ.Res.* **91**:525-531.
- Widnell CC, Pfenninger KH.** (1990) Muscle contraction and cell motility. *In Essential Cell Biology* p169-191 Williams&Wilkins: Baltimore

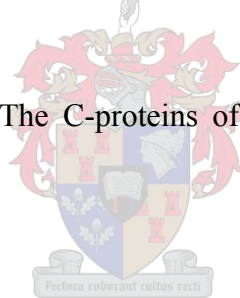
**Wilkinson, J. M. and Grand, R. J.** (1978). Comparison of amino acid sequence of troponin I from different striated muscles. *Nature* **271**:31-35.

**Winegrad, S.** (1984). Regulation of cardiac contractile proteins. Correlations between physiology and biochemistry. *Circ.Res.* **55**:565-574.

**Witt, C. C., Gerull, B., Davies, M. J., Centner, T., Linke, W. A. and Thierfelder, L.** (2001). Hypercontractile properties of cardiac muscle fibers in a knock-in mouse model of cardiac myosin-binding protein-C. *J.Biol.Chem.* **276**:5353-5359.

**Wyborny, L. E. and Reddy, Y. S.** (1978). Phosphorylated cardiac myofibrils and their effect on ATPase activity. *Biochem.Biophys.Res.Commun.* **81**:1175-1179.

**Yamamoto, K. and Moos, C.** (1983). The C-proteins of rabbit red, white, and cardiac muscles. *J.Biol.Chem.* **258**:8395-8401.



**Yamasaki, R., Berri, M., Wu, Y., Trombitas, K., McNabb, M., Kellermayer, M. S., Witt, C., Labeit, D., Labeit, S., Greaser, M. and Granzier, H.** (2001). Titin-actin interaction in mouse myocardium: passive tension modulation and its regulation by calcium/S100A1. *Biophys.J.* **81**:2297-2313.

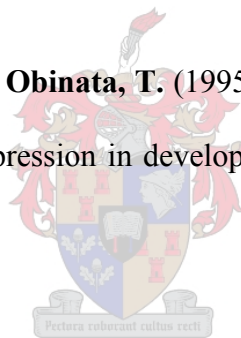
**Yamasaki, R., Wu, Y., McNabb, M., Greaser, M., Labeit, S. and Granzier, H.** (2002). Protein kinase A phosphorylates titin's cardiac-specific N2B domain and reduces passive tension in rat cardiac myocytes. *Circ.Res.* **90**:1181-1188.

**Yanaga, F., Morimoto, S. and Ohtsuki, I.** (1999). Ca<sup>2+</sup> sensitization and potentiation of the maximum level of myofibrillar ATPase activity caused by mutations of troponin T found in familial hypertrophic cardiomyopathy. *J.Biol.Chem.* **274**:8806-8812.

**Yang, Q., Sanbe, A., Osinska, H., Hewett, T. E., Klevitsky, R. and Robbins, J.** (1998). A mouse model of myosin binding protein C human familial hypertrophic cardiomyopathy. *J.Clin.Invest* **102**:1292-1300.

**Yang, Q., Sanbe, A., Osinska, H., Hewett, T. E., Klevitsky, R. and Robbins, J.** (1999). In vivo modeling of myosin binding protein C familial hypertrophic cardiomyopathy. *Circ.Res.* **85**:841-847.

**Yasuda, M., Koshida, S., Sato, N. and Obinata, T.** (1995). Complete primary structure of chicken cardiac C-protein (MyBP-C) and its expression in developing striated muscles. *J.Mol.Cell Cardiol.* **27**:2275-2286.



**Young, P., Ferguson, C., Banuelos, S. and Gautel, M.** (1998). Molecular structure of the sarcomeric Z-disk: two types of titin interactions lead to an asymmetrical sorting of alpha-actinin. *EMBO J.* **17**:1614-1624.

**Yu, B., French, J. A., Carrier, L., Jeremy, R. W., McTaggart, D. R., Nicholson, M. R., Hambly, B., Semsarian, C., Richmond, D. R., Schwartz, K. and Trent, R. J.** (1998). Molecular pathology of familial hypertrophic cardiomyopathy caused by mutations in the cardiac myosin binding protein C gene. *J.Med.Genet.* **35**:205-210.

**Zakhary, D. R., Moravec, C. S., Stewart, R. W. and Bond, M.** (1999). Protein kinase A (PKA)-dependent troponin-I phosphorylation and PKA regulatory subunits are decreased in human dilated cardiomyopathy. *Circulation* **99**:505-510.

**Zhang, R., Zhao, J. and Potter, J. D.** (1995). Phosphorylation of both serine residues in cardiac troponin I is required to decrease the Ca<sup>2+</sup> affinity of cardiac troponin C. *J.Biol.Chem.* **270**:30773-30780.

**Zot, A. S. and Potter, J. D.** (1987). Structural aspects of troponin-tropomyosin regulation of skeletal muscle contraction. *Annu.Rev.Biophys.Biophys.Chem.* **16**:535-559.

